High temperature felsic volcanism and the role of mantle magmas in Proterozoic crustal growth: The Gawler Range Volcanic Province

by

Kathryn P Stewart
B.Sc. Hons. (Adelaide 1985)

Submitted in fulfilment of the requirement
for the degree of Doctor of Philosophy

Department of Geology and Geophysics
The University of Adelaide
South Australia

June, 1992

Awarded 1994

Abstract

The volcanism of the Mesoproterozoic Gawler Ranges has been divided into two phases. The first phase, which was the initial volcanism in any particular area, was comprised of sequences of dominantly silicic ignimbrites and lavas of small to moderate volume, with a minor mafic lava component, which erupted at scattered, spatially distinct centres. The mafic rocks are basalts and basaltic andesites which are enriched in LILE and depleted in HFSE, a signature which was inherited from an earlier enrichment event in the sub-continental lithospheric mantle. The silicic volcanics of the developmental phase contained 0-15% phenocrysts, which were plagioclase ± pyroxene ± magnetite ± potassium feldspar (in rhyodacites and rhyolites) ± quartz (in rhyolites). Systematic variation of Nd isotope values with various chemical parameters indicate that the silicic magmas formed by a combined assimilation and fractional crystallization (AFC) process between a mantle-derived mafic endmember similar to the coeval basalts and continental crust, with the mantle component dominant in all cases. The result of the mixing process was the eruption of isotopically heterogeneous packages of volcanics with similar chemistry at any given silica level due to the dominant effect of fractional crystallization. Systematic variation in the position of the isotopic arrays from the northern developmental centres to those further south may indicate a younging of the basement age away from the exposed Archaean basement.

The second phase of volcanism, termed the mature phase, represented an abrupt change to eruptions of large volume ignimbrites which were mostly dacitic to rhyodacitic in composition, with only minor silicic lava flows. The magmas of the entire mature phase (minimum estimated volume approximately 4,000km^3) are isotopically homogeneous and mineralogical and chemical data indicate they represent a single evolutionary sequence which fractionated from a more mafic magma which was chemically and isotopically homogeneous. The early erupted units are chemically and mineralogically zoned, which was the result of fractional crystallization. The zoning was not repeated, indicating that once eruptions from the mature phase chamber began, the rate of eruption exceeded the rate at which zoning could be regenerated. The magmas evolved under high temperature (>950-1100°C), low fO_2 (≤FMQ), and low water activity conditions fractionating the phenocryst assemblage plagioclase + pigeonite + augite + magnetite + potassium feldspar ± quartz (in rhyolites) ± olivine (in rhyolites). The mature phase volcanics are interpreted to have been emplaced at near magmatic temperatures, resulting in a high degree of welding of the ignimbrites and common granophyric recrystallization of the matrices. The homogeneous isotopic nature of the magmas is a physical consequence of the vigorous convection which

followed the formation of the large mature phase chamber from a number of the smaller developmental phase chambers. The mature phase chamber was in the mid-crust (top at 8-15 kilometres) but the source vent area is still unknown, but it may be a subtle feature unlike the spectacular calderas of the western United States.

Two contrasting types of magmatic inclusions occur in the mature phase volcanics, each of which sheds light on magmatic processes in the province. Type 1, of basaltic andesitic composition, reveals that mantle derived mafic magmas were present in the magma system until the cessation of volcanism. The silicic andesitic type 2 inclusions are interpreted to be a remnant of a more mafic precursor in the mature phase evolutionary sequence ripped from a mushy zone on the periphery of the magma chamber during eruption, and as such lend support to the interpretation that the mature phase volcanics are the result of an extensive fractionation history.

The exposed dominantly silicic magmatism of the Gawler Range province is demonstrated to have been contemporaneous with the intrusion of a very large mid-crustal gabbroic body, which provides evidence for the large volume of mafic magma needed to produce the silicic volcanics by AFC processes. The magmatism resulted in considerable modification of the lithosphere and in particular in the hybridization of the crustal volume beneath the Gawler Ranges, the net result of which was considerable crustal growth.

It is suggested that fractionation dominated AFC processes between basalts and crust is a mechanism, for the production of anorogenic granites and volcanics which may be obscured in many cases by the convective homogenization within large silicic magma chambers.

Statement of Originality:

I hereby certify that this thesis does not incorporate, without acknowledgement, any material which has been previously submitted for a degree or diploma in any university, and to the best of my knowledge and belief, it does not contain any written or published material by another person, except where due reference is made in the text.

Kathryn Patricia Stewart
June, 1992

I, Kathryn Stewart, give consent to this copy of my thesis, when deposited in the University Library, being available for loan and photocopying.

Signature

Acknowledgements

I would like to thank my supervisor, John Foden, for his friendship, enthusiasm and help. Numerous ideas in this thesis evolved from discussions with John. Everyone should find a PhD supervisor whose expertise extends from geology to gourmet cooking, it is a great combination. Many memorable meals were whipped up by John and Di, and some great evenings were spent in the abode at Belair, both before and after its conversion into a mansion.

Critical technical assistance was provided by many staff including: D. Bruce, G. Trevelyan, P. McDuie, J. Willoughby, J. Stanley, R. Barrett and W. Mussared, all of whom had to put up with the occasional hassling from me in one of my more harried moods. I have enjoyed many discussions with geologists from the South Australian Geological Survey, particularly Sue Daly of the Regional Geology section whose enthusiasm for geology was infectious and whose extensive knowledge of the geology of the Gawler Craton and the Gawler Range Volcanics made hers a brain to pick.

The fact that the usual onerous nature of microprobe work was transformed into a much more enjoyable task was entirely due to that always cheerful Welshman, Huw Rosser. No amount of trouble with the microprobe seemed to dim his view of life. He should be cloned!

The research was carried out against a backdrop of constant support, advice (not always good!), and general good cheer provided by friends including Sophie, Andy, Mike B., Tania, Graham, Jane, Karen, Kurt, Thomas, Jo, Bunge, Simone, Liz, Nat, Anna, Mike S., Bridget, Pru, Andrew, Nick, Meredith, Huw, Jim, Pandy, Alan, Phil, Mike, Libby and Nigel. All of these people have helped make the last few years the most memorable of my life.

The love and support provided by my parents not only during the production of this thesis but throughout my university career has been unfailing, and I cannot thank them enough for their care in looking after this wayward daughter who decided to enter university and the financially uncertain world of the student rather than remain in the secure environs of employment. Thanks also to the rest of my family who have also patiently endured the highs and lows of having a uni student in their midst, including the grumpy pre-exam periods, the weird hours, and the terminal forgetfulness of anything outside of geology.

Finally, boundless thanks to Simon who has acted as sounding board, blow-out preventer, who has cheered me on every time the going got tough, and who has shared the adventures of travel, geology, cooking and life in general - I made it!

Table of Contents

Chapter 3. Evidence for the eruptive mechanism of the mature phase volcanics: the lava versus ignimbrite debate

Chapter 4. The characterization, evolution and genesis of a large volume, high temperature, silicic magma chamber, Part 1: mineralogy, petrology and magmatic conditions.

Chapter 5. The characterization, evolution and genesis of a large volume, high temperature, silicic magma chamber, Part 2: geochemical and isotopic constraints.

Chapter 7. The fundamental role of mafic magma in the generation of high temperature felsic magmas and the case for crustal growth

List of Figures

Chapter 1.

Chapter 2.

Chapter 3.

Chapter 4.

Chapter 5.

Chapter 6.

Chapter 7.

List of Tables

Chapter 2

Chapter 3

Chapter 4

Chapter 5

Chapter 6

Chapter 7

Chapter 1 - Introduction

1.1 - General introduction

The roles played by the different chemical and isotopic reservoirs of the earth in the generation of continental magmas is one of the key issues in modern igneous petrology. Continental volcanics, both mafic and felsic, may be sourced partly or totally from the asthenosphere, or the mantle or crustal components of the lithosphere. The recognition of sources of continental magmatism and the processes by which components from those different sources interact has, in recent years, been a subject of considerable scientific debate. Of particular interest are provinces which contain both mafic and silicic portions, for these compound the questions of source regions and in addition present a further problem to be unravelled, namely the relationship of felsic to mafic volcanism. This type of province represents the best chance for studying many of the complex problems associated with continental magmatism.

Large volume silicic volcanic provinces provide a unique chance to study the fluxes of, and temporal changes in, source components during the evolution of silicic continental magmatic systems. In the plutonic environment, time or space related compositional and/ or source variation may be muted if not totally obscured by convective homogenization and diffusion during an extended crystallization history. Because volcanic eruptions represent time slices in the history of a magmatic system, they represent a chance to study the relative effects of many physical and chemical processes such as fractionation, contamination, convection and zonation. Finally the resolution of source components and processes operative in the evolution of a magmatic province can, in turn, allow insights into crustal addition, and tectonic processes operative at the time of magmatism.

The setting for this thesis is the Gawler Craton and specifically the Mesoproterozoic Gawler Range Volcanics of the central craton which represent the final major magmatic event on the craton. The Gawler Range Volcanic province is an excellent locality in which to study continental volcanism and the development of large volume silicic magma systems. It is comprised of a number of early, well exposed areas of volcanic activity whose units exhibit considerable compositional diversity, which are overlain by later, areally extensive,

large volume silicic units. This provides an exceptional chance to determine the relative change in source components during the development of the province.This thesis documents a study of the volcanic portion of this magmatism and has the following aims:

1) to determine the chemical and isotopic characteristics of the volcanism, and to document spatial and temporal variations;

2) to assess the crustal and mantle contributions to the volcanism and the flux of components through time;

3) to study in detail the largest volume units and develop a model for their evolution and their relationship to each other;

4) to assess the evidence for the processes responsible for the initiation of melting and the continuance of magmatism;

5) to further understanding of lithospheric scale processes in large volume felsic magmatic provinces;

6) to determine whether any inferences can be drawn as to the tectonic regime in which the volcanism was generated.

1.2 - Current areas of interest in continental magmatism

A primary concern of igneous petrology is to define and understand the processes which initiate and contribute to magmatism within continents. This is a considerably more difficult task for continental magmatism than for the more intensively studied field of oceanic mafic magmatism due in large part to the added complexities of a greater possible number of separate source components coupled with the actions of various mixing processes which separately, or together, may obscure the origin of the magmas.

Continental flood basalt volcanism is the best known and most intensively studied type of intracontinental mafic magmatism. A general consensus at present links most such volcanism with the presence of mantle plumes and lithospheric extension, e.g. Carlson, (1991); White and McKenzie (1989). There is however still some uncertainty as to the relative importance of these two factors in the production of flood basalts, in particular whether the volcanism is a direct response of the impingement of a plume on the base of continental crust, or whether extension is initiated by changing boundary conditions and the volcanism results from extension of lithosphere which had been heated by the plume. Vigorous debate also continues on the question of source regions for continental flood basalt volcanism, whether they are derived solely from the plume or whether significant components are derived from the overlying lithospheric mantle and/or continental crust.

Studies of xenoliths from the lithospheric mantle of various ages have shown that much of the subcontinental lithosphere is variably enriched relative to depleted mantle regions such as those which source MORB (e.g. Erlank *et al.*, 1982, 1987; Menzies, 1983; Menzies *et al.*, 1983, 1987; Menzies and Halliday, 1988; Richardson *et al.*, 1985; Waters and Erlank, 1988). This type of enriched lithospheric component has been argued to be a significant component in flood basalts (e.g. Allegre *et al.*, 1981, 1982; Ellam and Cox, 1989, 1991; Peate *et al.*, 1990) and has been argued to be the sole recognised source in some cases (e.g. Hergt *et al.*, 1989, 1991). In addition continental flood basalts may be contaminated during their passage through the continental crust (e.g. Cox and Hawkesworth, 1984) further complicating their chemical and isotopic signature.

Many of the postulated sources and modification processes which have been outlined above in their connection with continental flood basalt volcanism have also been interpreted for smaller volume mafic magmatism within continents, including those in provinces which also have silicic members. For example mafic volcanism at least partly sourced from enriched or metasomatized mantle has been recognised in the western U.S.A. (Fitton *et al.*, 1991; Kempton *et al.*, 1991; Leat *et al.*, 1989; Lum *et al.*, 1989; Ormerod *et al.*, 1988; Thompson *et al.*, 1990). Thus the identification of components which may be derived from the sub-continental lithosphere and from the continental crust is a major task when dealing with continental basaltic rocks.

The identification of source(s) and mechanisms of differentiation of felsic magmas are equally complex and not a little controversial. These questions are particularly difficult to answer for large volume felsic magmas which often are chemically and mineralogically homogeneous (the monotonous intermediates of Hildreth, 1981). Therefore there are number of problems which must be solved in any study of a large volume felsic magmatic province, the answers to which may well shed light on continental magmatism in a more general sense. These include what initiates melting of the source regions, the identification of source components of the felsic magmas and whether they show temporal and spatial variation during the development of a volcanic province. One mechanism mooted for crustal melting has been crustal thickening. Recent modelling (e.g. Sandiford and Powell, 1990) has shown however that in many cases crustal thickening will not provide the requisite heat for partial melting of the crust, due to a number of factors such as slow thermal rebound due to the low inherent thermal conductivity of rocks and the lengthy period of time over which thickened crust must be maintained to generate the required heating by radiogenic means. Thus crustal thickening is unlikely to result in melting of the lower crust unless it is accompanied by significant thinning of the mantle lithosphere (Sandiford and Powell, 1990). Initiation of crustal melting by the intrusion into the crust of

basaltic melts is an alternative mechanism, and has been advocated by Hildreth (1981) and Huppert and Sparks (1988) amongst others. Continued input of mafic mantle magmas would also seem necessary to sustain felsic magmatism over long time periods, for recent fluid dynamical studies (e.g. Huppert and Sparks, 1988; Worster *et al.*, 1990) indicate that basaltic magma emplaced into the continental crust will solidify in the time range of 10^2-10^3 years (the exact time depending on a combination of factors including the temperature, composition and volume of the mafic melt, the temperature of the crust, and whether crustal melting is triggered). This is several orders of magnitude less than the 10^5-10^6 years which are considered to be required to form a felsic magma chamber of very large dimensions (Hildreth *et al.*, 1991; Shaw, 1985).

The necessity of a heat flux from the asthenosphere is less controversial than the idea that mantle lithologies may also be a partial source for continental silicic magmas. A traditional view is that such silicic magmatism is entirely derived from the melting of lithologies residing within the crust. This has been particularly emphasised for the granites and volcanics of the Lachlan Fold Belt, which have been divided into I- and S- types, interpreted to be the products of melting of igneous and metasedimentary rocks respectively, and which contain no source component derived from the contemporary mantle (Chappell, 1984; Chappell and White, 1974, 1984; Chappell and Stephens, 1988). In contrast, many recent studies have proposed that mantle mafic melts form a significant source component for felsic magmas (Feeley and Grunder, 1991; Gans *et al.*, 1989; Hildreth *et al.*, 1991; Johnson, 1991; Sharma *et al.*, 1991), and in some cases are the dominant, if not only source, with the felsic magmas generated by extreme differentiation (Foland *et al.*, 1988; Mahood and Halliday, 1988; Musselwhite *et al.*, 1989; Sparks, 1988; Turner *et al.*, 1992a). Therefore it would seem that there can be no single model which accounts for all continental felsic magmatism, rather each volcanic province must be evaluated individually. An approach which has proven effective in discriminating different source components is that which utilizes both major and trace element chemistry and radiogenic isotopes (Johnson and Lipman, 1988; McMillan and Dungan, 1988; Thompson *et al.*, 1986; Thompson and Morrison, 1988).

The determination of source(s) for continental magmatism, both mafic and felsic varieties, may, when considered in concert with other factors such as evidence for contemporaneous tectonism, allow some interpretation of current models of crustal growth and for the tectonic settings of magmatism. It has been shown that previous tectonic settings inferred on the basis of chemistry alone are prone to error (see Arculus (1987) and Duncan (1987) for discussion on this point).

1.3 - Geological setting and previous work

The Gawler Range Volcanic province is an areally extensive Mesoproterozoic sequence of volcanics which outcrop in the central part of the Gawler Craton (see inset Figure 1.1). The province is named after the physiographic range of rounded hills which form the southern portion of the province. The following summary of the tectonic evolution of the Gawler Craton is drawn predominantly from Fanning *et al.* (1988), Parker and Lemon (1982), Parker *et al.* (1985) and Webb *et al.* (1986). The development of the Gawler Craton has been divided into three megacycles. The first megacycle produced two metamorphic complexes, the Sleaford Complex in the south of the craton and the Mulgathing Complex in the north. These complexes formed by the deposition of a sequence of Late Archaean to Palaeoproterozoic sediments with some accompanying volcanism, all of which were metamorphosed to upper amphibolite-granulite facies and intruded by granitoids during the Sleafordian Orogeny. The resultant metamorphic complexes contain quartzofeldspathic gneisses, iron formation, garnetiferous gneisses, cordierite gneiss, together with some marble and calc-silicate and meta-basalt. The deformation associated with the Sleafordian orogeny had ceased by approximately 2300Ma. Megacycle 2 saw the deposition, somewhere between ≈1960Ma and ≈1840Ma, of a sequence of mixed clastic and chemical sediments on the basement metamorphic complexes. These sediments, which comprise the Hutchinson Group, include calc-silicate, quartzite, dolomite, iron formation, and various schist types. Layer parallel, interbedded amphibolites have been interpreted as basaltic flows (Parker and Lemon, 1982). The Hutchinson group occurs only in the eastern third of the craton. Subsequent sedimentation and volcanism was restricted to small scale basin development on the easternmost part of the craton and as a result units belonging to this phase of megacycle 2 are areally restricted. Episodic bimodal volcanism occurred, and resulted in interbedded volcanics and basin sediments. These volcanic sequences include the Myola, Tidamurkana and McGregor Volcanics. The sedimentation and accompanying volcanism of Megacycle 2 was punctuated by the three deformation phases of the Kimban Orogeny and associated acidic and basic plutonism. The earliest intrusives are represented by the ≈1850Ma. Donington Granitoid Suite, which occur on the south-eastern portion of the craton. Extensive granite plutonism occurred in later in the Kimban orogeny, and these granitoids are variably foliated depending on the exact time of intrusion relative to the Kimban orogenic cycle. The dominant event in Megacycle 3 was the eruption of the Gawler Range Volcanics and the

associated subvolcanic Hiltaba Granite Suite. No deformation appears to have been associated with this widespread magmatism.

Much of the study of the Gawler Range Volcanics has been carried out by members of the South Australian Geological Survey over a period of over twenty years, particularly Hugh Blissett and Sue Daly, who have carried out mapping of the province and division of the volcanics into units. Detailed study of the volcanics have been thus far restricted those in the Kokatha area (Branch, 1978; Robertson, 1989) and the Lake Everard area (Giles, 1980). A summary of some of the features of the Yardea Dacite (Creaser and White, 1991) is the most recent published work on the province.

In this study volcanism in the Gawler Range volcanic province has been divided into two phases, termed the developmental and mature phases. These two phases were originally defined on stratigraphic, spatial and volumetric grounds, and this study indicates that the two phases are also characterized by quite different chemical and isotopic characteristcs. The developmental phase includes all the volcanics which occur in the Tarcoola, Kokatha and Lake Everard areas and in addition the Bittali Rhyolite and units which stratigraphically underlie it. The mature phase is comprised of the remaining uppermost part of the volcanic sequence from the Nonning Rhyodacite to the Yardea Dacite.

The developmental phase comprises three discrete centres exposed along the western margin of the province, the Tarcoola, Kokatha and Lake Everard centres, and a fourth area, termed herein the southern Gawler Range area (SGRA) which takes the form of a thin, discontinuous band of outcrops along the south-western and southern edge of the province (Figure 1.2).

The developmental phase volcanism in each of the four areas was composed of chemically and isotopically heterogeneous sequences of lavas and ignimbrites of relatively small to modest volumes, containing low to moderate phenocryst contents. At the onset of the mature phase, the character of volcanism changed to large ignimbrite sheets with relatively a relatively minor lava component. The units erupted during the mature phase were mostly large volume eruptions (up to 3,000km^3 of magma in a single unit) which contain a higher average proportion of phenocrysts than the developmental phase volcanism, and which formed an isotopically homogeneous and chemically well defined fractionation sequence.

All four developmental volcanic areas are dominated by silicic members, and basalts occur in all centres with the exception of the SGRA. Small inliers of presumed developmental phase volcanism outcrop through Quaternary cover to the south of the main province, and further volcanic centres of the developmental phase are likely to be concealed

beneath the blanketing mature phase sequence. In each of the four areas discussed in this chapter, the developmental phase volcanics represent the initiation of Gawler Range magmatism.

The Tarcoola volcanic centre is the northernmost of the areas discussed in this thesis (Figure 1.2), and is made up of three units, the Konkaby Basalt, the Ealbara Rhyolite and the Carnding Rhyodacite (Figure 1.1; Daly, 1985). The underlying rocks in this area belong chiefly to the Archaean Mulgathing Complex and the Palaeoproterozoic Tarcoola Formation. The Mulgathing Complex comprises granite gneisses, metasediments including garnet gneiss, banded iron formation, quartzite, marble and calc-silicate, and meta-gabbroic bodies. The Tarcoola Formation is a metasedimentary sequence of siltstone, quartzite and conglomerate containing minor silicic to basaltic tuffs (Daly, 1985). The Ealbara Rhyolite and Konkaby Basalt are each composite units, the former is dominantly ignimbritic with some lava flow component whereas the latter is composed of lavas, agglomerates, some lapilli tuff (Cowley and Martin, 1991; Daly, 1985) with minor interbedded dacite (Daly, 1985) in places.

The Kokatha volcanic centre is situated on the north-western shore of Lake Gairdner (Figure 1.2). Granite gneiss, calc-silicates and metamorphosed pillow basalts belonging to the Mulgathing Complex form the basement to the volcanic sequence in this area. The volcanic sequence at Kokatha is well exposed and eastward dipping, the stratigraphy of which is illustrated in Figure 2.1. The stratigraphic names used in this study for the Kokatha area are a modified version of those defined by Robertson (1989), rather than those of previous workers (Branch, 1978; Blissett, 1975). The Kokatha volcanic sequence is also predominantly silicic, but it does contain considerable thicknesses of basalt and basaltic andesite, which are herein divided into three types - low phosphorous (LP), high phosphorous (HP) and intermediate phosphorous (IP). The LP and HP basalt/basaltic andesite groups outcrop in the lower part of the succession, and are both reasonably thick piles (each in the order of hundreds of metres thick). In contrast the IP basaltic andesite is only quite a thin unit and was erupted within the large package of felsic eruptives which succeeded the HP basaltic andesites (Figure 2.1). Felsic volcanics in the Kokatha area occur throughout the sequence, but whereas they are subordinate in the lower section where the LP and HP basalts occur, they dominate the succession above the level of the HP basaltic andesites (Figure 2.1). Most of the felsic lithologies are interpreted to have erupted as ignimbrites, with some extruded as lavas. The volcanics at Kokatha are interpreted to have erupted in two cycles, based on chemical and isotopic data which are discussed in later sections.

The Lake Everard volcanic centre, located on the southern edge of Lake Everard (Figure 1.2) is a complex volcanic pile of felsic ignimbrites and lava domes with a very minor outcropping basaltic component. The stratigraphy of the area is illustrated in Figure 2.1, the units are as defined by Giles (1980, 1988). No basement rocks outcrop in this area, and it is therefore uncertain whether the lowermost unit, the Childera Dacite, is underlain by basement or earlier erupted volcanics.

The southern Gawler Range area is defined in this thesis as all volcanics south of latitude 32°00' which lie stratigraphically below the Eucarro Dacite in the west of the province or below the Nonning Rhyodacite in the east of the province. They form a curvilinear belt along the south-west and southern edges of the mature phase volcanism. The units which comprise the SGRA are the Bittali Rhyolite, the Waganny Dacite, both of which are unit names for a complex grouping of lavas and ignimbrites, and a rarely outcropping rhyolite termed PaO1. All of these names are those defined by Blissett (1986). In much of the SGRA, a single unit is all that outcrops in any one area (Figure 1.1). However in the Toondoolya Bluff area, east of Lake Acraman (Figure 1.2), a small sequence composed of three sub-units each of the Waganny Dacite and the Bittali rhyolite underlie the mature phase (Eucarro Dacite). The study of the SGRA is concentrated on this area as variations in chemistry and isotopic values can be related to the known stratigraphy, which facilitates comparison with the other three areas. The age and makeup of the basement in the Toondoolya Bluff area is unknown, the nearest outcropping basement is approximately 80 kilometres to the south-east. Indeed in this area it is not known if the Waganny Dacite represents the first erupted member of the volcanic sequence. In the remainder of the SGRA, along the southern margin of the GRV province, the Bittali Rhyolite can be observed intruding metasediments belonging to the Palaeoproterozoic (≈1850-1920 m.a.) Hutchinson Group which is thus defined as basement to the volcanics in this region.

The mature phase of the Gawler Range volcanism is dominated by large volume dacitic and rhyodacitic units, with minor rhyolitic to rhyodacitic lava flows, all of which are interpreted to have tapped a single, zoned, evolving magma chamber. The units which erupted from this final magma reservoir are, in interpreted stratigraphic order, the Nonning Rhyodacite, the Eucarro Dacite, the Yannabie Rhyodacite, the Paney Rhyolite and the Yardea Dacite. All names are taken from the formal stratigraphic nomenclature defined by Blissett (1975, 1986).

The subdivision of the volcanics into developmental and mature phases as outlined above is a significant departure from previous attempts to correlate from one volcanic area within the province to another. The most recent published correlation is shown in Figure

1.1, where the basal member of the mature phase, the Nonning Rhyodacite, is correlated with the Bunburn Dacite at Lake Everard, the Chandabooka Dacite at Kokatha and the Carnding Rhyodacite at Tarcoola. Work carried out during the course of this research has proven this correlation to be incorrect.

The known basement distribution around the Gawler Range Volcanic province has been outlined in the above discussion of the developmental volcanism. The extent of Proterozoic and Archaean basement under the extensive blanket of the mature phase units is unknown. The current extent of the volcanics probably represents only a portion of their original distribution. To the north-northeast the volcanics are covered by younger sediments including the Mesoproterozoic Pandurra Formation (ca. 1420 Ma., Fanning *et al.*, 1983), while blanketing Quaternary sediments occur to the west and south.

1.4 - Aims and structure of this thesis

This thesis is based on an extensive but by no means exhaustive sampling of the volcanics of the Gawler Range Volcanic province for petrographic, chemical and isotopic study. The sheer size of the province prohibits sampling of every single unit or facies thereof for a regionally based project such as this. Field mapping did not form a part of this project, a decision which was based on two factors: field observations (later backed up by petrographic and chemical data) indicated the mapping program by the South Australian Geological Survey had in all but a few cases ascribed the boundaries between units correctly, and that the unit divisions were fundamentally sound; the time necessary to map the province would be prohibitive (the Geological Survey mapping program of the Gawler Ranges had lasted more than 15 years).

All of the thin sections, polished thin sections, hand specimens and rock powders are kept at the University of Adelaide, Department of Geology and Geophysics under the accession number A884- .

This research project was initiated to document the temporal variations in geochemistry and isotopic characteristics of the province, to use this information to synthesize a model for the formation of this volcanic province as a whole, and to assess the general applicability of the model thus generated for other large felsic volcanic provinces. Early research work on the thesis focussed on collecting samples from throughout the province to create a chemical database. The sheer size of the province resulted in a decision, made relatively early in the work, to focus the thesis on the western half of the province, as this was where most of the earlier volcanism outcropped. Isotopic determinations were then made on a selected group of samples from the overall database, chosen so as to reveal any temporal and/or spatial changes in isotopic values.

The early chemical and isotopic evolution of the province is documented in Chapter 2, together with spatial and temporal variations both within and between individual areas of volcanism. This is then used to develop a general model for the sources and processes involved in the developmental phase volcanism. The volcanological features of the mature phase volcanics are outlined in Chapter 3, and are used to interpret whether they represent ignimbrites or lavas, which is currently a controversial topic for high temperature silicic volcanics. The mineralogical, chemical and isotopic characteristics of the voluminous mature phase volcanics are presented in Chapters 4 and 5, the relationships between the various mature phase units is determined and the evolution of the mature phase magma chamber is unravelled.The unexpected discovery during field work of magmatic inclusions within units of the mature phase resulted in Chapter 6, which documents their physical, petrographic and chemical features which together with some isotopic work, allow the distinction of two inclusion types with different petrogenetic histories and different relationships to the mature phase magmatism. Chapter 7 presents isotopic data on a large mid-crustal gabbroic body which provides a link between the magmatism and a major influx of mantle derived mafic magma into the lower crust, and finally outlines a preferred petrogenetic model for the evolution of the Gawler Range Volcanic province.

Figure opposite:

Figure 1.2 - Simplified map of the Gawler Ranges volcanic province showing the various developmental centres and the mature phase units

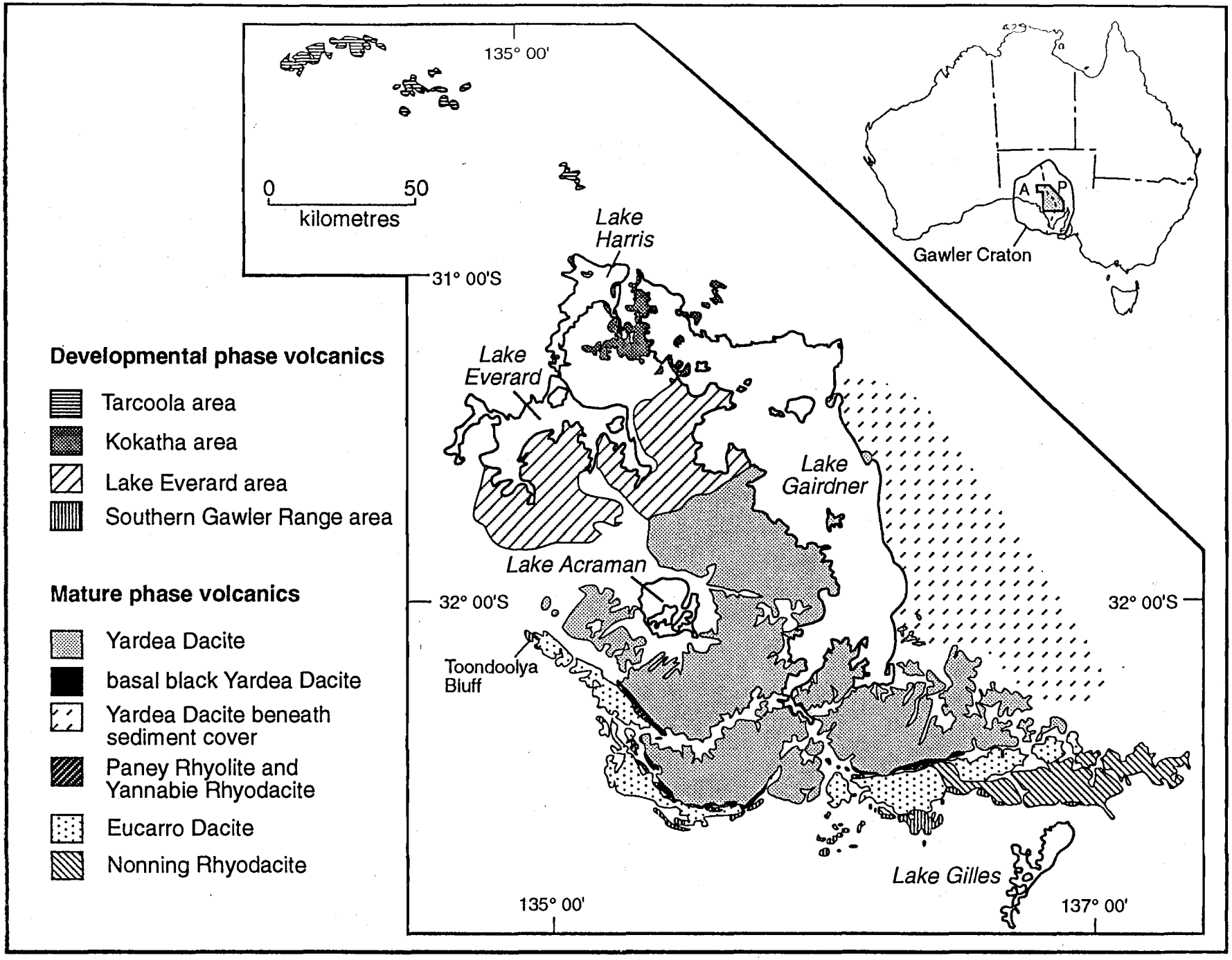
135° 00'
0
50
kilometres
Lake Harris
31° 00'S
Lake Everard
Lake Gairdner
Lake Acraman
32° 00'S
32° 00'S
Toondoolya Bluff
Lake Gilles
135° 00'
137° 00'
A
P
Gawler Craton
Developmental phase volcanics
Tarcoola area
Kokatha area
Lake Everard area
Southern Gawler Range area
Mature phase volcanics
Yardea Dacite
basal black Yardea Dacite
Yardea Dacite beneath sediment cover
Paney Rhyolite and Yannabie Rhyodacite
Eucarro Dacite
Nonning Rhyodacite

Chapter 2 : Chemical and isotopic evidence for the genesis of a dominantly felsic volcanic province by contamination and mixing of basaltic magma.

2.1 - Introduction

Numerous recent studies have attempted to define the roles of mantle derived and continental crustal sources in the formation of relatively large volumes of felsic magma in continental settings (e.g. Musselwhite *et al.*, 1989; Hildreth *et al.*, 1991; Johnson *et al.*, 1990; Riciputi and Johnson, 1990; Sharma *et al.*, 1991). This chapter presents a chemical and isotopic study of the four spatially separate volcanic areas of the developmental phase of Gawler Range volcanism as defined in Chapter 1. The object of the study is to compare and contrast the geochemical and isotopic evolution of the developmental phase volcanism, to identify the sources of the volcanics and to reveal the mechanisms involved in their petrogenesis.

2.2 - Geological Setting

The volcanic stratigraphy of each of the developmental phase areas is given in Figure 2.1. The most complex sequences are those at Kokatha and Lake Everard, whereas at Tarcoola and in the SGRA the developmental phase is represented by only a few units. Basalts occur in three areas, at Tarcoola, Kokatha and Lake Everard, but are absent in the SGRA. Because of the large number of units being dealt with in this chapter, and the highly variable state of preservation of their phenocryst assemblages (see below), the study of the evolution of each of the four provinces, and that of the developmental phase volcanism as a whole, is focussed on chemical and isotopic data.

2.3 - Petrography of the developmental phase volcanics

The average percentage of phenocrysts in the developmental phase volcanics is low to moderate, with most units containing between 1% and 15% phenocrysts. Units which contain a greater proportion of phenocrysts (>15%) are mostly rhyolite.

Figure opposite:

Figure 2.1- Simplified stratigraphic columns of the four areas of developmental volcanism. The diagram is schematic and is not intended to indicate real or inferred unit thicknesses. The units below and above the dashed line belong to the developmental phase and mature phase respectively. It is not known whether the non-occurrence of mature phase units indicates they were never deposited in the Kokatha and Tarcoola areas or whether they have been eroded away.

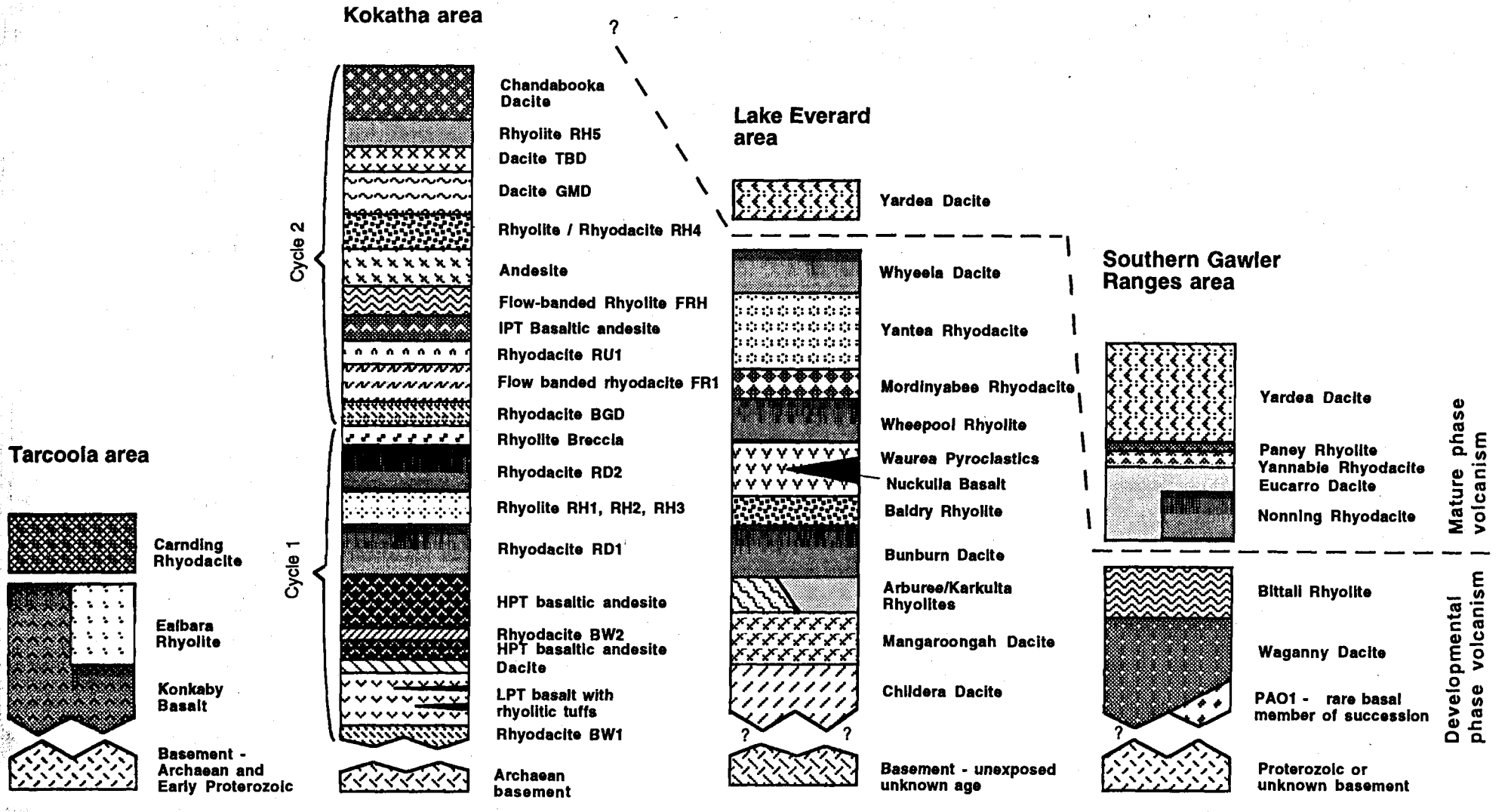
Kokatha area
Tarcoola area
Lake Everard area
Southern Gawler Ranges area
Cycle 2
Cycle 1
Chandabooka Dacite
Rhyolite RH5
Dacite TBD
Dacite GMD
Rhyolite / Rhyodacite RH4
Andesite
Flow-banded Rhyolite FRH
IPT Basaltic andesite
Rhyodacite RU1
Flow banded rhyodacite FR1
Rhyodacite BGD
Rhyolite Breccia
Rhyodacite RD2
Rhyolite RH1, RH2, RH3
Rhyodacite RD1
HPT basaltic andesite
Rhyodacite BW2
HPT basaltic andesite
Dacite
LPT basalt with rhyolitic tuffs
Rhyodacite BW1
Archaean basement
Carnding Rhyodacite
Ealbara Rhyolite
Konkaby Basalt
Basement - Archaean and Early Proterozoic
Yardea Dacite
Whyeela Dacite
Yantea Rhyodacite
Mordinyabee Rhyodacite
Wheepool Rhyolite
Waurea Pyroclastics
Nuckulla Basalt
Baldry Rhyolite
Bunburn Dacite
Arburee/Karkulta Rhyolites
Mangaroongah Dacite
Childera Dacite
Basement - unexposed unknown age
Yardea Dacite
Paney Rhyolite
Yannabie Rhyodacite
Eucarro Dacite
Nonning Rhyodacite
Bittali Rhyolite
Waganny Dacite
PAO1 - rare basal member of succession
Proterozoic or unknown basement
Mature phase volcanism
Developmental phase volcanism

Preservation of primary mineralogy is extremely variable; Fe-Ti oxides are invariably exsolved and/or oxidized, plagioclase grains vary from slightly to totally sericitized, potassium feldspars may be partly to wholly sericitized and/or turbid or have undergone fine to relatively coarse unmixing of albite and orthoclase phases, while pyroxenes, although they are commonly the most well preserved mineral, have most often been replaced by chlorite, either partially or completely. The mineralogy is dominated by feldspar-pyroxene assemblages, with hydrous phenocrysts much less common.

A brief summary of the major phenocryst assemblages for different lithological groupings is given below.

2.3.1 - Basalts and basaltic andesites

The mafic volcanic units have been divided into three basic types, based on chemical grounds. The three groupings, whose chemical characteristics are discussed in a later section are 1) low phosphorous (LP) basalts, 2) high phosphorous (HP) basaltic andesites, and 3) intermediate phosphorous (IP) basaltic andesites. LP basalts occur in the Tarcoola, Kokatha and Lake Everard areas, whereas the HP and IP basaltic andesites occur at Kokatha only. No mafic volcanics are present in the SGRA.

The phenocryst assemblage of the LP basalts is typically augite ± plagioclase ± magnetite, with the total percentage of phenocrysts ranging from 2-10%. The phenocrysts are set in a matrix of fine plagioclase laths which may exhibit flow alignment. Some contaminated basalts from the Tarcoola area also contain xenocrysts of various types, e.g. quartz grains, or large (up to 10mm diameter) potassium feldspar xenocrysts with conspicuous reaction rims. Augite phenocrysts are often fresh and may show evidence of concentric and/or sector zoning. Plagioclase phenocrysts and groundmass laths are variably altered, while magnetite is unmixed and may be also oxidised.

The HP and IP basaltic andesites each have only rare phenocrysts of plagioclase set in a groundmass which contains fine pyroxene grains and a significant proportion of skeletal iron-titanium oxides (both magnetite and ilmenite). Some fresh pyroxene may occur but often most other phases are altered.

2.3.2 - Andesites

Rocks of andesitic composition occur in both the Kokatha and Lake Everard areas. The petrography of these andesites are alike, with augite + plagioclase + magnetite ± pigeonite as the main phenocryst phases. In addition the Kokatha andesite contains common quartz xenocrysts which are invariably surrounded by a reaction rim of pyroxene. The proportion of phenocrysts is variable up to a maximum of approximately 20%.

2.3.3 - Dacites and Rhyodacites

Dacites occur in all of the developmental volcanic areas, with the exception of Tarcoola. The almost ubiquitous mineral assemblage for the dacites is plagioclase + clinopyroxene ± magnetite, although the Bunburn Dacite at Lake Everard contains only rare phenocrysts of plagioclase.

Rhyodacites are present in all four developmental volcanic areas, and the most common phenocryst phases are plagioclase + pyroxene ± potassium feldspar ± magnetite. Hydrous ferromagnesian silicates are rare, and when they occur are almost certainly of secondary origin, e.g. calcic amphibole in the Carnding Rhyodacite, possibly having formed during slow cooling after eruption. Ragged rather than euhedral morphology of both phenocrysts and groundmass grains is a typical feature of this secondary hornblende, and a detailed morphologic and chemical description of this type of hornblende is given in Chapter 4 where it occurs in the Eucarro Dacite from the mature phase of volcanism.

2.3.4 - Rhyolites

Potassium feldspar becomes a dominant phenocryst phase in many of the rhyolites and the typical phenocryst assemblage is potassium feldspar + plagioclase + quartz ± pyroxene ± magnetite. Biotite, or pseudomorphs after biotite, have been observed in very few units, typically occurring in rather silicic rocks (>70% SiO_2) where its occurrence may be due to the build up of volatiles during crystallization and fractionation. The rhyolites often have well preserved primary volcanic textural features, such as perlitic cracking, flow banding, and pyroclastic textures. Examples of preserved pyroclastic textures from the developmental volcanics are shown in Figure 3.2b-d.

2.4 - The geochemistry of the developmental phase volcanics

Whole rock and trace element analyses of a total of 161 samples from the developmental phase of volcanism are presented in Tables 2.1-2.4. These analyses include those analysed as part of this study plus analyses from Giles (1980), Jagodzinski (1985), and Robertson (1989). All analyses were carried out at the University of Adelaide and inter-study agreement is excellent. This large data base has enabled a clear picture of the chemical character of each of the four provinces to be determined and comparisons between the four areas to be made.

2.4.1 - Terminology

The IUGS recommended QAFP modal terminology used for naming volcanic rocks, which is based on phenocryst phases and their proportions, has not been used in this study because of the difficulties encountered when dealing with sparsely phyric or aphyric units, coupled with the above-mentioned fact that preservation of the phenocrysts is highly variable both between and within individual units, and that alteration can make mineral identification difficult.

The secondary method nominated by IUGS for nomenclature of volcanics is illustrated in Figure 2.2, with the data for the developmental phase volcanics plotted. The official nomenclature was rejected in preference to the simpler scheme shown along the bottom of the diagram for two reasons - 1) it was considered that the scheme did not allow enough discrimination of the volumetrically dominant felsic rocks; 2) the mafic volcanics tended to straddle across the IUGS fields of basalt, trachy-basalt, basaltic andesite and basaltic trachy-andesite, and it was considered that better divisions for the mafic rocks were high, intermediate and low phosphorous (HP, IP and LP respectively) basaltic (sensu lato) rocks. Many of the units illustrated in the stratigraphic sections in Figure 2.2 straddle two divisions of the preferred scheme, in which case the unit name indicates the dominant chemical type.

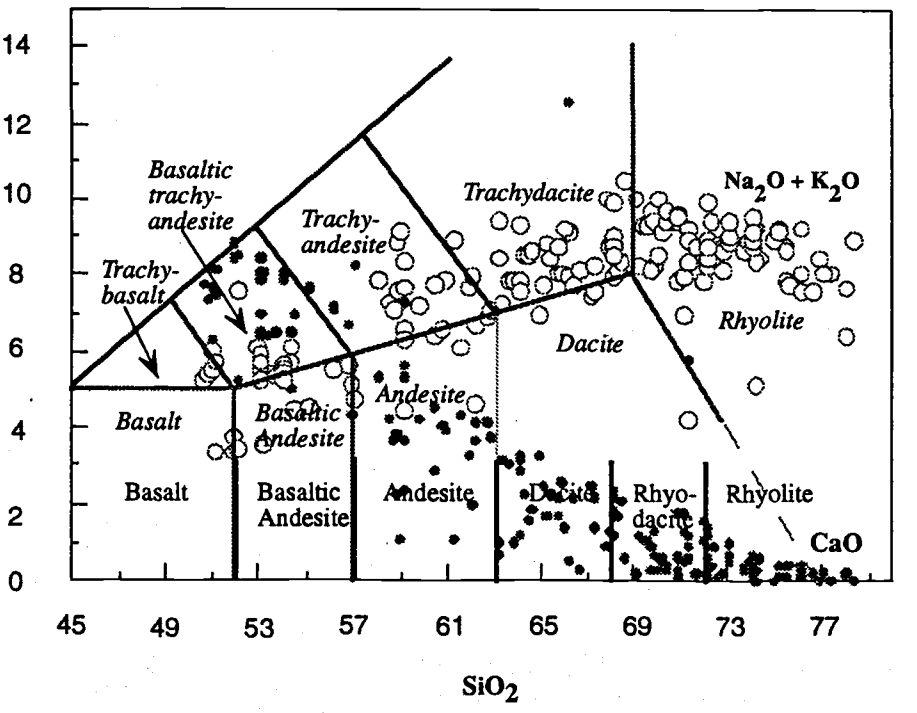

Figure 2.2 - Alkali-lime variation diagram for the developmental phase volcanics. CaO is plotted as filled circles, Na_2O+K_2O is plotted as open circles. IUGS classification (from Le Bas et al., 1986) is shown in grey lines with the fields labelled in italics. The classification used here is represented at the bottom of the figure, with solid lines separating the fields.

2.4.2 - The geochemistry of the Kokatha area

The Kokatha area has been studied in the most detail because it has the largest number of mappable stratigraphic units, which results in finer time divisions when looking at its chemical and isotopic evolution. The volcanics in this area erupted in two cycles (Figures 2.1, 2.3), based chemical and isotopic data as well as stratigraphic evidence.

Figure 2.1 illustrates the stratigraphy of the Kokatha area, and chemical analyses are listed in Table 2.1. Major element variation in the Kokatha volcanics is illustrated in Figure 2.3. For clarity in this and following diagrams the silicic rocks of the Kokatha province (those with > 63% SiO_2) are considered in three groups, cycle 1 volcanics, cycle 2 volcanics and the final eruptive unit, the Chandabooka Dacite (Figure 2.1). Major element variation with increasing SiO_2 content does not reveal a smooth pattern indicative of a single line of descent, and the same observation is made when major elements are plotted versus MgO. CaO, Al_2O_3 and MgO all decrease with increasing SiO_2. Fe_2O_3*, TiO_2, P_2O_5, and K_2O all show linear to curvilinear variation with increasing SiO_2 except the HP and IP basaltic andesites which define a much steeper trend. Na_2O first increases and then decreases with increasing SiO_2. The second phase felsic volcanics form two groupings, those with between 63 and 66% SiO_2 have Na_2O contents from 3.5-4.2% whereas those with more than 70% SiO_2 show a large variation in Na_2O content, from 2.5 to almost 5% with little change in SiO_2. This latter grouping exhibits antithetic behaviour between K_2O and Na_2O and some of this variation may be due to post-emplacement alkali movement. The first cycle felsic volcanics in contrast show a relatively coherent trend in both alkalis, Na_2O decreases whereas K_2O contents rise and then plateau from approximately 69% SiO_2 upwards where potassium feldspar becomes an important fractionating phase and buffers the level of K_2O.

Trace element variation diagrams are presented as Figure 2.4. With the exception of the Pb-SiO_2 diagram, all the graphs in Figure 2.4a illustrate much the same type of variation and the same chemical groupings. The LP basaltic andesites plot at lower contents of Zr, Nb, REEs, Y and Th than the LP and IP rocks of similar SiO_2 content, and the andesites plot in a cluster at much the same level as the more mafic rocks (again with the exception of Pb). The first cycle felsic volcanics plot in a semi-linear to curvilinear array which either decreases with increasing SiO_2 as with Zr, Nb and Y, or with a few exceptional samples the array stays at much the same level with increasing SiO_2 e.g. REEs, Th. The second cycle felsic volcanics on the other hand plot typically in three groups. The first of these groups plots between the andesites and the Chandabooka Dacite, and these samples are from the small volume units which lie spatially and

Table 2.1 - Major and trace element compositions of volcanics from the Kokatha volcanic centre

Sample§	*908-122*	*K101*	*884-K8*	*908-123*	*908-120*	*908-119*	*908-118*	*K33*	*K110*	*884-K4*	*884-K7*	*884-K3*	*884-K5*	*908-21*	*908-72*	*908-150*	*K122*
Lithology	*Rhyodacite BW1*	*LPT basalt*	*LPT basalt*	*LPT basaltic andesite*	*LPT basaltic andesite*	*Rhyolitic Tuff*	*LPT basaltic andesite*	*LPT basalt*	*LPT basalt*	*Dacite*	*Rhyodacite*	*HPT basalt*	*HPT basaltic andesite*	*HPT basaltic andesite*	*HPT basaltic andesite*	*HPT basaltic andesite*	*HPT basaltic andesite*
SiO2	71.91	51.91	51.00	54.50	56.90	74.07	53.11	52.01	51.94	63.14	70.78	52.96	54.22	53.32	53.02	52.99	54.28
TiO2	0.26	0.64	0.62	0.96	0.96	0.18	1.18	0.82	0.85	0.72	0.45	2.21	2.04	2.22	2.18	2.20	2.32
Al2O3	13.84	13.65	14.14	14.93	12.95	14.47	15.63	16.02	15.87	15.99	14.81	14.23	14.07	14.36	14.14	14.23	14.64
Fe2O3*	2.07	9.66	9.62	8.92	7.96	1.04	9.61	10.79	10.18	5.11	1.98	12.07	13.47	12.06	12.20	12.22	12.02
MnO	0.07	0.18	0.17	0.15	0.14	0.05	0.15	0.19	0.18	0.11	0.04	0.25	0.18	0.23	0.22	0.20	0.23
MgO	0.74	11.77	10.96	6.54	7.92	3.05	6.16	8.44	7.72	2.26	0.87	3.28	2.41	3.36	3.53	3.57	3.27
CaO	1.70	8.55	7.54	7.09	4.38	0.36	8.18	8.62	8.88	3.21	0.66	7.05	5.14	6.48	6.45	6.56	6.57
Na2O	3.61	2.15	3.15	3.32	2.10	2.19	2.75	2.51	2.59	5.13	4.35	2.70	2.69	2.77	3.27	3.27	3.01
K2O	4.34	1.27	0.28	1.23	3.07	3.04	0.86	1.06	1.23	2.24	5.33	3.14	3.51	2.74	2.73	2.63	2.75
P2O5	0.09	0.18	0.18	0.31	0.94	0.03	0.44	0.25	0.24	0.14	0.05	1.33	0.82	1.36	1.33	1.34	1.07
LOI	0.67	1.51	1.97	1.29	1.40	2.13	1.32	1.46	2.12	1.39	0.60	0.53	1.21	0.64	0.49	0.28	0.80
Total	99.30	101.47	99.63	99.24	98.72	100.61	99.39	102.17	101.80	99.44	99.92	99.75	99.76	99.54	99.56	99.49	100.96
Zr	156.0	102.0	102.0	164.0	328.0	104.0	170.0	124.0	119.0	417.0	392.0	233.0	220.0	231.0	224.0	226.0	234.0
Nb	11.9	5.3	4.8	8.1	13.5	10.0	8.0	5.9	5.6	19.3	17.8	9.6	8.8	9.2	9.8	9.9	11.0
Sr	296.0	510.0	427.0	995.0	749.0	650.0	714.0	480.0	547.0	432.0	162.0	635.0	529.0	547.0	506.0	491.0	519.0
Rb	133.0	45.0	9.7	34.0	130.0	154.0	25.0	36.0	42.0	32.0	155.0	72.0	69.0	121.0	87.0	74.0	82.0
Y	17.0	19.0	19.7	23.0	38.0	16.0	27.0	23.0	24.0	56.0	40.0	51.0	45.0	49.0	48.0	49.0	52.0
Ba	933.0	1005.0	492.0	830.0	1578.0	1531.0	651.0	718.0	842.0	1366.0	1373.0	2135.0	2456.0	1382.0	1585.0	1462.0	1700.0
Sc	5.2	29.0	31.0	25.0	24.0	2.8	26.0	30.0	32.0	12.0	7.2	31.0	31.0	30.0	26.0	26.0	32.0
Ga	n.a.	n.a.	19.0	n.a.	n.a.	n.a.	n.a.	n.a.	n.a.	21.0	19.0	23.0	21.0	23.0	21.0	n.a.	n.a.
Ni	9.0	362.0	289.0	102.0	151.0	7.0	107.0	192.0	197.0	4.0	0.0	5.0	6.0	3.0	3.0	7.0	8.4
Th	16.0	n.a.	5.7	4.0	19.0	15.0	6.0	n.a.	n.a.	29.0	27.0	9.4	11.0	13.0	9.9	8.0	n.a.
Pb	20.0	n.a.	12.0	9.0	19.0	10.0	11.0	n.a.	n.a.	24.0	35.0	15.0	12.0	14.0	12.0	9.0	n.a.
U	5.0	n.a.	2.8	5.0	6.0	5.0	3.0	n.a.	n.a.	7.8	5.2	6.0	3.5	5.4	4.0	3.0	n.a.
Ce	80.0	78.0	66.0	77.0	195.0	93.0	66.0	58.0	54.0	149.0	155.0	133.0	108.0	107.0	114.0	127.0	120.0
Nd	29.0	36.0	32.0	43.0	103.0	33.0	47.0	n.a.	21.0	63.0	59.0	66.0	41.0	66.0	64.0	65.0	63.0
La	16.0	n.a.	27.0	43.0	90.0	50.0	37.0	n.a.	n.a.	71.0	78.0	57.0	44.0	56.0	59.0	56.0	n.a.
V	29.0	180.0	182.0	176.0	157.0	7.0	189.0	176.0	179.0	20.0	19.0	156.0	217.0	155.0	143.0	152.0	167.0
Cr	11.0	1050.0	941.0	278.0	490.0	9.0	210.0	600.0	619.0	<5	5.0	<5	<5	1.0	1.0	1.0	14.0

§ Samples prefixed 884- and 908- were analysed for this study and for Robertson (1989) respectively. Samples without a prefix, viz. K101 are from Giles (1980).
n.a. - indicates element not analysed
** all iron as Fe2O3*

Table 2.1 - (continued)

Sample	*884-K28*	*884-K10*	*908-79*	*908-80*	*908-111*	*908-132*	*908-137*	*908-152*	*908-83*	*908-47*	*908-20*	*908-45*	*884-K11*	*884-K24*	*884-K25*	*908-44*
Lithology	*HPT basaltic andesite*	*Rhyodacite RD1*	*Rhyodacite RD1*	*Rhyodacite RD1*	*Rhyodacite RD1*	*Rhyodacite RD1*	*Rhyodacite RD1*	*Rhyodacite RD1*	*Air Fall Tuff TU1*	*Dacite RD2*	*Rhyodacite RD2*	*Air Fall Tuff TU2*	*Rhyolite RH1*	*Rhyolite RH1*	*Rhyolite RH1*	*Rhyolite RH1*
SiO2	53.49	72.24	69.46	69.33	70.74	70.13	69.67	71.19	69.78	67.76	69.71	77.85	75.29	76.54	75.34	74.18
TiO2	2.18	0.38	0.46	0.47	0.37	0.39	0.44	0.37	0.55	0.64	0.43	0.10	0.18	0.14	0.18	0.17
Al2O3	14.25	13.36	14.38	14.43	13.84	14.04	14.09	13.84	14.11	15.10	14.09	12.27	12.90	12.43	12.54	12.49
Fe2O3*	12.12	2.82	3.31	3.16	3.07	3.16	3.22	2.97	3.69	3.23	3.38	1.24	2.18	1.82	2.24	2.36
MnO	0.22	0.04	0.14	0.09	0.11	0.10	0.12	0.08	0.13	0.06	0.12	0.03	0.04	0.03	0.01	0.11
MgO	3.39	0.21	0.45	0.49	0.43	1.45	0.41	0.41	0.69	0.26	0.75	0.35	0.27	0.35	0.23	0.38
CaO	6.63	0.47	1.20	1.15	0.81	0.67	0.99	0.64	1.42	1.01	0.74	0.30	0.45	0.32	0.18	0.66
Na2O	2.76	4.39	4.26	4.58	4.26	4.25	4.02	4.17	4.17	4.83	4.21	2.33	2.91	2.62	3.15	3.72
K2O	2.51	5.12	5.14	4.79	5.24	4.99	5.79	5.16	4.14	5.31	5.33	4.11	5.07	5.03	5.71	4.78
P2O5	1.37	0.03	0.07	0.08	0.05	0.07	0.07	0.05	0.15	0.11	0.08		0.01	0.01	0.02	0.02
LOI	0.65	0.53	0.45	0.45	0.34	0.65	0.47	0.55	0.46	0.37	0.61	0.92	0.71	0.64	0.28	0.31
Total	99.57	99.59	99.32	99.02	99.26	99.90	99.29	99.43	99.29	98.68	99.45	99.50	100.01	99.93	99.88	99.18
Zr	230.8	346.0	360.0	365.0	372.0	377.0	367.0	372.0	365	367.0	370.0	145.0	297.0	239.0	301.0	303.0
Nb	10.1	17.3	17.3	18.2	17.4	17.9	18.7	17.0	17	19.4	17.5	21.0	14.2	12.3	13.2	15.5
Sr	552.6	120.0	210.0	211.0	121.0	130.0	186.0	116.0	200	222.0	152.0	33.0	51.0	36.0	60.0	44.0
Rb	117.9	170.0	171.0	147.0	172.0	160.0	191.0	214.0	153	183.0	174.0	231.0	196.0	211.0	193.0	168.0
Y	49.9	52.0	52.0	49.0	52.0	51.0	54.0	50.0	52	67.0	51.0	43.0	38.0	43.0	36.0	35.0
Ba	1377.9	1750.0	2338.0	2412.0	1982.0	2035.0	2251.0	1905.0	1793	1946.0	2188.0	237.0	963.0	642.0	968.0	901.0
Sc	26.6	11.0	12.0	12.6	10.0	10.5	11.1	10.5	12	10.7	10.7	2.4	6.6	4.8	4.3	6.3
Ga	19.8	14.0	20.0	18.0	n.a.	n.a.	n.a.	n.a.	n.a.	n.a.	19.0	n.a.	18.0	19.0	18.0	
Ni	2.2	4.0	3.0	2.0	3.0	4.0	4.0	3.0	1	2.0	2.0	2.0	3.0	2.0	4.0	3.0
Th	10.4	26.0	26.0	25.0	24.0	26.0	22.0	25.0	25	27.0	25.0	43.0	26.0	27.0	25.0	25.0
Pb	10.8	20.0	38.0	30.0	29.0	27.0	44.0	24.0	29	25.0	31.0	28.0	27.0	23.0	28.0	69.0
U	2.6	8.6	4.5	6.2	9.0	7.0	7.0	9.0	7	6.2	6.6	10.0	9.6	5.0	4.7	9.0
Ce	129.3	159.0	153.0	147.0	152.0	152.0	149.0	150.0	153	162.0	34.0	144.0	137.0	131.0	148.0	149.0
Nd	65.9	67.0	66.0	60.0	62.0	66.0	64.0	66.0	73	71.0	47.0	72.0	53.0	54.0	63.0	64.0
La	62.0	79.0	75.0	69.0	74.0	74.0	74.0	72.0	76	82.0	76.0	77.0	70.0	67.0	85.0	75.0
V	129.7	5.0	3.0	4.0	5.0	5.0	5.0	5.0	15	10.0	3.0	2.0	2.0	2.0	2.0	3.0
Cr	0.0	<5	1.0	1.0	1.0	1.0	6.0	1.0	1	1.0	1.0	1.0	<5	5.0	<5	1.0

Table 2.1 - (continued)

Sample § Lithology	*908-74 Rhyolite RH2*	*908-1 Rhyolite RH2*	*908-29 Rhyodacite BGD*	*908-12 Rhyodacite FR1*	*908-41 Rhyodacite RU1*	*K153 IPT basaltic andesite*	*908-61 IPT basaltic andesite*	*908-90 Rhyolite FRH*	*884-K12 Andesite*	*884-K15 Andesite*	*884-K16 Andesite*	*884-K26 Andesite*	*908-18 Andesite*	*908-51 Andesite*	*908-52 Andesite*	*908-53 Andesite*	*884-K13 Rhyolite RH4*
SiO2	75.46	76.00	71.77	72.08	72.32	53.69	52.91	73.57	62.12	62.50	62.69	60.21	60.33	59.68	61.39	60.88	73.70
TiO2	0.16	0.16	0.49	0.47	0.50	1.74	1.77	0.30	0.93	0.91	0.89	1.03	1.03	1.02	0.98	0.94	0.32
Al2O3	12.53	12.11	12.74	12.58	12.79	14.81	14.79	12.44	14.16	14.05	14.00	14.15	14.10	13.89	14.05	13.81	12.68
Fe2O3*	2.08	2.05	3.70	3.38	3.06	13.57	13.60	2.73	8.01	7.71	7.47	9.01	9.06	8.91	8.31	8.12	2.83
MnO	0.07	0.06	0.09	0.10	0.09	0.21	0.24	0.05	0.15	0.14	0.12	0.15	0.16	0.18	0.15	0.16	0.04
MgO	0.23	0.21	0.29	0.45	0.62	3.53	3.30	0.64	2.40	2.22	2.11	2.78	2.98	2.84	2.72	2.59	0.36
CaO	0.51	0.52	1.16	0.70	0.99	6.54	5.18	0.42	4.20	4.24	3.84	4.64	4.59	4.34	4.45	4.04	0.55
Na2O	2.43	2.41	3.08	3.66	3.84	3.23	3.65	3.39	3.59	3.75	3.89	3.64	3.64	4.41	4.31	4.53	4.08
K2O	5.38	5.21	5.52	5.31	4.71	2.20	2.51	5.46	3.21	3.20	3.31	2.70	2.82	2.88	1.86	3.37	4.93
P2O5	0.01	0.03	0.10	0.10	0.09	0.40	0.43	0.04	0.19	0.20	0.20	0.21	0.22	0.22	0.21	0.21	0.04
LOI	0.59	0.64	0.31	0.46	0.46	0.70	1.36	0.33	1.08	1.02	0.97	1.15	1.17	0.80	1.22	0.70	0.33
Total	99.45	99.40	99.25	99.29	99.47	100.62	99.74	99.37	100.04	99.94	99.49	99.67	100.10	99.17	99.65	99.35	99.86
Zr	263.0	266.0	471.0	464.0	231.0	229.0	233.0	325.0	211.0	210.0	218.0	208.9	207.0	212.0	212.0	211.0	322.0
Nb	14.7	14.1	24.0	25.0	10.9	9.5	8.8	14.8	8.7	9.5	9.6	8.6	8.9	8.0	8.2	8.2	14.4
Sr	40.0	41.0	73.0	70.0	191.0	433.0	432.0	82.0	368.0	355.0	375.0	390.6	389.0	381.0	352.0	382.0	104.0
Rb	203.0	185.0	246.0	214.0	143.0	67.0	98.0	173.0	110.0	108.0	102.0	100.0	103.0	111.0	67.0	121.0	159.0
Y	38.0	35.0	70.0	71.0	25.0	40.0	38.0	34.0	29.0	29.0	29.0	29.7	29.0	30.0	30.0	28.0	36.0
Ba	895.0	919.0	739.0	675.0	1679.0	976.0	1096.0	1346.0	1079.0	1003.0	1084.0	1013.0	1046.0	975.0	635.0	1046.0	1311.0
Sc	5.5	5.3	9.3	8.5	8.0	28.0	27.0	6.5	19.0	19.0	20.0	19.2	22.0	24.0	20.0	20.0	6.7
Ga	n.a.	n.a.	n.a.	n.a.	n.a.	n.a.	23.0	n.a.	22.0	20.0	20.0	21.1	19.0	21.0	20.0	21.0	18.0
Ni	4.0	2.0	4.0	3.0	5.0	8.4	5.0	2.0	10.0	11.0	8.0	12.1	14.0	15.0	11.0	13.0	3.0
Th	24.0	23.0	35.0	34.0	10.0	n.a.	7.6	17.0	9.8	12.0	11.0	11.7	8.9	9.7	12.0	11.0	17.0
Pb	50.0	44.0	34.0	42.0	28.0	n.a.	19.0	10.0	40.0	29.0	25.0	44.3	44.0	40.0	34.0	38.0	15.0
U	7.0	10.0	8.0	11.0	2.0	n.a.	2.5	6.0	3.0	4.9	3.8	1.3	4.1	3.4	4.2	3.3	1.6
Ce	129.0	133.0	189.0	189.0	79.0	86.0	85.0	112.0	89.0	87.0	110.0	82.3	83.0	81.0	75.0	87.0	120.0
Nd	53.0	5.0	81.0	81.0	31.0	45.0	45.0	45.0	34.0	35.0	36.0	34.4	34.0	35.0	33.0	39.0	46.0
La	67.0	67.0	94.0	94.0	43.0	n.a.	43.0	57.0	44.0	45.0	46.0	45.4	47.0	42.0	41.0	46.0	61.0
V	3.0	3.0	15.0	13.0	20.0	280.0	282.0	8.0	162.0	155.0	159.0	191.0	193.0	188.0	176.0	172.0	11.0
Cr	1.0	1.0	1.0	1.0	1.0	8.1	1.0	1.0	8.0	<5	<5	8.7	1.0	8.0	5.0	12.0	<5

Table 2.1 - (continued)

Sample	*884-K14*	*908-55*	*884-K17*	*884-K18*	*908-93*	*908-94*	*908-64*	*908-104*	*908-67*	*884-K19*	*884-K20*	*884-K22*	*884-K23*	*908-105*	*908-106*
Lithology	*Rhyolite RH4*	*Rhyolite RH4*	*Rhyodacite RH4*	*Rhyodacite RH4*	*Rhyodacite RH4*	*Rhyodacite RH4*	*Dacite GMD*	*Dacite GMD*	*Dacite TBD*	*Chandabooka Dacite*	*Chandabooka Dacite*	*Chandabooka Dacite*	*Chandabooka Dacite*	*Chandabooka Dacite*	*Chandabooka Dacite*
SiO2	72.04	73.60	70.98	70.71	71.25	71.19	64.09	65.65	65.71	67.97	67.00	67.14	68.17	68.00	68.38
TiO2	0.47	0.29	0.50	0.49	0.45	0.39	0.98	0.84	0.85	0.73	0.64	0.61	0.59	0.62	0.65
Al2O3	13.13	12.43	13.50	13.36	13.05	12.41	13.90	13.95	13.80	14.00	13.78	13.52	13.69	13.76	13.95
Fe2O3*	3.25	2.61	3.67	3.55	3.30	3.48	6.93	5.86	6.01	5.00	4.25	4.42	4.25	4.75	4.80
MnO	0.08	0.08	0.09	0.09	0.08	0.09	0.16	0.14	0.17	0.11	0.11	0.09	0.09	0.14	0.10
MgO	0.50	0.42	0.70	0.75	0.63	0.72	1.59	1.45	1.27	0.99	0.91	0.91	0.79	1.00	0.79
CaO	1.30	0.52	1.83	1.86	1.02	5.89	2.98	2.24	2.67	2.26	2.52	2.23	1.73	1.93	2.18
Na2O	3.75	3.45	3.98	4.04	4.80	2.81	4.05	4.12	3.55	3.79	3.44	3.28	3.48	3.63	3.30
K2O	4.54	5.27	4.07	3.95	3.64	1.54	3.62	3.97	4.61	4.29	4.08	4.41	4.78	4.43	5.15
P2O5	0.10	0.05	0.13	0.12	0.10	0.16	0.27	0.26	0.26	0.20	0.17	0.17	0.14	0.16	0.17
LOI	0.61	0.58	0.35	0.54	1.14	1.09	0.85	1.09	0.69	0.68	2.86	2.66	1.59	0.81	0.30
Total	99.77	99.30	99.80	99.46	99.46	99.77	99.42	99.57	99.59	100.02	99.76	99.44	99.30	99.23	99.77
Zr	250.0	327.0	218.0	220.0	243.0	214.0	239.0	238.0	399.0	386.0	352.0	330.0	330.0	350.0	345.0
Nb	11.9	14.4	11.5	11.2	12.3	9.6	9.8	10.6	18.6	17.3	14.5	14.0	13.8	14.0	14.3
Sr	188.0	82.0	287.0	279.0	190.0	341.0	359.0	322.0	208.0	187.0	209.0	212.0	247.0	209.0	225.0
Rb	156.0	180.0	131.0	110.0	120.0	60.0	141.0	136.0	181.0	156.0	142.0	134.0	165.0	157.0	166.0
Y	29.0	35.0	27.0	27.0	28.0	22.0	30.0	29.0	57.0	53.0	41.0	39.0	39.0	39.0	40.0
Ba	1277.0	1357.0	1210.0	1227.0	1109.0	586.0	1145.0	1213.0	1194.0	1225.0	1154.0	1620.0	1262.0	1203.0	1332.0
Sc	8.1	8.4	9.5	8.8	8.0	9.3	17.0	13.6	15.0	14.0	12.0	11.0	11.0	12.4	11.6
Ga	19.0	n.a.	18.0	18.0	n.a.	n.a.	20.0	n.a.	n.a.	19.0	19.0	20.0	20.0	n.a.	n.a.
Ni	1.0	1.0	2.0	3.0	4.0	5.0	4.0	4.0	7.0	6.0	3.0	2.0	5.0	8.0	4.0
Th	14.0	19.0	12.0	13.0	11.0	12.0	13.0	16.0	25.0	26.0	21.0	20.0	20.0	19.0	19.0
Pb	19.0	19.0	25.0	27.0	20.0	15.0	26.0	33.0	35.0	27.0	34.0	45.0	24.0	22.0	27.0
U	4.3	3.0	2.7	2.4	4.0	4.0	4.0	4.0	5.0	7.4	3.8	5.6	6.5	5.0	8.0
Ce	101.0	110.0	86.0	91.0	91.0	78.0	93.0	95.0	151.0	161.0	132.0	123.0	121.0	125.0	122.0
Nd	42.0	55.0	37.0	38.0	36.0	38.0	43.0	43.0	66.0	58.0	48.0	47.0	52.0	54.0	52.0
La	49.0	56.0	42.0	41.0	47.0	45.0	54.0	52.0	76.0	74.0	61.0	60.0	61.0	63.0	67.0
V	27.0	7.0	41.0	41.0	28.0	74.0	105.0	81.0	46.0	40.0	40.0	38.0	33.0	38.0	40.0
Cr	6.0	5.0	5.0	<5	1.0	6.0	1.0	6.0	7.0	<5	5.0	<5	<5	8.0	8.0

Figure opposite:

Figure 2.3 - Variation of major elements vs. SiO_2 for volcanics of the Kokatha area. Symbols: open squares, LPT basalts; open triangles, HPT and IPT basaltic andesites; filled squares, andesite of the second cycle; small crosses, silicic volcanics of the first phase; large crosses, silicic volcanics of the second phase excluding the Chandabooka Dacite; barred squares, Chandabooka Dacite.

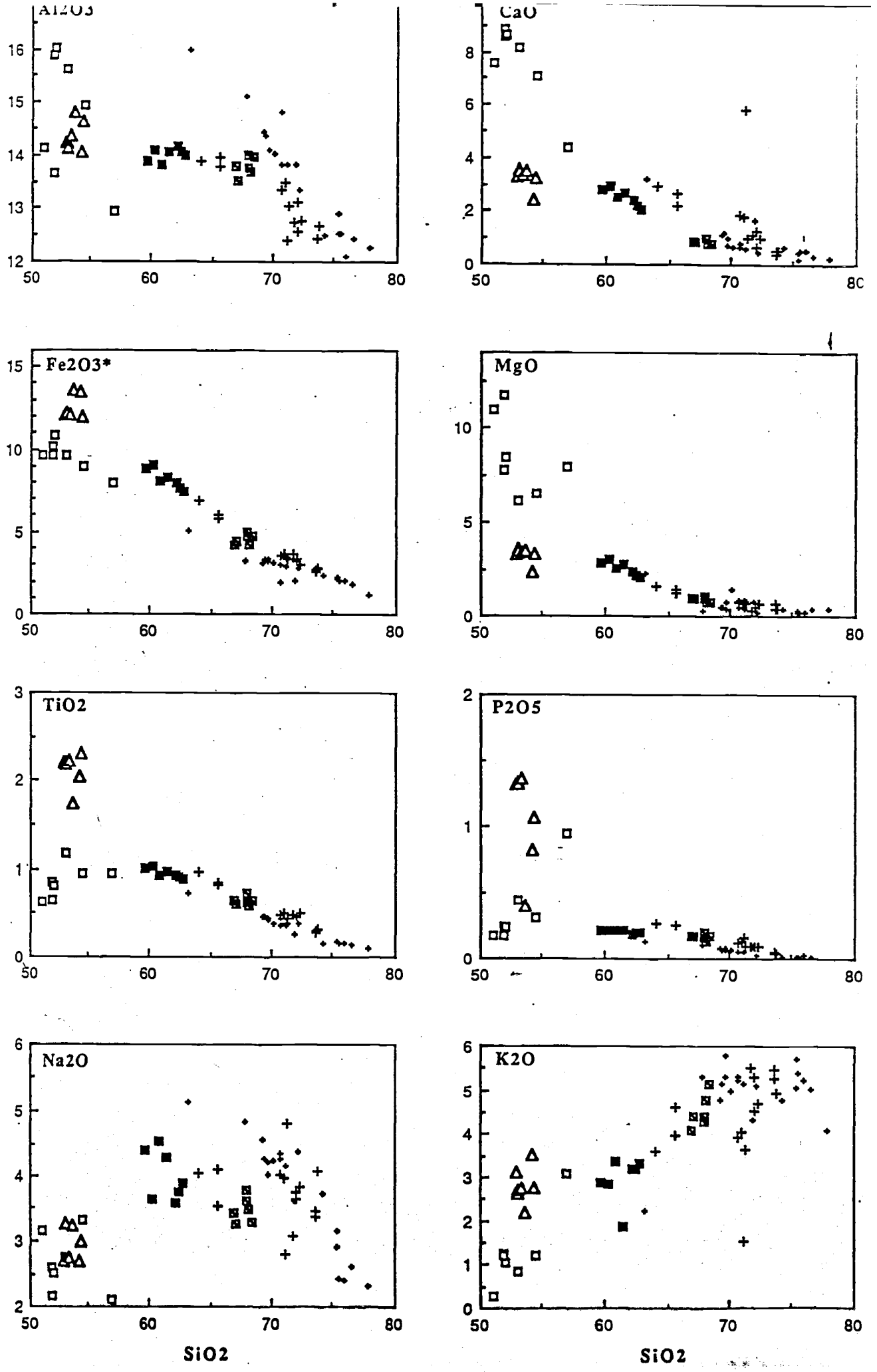
Al2O3
CaO
Fe2O3*
MgO
TiO2
P2O5
Na2O
K2O
SiO2
SiO2

temporally beneath the Chandabooka Dacite. A second group belong to a single unit (Rhyolite BGD) and have high contents of Zr, Nb, REEs, Y, and Th compared to all other silicic volcanics from Kokatha at the SiO_2 content of 72%. The third group, which are all samples from units Rhyolites FRH and RH4, have lower contents of the above-mentioned elements at their SiO_2 values than comparable first cycle felsic rocks. Ba and Rb show contrasting behaviour for the Kokatha volcanics. The HP and IP basaltic andesites have more Rb and much more Ba than the LP rocks. The andesites form a tight cluster between the mafic rocks (of moderate Ba content) and the Chandabooka Dacite. The felsic rocks of the first cycle show a broad increase in Rb but a strong linear decrease in Ba with increasing SiO_2. The felsic rocks of the second cycle fall into the same three groups as previously outlined and plot either between the andesites and the Chandabooka Dacite or in a sub-vertical array on both Ba and Rb plots with variable LILE contents with only a small increase in SiO_2. The compatible trace elements Sr, Sc, and V show variability with SiO_2 which corresponds roughly to the major elements CaO, Fe_2O_3* and TiO_2, and are thought to illustrate the removal of plagioclase, pyroxene and magnetite respectively. High to moderate Ni contents occur only in the in the LP mafic rocks and Ni is rapidly depleted with little increase in SiO_2. A positive linear correlation between MgO and Ni and between Cr and Ni, indicates that Ni is being removed by the fractionation of olivine ± pyroxene and Cr by olivine ± chrome spinel. Indeed the most mafic basalt has been found to contain spinel grains which have chrome spinel cores and Cr bearing magnetite rims indicating that chrome spinel was a crystallizing phase in at least the most mafic lavas.

2.4.3 - The geochemistry of the Lake Everard area

Major and trace element analyses for the volcanics from the Lake Everard volcanic area are presented as Table 2.2 and selected element and element ratio versus SiO_2 diagrams are given as Figure 2.5 and 2.6. With increasing amounts of differentiation the analyses plot as broad trends for the volcanic sequence as a whole, however quite a degree of scatter is produced by the rather variable trends followed by individual units. The overall patterns show Al_2O_3, TiO_2, CaO, MgO, Fe_2O_3*, MnO, P_2O_5, Sr, Sc, and V all decrease, and K_2O, Rb, Y and the REEs and Nb increase with increasing SiO_2. Na_2O concentrations are highly scattered both between and within units. Zr and Ba both exhibit complex behaviour with different units following different trends, which may be the result of differing timing of the onset of zircon and alkali feldspar crystallisation. The Mangaroongah and Whyeela Dacites and the Yantea Rhyodacite form a trend to high Zr levels with increasing SiO_2, Zr in the Childera Dacite decreases slightly with differentiation, whereas in the remainder of the felsic units of the area the Zr concentration remains relatively constant up to approximately 70% SiO_2, beyond which it decreases.

Figure opposite:

Figure 2.4a - Variation of trace elements vs. SiO_2 for volcanics of the Kokatha area. Symbols as for Figure 2.3.

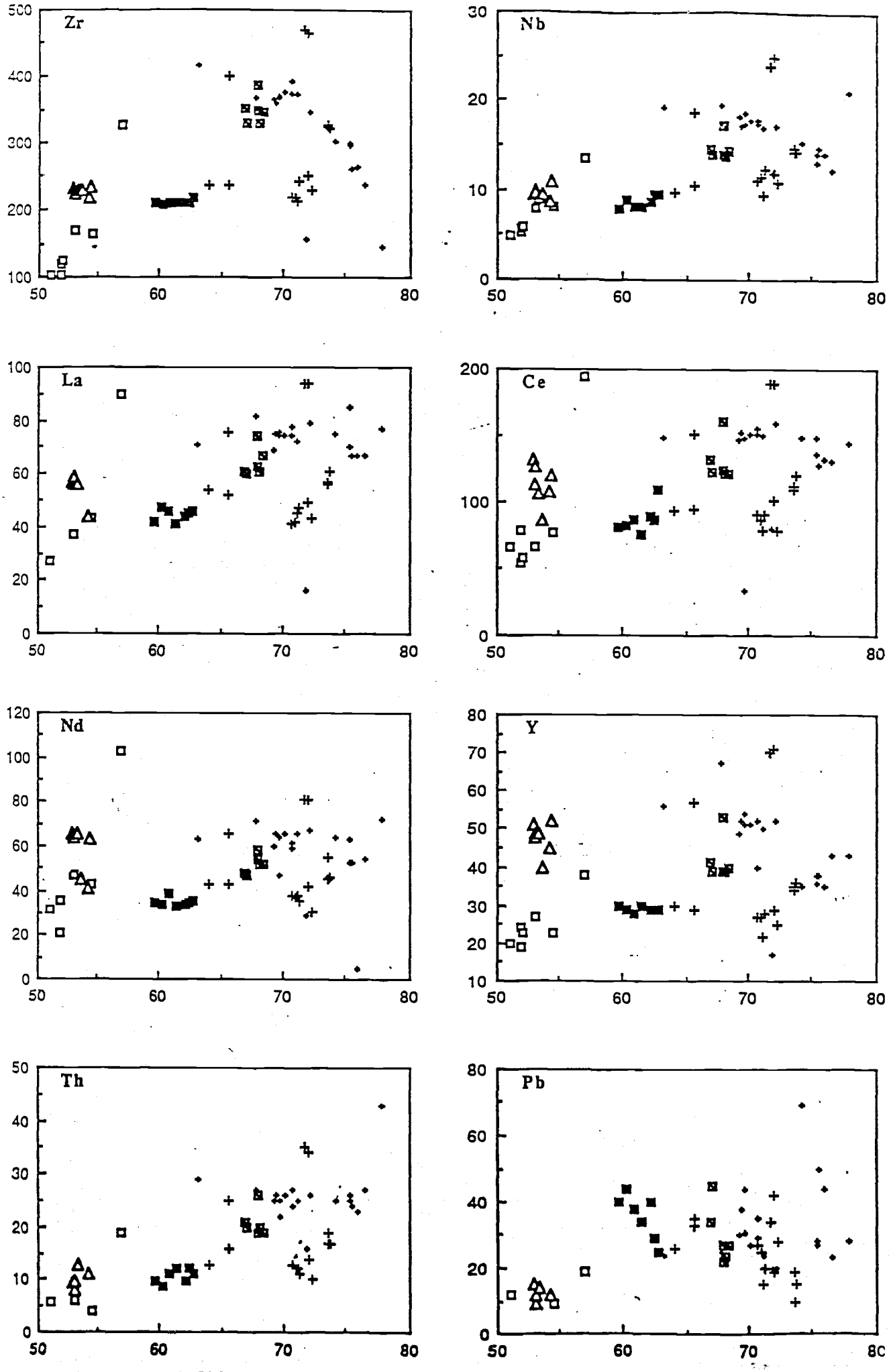
Zr
Nb
La
Ce
Nd
Y
Th
Pb
SiO2
SiO2

Figure opposite:

Figure 2.4b - Variation of trace elements vs. SiO_2 for volcanics of the Kokatha area. Symbols as for Figure 2.3.

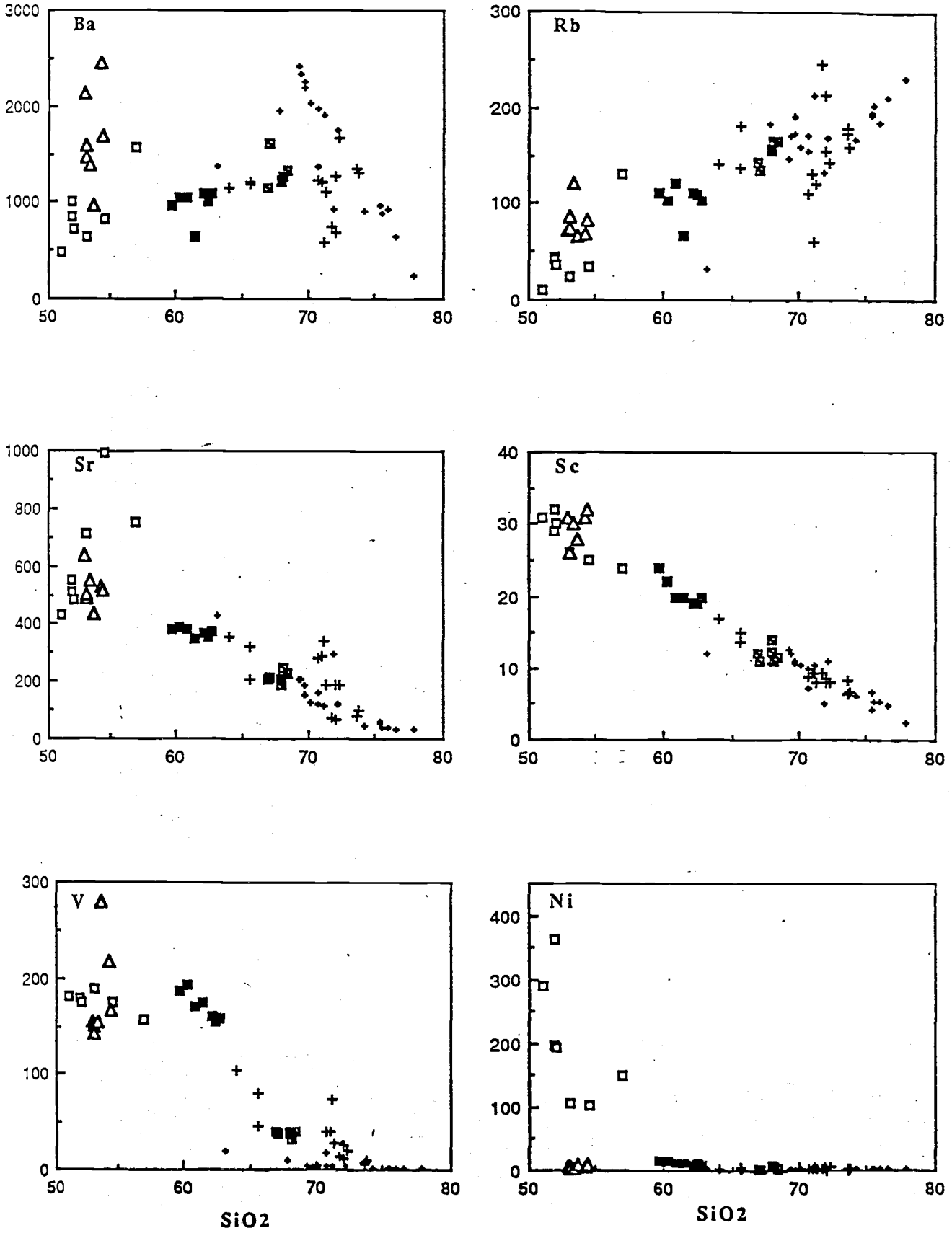
Ba
3000
2000
1000
0
50
60
70
80
Rb
300
200
100
0
50
60
70
80
Sr
1000
800
600
400
200
0
50
60
70
80
Sc
40
30
20
10
0
50
60
70
80
V
300
200
100
0
50
60
70
80
SiO2
Ni
400
300
200
100
0
50
60
70
80
SiO2

Table 2.2 - Major and trace element compositions of volcanics from the Lake Everard volcanic centre

Sample§ Lithology	*884-GH8 Childera Dacite*	*E278 Childera Dacite*	*E500 Childera Dacite*	*E50 Childera Dacite*	*E468 Childera Dacite*	*E494 Childera Dacite*	*884-GH5 Mangaroongah Dacite*	*884-GH10 Mangaroongah Dacite*	*884-GH4 ?Mangaroongah Dacite*	*E532 Mangaroongah Dacite*	*E524 Mangaroongah Dacite*	*E33 Mangaroongah Dacite*	*E747 Mangaroongah Dacite*
SiO2	60.36	60.61	61.79	63.57	64.16	64.34	58.71	64.55	69.17	56.67	58.58	59.07	61.91
TiO2	1.29	1.37	1.16	1.02	0.74	1.21	1.20	0.91	0.57	1.12	1.20	1.18	1.11
Al2O3	14.00	13.87	13.76	14.74	13.74	14.16	15.04	14.42	13.42	15.74	15.30	15.04	15.08
Fe2O3*	7.62	7.95	6.57	6.36	4.73	7.06	8.09	5.07	3.69	8.09	8.59	8.21	7.49
MnO	0.20	0.23	0.17	0.13	0.14	0.14	0.18	0.17	0.14	0.16	0.16	0.17	0.17
MgO	2.84	2.08	1.79	2.22	1.64	1.12	3.32	2.19	1.98	2.72	2.83	3.03	2.29
CaO	2.92	4.16	3.30	3.09	2.32	1.71	3.92	1.92	1.28	6.81	3.75	2.41	2.01
Na2O	3.07	4.80	4.61	3.41	3.41	3.85	3.75	3.90	3.65	3.74	3.33	2.82	3.06
K2O	4.79	1.87	3.17	4.55	5.22	4.76	3.85	4.86	4.71	1.92	3.83	4.94	4.98
P2O5	0.70	0.73	0.60	0.41	0.31	0.71	0.47	0.31	0.24	0.42	0.48	0.46	0.40
LOI	1.72	1.71	2.48	0.63	2.77	1.33	1.73	1.27	1.27	2.63	1.80	2.18	1.57
Total	99.51	99.38	99.40	100.13	99.18	100.39	100.26	99.57	100.12	100.02	99.85	99.51	100.07
Zr	273.0	281.0	251.0	282.0	243.0	n.a.	309.0	497.0	202.0	294.0	310.0	315.0	371.0
Nb	16.3	17.0	19.0	16.0	16.0	n.a.	11.7	14.8	16.1	13.0	12.5	14.0	13.0
Sr	351.0	340.0	286.0	404.0	250.0	n.a.	461.0	262.0	219.0	308.0	454.0	540.0	453.0
Rb	189.0	63.0	117.0	149.0	170.0	n.a.	118.0	140.0	168.0	77.0	117.0	193.0	155.0
Y	48.0	50.0	48.0	43.0	44.0	n.a.	44.0	46.0	45.0	42.0	43.0	41.0	47.0
Ba	2044.0	975.0	1240.0	1670.0	1160.0	n.a.	1424.0	2722.0	738.0	1000.0	1460.0	1780.0	2830.0
Sc	22.0	22.0	19.0	16.0	12.0	n.a.	21.0	16.0	11.0	21.0	n.a.	20.0	20.0
Ga	19.0	n.a.	n.a.	n.a.	n.a.	n.a.	20.0	19.0	16.0	n.a.	n.a.	n.a.	n.a.
Ni	9.0	17.0	15.0	19.0	n.a.	n.a.	18.0	8.0	7.0	21.0	23.0	28.0	25.0
Th	14.0	n.a.	n.a.	n.a.	n.a.	n.a.	12.0	14.0	19.0	n.a.	n.a.	n.a.	n.a.
Pb	10.0	n.a.	n.a.	n.a.	n.a.	n.a.	26.0	37.0	30.0	n.a.	n.a.	n.a.	n.a.
U	2.2	n.a.	n.a.	n.a.	n.a.	n.a.	2.5	2.4	3.4	n.a.	n.a.	n.a.	n.a.
Ce	101.0	104.0	84.0	106.0	115.0	n.a.	120.0	134.0	106.0	104.0	106.0	112.0	122.0
Nd	48.0	n.a.	n.a.	48.0	n.a.	n.a.	52.0	56.0	48.0	n.a.	n.a.	n.a.	55.0
La	42.0	n.a.	n.a.	n.a.	n.a.	n.a.	51.0	65.0	48.0	n.a.	n.a.	n.a.	n.a.
V	108.0	119.0	98.0	97.0	n.a.	n.a.	133.0	62.0	49.0	160.0	138.0	133.0	109.0
Cr	<5	n.a.	n.a.	n.a.	n.a.	n.a.	10.0	<5	6.0	n.a.	n.a.	24.0	n.a.

** all iron as Fe2O3*
§ Samples wothout prefixes from Giles (1980)
n.a. indicates element not analysed

Table 2.2 - (continued)

Sample	*E290*	*E126*	*E48*	*E554*	*E78*	*E627*	*884-GH11*	*E689*	*E227*	*E512*	*E62*	*E168*	*E540*	*884-GH20*
Lithology	*Mangaroongah Dacite*	*Mangaroongah Dacite*	*Mangaroongah Dacite*	*Arburee Rhyolite*	*Arburee Rhyolite*	*Karkulta Rhyolite*	*Bunburn Dacite*	*Bunburn Dacite*	*Bunburn Dacite*	*Bunburn Dacite*	*Bunburn Dacite*	*Bunburn Dacite*	*Bunburn Dacite*	*Baldry Rhyolite*
SiO2	62.18	63.01	64.03	74.06	74.97	72.71	58.82	58.86	61.11	63.02	65.08	66.08	68.97	78.20
TiO2	1.08	0.95	0.95	0.32	0.31	0.14	0.99	1.14	0.93	0.77	0.71	0.66	0.36	0.14
Al2O3	15.16	15.30	14.81	12.97	12.28	13.53	16.94	16.85	17.34	17.27	16.01	15.64	15.11	10.82
Fe2O3*	6.93	6.01	5.19	2.38	1.44	1.82	6.17	7.11	5.49	4.92	3.86	4.64	2.67	0.82
MnO	0.15	0.14	0.15	0.04	0.04	0.04	0.18	0.21	0.16	0.14	0.11	0.11	0.06	0.03
MgO	2.15	2.59	2.31	0.36	0.32	0.37	3.09	2.17	2.58	1.47	1.60	1.53	0.04	0.04
CaO	3.72	1.05	1.24	0.09	0.18	0.34	2.38	1.16	1.18	0.78	1.77	0.56	0.28	0.09
Na2O	4.34	4.13	3.98	2.26	2.09	3.85	4.46	5.57	5.38	4.89	4.07	4.32	4.78	1.03
K2O	0.40	4.40	5.42	7.09	7.20	4.83	4.43	3.65	3.62	4.59	4.87	4.94	5.29	7.96
P2O5	0.41	0.32	0.26	0.06	0.04	0.02	0.52	0.70	0.54	0.32	0.20	0.26	0.02	0.00
LOI	1.87	2.27	1.54	0.69	0.95	1.62	2.02	2.12	1.78	2.23	1.65	1.40	1.88	0.48
Total	98.39	100.17	99.88	100.32	99.82	99.27	100.00	99.54	100.11	100.40	99.93	100.14	99.46	99.61
Zr	408.0	n.a.	542	312.0	298.0	132.0	268.0	311.0	273.0	365.0	334.0	314.0	426.0	157.0
Nb	14.0	n.a.	16	24.0	23.0	14.0	12.4	15.0	13.0	16.0	16.0	14.0	19.0	19.8
Sr	298.0	n.a.	220	50.0	85.0	131.0	753.0	395.0	493.0	476.0	500.0	430.0	296.0	15.1
Rb	126.0	n.a.	142	210.0	211.0	133.0	142.0	113.0	127.0	176.0	159.0	156.0	155.0	304.0
Y	14.0	n.a.	48	53.0	60.0	23.0	37.0	47.0	37.0	40.0	35.0	36.0	45.0	66.0
Ba	2170.0	n.a.	2940	676.0	2010.0	2120.0	1554.0	1765.0	1340.0	2945.0	1870.0	1730.0	1940.0	138.0
Sc	20.0	n.a.	15	6.0	5.0	2.4	15.0	14.0	14.4	8.0	11.0	11.5	6.0	3.1
Ga	n.a.	n.a.	n.a.	n.a.	n.a.	n.a.	20.0	n.a.	n.a.	n.a.	n.a.	n.a.	n.a.	12.0
Ni	n.a.	n.a.	15.6	n.a.	n.a.	n.a.	4.0	11.0	9.0	n.a.	n.a.	n.a.	n.a.	3.0
Th	n.a.	n.a.	n.a.	n.a.	n.a.	n.a.	13.0	n.a.	n.a.	n.a.	n.a.	n.a.	n.a.	23.0
Pb	n.a.	n.a.	n.a.	n.a.	n.a.	n.a.	14.0	n.a.	n.a.	n.a.	n.a.	n.a.	n.a.	24.0
U	n.a.	n.a.	n.a.	n.a.	n.a.	n.a.	2.5	n.a.	n.a.	n.a.	n.a.	n.a.	n.a.	3.9
Ce	n.a.	n.a.	115	143.0	117.0	n.a.	112.0	144.0	136.0	n.a.	125.0	n.a.	n.a.	220.0
Nd	n.a.	n.a.	n.a.	50.0	45.0	n.a.	51.0	59.0	62.0	n.a.	52.0	n.a.	n.a.	74.0
La	n.a.	n.a.	n.a.	n.a.	n.a.	n.a.	51.0	n.a.	n.a.	n.a.	n.a.	n.a.	n.a.	85.0
V	n.a.	n.a.	68	n.a.	n.a.	n.a.	67.0	80.0	61.0	n.a.	24.0	n.a.	n.a.	2.0
Cr	n.a.	n.a.	n.a.	n.a.	n.a.	n.a.	<5	n.a.	n.a.	n.a.	n.a.	n.a.	n.a.	<5

Table 2.2 - (continued)

Sample	*E197*	*884-GH1*	*884-GH2*	*E231*	*E459*	*E434*	*884-GH15*	*E607*	*E615*	*E714*	*E599*	*884-GH12*	*884-GH18*	*884-GH14*	*E528*
Lithology	*Waurea Pyroclastics*	*Nuckulla Basalt*	*Nuckulla Basalt*	*Nuckulla Basalt*	*Nuckulla Basalt*	*Wheepool Rhyolite*	*Wheepool Rhyolite*	*Wheepool Rhyolite*	*Wheepool Rhyolite*	*Wheepool Rhyolite*	*Mordinyabee Rhyodacite*	*Yantea Rhyodacite*	*Yantea? Rhyodacite*	*Yantea Rhyodacite*	*Yantea Rhyodacite*
SiO2	75.38	50.85	50.65	50.85	50.76	72.06	72.44	72.71	74.03	77.36	67.23	70.31	65.55	70.27	68.45
TiO2	0.16	1.17	1.15	1.15	1.18	0.35	0.34	0.35	0.28	0.20	0.64	0.42	0.60	0.42	0.83
Al2O3	12.67	17.13	17.01	16.71	17.02	12.90	12.93	13.08	12.83	11.58	13.61	13.67	13.87	13.89	14.12
Fe2O3*	1.05	10.18	10.15	10.22	9.90	3.54	2.31	2.45	3.34	1.82	5.06	3.19	4.99	3.40	4.38
MnO	0.03	0.18	0.18	0.16	0.16	0.06	0.06	0.05	0.03	0.02	0.11	0.04	0.16	0.08	0.09
MgO	0.61	4.68	5.45	5.45	5.02	0.75	0.87	0.74	0.20	0.33	1.01	0.64	0.77	0.84	0.72
CaO	0.21	7.78	7.80	6.40	7.45	0.20	0.23	0.28	0.12	0.13	1.46	0.39	1.73	0.52	0.69
Na2O	2.92	3.14	3.56	3.70	3.59	2.51	2.60	2.66	2.62	2.18	2.92	2.61	3.86	3.43	4.72
K2O	5.80	2.46	1.71	2.33	1.92	6.47	6.36	6.19	5.84	5.91	5.44	7.19	4.95	6.11	5.90
P2O5	0.01	0.22	0.22	0.21	0.20	0.03	0.04	0.03	0.06	0.07	0.19	0.06	0.13	0.06	0.20
LOI	1.31	2.03	2.23	2.52	2.54	1.11	1.01	1.04	0.86	0.60	1.94	0.83	2.28	0.91	1.03
Total	100.15	99.82	100.11	99.70	99.74	99.98	99.19	99.58	100.21	100.20	99.61	99.35	98.89	99.93	101.13
Zr	168.0	163.0	162.0	159.0	158.0	412.0	425.0	413.0	348.0	289.0	432.0	678.0	525.0	667.0	600.0
Nb	24.0	8.5	8.9	8.6	9.3	20.0	19.8	22.0	20.0	20.0	22.0	20.0	16.5	19.9	16.0
Sr	19.0	401.0	450.0	529.0	446.0	45.0	47.0	38.0	44.0	26.0	168.0	97.0	87.0	61.0	137.0
Rb	241.0	99.0	56.0	85.0	58.0	205.0	217.0	198.0	214.0	215.0	219.0	211.0	126.0	185.0	163.0
Y	42.0	28.0	28.0	28.0	28.0	48.0	52.0	48.0	49.0	54.0	66.0	51.0	53.0	51.0	50.0
Ba	87.0	781.0	482.0	695.0	619.0	1005.0	1462.0	940.0	888.0	480.0	1710.0	1329.0	2235.0	1047.0	3270.0
Sc	3.0	25.0	23.0	24.0	23.0	8.0	8.8	8.0	6.0	4.0	14.0	10.0	16.0	11.0	14.0
Ga	n.a.	19.0	20.0	n.a.	n.a.	n.a.	18.0	n.a.	n.a.	n.a.	n.a.	19.0	19.0	20.0	n.a.
Ni	n.a.	96.0	93.0	112.0	98.0	n.a.	4.0	n.a.	n.a.	n.a.	n.a.	2.0	3.0	2.0	n.a.
Th	n.a.	6.2	6.2	n.a.	n.a.	n.a.	29.0	n.a.	n.a.	n.a.	n.a.	24.0	18.0	24.0	n.a.
Pb	n.a.	12.0	9.0	n.a.	n.a.	n.a.	6.0	n.a.	n.a.	n.a.	n.a.	32.0	7.0	8.0	n.a.
U	n.a.	0.3	3.6	n.a.	n.a.	n.a.	2.7	n.a.	n.a.	n.a.	n.a.	6.5	5.5	6.4	n.a.
Ce	n.a.	60.0	63.0	52.0	n.a.	n.a.	182.0	125.0	n.a.	n.a.	180.0	156.0	141.0	158.0	n.a.
Nd	n.a.	27.0	35.0	25.0	n.a.	n.a.	79.0	46.0	n.a.	n.a.	69.0	69.0	57.0	66.0	n.a.
La	n.a.	27.0	28.0	n.a.	n.a.	n.a.	97.0	n.a.	n.a.	n.a.	n.a.	73.0	66.0	75.0	n.a.
V	n.a.	203.0	198.0	188.0	183.0	n.a.	5.0	9.6	n.a.	n.a.	n.a.	5.0	9.0	5.0	n.a.
Cr	n.a.	63.0	61.0	106.0	86.0	n.a.	<5	n.a.	n.a.	n.a.	n.a.	<5	<5	<5	n.a.

Table 2.2 - (continued)

Sample	*E530*	*E294*	*E402*	*E395*	*E312*	*E742*	*E561*	*E515*	*E516*	*884-GH9*	*E705*	*I84*	*E417*	*E225*	*E230*
Lithology	*Yantea Rhyodacite*	*Yantea Rhyodacite*	*Yantea Rhyodacite*	*Yantea Rhyodacite*	*Whyeela Dacite*	*Whyeela Dacite*	*Whyeela Dacite*	*Yandoolka Rhyolite*	*Palthrubie Granophyre*	*Moonamby Dyke Suite*	*Moonamby Dyke Suite*	*Moonamby Dyke Suite*	*Moonamby Dyke Suite*	*Moonamby Dyke Suite*	*Moonamby Dyke Suite*
SiO2	70.01	70.72	70.80	72.58	58.49	64.78	63.76	71.26	76.77	74.81	65.24	66.56	67.78	71.57	76.07
TiO2	0.40	0.44	0.41	0.36	1.21	0.99	0.98	0.37	0.19	0.19	0.59	0.74	0.62	0.42	0.18
Al2O3	14.12	13.80	13.32	13.99	15.04	15.08	14.45	13.88	11.78	12.35	16.17	13.76	14.25	13.44	12.43
Fe2O3*	3.55	3.40	3.46	2.45	7.98	5.90	6.21	2.20	1.47	1.58	3.81	5.75	5.11	2.94	1.93
MnO	0.07	0.06	0.05	0.04	0.15	0.16	0.15	0.06	0.01	0.02	0.14	0.09	0.09	0.07	0.00
MgO	0.42	0.50	0.44	0.28	2.64	1.76	2.17	0.35	0.00	0.53	1.22	2.29	0.75	0.98	0.45
CaO	0.64	0.37	0.17	0.29	4.28	3.34	1.04	1.32	0.12	0.13	2.36	0.40	1.35	0.29	0.15
Na2O	4.20	3.64	3.27	5.82	3.63	2.88	3.26	3.56	2.53	2.71	3.26	3.05	3.70	3.53	2.61
K2O	5.93	6.07	6.35	2.45	3.76	4.19	4.70	5.42	6.04	6.29	5.23	5.23	5.15	5.30	5.55
P2O5	0.08	0.05	0.04	0.04	0.49	0.34	0.37	0.10	0.01	0.02	0.22	0.18	0.16	0.10	0.12
LOI	1.12	0.92	1.00	1.02	2.06	0.55	2.59	1.07	0.78	0.73	1.35	1.90	1.12	1.07	0.85
Total	100.54	99.97	99.31	99.32	99.73	99.97	99.68	99.59	99.70	99.36	99.59	99.95	100.08	99.71	100.34
Zr	653.0	654.0	643.0	569.0	309.0	476.0	402.0	239.0	239.0	232.0	324.0	406.0	418.0	347.0	191.0
Nb	21.0	20.0	20.0	17.0	12.0	16.0	14.0	19.0	20.0	17.5	17.0	21.0	24.0	20.0	21.0
Sr	65.0	49.0	58.0	76.0	486.0	336.0	339.0	240.0	58.0	51.0	405.0	79.0	188.0	84.0	45.0
Rb	186.0	174.0	174.0	70.0	104.0	139.0	139.0	209.0	283.0	276.0	174.0	167.0	196.0	220.0	321.0
Y	53.0	49.0	47.0	41.0	42.0	52.0	44.0	33.0	50.0	53.0	41.0	60.0	65.0	51.0	47.0
Ba	1240.0	1170.0	1160.0	550.0	1450.0	2390.0	4110.0	930.0	595.0	1603.0	1610.0	1270.0	1520.0	997.0	443.0
Sc	10.0	11.0	8.0	9.0	20.0	17.0	17.0	5.0	4.0	4.5	8.0	13.0	14.0	7.5	3.0
Ga	n.a.	n.a.	n.a.	n.a.	n.a.	n.a.	n.a.	n.a.	n.a.	17.0	n.a.	n.a.	n.a.	n.a.	n.a.
Ni	n.a.	n.a.	n.a.	n.a.	24.0	n.a.	n.a.	n.a.	n.a.	7.0	n.a.	10.0	n.a.	n.a.	n.a.
Th	n.a.	n.a.	n.a.	n.a.	n.a.	n.a.	n.a.	n.a.	n.a.	39.0	n.a.	n.a.	n.a.	n.a.	n.a.
Pb	n.a.	n.a.	n.a.	n.a.	n.a.	n.a.	n.a.	n.a.	n.a.	8.0	n.a.	n.a.	n.a.	n.a.	n.a.
U	n.a.	n.a.	n.a.	n.a.	n.a.	n.a.	n.a.	n.a.	n.a.	2.9	n.a.	n.a.	n.a.	n.a.	n.a.
Ce	n.a.	144.0	n.a.	n.a.	113.0	136.0	118.0	139.0	136.0	149.0	165.0	160.0	174.0	n.a.	n.a.
Nd	n.a.	61.0	n.a.	n.a.	54.0	n.a.	52.0	n.a.	n.a.	38.0	68.0	n.a.	n.a.	n.a.	n.a.
La	n.a.	n.a.	n.a.	n.a.	n.a.	n.a.	n.a.	n.a.	n.a.	40.0	n.a.	n.a.	n.a.	n.a.	n.a.
V	n.a.	8.0	n.a.	n.a.	131.0	65.0	93.0	n.a.	n.a.	3.0	53.0	47.0	n.a.	n.a.	n.a.
Cr	n.a.	n.a.	n.a.	n.a.	n.a.	14.0	n.a.	n.a.	n.a.	<5	n.a.	n.a.	n.a.	n.a.	n.a.

Figure opposite:

Figure 2.5 - Variation of major elements vs. SiO_2 for volcanics of the Lake Everard area. Symbols: open diamonds, Childera Dacite; filled triangles, Mangaroongah Dacite; diagonal crosses, Bunburn Dacite; open triangles, Yantea Rhyodacite; barred squares, Whyeela Dacite; open circles, Yardea Dacite (of the mature phase); crosses, other silicic units.

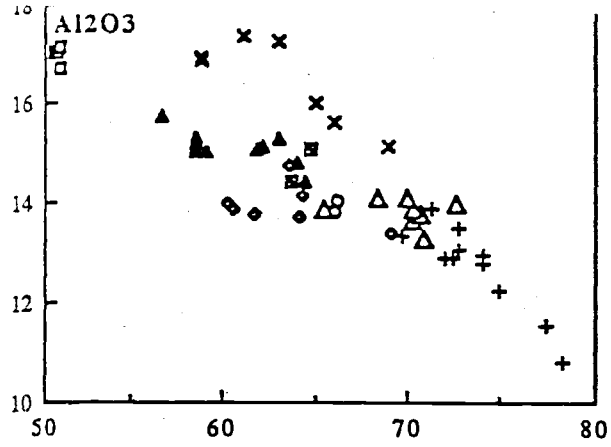
Al2O3
16
14
12
10
50
60
70
80

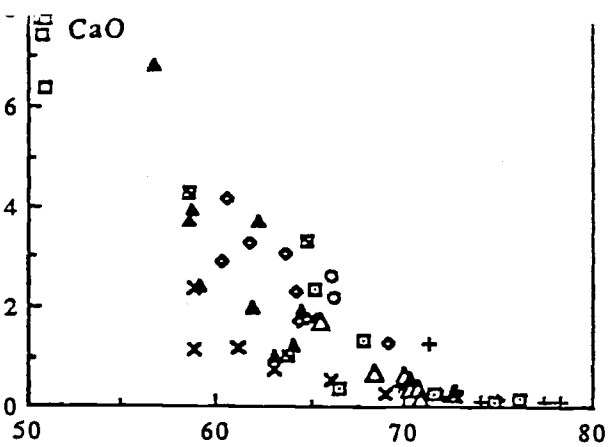
CaO
6
4
2
0
50
60
70
80

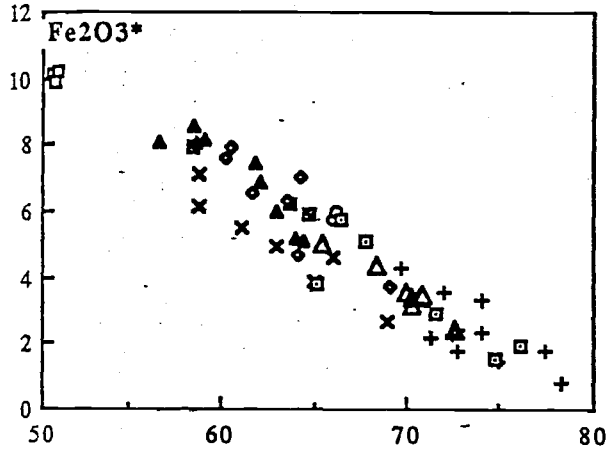
Fe2O3*
12
10
8
6
4
2
0
50
60
70
80

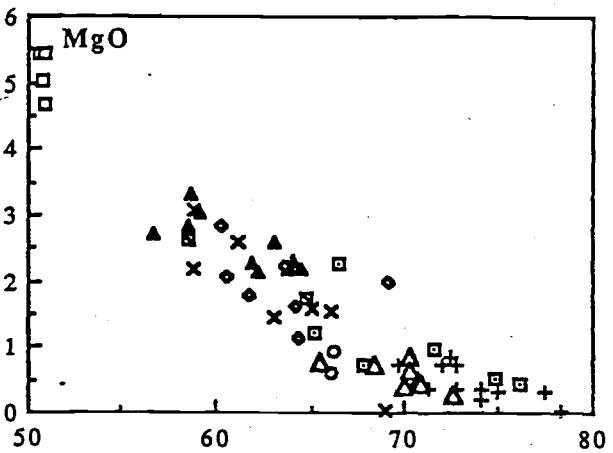
MgO
6
5
4
3
2
1
0
50
60
70
80

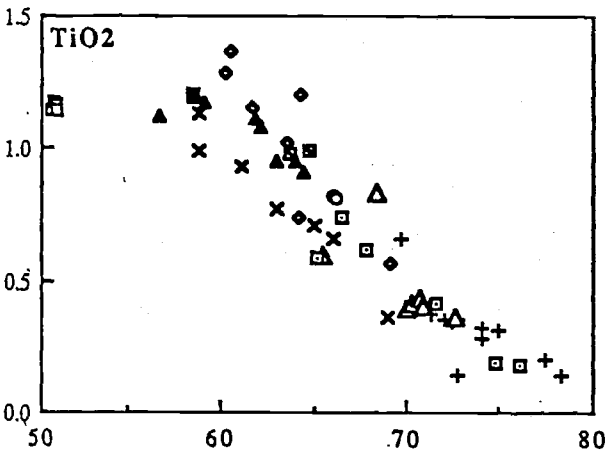
TiO2
1.5
1.0
0.5
0.0
50
60
70
80

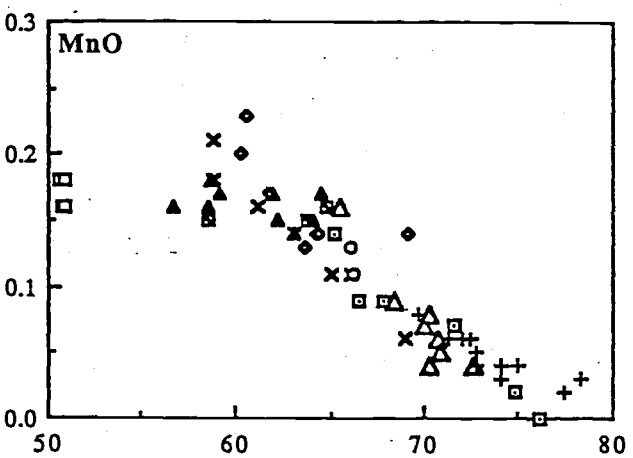
MnO
0.3
0.2
0.1
0.0
50
60
70
80

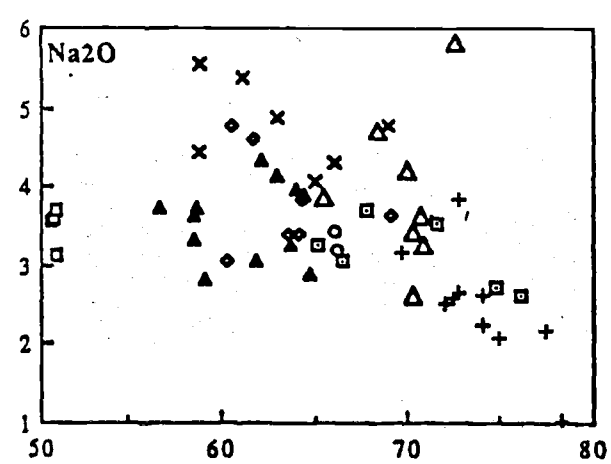
Na2O
6
5
4
3
2
1
50
60
70
80
SiO2

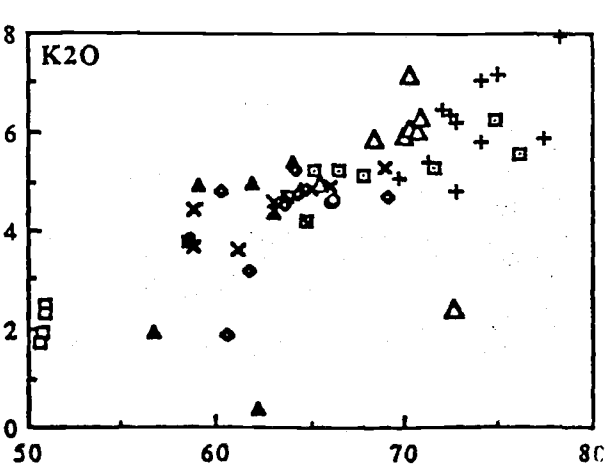
K2O
8
6
4
2
0
50
60
70
80
SiO2

Figure opposite:

Figure 2.6a - Variation of trace elements vs. SiO_2 for volcanics of the Lake Everard area. Symbols as for Figure 2.5.

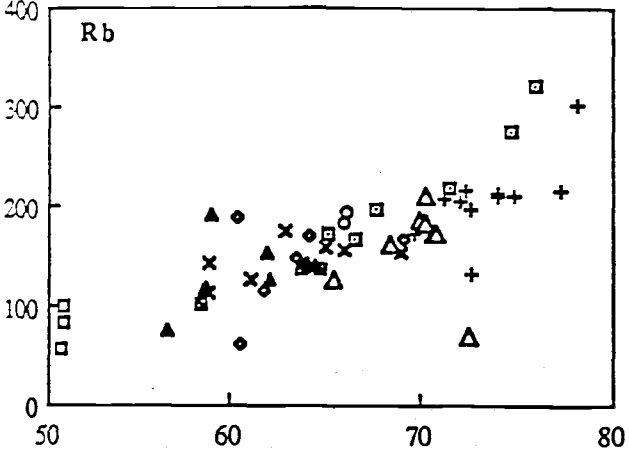
Rb
400
300
200
100
0
50
60
70
80

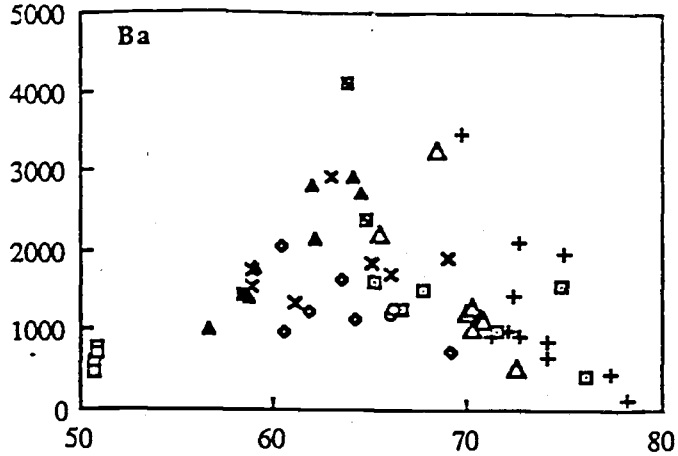
Ba
5000
4000
3000
2000
1000
0
50
60
70
80

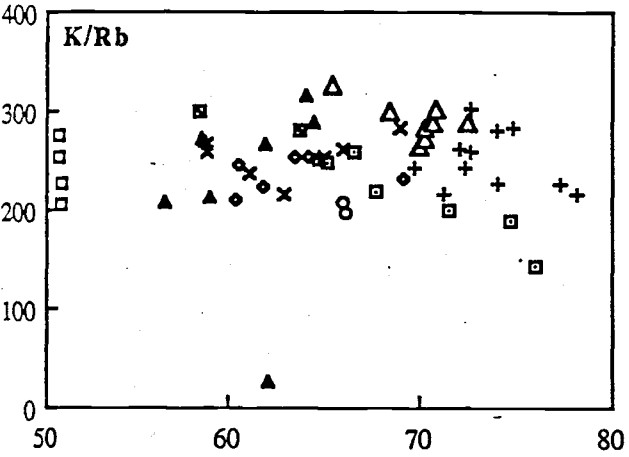
K/Rb
400
300
200
100
0
50
60
70
80

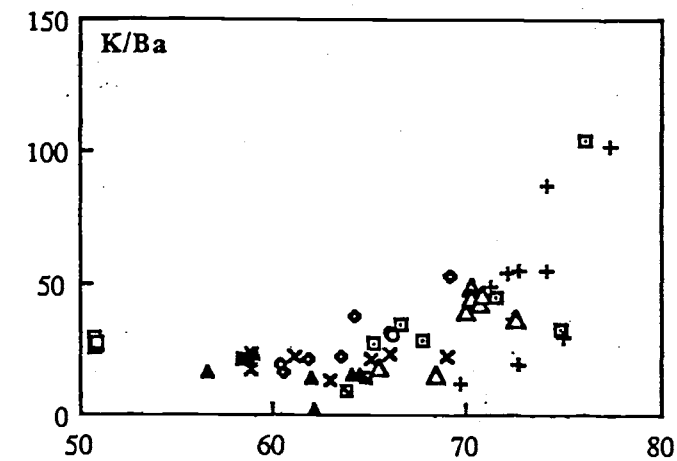
K/Ba
150
100
50
0
50
60
70
80

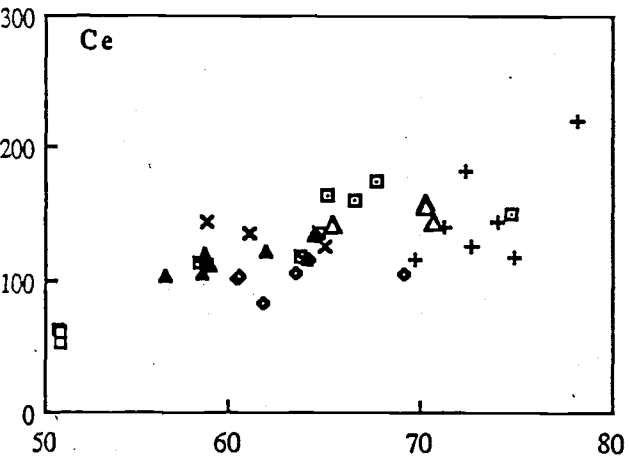
Ce
300
200
100
0
50
60
70
80

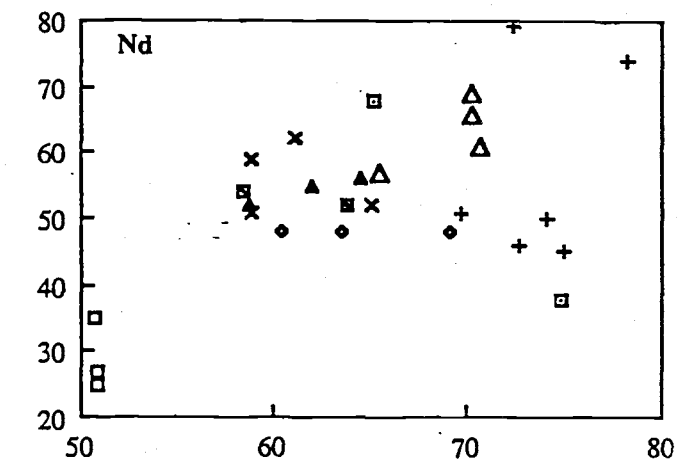
Nd
80
70
60
50
40
30
20
50
60
70
80

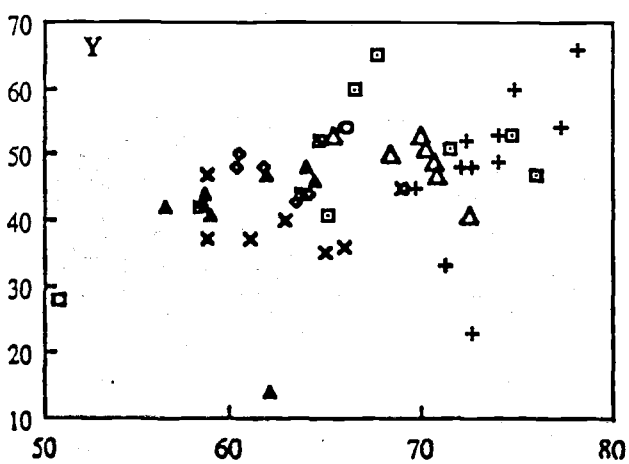
Y
70
60
50
40
30
20
10
50
60
70
80
SiO2

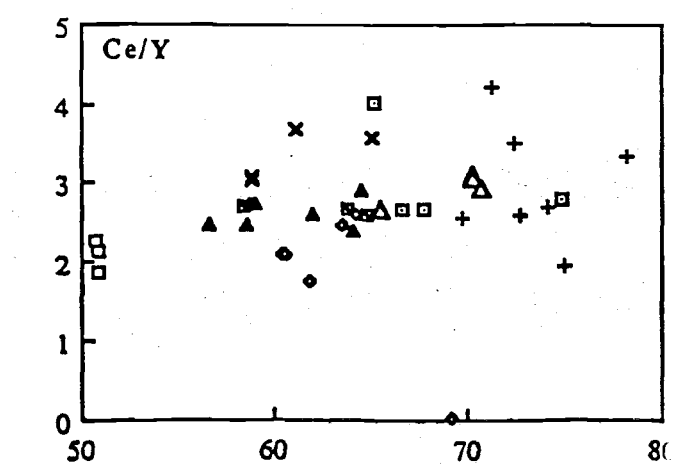
Ce/Y
5
4
3
2
1
0
50
60
70
80
SiO2

Figure opposite:

Figure 2.6b - Variation of trace elements vs. SiO_2 for volcanics of the Lake Everard area. Symbols as for Figure 2.5.

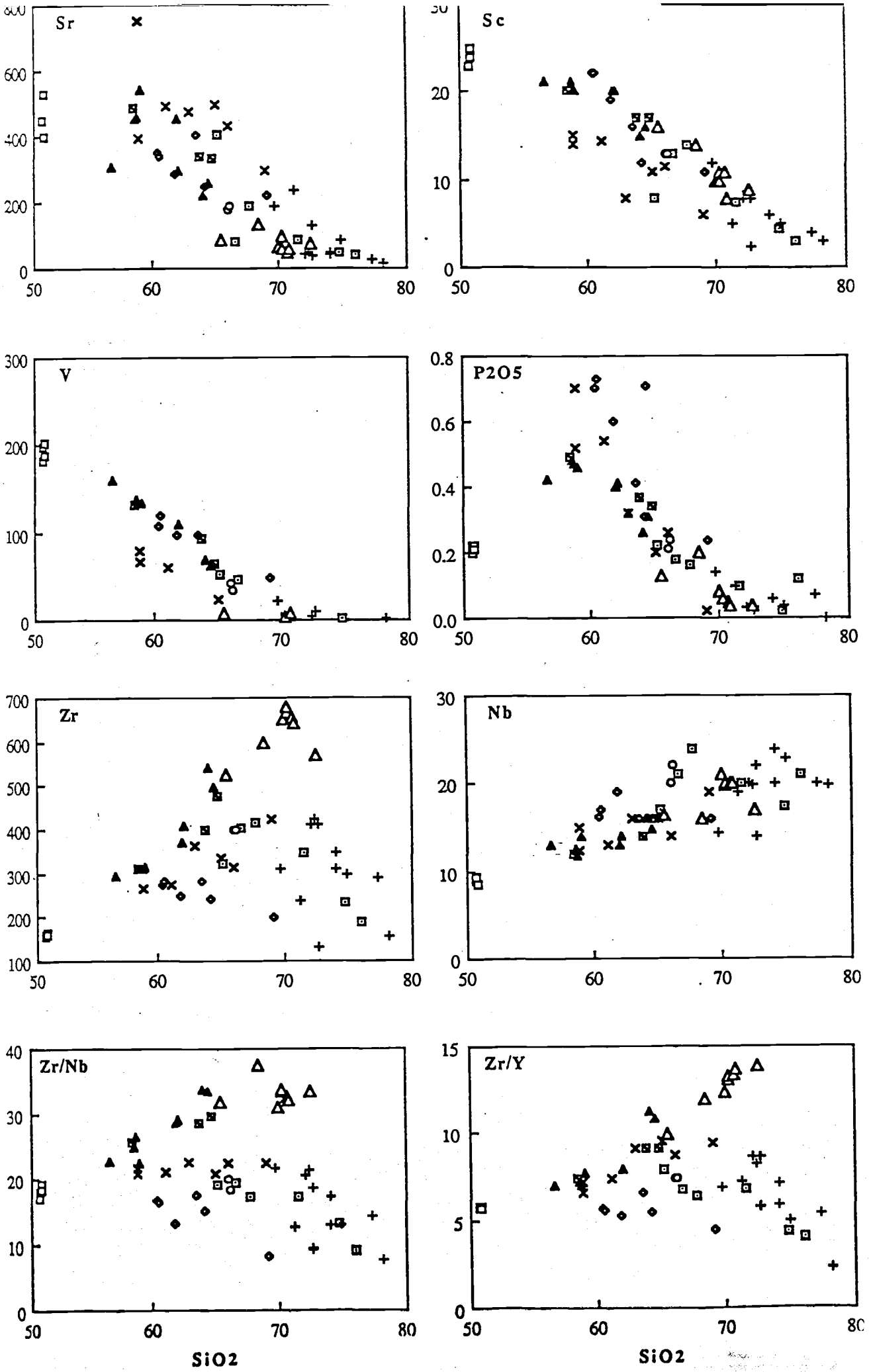
Sr
Sc
V
P2O5
Zr
Nb
Zr/Nb
Zr/Y
SiO2
SiO2

Different element variation trends between various units cannot be simply the effect of presence or absence of phenocrysts, for example considerably different trends are shown by the Childera, Mangaroongah and Bunburn Dacites, all of which span much the same silica range and are aphyric to sparsely phyric. The Bunburn Dacite contains comparatively high amounts of Al_2O_3, Na_2O and Sr, and low levels of CaO, TiO_2, Sc, V and exhibits moderate zircon enrichment but without an increase in Zr/Nb with more SiO_2. The Mangaroongah Dacite has moderate amounts of Al_2O_3 and TiO_2, low Na_2O and strong increases in both Zr and Zr/Nb with greater differentiation. Finally the Childera Dacite has low Al_2O_3, high P_2O_5 and TiO_2, and shows a decrease in Zr and Zr/Nb with differentiation.

2.4.4 - The geochemistry of the Tarcoola area

Major and trace element compositions for the volcanics of the Tarcoola area are given in Table 2.3 and selected variation diagrams comprise Figure 2.7 and 2.8. Also included are analyses of inclusions found in the volcanic suite. The volcanism in Tarcoola is bimodal with an apparent gap between approximately 60 and 67% SiO_2, and only one of the inclusions plots within this gap. Analyses of both the Ealbara Rhyolite and Carnding Rhyodacite are reasonably tightly clustered, at approximately 67% and 73% SiO_2 respectively. For the former unit this may be due to sample bias as the formal description of the unit includes subordinate rhyodacite, however samples of the latter unit were taken over much of its outcrop area and it is considered that chemical homogeneity is characteristic. The clustering of data for the two felsic units limits interpretations of differentiation from rhyodacite to rhyolite, although the Ealbara Rhyolite does exhibit chemical characteristics consistent with generation by fractionation from rhyodacite, namely lower Al_2O_3, CaO, MgO, Fe_2O_3*, TiO_2, MnO, Sc, Sr, V, Ba, and higher concentrations of K_2O, Rb, Nb, Y, and REE.

None of the samples of the Konkaby Basalt analysed for this study actually fall in the basalt field of Figure 2.2, even those samples with up to 8% MgO and more than 800ppm chromium, rather they are dominantly basaltic andesites with minor andesites. They do not exhibit any single line of descent but instead often form irregularly shaped clusters. The basaltic andesites tend to either high Al_2O_3 and low MgO or vice versa, at similar levels of SiO_2. Three samples are relatively highly enriched in K_2O, Rb, Ba, have high La/Y values and are variably but strongly depleted in Na_2O. In addition they contain xenocrysts of K-feldspar and are obviously highly contaminated probably by both the ingestion of felsic crustal material and also by post-eruptive element mobility. In contrast, on variation diagrams involving the less mobile elements Sc, Nb, Zr, Y and the rare earths, all of the mafic samples from Tarcoola plot as a single group.

Table 2.3 - Representative major and treace element compositions of volcanics from the Tarcoola volcanic centre

Sample	*884-T1*	*884-T4*	*884-T6*	*884-T8*	*884-T11*	*884-T17*	*884-T18*	*884-T20*	*884-T22*	*884-T14*	*884-T15*	*884-T16*	*884-T19*	*884-T27*	*884-T28*	*884-T29*	*884-T30*	*884-T31*	*884-T32*	*884-T34*	*884-T35*
Lithology	*Konkaby Basalt (BA)*	*Konkaby Basalt (BA)*	*Konkaby Basalt (BA)*	*Konkaby Basalt (BA)*	*Konkaby Basalt (BA)*	*Konkaby Basalt (BA)*	*Konkaby Basalt (BA)*	*Konkaby Basalt (A)*	*Konkaby Basalt (A)*	*Konkaby Basalt (BA)*	*Konkaby Basalt (BA)*	*Konkaby Basalt (BA)*	*Konkaby Basalt (A)*	*Ealbara Rhyolite (R)*	*Ealbara Rhyolite (R)*	*Ealbara Rhyolite (R)*	*Ealbara Rhyolite (R)*	*Carnding Rhyodacite (RD)*	*Carnding Rhyodacite (RD)*	*Carnding Rhyodacite (RD)*	*Carnding Rhyodacite (RD)*
SiO2	53.49	53.76	54.19	55.47	53.69	52.89	53.01	58.23	59.08	55.95	56.31	56.74	58.94	73.87	73.15	73.47	73.78	68.26	68.48	68.22	68.15
TiO2	0.96	0.97	0.97	0.91	0.97	0.76	0.74	0.56	0.55	0.67	0.66	0.59	0.58	0.22	0.26	0.23	0.22	0.55	0.59	0.60	0.59
Al2O3	16.47	16.49	16.56	16.59	16.59	14.39	14.42	15.39	15.27	15.98	15.79	13.22	13.72	12.85	13.00	12.83	12.78	14.32	14.08	14.21	14.18
Fe2O3*	8.94	9.04	9.11	9.04	9.12	9.51	9.01	6.15	6.19	8.34	8.30	7.38	6.92	2.59	2.46	2.29	2.25	3.70	3.93	3.92	3.91
MnO	0.16	0.17	0.15	0.19	0.17	0.20	0.20	0.12	0.13	0.15	0.14	0.20	0.17	0.16	0.07	0.08	0.08	0.10	0.12	0.12	0.12
MgO	4.98	4.99	4.51	4.27	4.43	7.29	7.15	4.76	4.88	4.14	4.24	6.91	6.12	0.19	0.28	0.29	0.32	0.94	0.97	0.97	0.92
CaO	8.09	8.11	8.05	7.71	7.90	7.99	8.54	5.38	5.38	7.25	7.18	8.29	7.37	0.33	0.75	0.81	0.76	1.86	1.79	1.72	1.81
Na2O	2.98	2.94	3.10	3.13	3.07	3.59	2.46	1.42	3.63	2.86	2.91	0.58	0.55	3.47	3.73	3.62	3.62	4.11	3.79	3.90	3.95
K2O	2.58	2.56	2.19	1.43	2.61	2.19	2.82	6.48	3.02	2.72	2.68	4.24	3.96	5.28	5.20	5.27	5.35	4.97	5.04	5.04	4.89
P2O5	0.41	0.40	0.40	0.37	0.41	0.33	0.33	0.22	0.20	0.24	0.24	0.30	0.28	0.03	0.04	0.04	0.03	0.20	0.23	0.23	0.21
LOI	0.44	0.44	0.37	0.80	0.34	0.49	0.80	0.81	1.08	1.12	1.06	0.85	0.93	0.84	0.61	0.80	0.79	0.70	0.67	0.69	0.76
Total	99.50	99.87	99.60	99.91	99.30	99.63	99.48	99.52	99.41	99.42	99.51	99.30	99.54	99.83	99.55	99.73	99.98	99.71	99.69	99.62	99.49
Zr	136.0	137.0	137.0	193.0	139.0	143.0	139.0	208.0	215.0	136.0	135.0	170.0	181.0	384.0	395.0	391.0	378.0	411.0	416.0	404.0	432.0
Nb	7.4	7.2	6.6	8.5	6.8	6.3	6.3	8.6	8.5	6.7	7.0	9.6	9.8	23.0	22.0	22.0	23.0	15.6	16.3	16.5	15.9
Sr	762.0	756.0	788.0	770.0	764.0	705.0	719.0	721.0	519.0	532.0	546.0	422.0	401.0	63.0	88.0	72.0	66.0	205.0	182.0	212.0	193.0
Rb	74.0	74.0	63.0	68.0	68.0	76.0	84.0	208.0	112.0	107.0	104.0	213.0	225.0	209.0	204.0	215.0	219.0	157.0	158.0	177.0	168.0
Y	20.0	18.9	19.8	23.0	19.6	19.8	20.1	17.7	18.8	18.3	18.2	18.3	20.3	61.0	61.0	62.0	63.0	47.0	50.0	50.0	50.0
Ba	958.0	928.0	922.0	690.0	983.0	878.0	1073.0	2064.0	1389.0	934.0	969.0	555.0	433.0	269.0	335.0	271.0	257.0	1060.0	1162.0	1147.0	1115.0
Sc	27.0	27.0	27.0	27.0	28.0	34.0	34.0	19.0	20.0	28.0	29.0	24.0	23.0	6.8	6.6	6.9	6.6	12.0	12.0	24.0	23.0
Ga	20.0	19.0	20.0	20.0	19.0	16.0	16.0	16.0	18.0	17.0	17.0	15.0	17.0	20.0	21.0	19.0	20.0	20.0	19.0	21.0	19.0
Ni	29.0	29.0	28.0	17.0	28.0	65.0	63.0	64.0	70.0	33.0	32.0	212.0	225.0	2.0	3.0	3.0	3.0	6.0	2.0	3.0	4.0
Th	5.4	5.6	5.0	7.6	4.7	5.6	4.3	10.0	10.0	8.4	10.0	14.0	17.0	28.0	28.0	27.0	28.0	19.0	20.0	21.0	20.0
Pb	13.0	8.0	9.0	13.0	13.0	12.0	12.0	39.0	19.0	13.0	13.0	18.0	18.0	33.0	35.0	30.0	33.0	25.0	25.0	26.0	24.0
U	2.0	3.2	3.9	4.2	3.6	3.6	2.0	2.1	3.9	3.9	4.1	5.6	4.1	7.7	5.2	6.5	7.7	3.8	4.9	5.5	4.4
Ce	77.0	82.0	84.0	89.0	73.0	78.0	71.0	105.0	114.0	79.0	82.0	90.0	97.0	192.0	177.0	195.0	201.0	152.0	153.0	153.0	149.0
Nd	30.0	36.0	31.0	39.0	32.0	33.0	36.0	32.0	36.0	27.0	30.0	35.0	41.0	81.0	77.0	78.0	80.0	60.0	61.0	68.0	63.0
La	36.0	35.0	30.0	40.0	37.0	33.0	32.0	59.0	58.0	34.0	31.0	45.0	46.0	96.0	88.0	94.0	96.0	71.0	73.0	74.0	75.0
V	215.0	218.0	227.0	218.0	222.0	173.0	190.0	104.0	110.0	194.0	193.0	138.0	134.0	4.0	6.0	4.0	4.0	26.0	27.0	29.0	28.0
Cr	29.0	26.0	23.0	23.0	22.0	357.0	365.0	347.0	370.0	130.0	135.0	874.0	896.0	<5	<5	<5	<5	5.0	<5	5.0	<5

** all iron as Fe2O3*

(BA), (A), (RD) and (R) refer to basaltic andesite, andesite, rhyodacite and rhyolite respectively

Figure opposite:

Figure 2.7 - Variation of major elements vs. SiO_2 for volcanics of the both the Tarcoola and southern Gawler Range areas. Symbols for the Tarcoola area: dotted squares, Konkaby Basalt; small open squares, Ealbara Rhyolite; open circles, Carnding Rhyodacite. Symbols for the southern Gawler Range area: diagonal crosses, Waganny Dacite; small filled squares, Bittali Rhyolite.

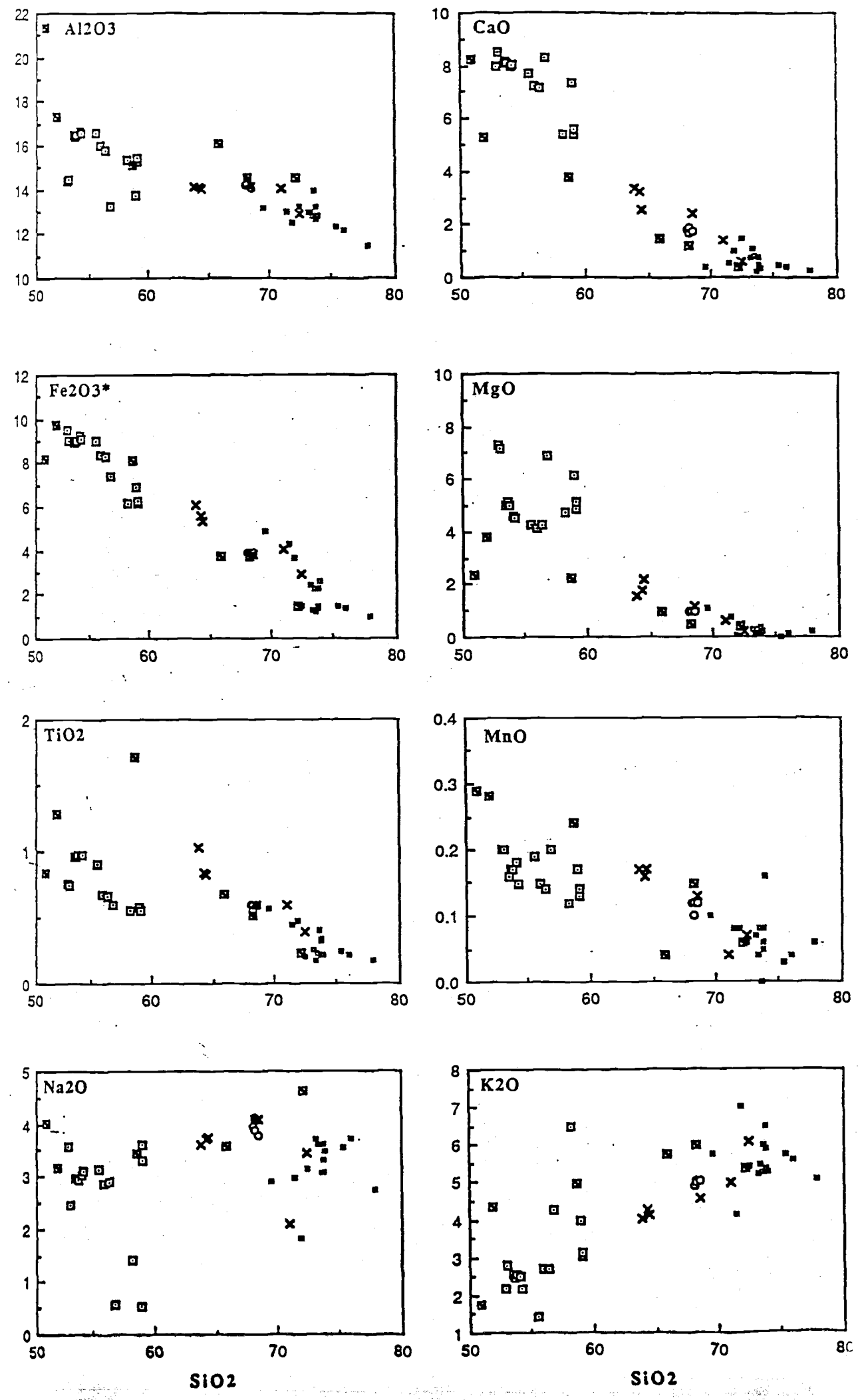
Al2O3
CaO
Fe2O3*
MgO
TiO2
MnO
Na2O
K2O
SiO2
SiO2

2.4.5 - The geochemistry of Southern Gawler Range area

Major and trace element analyses of samples from the southern Gawler Range volcanic area are presented as Table 2.4 and in Figure 2.7 and 2.8. The analyses represent mostly samples from the Toondoolya Bluff area with a few extra samples of Bittali Rhyolite from elsewhere in its outcrop area. The Waganny Dacite is mainly dacitic, with rhyodacitic and minor rhyolitic portions which Jagodzinski (1985) mapped as successive eruptive pulses. The Bittali Rhyolite is also interpreted to be a composite unit, formed by a number of eruptions of rhyolitic and rhyodacitic magma. The major element variation for these two units is quite regular with the greatest scatter occurring in K_2O and particularly Na_2O which tend to be more mobile and the most easily affected by post emplacement movement. K_2O increases with increasing differentiation. CaO, Al_2O_3, Fe_2O_3*, MgO, TiO_2, P_2O_5 all decrease with increasing SiO_2. The Waganny Dacite exhibits evidence of relatively rapid removal of TiO_2 and P_2O_5 in its dacitic portion, which lessened in the rhyodacitic to rhyolitic part.

The compatible trace elements Sc, Sr and V show quite regular behaviour within each unit although differences in actual concentrations between the units are apparent with the rhyodacitic portion of the Waganny having higher levels of Sr, and V than Bittali Rhyolite of a similar SiO_2 content.

REEs, Nb and Y all show a general increase with increasing SiO_2, with the exception of three samples from the Bittali Rhyolite. Two of these samples plot at relatively low levels of Y, Nb and Zr for the same SiO_2 content, compared with the main Bittali group. Both of these samples are from the Bittali Dam area and the collected specimens contained xenoliths of country rock. Although all observable xenolithic material was removed prior to analysis, it is possible the samples are nevertheless affected. The third anomalous sample was taken from the boundary between the Bittali Rhyolite and the overlying Eucarro Dacite (of the mature phase volcanism) and may be incorrectly assigned to the developmental phase volcanism although this was difficult to determine from field relations.

The large ion lithophile trace elements Rb and Ba exhibit contrasting behaviour with increasing SiO_2. Rb continues to increase whereas Ba has fairly constant levels up to approximately 70% SiO_2 and then decreases rapidly. Both elements show considerable scatter, but whether this is original or due to some post-emplacement movement of these elements is uncertain.

Figure opposite:

Figure 2.8a - Variation of trace elements vs. SiO_2 for volcanics of both the Tarcoola and southern Gawler Range areas. Symbols as for Figure 2.7.

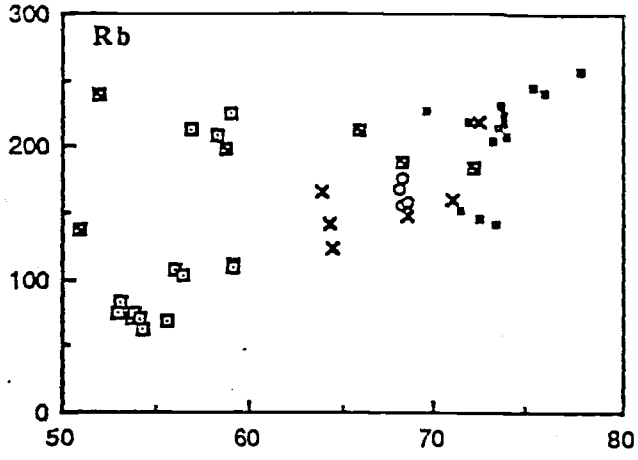
Rb
300
200
100
0
50
60
70
80

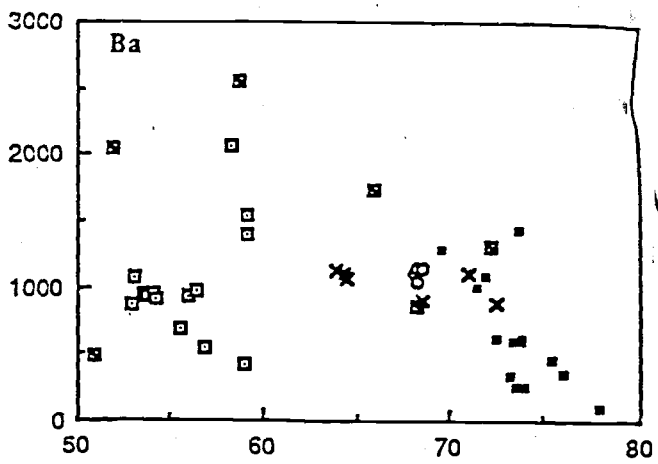
Ba
3000
2000
1000
0
50
60
70
80

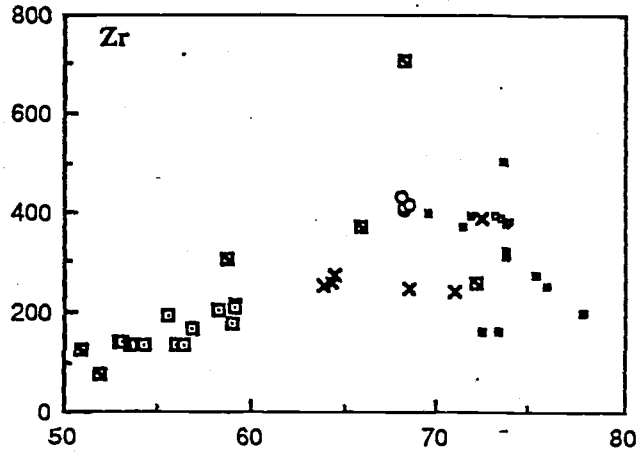
Zr
800
600
400
200
0
50
60
70
80

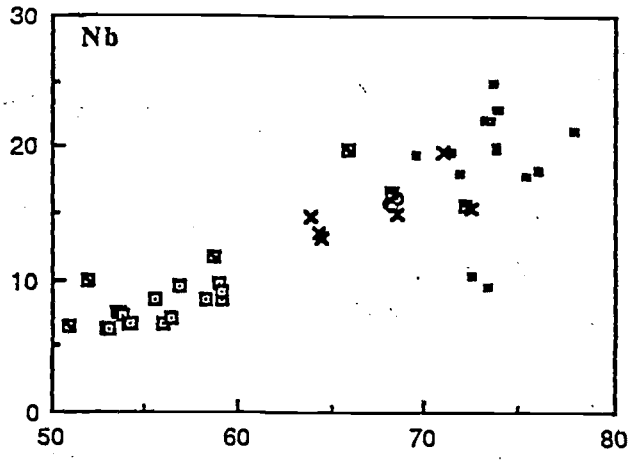
Nb
30
20
10
0
50
60
70
80

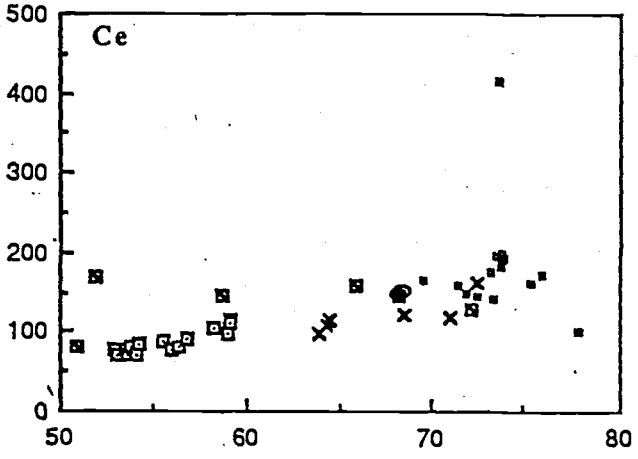
Ce
500
400
300
200
100
0
50
60
70
80

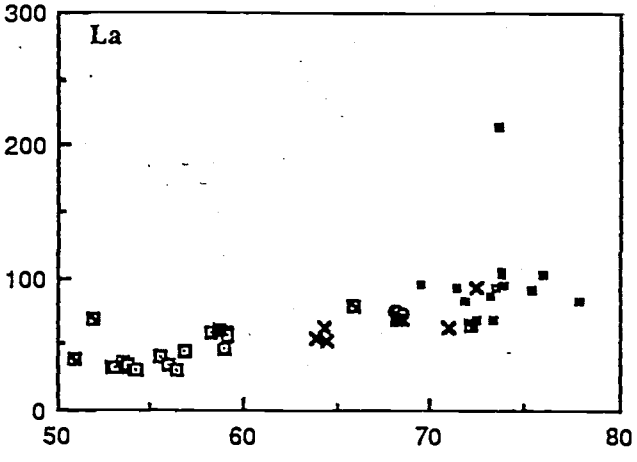
La
300
200
100
0
50
60
70
80

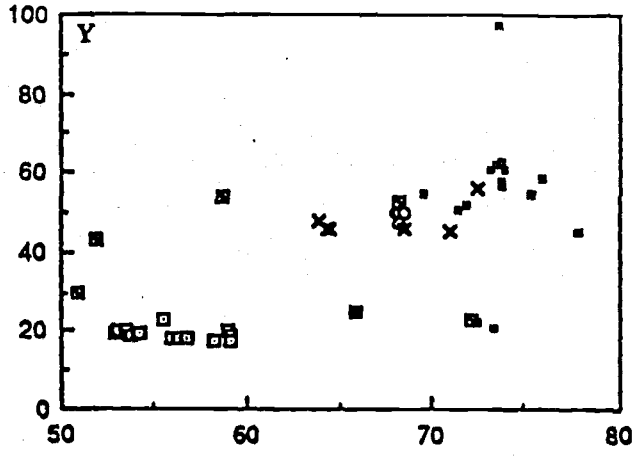
Y
100
80
60
40
20
0
50
60
70
80
SiO2

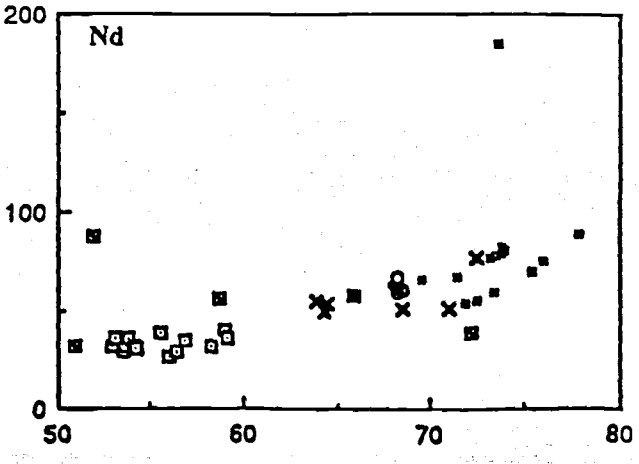
Nd
200
100
0
50
60
70
80
SiO2

Figure opposite:

Figure 2.8b - Variation of trace elements vs. SiO_2 for volcanics of both the Tarcoola and southern Gawler Range areas. Symbols as for Figure 2.7.

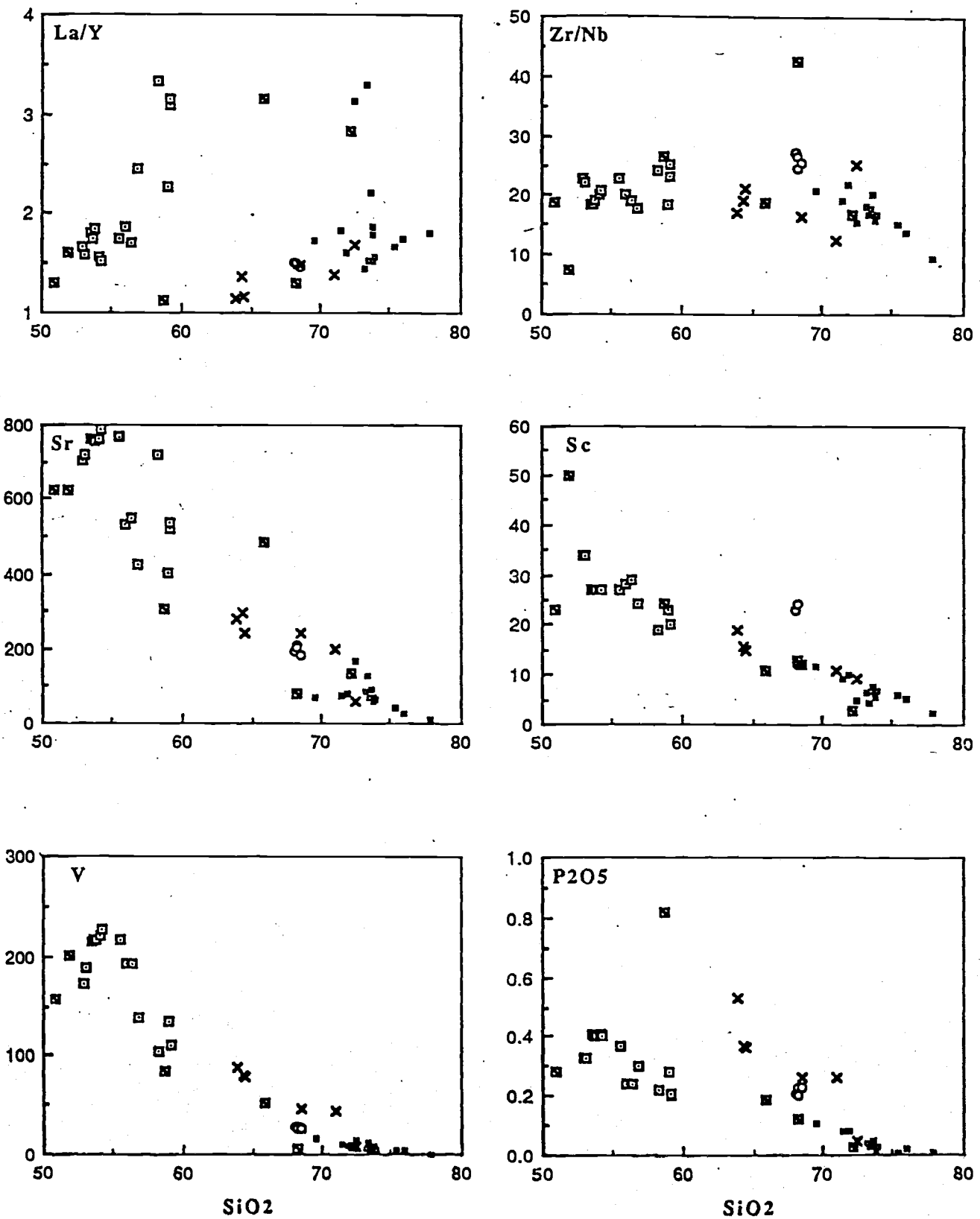
La/Y
Zr/Nb
Sr
Sc
V
P2O5
SiO2
SiO2

Table 2.4 - Major and trace element compositions of volcanics from the Southern Gawler Range volcanic area

Sample	*884-PAO1*	*849-29*	*849-34*	*849-24*	*849-11*	*849-82*	*849-64*	*884-Bi1*	*884-Bi2*	*884-Bi5*	*884-Bi6*	*849-21*	*849-26*	*849-80*	*849-49*	*849-94*	*849-85*	*849-87*
Lithology	*Rhyolite*	*Waganny*	*Waganny*	*Waganny*	*Waganny*	*Waganny*	*Waganny*	*Bittali*	*Bittali*	*Bittali*	*Bittali*	*Bittali*	*Bittali*	*Bittali*	*Bittali*	*Bittali*	*Bittali*	*Bittali*
	(R)	*Dacite (D)*	*Dacite (D)*	*Dacite (D)*	*Dacite (RD)*	*Dacite (RD)*	*Dacite (R)*	*Rhyolite (R)*	*Rhyolite (R)*	*Rhyolite (R)*	*Rhyolite (R)*	*Rhyolite (R)*	*Rhyolite (R)*	*Rhyolite (RD)*	*Rhyolite (RD)*	*Rhyolite (RD)*	*Rhyolite (R)*	*Rhyolite (R)*
SiO2	77.06	63.85	64.33	64.52	68.48	71.02	72.51	73.31	73.61	72.44	77.81	75.42	75.88	69.59	71.46	71.88	73.81	73.83
TiO2	0.16	1.03	0.84	0.83	0.60	0.60	0.39	0.18	0.40	0.20	0.18	0.24	0.22	0.57	0.45	0.47	0.34	0.32
Al2O3	11.80	14.13	14.13	14.08	14.16	14.02	12.89	12.99	14.01	13.25	11.46	12.37	12.15	13.16	12.98	12.49	13.23	12.64
Fe2O3*	1.28	6.12	5.58	5.34	3.79	4.03	2.93	1.32	1.18	1.48	1.01	1.44	1.34	4.84	4.26	3.61	1.47	1.41
MnO	0.05	0.17	0.16	0.17	0.13	0.04	0.07	0.04	0.00	0.06	0.06	0.03	0.04	0.10	0.08	0.08	0.05	0.06
MgO	0.27	1.58	1.79	2.16	1.15	0.64	0.23	0.16	0.13	0.26	0.18	0.02	0.11	1.08	0.72	0.07	0.14	0.12
CaO	0.34	3.37	3.21	2.56	2.43	1.42	0.58	1.08	0.19	1.51	0.28	0.49	0.38	0.39	0.57	0.98	0.45	0.41
Na2O	2.61	3.63	3.70	3.75	4.09	2.11	3.43	3.62	3.06	3.15	2.72	3.54	3.73	2.89	2.96	1.84	3.08	3.30
K2O	5.54	4.01	4.28	4.10	4.54	4.98	6.05	5.46	5.96	5.38	5.06	5.72	5.58	5.74	4.14	7.03	6.49	5.88
P2O5	0.01	0.53	0.37	0.36	0.26	0.26	0.05	0.03	0.05	0.05	0.01	0.01	0.02	0.11	0.08	0.08	0.01	0.01
LOI	0.64	1.31	1.37	1.64	0.62	1.09	0.81	1.23	0.97	1.81	0.41	0.48	0.86	1.37	1.18	0.81	0.71	1.67
Total	99.77	99.73	99.76	99.51	100.25	100.21	99.94	99.42	99.56	99.59	99.18	99.76	100.31	99.84	98.88	99.34	99.78	99.65
Zr	211.0	253.0	259.0	275.0	249.0	245.0	388.0	160.0	503.0	160.0	197.6	273.0	253.0	401.0	375.0	396.0	322.0	313.0
Nb	23.0	14.7	13.5	13.1	15.1	19.7	15.4	9.6	25.0	10.3	21.3	17.9	18.2	19.4	19.7	18.1	20.1	19.8
Sr	54.0	281.0	297.0	243.0	242.0	198.0	57.0	129.0	91.0	167.0	10.5	41.0	26.0	68.0	75.0	78.0	69.0	60.0
Rb	303.0	167.0	142.0	123.0	148.0	160.0	218.0	141.0	231.0	146.0	257.0	245.0	241.0	228.0	153.0	219.0	225.0	219.0
Y	65.0	48.0	46.0	46.0	46.0	45.0	56.0	21.0	97.0	22.0	45.4	55.0	59.0	55.0	51.0	52.0	57.0	58.0
Ba	193.0	1143.0	1113.0	1069.0	915.0	1123.0	902.0	618.0	1433.0	624.0	102.0	470.0	364.0	1293.0	1019.0	1087.0	638.0	600.0
Sc	4.1	19.1	15.9	14.8	11.9	11.0	9.3	4.4	7.7	4.7	2.4	6.0	5.1	11.8	9.4	9.9	5.9	5.8
Ga	19.0	20.0	19.0	18.0	17.0	18.0	19.0	15.0	21.0	16.0	16.4	17.0	17.0	21.0	20.0	18.0	17.0	17.0
Ni	2.0	13.0	14.0	13.0	8.0	10.0	5.0	5.0	1.0	4.0	0.0	1.0	3.0	4.0	4.0	6.0	2.0	4.0
Th	39.0	n.a.	n.a.	n.a.	n.a.	n.a.	n.a.	29.0	37.0	26.0	30.0	n.a.	n.a.	n.a.	n.a.	n.a.	n.a.	n.a.
Pb	131.0	n.a.	n.a.	n.a.	n.a.	n.a.	n.a.	30.0	34.0	17.0	40.3	n.a.	n.a.	n.a.	n.a.	n.a.	n.a.	n.a.
U	9.3	n.a.	n.a.	n.a.	n.a.	n.a.	n.a.	4.1	11.0	5.1	8.2	n.a.	n.a.	n.a.	n.a.	n.a.	n.a.	n.a.
Ce	166.0	97.0	109.0	115.0	122.0	117.0	163.0	141.0	416.0	144.0	101.4	161.0	172.0	164.0	159.0	148.0	193.0	184.0
Nd	74.0	55.0	50.0	54.0	52.0	52.0	77.0	60.0	185.0	55.0	89.7	70.0	76.0	66.0	68.0	54.0	83.0	80.0
La	74.0	55.0	63.0	53.0	68.0	62.0	94.0	69.0	214.0	69.0	82.3	92.0	103.0	95.0	93.0	83.0	106.0 *	103.0
V	2.0	88.0	80.0	78.0	47.0	44.0	8.0	13.0	6.0	15.0	0.3	4.0	4.0	16.0	11.0	9.0	9.0	8.0
Cr	<5	<5	5.0	5.0	<5	n.a.	n.a.	6.0	<5	9.0	0.6	<5	<5	n.a.	n.a.	n.a.	n.a.	n.a.

** - all iron as Fe2O3*
Samples prefixed 849- are from Jagodzonski (1985)
(D), (RD) and (R) indicate dacite, rhyodacite and rhyolite respectively

Figure opposite:

Figure 2.9 - Variation diagrams vs. SiO_2 for all developmental volcanics. Symbols: red squares, Lake Everard; blue diamonds, Kokatha; green squares, Tarcoola; pink diamonds, Southern Gawler Range.

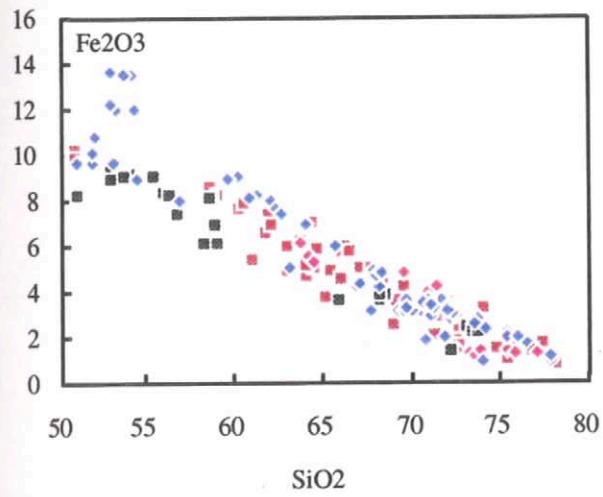
Fe2O3
16
14
12
10
8
6
4
2
0
50 55 60 65 70 75 80
SiO2

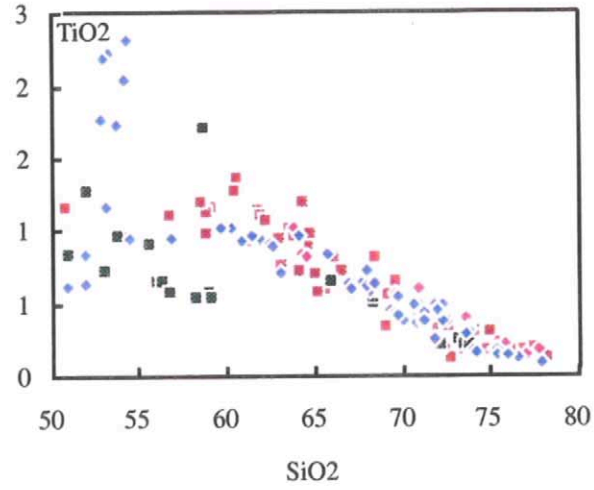
TiO2
3
2
2
1
1
0
50 55 60 65 70 75 80
SiO2

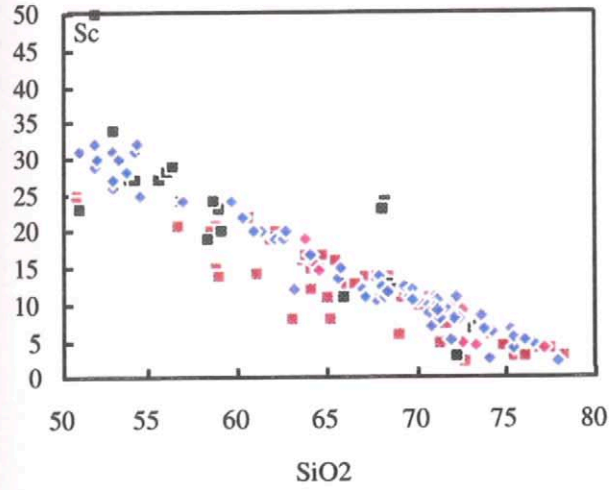
Sc
50
45
40
35
30
25
20
15
10
5
0
50 55 60 65 70 75 80
SiO2

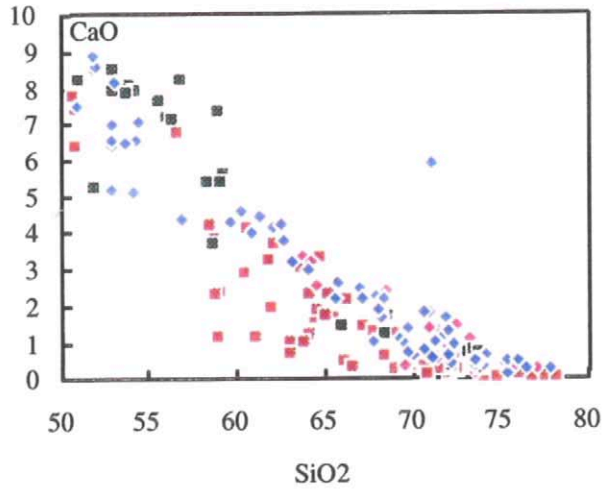
CaO
10
9
8
7
6
5
4
3
2
1
0
50 55 60 65 70 75 80
SiO2

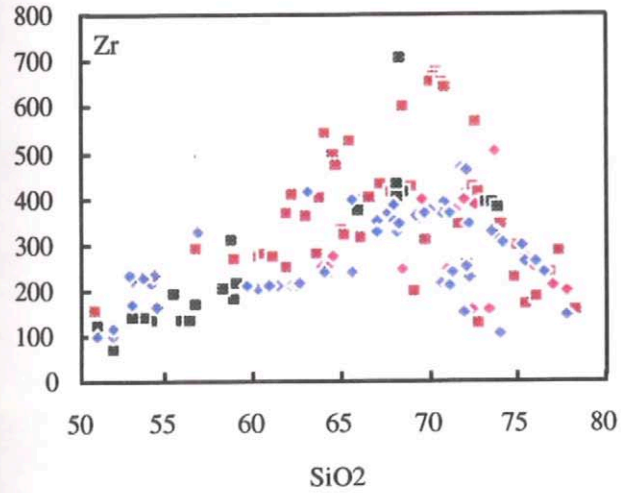
Zr
800
700
600
500
400
300
200
100
0
50 55 60 65 70 75 80
SiO2

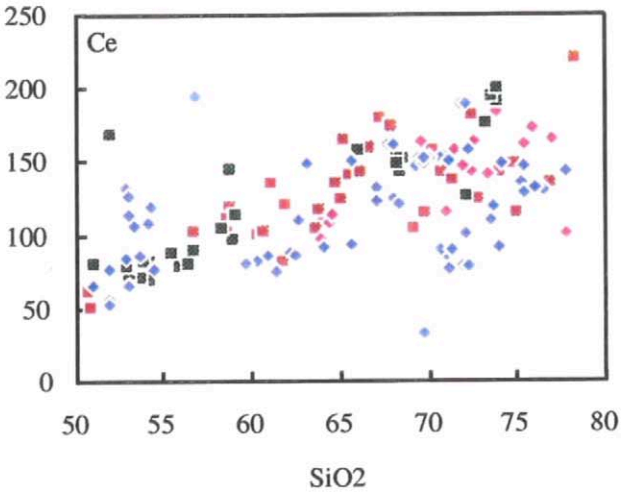
Ce
250
200
150
100
50
0
50 55 60 65 70 75 80
SiO2

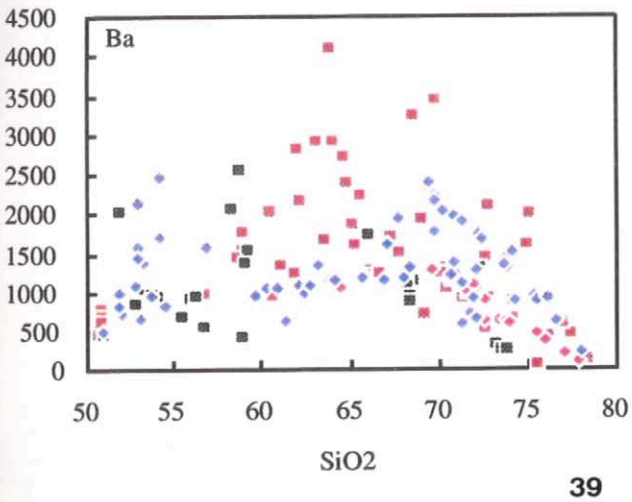
Ba
4500
4000
3500
3000
2500
2000
1500
1000
500
0
50 55 60 65 70 75 80
SiO2

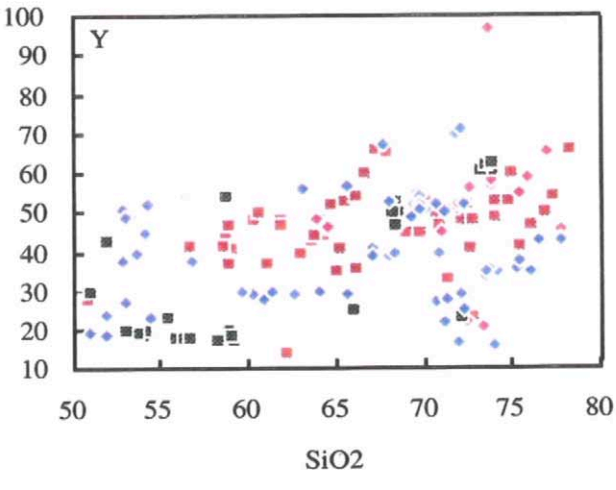
Y
100
90
80
70
60
50
40
30
20
10
50 55 60 65 70 75 80
SiO2

2.4.6 - A comparison of the geochemistry of the developmental volcanic areas

Selected major and trace element variation diagrams illustrating the combined chemistry of the four areas of developmental volcanism are presented as Figure 2.9. These Harker diagrams show that elements which are strongly controlled by the almost ubiquitous phenocryst phases pyroxene and magnetite (e.g. Sc, Fe_2O_3*), tend to form well defined decreasing trends with increasing SiO_2. Also relatively tightly constrained are the variations of the rare earths which increase steadily with SiO_2.

The largest scatter is seen in variation diagrams of elements such as Ba, and Zr. Although some scatter in Ba could be due to its mobility this is unlikely because of the coherent trends versus SiO_2 shown by individual units (see Figure 2.4b Ba-SiO_2). Instead the scatter is the likely result of one or both of the following mechanisms: 1) element concentrations are controlled by the removal of crystal phase(s) whose appearance on the liquidus occurs at different points in the differentiation of each unit controlled by the prevailing magma chamber conditions (which were probably different between units and between volcanic areas) and the scatter is due to many slightly different trends being superimposed; 2) scatter is introduced by mixing processes such that the resultant mix moves off of the fractional crystallization trend. Many of these mixing processes result in subhorizontal trends because enrichment is stopped by the mixing process. These two processes will be further evaluated in the discussion of mechanisms and sources.

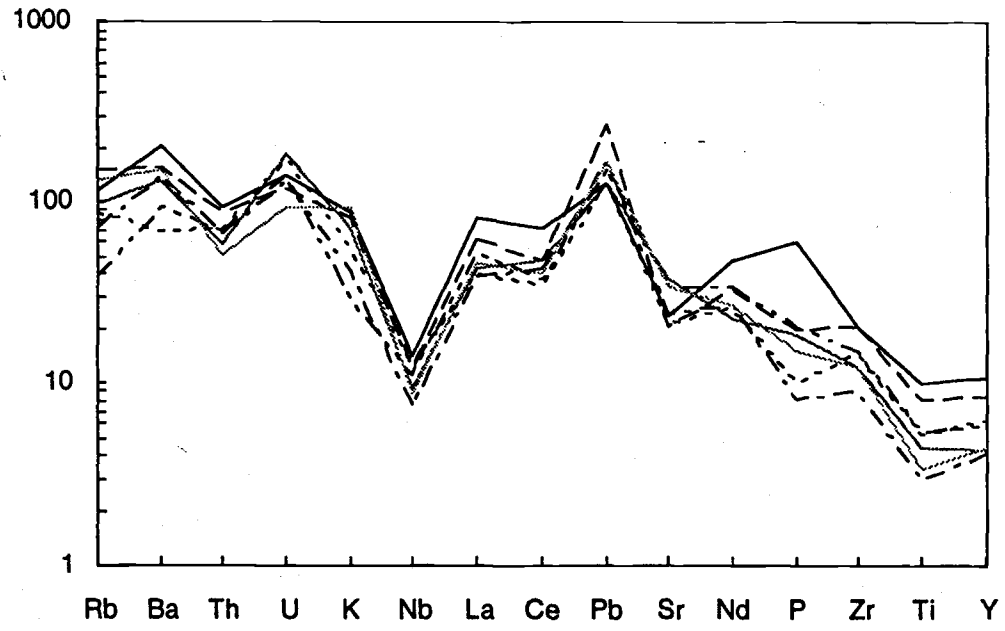

Figure 2.10 - Primitive mantle normalized multi-element diagram for the basalts and basaltic andesites of the developmental phase volcanics. Normalizing factors are from Sun and McDonough (1989).

Figures opposite:

Figure 2.11a - Primitive mantle normalized (PMN) diagram of felsic volcanics with approximately 65-66% SiO_2.

Figure 2.11b - Primitive mantle normalized (PMN) diagram of felsic volcanics with approximately 68% SiO_2.

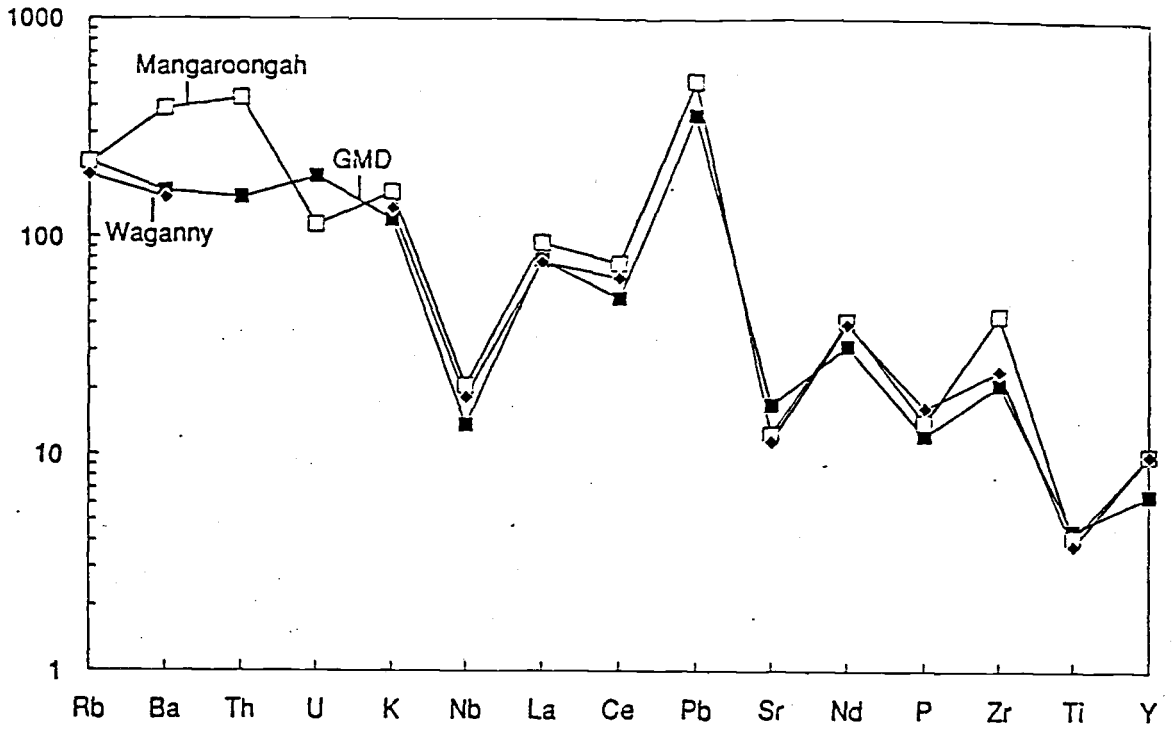
1000
100
10
1
Mangaroongah
GMD
Waganny
Rb
Ba
Th
U
K
Nb
La
Ce
Pb
Sr
Nd
P
Zr
Ti
Y

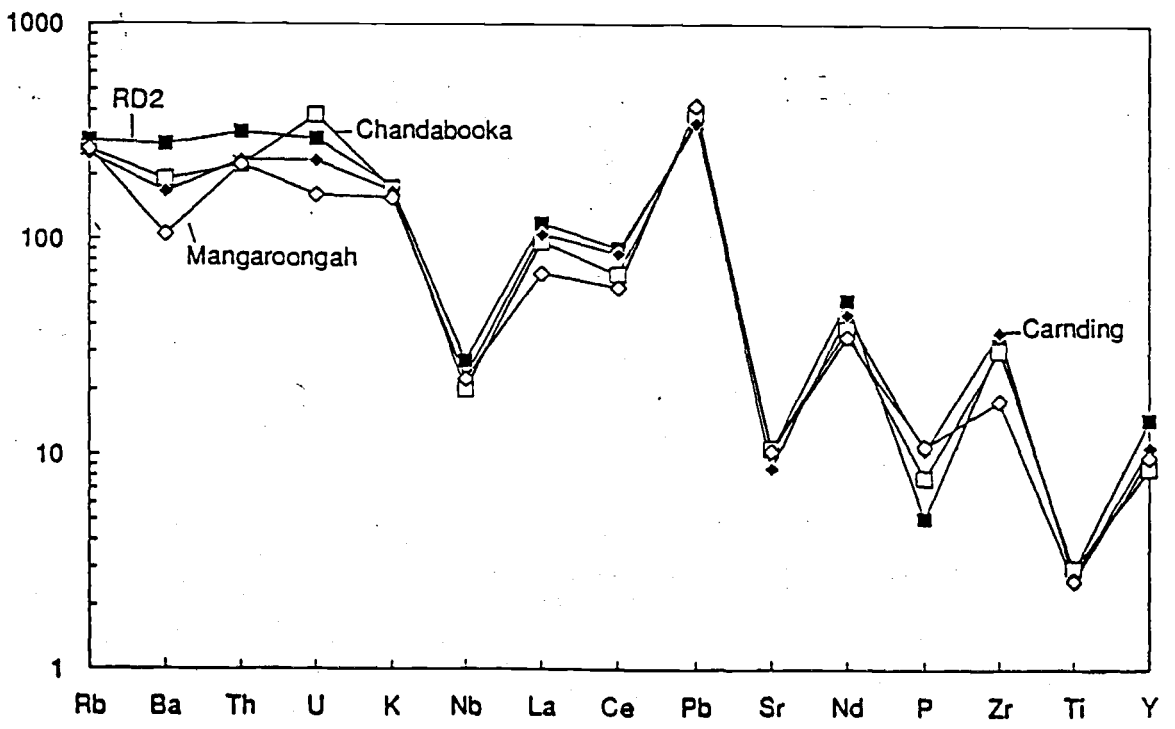
1000
100
10
1
RD2
Chandabooka
Mangaroongah
Carnding
Rb
Ba
Th
U
K
Nb
La
Ce
Pb
Sr
Nd
P
Zr
Ti
Y

Figures opposite:

Figure 2.12a - Primitive mantle normalized (PMN) diagram of felsic volcanics with approximately 70% SiO_2.

Figure 2.12b - Primitive mantle normalized (PMN) diagram of felsic volcanics with approximately 74-78% SiO_2.

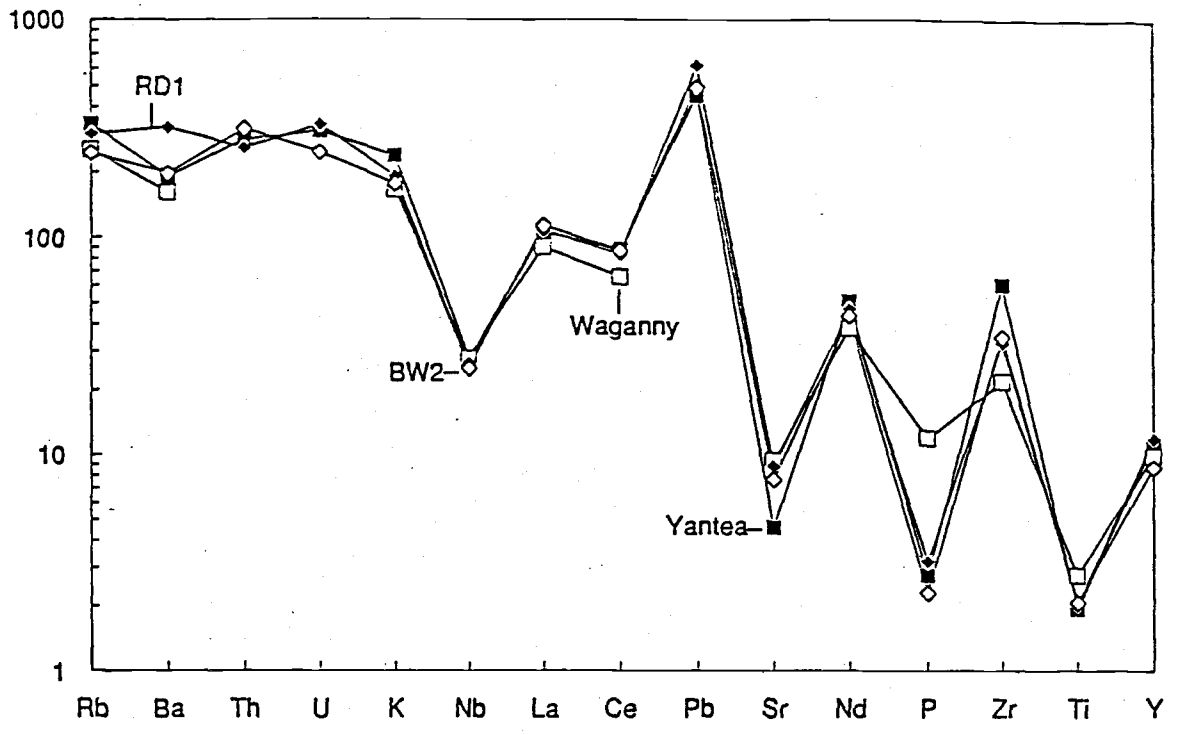
1000
100
10
1
RD1
BW2
Waganny
Yantea
Rb
Ba
Th
U
K
Nb
La
Ce
Pb
Sr
Nd
P
Zr
Ti
Y

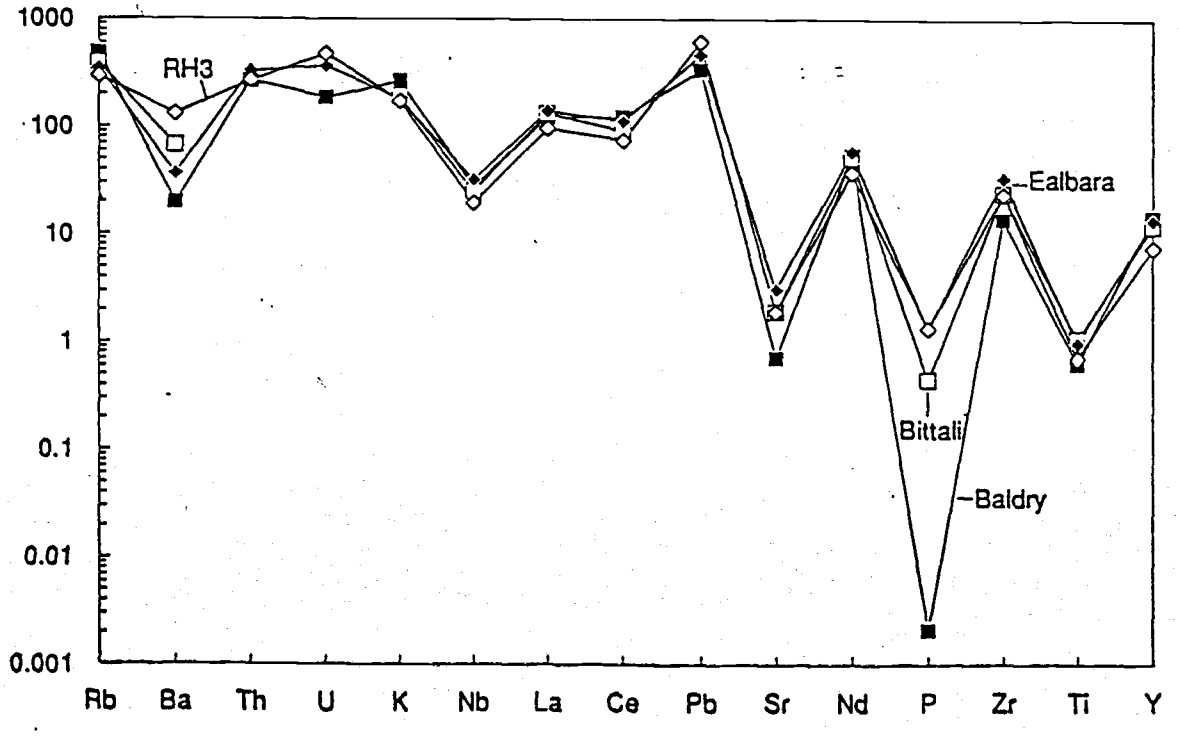
1000
100
10
1
0.1
0.01
0.001
RH3
Ealbara
Bittali
Baldry
Rb
Ba
Th
U
K
Nb
La
Ce
Pb
Sr
Nd
P
Zr
Ti
Y

A second way to compare the chemistry of the four developmental areas is to use primitive mantle normalized (PMN) diagrams (Sun and McDonough, 1989). The PMN diagram of representative basalts and basaltic andesites from the developmental volcanism is presented as Figure 2.10 and the general overall similarity of shape is striking, even though absolute abundances vary by a considerable amount. The basalts do not geochemically resemble either MORB or OIB type basalts (Figure 2.19). Instead the geochemical features of all the developmental phase basalts are their high ratios of large ion lithophile (LIL) elements to high field strength (HFS) elements, distinctive Nb and Sr depletions and strong Pb enrichments.

Another distinctive feature illustrated in the PMN patterns of the basalts is the similarity of relative proportions of LIL elements which plot on the left hand side of primitive mantle normalised (PMN) diagrams i.e. Rb, Ba, Th, U, and K. Most of the analysed basalts exhibit an 'M-shaped' pattern with relative enrichment of Ba and U compared with Rb, Th and K (Figure 2.10). There are significant differences in the relative concentrations of P, Zr, Ti and Y between the various mafic volcanic types.

There are some similarities between the PMN patterns of the basaltic and felsic rocks (compare Figures 2.10, 2.11, 2.12), in particular negative Nb and Sr anomalies and a positive Pb anomaly. However unlike the basaltic rocks the felsic rocks have negative Ti and P anomalies indicating magnetite and apatite crystallisation. In an attempt to compare rocks at similar levels of differentiation PMN patterns for the felsic volcanics have been grouped according to SiO_2 content of samples from the different areas (Figures 2.11 and 2.12). At each of the four silica levels selected the patterns are very similar. Variation in the element sequence Rb through to U may in part be to post-emplacement alteration, although in the samples plotted this seems to be a major factor in only a single sample, with most of the variation in Ba attributable to depletion by its removal in sanidine in rhyodacites and rhyolites. The other major differences in the patterns at any particular silica level is in P and to a lesser degree Sr, which are controlled by the fractionation of apatite and plagioclase respectively.

2.4.7 - Rare earth elements

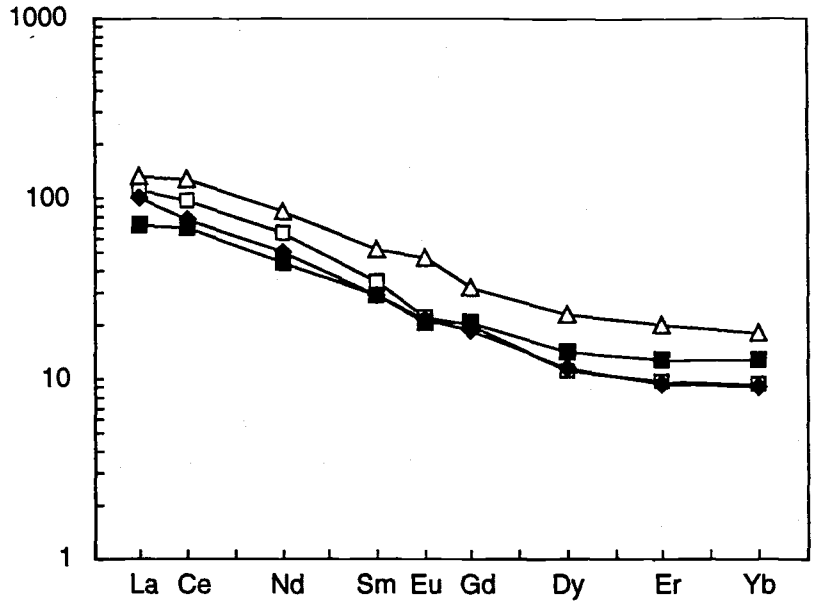

Figure 2.13 - Chondrite normalized abundances of rare earth elements in Gawler Range basalts and basaltic andesites. Symbols: open triangle, HPT basaltic andesite (884-K5); open square, LPT basalt (884-K8); filled square, Nuckulla Basalt (884-GH2); filled diamond, Konkaby basalt (884-T18).

Rare earth patterns for mafic rocks from the Kokatha, Tarcoola and Lake Everard are shown in Figure 2.13. The patterns reveal that the mafic rocks are ubiquitously light rare earth enriched. The Nuckulla basalt from Lake Everard exhibits the least enriched pattern with $La_N/Yb_N = 5.6$ and approximately 70x chondrite La. The HP basalts from Kokatha are more LREE enriched with $La_N/Yb_N = 7.4$, and with 18x chondritic Yb, these basaltic andesites have higher total REE levels than the other mafic rocks. The LP basalts from Kokatha and the Konkaby basaltic andesite from Tarcoola have similar patterns, higher in LREE and lower in HREE than the Nuckulla Basalt, with La_N/Yb_N =11-12. The three LP basalt patterns (for the Nuckulla and Konkaby Basalts and the Kokatha LP basalts) fan about a pivot point at approximately 20x chondrite Eu, and each of these three patterns has a small Eu anomaly. In contrast the HP basalt from Kokatha has a small positive Eu anomaly. HREE concentrations in each of the patterns are too high for residual garnet to have been present in the mantle source.

2.5 - Isotopic variations in the developmental phase volcanics

Representative samples from each of the four volcanic centres were selected for isotopic analysis. Samples were selected such that they were representative of their respective unit and were thought on visual, petrographic and chemical grounds to be unaltered. Thirty four samples were analysed for Nd-Sm isotopes and twenty nine for Rb-

Sr isotopes, with concentrations of Nd and Sm obtained by isotope dilution and concentrations of Rb and Sr by isotope dilution and/or extended XRF. The isotopic and concentration data are given in Table 2.5, and summary of the isotopic techniques together with the constants used in the isotopic calculations are listed in appendix B.

It rapidly became apparent after the isotopic study was commenced that the Sr isotopic systematics of many of the more siliceous volcanics had been disturbed, and it was obvious that the results from samples with less than 100ppm Sr are at the very least highly suspect, often yielding unrealistically low initial ratios (Figure 2.14). For this reason the strontium results were culled and those samples containing less than 100ppm Sr together with those whose initial ratios were considered to be unacceptably low (<0.7015) were removed prior to further evaluation of the Sr data, and will not be referred to here.

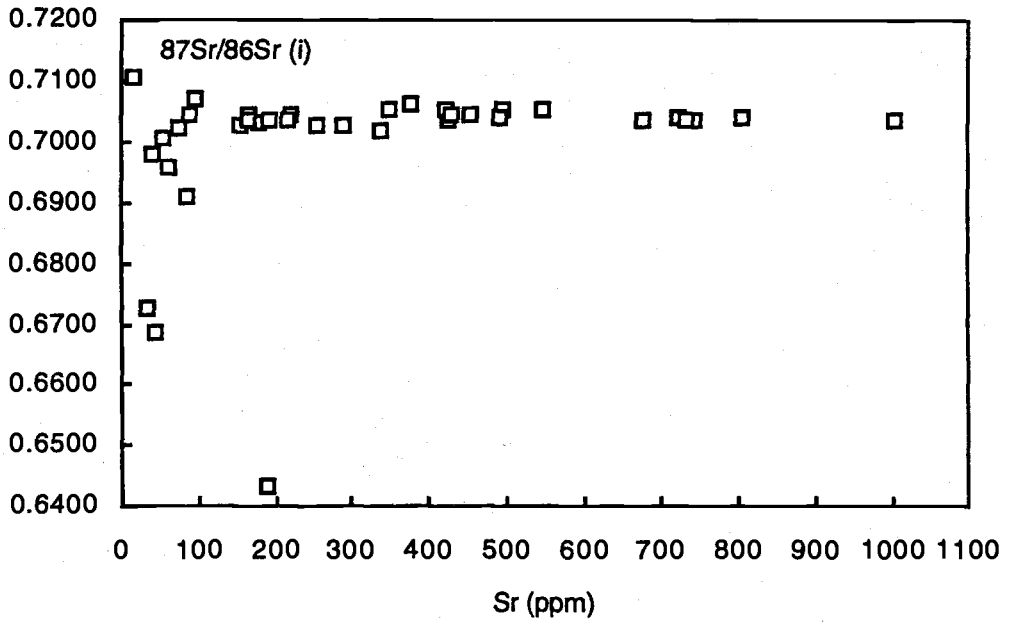

Figure 2.14 - Plot of $^{87}Sr/^{86}Sr$ initial ratio (calculated at 1592 Ma.) against Sr concentration for all the isotopic data (both the developmental and mature phase volcanics) illustrating the tendency for low values in some samples which have low Sr levels.

2.5.1 - Isotopic variation in the Kokatha area

The volcanics from the Kokatha area exhibit the greatest variation in ε_{Nd} of all the developmental areas, ranging from -1.6 for a LP basalt to -7.4 for the rhyolite RH3. The HP and IP basaltic andesites have ε_{Nd} values of -3.5 and -3.0 respectively. When the Kokatha Nd data are viewed all together, the volcanics exhibit a general trend of decreasing ε_{Nd} when plotted against indices of increasing differentiation. For example there is a general trend of decreasing ε_{Nd} with decreasing MgO (Figure 2.16). In addition, the volcanics from the Kokatha area exhibit a strong link between the stratigraphic level

Table 2.5 - Nd and Sr isotopic data for the developmental phase volcanics, Gawler Range Volcanic Province

Volcanic area	*Sample Number*	*Unit*	*Nd ppm*	*Sm ppm*	*143/144 Nd measured*	*147Sm/144Nd*	*TChur Ga*	*TDm Ga*	*143/144(T)*	*e Nd (T)*	*Sr87/86 measured*	*Sr ppm*	*Rb ppm*	*87Rb/86Sr*	*87Sr/86Sr initial*
Southern Gawler Range															
Toondoolya Bluff	849-24	Waganny Dacite - B	56.94	10.90	0.511854 ±24	0.1158	1.52	1.80	0.510642	0.8					
Toondoolya Bluff	849-82	Waganny Dacite - A	49.70	9.67	0.511846 ±15	0.1177	1.57	1.85	0.510615	0.2					
Toondoolya Bluff	849-85	Bittali Rhyolite	78.70	13.07	0.511613 ±17	0.1005	1.66	1.88	0.510562	-0.8					
NE of Mt. Sturt	884-Pao1	Pao1 Rhyolite	63.39	10.32	0.511654 ±6	0.0985	1.56	1.80	0.510624	0.4	1.07634 ±2	54.0	303.0	16.436	0.70055
NE of Bittali Dam	884-Bi5	Bittali Rhyolite	70.00	12.00	0.511431 ±6	0.1037	2.02	2.16	0.510346	-5.0	0.76320 ±2	167.0	146.0	2.561	0.70464
Lake Everard															
	884-GH8	Childera Dacite	50.94	10.11	0.511821 ±12	0.1200	1.67	1.93	0.510565	-0.7	0.73824 ±4	339.5	185.4	1.599	0.70167
	884-GH5	Mangaroongah Dacite	51.58	10.23	0.511822 ±12	0.1199	1.66	1.92	0.510567	-0.7	0.72156 ±5	455.3	116.9	0.752	0.70436
	884-GH10	Mangaroongah Dacite	62.76	11.53	0.511712 ±12	0.1112	1.69	1.92	0.510548	-1.0	0.73799 ±4	256.8	136.2	1.554	0.70247
	884-GH11	Bunburn Dacite	58.10	10.79	0.511745 ±13	0.1123	1.65	1.90	0.510569	-0.6	0.71619 ±3	743.7	138.7	0.546	0.70369
	884-GH20	Baldry Rhyolite	58.81	13.25	0.511844 ±15	0.1363	2.07	2.25	0.510418	-3.6	1.95625 ±10	15.7	292.9	54.489	0.71042
	884-GH2	Nuckulla Basalt	26.46	5.48	0.511975 ±23	0.1253	1.46	1.79	0.510664	1.2	0.71308 ±10	499.0	56.4	0.331	0.70551
	884-GH15	Wheepool Rhyolite	75.19	12.74	0.511555 ±39	0.1025	1.79	1.98	0.510482	-2.3	0.97221 ±4	46.3	210.1	13.290	0.66834
	884-GH12	Yantea Rhyodacite	72.43	12.70	0.511572 ±13	0.1061	1.83	2.02	0.510462	-2.7	0.84707 ±4	97.8	204.7	6.133	0.70685
Kokatha															
	908-122	Rhyodacite BW1	30.29	4.82	0.511487 ±24	0.0962	1.78	1.96	0.510480	-2.4	0.73316 ±1	291.3	133.0	1.337	0.70258
	884-K8	LPT Basalt	27.18	5.68	0.511805 ±28	0.1263	1.86	2.08	0.510483	-2.3	0.70511 ±2	427.0	9.7	0.067	0.70359
	908-118	LPT Basalt	35.42	6.64	0.511700 ±18	0.1135	1.76	1.98	0.510512	-1.8	0.70643 ±5	723.5	27.9	0.113	0.70385
	908-123	LPT Basalt	38.38	7.42	0.511743 ±22	0.1169	1.75	1.98	0.510520	-1.6	0.70590 ±1	1005.7	35.8	0.104	0.70352
	884-K4	Dacite BW	64.42	11.57	0.511528 ±17	0.1086	1.96	2.12	0.510391	-4.1	0.71038 ±1	423.5	31.6	0.219	0.70538
	884-K5	HPT Basaltic andesite	49.76	9.95	0.511690 ±23	0.1210	1.96	2.14	0.510424	-3.5	0.71390 ±10	549.7	70.6	0.376	0.70530
	908-150	HPT Basaltic andesite	57.90	11.50	0.511681 ±30	0.1201	1.95	2.14	0.510424	-3.5	0.71460 ±6	494.9	76.9	0.455	0.70419
	884-K7	Rhyodacite BW2	55.10	9.82	0.511514 ±14	0.1079	1.97	2.13	0.510385	-4.2	0.76634 ±1	158.0	150.4	2.789	0.70258
	908-137	Rhyodacite RD1	63.14	11.56	0.511591 ±32	0.1107	1.90	2.08	0.510432	-3.3	0.71144 ±1	189.8	193.7	2.989	0.64310
	908-47	Rhyodacite RD2	71.05	13.28	0.511524 ±37	0.1131	2.08	2.22	0.510341	-5.1	0.75867 ±1	218.1	179.6	2.412	0.70352
	908-1	Rhyolite RH3	51.11	8.06	0.511224 ±30	0.0954	2.16	2.27	0.510226	-7.4	0.98986 ±6	42.2	183.8	12.765	0.69801
	908-29	Rhyodacite BGD	77.33	13.66	0.511561 ±14	0.1069	1.87	2.05	0.510443	-3.1	0.92294 ±1	75.2	247.8	9.657	0.70214
	908-61	IPT basaltic andesite	39.27	7.88	0.511719 ±18	0.1214	1.91	2.11	0.510449	-3.0	0.71979 ±1	431.4	99.1	0.673	0.70441
	908-18	Andesite	33.60	6.13	0.511461 ±30	0.1104	2.12	2.25	0.510305	-5.8	0.72413 ±6	379.7	101.3	0.781	0.70627
	884-K14	Rhyolite RH4	36.96	6.36	0.511361 ±18	0.1041	2.14	2.26	0.510271	-6.5	0.75845 ±1	182.4	150.1	2.411	0.70333
	908-64	Dacite GMD	42.17	7.17	0.511321 ±21	0.1029	2.18	2.28	0.510244	-7.0	0.73203 ±1	352.2	140.8	1.171	0.70525
	908-106	Chandabooka Dacite	47.20	8.64	0.511450 ±30	0.1107	2.15	2.27	0.510291	-6.1	0.75421 ±6	223.5	165.4	2.168	0.70464
Tarcoola															
	884-T6	Konkaby Basalt	30.30	5.70	0.511626 ±27	0.1138	1.90	2.09	0.510435	-3.3	0.70931 ±3	807.5	65.3	0.237	0.70389
	884-T18	Konkaby Basalt	30.38	5.70	0.511677 ±23	0.1134	1.80	2.01	0.510490	-2.2	0.71117 ±10	732.5	85.5	0.342	0.70335
	884-T30	Balbara Rhyolite	73.66	12.47	0.511527 ±17	0.1024	1.83	2.02	0.510456	-2.9					
	884-T31	Carnding Rhyodacite	57.35	10.09	0.511596 ±31	0.1064	1.80	1.99	0.510483	-2.3					

Errors quoted are calculated as 2 standard error of the mean
Time (T) is 1.592 Ma.

and Nd isotopic value (Figure 2.15). It is this relationship which most strongly defines the two phases of volcanism at Kokatha. In both phases early erupted units, whether mafic or felsic, have relatively high (for the area) ε_{Nd}, and as stratigraphically higher levels are reached the ε_{Nd} becomes progressively more negative.

The initial $^{87}Sr/^{86}Sr$ ratios of the Kokatha volcanics (for the data which survived the culling procedure) range from 0.70258 for two different rhyodacites erupted within the first cycle mafic rocks to 0.70627 for the second cycle andesite. There is no clear correlation between calculated initial $^{87}Sr/^{86}Sr$ ratio and any index of differentiation or stratigraphic height. Nor is there any observable correlation between εNd and the initial initial $^{87}Sr/^{86}Sr$ ratio.

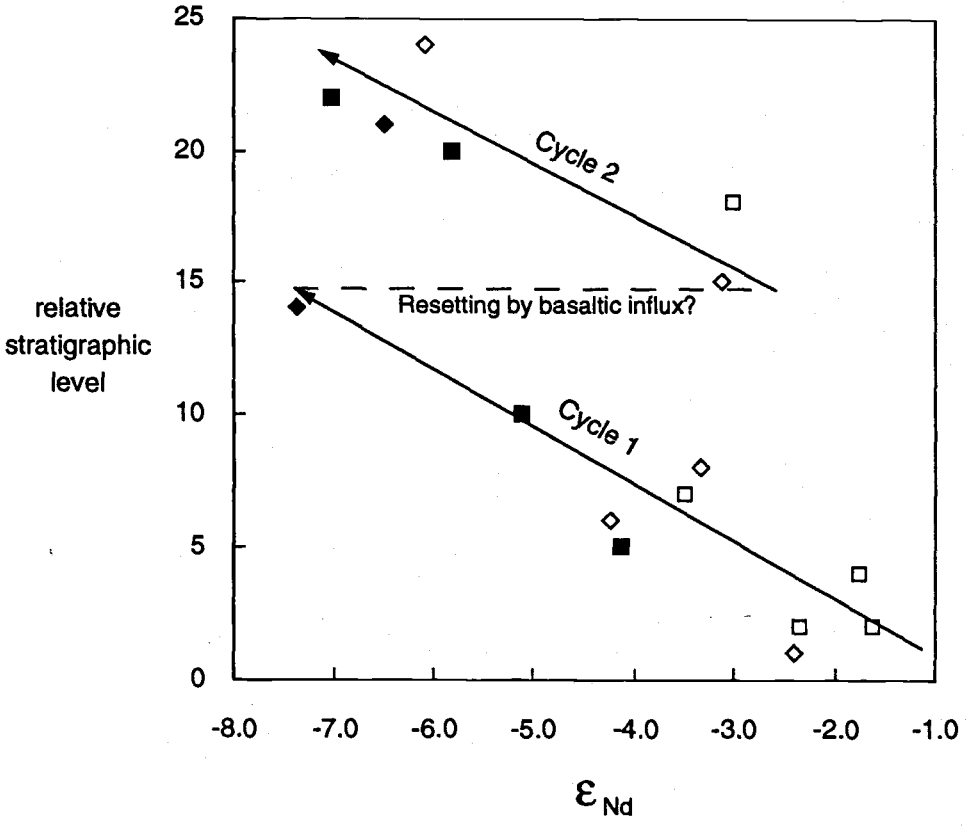

Figure 2.15 - The variation of ε_{Nd} plotted against relative stratigraphic level for the volcanics at Kokatha. Symbols define lithological type according to the silica scheme shown in Figure 2.2: open squares, basalt, basaltic andesite and andesite; filled squares, dacite; open diamonds, rhyodacite; filled diamonds, rhyolite.

2.5.2 - Isotopic variation in the Lake Everard area

The ε_{Nd} values for the volcanics from Lake Everard range from +1.2 for the Nuckulla Basalt to -3.6 for the Baldry Rhyolite. In a similar manner to the pattern seen for Kokatha, the ε_{Nd} values decrease with various indices of increasing differentiation (e.g. decreasing MgO, Figure 2.16), however the position of the pattern is removed to higher values than that of the Kokatha rocks. Of the initial $^{87}Sr/^{86}Sr$ ratios which survived the

culling process, the lowest value of 0.70167 belongs to a sample of the Childera Dacite while the highest value of 0.70551 is for the Nuckulla Basalt. There is no apparent systematic variation in ε_{Nd} or initial $^{87}Sr/^{86}Sr$ with stratigraphic height for the Lake Everard volcanics.

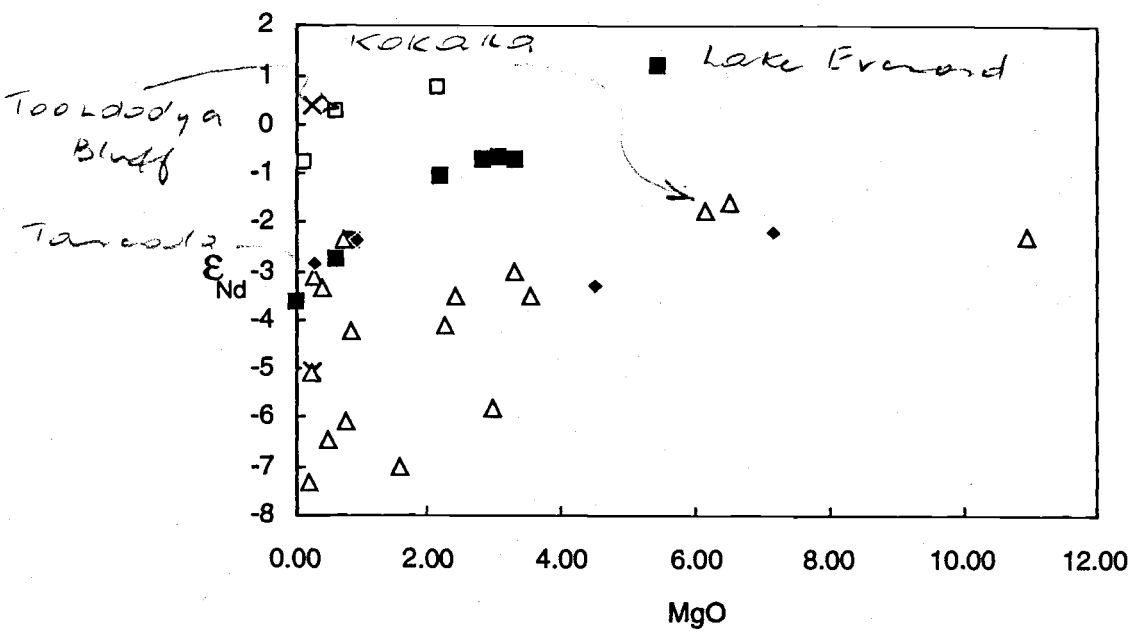

Figure 2.16 - ε_{Nd} v MgO for the developmental phase volcanics illustrating the tendency towards decreasing eNd with decreasing MgO within individual volcanic areas. Symbols: filled squares, Lake Everard area; open triangles, Kokatha area; open squares, Toondoolya Bluff locality of the SGRA; crosses, volcanics from SGRA other than from Toondoolya Bluff; filled diamonds, Tarcooola area.

2.5.3 - Isotopic variation in the Tarcoola area

Only four samples of the volcanic sequence were analysed for Nd isotopes, because it was difficult to determine relative stratigraphic positions of the samples from the scattered outcrops and because the number of units present is small, both factors which make comparison with the above areas difficult. The two ε_{Nd} values for the Konkaby Basalt are -2.2 and -3.3, that of the Ealbara Rhyolite is -2.9 while the Carnding Rhyodacite has a value of -2.3. Strontium isotopes for the two basalt samples analysed are 0.70335 and 0.70389. There is no simple covariation of ε_{Nd} with MgO or any other indicator of differentiation.

2.5.4 - Isotopic variation in the Southern Gawler Range area

Five samples from the Southern Gawler Range area have been analysed for Nd isotopes, three from the two units exposed at Toondoolya Bluff and two from the remainder of the area. The three samples from Toondoolya Bluff range from ε_{Nd}=+0.8

for the Waganny Dacite to ε_{Nd}=-0.8 for a sample of the Bittali Rhyolite. The sample PaO1 has an ε_{Nd} of +0.4 while that of the Bittali Rhyolite from Bittali Dam is -5.0. The large difference in values for the two Bittali Rhyolite samples from the two localities is surprising, however an explanation may lie in the linear nature of the southern Gawler Range volcanic area, which along its length may be underlain by different basement types. The samples from Toondoolya Bluff do form a trend of decreasing ε_{Nd} with decreasing MgO (Figure 2.16). The two samples from outside Toondoolya Bluff were analysed for Sr isotopes, and only one of these values passes the culling criteria. This sample has an initial $^{87}Sr/^{86}Sr$ of 0.70464.

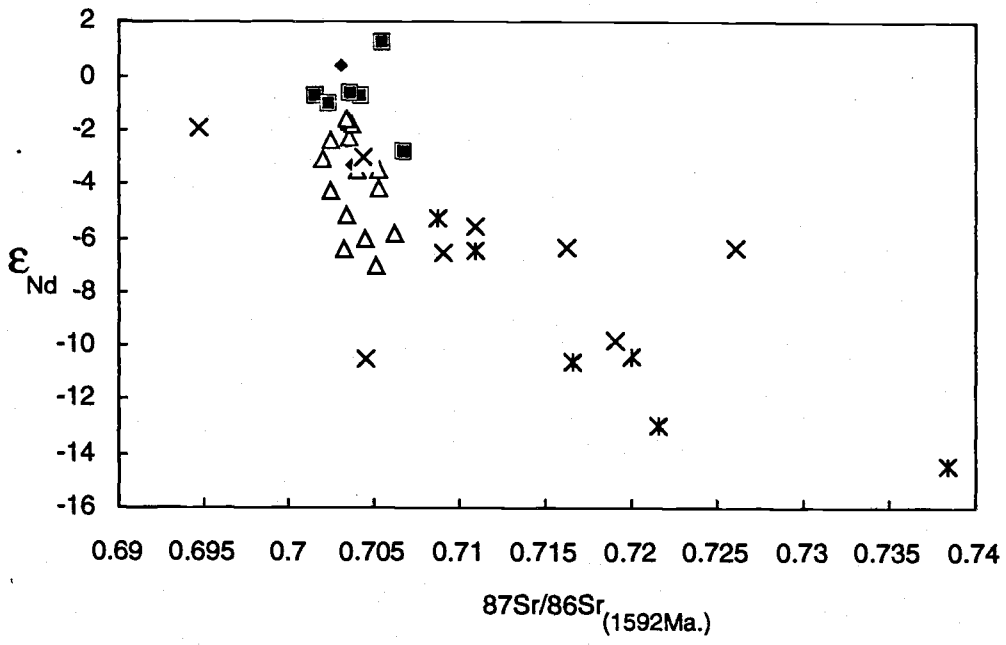

Figure 2.17 - Plot of ε_{Nd} against $^{87}Sr/^{86}Sr$ (at 1592Ma.) for the developmental volcanics and some Archaean and Palaeoproterozoic basement lithologies. Isotopic data for the basement rocks is given in Table 2.6. Symbols: open triangles, Kokatha volcanics; filled squares, Lake Everard volcanics; filled diamonds, Konkaby Basalt from Tarcoola; crosses, Palaeoproterozoic basement lithologies; barred crosses, Archaean basement lithologies.

2.5.5 - Discussion of the isotope data

A recurring feature of the Nd isotope data is the correlation between geochemical and isotopic variation as illustrated by Figure 2.16 which shows the variation of εNd and MgO. In contrast no easily interpretable correlations are evident between the ε_{Nd} and the initial $^{87}Sr/^{86}Sr$ for the developmental volcanics from any area. Also no correlations are observed between either chemistry or stratigraphic grouping and the initial $^{87}Sr/^{86}Sr$ ratios for any area, whereas definite correlations with one or other of these parameters is seen for all the areas with respect to the Nd isotopic system. The Nd-Sm system is much less prone to resetting and post-emplacememt mobility than the Rb-Sr system and therefore

one way of assessing the Sr data is to view it with respect to the Nd isotope results. If the isotopic characteristics of the developmental phase volcanics are viewed with respect to analysed Archaean and Palaeoproterozoic rocks of the Gawler Craton, which may represent possible sources, it is obvious that their variation is comparatively small (Figure 2.17). Therefore the Sr isotope behaviour may be explained in a number of different ways:

1) it may be caused by mixing between two endmembers with similar, low Sr isotopic values but highly different Nd isotopic values.

2) it may be due to a two endmember AFC process whose products contain only a small proportion of a crustal component with low εNd and high Sr initial ratio.

3) the Sr isotopic system has been disturbed and the initial ratios are not correct. The first explanation neccesitates a crustal endmember for the mixing process with a low Sr ratio at Gawler Range time and a low ε_{Nd} value. One way of producing these characteristics is for the crustal endmember to have had a long residence time in the crust during which it had at some stage lost Rb. However none of the chemical signatures of the felsic volcanic rocks or any of the analysed basement lithologies exhibits Rb depletion of crustal rocks of this type (Table 2.7) e.g. the granulite facies Lewisian gneisses, and this mechanism for generating the observed Sr ratios is considered to be unlikely. While the second explanation is feasible, the third listed possibility gains credence from the fact that previous published Sr isotope work on the Gawler Craton (e.g. Webb *et al.*, 1986) has repeatedly proven to yield ages far younger than actual crystallization ages later determined by U-Pb dating (with age discrepancies often in the range 100-200Ma.), and from the previously illustrated variation of initial ratios in volcanics of low Sr content. It is therefore considered that the Sr isotopes may well be suspect of little value in identifying and quantifying the processes which produced the volcanics.

2.6 - Chemistry and isotopic ratios of basement rocks

Before any discussion of the sources of any of the developmental volcanics can be determined, the characteristics of potential crustal source lithologies must be determined. Six Archaean and six Palaeoproterozoic rocks have been analysed to determine their Nd (and Sr) isotopic values at Gawler Range time, and their chemistry. This data is presented as Tables 2.6 and 2.7. For each group the samples were chosen to satisfy two basic criteria, that they cover a wide range of chemical composition and that they had been previously dated such that there was some certainty as to which basement age group they belonged. In many cases the samples thus chosen had previously been run for their Sr isotopes (see footnote to Table 2.6).

Table 2.6 - Nd and Sr isotopic data for selected Archaean and Palaeoproterozoic rocks from the Gawler Craton

	Locality or unit	Age (Ga)	Lithology	Sample Number	Nd ppm	Sm ppm	143Nd/144Nd measured	147Sm/144Nd	TChur Ga	TDm Ga	143Nd/144Nd(T)	eps Nd (T)	87Sr/86Sr measured	Sr ppm	Rb ppm	87Rb/86Sr (1592Ma)	87Sr/86Sr (1592Ma)
Proterozoic	McGregor Volcanics	1.740 †	Basalt	884-MG2	33.46	5.12	0.511418 ±16	0.0926	1.82	1.99	0.510448	-3.0	0.71011 ±9	643	54	0.246	0.70447
		1.740 †	Dacite	884-MG4	55.53	9.82	0.511440 ±31	0.1070	2.08	2.21	0.510320	-5.5	0.78493 ±3	218	241	3.234	0.71098
	Donington Suite	1.823 *	Hypersthene Granite	515-B143	50.90	9.58	0.511469 ±13	0.1138	2.20	2.31	0.510277	-6.4	0.79508 ±4	171	201	3.443	0.71636
	Cape Donington	1.850 *	Meta-basaltic dyke	515-B26	23.30	4.48	0.511284 ±13	0.1163	2.62	2.62	0.510067	-10.5	0.71087 ±3	320	30	0.275	0.70459
	Donington Suite	1.820 *	Alkali Granite	515-B152	33.80	5.74	0.511728 ±16	0.1027	1.51	1.77	0.510653	1.0	4.35480 ±4	12	413	100.815	2.04979
	Donington Suite	1.896 *	Quartz Gabbronorite	468-B201	28.80	5.68	0.511518 ±24	0.1194	2.26	2.36	0.510269	-6.5	0.73871 ±5	231	102	1.293	0.70914
	Tarcoola Formation	1.654 ◊	Shale	939-90-14	26.67	4.94	0.511679 ±20	0.1121	1.77	1.98	0.510506	-1.9	0.99480 ±4	36	162	13.121	0.69481
	Cook Gap Schist	1.850 ◊	Schist	939-90-13	37.48	6.68	0.511405 ±31	0.1077	2.16	2.27	0.510277	-6.4	0.94741 ±6	69	229	9.674	0.72622
	Broadview Schist	1.800 ◊	Schist	6131RS147	14.29	3.05	0.511456 ±47	0.1292	2.74	2.71	0.510103	-9.8	0.80340 ±6	109	181	4.867	0.71913
Archaean	Sleaford Complex	2.640 §	Basic granulite	466-C142	8.34	2.32	0.511820 ±26	0.1679	4.63	3.62	0.510062	-10.6	0.73215 ±7	82	19	0.679	0.71663
	Sleaford Complex	2.837 §	Leucogneiss	466-JC3	17.12	2.64	0.510916 ±28	0.0933	2.58	2.59	0.509940	-13.0	0.74300 ±3	135	43	0.933	0.72167
	Sleaford Complex	2.643 §	Augen Gneiss	466-256	40.24	6.78	0.510933 ±28	0.1019	2.79	2.75	0.509867	-14.4	0.79880 ±2	140	126	2.636	0.73852
	Sleaford Complex	2.640 §	Basic granulite	466-F30	28.80	7.49	0.511981 ±26	0.1572	2.67	2.65	0.510336	-5.2	0.71321 ±1	62	4	0.189	0.70889
	Devils Peak	2.525 #	Rhyolite	884-DPA	26.46	6.09	0.511528 ±36	0.1392	3.04	2.90	0.510071	-10.4	0.78384 ±7	48	46	2.789	0.72006
	Volcanics	2.525 #	Andesite	884-DPB	28.56	5.93	0.511589 ±27	0.1255	2.31	2.40	0.510275	-6.4	0.72274 ±6	78	14	0.513	0.71100

Errors quoted are calculated as 2 standard error of the mean
Time (T) is 1.592 Ma.
*Ages are from the following sources- † Fanning et al., 1986; * Mortimer, 1984; § Fanning, 1975; # Cowley and Fanning, 1991; ◊ R. Flint (pers comm.).*
Strontium isotope values for samples prefixed 515- and 468- are from Mortimer (1984)
Strontium isotope values for samples prefixed 466- are from Fanning (1975)

Table 2.7 - Major and trace element data for selected basement lithologies from the Gawler Craton §

	Archaean						*Palaeoproterozoic*								
	Sleaford Complex	*Sleaford Complex*	*Sleaford Complex*	*Sleaford Complex*			*Cape Donnington*	*Cape Donnington*	*Cape Donnington*	*Cape Donnington*	*Cook Gap Schist*	*Broadview Schist*	*McGregor Volcanics*	*McGregor Volcanics*	*Tarcoola Formation*
Sample #	*JC3*	*446/256*	*446/F30*	*446/C142*	*DPA*	*DPB*	*515-B201*	*515-B26*	*515-B143*	*515-B152*	*939-90-13*	*6131RS147*	*MG2*	*MG4*	*939-90-14*
Lithology	*Leucogneiss*	*Augen gneiss*	*Basic granulite*	*Basic granulite*	*Rhyolite*	*Basalt*	*Qtz-gabbronorite*	*M-Basaltic dyke*	*Fe-hypersth Gt*	*Alkali granite*	*Schist*	*Schist*	*Basalt*	*Rhyodacite*	*Shale*
SiO2	76.75	70.08	47.54	50.69	73.15	58.13	55.96	52.89	65.37	77.01	61.85	61.89	47.44	65.59	72.50
TiO2	0.25	0.64	2.67	0.84	0.33	1.36	0.80	0.80	0.87	0.07	0.69	0.85	1.06	0.77	0.40
Al2O3	12.87	14.97	13.03	14.57	12.45	15.43	14.78	15.13	14.92	11.88	15.76	15.71	14.57	14.82	12.24
Fe2O3	1.77	3.59	17.77	12.94	4.25	11.01	9.93	10.67	6.09	1.04	8.07	8.23	11.78	5.29	4.18
MnO	0.02	0.04	0.26	0.21	0.06	0.16	0.15	0.17	0.10	0.03	0.18	0.15	0.21	0.13	0.04
MgO	0.40	2.08	6.83	7.77	1.53	5.50	5.95	7.04	1.57	0.18	2.92	1.97	8.63	1.56	1.64
CaO	2.02	1.32	10.04	11.76	0.83	0.78	6.94	9.88	3.37	0.74	0.66	1.05	12.12	2.17	0.61
Na2O	3.75	2.79	1.64	0.94	3.69	4.01	2.47	2.47	2.98	3.03	1.82	3.68	2.30	2.56	0.99
K2O	2.31	5.50	0.25	0.65	1.66	0.49	2.21	1.13	4.43	5.20	4.72	4.50	0.84	5.57	3.37
P2O5	0.03	0.09	1.09	0.06	0.05	0.26	0.20	0.19	0.24	0.00	0.13	0.18	0.29	0.23	0.08
LOI	0.33	0.15	-0.54	-0.01	2.31	3.58	0.44	-0.10	0.09	0.22	2.42	2.08	0.51	0.70	4.33
Total	100.50	101.25	100.58	100.42	100.31	100.71	99.83	100.27	100.03	99.40	99.22	100.29	99.75	99.39	100.38
Cr	398	434	223	368	146	39	575	345	16	1	204	159	657	13	88
Ni	11	21	65	87	7	5	111	79	22	11	35	50	262	7	20
Sc	4	6	42	43	7	18	29	35	16	1	12	18	33	15	7
V	17	60	460	278	10	140	157	228	58	1	96	154	225	53	41
Pb	14.9	40	3	6.6	4.5	4.9	15	6.4	26.4	48.6	1101	5.8	8	17	16
Rb	43.0	126.0	5.2	19.1	45.9	13.6	102.0	28.0	201.0	413.0	229.2	181.1	53.7	238.2	161.7
Sr	135.0	140.0	61.4	80.4	48.2	77.6	231.0	318.0	171.0	12.0	69.4	109.0	662.0	218.0	36.1
Ba	503	664	317	203	503	145	500	728	885	6	542	1126	183	887	585
Ga	13	19	20	17	15	18	16	6.4	17.4	16	26	19	16	19	15
Nb	6	7	17	4	12	7	12	6	17	6	17	13	13	16	13
Zr	171	275	170	51	300	166	168	113	288	118	193	177	91	305	144
Y	10	16	60	24	45	30	31	26.1	47	52	36	21	24	43	29
Th	11	52	1	1	11	4	8	2.2	17	36	24	12	4.7	20.3	16
U	0.2	2.3	0	0.7	1.8	0.6	7.6	0.5	4.9	13.3	6.1	2.9		4.5	2.7
La	39.000	88.295	37.000	6.578	28.000	23.000	38.000	23.900	58.500	39.000	50.000	17.246	39.000	67.000	41.012
Ce	70.000	214.637	70.000	16.918	59.000	36.000	74.000	50.900	120.000	74.000	93.000	52.589	75.000	134.000	75.752
Nd	17.118	96.628	28.800	8.116	26.462	28.564	28.800	23.300	50.900	33.800	37.479	16.678	33.464	55.529	29.195
Sm	2.639	16.159	7.485	2.318	6.088	5.928	5.684	4.480	9.580	5.740	6.675	3.613	5.152	9.825	5.375
Eu		1.057		0.649				1.280	1.770	0.163		0.793			0.867
Gd		7.487		2.860				4.470	8.600	6.450		3.321			4.846
Dy		3.411		3.861				4.220	7.930	7.130		4.088			4.434
Er		1.236		2.348				2.680	4.620	4.330		2.790			2.665
Yb		0.844		2.427				2.670	4.320	4.020		3.149			2.847

§ Data is from Turner et al., 1992b, with the exception of that for the McGregor Volcanics and the Archaean volcanics DPA and DPB

In the Archaean group two of the samples are from a recently discovered bimodal volcanic succession from within the Gawler Craton some 150 kilometres north-east of Tarcoola. As yet this volcanic suite is known only from drill hole intersection (Cowley and Fanning, 1991). The other Archaean samples are various meta-igneous, granulite facies, lithologies from the Sleaford Complex, the southern equivalent of the Mulgathing Complex, which outcrops at the southern end of the Gawler craton.The granulites analysed from the Sleaford Complex were metamorphosed under granulite facies conditions at approximately 2450 m.a. during the Sleafordian Orogeny (Daly and Fanning, 1990).

Four of the Palaeoproterozoic samples are from the Cape Donington area which outcrops on the south-east extremity of Eyre Peninsula, and comprise three members of the meta-igneous Donington Group (approximately 1850 Ma., Mortimer, 1984) including quartz gabbronorite, and orthopyroxene-bearing granitoids, and one meta-basaltic dyke all of which are interpreted to have undergone granulite facies metamorphism (Mortimer, 1984). Two samples are from the McGregor volcanics (≈1740Ma., Fanning *et al.*, 1986), a bimodal volcanic suite which is altered but only weakly metamorphosed. The remaining three Palaeoproterozoic samples are shales or schists, two from the Hutchinson Group and the third from the Tarcoola Formation. The shales/schists may be representative of average upper pre-Gawler Range crust (e.g. Taylor and McLennan, 1985).

Both groups of basement rocks, with few exceptions, have lower Nd ratios than the field defined by the developmental volcanics (Figure 2.17). At 1592 Ma. the Archaean crystalline basement would have had ε_{Nd} ranging from -5.2 to -14.4, whereas the Palaeoproterozoic crystalline basement would have had ε_{Nd} between -3.0 to -10.5. One anomalous Palaeoproterozoic sample, an alkali granite from Cape Donington, has a high ε_{Nd} of +1.0 (combined with a very high $^{87}Sr/^{86}Sr$ ratio; Table 2.6) and is not considered to represent typical isotopic compositions of crystalline basement beneath the Gawler Ranges. The Palaeoproterozoic shales and schists have εNd values which range from -1.9 for the Tarcoola Formation to -9.8 for the Broadview Schist. The Nd isotopic value for the Tarcoola Formation is high for a sediment deposited on (and sourced from?) Archaean basement, and this may indicate a large juvenile component in the formation.

2.7 - Origin of the basalts

The Nd isotopic data for the developmental phase volcanics indicates some relationship between the mafic and felsic volcanics within each area of developmental volcanism. Equally obvious is the chemical similarity between all of the basaltic (sensu lato) rocks of the province. However before the relationship between the basic and felsic

rocks can be evaluated, the sources and processes involved in the production of the basalts must be investigated. As outlined in sections 2.4.6 and 2.4.7 the basaltic rocks of the developmental phase are characterised by light rare earth enrichment, high LILE/HFSE ratios and a distinctive pattern of relative enrichment of the elements Rb, Ba, Th, U and K. This section attempts to identify the origin of this chemical signature.

Phenocrysts within the basalts are olivine, augite, and plagioclase (± magnetite?) with pigeonite also present as microphenocrysts in some of the more evolved mafic rocks. Pyroxene is the only one of these phases which could contribute to light rare earth enrichment during fractional crystallisation, having slightly larger partition coefficients for the HREE than for the LREE in basaltic systems. However LREE enrichment is observed even in the very magnesian basalts from Kokatha (e.g. K101, 884-K8), whose high Ni and Cr concentrations and high Mg numbers (up to 70) are chemical characteristics approximating those necessary for a liquid which formed in equilibrium with typical mantle olivine compositions (Frey *et al.*, 1978). Therefore the LREE enrichment observed in the basalts is unlikely to have been produced by extended crystal fractionation and must either be a feature inherited from the mantle source or caused by crustal assimilation.

Most crustal rocks are LREE enriched (Taylor and McLennan, 1985), however, to get the steep patterns of the Gawler Range mafic rocks from an unenriched basaltic parental magma would require either a) a crustal assimilant with an very high concentration of LREE or b) assimilation of a considerable amount of crust with average crustal REE. For example, to obtain the 110x chondritic enrichment in La in the most magnesian LP basalts from Kokatha would require either the addition of more than 100% of an assimilant with either average bulk or average upper crust composition being added to a typical MORB basaltic melt (using the average crustal compositions of Taylor and McLennan, 1985). Even if the assimilant was a partial melt with up to 400x chondrite La, 25% of this type of highly enriched crustal endmember would be required to produce the necessary LREE enrichment, but the resultant magma would neither have the high levels of MgO, nor the high compatible trace element (Ni, Cr) concentrations observed in the most primitive LP basalts. The LREE enrichment of the developmental phase basaltic rocks cannot have been produced by either fractionation or crustal contamination, and therefore must be a feature of the mantle source.

Could the distinctive chemical signature of the basaltic magmas, other than the LREE enrichment, result from crustal contamination during their ascent? Analyses of the pre-Gawler Range shales and Archaean to Palaeoproterozoic crystalline basement rocks (Table 2.7), together with estimates of average upper and lower crust from Taylor and McLennan (1985), have been used to evaluate the role of crustal contamination of the basalts. Figures 2.18a &b illustrate that the developmental basalts do not lie on mixing lines between asthenospherically derived basalts (OIB or MORB) and any of the possible

Figure opposite:

Figure 2.18 a & b - Chemical ratio plots illustrating some differences in chemistry between the mafic rocks of the Gawler Range volcanics, MORB and OIB, upper crust (UC) and lower crust (LC). Symbols: open squares, Kokatha LP basalts; open triangles, Kokatha HP basalts; filled squares, Nuckulla Basalt from Lake Everard; filled diamonds, Konkaby Basalt from Tarcoola; crosses, Palaeoproterozoic basement; barred crosses, Archaean basement.

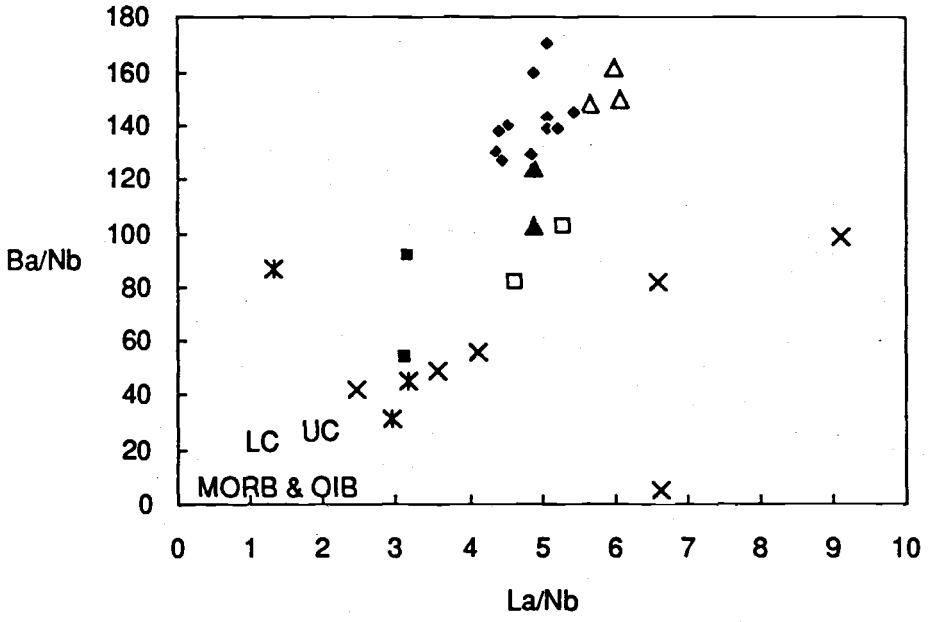
180
160
140
120
100
80
60
40
20
0
Ba/Nb
LC
UC
MORB & OIB
0
1
2
3
4
5
6
7
8
9
10
La/Nb

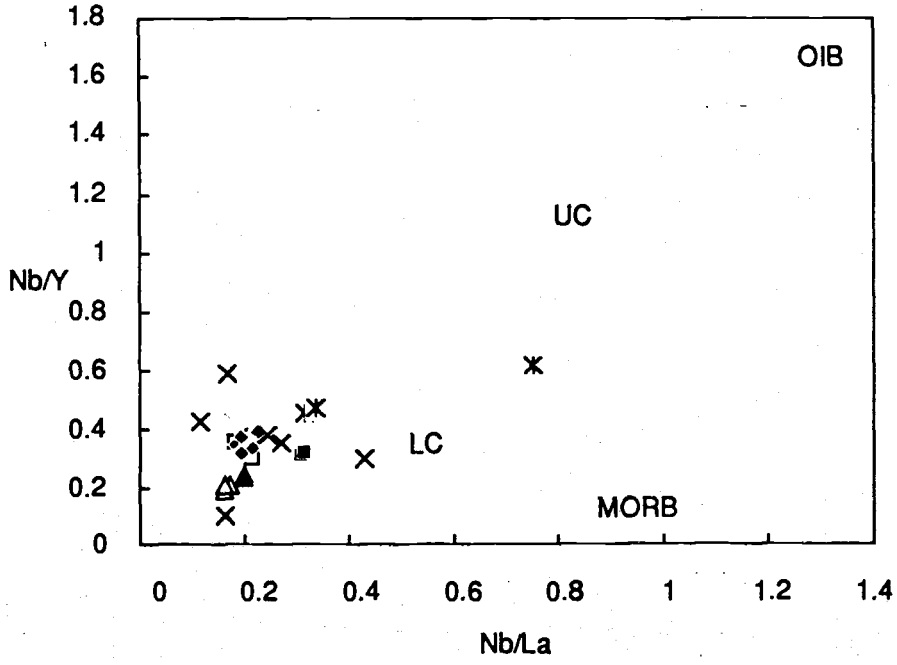
1.8
1.6
1.4
1.2
1
0.8
0.6
0.4
0.2
0
Nb/Y
OIB
UC
LC
MORB
0
0.2
0.4
0.6
0.8
1
1.2
1.4
Nb/La

crustal endmembers. In particular the high LILE/HFSE ratios (such as Ba/Nb) cannot be produced in this manner because the basalts have higher ratios than either crustal estimates or MORB or OIB. In addition the HP basaltic andesites have higher levels of Zr, P, Ti, REE, together with higher Ti/Zr and lower εNd than the LP basaltic rocks. Although the higher Zr and REE contents could be explained by crustal contamination, the HP basaltic andesites cannot be explained by crustal contamination of LP basalts because crustal lithologies have low concentrations of Ti, P and Sr. Figures 2.19a&b illustrate that regardless of whether an OIB type or MORB type asthenospheric component is chosen, contamination with crust fails to replicate the chemistry of the basalts. For example large proportions of crust ($\geq$ 50%) must be added to MORB to produce the incompatible element concentrations of the basalts, and then the level of Nb is much higher and the amount of Sr is far lower than that observed in the basalts (Figure 2.19a). Of course such large degrees of contamination are ruled out by the fact that the resultant magma would no longer be basaltic in composition. Conversely when an OIB parent is used, it is almost impossible to produce the observed Nb anomaly even when assuming the crust contained no Nb itself (Figure 2.19b).

A few basalts from the developmental volcanics do appear to have been substantially contaminated by continental crust, however they form a minor proportion of the basalts of the province. These samples typically contain some other evidence of contamination such as quartz or potassium feldspar xenocrysts, or a combination of high compatible element values, e.g. Ni, Cr, together with increased levels of SiO_2 and very high levels of incompatible elements such as Zr, Rb, and REEs compared with uncontaminated members of the same units.

In summary the distinctive chemistry of the basalts including their LREE enrichment and high LILE/HFSE ratios is not the result of crustal contamination of asthenospheric basalts. As no asthenospheric basalts (OIB, MORB) bear this type of chemical signature, it is inferred to be derived from the continental lithosphere. The affect of interaction of asthenospheric magmas with continental mantle lithosphere is now addressed.

The definition of the term mantle lithosphere, as used here, is that of McKenzie (1989), i.e. a mechanical boundary layer which lies beneath the continental crust and which has remained physically isolated from the convecting asthenosphere for significant periods of time. As the mantle lithosphere does not convect, it can preserve chemical and isotopic signatures previously emplaced within it. It seems quite probable that the continental lithosphere is highly variable in composition, reflecting the large variety of possible mechanisms by which it could be chemically and isotopically modified.

The preferred interpretation of the chemical and isotopic data for the basaltic rocks is that they represent different degrees of mixing between two mantle-derived

Figures opposite:

Figure 2.19 a & b - Primitive Mantle normalised diagrams comparing the chemistry of the LP basalt K101 from Kokatha, with a) mixtures of MORB and upper crust; and b) mixtures of OIB and upper crust.

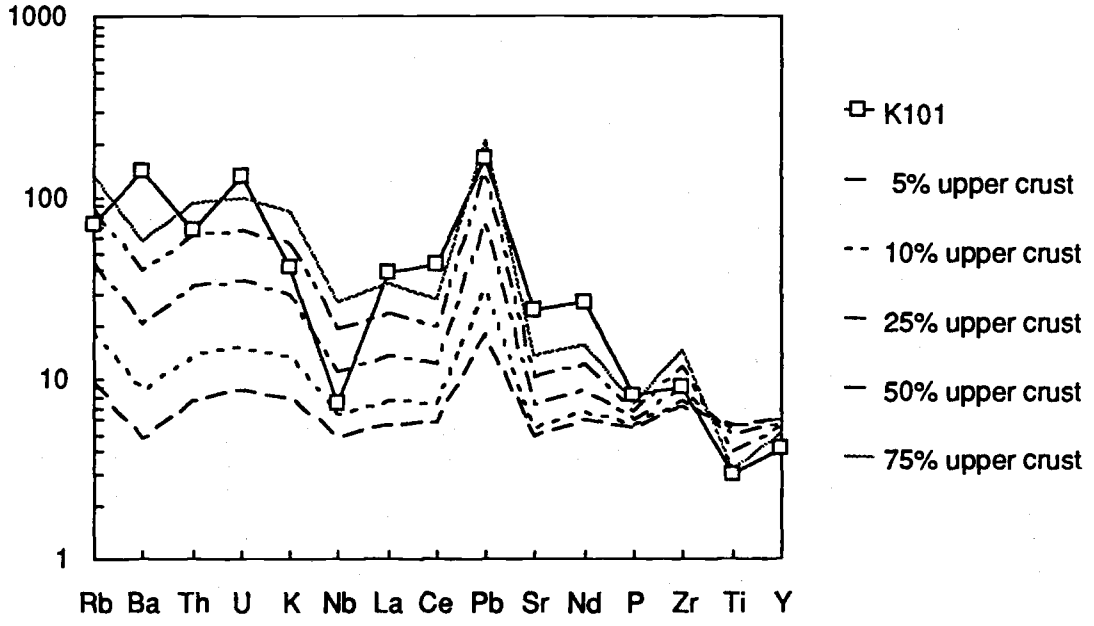
1000
100
10
1
Rb Ba Th U K Nb La Ce Pb Sr Nd P Zr Ti Y
K101
5% upper crust
10% upper crust
25% upper crust
50% upper crust
75% upper crust

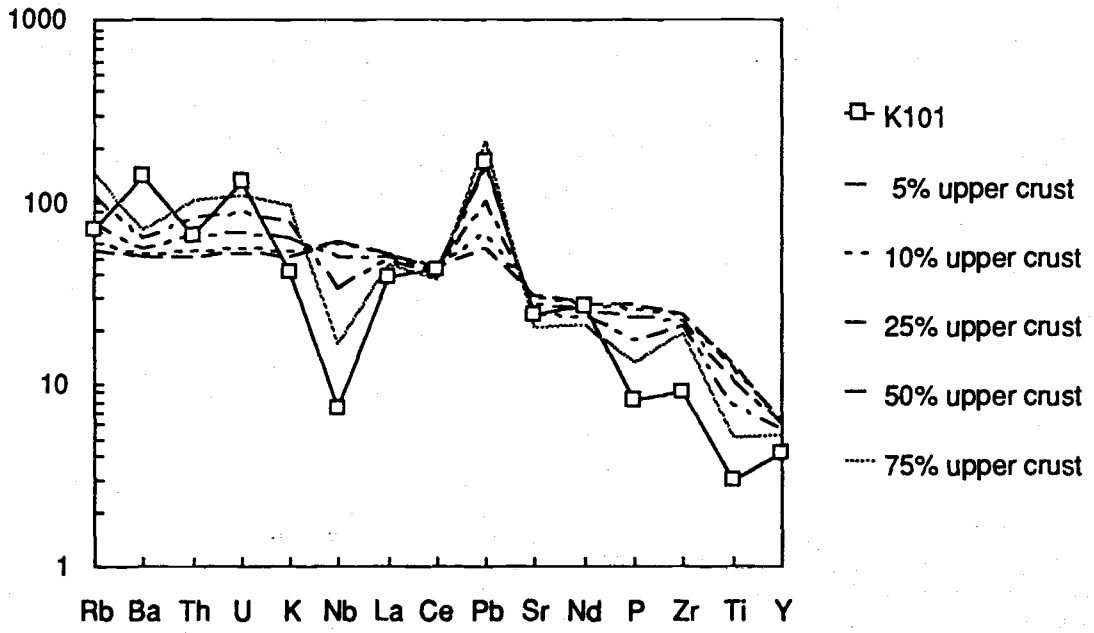
1000
100
10
1
Rb Ba Th U K Nb La Ce Pb Sr Nd P Zr Ti Y
K101
5% upper crust
10% upper crust
25% upper crust
50% upper crust
75% upper crust

endmembers. One endmember is derived from an enriched lithospheric source which contains high levels of REE and LILE, a distinctive LILE pattern enriched in Ba and U relative to Rb and Th, and low HFSE, while the other endmember may be either OIB- or MORB-like. The exact identification of the asthenospheric endmember is impossible without more precise knowledge of the lithospheric endmember. The enrichment of the mantle lithosphere cannot have been temporally related to the Gawler Range volcanism, for this would not allow evolution to low ε_{Nd}. Rather the enrichment must have occurred significantly before the Gawler Range volcanism, an interpretation which is consistent with the Nd model ages of the basalts ranging from 1760 to 2140 Ma (Table 2.5).

The basalts of the Gawler Ranges exhibit similar chemical variation to that seen in basalts of the Northeastern Transition Zone (NETZ), Southeastern Transition Zone (SETZ) and Western Great Basin (WGB) in the Southwestern United States (Figure 2.20). Each of these regions borders the Basin and Range Province,which has been extended by up to 250% in some areas (Gans *et al.*, 1988), and is transitional to areas of little/no extension, such as the Colorado Plateau and the Sierra Nevada Batholith. Basalts from within the Basin and Range province itself have a smooth, concave down pattern similar to those of ocean island basalts (OIB), and have been interpreted as having formed from an asthenospheric source without significant contamination from continental crust or mantle lithosphere (Menzies *et al.*, 1983; Kempton *et al.*, 1991). Basalts from the above listed areas which are transitional to the Basin and Range vary from being similar to those from the Basin and Range to those which have peaks at Ba relative to Rb and K, and Nb depletions, similar to the Gawler Range mafic volcanics. The distinctive chemistry of the SETZ, NETZ and WGB basalts has been shown by Ormerod *et al.*(1988) and Kempton *et al.*(1991) to be unable to be explained by crustal contamination. This interpretation has been reinforced by inverse modelling as applied to basalts from the WGB which demonstrated the trace element features were derived from the source and not artifacts of later crustal contamination (Ormerod *et al.*, 1991). This comparison illustrates that chemical signatures such as those of the developmental phase basalts can be derived from subcontinental lithospheric mantle.

That enriched mantle lithosphere may indeed be present beneath the Gawler Ranges is indicated by the recent recognition of altered phlogopite bearing basaltic rocks near Mount Gunson (approximately 160 kilometres north-northeast of Port Augusta) which have been tentatively correlated with the Gawler Range volcanics (Knutson *et al.*, 1992). In less altered parts the ferromagnesian phenocryst assemblage in these volcanics is clinopyroxene+ phlogopite ± olivine ± hornblende. Chemically the basalts have high LILE and REE concentrations, and they also have very similar levels of P, Ti and Y to the HP basaltic andesites from Kokatha. Although the relative enrichments in LILE of the phlogopitic basalts is not the same as that typical of the developmental phase basalts, the

degree of alteration present induces caution in interpreting too much from these analyses. The Mt. Gunson basic volcanics may represent the enriched lithospheric endmember of the mixing process which produced the basalts, indicating the presence of pockets of enriched metasomatised mantle within the lithosphere. Similarly the ultrapotassic rocks of the Colorado Plateau and Leucite Hills have been interpreted to represent the melts of enriched lithosphere (Thompson *et al.*, 1990) which mix with asthenospheric magmas to form the basalts of the Western Great Basin and North-east and South-east transition zones around the Colorado Plateau (Kempton *et al.*, 1991; Fitton *et al.*, 1991). The occurrence of phlogopite in the Mt. Gunson mafic volcanics is in accord with the work of Hawkesworth *et al.* (1990) who have identified phlogopite to be the phase within enriched lithosphere which to a large degree controls inter-element fractionation.

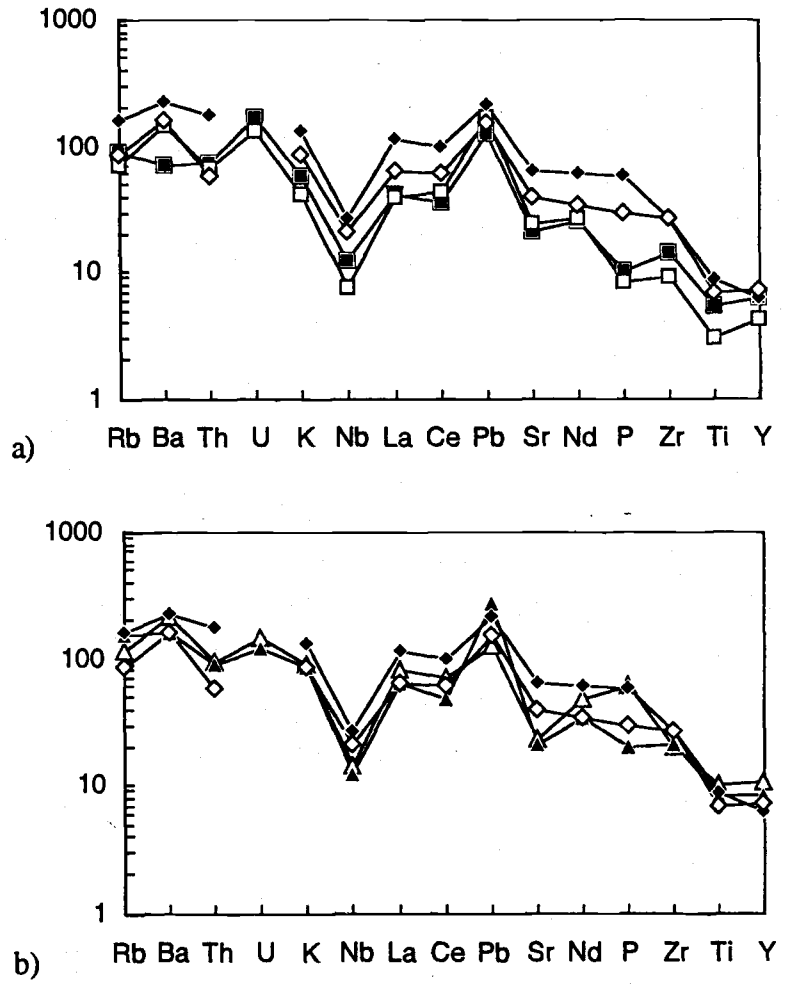

Figure 2.20 - PMN multi-element diagrams comparing a) LPT and b) HPT mafic rocks with basalts from the transition zones between the Basin and Range province and the Colorado Plateau. Normalizing factors are from Sun and McDonough (1989). Symbols: filled squares, Nuckulla Basalt; open squares, high-Mg LPT basalt Kokatha; open triangles, HPT basaltic andesite; filled triangles, IPT basaltic andesite; open and filled diamonds, transition zone basalts from Kempton et al. (1991).

One tectonic environment where lithospheric modification occurs and ultimately results in basaltic rocks which are enriched in LILE and depleted in HFSE is in subduction related areas (Ellam and Hawkesworth, 1988; Hildreth and Moorbath, 1988; Kempton *et al.*, 1991). These chemical characteristics are also features of the Gawler Range basalts. It is therefore suggested that much of the trace element variation seen in the Gawler Range basalts may be the result of interaction between asthenospheric melts and continental mantle lithosphere which had previously been enriched in LIL elements, and rare earths, and depleted in HFS elements such as Nb by an earlier subduction related event. It must be emphasized that this is not meant to imply that there was active subduction going on at Gawler Range time, for none of the features which typify arc systems are observed, such as accretionary wedge sediments, linearity of magmatism and volcanism volumetically dominated by andesites (or the plutonic equivalent - tonalite dominated intrusives of batholithic proportions). Rather the interpretation is that at some time prior to the initiation of Gawler Range volcanism, the sub-continental lithospheric mantle was modified, becoming enriched in rare earths and LIL elements but not in HFS elements. This interpretation is strengthened by the fact that peridotite xenoliths have been shown to have chemical features which are similar to subduction related basalts, e.g. high LILE to HFSE ratios (Erlank *et al.*, 1987; Salters and Shimizu, 1988), signatures which are interpreted to have been emplaced during the previous history of the lithosphere. It is likely that volatiles would be introduced at the same time, thereby lowering the solidus and allowing melting in the presence of an asthenospheric thermal anomaly even where there is little associated extension (e.g. Gallagher and Hawkesworth, 1992).

The paradox apparent in the interpretation that the mantle lithospheric enrichment took place during a previous subduction is that there are no known suites of volcanic or plutonic rocks on the Gawler Craton which represent the typical magmatic expression of a subduction zone. Possibly the enrichment took place by metasomatism which was not necessarily related to subduction, possibly by the movement of small degree, highly enriched melts, as outlined by McKenzie (1989). Alternatively the enrichment may be related to an Archaean event and the expression of subduction at this time was not identical to that seen in modern subduction settings. With the current data set the timing of the enrichment event must remain problematical, with the Nd model ages providing probable minimum estimates.

2.8 - Petrogenesis of the felsic volcanics

Felsic magmas may be generated by a number of different processes such as partial melting, fractionation, mixing, or some combination of processes. Any model for generating the felsic volcanics must account for: 1) the covariation of εNd with indices of differentiation; 2) the pattern of increasing εNd with stratigraphic level observed in the Kokatha area; 3) the dominance of silicic magma over other magma types. The objective of this section is to evaluate the various mechanisms for felsic magma generation and how well they can account for the observations.

2.8.1 Partial melting

Partial melting of crustal rocks may generate considerable volumes of felsic magma, and the presence of basalts in the Tarcoola, Lake Everard and Kokatha areas indicates that mantle derived mafic melts could have provided the heat necessary to promote crustal fusion. However most of the felsic developmental phase volcanics from the Kokatha and Tarcoola areas, which are each underlain by Archaean basement, plot above the region defined by Archaean age basement on a Nd isotope evolution curve (Figure 2.21). Thus it seems that these felsic volcanics cannot result from simple crustal fusion, unless there exists Archaean basement with far more primitive isotopic character than that sampled so far. Moreover, the systematic relationships between εNd and both indices of differentiation and stratigraphic height at Kokatha, point to the various silicic volcanics being genetically related. However, in the most simple partial melting model, initial low degrees of melting (as the source region begins to heat above its solidus) produce the most silicic magmas while later magmas are expected to be increasingly more mafic. For a single source region, both these early and later melts should be in isotopic equilibrium. Clearly, more complex models could be imagined, but the systematic relationships between εNd and indices of differentiation and stratigraphic height would have to be a remarkable coincidence if a partial melting model were correct.

Similarly, in Figure 2.22, the felsic volcanics of the Lake Everard and Toondoolya Bluff areas, whose basement may be either Archaean or Palaeoproterozoic, plot well above the Archaean basement envelope, and many also lie above that for Palaeoproterozoic age basement as well. This not only indicates that none of the felsic volcanics of these two volcanic areas can be partial melts of analysed Archaean crust, but also that most cannot be melts of Palaeoproterozoic crust. Again, strong correlations between Nd isotopic values and indices of differentiation such as MgO (Figure 2.16) indicate that the silicic volcanics within each area are related by some petrogenetic process, and therefore it is unlikely that any represent pure crustal melts.

Figures opposite:

Figure 2.21 - Nd evolution curve for the volcanics from the Tarcoola and Kokatha areas. The field for Archaean crust is shaded.

Figure 2.22 - Nd evolution curve for the volcanics from the Lake Everard area and the Toondoolya Bluff locality of the SGRA. The field for Archaean crust is shaded whereas that for Palaeoproterozoic crust is outlined.

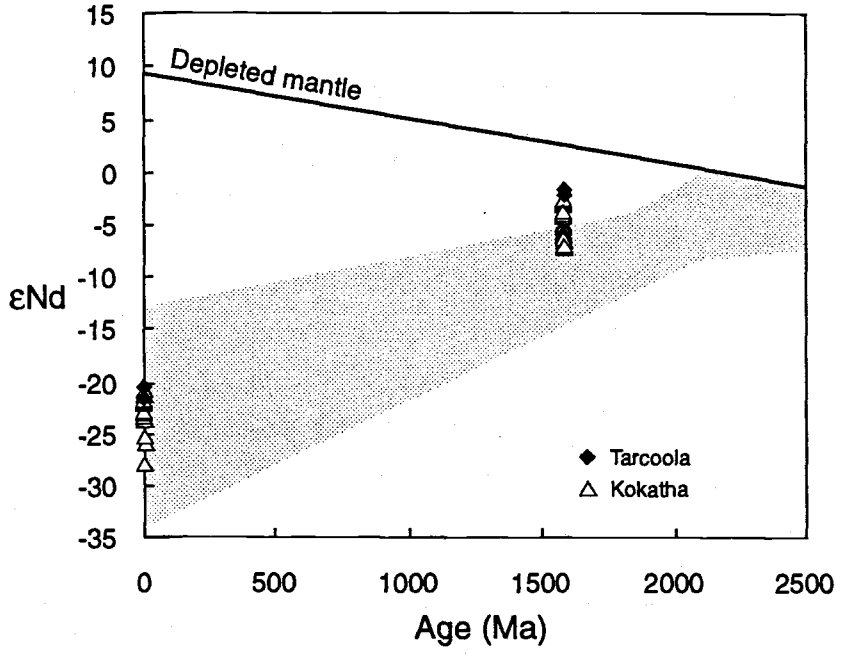
15
10
5
0
-5
-10
-15
-20
-25
-30
-35
εNd
Depleted mantle
Tarcoola
Kokatha
0
500
1000
1500
2000
2500
Age (Ma)

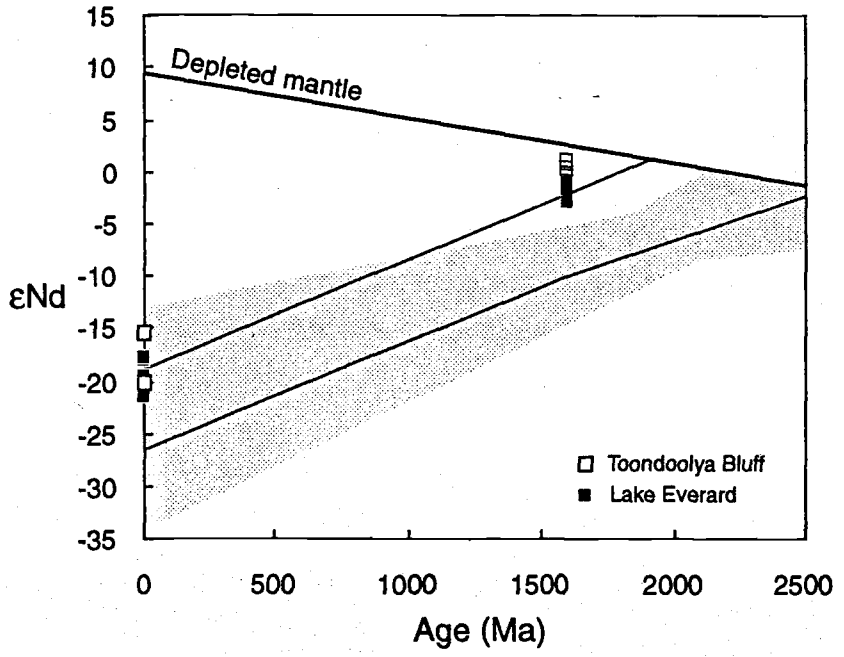
15
10
5
0
-5
-10
-15
-20
-25
-30
-35
εNd
Depleted mantle
Toondoolya Bluff
Lake Everard
0
500
1000
1500
2000
2500
Age (Ma)

The silicic developmental volcanics have high La/Y ratios (0.88-2.39, average 1.61), combined with high Y concentrations. During partial melting of crust the ratio La/Y in the melt will remain similar to that originally in the source, unless garnet is present in the residue after melting. Garnet as a residual phase would result in higher La/Y ratios in the melt compared to that in the source, with the high ratio due to low Y concentrations as Y and HREE are preferentially retained in garnet. However the high Y concentrations exhibited by the silicic developmental volcanics indicate that garnet could not have been present in the melt residue. A lack of garnet in melt residue fits with the results of melting experiments on intermediate and mafic crustal rocks, which indicate that for 30-50% melting (the amount necessary for a silicic melt to segregate from its source and rise; Wickham, 1987; van der Molen and Paterson, 1979; Miller et al., 1988), garnet is not a residual phase (Skjerlie and Johnson, 1992, Rutter and Wyllie, 1988, Rushmer, 1991). The La/Y ratios of the silicic developmental volcanics are considerably higher than those of bulk crust or lower crust estimates (La/Y = 0.8 and 0.58 respectively, from Taylor and McLennan, 1985), and higher than most of the Archaean mafic basement rocks from the Gawler Craton (La/Y=0.27-0.77) which could be considered sources for the intermediate and felsic developmental volcanics. Thus both isotopic and chemical observations argue against the crustal partial melting model.

2.8.2 Crystal fractionation

Crystal fractionation is one method which could produce the chemical variability observed in the felsic developmental volcanics. This process is particularly effective when differentiated liquids are convected or otherwise moved away from the crystal residue, which has been variously termed convective fractionation (Sparks *et al.*, 1984), liquid fractionation (McBirney *et al.*, 1985) or sidewall crystallisation, for it allows highly differentiated magma to accumulate even when the total proportions of crystals removed (in terms of chamber volume) is low. However although crystal fractionation can produce chemically varied magmas, it does not affect the isotopic ratios, and therefore some other mechanism is required to produce the felsic developmental volcanics.

2.8.3 Mixing processes

Neither partial melting of crust, nor crystal fractionation can fully explain the features of the developmental phase volcanics. The covariation of magma chemistry and isotopes (Figure 2.16) implies that the volcanics were formed by some sort of mixing process between two (or possibly more) isotopically distinct endmembers. Three possibilities will be considered, simple mixing, mixing followed by fractional crystallisation and combined assimilation and fractional crystallisation (AFC).

2.8.3.1 Mixing

Mixing between basalt and a crustally derived melt will produce systematic variations in chemistry and isotopes if the two endmembers have substantially different chemistry and isotopic values. However simple mixing results in linear element-element variation, whereas the chemical trends in the felsic developmental volcanics often exhibit inflexions which reflect changes in bulk distribution coefficients due to the onset of crystallisation of a new phase. Mixing between the basalts of the developmental phase and silicic basement lithologies (which will be the first to melt due to their lower temperature of fusion) cannot explain the element/isotope variation of the felsic developmental volcanics, particularly their incompatible element enrichments. This is illustrated in Figure 2.23 which plots mixing curves between basement (broadly granitic in composition) and basalt for the Kokatha, Lake Everard and Toondoolya bluff sequences. The Kokatha volcanics are modelled using an Archaean crustal endmember, as they are known to have erupted onto Archaean age crust. The age of the crust beneath Lake Everard and Toondoolya Bluff is unknown, therefore modelling for each of these areas was carried out using both Archaean and Palaeoproterozoic endmembers. A consistent feature of the plots is that bulk mixing results in considerable changes in the Nd isotopic ratio with only moderate corresponding changes in the concentrations of the more incompatible elements. Mixing cannot explain both the chemical and isotopic variations observed. A final point against mixing as a mechanism for producing the felsic volcanics is that rocks related by this process will plot as a straight line on a diagram of $^{143}Nd/^{144}Nd$ v 1/Nd, but this is not observed (Figure 2.24).

2.8.3.2 Mixing followed by fractionation

If the felsic magmas at any given developmental volcanic area formed by a process of bulk mixing followed by fractional crystallisation, the products of this combined process would be chemically variable but isotopically homogeneous magmas. However each developmental volcanic area erupted magmas which were both chemically *and* isotopically variable. An alternative is that each separate felsic volcanic unit in the developmental phase formed by a process of mixing followed by crystallisation. This model would not result in the observed covariance between isotopes and chemistry, for there should be no link between the amount of mixing, the amount of fractionation and the point at which the magma erupts. In addition the model fails to explain the two cycles of volcanism at Kokatha, and it does not fit well with current concepts of magma chamber processes.

Figures opposite:

Figure 2.24 - Plots of $^{143}Nd/^{144}Nd$ against several chemical parameters illustrating simple mixing curves between basalt and Gawler Craton crust. The mafic endmember for the Lake Everard and Toondoolya Bluff areas is the Nuckulla Basalt sample GH2; whereas the mafic endmember for the Kokatha area is the LP basalt K8. A represents the Archaean crustal endmember of the calculation, 466-256; and P represents the Palaeoproterozoic crustal endmember 515-B143. The ticks on the mixing curves are at intervals of 0.1. Symbols: open squares, Toondoolya Bluff volcanics; filled squares, Lake Everard volcanics; open triangles, cycle 1 Kokatha volcanics; filled triangles, cycle 2 Kokatha volcanics.

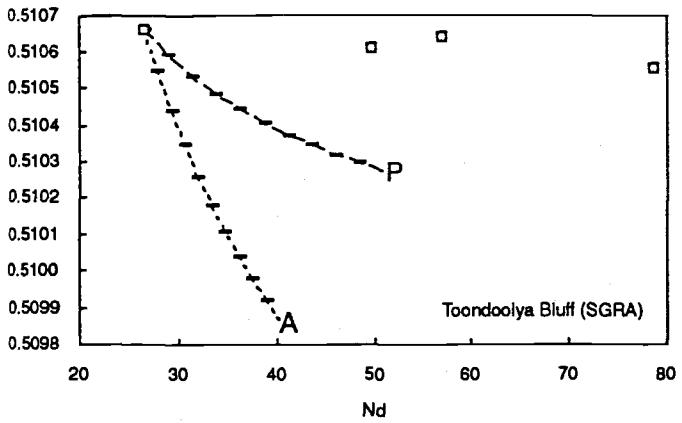
Toondoolya Bluff (SGRA)
P
A
Nd

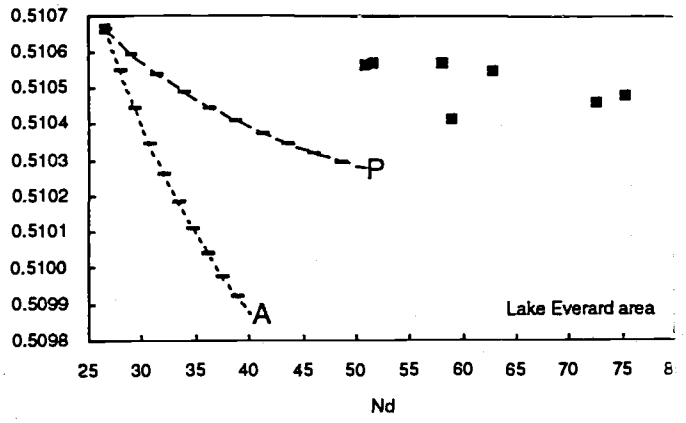
Lake Everard area
P
A
Nd

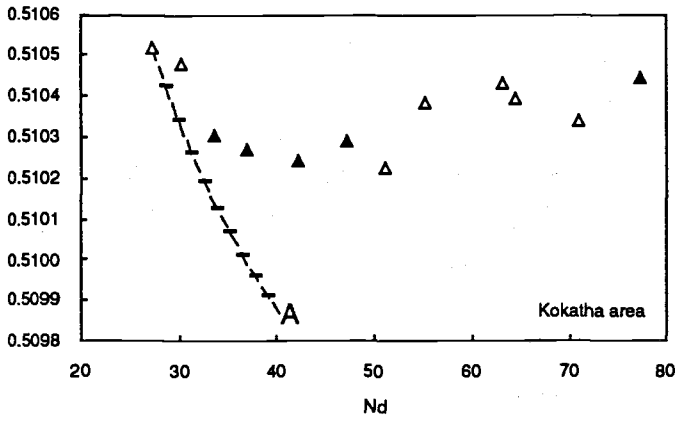
Kokatha area
A
Nd

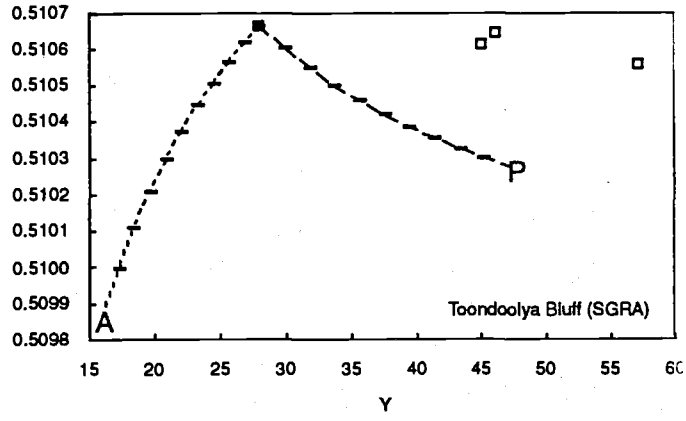
Toondoolya Bluff (SGRA)
P
A
Y

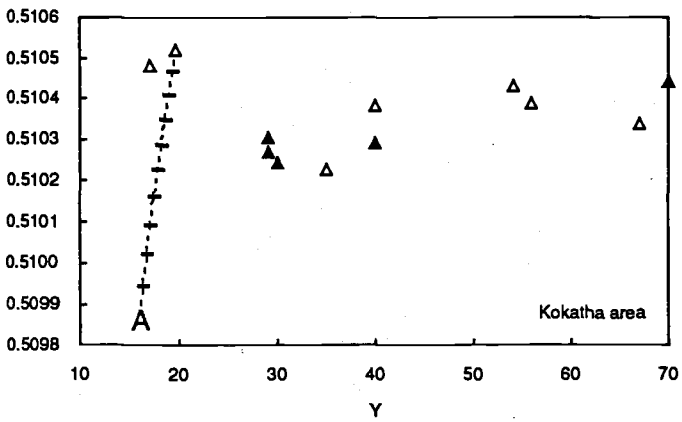
Kokatha area
A
Y

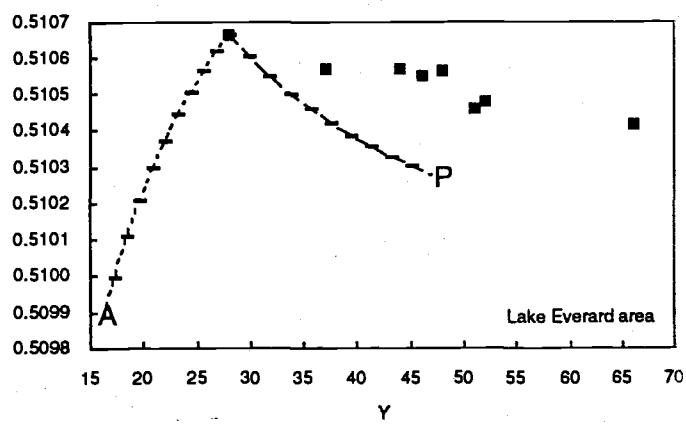
Lake Everard area
P
A
Y

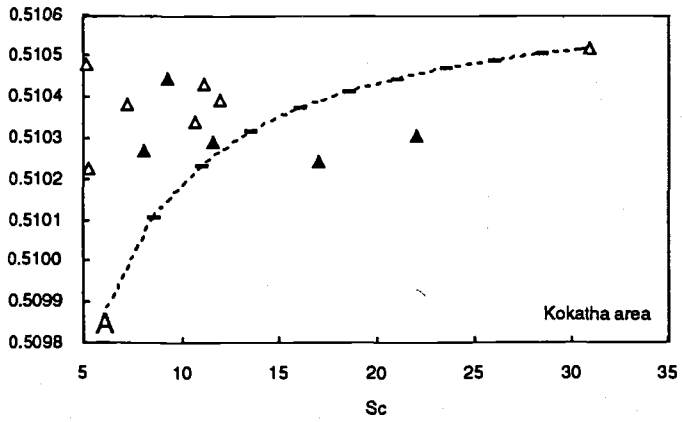
Kokatha area
A
Sc

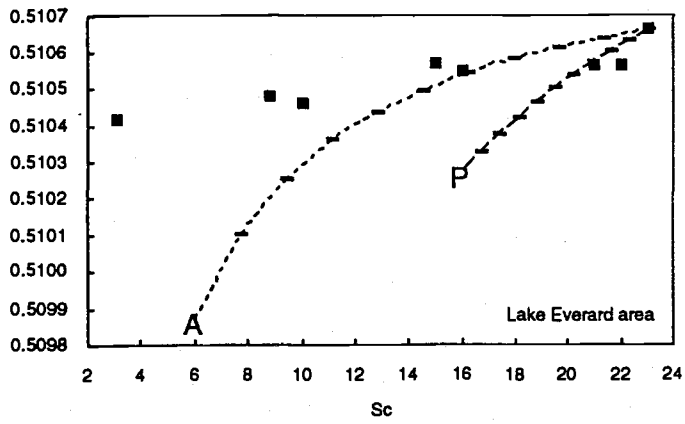
Lake Everard area
P
A
Sc

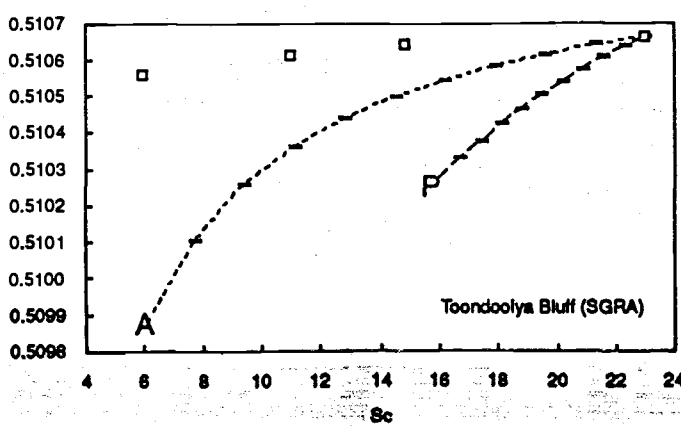
Toondoolya Bluff (SGRA)
P
A
Sc

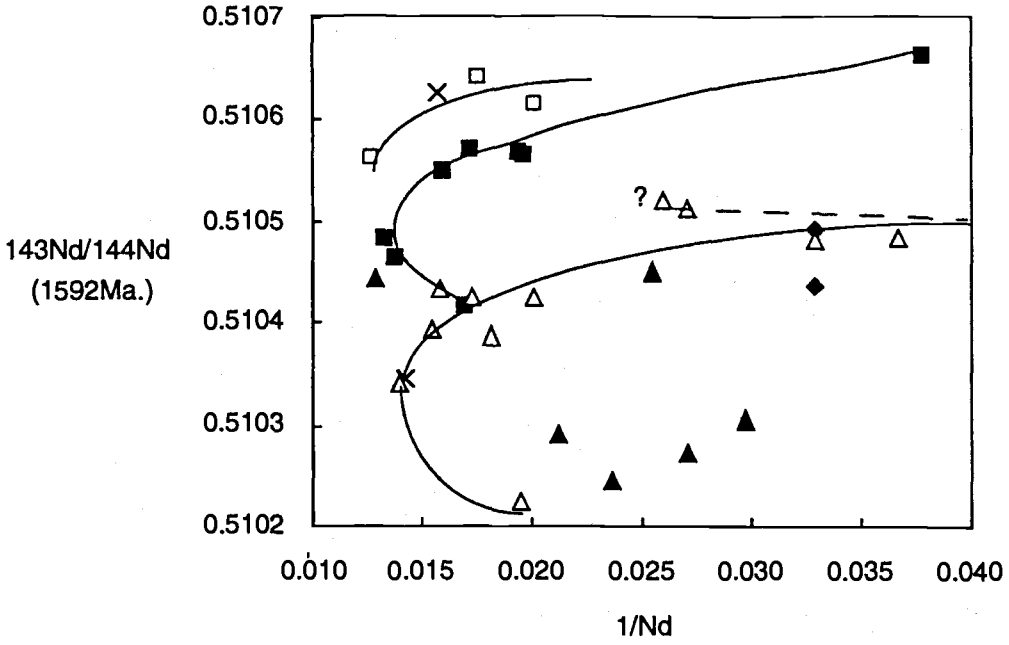

Figure 2.24 - Plot of $^{143}Nd/^{144}Nd$ v 1/Nd for the developmental phase volcanics. Symbols: open triangles, cycle 1 volcanics from Kokatha; filled triangles, cycle 2 volcanics from Kokatha; filled squares, Lake Everard volcanics; open squares, volcanics from the Toondoolya Bluff locality of the SGRA; crosses, other SGRA volcanics; filled diamonds, Konkaby Basalt, Tarcoola.

2.8.3.3 Assimilation Fractional Crystallisation (AFC)

The basic principle of AFC is a link between the amount of assimilation and fractional crystallisation during the evolution of a magma. This provides a mechanism for a covariation of isotopes and chemistry which is lacking in the other petrogenetic processes discussed previously. In AFC, as magma evolves in a magma chamber it continually assimilates country rock and fractionates crystals, therefore the most differentiated magmas should have the lowest $^{143}Nd/^{144}Nd$ ratios, which is exactly what is observed (Figure 2.16). The observed decrease in $^{143}Nd/^{144}Nd$ up sequence within each of the two volcanic cycles at Kokatha may be explained by progressively larger proportions of crust in the magmas due to continued assimilation. If the fractionation part of the process occurred by a mechanism such as convective fractionation or sidewall crystallisation, the evolving magma chamber could yield progressively more contaminated magmas with variable chemistry.

As noted above on a plot of $^{143}Nd/^{144}Nd$ against 1/Nd a simple mixing array would plot as a straight line, whereas samples related by AFC would plot on some type of curve. The array for the Lake Everard rocks do fit a curve, as do those from Toondoolya Bluff (Figure 2.24). The rocks from Kokatha however do not form a single trend, instead they form two (or possibly three) main groups corresponding to the cycle 1 and cycle 2 felsic volcanics and the Chandabooka Dacite. The Kokatha cycle 1 volcanics form a curved trend similar to that of the Lake Everard rocks, but displaced to lower isotopic ratios. The Kokatha cycle 2 volcanics define an inclined array at low isotopic values

compared with cycle 1. Both cycle 1 and 2 contain felsic volcanic units which exhibit anomalous behaviour, and in each case these units are at the base of the cycle, closely associated with the basaltic rocks of the individual cycle. The basal unit of cycle 1 is a rhyodacite isotopically similar to the basaltic rocks, and at the base of cycle 2 rhyodacite BGD also has an anomalously high isotopic ratio for the cycle.

The increased curvature and the 'turn-around' seen in the Lake Everard and Kokatha cycle 1 trends on Figure 2.24 indicates a changing bulk distribution coefficient for Nd with increasing differentiation, which is also evidenced by a slight decrease in Nd concentrations at high SiO_2 for some felsic volcanics on Nd-SiO_2 variation diagrams (Figures 2.4a and 2.6a).The trend illustrated by the Toondoolya Bluff rocks does not 'turn-around'. This may be because the most siliceous sample analysed for this locality contained 73% SiO_2, compared to 78% and 76% SiO_2 respectively for the Baldry Rhyolite from Lake Everard and the rhyolite RH3 from Kokatha, i.e. the change in the bulk distribution coefficient for Nd does not occur until extreme differentiation is achieved. However the Nd-SiO_2 variation diagram (see Figure 2.8a) for the SGRA does not indicate any decrease in Nd at silica levels up to 78% SiO_2, and therefore there may have been no change in the bulk distribution coefficient of Nd in the magmatic evolution at Toondoolya Bluff.

2.8.3.4 Modelling of the AFC process

Quantitative modelling of the developmental phase magmas by AFC is hampered by a number of problems, including the poor mineralogical preservation of the volcanics, the lack of intermediate compositions in several of the developmental sequences, uncertainty as to the chemical and isotopic composition of the crustal and mantle endmembers of the process, and a wide range values in published partition coefficients. One method for modelling the AFC process requires least squares modelling of major element compositions to yield the amount of assimilant and the proportions of minerals removed, with the latter information then being used to calculate bulk partition coefficients for trace element modelling. This method is particularly useful in volcanic sequences where phenocryst modes and compositions can be accurately determined. Although this is not the case for the developmental phase volcanics, least squares modelling of the Lake Everard sequence and the Kokatha cycle 1 and cycle 2 sequences have been carried out for the compositional interval basalt to dacite to assess the utility of the method for the developmental sequences. The mineral compositions used in, and results of, the calculations are given Appendix C. Models were not able to be developed for the more felsic members of each sequence (dacite to rhyodacite and rhyolite) because mineral compositional data is not available due to very poor mineral preservation.

The two assimilants used in the calculations were both broadly granitic in composition, such felsic rocks would be likely crustal contaminants as they have lower temperatures of fusion than more mafic crustal rocks. One assimilant used the major element composition of the Archaean augen gneiss 466-256, chosen to represent a granitic composition. The second assimilant had a very silicic composition, chosen to approximate a small degree partial melt of crust (Appendix C).

The least squares modelling shows that the major element compositions of the dacitic rocks can be closely approximated by AFC models. However when all the models are considered, it becomes obvious that the lack of knowledge of both mineral and assimilant compositions drastically limits the usefulness of the technique for constraining AFC parameters. For example, in some models changing the composition of just one of the fractionating phases can radically alter the amount of assimilation required, but with little associated change in either the amount of fractionation required or the relative proportions of minerals removed (e.g. compare models K2d and K2e). Changing the composition of the assimilant can also drastically change the amount of assimilation required, again with little change in the relative proportions of the fractionating phases or the degree of fractionation (e.g. compare models G2a and G2b).

Thus it would seem that although the least squares method is well suited to young volcanic sequences which are unaltered, it is not easily applicable to the developmental phase volcanics because the poor mineral preservation makes assessment of the 'correct' phenocryst phases and their compositions difficult, if not impossible. Although the differentiating mineral assemblage can be estimated, the modelling illustrates that a wrong choice in mineral type or composition can introduce large errors. For example at any particular stage the pyroxene being removed could be augite or pigeonite or orthopyroxene, or augite+orthopyroxene or augite+pigeonite. If the compositions of the minerals were poorly constrained there would be considerable doubt that the most numerically correct result would necessarily be the right one. As noted by Defant and Nielsen (1990) in badly constrained situations least squares modelling may yield answers which are numerically correct but geologically irrelevant. Another problem with the method is that unless the modelling is carried out in very small incremental steps, least squares mixing models equilibrium crystallisation rather than fractional crystallisation, however such small compositional increments are impossible for many of the sequences within the developmental phase volcanism which contain large compositional gaps. It should also be noted that even in young volcanic systems where good data is available on the mineral compositions, least squares modelling may not be particularly useful in quantifying assimilation (e.g. Ferriz and Mahood, 1987) in AFC processes. Therefore the only information which can be drawn from the least squares modelling are perhaps general points which apply for most models, such as the fact that most models indicate a

low amount of assimilation, and that the mineral assemblages for the compositional interval basalt to dacite would be mainly composed of plagioclase, clinopyroxene, and magnetite ± olivine.

Given the above information and the poorly defined constraints which can be defined for AFC, the rationale behind further modelling was not so much to prove absolutely that AFC was the petrological process by which the felsic developmental volcanics formed, for given the available data there can be no such thing as absolute proof. Instead the modelling attempts to show that unlike the other petrogenetic processes which have been discounted above, AFC can produce both the systematic variations in isotopes and chemistry and the high incompatible element concentrations observed in the developmental phase felsic volcanics.

The variation of Nd concentration with Nd isotopic composition was chosen to provide a test of whether AFC could produce the observed correlation between chemistry and isotopes and the high levels of REE observed in the silicic developmental phase volcanics. Nd was chosen because: 1) the concentration of Nd had been accurately determined by isotope dilution; 2) Nd is relatively incompatible and as noted in section 2.8.3 the enrichment of incompatible elements in the felsic volcanics could not be explained by simple mixing, and; 3) partition coefficient data for the REE is more plentiful and probably more accurate than that available for most other elements. Using incompatible element concentrations and Nd isotopes as an index of contamination is a method which been used for other ancient volcanic suites (e.g. the Archaean Huronian volcanics, Jolly *et al.*, 1992).

It was not possible to effectively model those elements which were compatible in the felsic volcanic sequences such as Sc and Sr. Partition coefficients for Sc vary not only with temperature and melt composition but also with the Ca content of the pyroxene (Sisson, 1990; Nielsen *et al.*, 1992), with augite, pigeonite and orthopyroxene exhibiting widely different partition coefficient values for Sc (although few high quality values have been published for pigeonite). Any estimate of the bulk partition coefficient for Sc could therefore easily be in error by a considerable amount because the pyroxene assemblages and temperatures cannot be determined with any certainty for many of the rocks. Recent experimental and thermodynamic work indicates that the mineral partition coefficient for Sr in plagioclase is also highly temperature dependent (J. Blundy pers. comm.) and any estimate made without knowledge of both temperature and proportions of fractionating phases may again lead to large errors in calculations.

The modelling was undertaken using two bulk partition coefficients for Nd, 0.21 and 0.42, which were chosen because they bracket most of the values calculated from the least squares modelling results (Appendix C). The mineral partition coefficients used to calculate bulk partition coefficients for Nd for the compositional range basalt to rhyodacite

Figures opposite:

Figure 2.25 - Plots of $^{143}Nd/^{144}Nd$ against Nd illustrating the results of AFC/mixing calculations for the developmental phase volcanics. Tickmarks on calculated curves are at a multiple of 0.1 except where marked differently. The endmembers for the different areas are as listed for Figure 2.23.

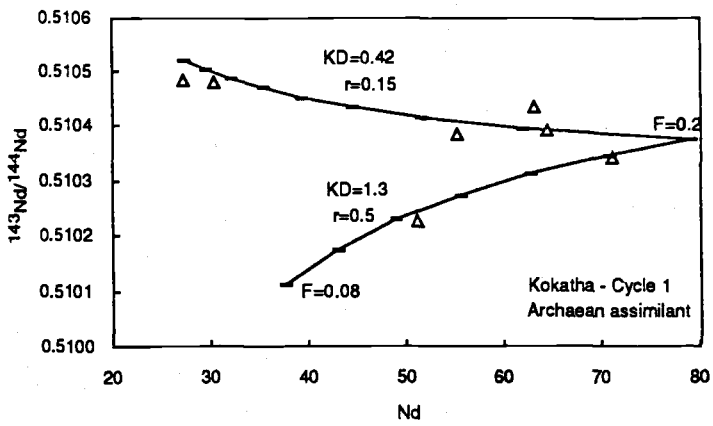
KD=0.42
r=0.15
F=0.2
KD=1.3
r=0.5
F=0.08
Kokatha - Cycle 1
Archaean assimilant
143Nd/144Nd
Nd

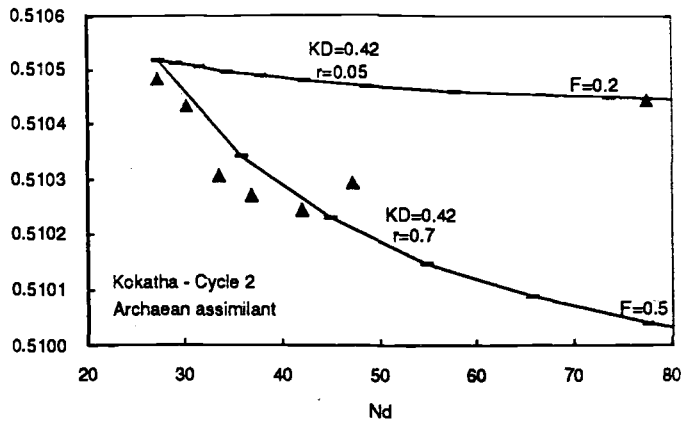
KD=0.42
r=0.05
F=0.2
KD=0.42
r=0.7
F=0.5
Kokatha - Cycle 2
Archaean assimilant
Nd

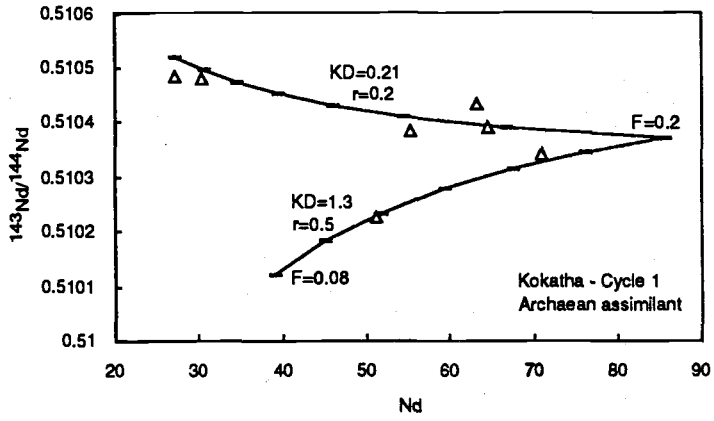
KD=0.21
r=0.2
F=0.2
KD=1.3
r=0.5
F=0.08
Kokatha - Cycle 1
Archaean assimilant
143Nd/144Nd
Nd

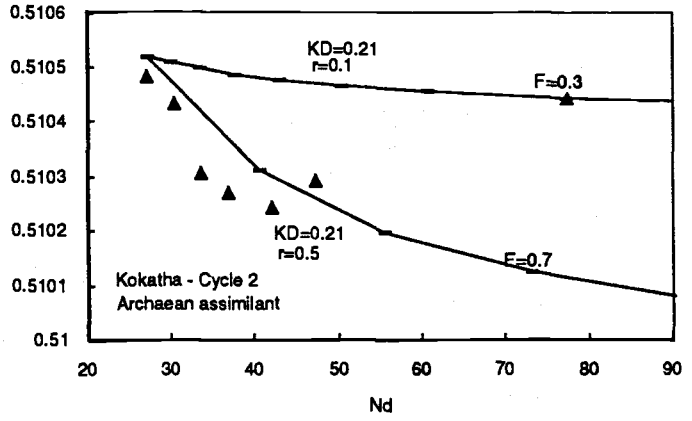
KD=0.21
r=0.1
F=0.3
KD=0.21
r=0.5
F=0.7
Kokatha - Cycle 2
Archaean assimilant
Nd

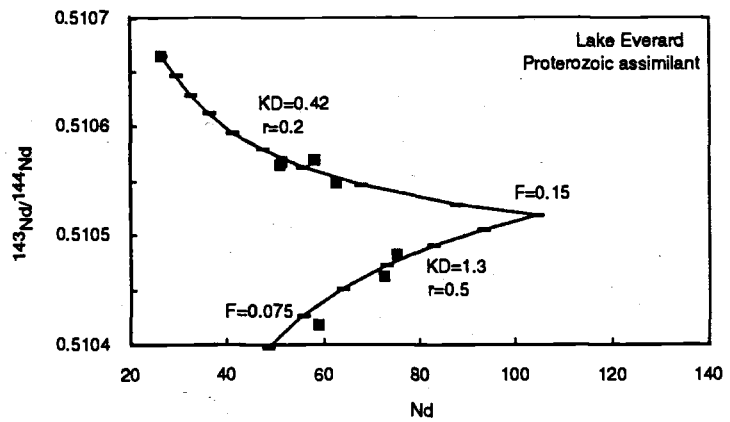
Lake Everard
Proterozoic assimilant
KD=0.42
r=0.2
F=0.15
KD=1.3
r=0.5
F=0.075
143Nd/144Nd
Nd

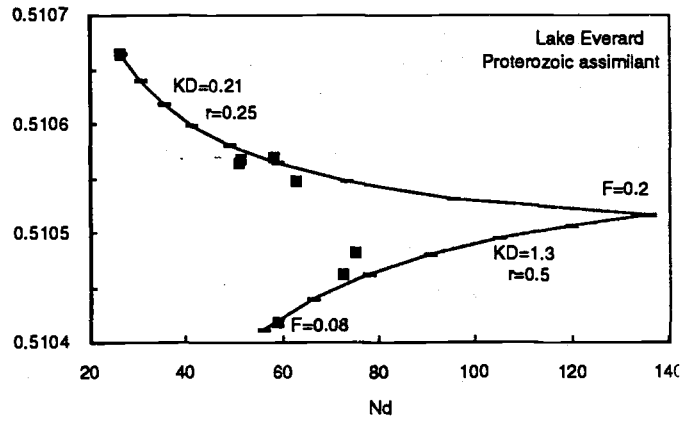
Lake Everard
Proterozoic assimilant
KD=0.21
r=0.25
F=0.2
KD=1.3
r=0.5
F=0.08
Nd

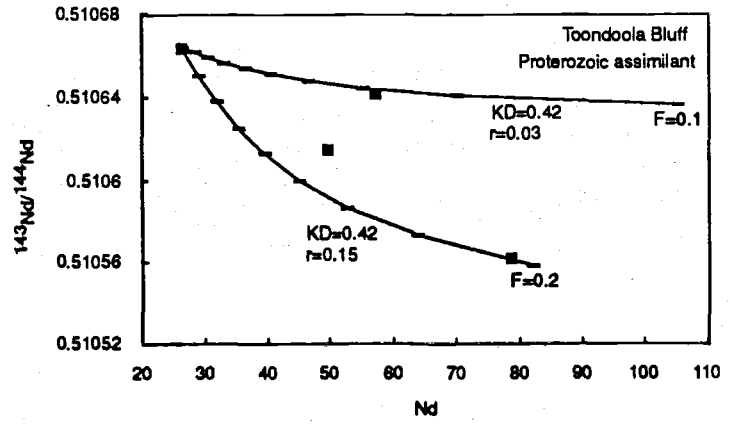
Toondoola Bluff
Proterozoic assimilant
KD=0.42
r=0.03
F=0.1
KD=0.42
r=0.15
F=0.2
143Nd/144Nd
Nd

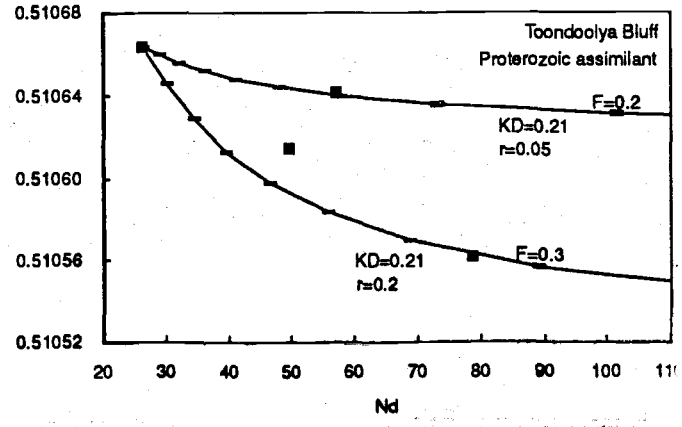
Toondoolya Bluff
Proterozoic assimilant
F=0.2
KD=0.21
r=0.05
KD=0.21
r=0.2
F=0.3
Nd

were those given for intermediate rocks by Feeley and Grunder (1990). At higher degrees of differentiation, even small amounts of accessory phase fractionation can radically change the bulk partition coefficients for REE. Where the chemical data indicated a decrease in REE for these higher SiO_2 rocks, due to accessory phase fractionation, an appropriate bulk partition partition coefficient was chosen to pass through the data points.

The Nuckulla Basalt from the Lake Everard area was chosen as the basaltic endmember for modelling the sequences at Lake Everard and Toondoolya Bluff (no basalt is present in the Toondoolya Bluff sequence). The choice of basaltic endmember for modelling the Kokatha sequence is a little more problematical, for the most primitive basalt does not have the highest εNd value for the area. For this reason, modelling of the Kokatha volcanics was undertaken using a basalt with a $^{143}Nd/^{144}Nd$ ratio (at 1592Ma.) of 0.51052 (similar to the most positive εNd LP basalt at Kokatha) and with the chemical composition of the basalt 884-K8/K101. As the Kokatha volcanics erupted onto basement known to be Archaean in age, the assimilant for the Kokatha calculations is the Archaean augen gneiss 466-256 which is broadly granitic in composition. The basement age for the Lake Everard and Toondoolya Bluff sequences is unknown, so the calculations used the Palaeoproterozoic hypersthene granite gneiss 515-B143 as the assimilant. If the basement for these two areas was in fact Archaean the amount of crustal assimilation calculated would be less, for Archaean granitic crust would have lower $^{143}Nd/^{144}Nd$ (e.g. gneiss 466-256). Therefore the amount of assimilation calculated using the Palaeoproterozoic gneiss can be considered to be a maximum.

The results of the modelling are plotted on Figure 2.25 and illustrate several points. Firstly the process of AFC can readily explain the variations in isotope compositions of the developmental phase volcanics and their high incompatible element concentrations. Secondly, for the Toondoolya Bluff, Lake Everard and cycle 1 Kokatha rocks the ratio of assimilation to fractional crystallisation (r) has to be low (0.03-0.25) in the basaltic to dacitic rocks to produce the required high levels of incompatible elements. For each area the lower bulk distribution coefficient required a slightly higher amount of assimilation (higher r). However the total amount of assimilation is approximately the same for both assemblages, for calculations which indicate a lower r value also result in a lower value of F (the proportion of original melt remaining), i.e. more fractionation has taken place accompanied by fractionation. A third point is that the second cycle volcanics of the Kokatha area (excepting the basal rhyodacite BGD) require much higher values of r than any of the other volcanic sequences modelled. The fit for the cycle 2 rocks is improved if the mafic endmember for the second cycle mixing has a lower level of Nd, e.g. 23ppm Nd and the same $^{143}Nd/^{144}Nd$ ratio of 0.51052 (Figure 2.25), however regardless of the mafic endmember required, the intermediate and felsic volcanics of cycle 2 require a much greater degree of assimilation (r= 0.5 to 0.7) and much smaller amounts

of fractionation (F>0.7). This requirement for a higher degree of assimilation correlates well with both petrographic and chemical features of the cycle 2 volcanics and also makes thermal sense, i.e. the crust is getting hotter and melting more. For example the second cycle andesite contains common quartz xenocrysts rimmed by augite reaction rims. This indicates the andesite may have formed from a more mafic magma by the ingestion of granitic country rock. In addition many of the variation diagrams the second cycle volcanism (again excluding the basal rhyodacite BGD) forms a rather flat array with little change in element concentration with increasing SiO_2, consistent with assimilation of a contaminant with relatively low levels of incompatible elements combined a low amount of fractionation which does little to increase the incompatible element concentrations. The modelling indicates that rhyodacite BGD at the base of cycle 2 is the product of a large amount of fractionation (F=0.1-0.3) combined with a low rate of assimilation (r=0.05-0.1) which is consistent with its very high incompatible element concentrations.

2.9 Discussion

Isotopic and chemical data indicate that partial melting, magmatic differentiation, and mixing are individually unable to explain the paired isotopic and chemical variation of the developmental felsic volcanics. The modelling indicates that AFC may be the process which produced the covariations in isotopes and chemistry exhibited by the developmental phase volcanics, however the previously discussed limitations of the models means that it does not provide absolute proof that the volcanics formed in this way. The nature of the alternative models is such that any systematic temporal variation in isotopes such as that seen at Kokatha is unlikely, while any correlation between chemistry and isotopes would be coincidental. That such a coincidence occurred at three separate volcanic centres is scarcely credible, and AFC appears to be the only realistic mechanism by which the systematic chemical and isotopic variations which characterise the developmental phase volcanics could have developed. If AFC is indeed correct, the predominantly low values for r indicate that the developmental volcanism is dominated by a mantle component. The amount of Archaean crust calculated as present in the Kokatha cycle 1 felsic volcanics can be crudely calculated as 10-12% in dacite, 17-22% in rhyodacite and 42-43% in high silica rhyolite, (the ranges cover the two endmember bulk partition coefficients used in the modelling). In the Kokatha cycle 2 volcanics the main sequence has a maximum of 18% Archaean crust, whereas the dacite BGD a maximum of 8% Archaean crust. The amount of Palaeoproterozoic crust calculated to be present in the Lake Everard felsic volcanics is 12-13% in dacites, to 42-43% in the high silica Baldry Rhyolite. The volcanics at Toondoolya Bluff are calculated to contain between <1-13% of Palaeoproterozoic crust. As previously stated if the assimilant for the AFC process at Lake Everard and

Toondoolya Bluff was Archaean rather than Proterozoic the amounts of crust required would be less.

Two features of the silicic volcanics of the developmental phase are notable. One feature is that silicic volcanics of very different isotopic values tend to have very similar chemistry (Figures 2.11 and 2.12). The second feature is that although the isotopic modelling shows that the ratio of assimilation to fractional crystallization is low, and therefore the mantle endmember is volumetrically dominant in all modelling, the chemistry of the felsic volcanics is 'crustal'. The most probable assimilants are granitoids which have a strong 'crustal signature' (e.g. Hergt *et al.*, 1991). The basalt endmember to the mixing process has a similar, but not identical, signature derived largely from the mantle lithosphere. Therefore mixtures between the enriched basalts and granitoids would tend to look 'crustal', and similarities in chemistry of the felsic volcanics would be reinforced by the fractionation of the near ubiquitous phenocryst assemblage, plagioclase + pyroxene + magnetite ± sanidine ± quartz, and because fractionation always dominates over assimilation (hence the low r values in the AFC calculations).

Considerable variations in chemistry between different units of similar rock type are observed for the andesitic to dacitic rocks of the Lake Everard volcanic area, where the first three large ignimbritic units, the Childera, Mangaroongah and Bunburn Dacites, have quite individual chemical trends. However the isotopic and chemical covariation indicate that all of these units are somehow genetically related. The behaviour of elements such as Al_2O_3, CaO, TiO_2, Sr, Sc and V indicate that the Childera Dacite fractionated more plagioclase relative to the other two units, that the Bunburn Dacite fractionated less plagioclase and more clinopyroxene than either of the other two units, whereas the Mangaroongah Dacite fractionated intermediate amounts of these clinopyroxene and plagioclase. Therefore in the early evolution of the Lake Everard magma chamber as revealed by these three units, the relative proportions of plagioclase and clinopyroxene in the fractionating assemblage changed, with plagioclase decreasing and clinopyroxene increasing as the chamber developed, which could have been a response to a decrease in temperature and/or increasing water content in the magma system (Foden and Green, 1992). The behaviour of Zr in the various units of the Lake Everard volcanic area is one the most striking examples of differing chemical behaviour in the intermediate to silicic units of the Lake Everard area. This also may be attributable to changes in the intensive parameters of the evolving magma chamber, this time temperature, as zircon saturation calculations (Watson and Harrison, 1983) indicate that the units which exhibit strong enrichment with differentiation (Mangaroongah Dacite and Yantea Rhyodacite) must have had minimum temperatures of 900°C, whereas the Childera dacite, which has decreasing Zr with increasing SiO_2, must have had a minimum temperature of 800°C. Therefore the chemistry of the intermediate to silicic volcanics at Lake Everard, while exhibiting greater

variation between units than is observed in other areas, nevertheless appears to reveal more about the fractionating mineral assemblage than the source, as is the case in the other developmental areas.

2.9 - A general model for the genesis of the intermediate and felsic developmental phase volcanics

Isotopic and mineralogical evidence from volcanics of the developmental phase indicate that three sources were involved in their formation. The basalts and basaltic andesites represent different degrees of melting and mixing of enriched mantle lithosphere and asthenosphere. These mafic magmas then rose into the crust, initiating crustal melting. The volcanics of andesitic and more silicic compositions have systematic covariations in chemistry and isotopes which are most successfully interpreted as having formed by AFC processes. The following interpretation of a cycle of magmatism in the developmental phase volcanism is based on the complex isotopic array shown by the volcanics of the Kokatha area, but as a general model is considered to apply for all developmental areas.

A general observation is that where basalts outcrop, they tend to be located low in the stratigraphic sequence of any particular area, or low in a cycle where volcanism is multicyclic. This indicates that the input of heat from the mantle occurred in the form of basaltic melt and this then initiated local crustal melting. What then happened was the result of a number of competing mechanisms which between them determined the amount of assimilation in any felsic volcanic unit. The amount of assimilation was in part likely to be controlled by the volume of basaltic melt input into the system at any time (e.g. Vosage *et al.*, 1990), the larger the basalt volume, the greater the amount of heat (derived both initially from the physical heat of the basalt and later by the latent heat of crystallization) available to melt the enclosing mid- to lower crustal wall rocks. A second, partially interactive parameter controlling the amount of assimilation is the length of time between basaltic influx and the eruption of a unit. The longer this time, the greater the total amount of assimilation is likely to be, both because of a physically longer time for ingestion of country rock, and because the enclosing lithologies will heat up, becoming closer to their respective solidi, and more crustal melting and assimilation will result. A greater degree of crustal assimilation is likely to take place following a second input of basalt than occurs with the first, again due to the heating of the crustal rocks to (or closer to) their solidi by the first basalt emplacement. As an overall result of this complex interaction (at least in the Kokatha area) early erupted felsic volcanics in any cycle will have less crustal component than those erupted later, and overall second cycle felsic volcanics will tend to have a

greater crustal component than those of an initial cycle. As the magma chamber evolves it continually assimilates crustal material and fractionates whilst periodically erupting.

It would therefore seem that a model for the formation of the developmental volcanics has interactive controlling parameters including basalt volume, heat of country rocks and length of 'gestation' in the magma chamber prior to eruption. Although no systematic variation of Nd isotopic values with stratigraphic height has been observed for areas other than Kokatha, a similar counterbalancing of mechanisms may have occurred there, however either the number of units is too small to allow this type of detailed section to be collected (as is the case for the Tarcoola area and the southern Gawler Range area), or a larger number of samples need to be run for this type of signature to be revealed (e.g. the Lake Everard area).

An alternative explanation for the chemical variability but systematic isotopic variation observed particularly for the Lake Everard volcanics lies with the process of convective fractionation or sidewall crystallisation. Liquid residual from AFC is less dense than the original magma and moves to higher levels in the magma chamber. The mineral assemblage which fractionates from the magma will be determined by the intensive magmatic parameters of the chamber (or of the double diffusive convection cell) , such as magmatic temperature and volatile content, magma composition and amount of fractionation, whereas the amount of assimilation will depend mainly on the temperature of the magma and the solidus of the enclosing rocks. Therefore such a magma chamber can erupt a sequence of magmas which are the products of AFC from the same two endmembers but which are chemically variable because of different fractionated assemblages and amounts of assimilation.

Figure 2.26 represents an interpretation of the isotopic/chemical variation of the developmental volcanics.

2.10 - Implications for crustal structure of the Gawler Craton

As has been previously stated, the volcanics from each of the Kokatha, Lake Everard and Toondoolya Bluff areas form distinct arrays on diagrams of εNd versus any index of differentiation such as MgO (e.g. Figure 2.16). In addition the Lake Everard array lies at higher εNd than that of the Kokatha rocks, and the Toondoolya Bluff array is at still higher εNd. Two possible explanations for this are: 1) each of the developmental volcanic areas lies on Archaean crust, and the arrays indicate that from Kokatha to Lake Everard and then to Toondoolya Bluff increasingly smaller amounts of assimilation accompanied fractionation during formation of the felsic volcanics, or 2) the volcanics of

Figure opposite:

Figure 2.26 - An example of the interpretation of the systematic correlations and variations of Nd isotopic values and chemical parameters observed in the developmental phase volcanics of the Gawler Range volcanic province. Upper diagram shows the variation in ε_{Nd} with MgO, and the lower diagram is an interpretation of the trends observed. The silicic magmas are formed by AFC processes, the exact controlling parameters of which are determined by a number of interacting factors. With an elemental axis such as the one chosen here, the consistently compatible nature leads to downward curving trends which do not reverse direction. In the case of some elements however, which change from incompatible to compatible during the differentiation sequence, the trends become more strongly curved and both increases and decreases in elemental abundance occur.

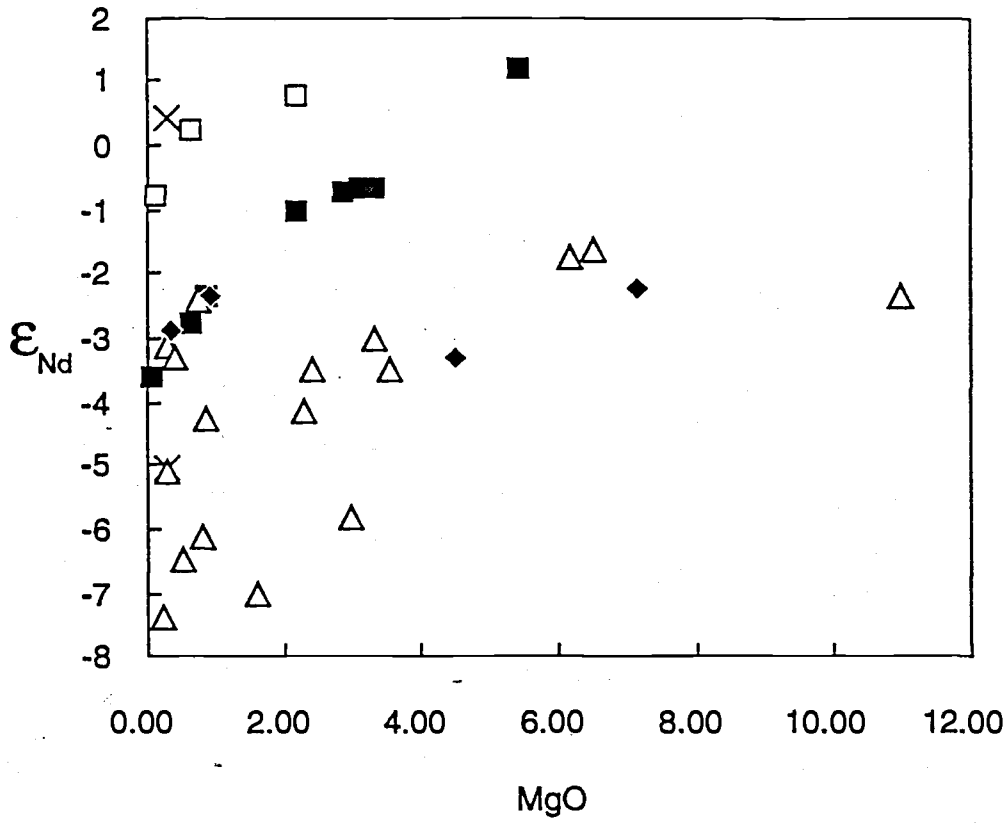

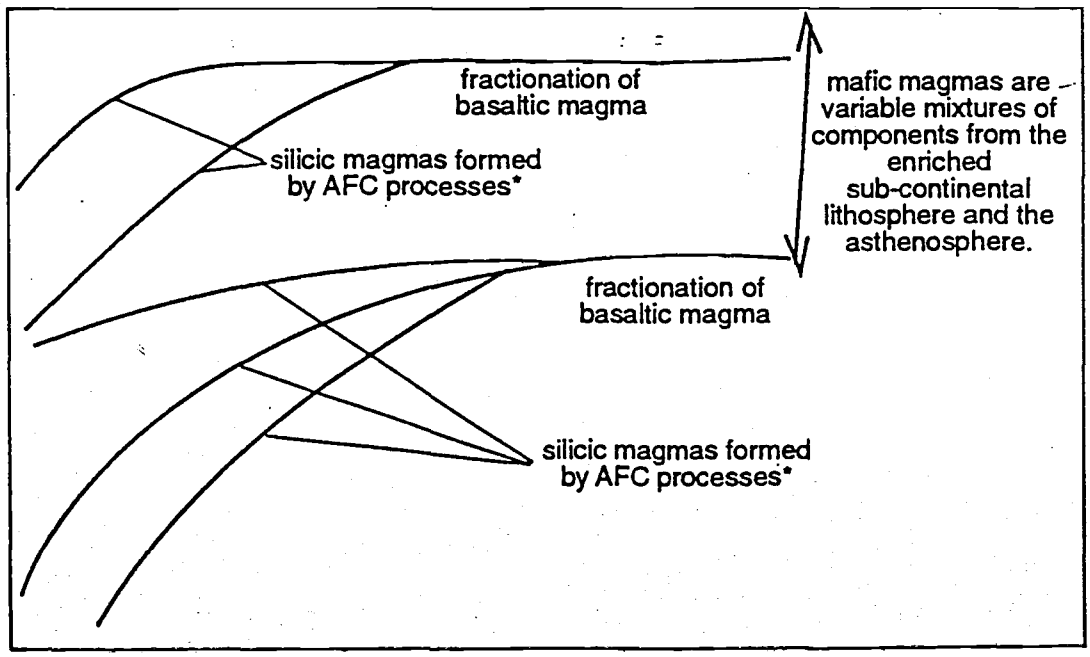

*The position in which a given silicic unit plots depend on: the original isotopic composition of both the basaltic melt and the crust assimilated, the residence time in the magma chamber, and the temperature of the country rocks (see text for discussion)..

each developmental area were the result of an AFC process, but with different endmembers.

Both the Tarcoola and Kokatha areas demonstrably lie upon Archaean basement, and correspondingly have arrays which have lower $^{143}Nd/^{144}Nd$ ratios at any given value of a compositional or differentiation index. South of Kokatha is the Lake Everard area and south again of this is the Toondoolya Bluff locality of the SGRA. As previously stated, no basement is known from these areas, however it is striking that the entire volcanic sequences *from basalt to rhyolite* are displaced to higher and higher levels of $^{143}Nd/^{144}Nd$ in each successive volcanic centre as you go south. This may indicate a younging of the basement from north to south along the western margin of the Gawler Range province. If this is correct, it provides an explanation for the different Nd isotopic values of the basalts as well as the felsic rocks. This model has an added attraction in that it also happens to correlate with known basement age distribution, from Archaean near Kokatha to Palaeoproterozoic along the southern margin of the province.

The crustal mixing endmember for the Lake Everard area may be either Proterozoic crust older than that in the Toondoolya Bluff area, or it may be a mixed Archaean/Proterozoic crustal component, with the Toondoolya Bluff volcanics containing a more purely Proterozoic component. The Tarcoola and Kokatha basalts consistently have lower εNd than the Nuckulla basalt from Lake Everard, which is not attributable to crustal contamination (see section 2.7). If the enrichment of the subcontinental lithospheric mantle was primarily associated with the Archaean Mulgathing Complex now exposed around Tarcoola and Kokatha, basalts in these areas formed by later melting would be expected to have a combination of lower εNd and higher LILE/HFSE ratios compared to basalts erupted on the edge of, or moving away from, this crustal segment. This is precisely what is observed, for the Nuckulla Basalt from Lake Everard, which may be on the edge of the Archaean crustal segment and have both Archaean and Palaeoproterozoic mantle inputs, has higher εNd and lower Ba/Nb than any of the Tarcoola or Kokatha mafic volcanics. Thus although basement does not outcrop at either Lake Everard or Toondoolya Bluff, isotopic evidence indicates a hitherto undocumented boundary between Archaean and Palaeoproterozoic crustal segments is present along the western Gawler Range Volcanic province.

Chapter 3 - Evidence for the eruptive mechanism of the mature phase magmas: the lava versus ignimbrite debate

3.1 - Introduction

Large volume, high temperature felsic volcanic units have recently become the focus of a number of studies which have attempted to determine whether they erupted as lavas or ignimbrites (Ekren *et al.*, 1984; Bonnischen and Kauffmann, 1987; Henry *et al.*, 1988 and Henry *et al.*, 1990; Branney *et al.*, 1992; Henry and Wolff, 1992; Milner *et al.*, 1992). The mature phase volcanism of the Gawler Range Volcanic province is dominated by large volume silicic eruptive units of the type central to the above debate, and this chapter attempts to establish their mode of eruption. Following chapters deal with chemical and isotopic development of the mature phase magmas.

Early observations of the volcanics from the Gawler Ranges were predominantly concerned with those units grouped in this study into the mature phase volcanism and indicate that there was considerable uncertainty as to their origin. Jack (1912) considered them to be "either an enormous sill or an extensive surface flow", although later he plumped for an extrusive origin (Jack, 1917). Turner (1975) noted an extensive porphyritic rhyolite to rhyodacite in the far eastern Gawler Ranges which he interpreted as a 'welded tuff sheet'. Further work by Blissett (1975, 1986) resulted in the division of this sheet into the three major units of what has been termed in this study the mature phase volcanism, i.e. the Nonning Rhyodacite and the Eucarro and Yardea Dacites. An ignimbritic origin has been postulated for all of these units, however little evidence for such an origin has been documented, with the interpretations largely resting on their extensive size (Blissett, 1975) and some petrographic indications of a pyroclastic origin (Giles, 1980). The recent debate mentioned above has renewed speculation as to the eruptive process responsible for the mature phase sequence (Creaser and White, 1991; R. Creaser pers. comm., A. Ewart pers. comm.).

This chapter aims to examine and discuss physical features which can shed light on models of eruptive mechanisms of the major units of the mature phase volcanism. The units under discussion are primarily the Eucarro and Yardea Dacites as these are the best preserved and most intensively studied (Chapters 3 and 4), however the interpretations made also apply to the Nonning Rhyodacite and to some extent the Yannabie Rhyodacite.

3.2 - Stratigraphy and volume estimates

As noted in Chapter 1, the mature phase volcanism is composed of the Nonning Rhyodacite, the Eucarro Dacite, the Yannabie Rhyodacite, the Paney Rhyolite and the Yardea Dacite (Figure 3.1). The preserved record of volcanic activity from the mature phase magma chamber is interpreted to begin with the Nonning Rhyodacite, followed (?) by the Eucarro Dacite. The exact stratigraphic relationship between the Nonning and the Eucarro is unclear. The Nonning outcrops only in the easternmost Gawler Ranges, where it is interpreted to be overlain by the Eucarro (Blissett, 1986), however they may represent eruptions of the uppermost, zoned magma from the chamber from two spatially separate vents. The focus of this study has been the western half of the province and so this question remains to be answered by a detailed study of these two units. The next unit erupted was the smaller volume Yannabie Rhyodacite, followed by the extrusion of the Paney Rhyolite. The culminative event of the province and of the mature phase volcanism was the evisceration of the chamber which produced the Yardea Dacite.

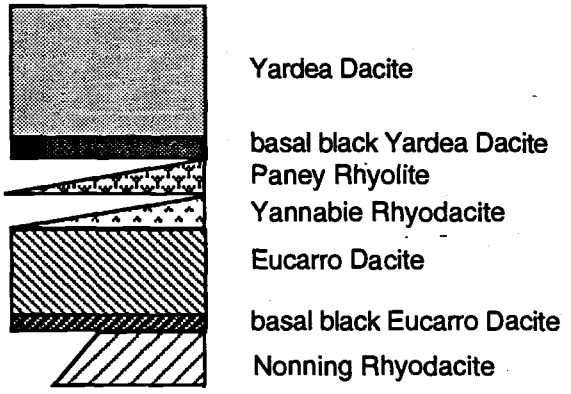

Figure 3.1 - A similified stratigraphic column of the mature phase volcanism. The diagram is schematic ans is not intended to indicate real or inferred unit thicknesses.

The Yardea and Eucarro Dacites and the Nonning Rhyodacite all outcrop as rounded hills (Figure 4.1a), and together form the physiographic range of hills from which the volcanic province takes its name. Columnar jointing is a common feature of each of these three units (Figure 4.1 b &c), indicating they underwent slow cooling after their emplacement. As previously mentioned the Eucarro and Nonning together form a band of outcrop along the south and west of the Yardea Dacite, which itself is interpreted to be an areally extensive, relatively flat-lying sheet. The Yannabie Rhyodacite has a much

more restricted outcrop distribution, forming isolated low hillocks. The Paney Rhyolite forms isolated, domal and sheet-like outcrops which occur irregularly between the underlying Eucarro and Yannabie units and the overlying Yardea Dacite. The distribution of the units in the mature phase is illustrated in Figures 1.1 and 1.2.

Volume estimates for the four main units of the mature phase volcanism are presented as Table 3.1. Volumes have been calculated using two different methods for determining the area of the units. The first method took the area of currently exposed outcrop (combined with intersections in drill holes in the case of the Yardea Dacite) as representing the original area of the unit. However this method very likely underestimates the actual original area, because all units stratigraphically beneath the Yardea Dacite dip beneath it and have unknown extents. Therefore a second method was employed, which assumed that each of the units had an original circular plan form, with a diameter equal to the current maximum strike length of the unit. The areas obtained by each of these methods were then converted to volumes using the thicknesses given by Blissett (1975, 1986). The first and second methods of area calculation can be considered to yield minimum and maximum values respectively, therefore the actual eruptive volume of each unit should be bracketed by the two volume estimates (Table 3.1).

Table 3.1 - Volume estimates for the ignimbritic units of the mature phase Gawler Range Volcanics

Unit	Outcrop area (square km)	Volume (cubic km)§	Area assuming circular shape* (square km)	Volume (cubic km)§
Yardea Dacite	12000	3000	31416	7854
Yannabie Rhyodacite	50	5	12272	1227
Eucarro Dacite	2100	735	31416	10996
Nonning Rhyodacite	1250	375	7854	2356
		Total 4115		Total 22433

*Calculated using the present known strike length of the unit as the diameter of the circle. Used as an estimate to account for the fact that all of the units stratigraphically below the Yardea Dacite dip north beneath it.
§Volumes calculated using the thicknesses given in Blissett (1975, 1986).

3.3 - Evidence for an ignimbritic origin

Silicic ignimbrites and lava flows are each characterised by specific features, the use of which has enabled, in many provinces, the distinction of these two eruptive types. These characteristic features are listed in Table 3.2. The distinction between the two types becomes blurred however when the silicic volcanics are high temperature.

Table 3.2 - Features often used to distinguish ignimbrites and lavas

Silicic ignimbrites	Silicic lavas
Extensive sheet-like form	
Low aspect ratio	High aspect ratio
Fiamme	Autobreccias
Eutaxitic texture	
Abundant lithic fragments	Rare lithic fragments
Broken Phenocrysts	Unbroken phenocrysts
Glass shards	
	Flow banding
Non welded to densely welded	Elongation of vesicles
Fumarolic pipes	Ramp structures

Characteristics are similar to those outlined or used by Bonnischen and Kauffman (1987), Henry et al. (1988, 1990), Walker et al. (1980), Walker (1973, 1983).

Many of the physical features exhibited by the major mature phase units do not reliably distinguish lavas and ignimbrites. These features include columnar jointing, the apparent absence or paucity of fiamme, a basal 'vitrophyre' and rare flow folding. The interpretation of these units as ignimbritic rests rather on a few pieces of crucial evidence, the aforementioned features are then interpreted in line with this model.

3.3.1 - Pumice fragments

Although typical eutaxitic texture has not been observed in any outcrops of these large volume units, at one locality within the basal black Yardea highly flattened pumice fragments are observed. In outcrop these mimic flow banding (Figure 3.2a), due to combination of intense flattening and rather rubbly exposure. Indeed this was the interpretation of Creaser and White (1991) who reported flow banding in a sample from the same locality. Although thin sections of highly flattened pumice fragments can be misinterpreted as flow banding (as was probably the case for Creaser and White), many sections reveal textural evidence that these features are in fact pumice fragments (Figure 3.2 b,c and d). Lenticular, ragged forms are common, as are features interpreted to represent wispy tube pumice (Figure 3.2b). It is probable that recognition of pumice is only possible in the fine grained basal Yardea for in the main part of the unit, relatively slow cooling, recrystallization and welding resulted in an almost ubiquitous groundmass texture of graphic to granophyric intergrowths of alkali feldspar and quartz, which is generally as coarse as the recrystallized pumice. It is likely that the pumice would therefore be indistinguishable in such a coarsely crystalline groundmass and was probably also recrystallized during the cooling process. A similar obliteration of ignimbritic textures

a

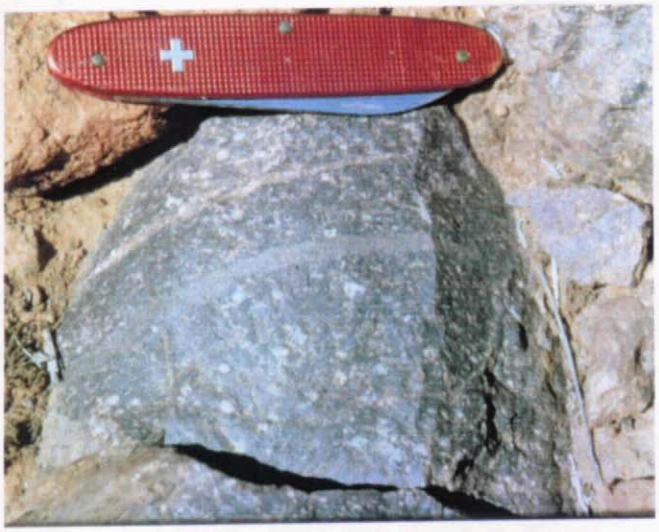

b

c

d

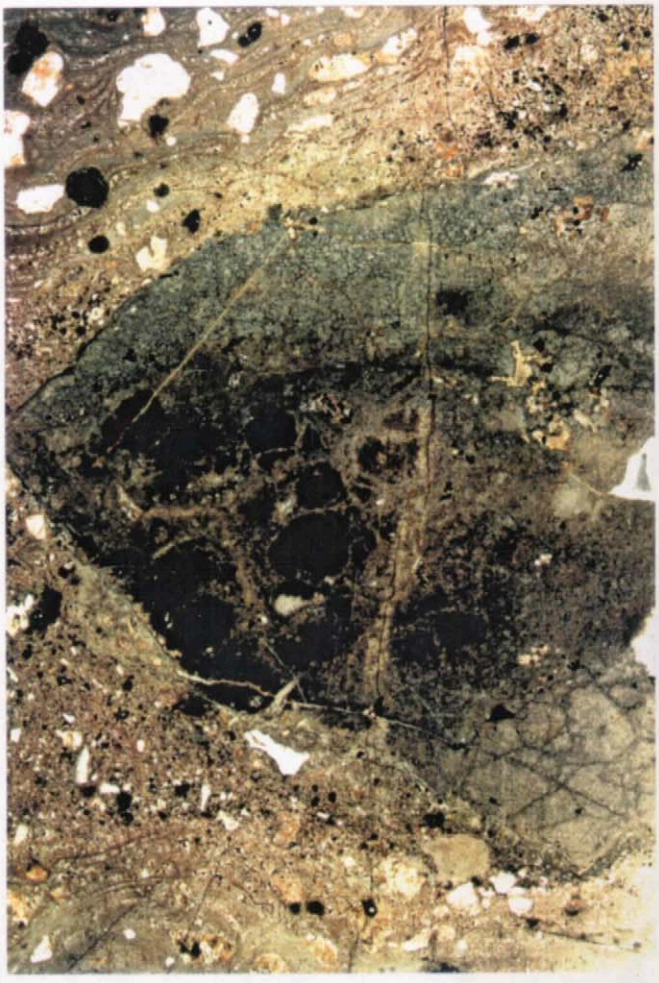

has been reported for the thick intracaldera sequences of both the Otowi and Tshirege Members of the Bandelier Tuff (Nielson and Hulen, 1984) and for rhyolitic ignimbrites of the Keeweenawan Midcontinent Rift plateau volcanics (Green and Fitz, 1993). In the Bandelier Tuff high degrees of welding, devitrification and recrystallization have resulted in thick granophyrically crystallized core zones where eutaxitic texture and shards cannot be identified, whereas the outflow sheets of both units exhibit well developed eutaxitic texture and readily identifiable shards. This does not imply that the major units of the mature phase volcanism represent intracaldera deposits, rather that their high temperature resulted in granophyric texture being developed in the sheets. The Keeweenawan rhyolitic rheoignimbrites, which are of similar thicknesses to the mature phase units, have fiamme and eutaxitic texture preserved only in their upper and lower levels, textures which have been obliterated in the more coarsely crystallized central sections.

The question must then be asked 'Is the apparent paucity of pumice fragments simply a reflection of their poor preservation or a primary feature?'. Pumice fragments of the type shown in Figure 3.2a-c have been found from only one locality in the Yardea vitrophyre and not at all in the Eucarro vitrophyre. A much more common texture in both vitrophyres is the rather subdued, wispy texture arrowed in Figure 3.3a. The preferred interpretation of this texture is that it represents a highly welded ignimbrite in which rare and small pumice fragments have been highly flattened and possible fine ghosts of welded shards. The apparent small amount of pumice is therefore considered to be a primary feature, and although unusual, this is not unknown in large volume ignimbrites. For instance Whitney and Stormer (1985) note that no large pumice blocks occur in the large Fish Canyon Tuff of the Central San Juan Volcanic Field, while Francis *et al.* (1983) and Sparks *et al.* (1985) report that the Cerro Galan ignimbrite contains only rare and small pumice clasts.

Pseudo-pyroclastic textures have been reported in silicic lavas, produced either by hydrothermal alteration (Allen, 1988) or by a combination of metamorphism and tectonism (Cas and Wright, 1987; Allen, 1988), however the textures reported here are from the unmetamorphosed and unaltered base of the unit, so a secondary origin for the textures is improbable.

3.3.2 - Chemical zonation

Chemical data from the Eucarro Dacite also provide evidence for a pyroclastic origin. This unit is zoned both chemically and mineralogically from base to top, as detailed in Chapters 4 and 5. Such chemical zonation is common in ignimbrites (Hildreth, 1981) but is unknown in lavas, and in fact a lack of chemical and mineralogical zonation is amongst the diagnostic features of silicic lava flows as outlined by both Henry *et al.* (1990) and Bonnischen and Kaufmann (1987). A recent reappraisal of transport and

Figures opposite:

Figure 3.3a - Photograph of a thin section from the black Eucarro 'vitrophyre'. Note that the section contains both entire phenocrysts and fragments thereof. Arrowed are the fine wispy textural features which are interpreted to represent highly flattened pumice. Width of field of view is 2 centimetres.

Figure 3.3b,c and d - Photographs of thin sections from various developmental phase volcanics which are interpreted as ignimbrites both in this study and by previous work (Giles, 1980; Robertson, 1989). The units are b) the Baldry Rhyolite and c) the Mangaroongah Dacite both from the Lake Everard area, and d) rhyolite RH3 from the Kokatha area. Width of field of view is 2 centimetres for each photograph.

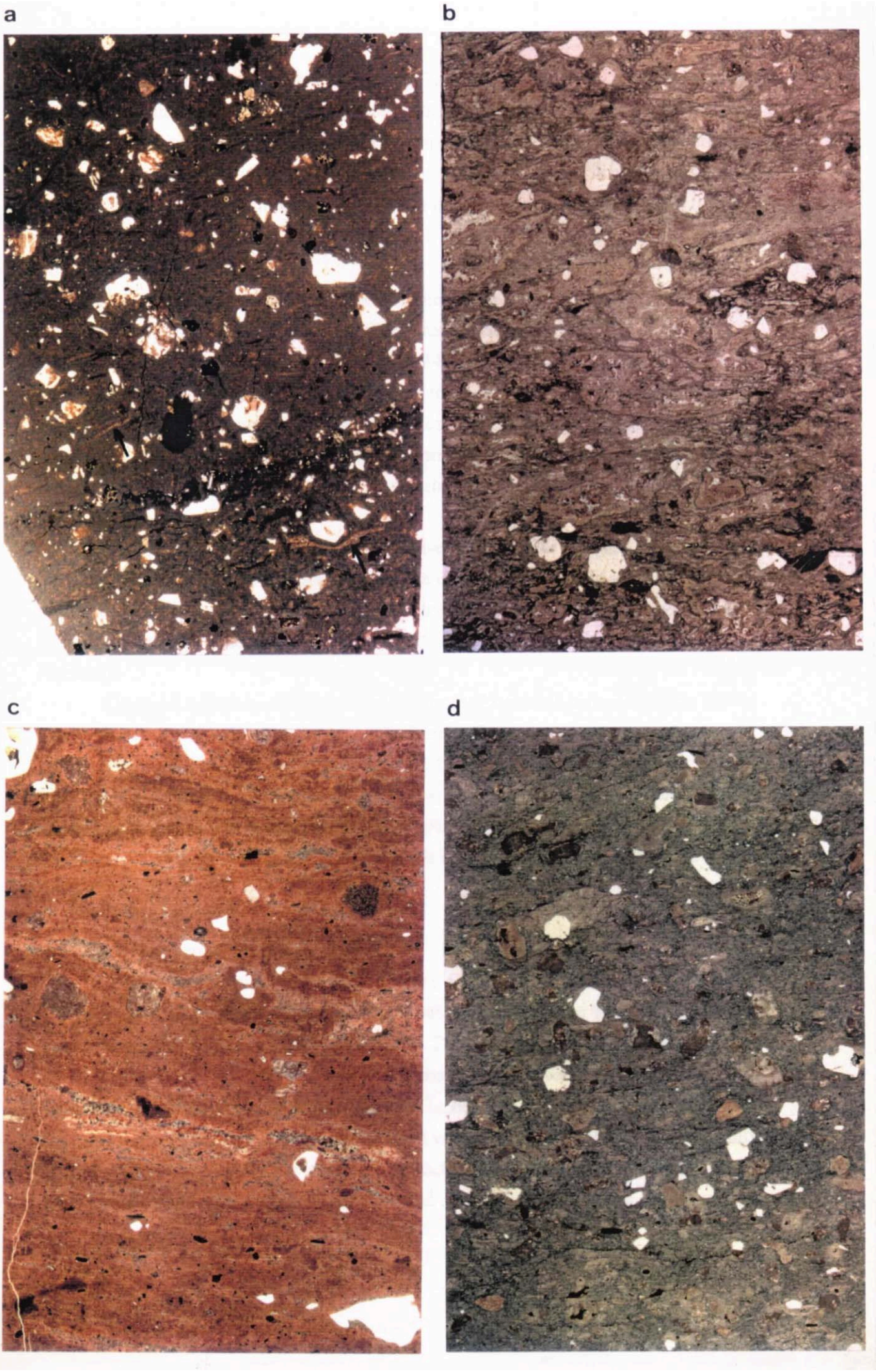
a
b
c
d

deposition from ignimbrites by Branney and Kokelaar (1992) provides a mechanism by which ignimbrites may produce vertical gradients in composition. Material is carried long distances in the ignimbrite in the transport system, and is deposited from the underlying, more dense depositional system. Sedimentation from the ignimbrite is by progressive aggradation from the depositional system, rather than by mass deflation of the entire ignimbrite, which allows a single layer to be built up which may be compositionally zoned from base to top.

In contrast to the vertical zonation, samples taken from the Eucarro vitrophyre over a strike length of over seventy five kilometres are chemically and mineralogically almost identical (samples 884-Eu7, 884-Eu20, 849-36; see Chapters 5 and 6). It would seem more likely if any chemical variation were to be observed in a lava flow that the variation would be in a lateral rather than a vertical sense (although Bonnischen and Kauffmann reject any chemical zonation being present in silicic lavas). The observed vertical and not lateral zonation therefore represents strong evidence for the ignimbritic origin of this unit.

The study by Turner (1975) of the south-eastern Gawler Ranges indicates that of the unit now defined as the Nonning Rhyodacite is zoned from rhyolite to rhyodacite from base to top, a similar zonation to that exhibited by the Eucarro Dacite. The arguments for an ignimbritic rather than lava flow origin for the Eucarro therefore also apply to the Nonning.

Chemical variation of the type observed in the Eucarro is not seen for the Yardea Dacite. However as outlined in Chapter 6 the Yardea Dacite is fairly homogeneous and although its base is defined by vitrophyre, the flat lying nature of the unit makes it impossible determine the height above the base at any particular locality. Therefore relating chemical variation in the Yardea to height above the vitrophyre is difficult. Chemical variation in the Yardea therefore sheds little light on the possible origin of this unit.

3.3.3 - Occurrence of basal breccia

A basal breccia was considered by Henry *et al.* (1990) to be the most diagnostic feature of lava flows. Not a single instance of basal brecciation has been observed at the base of either the Yardea or the Eucarro Dacite. The contact between the basal vitrophyre of the Yardea Dacite and underlying units is almost always covered by Quaternary sediments. A basal breccia could be inferred to lie beneath this sedimentary veneer, having been more readily eroded than the unbrecciated vitrophyre. Although this is a possibility it is considered to be unlikely, for where the contact between the Yardea and underlying units may be seen, no breccia is present. Instead a less resistant volcanic deposit such as a

pre-Yardea plinian deposit, or a small volume, less welded unit may be beneath this cover.

In contrast, where the Eucarro vitrophyre outcrops, it is observed to be in direct contact with the underlying Bittali Rhyolite, and no breccia has been observed at any locality above this contact. Although Henry *et al*. (1990) report local absence of basal breccia, its total absence in the case of the Eucarro and Yardea Dacites is considered to be another good piece of evidence for a pyroclastic origin for these units.

It should be noted that the apparent attribution of both a basal *and* an upper breccia to the Yardea Dacite which appears in Table 2 of Henry and Wolff (1992) is absolutely incorrect. As stated above, no basal breccia has been observed for the Yardea, and its upper section has been completely removed by subsequent erosion!

3.3.4 - Lithic fragments

The extensive silicic units which have been interpreted to be lava flows by Bonnischen and Kaufmann (1987) and Henry *et al*.. (1990) all have a marked absence of lithic fragments, in contrast to their common occurrence in ignimbrites. Examination of many specimens of Eucarro and Yardea Dacites has revealed that lithic fragments, whilst not abundant, are reasonably common, in agreement with Giles (1980) comment that the Yardea contained "abundant acid and basic xenoliths". It is difficult to determine their abundance but a tentative estimate of <0.01-0.05% lithics is made for both the Yardea and Eucarro Dacites. Their average size is small (< 2 centimetres in diameter), and recognition of them in outcrop or hand specimen can be difficult as many of them are of igneous derivation and may superficially resemble glomerophenocrysts. Typical lithic fragment types are dolerite, metasediment (Figure 3.2d, see also Figure 6.3a) granite and felsic gneiss. More than one lithic fragment type can occur in the same specimen although the dominant type in any outcrop area probably indicates the immediate basement type. The small average lithic fragment size may have been controlled by the intensity or rapidity with which the units erupted. Indeed small lithic size may be a feature of (at least some) very large volume (>1000km^3) ignimbrites, for Sparks *et al.*, 1985 report that the Cerro Galán ignimbrite contains <0.1wt.% lithic fragments which have a maximum diameter of 3.5cm, while Whitney and Stormer (1985) state the Fish Canyon Tuff has few lithic fragments of any size.

3.3.5 - Phenocryst fracturing

The degree of fracturing of phenocrysts is a criterion which has been used to distinguish lavas from ignimbrites, with a low degree of phenocryst fracturing taken to imply emplacement as a lava and a high amount to indicate a pyroclastic origin (Bonnischen and Kauffmann, 1987; Henry *et al.*, 1988; 1990). With respect to the Yardea

Dacite, Creaser and White (1991) report some samples which look typically pyroclastic and other samples which are more lava-like, and raise the possibility that an eruptive style unlike either typical ignimbrites or lava flows is responsible.

Careful examination of thin sections made for this study reveal that both the Yardea and Eucarro almost ubiquitously contain both totally intact phenocrysts and highly fractured grains in the same section e.g. Figure 3.3a. Phenocrysts may be fractured but with the pieces in situ (Figure 4.1d & e) or be tiny, angular fragments isolated within the groundmass (Figure 4.1g, 3.3a). Sometimes phenocryst fragments are concentrated in a thin horizon (Figure 3.3a) which may be related to the physical processes of eruption but this is problematical. Fractured phenocrysts are almost always feldspars, presumably due to their greater size with respect to other grains such as pyroxene. As noted above, granophyric recrystallization of the groundmass in the main part of the Yardea, and in much of the Eucarro tends to obscure fine features so these observations are from the basal vitrophyric Yardea and Eucarro.

A lack of or low degree of phenocryst fracturing has also been noted in units from the developmental phase of Gawler Range which have been interpreted as ignimbrites, (Figure 3.3b,c &d; this study; Giles, 1980; Robertson, 1989), and from the quartz latites of the Goboboseb Mountain volcanics (Milner and Ewart, 1989). All of these units and the Eucarro and Yardea Dacites are interpreted to have been erupted at high temperatures, therefore the degree of such fracturing could be in part controlled by the temperature of the magma (possibly combined with other physical or chemical parameters of the magmas) by affecting the mechanics of the eruptive process. This is similar to the conclusion reached by Creaser and White (1991). However when the Yardea and Eucarro Dacites are compared with other ignimbritic units, such as the Taupo ignimbrite, the proportion of entire phenocrysts to fragments thereof is similar, and therefore a different mechanism may not need to be invoked, and such high temperature ignimbrites may represent simply one member of a spectrum of ignimbritic eruptive types. The extreme may be represented by ignimbrites such as the Green Tuff of Pantelleria which contains few broken phenocrysts (Henry and Wolff, 1992).

3.3.6 - Viscosity and considerations on the magmas ability to flow

Another factor which argues against a lava flow origin is the large areal extent of the units, particularly the Yardea Dacite which is estimated to cover more than 12,000 km^2, and whose original extent may have been far greater. This is an order of magnitude more extensive than the area estimated for the Bracks Rhyolite lava (1000 km^2, Henry *et al.*, 1990) and for the biggest rhyolitic lava flow reported by Bonnischen and Kauffman (1987) in southwestern Idaho (approximately 500 km^2). Although the eruptive centre for the mature phase volcanism is unknown, if for arguments sake they erupted as lavas from

a single source placed at the centre of the current outcrop area, the Yardea would have to flow 90 kilometres (or more if the distal parts of the unit have been eroded), which seems unlikely for a magma containing up to 40% phenocrysts and with a highly siliceous matrix (76% SiO_2). The Bracks Rhyolite was interpreted by Henry *et al.* (1990) to have flowed up to 55 kilometres, which was partially attributed to the unit having lower than typical viscosity for a silicic lava. However the viscosities they calculated for the Bracks Rhyolite, using the method of Shaw (1972), did not account for the effect of phenocrysts contained within the magma.

The calculation of viscosities of silicic magmas is fraught with difficulty. For example, one commonly used method, that of McBirney and Murase (1984) has recently been reviewed and found to be inappropriate (Pinkerton and Stevenson, 1992) because it is based on emulsions which behave as Newtonian fluids, whereas silicic magmas do not exhibit Newtonian behaviour. As a result the McBirney and Murase calculation results unrealistically high apparent viscosities when anything but very small particle sizes are used. At crystal contents less than 30% Pinkerton and Stevenson (1992) reaffirmed the validity of another equation used to determine the effect of crystals on melt viscosity,

$$\eta_r = \eta_s/\eta_l = (1-R\phi)^{-2.5} \qquad (1)$$

where η_l is the viscosity of the phenocryst free melt calculated using the method of Shaw (1972), η_s is the viscosity of the phenocryst bearing melt, η_r the relative viscosity, R is the inverse of the maximum concentration that can be attained by the solids, and ϕ is the concentration (by volume) of phenocrysts in the magma. Where crystal contents exceed 30% Pinkerton and Stevenson (1992) outline a series of calculations to determine the viscosity of magmas which include terms for, among other things, yield strength, shape of crystals, crystal size and the geometric standard deviation of crystal size, shear stress and strain rate. In the case of calculating the viscosity of lava flows, which is the topic of interest here, the latter term is itself dependent on the effusion rate of magma and the velocity and thickness of flow. Therefore to apply this series of calculations to the mature phase volcanic units, values for a number of these terms would have to be assumed, introducing the possibility of erroneous results. However if apparent viscosities are calculated for Mount St Helens Dacite and porphyritic rhyolite from Inyo Domes using the data given in Pinkerton and Stevenson (1992) and equation (1), the results are often very close (and always in the same order of magnitude) as the results given in the paper which were calculated by their more complex method. The following discussion is therefore based on effective viscosities calculated using equation (1) which is, on the basis of crystal content, the appropriate method for all lithologies excepting the Yardea Dacite.

The viscosity of the Bracks Rhyolite calculated from the whole rock compositions given by Henry *et al.*, (1990) using the method of Shaw (1972) range from approximately $2.2x10^6$ Pa s for an anhydrous melt to $1.0x10^5$ Pa s for a melt containing 2% volatiles (H_2O+F). These viscosities are likely to be lower than the actual values because they are calculated on whole rock compositions rather than the compositions of the glass or matrix to the phenocrysts. The effect including the 10-15% phenocrysts which occur in the Bracks Rhyolite doubles these apparent viscosities to $4.4x10^6$ and $2.1x10^5$ respectively.

The effect of phenocrysts on the viscosities of the mature phase magmas is similar. This is illustrated in Figure 3.4 which has been plotted from the results of calculations using equation 1 (1984; Table 3.3). At any given volatile content apparent viscosities for the Eucarro Dacite approximately triple when the effect of phenocrysts are incorporated compared to levels calculated excluding any phenocryst effect. Similarly the apparent viscosity of the Yardea Dacite when calculated to include the effect of the phenocrysts are nearly nine times higher than those calculated for the melt composition without crystals (Table 3.2; Figure 3.4), at any of the volatile contents.

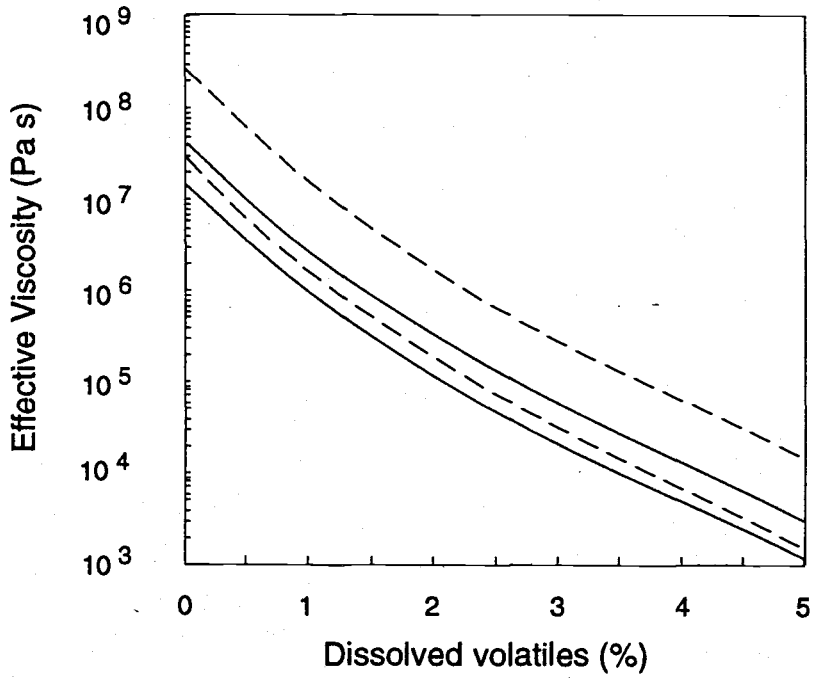

Figure 3.4 - The effective viscosity variation in the Eucarro and Yardea Dacites with % volatiles. Solid curves represent the Eucarro Dacite and dashed curves the Yardea Dacite. For each unit the lower curve represents the viscosity of a phenocryst-free melt, and the upper curve represents the viscosities calculated taking into account the effect of suspended crystals.

The calculations indicate that the presence of volatiles in the magma has the effect of decreasing the viscosity. Both H_2O and F have the effect of decreasing the viscosity of magmas by depolymerising the melt (Manning and Pichavant, 1983). Low dissolved

volatile contents have been estimated for both the Yardea and Eucarro magmas (Chapter 5), which would have been lowered even further by syn-eruptive degassing. Therefore the magma after eruption, were it to flow as a lava, would have very low levels of volatiles and the apparent viscosity of each unit upon eruption is likely to be described by the left hand portion of the upper viscosity curve for that unit on Figure 3.4. In addition recent experimental work indicates that the actual bulk viscosity of lava flows is heavily weighted towards the viscosity of their cool, viscous skins rather than their effective magmatic viscosity such as that calculated above (Stasiuk *et al.*, 1993). Therefore the viscosities in Table 3.4 can be considered to be absolute minima. The distances which the Eucarro Dacite would have needed to flow if it were extruded as a lava are not well constrained, for an unknown proportion of its extent is blanketed by the Yardea Dacite. An estimate of 90 kilometres has been made (see above) for the minimum distance which must have been travelled by the Yardea if erupted as a lava. It is considered that the calculated viscosity of each of the units is too great for them to be considered to have been erupted as lavas, for they are much higher than the viscosities of flood basalts (≈ 500 poise ≡ 50 Pa s, Shaw and Swanson, 1970).

Other features which have been used to distinguish rheomorphic ignimbrites from lava flows, such as the geometry of the flow margins (Bonnichsen and Kauffman, 1987) simply cannot be evaluated for the mature phase units because of the unknown amount of erosion which has occurred and the uncertainties in estimating the original distribution of each of the units.

Table 3.3- Viscosity calculations for the Eucarro and Yardea Dacites

Unit	*Modelled magma parameters*	*Dissolved volatile content*	*Viscosity phenocryst free melt (Pa s)*	*Effective viscosity with phenocrysts (Pa s)*
Yardea Dacite	Temperature = 1000°C			
	Volume fraction of phenocrysts =0.35	Dry magma	3.16×10^7	3.84×10^8
		1%	1.58×10^6	1.42×10^7
	Melt composition from Yardea	2%	2.00×10^5	1.8×10^6
	vitrophyre groundmass	5%	1.58×10^3	1.42×10^4
Eucarro Dacite	Temperature = 1000°C			
	Volume fraction of phenocrysts =0.2	Dry magma	1.58×10^7	4.36×10^7
		1%	1.00×10^6	2.76×10^6
	Melt composition from Eucarro	2%	1.26×10^5	3.48×10^5
	vitrophyre groundmass	5%	1.26×10^3	3.48×10^3

3.4 - Other features of the mature phase volcanics

All of the abovelisted features have been shown to be more consistent with the Eucarro and Yardea Dacites having been erupted as ignimbrites rather than lavas, and some of the features mentioned may be typical of very large volume ignimbrites (>1000 km^3), rather than of all ignimbrites. A similar origin is suggested for the Nonning and Yannabie Rhyodacites, with the reported chemical and mineralogical zonation in the former unit (Turner, 1975) making a strong argument for this interpretation. Little evidence has been garnered for the Yannabie Rhyodacite, due in part to its relatively small size, rather rubbly outcrop character and variable but often high degree of alteration, and so an ignimbritic origin for this unit is at best a tentative interpretation.

If then the Eucarro, Nonning, Yannabie and Yardea were all erupted not as lavas but as ignimbrites, various other features from these units of the mature phase volcanism can be interpreted in line with this origin.

The Eucarro Dacite exhibits evidence of flowage near its exposed top which is interpreted to be caused by rheomorphic flow after welding of the unit occurred. Textural evidence of the flow banding in the Eucarro is absent in thin section and is only observable in outcrop where weathering has etched the surface. When broken open, fresh surfaces are featureless. This evidence for rheomorphic flow has been observed only near the top of the Eucarro and may be due to the higher temperature of this upper part of the unit as deeper and hotter parts of the magma reservoir were tapped during the course of the eruption, as is indicated by pyroxene thermometry (Chapter 4). Such increases in temperature in zoned ignimbrites have been previously described by Hildreth (1979, 1981) and Grunder and Mahood (1988). Many cases of rheomorphic flow in ignimbrites have also been previously documented e.g. Gran Canaria (Schmincke and Swanson, 1967), the Eastern Snake River Plain (Morgan *et al*, 1984), the San Juan Volcanic Field (Varga and Smith, 1984) and the Marysvale Volcanic Field (Steven *et al.*, 1984), and is commonly attributed to a high emplacement temperature allowing flowage subsequent to welding. Although the Yardea Dacite was likely to have been erupted at a similar temperature, no evidence of flowage has been observed in this unit, an observation which is in line with its much higher viscosities relative to the Eucarro (see above), its higher crystal content (Chapter 4) which may have effectively prevented any post-emplacement rheomorphic flow.

The Yardea, Eucarro and Nonning all exhibit well defined columnar jointing in much of their outcrop distribution (Figure 4.1a, b). In highly welded zones of ignimbrites, columnar jointing is a common feature (e.g. Cas and Wright, 1987). The

occurrence and degree of welding is dependent on emplacement temperature, composition of the ignimbrite, and the thickness of the deposit (e.g. Cas & Wright, 1987). The common occurrence of columnar jointing in each of the major units indicates they underwent a high degree of welding, a consequence of their reasonable thicknesses (up to 200 metres thick, Blissett, 1975, 1986) and high emplacement temperatures (Chapter 4). Emplacement temperatures have been estimated to approach magmatic values for densely welded sheets (Sheridan, 1979) and for the units under consideration here this implies emplacement temperatures approaching 900-1000°C. The amount of time for a high degree of welding to occur can be very small - e.g. Bierworth (1982 - quoted in Cas & Wright 1987) calculated a rhyolitic ignimbrite of 100 m thickness emplaced at 850° C would undergo dense welding within one week. The higher temperatures and greater thicknesses estimated for both the Yardea and Eucarro Dacites, and by inference for the Nonning Rhyodacite, imply that they would have become highly welded in a time period of the same order of magnitude or less. In contrast the Yannabie Rhyodacite does not exhibit the columnar jointing typical of the other units. Petrographically it also differs, with no examples showing the granophyric groundmass texture so prevalent in the other units rather it has microcrystalline groundmass textures, and in addition, the Yannabie is the only unit to exhibit textures which are interpreted to relatively unflattened pumice and an open framework resulting from a low degree of welding. In many places where less welded, the Yannabie Rhyodacite is also more highly altered than other mature phase units. All of the above features of the Yannabie result from the fact that it is much thinner than any of the other mature phase units, which resulted both a lower degree of welding and a faster cooling rate for the Yannabie relative to the other units. Each of the major mature phase units may have had thinner distal portions, which did not undergo such intense welding and crystallization, and which have been removed by erosion. In particular the Yardea Dacite, whose entire outcrop above the basal vitrophyre is granophyrically recrystallized, may have had removed by erosion a significant, but indefinable, proportion of its original volume. Sedimentary sequences at least partly sourced from the Gawler Range volcanics include the fluvial sediments of the Mesoproterozoic Pandurra Formation, the minimum age of which has been estimated as approximately 1423 Ma. (Fanning *et al.*, 1983).

The widespread high degree of welding in the three main eruptive units of the mature phase volcanism indicate that the amount of heat lost during eruption was minimal, such that the emplacement temperatures were close to the pre-eruptive magmatic temperature. A high density eruption column with a low collapse height would best retain its heat, and this type of column has been modelled by Sparks *et al.* (1978) and Woods, (1988) as depending on a number of interrelated factors including a low estimated fluid

content of the magma, a wide vent area, a high rate of eruption, and high initial vent velocities.

The basal black part of the Eucarro Dacite, where exposed, immediately overlies flow banded rhyolite of the Bittali Rhyolite. Thus it seems there was no unwelded portion at the base of the Eucarro, unlike many large scale ignimbrites e.g. The Carpenter Ridge Tuff (Whitney *et al.*, 1988) the Fish Canyon Tuff (Whitney and Stormer, 1985), the Bishop Tuff (Hildreth, 1979), and the Bandelier Tuff (Self and Wright, unpublished data, quoted in Cas and Wright, 1987). However the large Cerro Galan ignimbrite is one example which also lacks a basal unwelded plinian deposit, suggested by Francis *et al.* (1983) to be due to an unusually rapid eruption rate. Such a high eruption rate would make a convecting column unstable, e.g. Cerro Galan (Francis *et al.*, 1983), and would have the effect of collapsing the column, thus limiting the interaction with air and leading to higher emplacement temperatures. As noted previously in almost all exposures Quaternary sediments obscure the sequence between the Yardea vitrophyre and the underlying units. Therefore it is difficult to make a similar statement about the presence or absence of a basal plinian deposit for the Yardea. One possible explanation for this gap in the volcanic outcrop at this level in the stratigraphy may be the preferential erosion of unwelded or partly welded plinian deposits erupted prior to the main Yardea unit. Alternatively it may be due to the presence at this horizon of other less resistant rock types.

3.5 - Source vents of the mature phase magmas

No known caldera subsidence-type feature has been found which could be interpreted as the source of the mature phase volcanics. In other provinces where the felsic volcanism is similarly high temperature, such as southwestern Idaho (Ekren *et al.*, 1984; Bonnichsen and Kauffman, 1987) and the Goboboseb Mountains of the Etendeka Province (Milner and Ewart, 1989), the eruptive centres are either entirely unknown or are subtle features such as the Messum complex in the Goboboseb Mountains, features quite unlike the quite unlike the spectacular calderas from which ignimbrite sheets are usually considered to have erupted (Lipman, 1984). Where eruptives of this high temperature type cannot be linked to a caldera structure, one hypothesis is that they were sourced from fissures (e.g. Bonnichsen and Kauffman, 1987; Henry *et al.*, 1989). However this source interpretation is sometimes based more on the lack of a caldera or other recognisable vent area than on direct observation for fissures (Bonnichsen and Kauffman, 1987), although feeder dykes to some extensive silicic lavas have been documented (Henry and Wolff, 1992).

In observed and reconstructed basaltic fissure eruptions, the locus of eruption changes relatively rapidly from the entire length of the fissure to point sources along the fissure. The same reduction in source length is probable in silicic fissure eruptions, and therefore the appeal of a fissure eruption model to explain widespread, voluminous, silicic volcanism is diminished, particularly when combined with high viscosities of the eruptive products. Consistent base to top geochemical and mineralogical trends in the Eucarro Dacite and Nonning Rhyodacite over long distances, which is difficult to explain via fissure type eruption without invoking a combination of high eruption rate and low viscosities, the combined effect of which would allow flowage over extreme distances as is the case with continental flood basalt provinces. Low viscosities have been discounted for the mature phase magmas, again rendering their eruption from fissures improbable.

Having discounted eruption of the mature phase magmas via fissures, each unit of the mature phase volcanism is considered to have erupted from a single vent area. All of the units may have erupted from a single vent, alternatively the vents may have been nested as are the calderas in the San Juan volcanic province and those in the Yellowstone volcanic area, with each major unit having a unique vent. The location of the eruptive vent(s) for the major mature phase units is problematical. They could lie to the north or north-east of the current outcrop area beneath later sediments (which range in age from Mesoproterozoic through Cretaceous and Tertiary), or even beneath Lake Gairdner which could be in part a physiographic depression over the vent area. Gravity data has not been useful in outlining possible vent areas because the signature is dominated by a mid-crustal body, the significance of which is discussed in Chapter 7.

In short there is no evidence for a typical caldera or cauldon structure which can be easily associated with the mature phase volcanics. However its absence does not imply that they erupted from anything other than a single source vent, for the alternative option, eruption from fissures, is regarded as highly improbable and cannot explain observed unit characteristics. As noted above the vent may or may not be currently exposed, however if it is, it does not resemble a typical caldera, and its more subtle nature may have prevented its identification thus far.

Milner *et al.* (1992) suggest that the subtle nature of the source vent of the Etendeka quartz latites, compared with the caldera stuctures of the western U.S.A., may be due to eruption from deeper magma chamber and a deeper drawdown of magma. This may indeed be true for the ***minimum*** depth to the top of the pre-Eucarro magma chamber is estimated to be between 8 and 13 kilometres (Chapter 4), the larger value is somewhat deeper than typical estimates for ignimbrites from caldera sources (e.g. Grunder and Mahood, 1988; Smith and Braile, 1983; Lipman, 1984). Another controlling factor in the morphology of the vents for these type of eruptions may be the high magmatic temperature of the erupted material.

3.6 - Variations on the theme of ignimbrite/lava discrimination

The above discussion on the interpretation of ignimbrites is predominantly based on the criteria put forward by Henry *et al.*, (1988, 1990) and Bonnischen and Kauffman (1987). However the criteria of some of the main protagonists in this debate appear to be changing. Henry and Wolff (1992) change tack rather in their approach to discrimination, and now insist that silicic lavas can contain pumice and shards. Their revised and preferred criteria now such things as distal thinning of units, the appearance of unit margins, the units response to topography and the source. Such factors cannot be determined for the mature phase volcanics. Erosion has almost certainly removed the peripheral portions of many/all of the larger units, as well as an unknown thickness of the upper part of the Yardea Dacite. This would be expected as the distal portions would be less welded (or even unwelded) and therefore less resistant. Also the flat lying, undissected nature of the Yardea Dacite, which blankets the earlier erupted mature phase units, makes any interpretations as to thickess variations and response to topography impossible. Finally ignimbrites generally thin radially away from their source. As no source for the mature phase volcanics has been thus far located, even if thickness variations could be observed, it is unclear what interpretations could be drawn from them. One of the factors which Wolff and Henry (1992) consider an equivocal discriminant is compositional zoning, although they concede that ignimbrites are often zoned and silicic lavas are often homogeneous. However as noted in section 3.3.2, it is difficult to conceive a mechanism for silicic lava eruption which would result in strong base to top chemical zoning combined with identical basal compositions over 80 kilometres apart.

Overall although it is agreed that discriminating high temperature ignimbrites from silicic lavas is a difficult task, it is considered that the recent publication by Henry and Wolff (1992) has an air of special pleading. The changing criteria has enabled these authors to interpret more high temperature silicic volcanics as lavas, but their methods may be open to question. Many of these interpretations have been made without the authors visiting the areas upon which they pass judgement, and their previously noted mis-attribution of upper and basal breccias to the Yardea Dacite, combined with a reference to a volcanic province named Australia which contains apparently both Palaeozoic rhyolites from New South Wales (Cas, 1978) and the Yardea Dacite, makes their care in data collection somewhat questionable.

3.7 - Conclusions

All units of the mature phase volcanic sequence, with the exception of the Paney Rhyolite, have been interpreted as having erupted as ignimbrites. The temperature of emplacement was likely to have been close to magmatic temperature. In the Nonning Rhyodacite and the Eucarro and Yardea Dacites this high temperature, in combination with the unit thicknesses, commonly resulted in a granophyric textured groundmass which has obscured much of the evidence for an ignimbritic origin. However many of the physical features observed have been found to be consistent with these units being ignimbrites and inconsistent with them being lavas. In particular the features show considerable similarities to some of those documented for very large volume ignimbrites. It is therefore not considered necessary to invoke a mode of eruption for these units which is significantly different to that of more 'normal' ignimbrites, except perhaps a lower collapse height for the convecting ash column. Many of the features of the three main units have been wholly or partly ascribed to be due to them having high emplacement temperatures and/or a high eruption rate, two factors which are interactive to a degree. It is considered that they both were fundamental in determining many of the observable physical features of the mature phase volcanics by influencing or controlling post-eruptive processes such as welding and recrystallization.

Although a source for the mature phase magmas has not been located as yet, it is considered that a single source vent is much more likely than eruption from fissures. However difficulty in identifying sources seems to be a common problem with high temperature felsic volcanics, and the answer may lie in the relatively subtle form of these vents compared with the typical caldera structure.

Chapter 4. The characterization, evolution and genesis of a large volume, high temperature, silicic magma chamber, Part 1: mineralogy, petrology and magmatic conditions.

4.1 - Introduction

Voluminous volcanic eruptions represent time slices in the development of their parent magmatic systems, and as such allow determination of the chemical, mineralogical and isotopic history, and the intensive parameters present in a system prior to eruption.

The mature phase of the Gawler Range volcanism is dominated by large volume, isotopically homogeneous units (Chapter 5), and is quite different from the earlier developmental phase volcanism, whose products were smaller volume chemically and isotopically heterogeneous units erupted from several scattered centres.

This chapter presents mineralogical data for the two largest units of the mature phase volcanism and this data is then used to constrain some magmatic parameters for these units. Chemical and isotopic data for the mature phase volcanics are examined in the following chapter.

Consideration of the mineralogical, chemical and isotopic data indicate that the mature phase units represent the periodic tapping of a single, large evolving magma chamber.

4.2 - Geological Setting

The geological setting for the Gawler Range volcanism as a whole has been previously outlined in Chapter 1. In summary units of the mature phase volcanism are only rarely juxtaposed against basement lithologies. Along the southern and south-western margins of the province, the Nonning Rhyodacite and the Eucarro and Yardea Dacites each only outcrop in close proximity to lithologies belonging to either metasediments of the Hutchinson Group or gneisses and granitoids of the Lincoln Complex, although the juxtaposition is often attributed to faulting (Figure 1.1). Along the southern and western margins of the Gawler Ranges, the basal units assigned to the mature phase volcanism more often overlie scattered outcrops of a complex series of rhyolitic to rhyodacitic flow folded lavas and small scale pyroclastics collectively named the Bittali Rhyolite (Blissett, 1986) the final unit of the developmental phase of the southern Gawler Ranges area. At Lake Everard the uppermost exposed unit of the mature

phase volcanic sequence, the Yardea Dacite, overlies the Wheepool Rhyolite and the Yantea Rhyodacite both which belong to the developmental phase in this area.

The ages of the various units, and therefore the repose times between eruptions, cannot be resolved, as was demonstrated by Fanning *et al.* (1986) whose U-Pb zircon ages for the Waganny Dacite (the lowermost exposed unit in the south-western Gawler Ranges which belongs to the developmental phase of volcanism, see Chapter 2) and for the vitrophyre of the Yardea Dacite were identical within error at 1592 ± 2 Ma. Thus all that is known is that the mature phase of volcanism took place in less than 2 million years. This is not unusual, however, as is demonstrated by Yellowstone (Hildreth *et al*, 1991), and the San Juan Mountains (Steven and Lipman, 1976), both of which volcanic fields erupted enormous quantities of felsic magma as a series of ignimbrites within a few million years.

4.3 - Petrography

Due in large part to the age of the province, preservation of minerals in the mature phase volcanic sequence is poor in most samples, although the degree of preservation varies from unit to unit. Examination of thin sections from each of the units does however reveal an overall mineralogical coherency. All units of the mature phase are porphyritic, and feldspars are ubiquitously the dominant phenocryst type. The relative proportions of sanidine and plagioclase vary with rock type, this variation is subtle and gradational, and both feldspars are present in all sections examined. Plagioclase is slightly dominant over sanidine in dacitic rocks, the two phases are present in subequal proportions in rhyodacites, and in rhyolites sanidine is more common than plagioclase. The major ferromagnesian silicate is pyroxene, which has been in many cases totally pseudomorphed by chlorite and/or complexly intergrown iron rich clays. In addition to pyroxene some samples of the Eucarro Dacite and the Paney Rhyolite, typically those with more than 72% SiO_2, also contain olivine which is rarely fresh, more commonly it has been pseudomorphed iddingsite. Magnetite, minor ilmenite and quartz in variable proportions complete the phenocryst assemblage. The general petrography of each of the lithologies of the mature phase of Gawler Range Volcanism is described in Table 4.1.

Mineral assemblages and compositions may be used to provide information on magma chamber conditions. As outlined above the degree of preservation of the mineral phases makes extraction of this type of information for the mature phase volcanics difficult. However both the Eucarro and Yardea Dacites have basal black, flinty sections which are interpreted to be crystallized vitrophyres, which contain almost pristine mineralogical assemblages. In addition both of these units also exhibit a reasonable degree

Figures opposite:

Figure 4.1a - Photograph of typical outcrop of the Yardea Dacite as a rounded hill. Several levels of columnar jointed dacite can be seen on the hill.

Figure 4.1b - Photograph of well developed columnar jointing in the Yardea Dacite. Man on left hand side of photograph for scale.

Figure 4.1c - Photograph of the tops of columnar jointed Yardea Dacite illustrating the well developed polygonal jointing pattern. Hammer is approximately 40 centimetres in length.

Figure 4.1d - Photomicrograph of a fractured plagioclase-pyroxene glomerophenocryst from the Yardea Dacite. The plagioclase grain is euhedral and zoned. Width of view is approximately 2 millimetres.

Figure 4.1e - Photomicrograph of highly fractured plagioclase phenocryst in the Yardea Dacite. Width of view is approximately 2 millimetres.

Figure 4.1f - Photomicrograph of plagioclase phenocryst from the Yardea Dacite with a strongly resorbed core. Width of view is approximately 2 millimetres.

Figure 4.1g - Photomicrograph of angular fragments of feldspar from the Eucarro Dacite, resulting from fracturing of larger grains. Width of view is approximately 2 millimetres.

Figure 4.1h - Photomicrograph of a resorbed quartz grain from the Yardea Dacite. Width of view is approximately 1 millimetre.

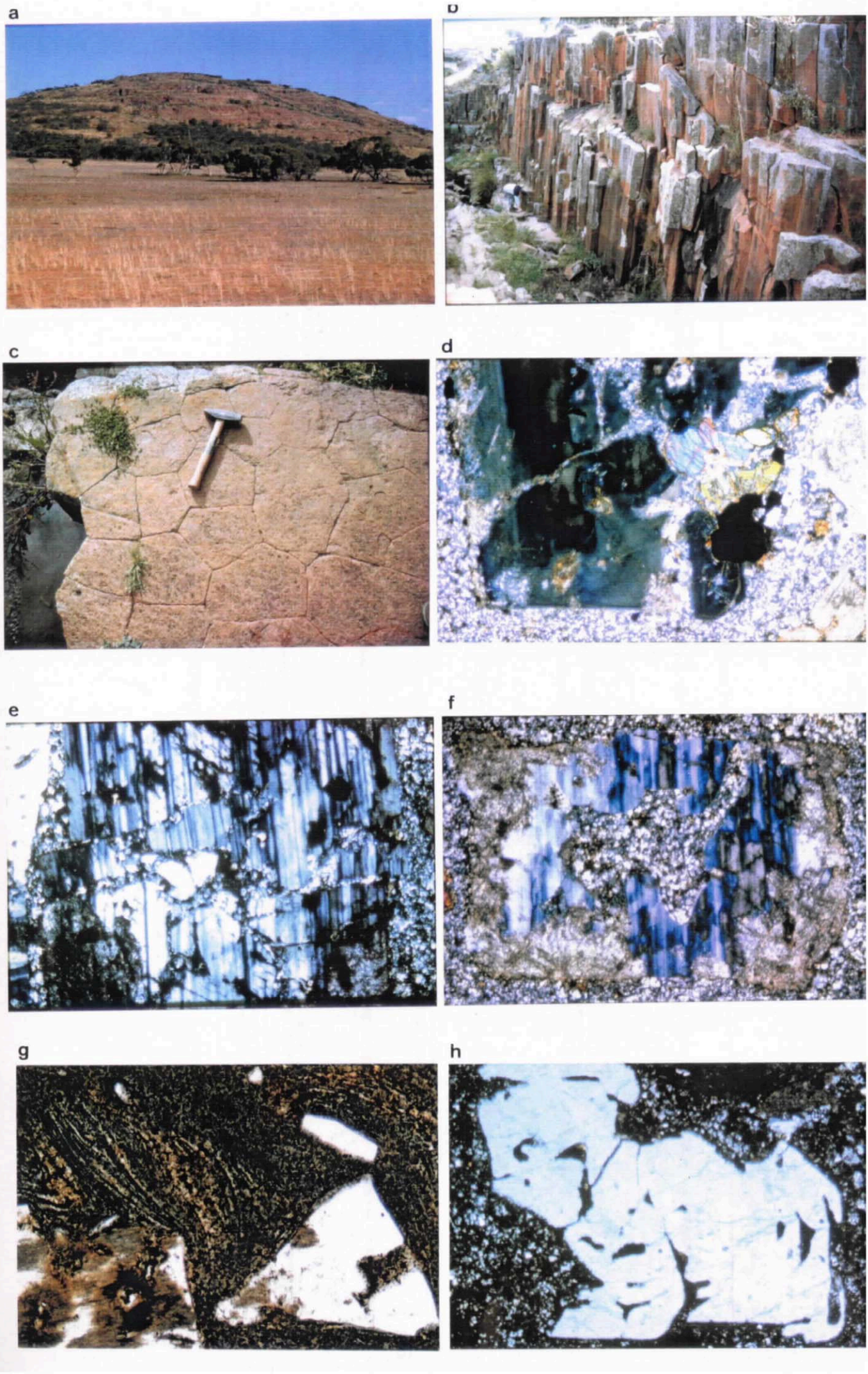
a
b
c
d
e
f
g
h

Table 4.1 - Observed or interpreted primary mineralogy of mature phase volcanic units

Unit	*% phenocrysts*	*Major Phenocrysts*	*Minor phenocrysts*	*Accessory minerals*	*Groundmass Textures*	*Comments*
Yardea Dacite	25 - 40	Plagioclase ≥ Sanidine> Clinopyroxene≥ Fe-Ti oxides	Quartz	Apatite > Zircon	Microgranular in black basal section Granophyric in main section	Mineralogy well preserved in basal 'vitrophyre'. In main section plagioclase is variably sericitized, sanidine may be turbid, augite is commonly preserved, pigeonite is altered to chlorite, Fe-Ti oxides are exsolved ± oxidized.
Paney Rhyolite - rhyolitic	15 - 25	Sanidine > Quartz > Plagioclase	Clinopyroxene, Olivine? Fe-Ti oxides	Apatite » Trace Zircon	Microgranular to microspherulitic	Mafic silicates totally replaced by chlorite and complex Fe clays feldspars sericitized ± turbid and oxidized. Trachytic texture of aligned feldspars is common.
- rhyodacitic	10 - 15	Sanidine > Plagioclase » Quartz ≈ Clinopyroxene	Olivine?, Fe-Ti oxides	Apatite » Trace Zircon	Microgranular, Perlitic, Microspherulitic	Some samples slightly vesicular, round vesicles filled with quartz, mafic minerals replaced variously by chlorite and complex Fe clays feldspars highly sericitized ± turbid due to iron oxidation
Yannabie Rhyodacite	10 - 20	Sanidine > Plagioclase > Clinopyroxene » Quartz	Fe-Ti oxides	Apatite > Zircon	Patchy microgranular	Lensoid cavities lined with axiolitic quartz and infilled with quartz, 'open ' groundmass compared to other units. Mafic silicates totally replaced by chlorite, Fe-Ti oxides oxidized, feldspars sericitized ± turbid
Eucarro Dacite	12 - 20	Top of unit - Plagioclase≥ Sanidine » Clinopyroxene > Fe-Ti oxides, gradational to base of unit where Sanidine > Plagioclase » Clinopyroxene or Amphibole	± Quartz Quartz	Apatite > Zircon Apatite > Zircon » Allanite	Microgranular to granophyric	Groundmass textures vary systematically with stratigraphic height, microgranular at base, coarsening to granophyic in centre of unit, then fining upwards to microgranular at top of unit. Mineralogy well preserved at and near base. In main unit some pyroxene preserved, plagioclase mostly sericitized, sanidine is often turbid and Fe-Ti oxides are variously exsolved ± oxidized
Nonning Rhyodacite	10 - 20	As for Eucarro Dacite	± Quartz	Apatite > Zircon	Microgranular to patchy microgranular	Plagioclase sericitized, Sanidine turbid due to Fe oxidation, mafic silicates altered to chlorite ± carbonate, Fe-Ti oxides oxidized

Figures opposite:

Figure 4.2a & b - Photomicrographs of a pyroxene phenocryst from the Yardea Dacite both under plane polarized light (a) and crossed polars (p). The grain is a composite with pigeonite (p) which has a euhedral optically oriented overgrowth of augite (a). The long dimension of the composite grain is a little over 1 millimetre.

Figure 4.2c - Electron microprobe photograph of the same grain as illustrated in a) and b), showing pigeonite remnants in the augite overgrowth. The entire grain has a very thin rim of amphibole which has an irregular margin against the surrounding matrix. The amphibole has much the same grey scale shade as augite.

Figure 4.2d - Photomicrograph of a plagioclase-pyroxene-oxide glomerophenocryst in the Yardea Dacite. Width of view is approximately 2 millimetres.

Figure 4.2e - Closer view of the large pyroxene grain in the glomerophenocryst illustrated in d), showing augite exsolution lamellae (green) parallel to the (001) plane in the host pigeonite (pink). Width of view is approximately 1 millimetre.

Figure 4.2f - Altered pigeonite grain from the main unit of the Yardea Dacite (above the 'vitrophyre'), which contains exsolution lamellae of augite parallel to the (001) plane. Width of view is approximately 1 millimetre.

Figure 4.2g - Herringbone exsolution texture of pigeonite preserved by replacement chlorite from the main unit of the Yardea Dacite. Width of view is approximately 1 millimetre.

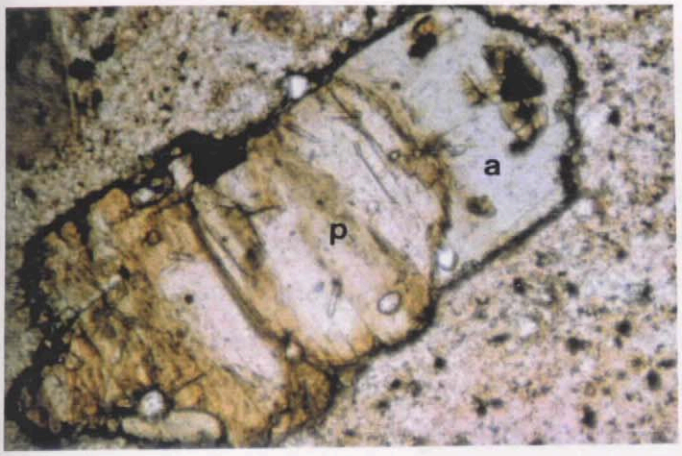

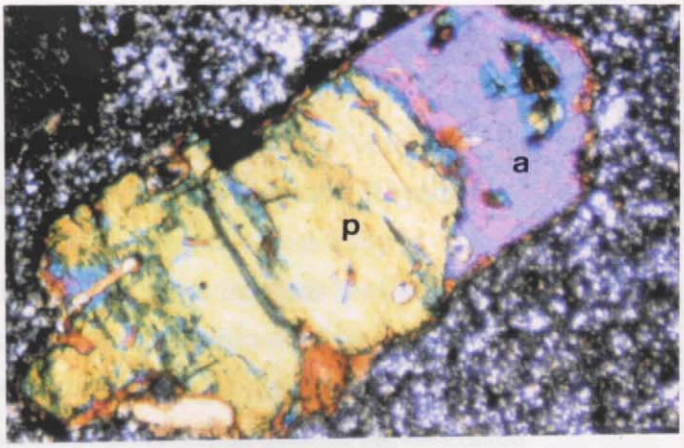

c

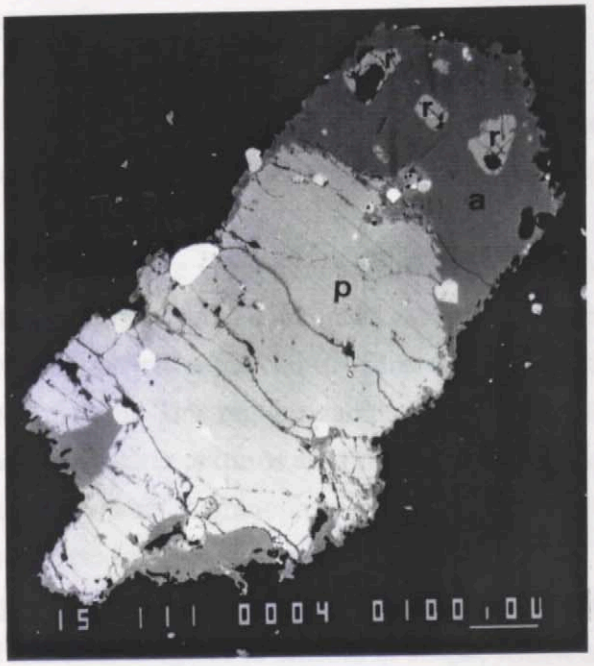

d

e

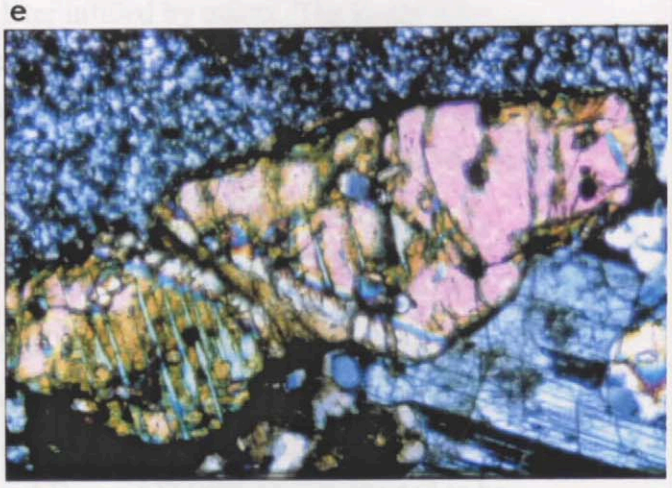

f

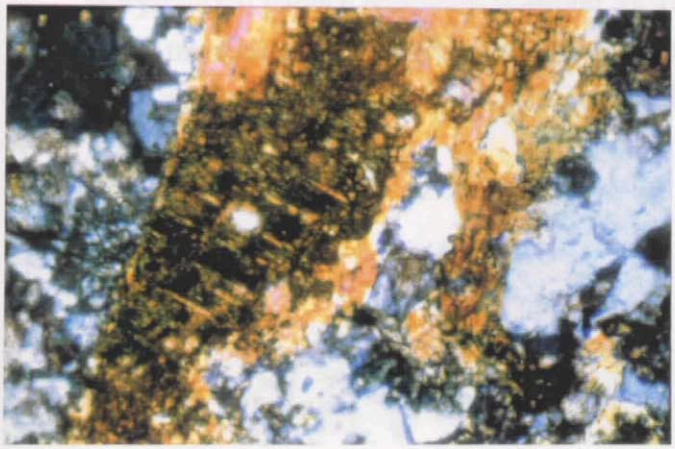

g

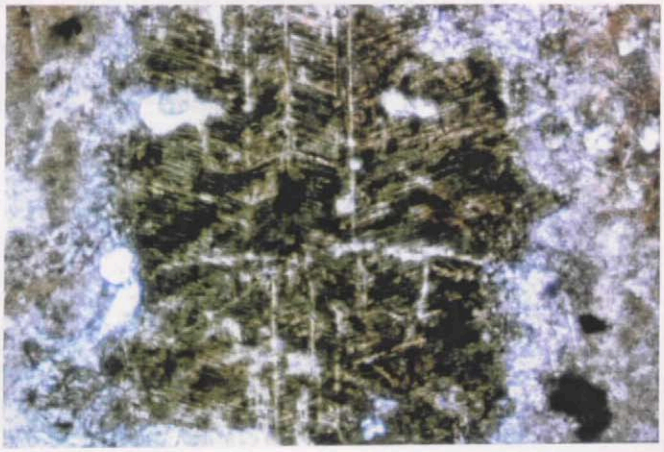

of mineral preservation in their main sections (above the vitrophyre). No 'vitrophyre' has been observed for the Nonning Rhyodacite, and it along with the Yannabie Rhyodacite and Paney Rhyolite are highly altered. For this reason the mineralogical study to determine some of the intensive parameters of the mature phase magmas has been concentrated on the Yardea and Eucarro units only. This is considered to be quite reasonable however as these two units, along with the Nonning Rhyodacite which is considered to be an analogue of the Eucarro, represent greater than 99% of the estimated total eruptive products of the mature phase magma chamber (Table 3.1). In addition the Yardea and Eucarro have mineral assemblages like those of the other units (see Table 4.1), and their compositions overlap are representative of the entire mature phase range with the exception of the few samples containing > 74% SiO_2, all of which are from the Paney Rhyolite.

The matrix of the Eucarro Dacite vitrophyre has a very fine microgranular texture consistent with very fast cooling. Above this the matrix textures gradually coarsen through microgranular to granophyric at the centre of the unit, and the fine again to microgranular at the top of the unit. This regular variation is accompanied by colour changes in outcrop. Where the matrix textures are fine, the outcrop is chocolate brown, grading to brick red where the matrix is granophyric. These observations indicate that the Eucarro Dacite can be interpreted to be a single cooling unit.

The Yannabie Rhyodacite has a matrix which is patchy microgranular, and some samples exhibit textural features, irregular to lensoid in shape, which may be voids in the original texture left by incomplete welding and later infilled by quartz. The Paney Rhyolite has many petrographic features typical of silicic lava flows including trachytic texture defined by alignment of feldspar laths (seen mostly in the rhyolitic member) and flow lineations and flow folding which is evident in outcrop, specimen and thin section scale. Textural variation in the rhyolitic member grades from micro-spherulitic to micro-granular, while the rhyodacitic member exhibits both of these plus occasional perlitic devitrification.

Little textural variation is seen in much of the Yardea Dacite, specimens above the vitrophyre ubiquitously have granophyric matrices, while those of the vitrophyre are fine microgranular. Ragged ended lenses of coarser crystalline material with axiolitic quartz observed in the vitrophyres of both the Yardea and Eucarro Dacites are interpreted to be recrystallized pumice fragments (Chapter 3). These features have been obliterated in the main, more coarsely crystalline portions of these two units by the development of coarse, granophyric matrix textures, which is the result of slow cooling.

Figures opposite:

Figure 4.3a - Electron microprobe photograph showing exsolution lamellae in pyroxenes of a pyroxene-plagioclase glomerophenocryst from the Yardea Dacite. Augite grains contain exsolution lamellae of pigeonite and likewise pigeonite grains contain lamellae of augite. Mineral abbreviations for all photographs in this plate: augite (a), pigeonite (p), Fe-Ti oxide (o), apatite (ap), amphibole (h).

Figure 4.3b - Higher magnification view of a portion of the same glomerophenocryst. Coarse pigeonite lamellae in augite host themselves contain very fine augite lamellae. Note zoning in some apatite grains, and altered Fe-Ti oxide.

Figure 4.3c - Electron microprobe photograph of an isolated small pigeonite grain from the Yardea Dacite. Surrounding the grain, between it and the enclosing matrix is a rim of amphibole.

Figure 4.3d - Electron microprobe photograph of a euhedral to subhedreal pigeonite grains from the Eucarro Dacite. The larger grain has two sets of augite exsolution lamellae (see text for discussion).

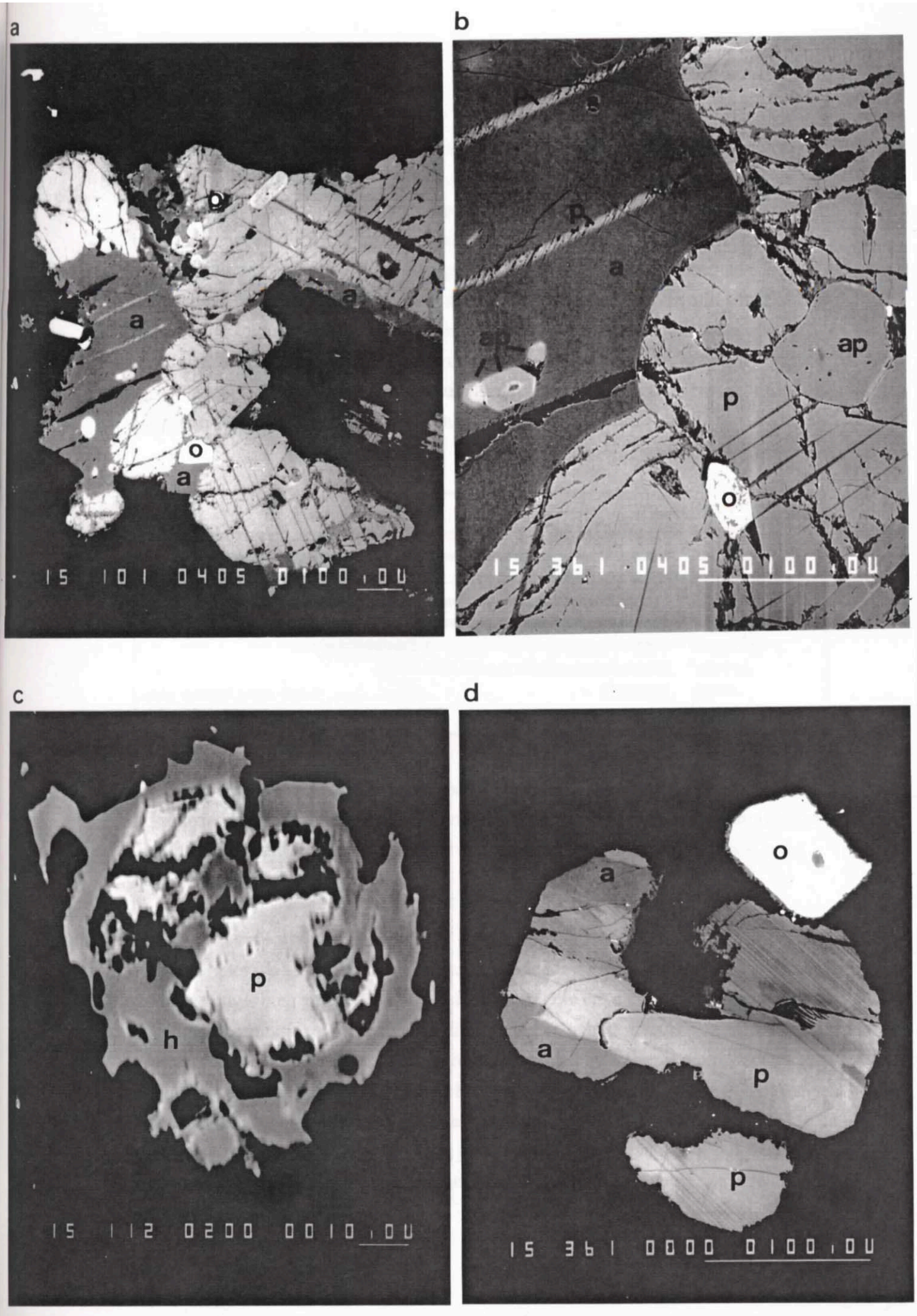
a
o
a
a
o
a
15 101 0405 0100.00
b
a
ap
ap
p
o
15 361 0405 0100.00
c
p
h
15 112 0200 0010.00
d
o
a
a
p
p
15 361 0000 0100.00

4.4 - Mineralogy

Plagioclase is the most abundant phenocryst phase in the Yardea Dacite and in the upper, dacitic (latitic) parts of the Eucarro Dacite. In the middle, rhyodacitic parts of the Eucarro, plagioclase and sanidine are equiproportional grading into the lower rhyolitic portion where sanidine is dominant over plagioclase. In both units the main ferromagnesian silicates are greenish pigeonite and augite present in subequal proportions. Iron-rich olivine occurs in some samples of the lower, rhyolitic part of the Eucarro Dacite. In an areally restricted area of the Eucarro, in the south-westernmost outcrops, the ferromagnesian silicate is amphibole, and no pyroxene has been observed.

The typical phenocryst crystallization sequence, as determined from inclusion relationships within the mature phase units, is illustrated below.

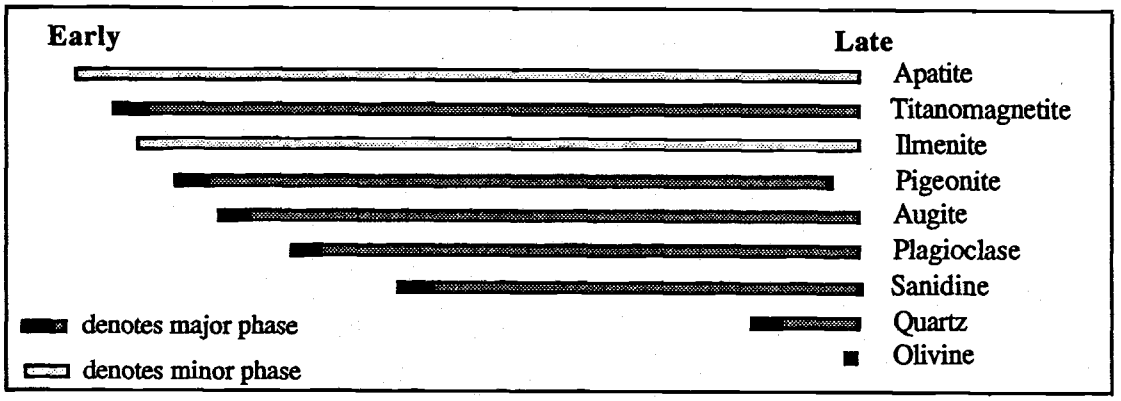

In addition to the relationships shown above, igneous amphibole occurring in the Yardea crystallized late, probably just prior to eruption. Where present in the Eucarro igneous amphibole crystallized in the same relative position as the pyroxenes, i.e. prior to the crystallization of the feldspars.

4.4.1 - Plagioclase

Samples of the Yardea Dacite contain euhedral to subhedral plagioclase phenocrysts which occur as both whole and fractured grains (Figure 4.1 d & e), as isolated grains or in glomeroporphyritic clots with pigeonite, augite, magnetite ± sanidine (Fig 4.1d, 4.2d). Normal zonation is ubiquitous and may be accompanied by some oscillatory zonation (Figure 4.1d). Occasionally plagioclase laths have resorbed cores (Figure 4.1f). Analysis of plagioclase compositions of the Yardea Dacite has been almost entirely restricted to the vitrophyre as those occuring in the main portion of the unit above the vitrophyre have undergone varying amounts of sericitization. Analyses reveal a limited range of compositions, with cores containing An $_{30-35}$ and rims An $_{25-31}$ (Table 4.2 and Figure

Figures opposite:

Figure 4.4a - Photomicrograph showing the typical subspherical morphology of primary igneous amphibole in the matrix of the Eucarro Dacite. Width of view is approximately 1 millimetre.

Figure 4.4b - Photomicrograph illustrating the blocky, irregular shape of amphibole in the matrix of the Eucarro Dacite where the grains are secondary and not of igneous origin. Width of view is approximately 1 millimetre.

Figure 4.4c - Photomicrograph illustrating the various secondary ferromagnesian phases which occur in the Eucarro Dacite. A large fe-Ti oxide grain (o) is rimmed by an inner rim of fibrous, colourless grunerite (g), and an outer rim of intergrown secondary calcic amphibole (h) and biotite (b). Width of view 4 millimetres.

Figure 4.4d - Photomicrograph of olivine phenocryst in Eucarro Dacite. Plane polarized light. Width of view 1.5 millimetres.

Figure 4.4e - Euhedral, zoned allanite (A) and fluorite (f) in the rhyodacitic portion of the Eucarro Dacite. Width of view is approximately 1 millimetre.

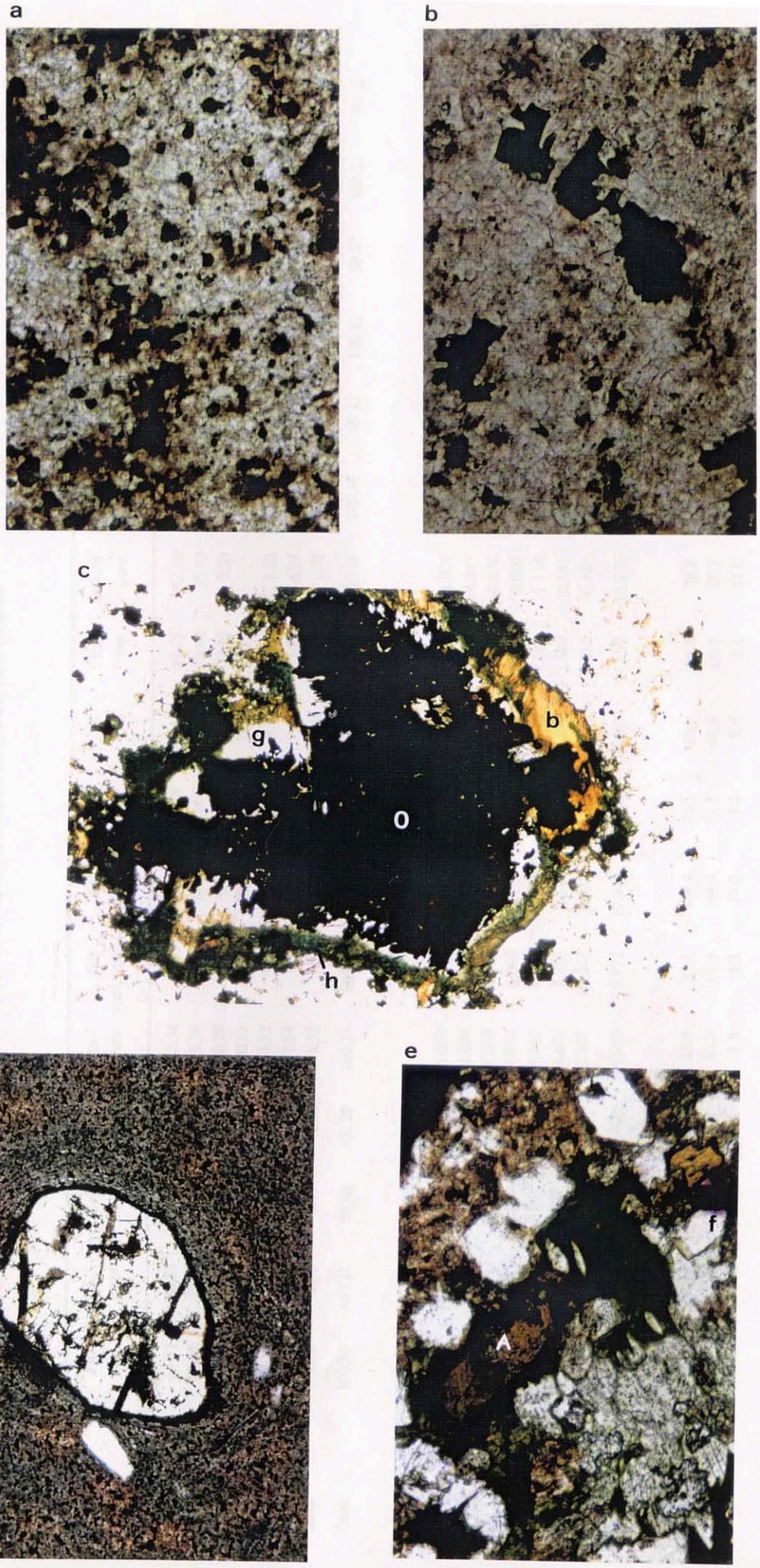
a
b
c
g
b
0
h
d
e
f
A

Table 4.2 - Representative plagioclase analyses, Eucarro and Yardea Dacites

Sample	*Eu7* *core*	*Eu7* *core*	*Eu7* *core*	*Eu7* *mid-grain*	*Eu7* *mid-grain*	*Eu7* *mid-grain*	*Eu7* *mid-grain*	*Eu7* *rim*	*Eu7* *rim*	*Eu7* *rim*	*849-36* *core*	*849-36* *core*	*849-36* *mid-grain*	*849-36* *mid-grain*	*849-36* *mid-grain*	*849-36* *rim*	*849-36* *rim*
SiO2	61.31	62.21	61.24	62.68	62.34	62.59	62.36	62.49	62.05	62.22	62.10	61.92	61.75	62.47	61.91	62.73	61.94
Al2O3	24.08	23.22	23.33	23.30	23.38	23.13	23.30	23.66	23.57	23.49	23.15	23.60	23.07	23.08	22.71	22.81	23.04
FeO	0.22	0.21	0.39	0.18	0.29	0.23	0.25	0.19	0.34	0.33	0.39	0.25	0.23	0.37	0.31	0.27	0.19
MgO	0.20				0.13		0.08		0.14	0.12							
CaO	6.12	5.40	6.07	4.96	4.92	4.81	5.01	5.14	5.14	5.32	5.83	6.11	5.53	5.25	5.46	5.33	5.34
Na2O	7.04	7.08	6.89	7.36	7.64	7.77	7.31	8.08	7.54	7.83	6.74	7.07	7.02	7.75	6.90	7.45	7.58
K2O	1.33	2.15	1.71	1.80	1.53	1.62	1.93	0.58	1.48	0.93	1.87	1.70	1.82	1.30	2.28	1.63	1.27
Total	100.30	100.27	99.63	100.28	100.23	100.15	100.24	100.14	100.26	100.24	100.08	100.65	99.42	100.22	99.57	100.22	99.36
							Structural formulae calculated to 32 O										
Si	10.905	11.080	10.989	11.124	11.076	11.128	11.091	11.067	11.029	11.042	11.075	10.992	11.078	11.104	11.116	11.153	11.094
Al	5.048	4.875	4.934	4.874	4.896	4.847	4.884	4.939	4.938	4.914	4.866	4.938	4.878	4.836	4.806	4.780	4.864
Fe	0.033	0.031	0.059	0.027	0.043	0.034	0.037	0.028	0.051	0.049	0.058	0.037	0.035	0.055	0.047	0.040	0.028
Mg	0.053	0.000	0.000	0.000	0.034	0.000	0.021	0.000	0.037	0.032	0.000	0.000	0.000	0.000	0.000	0.000	0.000
Ca	1.166	1.031	1.167	0.943	0.937	0.916	0.955	0.975	0.979	1.012	1.114	1.162	1.063	1.000	1.050	1.015	1.025
Na	2.428	2.445	2.397	2.533	2.632	2.679	2.521	2.775	2.599	2.694	2.331	2.434	2.442	2.671	2.402	2.568	2.633
K	0.302	0.488	0.391	0.407	0.347	0.367	0.438	0.131	0.336	0.211	0.425	0.385	0.416	0.295	0.522	0.370	0.290
Total	19.936	19.950	19.938	19.909	19.965	19.972	19.947	19.916	19.969	19.953	19.870	19.948	19.912	19.961	19.943	19.926	19.935
Mol per cent An	29.9	26.0	29.5	24.3	23.9	23.1	24.4	25.1	25.0	25.8	28.8	29.2	27.1	25.2	26.4	25.7	26.0
Ab	62.3	61.7	60.6	65.2	67.2	67.6	64.4	71.5	66.4	68.8	60.2	61.1	62.3	67.4	60.4	65.0	66.7
Or	7.7	12.3	9.9	10.5	8.9	9.3	11.2	3.4	8.6	5.4	11.0	9.7	10.6	7.4	13.1	9.4	7.4

Table 4.2 - (continued)

Sample	*Eu21 core*	*Eu20 core*	*Eu21 rim*	*Eu20 rim*	*Eu2 core*	*Eu2 core*	*Eu2 mid-grain*	*Eu2 mid-grain*	*Eu2 rim*	*Eu2 rim*	*Eu2 rim*	*Eu5 core*	*Eu5 core*	*Eu5 mid-grain*	*Eu5 mid-grain*	*Eu5 mid-grain*	*Eu5 rim*
SiO2	60.56	61.67	62.02	61.69	60.46	62.41	62.02	61.46	63.07	62.24	62.94	62.54	62.06	62.51	62.50	62.69	63.43
Al2O3	24.20	23.50	23.54	23.46	24.83	23.38	24.14	24.19	23.18	23.70	23.25	23.19	23.65	23.31	23.52	23.22	23.22
FeO	0.01	0.22	0.14	0.16	0.21	0.21		0.28		0.26	0.22	0.13	0.35	0.26	0.14	0.21	0.12
MgO	0.03															0.16	0.12
CaO	6.34	5.48	5.14	5.56	6.62	4.33	5.63	5.95	5.00	5.44	4.95	4.98	5.37	5.12	5.02	4.78	4.44
Na2O	7.39	6.99	7.32	7.36	7.50	7.95	7.73	7.73	8.54	8.03	8.47	7.54	7.62	7.57	7.72	8.33	8.53
K2O	1.38	2.00	1.67	1.63	0.57	0.74	0.71	0.67	0.39	0.62	0.49	1.78	1.21	1.51	1.18	0.61	0.48
Total	99.91	99.86	99.83	99.86	100.19	99.02	100.23	100.28	100.18	100.29	100.32	100.16	100.26	100.28	100.08	100.00	100.34
							Structural formulae calculated to 32 O										
Si	10.839	11.025	11.060	11.021	10.765	11.148	10.983	10.913	11.150	11.028	11.128	11.120	11.024	11.098	11.092	11.118	11.182
Al	5.105	4.952	4.948	4.940	5.211	4.922	5.039	5.063	4.830	4.949	4.845	4.860	4.952	4.878	4.920	4.854	4.825
Fe	0.001	0.033	0.021	0.024	0.031	0.031	0.000	0.042	0.000	0.039	0.033	0.019	0.052	0.039	0.021	0.031	0.018
Mg	0.008	0.000	0.000	0.000	0.000	0.000	0.000	0.000	0.000	0.000	0.000	0.000	0.000	0.000	0.000	0.042	0.032
Ca	1.216	1.050	0.982	1.064	1.263	0.829	1.068	1.132	0.947	1.033	0.938	0.949	1.022	0.974	0.955	0.908	0.839
Na	2.565	2.423	2.531	2.549	2.589	2.753	2.654	2.661	2.927	2.759	2.904	2.600	2.625	2.606	2.657	2.865	2.916
K	0.315	0.456	0.380	0.371	0.129	0.169	0.160	0.152	0.088	0.140	0.110	0.404	0.274	0.342	0.267	0.138	0.108
Total	20.049	19.939	19.922	19.970	19.989	19.852	19.905	19.962	19.943	19.947	19.957	19.952	19.949	19.937	19.910	19.956	19.918
Mol per cent An	29.7	26.7	25.2	26.7	31.7	22.1	27.5	28.7	23.9	26.3	23.7	24.0	26.1	24.8	24.6	23.2	21.7
Ab	62.6	61.7	65.0	64.0	65.0	73.4	68.4	67.5	73.9	70.2	73.5	65.8	66.9	66.4	68.5	73.2	75.5
Or	7.7	11.6	9.8	9.3	3.3	4.5	4.1	3.8	2.2	3.6	2.8	10.2	7.0	8.7	6.9	3.5	2.8

Table 4.2 - (continued)

Sample	*Y31 core*	*Y31 core*	*Y31 rim*	*Y31 rim*	*A2 core*	*A2 core (resorbed)*	*A2 core*	*A2 mid-grain*	*A2 mid-grain*	*A2 rim*	*A2 rim*	*WA4 core*	*WA4 core*	*WA4 mid-grain*	*WA4 mid-grain*	*WA4 mid-grain*	*WA4 rim*	*WA4 rim*
SiO2	61.29	60.89	61.33	61.33	60.54	60.39	60.40	60.18	59.87	60.63	61.00	60.67	61.02	60.35	60.19	60.68	61.06	60.83
Al2O3	23.99	25.09	24.09	24.18	23.59	24.94	24.96	23.70	25.12	24.04	24.63	24.51	24.52	24.62	24.99	24.80	24.16	24.12
FeO	0.30	0.30	0.32	0.39	0.22	0.21	0.44	0.25	0.24	0.37	0.14	0.21	0.27	0.27	0.26	0.22	0.19	0.21
MgO	0.09			0.13		0.19	0.10					0.19	0.15	0.10				0.16
CaO	5.99	6.85	6.22	6.14	6.36	6.99	6.79	6.75	7.05	6.85	6.33	6.38	6.44	6.65	6.72	6.64	5.84	5.89
Na2O	7.11	6.90	7.25	7.58	6.83	6.73	6.77	6.80	6.71	7.07	7.09	6.94	7.12	7.05	6.76	7.32	7.87	7.45
K2O	1.32	0.93	1.05	0.80	1.46	1.27	1.12	1.39	1.10	0.98	1.30	1.43	1.05	1.22	1.21	1.18	0.90	1.23
Total	100.09	100.96	100.26	100.55	99.00	100.72	100.58	99.07	100.09	99.94	100.49	100.33	100.57	100.26	100.13	100.84	100.02	99.89
							Structural formulae calculated to 32 O											
Si	10.924	10.764	10.910	10.881	10.924	10.727	10.738	10.869	10.696	10.845	10.835	10.809	10.829	10.768	10.742	10.766	10.888	10.872
Al	5.040	5.228	5.051	5.056	5.017	5.221	5.230	5.045	5.290	5.069	5.157	5.147	5.129	5.178	5.257	5.186	5.078	5.081
Fe	0.045	0.044	0.048	0.058	0.033	0.031	0.065	0.038	0.036	0.055	0.021	0.031	0.040	0.040	0.039	0.033	0.028	0.031
Mg	0.024	0.000	0.000	0.034	0.000	0.050	0.027	0.000	0.000	0.000	0.000	0.050	0.040	0.027	0.000	0.000	0.000	0.043
Ca	1.144	1.298	1.186	1.167	1.230	1.330	1.293	1.306	1.350	1.313	1.205	1.218	1.225	1.271	1.285	1.262	1.116	1.128
Na	2.457	2.365	2.501	2.608	2.390	2.318	2.334	2.381	2.324	2.452	2.442	2.398	2.450	2.439	2.339	2.518	2.721	2.582
K	0.300	0.210	0.238	0.181	0.336	0.288	0.254	0.320	0.251	0.224	0.295	0.325	0.238	0.278	0.275	0.267	0.205	0.280
Total	19.934	19.909	19.934	19.985	19.930	19.966	19.941	19.959	19.947	19.958	19.954	19.978	19.950	20.001	19.937	20.033	20.036	20.018
Mol per cent An	29.3	33.5	30.2	29.5	31.1	33.8	33.3	32.6	34.4	32.9	30.6	30.9	31.3	31.9	33.0	31.2	27.6	28.3
Ab	63.0	61.1	63.7	65.9	60.4	58.9	60.1	59.4	59.2	61.5	62.0	60.8	62.6	61.2	60.0	62.2	67.3	64.7
Or	7.7	5.4	6.1	4.6	8.5	7.3	6.5	8.0	6.4	5.6	7.5	8.2	6.1	7.0	7.1	6.6	5.1	7.0

4.5a). More calcic compositions, cores with up to An_{44} and rims up to An_{35}, are encountered in grains which are internal to some of the larger glomerphenocrysts (Table 4.4, Figure 4.2d). Compositions of plagioclases in the outer portions of these glomerophenocrysts are indistinguishable from the population of phenocrysts which occur as isolated grains within the groundmass (Table 4.4).

Plagioclase is present in the Eucarro Dacite as euhedral to slightly resorbed grains, which range from entire phenocrysts up to 6mm in length to small,broken, angular fragments (Figure 4.1g). Core to rim microprobe traverses of plagioclase phenocrysts in the Eucarro Dacite reveal quite complex zonation patterns, and markedly different compositional ranges for the amphibole bearing and the pyroxene ± olivine portions of the unit. In the pyroxene ± olivine bearing Eucarro cores range from An $_{24-31}$ and Or $_{5-12}$ with rim variation An $_{20-26}$ and Or_{3-10} (Figure 4.5a). An contents generally decrease in a regular manner from core to rim with minor oscillatory reverses, but accompanying this is a marked but irregular decrease in Or component (Figure 4.5b). Indeed some grains, with relatively low An cores, have decreases in Or of up to 8 mol per cent at almost constant An. This is somewhat contrary to the expected change in plagioclase composition of progressive increase in the Or component accompanied by depletion in the An component. A possible explanation for this behaviour is that the plagioclases are evolving along paths which are the result of two competing pathways as discussed by Nevaskil (1991); one which is driven by changing magma composition and involves a decrease in the An component and increase of the Or component, and another which results in a decrease of the Or component due to the expansion of the solvus with decreasing temperature. Relatively static Or levels in the interiors of some plagioclase phenocrysts implies that for part of the crystallization history a balance of the two pathways was maintained. In the later stages of crystallization of the Eucarro plagioclases domination of the latter pathway caused the observed decrease in Or component towards the grain rims with sometimes little change in the An component. Due to the typically poor preservation of plagioclase in the main part of the Eucarro sequence it cannot be determined if the same type of zoning occured in plagioclases deeper in the chamber, but it is considered that any magma cooling would be of lesser degree and slower, therefore plagioclases from deeper levels of the chamber would not be expected to show this zoning as strongly, if at all.

In contrast to the compositional variations noted above, where the Eucarro contains primary igneous amphibole and no pyroxene or olivine, the plagioclase phenocrysts have very much less Or component ; core compositions vary from An_{25-31}, Or_{3-4} and rims have An_{20-26} and Or $_{2-4}$, and there is decrease in Or from core to rim is minimal (Table 4.2 and Figure 4.5b). This is interpreted to indicate that the amphibole bearing portion of the Eucarro Dacite evolved in a cooler part of the magma chamber, the lower temperature resulting in less Or component being able to be accommodated in the plagioclase.

Figure opposite:

Figure 4.5a - Ternary projection of feldspar compositions of the Eucarro and Yardea Dacites. Symbols : filled circles = analyses from phenocrysts, open diamonds = analyses from grains interior to glomerophenocrysts.

Figure 4.5b- Ternary projection of feldspar compositions illustrating zoning seen in the feldspar. Symbols : filled circles = pyroxene bearing Eucarro Dacite, open triangles = amphibole bearing Eucarro Dacite.

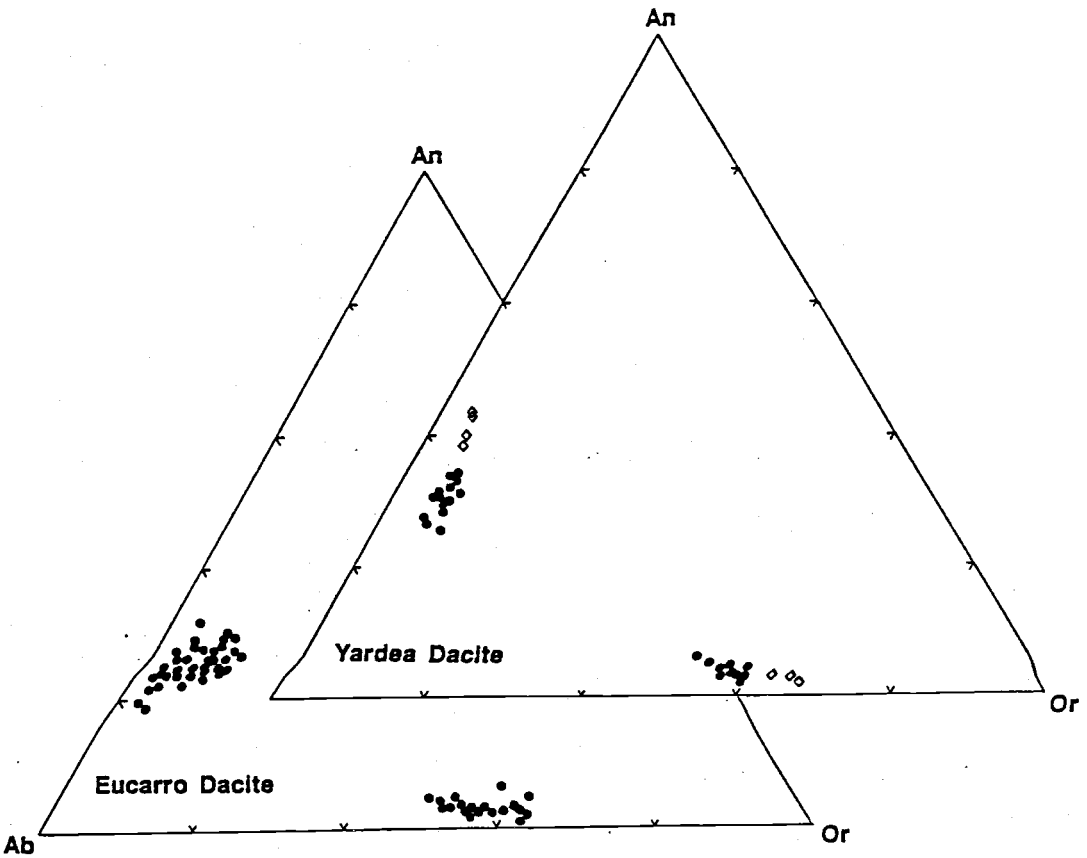
An
An
Yardea Dacite
Or
Eucarro Dacite
Ab
Or

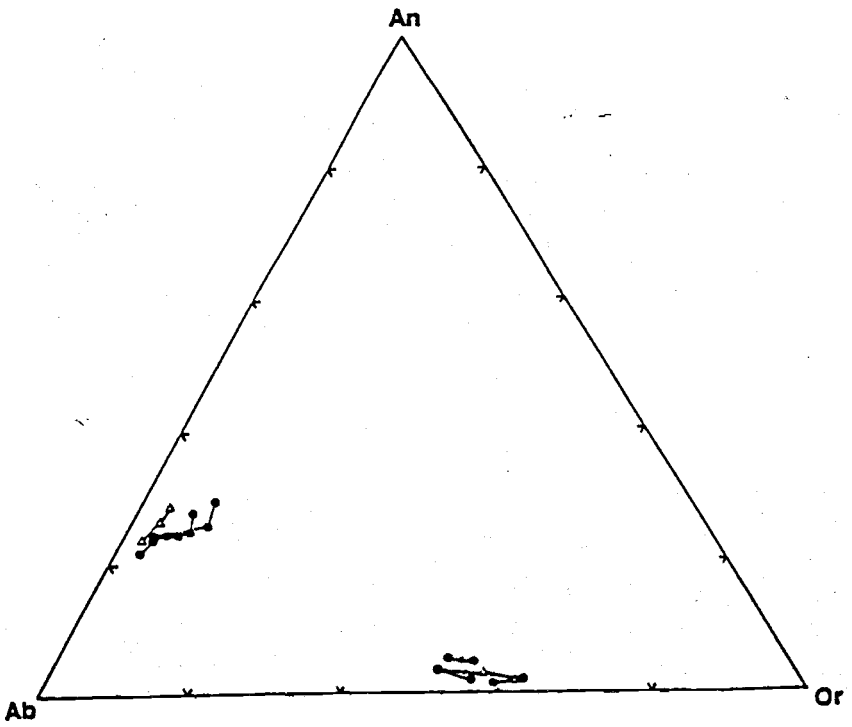
An
Ab
Or

Table 4.3 - Representative microprobe analyses of sanidine phenocrysts, Eucarro and Yardea Dacites

Sample	*Eu5* *p-r*	*Eu5* *p-m*	*Eu5* *p-c*	*Eu5* *p-r*	*Eu5* *p-m*	*Eu5* *p-m*	*Eu5* *p-c*	*Eu7* *p-c*	*Eu7* *p-m*	*Eu7* *p-r*	*Eu7* *p-c*	*Eu7* *p-m*	*Eu7* *p-r*	*Eu20* *Ep-c*	*Eu20* *Ep-c*	*Eu20* *Ep-m*	*Eu20* *Ep-r*	*849-70* *Ep-c*
SiO2	63.67	64.33	64.34	64.76	64.74	64.04	65.08	64.21	63.35	63.50	63.25	63.51	63.27	64.81	64.78	65.43	64.71	63.25
Al2O3	19.93	20.06	19.99	19.47	19.07	19.05	19.15	18.53	17.81	18.93	18.18	18.93	18.44	19.13	19.47	19.65	19.26	19.12
CaO	0.59	0.59	0.59	0.48	0.32	0.42	0.47	0.51	0.53	0.81	0.58	0.63	0.72	0.10	0.50	0.48	0.24	0.74
Na2O	5.50	5.57	5.49	5.08	5.05	4.92	5.01	4.95	5.13	5.75	5.26	5.40	5.54	5.86	6.39	6.67	6.62	6.76
K2O	9.16	8.91	8.79	9.76	10.18	9.90	9.73	10.09	10.08	9.13	9.77	9.49	9.31	9.66	8.71	8.45	8.91	8.56
BaO	0.59	0.80	0.81	0.64	0.73	0.71	0.77	1.00	0.95	1.07	0.97	0.97	0.76	0.48	0.76	0.80	0.60	1.00
Total	99.44	100.26	100.01	100.19	100.09	99.04	100.21	99.29	97.85	99.19	98.01	98.93	98.04	100.04	100.61	101.48	100.34	99.43
							Structural formulae (calculated to 32O)											
Si	11.668	11.686	11.705	11.784	11.824	11.806	11.840	11.853	11.888	11.735	11.838	11.759	11.804	11.812	11.740	11.744	11.761	11.666
Al	4.305	4.295	4.286	4.176	4.105	4.140	4.107	4.032	3.939	4.124	4.011	4.131	4.055	4.109	4.159	4.157	4.126	4.157
Ca	0.116	0.115	0.115	0.094	0.063	0.083	0.092	0.101	0.107	0.160	0.116	0.125	0.144	0.020	0.097	0.092	0.047	0.146
Na	1.954	1.962	1.937	1.792	1.788	1.759	1.767	1.772	1.867	2.060	1.909	1.939	2.004	2.071	2.246	2.321	2.333	2.418
K	2.141	2.065	2.040	2.265	2.371	2.328	2.258	2.376	2.413	2.152	2.332	2.241	2.216	2.246	2.013	1.935	2.066	2.014
Ba	0.042	0.057	0.058	0.046	0.052	0.051	0.055	0.072	0.070	0.077	0.071	0.070	0.056	0.034	0.054	0.056	0.043	0.072
Total	20.227	20.180	20.140	20.157	20.204	20.167	20.119	20.205	20.282	20.309	20.277	20.265	20.278	20.292	20.310	20.306	20.375	20.472
Mol per cent An	2.7	2.7	2.8	2.2	1.5	2.0	2.2	2.3	2.4	3.6	2.6	2.9	3.3	0.4	2.2	2.1	1.0	3.1
Ab	45.9	46.7	46.7	42.7	41.8	41.7	42.4	41.0	41.9	46.3	43.1	44.3	45.4	47.4	50.9	52.7	52.0	52.0
Or	50.3	49.2	49.2	54.0	55.5	55.2	54.1	55.0	54.1	48.4	52.7	51.2	50.1	51.4	45.7	43.9	46.0	43.3
Cn	1.0	1.4	1.4	1.1	1.2	1.2	1.3	1.7	1.6	1.7	1.6	1.6	1.3	0.8	1.2	1.3	1.0	1.6

Table 4.3 - (continued)

Sample	*849-70 Ep-m*	*849-70 Ep-r*	*849-70 Ep-c*	*849-70 Ep-m*	*849-70 Ep-r*	*849-70 p-c*	*849-70 p-m*	*849-70 p-r*	*Wa3 Ep-c*	*Wa3 Ep-m*	*Wa3 Ep-r*	*Wa3 p-c*	*Wa3 p-r*	*A2 Ep-c*	*A2 Ep-m*	*A2 Ep-r*	*A2 Ep-r*	*A2 Ep-c*
SiO2	64.44	64.61	64.27	63.95	63.12	64.69	63.37	64.87	63.60	63.39	63.21	62.73	62.80	64.65	64.74	65.45	64.07	63.28
Al2O3	18.97	19.08	18.86	18.99	19.01	18.94	19.03	18.95	18.77	18.47	18.81	18.20	18.31	18.62	18.50	18.44	18.85	18.36
CaO	0.45	0.89	0.67	0.77	0.64	0.60	0.71	0.58	0.70	0.67	0.78	0.69	0.63	0.67	0.62	0.56	0.74	0.63
Na2O	9.39	7.27	6.46	6.52	6.46	6.45	6.61	6.38	5.07	4.87	5.26	4.95	4.84	5.74	5.82	5.78	5.68	5.76
K2O	6.28	8.06	8.81	8.66	8.85	8.90	8.89	8.81	9.68	9.93	9.77	9.85	10.17	9.32	9.43	9.68	6.36	9.34
BaO	0.99	0.35	1.06	1.02	0.90	0.90	0.91	0.86	0.94	1.00	0.59	1.13	1.00	1.05	0.97	0.75	1.50	1.35
Total	100.52	100.26	100.13	99.91	98.98	100.48	99.52	100.45	98.76	98.33	98.42	97.55	97.75	100.05	100.08	100.66	97.20	98.72
									Structural formulae (calculated to 32O)									
Si	11.690	11.732	11.759	11.724	11.689	11.776	11.682	11.794	11.792	11.821	11.755	11.815	11.806	11.831	11.846	11.888	11.892	11.789
Al	4.056	4.084	4.067	4.104	4.150	4.064	4.135	4.061	4.102	4.060	4.123	4.040	4.057	4.016	3.990	3.948	4.124	4.032
Ca	0.087	0.173	0.131	0.151	0.127	0.117	0.140	0.113	0.139	0.134	0.155	0.139	0.127	0.131	0.122	0.109	0.147	0.126
Na	3.303	2.560	2.292	2.318	2.320	2.277	2.363	2.249	1.823	1.761	1.897	1.808	1.764	2.037	2.065	2.036	2.044	2.081
K	1.453	1.867	2.056	2.025	2.090	2.066	2.090	2.043	2.289	2.362	2.317	2.366	2.439	2.176	2.201	2.243	1.506	2.219
Ba	0.070	0.025	0.076	0.073	0.065	0.064	0.066	0.061	0.068	0.073	0.043	0.083	0.074	0.075	0.070	0.053	0.109	0.099
Total	20.660	20.440	20.381	20.395	20.441	20.364	20.477	20.322	20.213	20.211	20.291	20.252	20.267	20.267	20.292	20.277	19.821	20.345
Mol per cent An	1.8	3.7	2.9	3.3	2.8	2.6	3.0	2.5	3.2	3.1	3.5	3.2	2.9	3.0	2.7	2.5	3.9	2.8
Ab	67.2	55.4	50.3	50.7	50.4	50.3	50.7	50.4	42.2	40.7	43.0	41.1	40.1	46.1	46.3	45.8	53.7	46.0
Or	29.6	40.4	45.1	44.3	45.4	45.7	44.9	45.7	53.0	54.6	52.5	53.8	55.4	49.2	49.4	50.5	39.6	49.1
Cn	1.4	0.5	1.7	1.6	1.4	1.4	1.4	1.4	1.6	1.7	1.0	1.9	1.7	1.7	1.6	1.2	2.9	2.2

Analytical conditions for the sanidine analyses were 20kV acceleration voltage, beam current of 30nA and a 10-20um spot size on a JEOL 733 microprobe using wavelength dispersive spectrometers
p denotes grain analysed is a phenocryst
E denotes an euhedral grain
-c, -m, -r denote analyses of core, mid-grain and rim areas respectively

Ba and Sr concentrations were measured in Eucarro and Yardea plagioclases using wave length dispersive spectrometers on a JEOL 733 microprobe. Concentrations of these trace elements in the plagioclases of both units were similar with average Sr levels of 550 and 675 ppm Sr and average Ba contents of 750 and 800ppm for Eucarro and Yardea plagioclases respectively. No difference was noted in Sr and Ba levels between plagioclases from the amphibole bearing versus the pyroxene±olivine bearing Eucarro Dacite. It should be noted that some of these analyses, particularly for Sr, were often approaching the detection limits and must be considered to be a crude estimate of true values.

In summary the observed correlation between plagioclase composition and mafic silicate type for samples of very similar composition is related to the different thermal history of the amphibole bearing Eucarro Dacite compared with the pyroxene phyric part of the unit.

4.4.2 - Alkali Feldspar

The alkali feldspars of the Yardea are euhedral to partly resorbed grains, a few of which are fractured. Preservation is best in the vitrophyre. In the main part of the unit they tend to be oxidized and sericitized and many have undergone a chequerboard unmixing to almost pure albite and orthoclase endmembers with loss of Ca, although some cores remain relatively unaltered. For this reason most analyses are from the vitrophyre. The analyzed compositional range is Or_{54-68} (Figure 4.5a) with most grains exhibiting normal core to rim zonation (Table 4.3, Figure 4.5b). The variation in any one grain is rarely more than Or_4. Small interstitial grains (<50μm) contained within the interior of reasonably large glomerophenocrysts are more Or rich than either individuals within the groundmass or grains on the outside of glomerophenocrysts (Table 4.4), indicating a trend towards more sodic sanidine with fractionation. Ba contents are uniformly high, averaging approximately 9,000ppm. The celesian component of the Yardea sanidines ranges from $Cn_{1-2.4}$.

Alkali feldspars in the Eucarro Dacite are present dominantly as euhedral phenocrysts up to 8 mm in length. Broken fragments are less common, occurring in specific areas of some samples. Preservation of the alkali feldspars within the Eucarro Dacite is similar to those in the Yardea, with very few unaltered grains occurring in much of the unit, but with well preserved grains found in the 'vitrophyre' and some samples from the lower section. These alkali feldspars are sanidine, many of which show oscillatory zoning (Figure 4.5b). Within individual samples, compositional variation between different grains is often greater than core to rim zonation in any individual grain. Most analyses of sanidine in the Eucarro fall within the compositional range compositional ranges Or_{40-55} and $An_{1-3.5}$ (Table 4.4). Representative analyses of Eucarro

sanidines in Table 4.4 show up to 1.7 per cent of celesian. Ba concentrations in the Eucarro sanidines are considerably more variable than in the Yardea, ranging from approximately 3,000ppm to 9,600ppm, and the average Ba content is ≈7,000ppm. Unlike the plagioclases, there is little compositional difference between alkali feldspars in the amphibole and pyroxene phyric Eucarro Dacite samples (Figure 4.5b).

4.4.3 - Pyroxene

Pyroxene was a ubiquitous phenocryst phase in all of the preserved section of the Yardea Dacite. Both pigeonite and augite were originally present throughout the erupted unit as euhedral to subhedral grains up to 2mm in length. Augite is fresh in the vitrophyre and partly to wholly preserved in almost all sections examined from the rest of the unit. Where alteration has occured, chlorite has replaced augite. Pigeonite has been preserved only in the vitrophyre, above which it is altered to chlorite, however its ubiquitous presence as a phenocryst phase is indicated by the preservation of herringbone exsolution textures by replacement chlorite (Figure 4.2g).These herringbone textures are common in the main part of the Yardea and totally absent in the vitrophyre, which substantiates the idea that the interior of the unit cooled slowly, allowing augite to exsolve from pigeonite along the (001) plane. Occasionally augite lamellae are preserved in these chlorite hosts (Figure 4.2f). Some of these lamellae have compositions indicating that they are products of high temperature exsolution, plotting on the pyroxene quadrilateral within the main spread of analyses. However other augite lamellae have compositions which suggest they were formed by exsolution at lower temperatures during cooling of the unit.

Pyroxene compositions in the Yardea exhibit little compositional variation, as shown by analyses listed in Table 4.5 and plotted in Figure 4.6, which is consistent with the chemical homogeneity of the unit (Chapter 5). The single exception to this is the relatively large range of augite compositions obtained from sample Y19 (pigeonite in this sample from the vitrophyre has been replaced by chlorite). As illustrated in Figure 4.6 these compositions extend from the main Yardea population to much more iron rich compositions along a trend which indicates cooling of up to 100°C associated with the iron enrichment. This sample of the Yardea Dacite has unusual chemical and isotopic characteristics and is thought to represent Yardea magma contaminated at the roof of the chamber (see Chapter 5), contamination which resulted in the observed disequilibrium pyroxene assemblage. Zoning in the Yardea pyroxene phenocrysts is uncommon and where present is seen as an increase in Wo_{1-2} and $Fs_{\leq 1}$ from core to rim. Groundmass pyroxenes often have slightly higher Fs components than phenocrysts from the same sample, indicating that iron enrichment of pyroxenes accompanied chemical differentiation.

Table 4.4 - Comparative compositions of feldspar grains from inner and outer portions of glomerophenocrysts and isolated phenocrysts from the Yardea Dacite (sample WA4)

Plagioclase

	Phenocrysts within glomerophenocrysts				*Grains on edge of glomerophenocrysts*		*Isolated phenocrysts within the sample WA4*							
			Core	*Rim*			*Cores*			*Mid-grain*		*Rims*		
SiO2	56.64	58.39	56.93	59.33	60.24	61.78	60.26	60.33	60.07	60.35	60.33	60.80	60.85	61.06
Al2O3	27.03	26.07	26.71	25.21	24.69	23.65	24.76	24.31	25.03	24.62	25.01	24.49	24.60	24.16
FeO	0.25	0.34	0.24	0.41	0.27	0.42	0.17	0.28	0.27	0.27	0.17	0.14	0.19	0.19
MgO	0.00	0.10	0.16	0.11	0.12	0.13	0.00	0.00	0.00	0.10	0.09	0.00	0.00	0.00
CaO	9.16	8.04	8.95	6.95	6.64	5.53	6.64	6.26	7.09	6.65	6.77	6.25	6.34	5.84
Na2O	6.13	6.50	6.16	6.75	6.98	7.73	7.23	7.13	7.02	7.05	6.83	7.31	7.27	7.87
K2O	0.71	0.93	0.74	1.11	1.21	1.14	0.96	1.28	1.12	1.22	1.15	1.23	1.20	0.90
Total	99.92	100.37	99.89	99.87	100.15	100.38	100.02	99.59	100.60	100.26	100.35	100.22	100.45	100.02
Si	10.212	10.449	10.260	10.640	10.758	10.979	10.762	10.827	10.695	10.768	10.739	10.834	10.820	10.888
Al	5.744	5.499	5.674	5.329	5.197	4.954	5.212	5.142	5.253	5.178	5.248	5.144	5.156	5.078
Fe	0.038	0.051	0.036	0.062	0.040	0.062	0.025	0.042	0.040	0.040	0.025	0.021	0.028	0.028
Mg	0.000	0.027	0.043	0.029	0.032	0.034	0.000	0.000	0.000	0.027	0.024	0.000	0.000	0.000
Ca	1.770	1.542	1.728	1.336	1.271	1.053	1.271	1.204	1.353	1.271	1.291	1.193	1.208	1.116
Na	2.143	2.256	2.153	2.347	2.417	2.664	2.504	2.481	2.423	2.439	2.358	2.526	2.507	2.721
K	0.163	0.212	0.170	0.254	0.276	0.258	0.219	0.293	0.254	0.278	0.261	0.280	0.272	0.205
Total	20.070	20.035	20.064	19.996	19.990	20.005								
Mol per cent An	43.4	38.5	42.7	33.9	32.1	26.5	31.8	30.3	33.6	31.9	33.0	29.8	30.3	27.6
Ab	52.6	56.3	53.1	59.6	61.0	67.0	62.7	62.4	60.1	61.2	60.3	63.2	62.9	67.3
Or	4.0	5.3	4.2	6.4	7.0	6.5	5.5	7.4	6.3	7.0	6.7	7.0	6.8	5.1

Sanidine

	Small interstitial grains within glomerophenocrysts		*Isolated phenocrysts within groundmass*								
			Cores			*Mid-grain*			*Rims*		
SiO2	65.69	65.79	66.24	66.17	66.16	65.09	63.59	66.32	66.18	66.21	66.10
TiO2	0.00	0.00	0.23	0.17	0.33	0.23	0.88	0.34	0.00	0.27	0.56
Al2O3	19.04	18.74	19.20	19.28	19.24	18.82	19.40	19.16	19.12	19.06	19.81
FeO	0.27	0.63	0.00	0.00	0.00	0.00	0.00	0.00	0.00	0.00	0.00
CaO	0.46	0.39	0.42	0.56	0.55	0.52	0.79	0.41	0.56	0.50	0.70
K2O	11.12	11.44	9.93	9.98	9.57	9.43	9.14	9.87	9.68	9.75	9.35
Na2O	3.54	3.40	4.09	4.12	4.34	4.19	4.33	4.14	4.43	4.22	4.37
Total	100.12	100.39	100.11	100.28	100.19	98.28	98.13	100.24	99.97	100.01	100.89
Si	11.924	11.945	11.964	11.937	11.945	11.965	11.806	11.972	11.949	11.973	11.872
Al	4.074	4.010	4.087	4.100	4.095	4.078	4.246	4.077	4.069	4.062	4.194
Fe	0.041	0.096	0.000	0.000	0.000	0.000	0.000	0.000	0.000	0.000	0.000
Mg	0.000	0.000	0.000	0.000	0.000	0.000	0.000	0.000	0.000	0.000	0.000
Ca	0.090	0.076	0.081	0.108	0.106	0.102	0.157	0.079	0.108	0.097	0.135
Na	1.246	1.197	1.432	1.441	1.519	1.493	1.559	1.449	1.551	1.480	1.522
K	2.575	2.649	2.288	2.296	2.204	2.211	2.165	2.273	2.229	2.249	2.142
Total	19.949	19.973	19.853	19.882	19.869	19.849	19.932	19.850	19.907	19.861	19.864
Mol per cent An	2.3	1.9	2.1	2.8	2.8	2.7	4.1	2.1	2.8	2.5	3.5
Ab	31.9	30.5	37.7	37.5	39.7	39.2	40.2	38.1	39.9	38.7	40.1
Or	65.8	67.5	60.2	59.7	57.5	58.1	55.8	59.8	57.3	58.8	56.4

Analytical methods as listed in table 4.3. Structural formulae calculated to 32 O.

Augite overgrowths on pigeonite are common (Figure 4.2a-c), but the reverse relationship is never seen, indicating that pigeonite preceded augite in the crystallization sequence. Irregular remnants of pigeonite can be seen preserved within augite phenocrysts (Figure 4.2c). For any particular sample these remnants are typically more magnesian than unexsolved phenocrystic pigeonite, indicating that pigeonite formed earlier in the crystallization history became unstable, being replaced with augite. Both pyroxenes are also present as small grains ($\leq 70\mu m$) in the groundmass (Figure 4.3c), therefore it seems that they were both phases crystallized from the magma for much of its crystallization history.

Exsolution textures of the Yardea pyroxenes are best studied in the vitrophyre where pigeonite lamellae hosted in augite and the converse both occur (Figure 4.3a & b). The lamellae vary in thickness, with relatively coarse examples (e.g. Figure 4.2e and 4.3a & b) almost certainly having formed during the magmas residence in its reservoir prior to eruption, whereas very fine lamellae (e.g. those in the pigeonite in Figure 4.2c) may have formed either before or after eruption. All lamellae which are thick enough to analyse by electron microprobe are compositionally similar to the main pyroxene populations which may indicate they all formed at high temperature, probably within the magma chamber. The presence of these lamellae therefore indicate re-equilibration of earlier formed pyroxene in response to a decrease in temperature within the magma chamber. Further cooling of the pyroxenes upon eruption was rapid and resulted in the avoidance, at least in the vitrophyre, of the pigeonite $\rightarrow$ orthopyroxene reconstructive transformation. The effect of further cooling can be seen in the pyroxenes however, by the occurrence of fine augite lamellae within the coarse, earlier formed pigeonite lamellae (Figure 4.3b). Although these secondary lamellae are too fine for their exact composition to be analysed, their presence is indicated by the displacement of analyses along a mixing chord between the compositions of the coarser pigeonite lamellae and the co-existing augite host.

Most samples of the Eucarro Dacite are, or were before alteration, pyroxene bearing, containing euhedral pigeonite and augite phenocrysts up to 1mm in length (Figure 4.3d). Textural evidence indicates that pigeonite began crystallizing before augite. Pigeonite is preserved only in the vitrophyre, however the common occurrence of herring-bone exsolution textures pseudomorphed by chlorite indicate that pigeonite was a phenocryst phase throughout the unit. Augite is preserved in the vitrophyre, and in the lower and upper parts of the unit which are interpreted to have cooled relatively rapidly and are identified by their chocolate brown colour in hand specimen. No preserved pyroxenes have been found in samples from the central section of the Eucarro Dacite which has a microgranophyric matrix, reddened by the oxidation of iron contained in the matrix.

Figure opposite:

Figure 4.6 - Projection of Eucarro and Yardea Dacite pyroxenes onto the pyroxene quadrilateral. Pyroxenes were recalculated according to and isotherms taken from Lindsley (1983). Symbols : filled circles = Yardea Dacite, open circles = sample 884-Y19, filled diamonds = unexsolved pyroxenes from Eucarro Dacite, open diamonds = re-integrated compositions of finely exsolved pyroxenes from Eucarro Dacite.

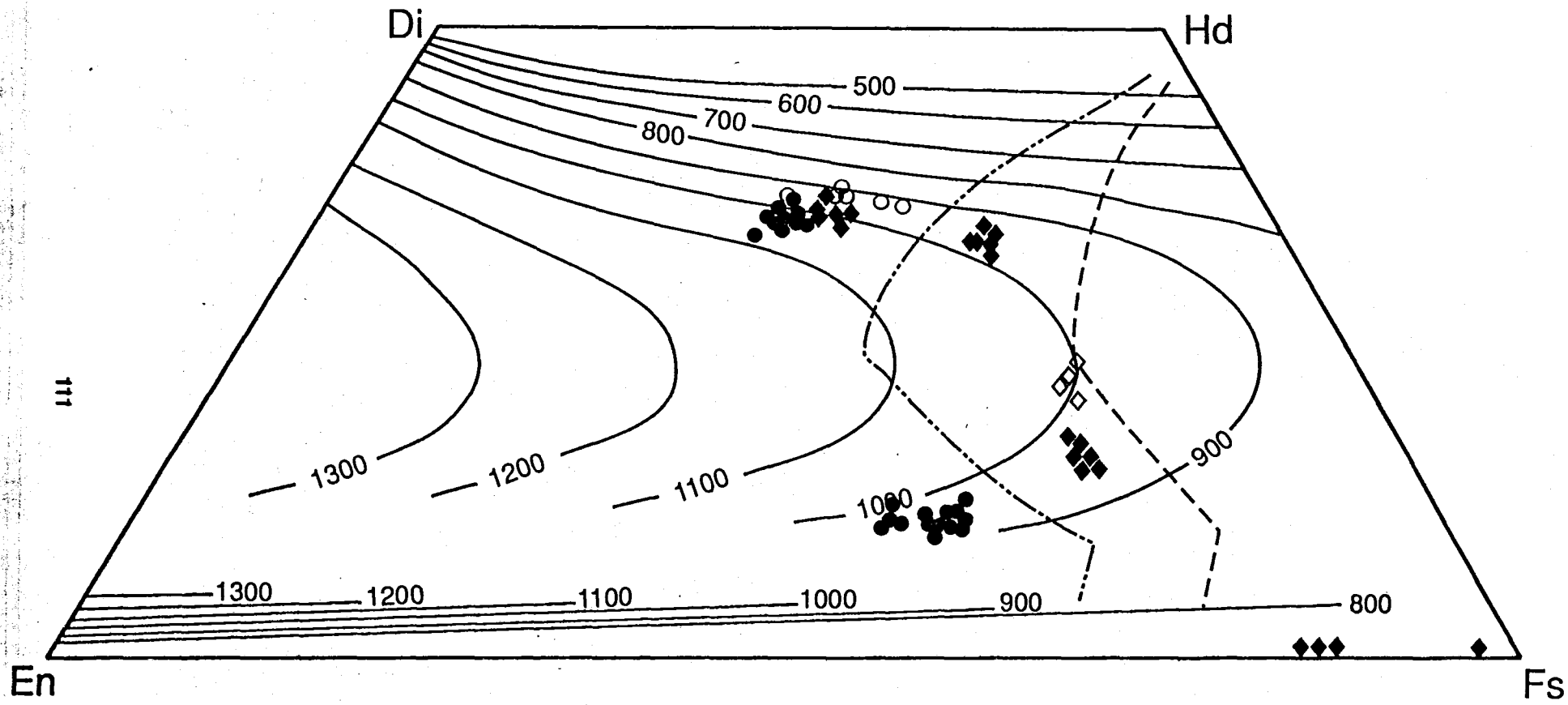
Di
Hd
En
Fs
500
600
700
800
900
1000
1100
1200
1300
1300
1200
1100
1000
900
800

Table 4.5 - Representative pyroxene analyses from the Eucarro and Yardea Dacites

Sample	*Y4 (m) aug*	*Y4 (m) aug*	*Y5 (m) aug - c*	*Y5 (m) aug - r*	*Y12 (m) aug*	*Y12 (m) aug*	*Y19(v) aug - c*	*Y19(v) aug - r*	*Y19(v) aug in plag*	*Y19(v) aug*	*Y31(v) pig a/s*	*Y31(v) aug f lam*	*Y31(v) pig a/s*	*Y31(v) aug no lam*	*Y31(v) pig gm a/s*	*Wa3(v) pig gm*	*Wa3(v) pig*	*Wa3(v) aug*	*Wa3(v) aug < a/s*
SiO2	50.10	50.32	50.18	50.47	49.71	50.48	49.31	50.14	50.84	50.29	49.67	50.02	49.60	50.67	49.21	49.07	49.06	49.84	50.15
TiO2	0.40	0.60	0.56	0.46	0.37	0.36	0.30	0.36	0.36	0.42	0.23	0.47	0.26	0.29	0.01	0.19	0.28	0.39	0.20
Al2O3	1.66	1.51	1.36	1.35	1.14	1.24	0.94	0.97	1.63	0.93	0.61	1.44	0.78	1.32	0.71	0.75	0.61	1.58	1.49
FeO	17.97	19.06	18.31	17.60	18.04	17.13	21.61	19.20	17.99	20.19	30.88	17.79	30.16	18.93	32.15	33.49	33.19	19.45	17.46
Fe2O3	1.26	0.53	1.30	1.50	1.04	1.67	0.83	1.09	0.35	0.00	0.50	1.79	0.69	0.73	1.09	0.78	0.39	0.49	2.53
MnO	0.86	0.75	0.78	0.85	1.09	1.17	1.30	1.11	0.76	1.16	1.13	0.73	1.16	0.78	1.63	1.65	1.39	0.84	0.74
MgO	10.95	10.58	10.40	10.99	10.22	10.42	7.93	9.29	10.19	8.93	12.90	10.46	12.68	10.64	11.33	10.44	11.44	10.64	10.64
CaO	16.85	17.19	17.17	17.31	18.10	18.06	17.30	17.80	18.73	18.02	4.09	17.28	4.53	17.30	3.94	4.19	3.66	16.14	17.23
Na2O	0.07	0.00	0.19	0.12	0.00	0.17	0.00	0.13	0.00	0.00	0.00	0.20	0.00	0.00	0.00	0.00	0.00	0.00	0.23
Total	100.12	100.54	100.25	100.65	99.71	100.70	99.52	100.09	100.85	99.94	100.01	100.18	99.86	100.66	100.07	100.56	100.02	99.37	100.67
Mg/(Mg+Fe2+)	52.1	49.7	50.3	52.7	50.2	52.0	39.5	46.3	50.0	44.1	42.7	51.1	42.8	50.0	38.6	35.7	38.1	49.4	52.0
Si	1.935	1.941	1.941	1.939	1.939	1.942	1.957	1.956	1.948	1.968	1.964	1.935	1.962	1.951	1.964	1.962	1.963	1.945	1.931
Ti	0.012	0.017	0.016	0.013	0.011	0.010	0.009	0.010	0.100	0.012	0.007	0.014	0.008	0.008	0.000	0.006	0.008	0.012	0.006
Al	0.076	0.069	0.062	0.061	0.052	0.056	0.044	0.045	0.740	0.043	0.029	0.066	0.036	0.060	0.034	0.035	0.029	0.073	0.068
Fe2+	0.580	0.615	0.592	0.565	0.589	0.551	0.717	0.626	0.583	0.661	1.021	0.576	0.997	0.610	1.073	1.120	1.110	0.635	0.562
Fe3+	0.037	0.015	0.038	0.043	0.030	0.048	0.025	0.032	0.010	0.000	0.015	0.052	0.021	0.021	0.033	0.024	0.012	0.014	0.073
Mn	0.028	0.025	0.026	0.028	0.036	0.038	0.044	0.037	0.025	0.039	0.038	0.024	0.039	0.025	0.055	0.056	0.047	0.028	0.024
Mg	0.630	0.608	0.599	0.629	0.594	0.598	0.469	0.540	0.582	0.521	0.760	0.603	0.747	0.611	0.674	0.622	0.682	0.619	0.610
Ca	0.697	0.710	0.711	0.713	0.757	0.745	0.735	0.744	0.769	0.755	0.173	0.716	0.192	0.714	0.169	0.179	0.157	0.675	0.711
Na	0.005	0.000	0.014	0.009	0.000	0.013	0.000	0.010	0.000	0.000	0.000	0.015	0.000	0.000	0.000	0.000	0.000	0.000	0.017
Wo	33.0	34.3	35.0	34.3	36.3	36.1	35.5	36.5	36.9	37.3	10.2	34.7	11.7	34.1	11.0	11.7	9.8	32.1	33.6
En	34.9	32.7	32.7	34.6	32.0	33.2	25.5	29.4	31.5	27.6	38.3	33.4	37.8	33.0	34.3	31.5	34.3	33.5	34.6
Fs	32.1	33.0	32.3	31.1	31.7	30.7	39.0	34.1	31.6	35.1	51.5	31.9	50.5	32.9	54.7	56.7	55.9	34.4	31.8

Table 4.5 (continued)

Sample	*Wa3 (v) pig a/s*	*Wa4 (v) pig rem in aug*	*Wa4 (v) aug<*	*Wa4 (v) pig*	*Wa4 (v) aug*	*A2 (v) pig a/s*	*A2 (v) aug a/s*	*A2 (v) pig a/s*	*A2 (v) pig gm*	*Y32 (m) aug a/s*	*Y32 (m)*	*Y45 (m)*	*Y45 (m)*	*Y46 (m)*	*Y46 (m)*	*Y47 (m)*	*Y47 (m)*	*Y49 (m) core*	*Y49 (m) <rim*
SiO2	49.80	48.98	50.22	49.35	50.57	49.43	50.66	49.35	49.20	50.20	50.39	49.94	50.13	50.01	50.13	50.50	50.09	49.95	49.99
TiO2	0.12	0.12	0.41	0.19	0.35	0.25	0.39	0.25	0.11	0.28	0.33	0.26	0.41	0.44	0.25	0.43	0.39	0.49	0.14
Al2O3	0.48	0.53	1.31	0.54	1.34	0.71	1.21	0.46	0.45	1.64	1.42	1.46	1.60	1.34	1.46	1.46	1.39	1.55	1.50
FeO	30.42	31.82	17.65	33.02	17.76	31.45	18.47	32.55	32.97	18.09	17.75	18.17	17.07	17.93	16.64	19.21	17.37	17.37	17.25
Fe2O3	0.52	0.02	1.22	0.72	0.89	0.61	0.80	0.34	0.49	0.80	1.24	1.68	2.01	1.86	2.50		1.83	1.98	1.92
MnO	1.32	1.38	1.03	1.42	1.01	1.20	0.69	1.25	1.54	0.93	0.70	0.98	0.97	0.89	0.9	0.77	0.84	0.7	0.73
MgO	12.94	11.72	10.13	10.83	10.41	12.09	10.82	11.93	11.26	10.16	10.99	10.6	10.8	10.5	10.6	10.7	11.0	10.8	10.8
CaO	4.46	3.56	17.92	3.72	17.56	4.15	17.53	3.87	3.93	17.85	17.07	17.05	16.95	16.98	17.46	16.95	17.13	17.09	17.29
Na2O	0.00	0.00	0.16	0.14	0.20	0.00	0.00	0.04	0.00	0.06	0.12	0.00	0.29	0.25	0.28	0.00	0.17	0.20	0.15
Total	100.06	98.13	100.05	99.93	100.09	99.89	100.57	100.04	99.95	100.01	100.00	100.17	100.20	100.20	100.26	100.00	100.17	100.13	99.79
Mg/(Mg+Fe2+)	43.1	39.6	50.6	36.9	51.1	40.7	51.1	39.5	37.8	50.0	52.3	51.0	52.9	51.1	53.3	49.8	52.9	52.6	51.1
Si	1.968	1.983	1.946	1.976	1.954	1.965	1.950	1.967	1.971	1.945	1.945	1.935	1.933	1.936	1.934	1.955	1.934	1.929	1.937
Ti	0.003	0.004	0.012	0.006	0.010	0.008	0.011	0.007	0.003	0.008	0.009	0.008	0.012	0.013	0.007	0.013	0.011	0.014	0.004
Al	0.022	0.025	0.060	0.025	0.061	0.033	0.055	0.022	0.021	0.075	0.065	0.067	0.073	0.061	0.066	0.066	0.063	0.071	0.068
Fe2+	1.005	1.078	0.572	1.106	0.574	1.045	0.595	1.085	1.105	0.586	0.576	0.589	0.551	0.581	0.537	0.622	0.561	0.561	0.599
Fe3+	0.015	0.001	0.035	0.022	0.026	0.018	0.023	0.010	0.015	0.023	0.036	0.049	0.058	0.054	0.073		0.053	0.058	0.056
Mn	0.044	0.047	0.034	0.048	0.033	0.040	0.023	0.042	0.052	0.031	0.023	0.032	0.032	0.029	0.029	0.025	0.027	0.023	0.024
Mg	0.762	0.707	0.585	0.646	0.600	0.716	0.621	0.709	0.672	0.587	0.632	0.614	0.619	0.606	0.612	0.616	0.631	0.622	0.625
Ca	0.189	0.155	0.744	0.160	0.727	0.177	0.723	0.165	0.169	0.741	0.706	0.708	0.700	0.704	0.722	0.703	0.709	0.707	0.718
Na	0.000	0.000	0.012	0.011	0.015	0.000	0.000	0.003	0.000	0.004	0.009	0.000	0.022	0.019	0.021	0.000	0.013	0.015	0.011
Wo	10.8	10.3	36.3	12.3	35.8	11.0	34.8	10.1	10.4	35.3	33.9	32.9	34.0	34.4	34.5	34.1	34.0	34.0	33.8
En	38.5	35.6	32.2	32.3	32.8	36.2	33.3	35.5	33.9	32.4	34.6	34.2	34.9	33.5	34.9	32.8	34.9	34.7	34.9
Fs	50.7	54.2	31.5	55.4	31.4	52.8	31.9	54.4	55.7	32.3	31.5	32.9	31.1	32.1	30.6	33.1	31.0	31.3	31.2

Conditions for microprobe analysis for all pyroxenes were 15kV and beam current 5nA.
Ternary components and Fe2O3 were calculated according to the method of Lindsley (1983)
-c and -r denote analyses from the core and rim of phenocrysts respectively, gm indicates the analysis is of a groundmass grain
a/s denotes the analysis was done using an area scan rather than a spot technique to minimise error induced by extremely fine lamellae which were not able to be analysed.
Arrowheads are used to indicate that adjacent analyses are from the same grain
(v) and (m) indicate the sample is from the vitrophyre or main portion of the unit respectively

Table 4.5 - Representative pyroxene analyses from the Eucarro and Yardea Dacites (continued)

Sample	*Eu10 (m) aug core*	*Eu10 (m) aug <rim*	*Eu10 (m)*	*Eu10 (m)*	*Eu7 (v)*	*Eu7 (v)*	*Eu7 (v)*	*Eu21 (m)*	*Eu20 (v)*	*Eu20 (v)*	*Eu20 (v) gm*	*849-36(v) gm*	*849-36(v)*	*849-36(v)*	*849-36(v)*	*849-36(v)*	*849-36(v)*
SiO2	49.57	49.86	50.12	49.81	48.33	49.19	49.58	48.96	47.34	48.50	48.77	47.89	49.17	49.06	47.57	48.36	49.67
TiO2	0.26	0.47	0.29	0.16	0.19	0.48	0.29	0.46	0.13	0.36	0.31	0.20	0.31	0.32	0.26	0.25	0.31
Al2O3	1.08	1.30	1.35	1.17	0.78	1.15	1.14	1.20	0.69	1.09	1.21	0.49	0.85	0.88	0.66	0.75	1.17
FeO	18.71	20.88	19.71	19.08	36.25	26.54	25.85	26.13	35.51	24.73	25.55	37.55	24.83	26.79	35.56	35.74	24.85
Fe2O3	2.31	0.18	1.39	2.25	0.38	0.03	0.18		1.44	1.86	1.31		2.04		0.51	0.23	
MnO	1.33	1.17	1.13	1.01	1.80	1.07	1.19	1.28	2.04	1.20	1.02	1.60	0.96	1.19	1.74	1.42	1.07
MgO	9.08	8.98	9.15	9.33	7.20	6.11	6.63	5.44	7.18	6.67	6.22	6.55	5.95	6.22	7.26	7.51	6.40
CaO	17.45	16.99	17.33	17.13	5.51	15.77	15.47	16.51	5.48	15.40	15.53	5.45	16.06	15.58	5.45	5.66	16.36
Na2O	0.44	0.05	0.18	0.28	0.00	0.11	0.24	0.00	0.24	0.34	0.22	0.25	0.51	0.43	0.00	0.05	0.20
Total	100.23	99.88	100.65	100.22	100.44	100.45	100.57	99.98	100.05	100.15	100.14	99.98	100.68	100.47	99.01	99.97	100.03
Mg/(Mg+Fe2+)	46.4	43.4	45.3	46.6	26.1	29.1	31.6	27.1	26.5	32.4	30.3	24.1	29.9	30.6	26.7	27.3	31.5
Si	1.938	1.955	1.947	1.943	1.970	1.962	1.964	1.965	1.946	1.939	1.951	1.969	1.957	1.954	1.967	1.973	1.976
Ti	0.008	0.014	0.008	0.005	0.006	0.015	0.009	0.014	0.004	0.011	0.009	0.006	0.009	0.010	0.008	0.008	0.009
Al	0.050	0.060	0.062	0.054	0.037	0.054	0.053	0.057	0.033	0.052	0.057	0.024	0.040	0.041	0.032	0.036	0.054
Fe2+	0.612	0.685	0.640	0.622	1.235	0.885	0.848	0.877	1.221	0.827	0.855	1.260	0.826	0.837	1.228	1.219	0.827
Fe3+	0.068	0.005	0.041	0.066	0.012	0.001	0.020		0.043	0.056	0.039	0.031	0.061	0.055	0.016	0.007	0.000
Mn	0.044	0.039	0.037	0.033	0.062	0.036	0.040	0.044	0.071	0.041	0.034	0.056	0.032	0.040	0.061	0.049	0.036
Mg	0.529	0.525	0.530	0.542	0.437	0.363	0.391	0.325	0.440	0.397	0.371	0.401	0.353	0.369	0.447	0.457	0.380
Ca	0.731	0.714	0.721	0.716	0.241	0.674	0.656	0.710	0.241	0.660	0.666	0.240	0.685	0.665	0.241	0.247	0.697
Na	0.034	0.004	0.013	0.022	0.000	0.009	0.018	0.000	0.019	0.026	0.017	0.020	0.039	0.033	0.000	0.004	0.015
Wo	36.5	35.0	34.9	34.6	15.4	33.3	32.8	34.8	16.7	32.8	32.6	17.4	35.1	33.8	15.4	15.8	34.4
En	29.5	28.2	29.5	30.4	22.1	19.4	21.2	17.7	22.1	21.8	20.4	20.0	19.4	20.3	22.6	22.9	20.7
Fs	34.0	36.8	35.6	34.9	62.5	47.3	46.0	47.6	61.3	45.4	47.0	62.7	45.5	45.9	62.0	61.3	45.0

Table 4.6 - reintegrated pyroxene compositions from the Eucarro Dacite

Sample	*849-36(v)*	*849-36(v)*	*849-36(v)*	*Eu7 (v)*	*Eu7 (v)*	*Eu7 (v)*	*Eu7 (v)*	*Eu21 (m)*	*Eu21 (m)*	*Eu20 (v)*
SiO2	47.80	48.34	48.45	49.44	49.43	50.22	49.22	48.18	48.51	47.42
TiO2	0.18	0.19	0.20	0.20	0.33	0.32	0.31	0.38	0.08	0.38
Al2O3	0.63	0.63	0.68	0.52	0.63	0.67	0.72	1.06	1.12	0.79
FeO	34.14	30.89	30.31	35.44	32.85	34.00	34.03	34.92	35.30	33.72
Fe2O3	1.74	1.84	1.95					0.53		0.94
MnO	1.60	1.38	1.24	1.49	1.46	1.34	1.49	1.52	1.70	1.47
MgO	6.47	6.22	6.21	6.59	6.33	6.68	6.53	6.90	6.78	6.74
CaO	7.20	10.55	10.96	6.71	8.91	6.45	7.28	6.32	6.11	8.23
Na2O	0.43	0.48	0.50	0.32	0.42	0.31	0.38	0.24	0.21	0.18
Total	100.19	100.52	100.50	100.71	100.36	99.99	99.96	100.05	99.81	99.87
Mg/(Mg+Fe2+)	25.3	26.4	26.8	24.9	25.6	25.9	25.5	26.0	25.5	26.3
Si	1.956	1.957	1.958	2.000	1.996	2.024	1.998	1.964	1.981	1.944
Ti	0.006	0.006	0.006	0.006	0.010	0.010	0.009	0.012	0.002	0.012
Al	0.030	0.030	0.032	0.025	0.030	0.032	0.034	0.051	0.054	0.038
Fe2+	1.168	1.046	1.024	1.199	1.109	1.146	1.155	1.191	1.206	1.156
Fe3+	0.054	0.056	0.059					0.016	0.000	0.029
Mn	0.055	0.047	0.042	0.051	0.050	0.046	0.051	0.052	0.059	0.051
Mg	0.395	0.375	0.374	0.397	0.381	0.401	0.395	0.419	0.413	0.412
Ca	0.316	0.458	0.475	0.291	0.386	0.279	0.317	0.276	0.267	0.361
Na	0.034	0.038	0.039	0.025	0.033	0.024	0.030	0.019	0.017	0.015
Wo	22.6	23.8	24.7	20.2	25.5	22.2	22.5	19.7	18.3	21.6
En	19.5	20.1	20.1	19.9	19.1	20.2	19.7	20.9	20.8	20.6
Fs	57.9	56.0	55.2	59.9	55.5	57.6	57.8	54.9	60.9	57.8

Analytical conditions were as given in Table 4.5
All analyses were obtained using an area scan technique, scanning as large an area as possible of the exsolved grain.

Compositions of the pyroxenes in the Eucarro vary systematically with whole rock composition. Those at the top of the unit have compositions which are more iron rich than those in the nearby Yardea vitrophyre, corresponding to the slightly more fractionated nature of the uppermost Eucarro compared with basal Yardea (see Chapter 5). Augites from the top of the Eucarro have the compositional range Wo_{36-37} En_{25-29} Fs_{34-38}. The iron enrichment trend defined by the Eucarro pyroxenes extends to very iron rich compositions in the lowermost Eucarro (Figure 4.6),where the compositional variation in pigeonite is Wo_{15-19} En_{19-21} Fs_{61-65} and that of augite is Wo_{32-35} En_{18-20} Fs_{34-38}, and the Mg numbers of the pigeonites cluster around 24-26 and those of the augites range from 29-30. The most iron rich pigeonite and augite have Mg numbers of 24 and 29 respectively. Some of the Eucarro pyroxenes in the vitrophyre contain fine lamellae (Figure 4.4), the individual lamellar compositions of which are consistent with the stable assemblage for the sample in which they occur. When the composition of the lamellae and host are reintegrated (Table 4.6), the range is Wo_{22-25} En_{19-21} Fs_{55-59}. Figure 4.3d shows a pyroxene from the Eucarro vitrophyre with two sets of exsolution lamellae, both of which are augite exsolved from a pigeonite host. The different orientations of the two sets of lamellae are due to phase-boundary lattice rotation. Pigeonite undergoes a large change in lattice parameters near the *C2/c* to $P2_1/c$ transition (Robinson 1980), such that the second set of augite lamellae were formed at a considerable angle to the first. The relative orientation of the lamellae indicate that both sets were formed above the aforementioned transition, i.e. that they are both products of exsolution at high temperatures (Robinson 1980).

4.4.4 - Olivine

Iron rich olivine is present as a minor phenocryst phase in some samples of the lowermost, rhyolitic part of the Eucarro Dacite in a number of localities, but is restricted to samples which have greater than 71% SiO_2, and which do not contain primary amphibole. Where present, olivine constitutes <1% of the phenocryst assemblage and forms a majority of the small (<30μm) ferromagnesian silicate grains in the groundmass. Samples where olivine occurs do not contain groundmass pigeonite but do have phenocrystic pigeonite, indicating that the assemblage Pig+Aug has become unstable, replaced by the assemblage Ol+Aug. Phenocrystic olivines are zoned (Table 4.7), with typical core to rim variation Fo_{15}-Fo_{12}. The groundmass olivines are considerably more iron-rich, with compositions of Fo_{2-3}.

Table 4.7 - Microprobe analyses of olivine from the Eucarro Dacite

Sample no.	*Eu20 p-core*	*Eu20 p-rim*	*Eu20 gm*	*Eu21 remnant p*
SiO2	30.85	30.85	30.26	31.22
TiO2	0.00	0.08	0.00	0.00
Al2O3	0.19	0.01	0.05	0.11
FeO	60.36	61.66	65.00	60.45
MnO	1.99	2.00	3.24	2.15
MgO	6.02	4.90	0.92	5.34
CaO	0.46	0.39	0.29	0.39
Total	99.87	99.89	99.76	99.66
Mg/Mg+Fe	15.1	12.4	2.5	13.6
	Structural formulae calculated to 4 oxygen			
Si	0.9979	0.9943	1.0153	1.0120
Ti	0.0000	0.0020	0.0000	0.0000
Al	0.0074	0.0004	0.0019	0.0044
Fe	1.6326	1.6624	1.8241	1.6388
Mn	0.0546	0.0546	0.0921	0.0591
Mg	0.2900	0.2353	0.0462	0.2581
Ca	0.0158	0.0133	0.0102	0.0135

p and gm denote phenocryst and groundmass grains respectively

4.4.5 - Amphibole

Pleochroic pale brown to pale green-brown amphibole is present in the Yardea predominantly as thin rims on phenocrysts and microphenocrysts of pyroxene (Figure 4.3h), less commonly as very small (<0.1mm) isolated grains within the groundmass. The amphiboles have a restricted compositional range (Table 4.8), and are catagorised as edenitic hornblende, ferro-edenitic hornblende and edenite using the classification scheme of Leake (1978). A striking feature about these amphiboles is their high halogen content, with fluorine content ranging from 2.1-2.8% and chlorine from 0.2-0.4%. Comparisons with amphiboles from chemically similar voluminous ignimbrites, the Cerro Galan ignimbrite (Francis *et al.*, 1989) and the Fish Canyon Tuff (Whitney and Stormer, 1985), reveal the Yardea amphiboles are significantly enriched in F, Cl, alkalis and less magnesian (Figure 4.7).

Amphibole occurs in a number of samples of the Eucarro Dacite. Both primary igneous and secondary amphibole have been found although both types have not been

Table 4.8 - Representative microprobe analyses of hornblende, Eucarro and Yardea Dacites

Sample	*Eu2*	*Eu2*	*Eu2*	*Eu11*	*Eu11*	*Eu11*	*Eu11*	*Eu5*	*Eu5*	*Eu5*	*Eu5*	*Eu5*	*Wa3*	*Wa3*	*A2*	*A2*	*A2*	*A2*	*A2*	*Y19*	*Y31*	*Y31*
Habit	*gm*	*Pc*	*Pr*	*P*	*P*	*gm*	*gm*			*gm*	*gm*	*grunerite*	*rA*	*rP*	*rP*	*rA*	*gm*	*gm*	*gm*	*rA*	*rA*	*rP*
SiO2	39.54	40.66	39.94	40.33	42.41	41.64	41.59	49.21	42.31	40.78	41.55	50.87	42.53	42.24	42.98	45.08	43.86	44.29	42.81	44.35	44.01	43.57
TiO2	1.31	0.16	1.18	1.21	1.18	1.37	1.29	0.36	0.56	1.37	0.91	0.00	0.92	0.85	0.57	0.49	1.08	0.71	0.42	0.30	1.04	1.19
Al2O3	7.81	7.32	7.63	9.30	7.50	8.62	8.29	1.79	6.82	7.48	6.30	0.20	6.71	6.81	6.71	6.26	6.25	6.26	7.16	6.17	6.13	6.63
FeO*	25.96	27.07	26.25	27.44	27.41	26.27	26.73	26.74	27.81	29.89	31.15	40.97	20.25	20.92	22.21	20.35	20.65	20.89	22.98	22.41	21.39	20.24
MnO	1.05	1.49	1.15	1.33	1.41	1.29	1.22	0.92	0.84	0.73	0.70	2.62	0.52	0.52	0.68	0.50	0.50	0.60	0.69	0.89	0.52	0.49
MgO	5.01	4.55	4.96	4.47	4.79	4.53	4.92	6.51	4.37	2.30	2.14	3.89	9.61	9.78	8.35	9.39	9.30	9.51	8.25	8.48	9.38	9.90
CaO	10.77	11.62	10.97	10.56	10.40	10.17	10.56	9.92	10.27	10.00	9.86	0.39	10.56	10.45	9.91	9.97	10.07	10.22	9.85	9.60	10.29	10.55
K2O	1.33	1.09	1.30	1.45	1.17	1.25	1.25	0.37	1.27	1.42	1.15	0.00	1.28	1.23	1.33	1.31	1.30	1.26	1.21	1.34	1.23	1.27
Na2O	2.47	2.22	2.41	2.93	2.78	2.84	2.95	1.27	2.49	2.51	2.40	0.31	2.74	2.70	2.75	2.67	2.83	2.64	2.71	2.76	2.65	2.73
Cl	0.20	0.11	0.19	0.17	0.12	0.14	0.12	0.15	0.69	0.80	0.68	n.d.	0.24	0.28	0.42	0.30	0.23	0.24	0.45	0.42	0.38	0.29
F	0.96	1.22	1.01	0.56	1.05	0.72	0.85	0.68	1.10	0.45	0.79	n.d.	2.60	2.25	2.48	2.56	2.28	2.23	2.16	2.22	2.21	2.31
Total	96.40	97.52	96.98	99.75	100.22	98.84	99.77	97.94	98.53	97.73	97.63	99.25	97.96	98.03	98.40	98.87	98.35	98.86	98.68	98.93	99.23	99.17
Mg#	0.28	0.25	0.28	0.26	0.27	0.26	0.27	0.35	0.24	0.13	0.12		0.52	0.55	0.47	0.50	0.50	0.52	0.48	0.48	0.50	0.52
Calculated formula **																						
Si	6.4414	6.6000	6.4798	6.3212	6.6107	6.5498	6.5098	7.5754	6.7692	6.6545	6.7941	not	6.6751	6.5831	6.7383	6.9558	6.8205	6.8245	6.6516	6.8646	6.7846	6.7128
Aliv	1.5008	1.4000	1.4590	1.7185	1.3783	1.5985	1.5298	0.3257	1.2308	1.3455	1.2059	recalculated	1.2415	1.2503	1.2404	1.0442	1.1463	1.1377	1.3111	1.1251	1.1141	1.2042
Alvi		0.0010							0.0560	0.0936	0.0079					0.0937						
Fe3+	0.4814	0.3914	0.4530	0.6264	0.5767	0.4326	0.4598	0.7154	0.4872	0.3288	0.5186		0.5505	0.8350	0.7141	0.4855	0.4933	0.6373	0.9513	0.8002	0.6420	0.5459
Fe2+	3.0560	3.2826	3.1080	2.9705	2.9971	3.0232	3.0393	2.7273	3.2333	3.7496	3.7419		2.1075	1.8915	2.1977	2.1402	2.1926	2.0545	2.0349	2.1012	2.1157	2.0620
Mn	0.1443	0.2042	0.1574	0.1766	0.1862	0.1719	0.1618	0.1203	0.1138	0.1006	0.0973		0.0697	0.0689	0.0903	0.0658	0.0654	0.0784	0.0905	0.1166	0.0679	0.0639
Mg	1.2160	1.1008	1.1984	1.0441	1.1127	1.0619	1.1477	1.4941	1.0420	0.5592	0.5222		2.2477	2.2714	1.9519	2.1584	2.1556	2.1847	1.9117	1.9570	2.1551	2.2732
Ti	0.1600	0.0200	0.1444	0.1426	0.1383	0.1621	0.1519	0.0418	0.0676	0.1682	0.1121		0.1081	0.0997	0.0672	0.0565	0.1263	0.0828	0.0489	0.0352	0.1206	0.1379
Ca	1.8792	2.0212	1.9061	1.7735	1.7370	1.7141	1.7711	1.6357	1.7607	1.7492	1.7270		1.7756	1.7447	1.6654	1.6482	1.6785	1.6868	1.6400	1.5918	1.6997	1.7417
K	0.2762	0.2262	0.2697	0.2899	0.2327	0.2508	0.2496	0.0732	0.2596	0.2952	0.2395		0.2555	0.2447	0.2670	0.2583	0.2572	0.2479	0.2396	0.2638	0.2419	0.2496
Na	0.7803	0.6991	0.7577	0.8904	0.8402	0.8662	0.8953	0.3799	0.7714	0.7931	0.7618		0.8350	0.8148	0.8367	0.7975	0.8527	0.7889	0.8170	0.8276	0.7921	0.8155
Cl	0.0558	0.0305	0.0528	0.0458	0.0321	0.0377	0.0322	0.0398	0.1891	0.2228	0.1906		0.0646	0.0753	0.1134	0.0793	0.0613	0.0635	0.1210	0.1121	0.1007	0.0766
F	0.4999	0.6316	0.5234	0.2814	0.5242	0.3616	0.4250	0.3363	0.5626	0.2339	0.4132		1.3061	1.1295	1.2490	1.2625	1.1335	1.1019	1.0839	1.1061	1.0927	1.1391
OH**	1.4443	1.3379	1.4239	1.6728	1.4437	1.6007	1.5428	1.6240	1.2484	1.5433	1.3962		0.6293	0.7952	0.6376	0.6582	0.8052	0.8345	0.7951	0.7818	0.8066	0.7843

Analytical conditions for microprobe analysis of hornblende were 20kV acceleration voltage, beam current approx. 30nA on a JEOL 733 microprobe.
Pc = phenocryst core, Pr = phenocryst rim, gm = groundmass phase, rA = rim on augite, rP = rim on pigeonite.
** Total iron measured as FeO.*
*** As suggested by Leake (1978) the formula was first calculated to 23O, assuming OH, F, Cl total 2, then normalized so that all cations except Ca,Na,K equal 13. Fe3+ was calculated to balance the anion charge to 46. OH is calculated by difference assuming F+Cl+OH=2*
n.d. = not determined

found in the same samples. The two types of amphibole are identified both by their chemistry and to some degree also by their morphology. Primary amphibole has been found only in samples from a relatively small part of the Eucarro Dacite, in the south-western section of its outcrop area, near Hiltaba Station. It is present both as subhedral to anhedral phenocrysts which often form glomerophenocrysts with plagioclase, sanidine and magnetite, and as small (<50μ) rounded grains within the groundmass (Figure 4.4a). It is pleochroic pale yellow-green to blue-green and when recalculated according to the recommendations of Leake (1978), is classified as hastingsitic hornblende. This primary amphibole is compositionally uniform (Table 4.8) with both phenocrysts and groundmass grains having Mg numbers which vary from 25-30. Halogen contents in the primary Eucarro amphiboles are quite a lot lower than those in the Yardea, however they are still higher than those from the Fish Canyon Tuff (Figure 4.7).

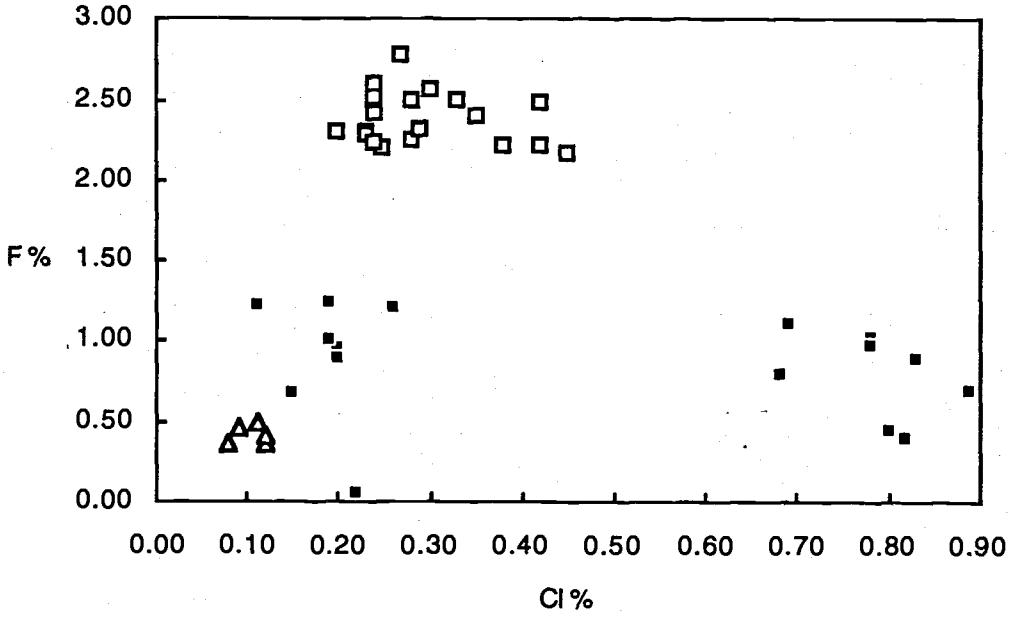

Figure 4.7 - F v Cl content for amphiboles from the Eucarro and Yardea Dacites compared with those from the Fish Canyon Tuff (Whitney and Stormer, 1985). Symbols : open squares, Yardea Dacite; filled squares, Eucarro Dacite; open triangles, Fish Canyon Tuff.

Two types of secondary amphibole occur in the Eucarro Dacite. The more common is a yellow to blue-green pleochroic calcic amphibole found as rims on partly to totally altered pyroxene or olivine and as small ragged anhedral grains within the groundmass (Figure 4.4b). This is ferro-edenitic hornblende to ferro-edenite, and differs from the primary amphibole in exhibiting a large variation in Mg-number between the rims on

phenocrysts and the groundmass grains (Table 4.8), with rims having Mg-numbers between 0.2 and 0.35 while the small grains in the groundmass having Mg-numbers as low as 0.12. This variation is attributed to the amount relative amount of Fe^{2+} to Mg available in any given area for the formation of amphibole, which in turn may be controlled by physical conditions such as fO_2 and chemical diffusion parameters. Rims forming around mafic silicate phases had a supply of Fe and Mg from the pre-existing grains, whereas secondary amphibole forming in the groundmass would form in an environment low in Fe and Mg. This secondary calcic amphibole has higher Cl content but approximately the same concentrations of F when compared to the primary type. This is interesting because Cl will not be incorporated by hydrous minerals if (OH) and F are present (Carmichael *et al.*, 1974). However Eichelberger and Westrich (1992) have shown that H_2O is almost completely released (>95%) from silicic melt during syneruptive degassing, whereas F and Cl are retained (<20% release). Post-emplacement degassing then occurs in response to the crystallization of volatile-free minerals, but only in thick lavas or pyroclastic flows which retain heat for extended time periods, and this phase of degassing releases most of the remaining H_2O and Cl, and some of the remaining F (Eichelberger and Westrich, 1992). These observations on modern silicic volcanics are directly applicable to the secondary calcic amphiboles in the Yardea Dacite. H_2O present in the system was lost during syn-eruptive degassing, and as post-eruptive crystallization released a greater proportion of Cl to F, the secondary calcic amphiboles contain more Cl than their primary counterparts.

A less common type of secondary amphibole is grunerite, which forms inner colourless fibrous rims between iron-rich phenocrysts (olivine and magnetite) and outer secondary calcic amphibole rims (Figure 4.4c) of the previously described type, a paragenetic association that confirms the compostion of secondary amphiboles was controlled by diffusional processes in the local chemical environment in which they formed. A typical composition of grunerite is given in Table 4.8.

4.4.6 - Biotite

No biotite has been observed in the Yardea Dacite, and the only biotite found in the Eucarro Dacite is intergrown with secondary calcic amphibole as rims on altered primary iron oxide or ferromagnesian silicate grains as illustrated in Figure 4.4c. The occurrence of biotite as discrete sections of such rims indicates that its formation and distribution is linked to its local chemical environment, where a little more potassium was present, biotite formed in preference to the more common secondary calcic amphibole. Thus it is clear that biotite is also secondary and cannot be used to determine any magma chamber conditions. Typical compositions of the secondary biotite are presented in Table 4.9.

Table 4.9 - Analyses of secondary biotite from the Eucarro Dacite

Sample	*Eu6*	*Eu6*	*Eu6*	*Eu5*	*Eu5*
SiO2	36.92	36.44	36.56	36.47	36.45
TiO2	3.40	3.55	3.27	2.44	1.87
Al2O3	11.48	11.29	11.42	10.77	10.09
FeO*	26.94	26.21	26.45	29.86	30.19
MnO	0.32	0.33	0.18	0.27	0.16
MgO	6.48	6.86	6.40	5.73	5.69
CaO			0.60		0.21
Na2O	0.37	0.16	0.21	0.29	0.40
K2O	9.24	9.15	9.10	8.69	7.86
Cl	0.38	0.31	0.39	0.42	0.38
Mg/Mg+Fe†	30.00	31.80	30.10	25.50	25.20
	Structural formulae, calculated to 22 Oxygen				
Si	5.887	5.869	5.884	5.934	6.038
Al iv	2.113	2.131	2.116	2.065	1.962
Al vi	0.045	0.012	0.051	0.000	0.007
Ti	0.408	0.430	0.396	0.299	0.233
Fe	3.593	3.530	3.560	4.063	4.182
Mn	0.043	0.045	0.025	0.037	0.022
Mg	1.540	1.647	1.535	1.390	1.405
Ca	0.000	0.000	0.103	0.000	0.000
Na	0.114	0.050	0.066	0.091	0.128
K	1.879	1.880	1.868	1.803	1.661
OH	3.897	3.915	3.894	3.884	3.893
Cl	0.103	0.085	0.106	0.116	0.107

** All iron as FeO*
† Calculated with all iron as FeO

4.4.7 - Iron-Titanium oxides

Ilmenite and titanomagnetite are present in all samples examined of both the Yardea and the Eucarro, however almost all grains are highly unmixed. Titanomagnetite is more common in both units, occurring as euhedral phenocrysts and microphenocrysts, as inclusions in all major phases and in glomeroporphyritic clots with pyroxene and feldspar (Figure 4.2d and 4.3a). Grains range from 0.05 to 0.5mm and typically form between 2 and 5% of the phenocryst population. The only mineral found as inclusions in magnetite is apatite. Ilmenite tends to form smaller (<0.1mm) rounded blebs within the groundmass, only rarely occuring as inclusions in pyroxene or other major phenocryst phases. It is typically present only in trace amounts. A single seemingly unexsolved titanomagnetite-ilmenite pair has been analysed from the freshest sample from the Yardea

vitrophyre. The grains occur as tiny (<10μ) inclusions in adjoining augite phenocrysts, and their compositions are given in Table 4.10. These analyses satisfy the Mg/Mn partitioning test of Bacon and Hirschmann (1988) for equilibrium between oxides.

Table 4.10 - Analyses of oxide minerals from the Yardea Dacite

Sample	*A2 (v) Ilmenite included in augite*	*A2 (v) Magnetite included in augite*
SiO2	0.00	0.72
TiO2	49.83	25.68
Al2O3	0.20	0.85
FeO	41.54	51.55
Fe2O3	5.11	14.88
V2O3	0.00	0.33
MnO	2.45	1.99
MgO	0.28	0.22
CaO	0.55	0.55
Na2O	0.25	0.20
Total	100.21	96.97
	*Cation proportions**	
Si	0.0000	0.2753
Ti	9.4374	7.3864
Al	0.0594	0.3831
Fe2+	8.7466	16.4847
Fe3+	0.9682	4.2816
V	0.0000	0.0834
Mn	0.5225	0.6445
Mg	0.1051	0.1254
Ca	0.1486	0.2257
Na	0.1220	0.1483

(v) indicates sample is from the vitrophyre
** ilmenite calculated to 3O, magnetite calculated to 4O*

4.4.8 - Quartz

Quartz is a rare phenocryst phase in the Yardea Dacite, particularly in the less siliceous samples, in which most quartz grains are polycrystalline aggregates thought to be xenocrysts included from the basement. In more siliceous samples of the Yardea, euhedral to rounded quartz grains typically less than 0.5 mm in diameter make up less than one per cent of the phenocryst population. Some of these grains are slightly resorbed as shown in Figure 4.1h.

Throughout much of the Eucarro sequence quartz is a sparse phenocryst phase, the rounded to slightly embayed grains constituting less than one per cent of the phenocryst

assemblage in most samples.The proportion of quartz increases anything up to 10% of the phenocryst population in a few more silicic samples, most of which have >73% SiO_2. Xenocrystic polycrystalline quartz has been noted in a number of sections of the Eucarro Dacite.

4.4.9 - Accessory Minerals

Euhedral, zoned apatite is a common accessory mineral in both the Yardea and Eucarro Dacites, occurring as inclusions in all major phenocryst phases, particularly magnetite and pyroxene and occasionally as isolated grains in the groundmass. Analyses of apatite are presented in Table 4.11. The apatites have few major constituents other than Ca and P. The zoning in the apatites can be seen from the analyses to be in response to quite subtle major element chemical changes, and may in fact be due to variations in trace element concentrations. Apatites analysed from the Yardea and from the pyroxene bearing portions of the Eucarro have comparable amounts of F (2.9-3.3%) and Cl (0.7-0.8%), whereas those from the amphibole bearing portion of the Eucarro have on average less F and Cl, 2.7% and 0.2% respectively. Chemically the greatest difference between the Yardea and Eucarro apatites and those from the FCT is the comparatively high chlorine content of the latter (0.7-1.1%, Whitney and Stormer, 1985).

Zircon occurs in both units as zoned, euhedral, prismatic crystals which are virtually always associated with magnetite grains. Fluorite is a common accessory mineral in the lower, more siliceous portion of the Eucarro Dacite and is most abundant in the section where primary amphibole is present, occurring as inclusions in sanidine and as free grains in the groundmass. Zoned, euhedral allanite is a rare accessory phase in the Yardea Dacite and has been noted in a few samples from the central rhyodacitic, granophyrically crystallized part of the Eucarro Dacite.

4.4.10 - Matrix Composition

Much of both major units have matrices which are too coarsely crystalline to be able to confidently determine their composition. The very fine microgranular matrix in the respective vitrophyres allow the best opportunity of analysing the groundmass, as an approximation of the composition of the melt which co-existed with the phenocryst assemblages outlined above. Table 4.12 lists matrix compositions analysed by electron microprobe using an area scan technique. The analyses are typically high silica rhyolite, with a relatively high iron content. The matrix of the Eucarro Dacite contains more Fe, K, and less Mg and Na than that of the Yardea Dacite, changes which are consistent with fractionation of the melt towards more evolved compositions.

Various studies have noted that alkali mobility and exchange occurs in volcanic rocks during cooling, devitrification and hydration (Lipman, 1965; Noble, 1970; Scott,

Table 4.11 - Analyses of apatite from the Yardea and Eucarro Dacites

Sample	*Y31 core*	*Y31 rim*	*Y31 core*	*Y31 rim*	*Eu20** core*	*Eu20** rim*	*Eu20** core*	*Eu20** rim*	*Eu20 gm*	*Eu11* core*	*Eu11* rim*	*Eu11† core*	*Eu11† rim*	*Eu11 core*	*Eu11 rim1*	*Eu11 rim2*	*Eu11 rim3*
SiO2	0.36	0.24	0.25	0.73	1.14	1.92	0.67	1.18	1.57	1.20	1.34	1.06	0.58	0.32	1.03	0.61	1.03
Al2O3	0.03	0.02	0.04	0.01	0.04	0.03	0.00	0.01	0.03	0.01	0.01	0.00	0.01	0.01	0.01	0.01	0.00
FeO	0.30	0.27	0.47	0.61	0.90	0.89	0.98	1.08	0.73	0.65	0.65	0.58	0.48	0.17	0.47	0.16	0.20
MgO	0.06	0.06	0.05	0.04	0.07	0.07	0.06	0.04	0.05	0.01	0.01	0.00	0.03	0.03	0.01	0.01	0.02
CaO	54.81	53.97	56.27	55.02	49.24	52.14	56.23	53.72	53.38	54.60	53.61	55.29	55.90	56.54	55.71	54.96	53.56
P	41.19	41.14	44.35	41.78	45.16	39.67	40.74	40.46	37.62	41.62	40.79	40.21	41.19	42.49	41.46	41.08	40.01
Cl	0.11	0.06	0.06	0.05	0.08	0.04	0.11	0.10	0.08	0.05	0.03	0.02	0.03	0.02	0.02	0.02	0.00
F	3.47	3.47	2.41	2.42	3.37	3.49	3.29	3.36	2.75	2.59	2.49	2.43	3.28	3.15	2.46	2.95	2.56
Total	100.33	99.23	103.90	100.66	100.00	98.25	102.08	99.95	96.21	100.73	98.93	99.59	101.50	102.73	101.17	99.80	97.38
							Structural formulae (calculated to 12 O and Ca+P=8)										
Si	0.031	0.021	0.020	0.062	0.100	0.171	0.057	0.102	0.141	0.103	0.117	0.091	0.049	0.027	0.087	0.052	0.090
Al	0.003	0.002	0.004	0.001	0.004	0.003	0.000	0.001	0.003	0.001	0.001	0.000	0.001	0.001	0.001	0.001	0.000
Fe	0.021	0.019	0.032	0.043	0.066	0.067	0.069	0.079	0.055	0.046	0.047	0.042	0.034	0.012	0.033	0.011	0.015
Mg	0.008	0.008	0.006	0.005	0.009	0.009	0.008	0.005	0.007	0.001	0.001	0.000	0.004	0.004	0.001	0.001	0.003
Ca	5.019	4.993	4.930	5.000	4.639	4.996	5.088	5.015	5.139	4.993	4.996	5.081	5.056	5.019	5.038	5.030	5.031
P	2.981	3.007	3.070	3.000	3.361	3.004	2.912	2.985	2.861	3.007	3.004	2.919	2.944	2.981	2.962	2.970	2.969
Cl	0.016	0.009	0.008	0.007	0.012	0.006	0.016	0.015	0.012	0.007	0.004	0.003	0.004	0.003	0.003	0.003	0.000
F	0.938	0.947	0.623	0.649	0.937	0.987	0.879	0.926	0.781	0.699	0.685	0.659	0.876	0.825	0.657	0.797	0.710
OH#	0.046	0.044	0.368	0.344	0.051	0.007	0.106	0.059	0.206	0.294	0.311	0.338	0.120	0.172	0.341	0.200	0.290

† denotes included in amphibole/plagioclase glomerophenocryst
** indicates grain included in amphibole*
*** signifies the grain is included in pyroxene*
 # OH calculated assuming one OH equivalent per formula unit

1971) however the presence and degree of alkali mobility varies considerably, from little or no alkali exchange (Lipman, 1965; Lipman *et al.*, 1969) to variable and complex behaviour within single units (Scott, 1971). It seems likely that in lava flows and highly welded ignimbrites, the possibility of alkali exchange is lessened due to their inherently low porosity inhibiting fluid movement through the volcanic pile. Although it can not be conclusively proven, the matrix compositions obtained for the Yardea and Eucarro Dacites are thought to be representative of the original glass. Evidence for this is: 1) the matrix compositions have slightly more K and less Na than their whole rock compositions which themselves exhibit little scatter in these elements above that expected due to the small variability in phenocryst content, the inference being that alkali mobility would induce greater scatter in the whole rock analyses; 2) When compared with analyses from the Fish Canyon Tuff (which shows considerable chemical similarities with the Yardea Dacite) of fresh glass and devitrified glass (Whitney and Stormer, 1985) and glass and melt inclusions in hornblende and quartz (Johnson and Rutherford, 1989) the Yardea and Eucarro matrix compositions more closely resemble the glass and melt inclusions rather than the devitrified glass which according to Whitney and Stormer (1985) has higher K_2O (av. 6.89% for 4 analyses) and less Na_2O (av. 2.04%). Using the FCT glass analysis of Johnson and Rutherford (1989) as the basis for more detailed comparison, the Yardea and Eucarro matrices contain comparatively more Fe, Ca, and less Na, and in addition the Eucarro matrix has less Mg and slightly higher K.

It is striking that the matrices of the Eucarro and Yardea vitrophyres are chemically so similar, given that the whole rock compositions are very different, dacitic for the Yardea and rhyolitic for the Eucarro. The obvious answer is the very different proportion of phenocrysts in the two units. An average phenocryst content of the Eucarro is about 18-20% and this is reasonably constant from the base to the top of the unit. At the top of the pre-Eucarro chamber the melt fraction was high silica rhyolite, and because of the constant amount of phenocrysts in the magma, it means that the melt in the last erupted part of the Eucarro was less siliceous, perhaps low silica rhyolite in composition. Continued crystallization of magma similar to this within the chamber, to a point where phenocrysts made up 35-40% of the magma, resulted in the Yardea Dacite vitrophyre having a bulk rock chemistry similar to the last erupted part of the Eucarro but with a matrix of high silica rhyolite.

Although the analyses obtained for the matrices are thought to represent reasonable estimates of magma in the top of the chamber just prior to the Yardea and Eucarro eruptive events, it is deemed not possible to use them to calculate the water pressure at which the melts equilibrated by comparing their normative compositions with the position of the eutectic or thermal minimum in the granite system (Tuttle and Bowen, 1958; Luth *et al.*, 1964, and Whitney, 1975). This is because even small variations in Na and K from the

true values, whether from even minimal amounts of alkali movement in the samples during their post-eruptive history, or from analytical errors in microprobe analysis, produce relatively large variations in normative albite and orthoclase content, ultimately resulting in an erroneous assessment of pressure.

Table 4.12 - Representative analyses of matrix compositions, Yardea and Eucarro vitrophyre

Sample	*Eu7*	*Eu7*	*849-36*	*849-36*	*A2*	*A2*
SiO2	76.32	75.62	75.93	75.93	75.93	77.30
TiO2	0.00	0.17	0.28	0.28	0.28	0.24
Al2O3	11.72	11.94	11.81	11.81	11.81	11.87
FeO*	2.12	1.96	2.13	2.13	2.13	0.98
MnO	0.00	0.00	0.00	0.00	0.00	0.00
MgO	0.00	0.00	0.00	0.00	0.00	0.18
CaO	0.87	0.80	0.81	0.81	0.81	0.70
Na2O	2.91	2.60	3.06	3.06	3.06	3.02
K2O	5.96	6.91	5.98	5.98	5.98	5.70
P2O5	0.11	0.00	0.00	0.00	0.00	0.00
Total**	100.00	100.00	100.00	100.00	100.00	100.00
Fe2O3†	0.20	0.19	0.20	0.29	0.11	0.09
FeO†	1.72	1.61	1.74	2.45	0.93	0.80
	CIPW Norm (from analyses recalculated to 100 per cent)					
q	34.12	32.19	33.24	31.73	32.41	35.86
hy	1.92	0.85	1.07	2.23	1.15	0.79
di	2.02	3.13	2.82	3.23	1.7	1.28
an	1.34	0.51	0.86	1.28	2.34	1.96
ab	24.53	22.16	25.97	21.91	26.05	25.46
or	35.08	41.11	35.49	38.57	35.38	33.54
mt	0.29	0.28	0.29	0.42	0.16	0.13
il	-	0.32	0.53	0.36	0.48	0.46
ap	0.26	-	-	-	-	-

FeO is all iron as FeO*
*** analyses recalculated to 100% volatile free*
† FeO and Fe2O3 calculated following Kilinic et al (1983) at T=1000°C and log fO2 = -11.5, the resultant values were used in the calculation of the norms
Each analysis was obtained using an area scan technique, with the beam scanning areas up to 500μm square for a total counting period of 50 seconds.

4.5 - Estimation of intensive parameters

4.5.1 - Thermometry and Oxygen Fugacity

The highly unmixed nature of most of the titanomagnetite and ilmenite phenocrysts from both the Yardea and Eucarro Dacites precludes their use in determining the temperature and oxygen fugacities of their respective magmas. Using Andersons (1985) thermometer on the single Fe-Ti oxide pair from the Yardea considered to have primary compositions yields a temperature of 1118°C. The common preservation of euhedral augite ± pigeonite allows some estimation of the magma temperature using pyroxene thermometry (Lindsley, 1983). Projection of pyroxene analyses yields temperatures of 1000-1100°C for the Yardea Dacite and 900-1000°C for the Eucarro Dacite. Sample Y19, as discussed previously, contains pyroxenes which have a relatively large compositional range, all of which upon recalculation yield temperatures 50-150°C lower than any other Yardea pyroxenes. In addition the trend to iron enrichment of these pyroxenes is also a trend down temperature, from approximately 950°C for the most magnesian pyroxene to 850°C for the most iron rich. The interpretation of this trend is that it represents a disequilibrium pyroxene assemblage formed when Yardea magma at the roof of the chamber assimilated silicic roof rock and, pyroxenes forming in this changing chemical environment had varying compositions.

A correlation between pyroxene temperature and composition is evident for the Eucarro Dacite. Augite phenocrysts from the upper part of the Eucarro Dacite give temperatures similar those from the Yardea, i.e. ≈1000°C, whereas those from the lower exposed parts give temperatures of 900-950°C, indicating a temperature gradient existed within the Eucarro chamber which was associated with variations in mineral composition and also to whole rock chemistry (Chapter 5). Re-integration of finely exsolved pyroxenes in the basal Eucarro vitrophyre results in compositions which yield temperatures of up to 1000°C, illustrating that the magma at the top of the chamber had cooled up to 100°C during the crystallization interval of pigeonite, prior to eruption.

High temperatures are also indicated by the occurrence of pigeonite rather than orthopyroxene which is the more common low-Ca pyroxene in felsic magmas (Carmichael, 1967; Warshaw and Smith,1988; Grunder and Mahood, 1988). Grove and Juster (1989) determined that for basaltic and andesitic compositions the pyroxene assemblage pigeonite+augite is stable at higher temperatures than orthopyroxene+ augite. If this is also true for more felsic magmas, it indicates higher temperatures for the Yardea/Eucarro sequence than those generally found in volcanics of this compositional range. Indeed the constant presence of pigeonite in these rocks is itself an indicator of high temperatures for the magmas, as the minimum stability of pigeonite gives a minimum

estimated temperature of approximately 890-970°C and 825°C (using Lindsleys 1983 curve) for the Yardea and Eucarro pigeonites respectively. The determination of pigeonite stability by Ishii (1975) produces higher temperatures for the Yardea pyroxenes of 980-1030°C , however this curve does not extend to the iron rich compositions of the Eucarro pyroxenes.

Application of the somewhat controversial plagioclase-amphibole geothermometer (Blundy and Holland, 1990) to the primary amphibole bearing Eucarro Dacite yields temperatures of 750°C and 715°C for assumed pressures of 2.5 kb and 5 kb respectively. These temperatures are considerably lower than those obtained for samples with pyroxene phenocrysts and if the method is sound, may indicate this part of the Eucarro erupted from a cooler, upper level of the magma chamber. However the effect of halogen substitution for OH in the amphibole structure is not accounted for by this thermometer, therefore the temperatures are likely to be minimum estimates only.

It is difficult given the few oxide phases interpreted to represent unaltered compositions to calculate the oxygen fugacity of the Yardea-Eucarro magmas with confidence. However using various methods and comparisons with other well studied volcanic areas a reasonable estimate can be made. A classic study by Carmichael (1967) on the relationship between ferromagnesian silicates and their co-existing iron-titanium oxides can be used to obtain a crude estimate of fO_2. It would be expected that samples from the Yardea and Eucarro Dacites would plot below the "pyroxene minus biotite" line on Carmichaels plot of oxygen fugacity vs temperature diagram (Figure 4.8), which at the temperatures of interest limits the maximum oxygen fugacity to approximately 0.75 log unit above the FMQ buffer. The occurrence of iron-rich olivine in basal parts of the Eucarro Dacite indicates the magma lay near or below the FMQ buffer in accordance with many previous studies of fayalite bearing volcanics (e.g.Carmichael, 1967, 1991; Warshaw and Smith, 1988; Mahood, 1981). Oxygen fugacities determined for other pigeonite + augite bearing felsic volcanic units including the Cougar Point Tuff (Hildreth, 1981) and quartz dacites from Chichi-jima (Kuroda *et al.*, 1988) have also all been below FMQ. This suggests that the mature phase chamber had a relatively low oxygen fugacity throughout its eruptive history. Indeed low oxygen fugacity conditions coupled with high temperatures seem to be necessary conditions for the formation of pigeonite in preference to orthopyroxene in felsic volcanics (Kuroda *et al.*, 1988; Warshaw and Smith, 1988).

A final piece of evidence for low oxygen fugacity in the Yardea-Eucarro magma system comes from the single oxide pair from the Yardea vitrophyre considered to retain primary compositions. This yields an oxygen fugacity of 0.77 log units below FMQ using Andersons (1985) oxide recalculation, a similar value to that obtained above by qualitative and comparative means.

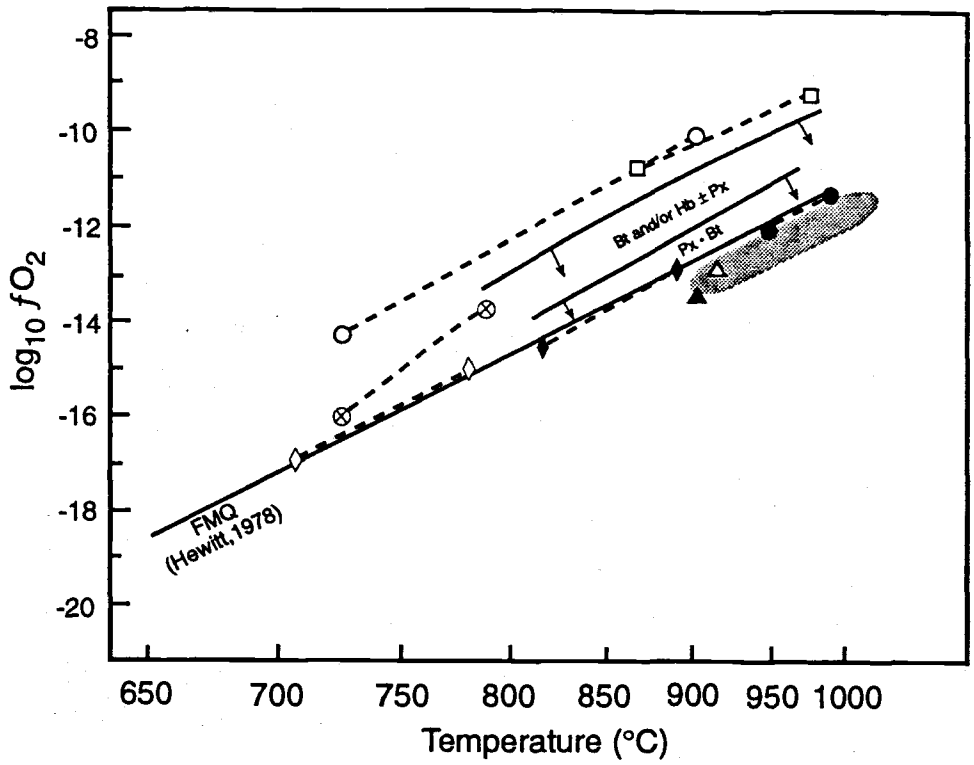

- ● Cougar Point Tuff - pig+aug, (Hildreth, 1981)
- ▲ Chichi-jima quartz dacite - pig+aug , (Kuroda et al,1988)
- ♦ Lava Creek Tuff - fa+hd or fa+aug, (Hildreth,1981)
- △ Obsidian, Iceland - fa±ferohd, (Carmichael, 1967)
- ⊗ Bishop Tuff - bt+aug+hy, (Hildreth,1981)
- ◊ Bandelier Tuff - hd+fa or aug+hy+fa, (Warshaw and Smith,1988)
- ○ Paintbrush Tuff - bt or bt+cpx+hb (Lipman, 1971; Lipman et al, 1966)
- □ Lassen dacite - hb+bt (Carmichael,1967)
- Estimated range for the Eucarro and Yardea Dacites

Figure 4.8 - log fO_2 v Temperature diagram illustrating the temperature-oxygen fugacity distributions of various silicic volcanic units, and the interpreted range for the Eucarro and Yardea Dacites. Also indicated are the ferromagnesian silicate assemblages for the represented volcanics. The lines marked Bt and/or Hb±Px and Px-Bt are taken from Carmichael (1967).

The relatively low oxygen fugacities obtained for the Yardea-Eucarro magma system are consistent with other mineralogical information such as the lack of sphene in the crystallizing assemblage. Sphene is regarded as an indicator of high magmatic oxygen fugacity (Whitney and Stormer, 1985) and was stabilized at only the higher oxygen fugacity experiments of Johnson and Rutherford (1989) which were at the MNO buffer, far higher than the fugacities postulated for the Yardea and Eucarro magmas.

4.5.2 - Pressure of phenocryst equilibration

There are typically few geobarometers available for use in felsic volcanics. However the presence of iron-rich pyroxenes allows the determination of a minimum pressure for the Eucarro Dacite. In the highly evolved compositions represented by the lowermost part of the Eucarro, pyroxenes without exsolution lamellae plot within the 1 atmosphere "forbidden zone" of Lindsley (1983), in positions indicating the minimum pressure for this two pyroxene assemblage is 2.5-3.5 kilobars (Figure 4.6).

When reintegration is attempted on those pyroxenes from the Eucarro which have fine lamellae, the resultant compositions form a mixing line between the equilibrium pyroxene assemblages, with most clustering close to Lindsleys (1983) 5 kilobar "forbidden zone", suggesting the Eucarro may have undergone polybaric crystallization, but this is difficult to determine as the pressures obtained by this method are minimum estimates only. Another interpretation of this data is that exsolution occurred as a response to a decrease in temperature at a relatively constant pressure of at least 4 kilobars.

Pressures cannot be calculated for the Eucarro Dacite which contains primary amphibole because of the lack of the requisite mineral assemblage of hornblende,biotite, plagioclase, sanidine, quartz, sphene and magnetite or ilmenite needed to apply the commonly used Al in hornblende barometer (Johnson and Rutherford, 1989; Hollister *et al*, 1987; Hammarstrom and Zen, 1986).

The pressures estimated for the Eucarro-Yardea magma system indicate that the magmas crystallized and possibly also erupted from 8-13 kilometres depth. This is considerably deeper than magma chamber depths invoked in general models of large scale eruptive, particularly ignimbritic, events. The lower end of this range does however overlap recent estimates for the Fish Canyon Tuff (Johnson and Rutherford, 1989), the Mount St. Helens Dacite (Rutherford and Devine, 1988), and the major ignimbritic units of the Loma Seca Tuff (Grunder and Mahood, 1988).

4.5.3 - Volatile contents of the magmas

In the absence of direct calculation methods such as that using the annite component of biotite (Wones, 1972), the magmatic volatile content for the Yardea and Eucarro Dacites can best be estimated by comparison with experimental phase equilibria determined for compositions most closely approximating the actual chemistry.

Phase relationships of the Fish Canyon Tuff as defined by Johnson and Rutherford (1989) are very useful due to the close approximation of their starting materials, Fish Canyon Tuff matrix and bulk rock, to the interpreted melt compositions of the Yardea and Eucarro Dacites (Table 4.12) and the bulk rock Yardea Dacite and the dacitic part of the Eucarro respectively. The differences between the experimental conditions and those

inferred for the Yardea-Eucarro system are the higher oxygen fugacities (the MNO and NNO buffers) and overall lower temperatures used for the experiments.

Results of the experimental work indicate that the degree of water undersaturation drastically affects the crystallization sequence. Figure 4.9, redrawn from Johnson and Rutherford (1989), illustrates this point. At water saturation sanidine and quartz do not crystallize at any of the experimental conditions, and plagioclase is a late crystallizing phase. In experiments where X_{H_2O}= 0.5 plagioclase, sanidine and quartz all begin to crystallize at temperatures which are considerably higher, but which are still much too low when compared with the estimated temperatures of the Yardea/Eucarro system under consideration.

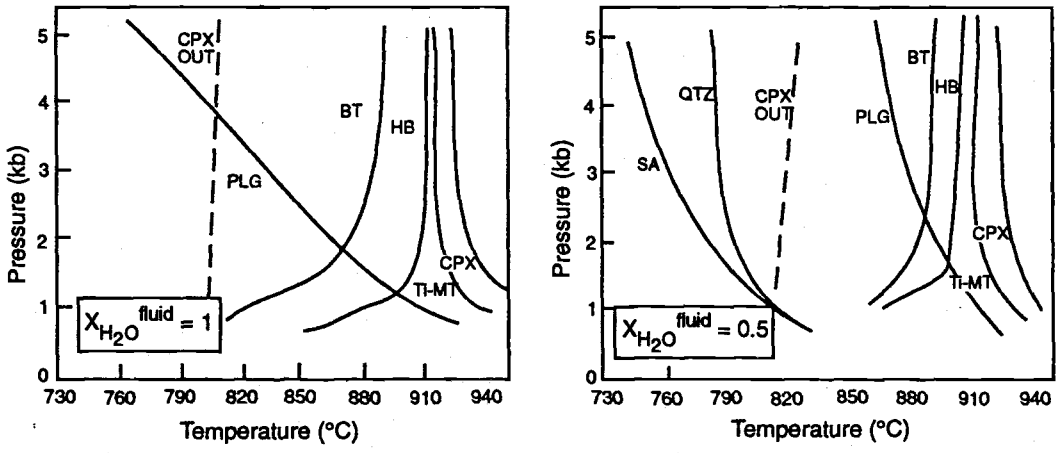

Figure 4.9 - P-T phase diagrams taken from Johnson and Rutherford (1989) illustrating that for the bulk Fish Canyon Tuff composition quartz and sanidine do not crystallize at all where X_{H_2O}=1.0, but do so when X_{H_2O}=0.5. Experiments were carried out at the MNO, NNO and AMQH oxygen buffers.

By inference with the experimental results it is considered that low aH_2O («1) is necessary to bring plagioclase, sanidine and quartz, in that order, onto the liquidus at the high temperatures of the Yardea and Eucarro Dacites, and more particularly to allow a large degree of crystallization (up to 40%) to occur whilst maintaining these temperatures. Note that this implies a reversal of crystallization order between sanidine and quartz from that shown in Figure 4.9. The T-X_{H_2O} (at 2 kb) diagram of Johnson and Rutherford for the Fish Canyon Tuff is presented as Figure 4.10. Quartz and sanidine begin to crystallize (Figure 4.10) at temperatures much lower than those interpreted for the Yardea and

Eucarro Dacites. However none of the experiments were carried out with water contents as low as interpreted for the Yardea and Eucarro.

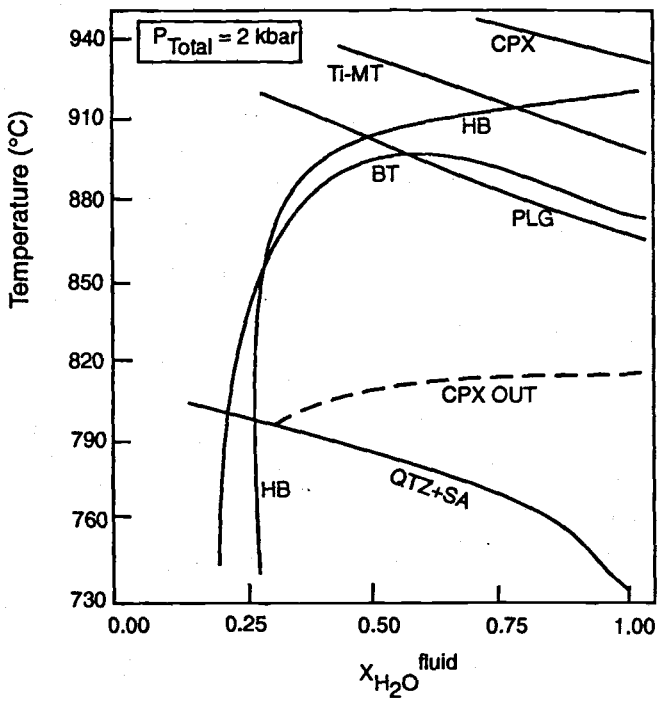

Figure 4.10- T-X_{H_2O} phase diagram from Johnson and Rutherford (1989) for the Fish Canyon Tuff at P_{total} = 2kbar and the oxygen buffers as noted for Figure 3.9. Note - no experiments were carried out at the lower oxygen fugacities estimated for the Eucarro and Yardea Dacites.

The control exerted on crystallization by the water content is well illustrated by the experimentally determined phase relationships on granite by Maaløe and Wyllie (1975). Their phase fields do show the appropriate crystallization order of salic minerals as seen in the Yardea and Eucarro dacites, that is plagioclase followed by alkali feldspar and then quartz, and their results indicate that to crystallize alkali feldspar at temperatures in excess of 1000°C, the system must contain less than ≈0.5 weight % of H_2O. Other experimental determinations of phase relationships for synthetic granite compositions (Naney, 1983; Whitney, 1975) all show the same features, with decreasing water content at constant pressure the temperature gap between liquidus and solidus increases markedly and the upper stability limits of pyroxenes, plagioclase, alkali feldspar and quartz all sweep upwards to high temperatures. Therefore to bring the phenocryst phases observed in the Yardea and Eucarro Dacites on to the liquidus in the observed sequence at the estimated temperature of more than 1000°C necessitates very low water contents similar to the estimation from the work of Maaløe and Wyllie (1975). At these low water contents there

is also a large temperature gap between liquidus and solidus, allowing a high degree of crystallization to take place while the magma remains well above the solidus.

Phase equilibria determined for the Mount St. Helens Dacite (Rutherford *et al.*, 1985; Rutherford and Devine, 1988) also indicate an upsweep of mineral stability curves to high temperatures when the melt is very undersaturated in water. This work is also difficult to apply to the Yardea and Eucarro Dacites, as plagioclase is the first phase to crystallize (prior to pyroxene and/or amphibole) under all experimental conditions except at relatively high water contents however the Mount St. Helens Dacite has more CaO and Al_2O_3 which could aid early stabilization of plagioclase.

Creaser and White (1991) estimated water contents for the Yardea magma, using the work of Nevaskil (1988), at <1% for a pressure of 2 kilobars or <2% for a pressure of 8 kilobars. The most silicic Eucarro Dacite has been shown to have the salic mineral assemblage of plagioclase, alkali feldspar and quartz, and a minimum magma temperature of 950°C. Using the phase diagrams of Nevaskil (1988), the water content at the top of the zoned pre-Eucarro magma chamber would have been approximately 1%. Estimates of water content for the lower, dacitic portion of the Eucarro and the most mafic Yardea must be less than this if the most silicic Eucarro formed by approximately 32% fractional crystallization from the latter (see Chapter 5). Therefore the water content estimates for the most mafic Yardea can only be approximately 0.6-0.7%, such that following the required amount of crystallization to produce the rhyolitic Eucarro, the water content has only risen to 1%.

Johnson and Rutherford (1989) also determined that highly water undersaturated conditions are necessary to stabilize pyroxene rather than amphibole, in experiments on the Fish Canyon Tuff. However the use of experimental phase relationships to determine the water content of the amphibole bearing Eucarro is hampered by a number of problems, including uncertain estimates of temperature and the large variations in amphibole stability which occur with changing composition and with substitution of F and/or Cl for OH in the amphibole structure. For example the work of Johnson and Rutherford, which is highly applicable to the pyroxene phyric magmas, indicates that the assemblage magnetite+hornblende+ plagioclase+sanidine+quartz does not occur at any of the experimental conditions without biotite. However the compositions of the primary Eucarro hornblendes are very different from those in the Fish Canyon Tuff, being much higher in FeO*, and with much higher halogen contents, factors which may result in a vastly different stability field from that determined experimentally by Johnson and Rutherford. The relatively high contents of F and Cl in the Eucarro igneous amphibole are likely to extend its stability to higher temperatures. The hornblende bearing Eucarro mineral assemblage also conflicts with the phase relations determined by Naney (1983)

for his synthetic granite composition, in which hornblende was never stabilized in any of the experimental runs, rather the ferromagnesian silicates were pyroxene and/or biotite.

Although the above discussion has tried to define the 'water content' of the magmas, it is almost certain that what was being defined was in fact the effect of a combination of dissolved volatiles (OH + halogens ± CO_2) in the magma. This is indicated by the halogen contents of both amphibole and apatite in the Yardea and Eucarro Dacites. The halogen content of magmatic apatite has been shown by Candela and Piccolo (1992) to be related to the halogen content of the magma from which they crystallised. Therefore the high F contents of the apatites (>3%), which leave little room in the respective mineral structures for (OH), argues for the dissolved volatile content in these fluid undersaturated magmas being rich in halogens, particularly F. The high halogen content of the Yardea amphiboles (2.1-2.8% F, 0.2-0.45% Cl) may reinforce this. In the Eucarro which contains igneous amphibole, interpreted as having been formed in equilibrium with melt, lower halogen contents are recorded for both amphibole (0.9-1.2% F, 0.1-0.2% Cl) and apatite (2.4-3.0% F, negligible Cl), possibly indicating that in the upper part of the chamber the proportion of OH to halogens dissolved in the melt was larger. Although both OH and F would have been concentrated near the roof of the chamber, (although the melt was still almost certainly fluid undersaturated) their proportions of may have been changing due to the removal of some F by the formation of fluorite as an accessory phase, that is the formation of fluorite was buffering the fugacity of HF in the melt. This correlates with the observation that fluorite is present in a far greater proportion in the amphibole bearing Eucarro than in its pyroxene bearing analogue. Direct measurement of bulk rock F and Cl contents for the Eucarro and Yardea Dacites were not carried out as they were not considered to represent reliable indicators of magmatic concentrations, because of the degassing during eruption.

Another possible volatile in the chamber, which would result in water undersaturation in the magma, is CO_2. However there is no method of determining the fugacity of CO_2 in the magma, and no mineralogical or analytical data which can be used to estimate it.

4.6 - Summary

The mature phase of the Gawler Ranges Volcanic Province, as documented above resulted in the eruption of a large volume of high temperature dacitic to rhyolitic magma. The dominant ferromagnesian silicate assemblage of the eruptives was pigeonite plus

augite. None of these factors, if taken individually, is particularly uncommon, however, when considered together they make this volcanism unusual.

Most products of very large volume eruptions (>1000km^3) which have been documented contain predominantly hydrous ferromagnesian phenocryst phases, and some systems have been estimated to have been close to water saturation e.g. the Timber Mountain and Paintbrush Tuffs (Warren *et al*, 1989). Magmas which have no hydrous phenocrysts, such as the Huckleberry Ridge Tuff and parts of the Lava Creek Tuff of the Yellowstone volcanic area, have estimated water contents which are well below water saturation but which are nevertheless considerably higher than those proposed for the Yardea and Eucarro Dacites. The effect of water content can be illustrated by looking at two well documented units which are chemically similar, but mineralogically different, to the Yardea and Eucarro Dacites (see Chapter 5), the Loma Seca Tuff (Grunder and Mahood, 1988) and the Fish Canyon Tuff (Whitney and Stormer, 1985). The Loma Seca Tuff contains plagioclase+augite+ orthopyroxene with no sanidine, and the Fish Canyon Tuff has sanidine+plagioclase+ quartz+biotite+hornblende, mineralogical differences which can be attributed to a greater magmatic water content in the case of the Loma Seca Tuff and to a combination of higher water content and lower temperature for the Fish Canyon Tuff (Johnson and Rutherford, 1989). The very low amount of fluid estimated to have been contained in the Yardea and Eucarro magmas relative to the Loma Seca Tuff resulted in the very different mineral assemblages, the upsweep of mineral saturation curves making sanidine and quartz liquidus phases in addition to plagioclase and pyroxene.

Continental volcanic areas whose silicic products exhibit mineralogical similarities to the mature phase units are the central Snake River Plain (SRP), Idaho, and the Etendeka Formation Volcanics, Namibia. In the central Snake River Plain the felsic volcanism is mostly rhyolitic, with subordinate rhyodacites and with the occasional exception such as the Cougar Point Tuff, the units are volumetrically small. The pyroxene assemblage of pigeonite + augite is virtually ubiquitous together with plagioclase± sanidine± quartz ± fayalite (Ekren *et al*, 1984; Bonnichsen and Kauffman, 1987; Honjo *et al.*, 1992). Basaltic volcanism immediately succeeded the eruption of silicic magmas in this region, indicating the presence of a mantle derived heat source for the felsic magmas.

In the Etendeka Volcanics, the silicic members have been described as being predominantly quartz latites with a small proportion of latites (Erlank *et al*, 1984; Milner and Ewart, 1989; Milner *et al.*, 1992), which are interbedded with large volumes of basalt. It should however be noted that the terms latite and quartz latite used by these authors do not correspond to the IUGS mineralogy based classification but instead refer to volcanics which contain >2-3% K_2O and 57-63% SiO_2 and >63% SiO_2 respectively. The quartz latites, which most closely correspond to the Gawler Range mature phase

volcanics, contain phenocrysts of plagioclase + pigeonite ± augite and in isolated cases ± orthopyroxene ± minor alkali feldspar (Erlank *et al.*, 1984; Milner and Ewart, 1989; Milner *et al.*, 1992). The small amount of alkali feldspar is in contrast to the GRV mature phase volcanics where sanidine is a major crystal phase, however the phenocryst content of the quartz latites is low (<10%), and as sanidine is a relatively late forming phase in the mature phase volcanics, it may be simply that the Etendeka quartz latites had not begun to crystallise this phase before they were erupted. Again, as noted for the Snake River Plain, the pigeonite bearing silicic volcanics are intimately associated with large volumes of basalt. This repeated association of large volumes of basalt with intracontinental felsic volcanics containing pigeonite implies that contemporaneous mafic magmatism often provides the high magmatic temperatures required to stabilize this pyroxene in preference to orthopyroxene, with or without co-existing augite. Magmatic parameters determined for the Yardea and Eucarro Dacites, and for other pigeonite + augite bearing felsic rocks (Figure 4.8) indicate that in addition to a high temperature, low water content and low oxygen fugacity may also be necessary to form the ferromagnesian silicate assemblage pigeonite + augite, and its apparent rarity in continental felsic volcanics is due to these conditions not often being met.

Although the volume of basalt erupted in the entire Gawler Range Volcanic Province is small relative to the amount of felsic erupted, and indeed that no basalts occur within or post-dating the mature phase volcanics, there is evidence that such a heat source was closely associated with the province. Further evidence for the presence of large volumes of mafic magma is presented in Chapter 7.

Destabilization of the two pyroxene assemblage in favour of olivine + augite was occurring in rhyolite at the top of the Eucarro magma reservoir just prior to eruption. It is possible therefore, that other large volume high silica rhyolites which bear olivine ± augite may have been underlain at depth by rhyodacitic to dacitic (or latitic) magmas of the pigeonite + augite type.

Chapter 5. The characterization, evolution and genesis of a large volume, high temperature, silicic magma chamber, Part 2: geochemical and isotopic constraints.

5.1 - Introduction

In recent years many studies have been conducted on silicic volcanic rocks, however despite this relatively little information is available on the sources of large volume silicic magma systems, or on the amount of, or mechanism for, their differentiation. Many previous chemical and isotopic studies of large volume silicic volcanism have looked at the voluminous units in isolation, thereby often forfeiting possible information available from preceding and intercalated eruptives, and have been inconclusive as to whether the magmas were derived by fractionation of mantle derived mafic melts, or by crustal melting, or by some combination of these processes.

This chapter presents a chemical and isotopic study of the volcanic units grouped into the mature phase of volcanism of the Gawler Range Volcanic Province with the aim of addressing these issues for this voluminous magmatic system (see Table 3.1). The mature phase volcanics bear many of the hallmarks of A-type rocks. Various hypotheses which have previously been advanced for the generation of A-type magmas are examined in the light of the information provided by the Gawler Range volcanic province as a whole. The mature phase magmas are interpreted to have formed as the ultimate product of an extended history of assimilation and fractional crystallization from a parental basaltic magma.

5.2 - Geology of the mature phase volcanic sequence

The Nonning Rhyodacite, the Eucarro Dacite, the Yannabie Rhyodacite, the Paney Rhyolite and the Yardea Dacite together comprise the mature phase volcanic sequence of the Gawler Ranges Volcanic province as described in Chapter 3. The eruptive products of the mature phase system are dominantly dacites and rhyodacites while rhyolitic material is volumetrically minor. The mature phase system developed upon the earlier developmental phase volcanism which erupted as spatially discrete centres (Chapter 2).

Although the eruptive history of the mature phase of Gawler Range volcanism cannot be put into an exact time frame, because all volcanism in the entire province occurs

within the resolution of U-Pb radiometric dating (Chapter 1), the changes in eruptive products with time can be viewed on a relative basis. The first two units to erupt, the Nonning Rhyodacite and Eucarro Dacite, are chemically very similar. Physically the Eucarro and Nonning have slightly different appearances, with the Nonning typically containing slightly larger, less well preserved phenocrysts than those in the Eucarro.

The Yannabie Rhyodacite is a small volume unit interpreted as having erupted in a minor pyroclastic event post-dating the Eucarro Dacite. It is generally much more poorly preserved than any of the three major units, interpreted to be the result of a lesser degree of welding which was, in turn, due to it being relatively thin (see Chapter 3). The Paney Rhyolite is a series of lavas both rhyolitic and rhyodacitic in composition which often are intimately co-mingled in outcrop, with flow banding and contorted flow folding prevalent. The final eruptive unit of the mature phase volcanism is the Yardea Dacite which is almost entirely dacitic in composition.

5.3 - Geochemistry

In the absence of material interpreted to be fiamme in any of the units sampled for analysis, bulk samples were analysed.

5.3.1 - Terminology

Application of the most recent IUGS recommendations on classification of volcanic rocks (Le Bas *et al.*, 1986) using modal phenocryst mineralogy defines the ubiquitously porphyritic products as latites, with minor quartz latites and rhyolites. There is throughout the sequence, with the exceptions of the volumetrically minor 'vitrophyres', variable preservation of feldspar phases, and the often high degree of turbidity in the feldspars makes identification of many grains difficult, thus limiting the usefulness of the modal classification. For this reason, classification has been undertaken using the alkali-silica diagram, to allow categorisation of all units and parts thereof. The modified classification outlined in Chapter 2 has been used for the mature phase volcanics (Figure 5.1), as it is more in line with the accepted formal stratigraphic nomenclature of the Gawler Range Volcanic Province, and removes the conflict between these stratigraphic names and the terminology used herein which would arise if the modal system were used.

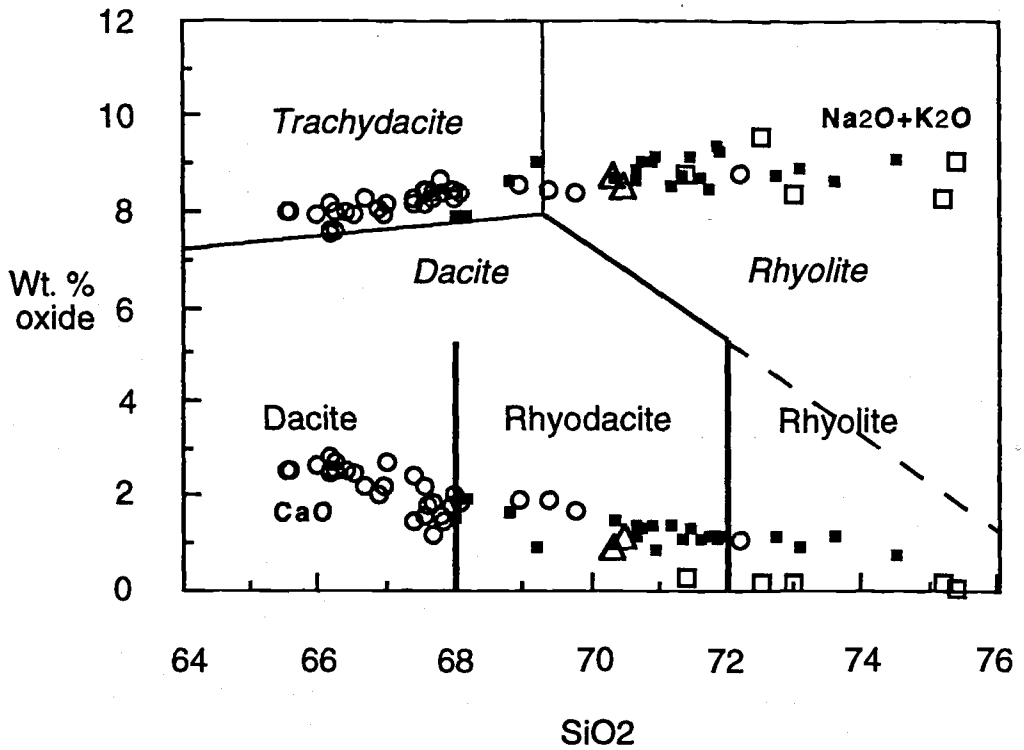

Figure 5.1 - Alkali-lime diagram for the mature phase volcanics. Symbols: filled squares - Nonning Rhyodacite and Eucarro Dacite, triangles - Yannabie Rhyodacite, open squares - Paney Rhyolite, circles - Yardea Dacite. Upper line of symbols = Na_2O+K_2O, lower line of symbols = CaO. The IUGS classification is shown for reference in italics but is not used here. The classification used here is in the lower part of the diagram in plain text.

5.3.2 - Whole Rock Chemistry

Major and trace element analyses were carried out on 53 samples by the X-ray fluorescence method. An additional 7 analyses from previous workers (Giles, 1980; Jagodzinski, 1985) were added to this data base. The chemical investigation sampled each of the units of the mature phase volcanism, but concentrated particularly on the Eucarro and Yardea Dacites, as these had been the focus of the mineralogical work described in Chapter 4.

The eruptive products from the mature phase volcanism are calc-alkalic as defined by Peacock (1931) and Irvine and Baragar (1971), in line with samples from the various developmental centres described in Chapter 2. All samples are metaluminous and have high Na_2O+K_2O. Representative whole rock and trace element analyses are presented in Table 5.1 and plotted in Figures 5.2 and 5.3.

5.3.3 - Assessment of the chemical effects of post-emplacement alteration

Little variation attributable to alteration has been detected when comparing samples taken from the basal black 'vitrophyres' and the red to brown main sections of the Yardea and Eucarro Dacites. Differences between selected samples from the vitrophyes and main

Table 5.1 - Chemical analyses of mature phase Gawler Range Volcanics

Sample No.	*884-Eu1*	*884-Eu2†*	*884-Eu3*	*884-Eu4*	*884-Eu5**	*884-Eu7*	*884-Eu10*	*884-Eu11†*	*884-Eu20**	*884-Eu21**	*884-Eu22*	*884-Eu23*	*884-Eu24*	*884-Eu25*	*849-36*	*849-2*	*849-70*	*849-38*	*849-72*	*884-N1*
Unit	*Eucarro Dacite*	*Eucarro Dacite*	*Eucarro Dacite*	*Eucarro Dacite*	*Eucarro Dacite*	*Eucarro Dacite (v)*	*Eucarro Dacite*	*Eucarro Dacite*	*Eucarro Dacite (v)*	*Eucarro Dacite*	*Eucarro Dacite*	*Eucarro Dacite*	*Eucarro Dacite*	*Eucarro Dacite*	*Eucarro Dacite (v)*	*Eucarro Dacite*	*Eucarro Dacite*	*Eucarro Dacite*	*Eucarro Dacite*	*Nonning Rhyodacite*
SiO2	73.58	70.73	70.36	69.20	71.62	71.35	68.82	71.17	72.71	71.70	70.88	70.69	68.01	68.18	71.47	71.91	71.86	73.09	74.54	70.66
TiO2	0.30	0.41	0.41	0.53	0.37	0.40	0.56	0.41	0.40	0.39	0.46	0.47	0.65	0.70	0.40	0.41	0.36	0.33	0.27	0.38
Al2O3	12.58	13.13	13.12	13.67	13.09	13.27	13.64	13.30	12.75	13.21	13.32	13.20	13.49	13.58	13.19	13.28	12.95	12.28	11.98	13.10
Fe2O3**	2.96	3.76	3.75	4.00	3.44	3.60	4.21	3.72	3.77	3.58	3.95	3.92	4.99	5.21	3.84	3.84	3.44	3.19	2.54	3.65
MnO	0.08	0.09	0.09	0.12	0.09	0.08	0.11	0.10	0.08	0.09	0.09	0.09	0.09	0.13	0.10	0.10	0.10	0.08	0.08	0.08
MgO	0.05	0.39	0.26	0.66	0.33	0.22	0.59	0.33	0.14	0.19	0.27	0.29	0.75	0.67	0.13	0.30	0.10	0.08	0.05	0.46
CaO	1.19	1.31	1.49	0.95	1.12	1.13	1.66	1.41	1.17	1.17	1.38	1.44	1.56	1.97	1.35	1.16	1.12	0.91	0.75	1.21
Na2O	2.86	3.32	3.22	3.56	3.22	3.26	2.66	3.20	3.30	3.20	3.50	3.10	3.10	3.20	3.52	3.35	3.48	3.17	3.19	3.06
K2O	5.76	5.71	5.49	5.49	5.49	5.52	6.00	5.34	5.45	5.30	5.54	5.49	4.85	4.76	5.62	5.89	5.91	5.81	5.88	5.78
P2O5	0.03	0.07	0.07	0.11	0.06	0.06	0.13	0.07	0.05	0.05	0.08	0.08	0.15	0.17	0.06	0.06	0.04	0.02	0.01	0.06
LOI	0.49	0.38	1.14	1.11	0.47	0.34	0.95	0.56	0.18	0.46	0.68	1.14	1.07	0.80	0.51	0.84	0.72	1.10	0.76	1.66
Total	99.88	99.30	99.40	99.40	99.30	99.23	99.33	99.61	100.00	99.34	100.15	99.91	98.71	99.37	100.19	101.14	100.08	100.06	100.05	100.10
Zr	449.0	485.0	479.0	405.0	465.2	499.5	392.5	485.2	516.1	470.2	444.1	462.3	430.7	414.4	508.0	480.0	462.0	506.0	427.0	491.0
Nb	26.0	24.0	24.0	20.0	25.2	25.7	20.8	24.1	27.9	25.5	23.2	24.2	22.4	21.8	24.1	23.0	24.1	25.2	26.3	24.0
Sr	65.0	98.0	102.0	107.0	74.6	78.2	155.0	93.1	59.6	93.7	106.7	102.2	107.7	149.5	96.0	100.0	90.0	52.0	45.0	67.0
Rb	256.0	246.0	232.0	213.0	223.0	221.1	263.3	207.2	214.0	230.0	230.0	228.1	210.0	196.8	221.0	233.0	254.0	235.0	284.0	230.0
Y	75.0	70.0	70.0	61.0	70.0	71.4	60.0	68.1	73.0	68.4	66.5	68.7	63.9	63.8	74.0	72.0	74.0	79.0	77.0	70.0
Ba	847.0	1208.0	1194.0	1317.0	1036.0	1252.0	1290.0	1206.7	857.0	1143.0	1209.0	1201.0	1319.0	1368.0	1214.0	1208.0	1127.0	652.0	436.0	1120.0
Sc	6.6	8.3	9.4	10.0	6.0	7.0	8.3	7.6	6.1	5.7	8.0	7.9	10.4	11.2	9.3	8.8	8.2	6.8	5.5	8.7
Ga	21.0	22.0	21.0	21.0	20.3	20.3	20.0	19.1	23.0	22.2	22.8	21.1	22.1	21.3	21.0	22.0	21.0	20.0	20.0	21.0
Ni	2.0	3.0	2.0	4.0	0.0	0.0	2.6	0.0	n.d.	n.d.	n.d.	n.d.	n.d.	n.d.	3.0	6.0	2.0	2.0	1.0	3.0
Th	41.0	37.0	35.0	30.0	36.4	36.2	29.0	33.3	38.9	33.6	34.3	34.5	29.3	29.9	n.d.	n.d.	n.d.	n.d.	n.d.	35.0
Pb	29.0	32.0	25.0	7.0	35.7	33.6	26.7	24.5	33.4	32.0	24.0	26.1	11.7	32.7	n.d.	n.d.	n.d.	n.d.	n.d.	6.0
U	11.0	11.0	10.0	8.0	7.1	8.9	7.2	8.5	8.0	8.4	6.9	9.2	8.4	5.6	n.d.	n.d.	n.d.	n.d.	n.d.	6.9
Ce	211.0	201.0	195.0	169.0	200.8	195.7	155.5	193.3	207.0	193.0	185.0	198.0	168.0	168.0	192.0	182.0	198.0	201.0	210.0	181.0
Nd	89.0	82.0	79.0	71.0	87.1	86.8	72.0	85.8	95.0	90.0	84.0	86.0	75.0	75.0	82.0	90.0	84.0	90.0	98.0	73.0
La	98.0	96.0	92.0	87.0	97.1	95.3	78.7	96.0	102.0	97.0	96.0	95.0	85.0	84.0	111.0	108.0	116.0	124.0	120.0	83.0
V	4.0	8.0	9.0	17.0	1.8	2.3	13.5	4.0	3.2	3.3	6.5	7.3	17.1	16.1	7.0	9.0	6.0	4.0	5.0	7.0
Cr	< 5	< 5	< 5	< 5	0.0	3.3	2.0	0.0	n.d.	n.d.	n.d.	n.d.	n.d.	n.d.	n.d.	< 5	n.d.	n.d.	n.d.	< 5
Mol. Na+K/Al	0.870	0.887	0.857	0.863	0.859	0.855	0.797	0.831	0.889	0.833	0.883	0.837	0.767	0.767	0.900	0.895	0.936	0.937	0.970	0.862
Mol Al/Na+K+Ca	0.960	0.936	0.941	1.011	0.986	0.991	0.982	0.978	0.948	1.006	0.934	0.966	1.023	0.970	0.921	0.949	0.915	0.933	0.923	0.971
Mg/Mg+Fe §	0.032	0.170	0.121	0.246	0.160	0.108	0.217	0.149	0.069	0.095	0.119	0.128	0.229	0.203	0.063	0.134	0.054	0.047	0.038	0.200

*** All Fe as Fe2O3*

† denotes analysis is of primary amphibole bearing Eucarro Dacite

** indicates the sample contains olivine phenocrysts or pseudomorphs*

(v) signifies the samples are from the vitrophyre of the listed unit

n.d. = not determined

§ - Mg ratio calculated with all Fe as FeO

Samples prefixed 849- are from Jagodzinski (1985)

Table 5.1 - (continued)

Sample No.	*884-N2*	*884-P1*	*884-P2*	*884-P3*	*884-P5*	*884-P6*	*884-YR1*	*884-Yan2*	*884-Yan4*	*884-Y*	*884-Y1A*	*884Y1B*	*884-Y2*	*884-Y4*	*884-Y5*	*884-Y10*	*884-Y11*	*884Y-12*	*884Y-13*	*884-Y14*
Unit	*Nonning Rhyodacite*	*Paney Rhyolite*	*Paney Rhyolite*	*Paney Rhyolite*	*Paney Rhyolite*	*Paney Rhyolite*	*Paney Rhyolite*	*Yannabie Rhyodacite*	*Yannabie Rhyodacite*	*Yardea Dacite (v)*	*Yardea Dacite (v)*	*Yardea Dacite (v)*	*Yardea Dacite*	*Yardea Dacite*	*Yardea Dacite*	*Yardea Dacite*	*Yardea Dacite*	*Yardea Dacite*	*Yardea Dacite*	*Yardea Dacite*
SiO2	70.95	72.96	71.37	72.51	75.37	75.19	74.49	70.48	70.31	69.76	66.71	66.93	67.39	65.53	65.61	68.02	67.92	68.01	67.84	67.60
TiO2	0.39	0.33	0.36	0.37	0.20	0.21	0.28	0.48	0.41	0.55	0.79	0.74	0.67	0.82	0.80	0.67	0.66	0.67	0.66	0.68
Al2O3	13.11	12.32	12.85	12.51	11.20	12.05	12.21	13.48	13.17	13.67	13.75	13.57	13.48	13.71	13.89	13.68	13.57	13.63	13.64	13.52
Fe2O3**	3.62	3.19	3.55	2.59	2.84	2.40	2.27	3.49	3.68	3.77	5.60	5.29	5.29	5.83	5.71	5.10	5.10	5.09	5.10	5.19
MnO	0.07	0.04	0.06	0.02	0.02	0.01	0.05	0.09	0.07	0.08	0.12	0.14	0.11	0.13	0.12	0.14	0.13	0.14	0.14	0.13
MgO	0.44	0.52	0.78	0.18	0.29	0.18	0.46	0.62	0.43	0.58	1.06	1.24	0.99	1.06	1.07	0.57	0.87	0.84	1.02	0.93
CaO	0.88	0.19	0.31	0.16	0.09	0.18	0.43	1.21	0.94	1.74	2.19	2.06	1.52	2.55	2.57	2.03	1.79	2.03	1.51	1.77
Na2O	3.65	2.58	1.79	0.91	0.41	2.98	2.73	3.37	3.13	3.27	3.32	3.17	3.02	3.47	3.47	3.29	3.21	3.24	3.12	3.26
K2O	5.50	5.79	7.03	8.69	8.67	5.31	5.54	5.15	5.65	5.14	4.96	4.90	5.27	4.54	4.52	5.19	5.27	5.11	5.27	5.21
P2O5	0.06	0.04	0.06	0.04	0.03	0.01	0.03	0.11	0.08	0.12	0.22	0.19	0.18	0.24	0.25	0.17	0.17	0.16	0.17	0.17
LOI	1.12	1.35	1.49	1.02	0.72	0.83	0.87	1.02	1.17	0.54	0.86	1.33	1.47	1.24	1.43	0.95	1.18	1.13	1.21	1.08
Total	99.79	99.31	99.65	99.00	99.84	99.35	99.36	99.50	99.04	99.22	99.58	99.56	99.39	99.12	99.44	99.81	99.87	100.05	99.68	99.54
Zr	481.0	471.0	490.0	492.0	296.0	315.0	384.7	335.8	467.7	400.2	412.0	419.0	425.0	402.0	393.0	432.0	420.0	412.0	430.0	431.0
Nb	24.0	25.0	23.0	24.0	24.0	25.0	26.5	19.1	23.9	19.3	19.2	19.6	21.0	18.6	18.9	21.0	21.0	21.0	21.0	21.0
Sr	166.0	40.0	41.0	66.0	25.0	34.0	29.6	122.3	120.5	149.0	229.0	140.0	159.0	196.0	169.0	167.0	150.0	158.0	155.0	149.0
Rb	224.0	271.0	320.0	417.0	374.0	252.0	258.3	211.2	218.9	211.7	205.0	197.0	219.0	182.0	180.0	212.0	215.0	208.0	213.0	207.0
Y	71.0	72.0	75.0	71.0	60.0	69.0	72.9	52.5	68.0	53.7	57.0	58.0	66.0	58.0	56.0	66.0	67.0	66.0	66.0	67.0
Ba	1686.0	1279.0	1549.0	2281.0	825.0	496.0	570.7	960.4	1255.1	1085.8	1189.0	1034.0	1381.0	1205.0	1165.0	1410.0	1421.0	1390.0	1371.0	1342.0
Sc	8.6	7.0	8.3	8.0	4.0	4.8	4.6	8.4	7.4	6.8	12.0	13.0	14.0	14.0	13.0	15.0	13.0	13.0	13.0	14.0
Ga	23.0	18.0	21.0	17.0	11.0	19.0	19.2	17.7	20.6	18.3	21.0	21.0	22.0	21.0	20.0	21.0	22.0	22.0	23.0	22.0
Ni	1.0	3.0	4.0	2.0	2.0	2.0	1.6	0.7	0.0	0.0	6.0	5.0	2.0	8.0	5.0	3.0	4.0	1.0	4.0	6.0
Th	34.0	36.0	34.0	35.0	39.0	43.0	42.1	26.3	35.0	30.2	27.0	29.0	27.0	26.0	26.0	31.0	30.0	29.0	29.0	30.0
Pb	41.0	3.0	3.0	4.0	3.0	6.0	17.7	9.2	24.5	28.9	27.0	32.0	28.0	25.0	26.0	26.0	29.0	28.0	28.0	30.0
U	9.1	7.4	9.0	8.8	6.6	8.0	9.0	5.0	8.9	7.9	7.8	6.0	7.0	6.9	6.4	8.5	7.4	7.6	7.5	3.2
Ce	185.0	183.0	194.0	156.0	313.0	292.0	222.3	149.6	187.2	153.7	158.0	161.0	170.0	158.0	156.0	178.0	180.0	183.0	176.0	177.0
Nd	75.0	46.0	75.0	59.0	140.0	112.0	94.8	67.1	81.4	66.0	67.0	70.0	74.0	70.0	58.0	71.0	70.0	70.0	73.0	74.0
La	91.0	46.0	88.0	85.0	163.0	122.0	112.0	75.5	94.2	77.7	79.0	78.0	87.0	75.0	70.0	84.0	82.0	89.0	87.0	86.0
V	6.0	5.0	7.0	7.0	1.0	3.0	0.9	16.7	4.1	14.9	38.0	40.0	24.0	44.0	44.0	20.0	20.0	20.0	20.0	21.0
Cr	< 5	8.0	< 5	< 5	< 5	< 5	3.9	2.3	3.4	1.4	5.0	7.0	< 5	5.0	< 5	< 5	6.0	< 5	< 5	< 5
Mol. Na+K/Al	0.912	0.853	0.822	0.872	0.898	0.884	0.859	0.825	0.856	0.801	0.788	0.775	0.792	0.775	0.763	0.806	0.810	0.797	0.795	0.814
Mol Al/Na+K+Ca	0.967	1.135	1.156	1.118	1.096	1.098	1.084	1.012	1.015	0.969	0.928	0.951	1.003	0.899	0.910	0.929	0.953	0.937	1.004	0.951
Mg/Mg+Fe	0.194	0.244	0.303	0.121	0.168	0.129	0.286	0.260	0.188	0.234	0.273	0.317	0.270	0.265	0.271	0.181	0.253	0.246	0.284	0.262

Table 5.1 - (continued)

Sample No.	*884-Y15*	*884-Y16*	*884Y-17*	*884-Y18*	*884-Y19*	*884-Y31*	*884-Y32*	*884-Y35*	*884-Y36*	*884-Y41*	*884-Y45*	*884-Y46*	*884-Y47*	*884-Y48*	*884-Y49*	*884-Y50*	*884-WA3*	*884-WA4*	*Y28¶*	*E725¶*
Unit	*Yardea Dacite*	*Yardea Dacite*	*Yardea Dacite*	*Yardea Dacite*	*Yardea Dacite (v)*	*Yardea Dacite (v)*	*Yardea Dacite*	*Yardea Dacite*	*Yardea Dacite*	*Yardea Dacite*	*Yardea Dacite*	*Yardea Dacite*	*Yardea Dacite*	*Yardea Dacite*	*Yardea Dacite*	*Yardea Dacite*	*Yardea Dacite (v)*	*Yardea Dacite (v)*	*Yardea Dacite*	*Yardea Dacite*
SiO2	67.56	67.78	67.66	68.07	72.14	67.41	66.51	67.65	67.57	66.18	66.20	66.18	65.99	66.24	66.43	66.22	69.36	68.91	66.97	67.03
TiO2	0.68	0.68	0.68	0.63	0.40	0.73	0.78	0.65	0.68	0.75	0.82	0.83	0.86	0.86	0.82	0.84	0.56	0.55	0.82	0.83
Al2O3	13.60	13.57	13.49	13.62	13.29	14.13	13.95	13.65	13.55	13.89	14.06	13.99	13.87	13.93	14.03	13.93	13.96	14.18	14.24	14.03
Fe2O3**	5.20	5.07	5.17	4.89	3.02	5.13	5.51	4.97	5.18	5.45	6.00	5.84	6.09	6.13	5.89	6.06	3.95	3.90	6.10	5.85
MnO	0.13	0.12	0.16	0.11	0.08	0.11	0.12	0.13	0.12	0.13	0.12	0.12	0.13	0.12	0.12	0.12	0.09	0.09	0.11	0.13
MgO	0.92	1.07	1.24	0.65	0.51	0.83	0.99	0.78	0.66	0.96	1.05	1.10	1.08	0.98	0.98	0.97	0.64	0.61	0.96	0.63
CaO	1.59	1.57	1.20	1.89	1.10	2.42	2.49	1.92	2.18	2.48	2.82	2.60	2.65	2.77	2.58	2.56	1.95	1.97	2.23	2.71
Na2O	3.06	3.23	3.08	3.27	3.54	3.44	3.26	3.17	3.25	3.52	3.30	3.30	3.30	3.40	3.40	3.40	3.35	3.42	3.25	3.48
K2O	5.42	5.44	5.21	5.09	5.22	4.70	4.65	5.22	4.87	4.60	4.24	4.29	4.64	4.23	4.61	4.62	5.14	5.12	4.70	4.68
P2O5	0.18	0.18	0.17	0.15	0.07	0.20	0.22	0.18	0.18	0.21	0.24	0.23	0.25	0.23	0.22	0.24	0.14	0.14	0.24	0.21
LOI	1.27	1.59	1.29	0.99	0.76	0.52	0.87	0.81	1.05	0.99	1.18	1.18	1.10	0.99	0.93	1.00	0.40	0.55	1.11	1.43
Total	99.61	100.30	99.35	99.36	100.13	99.62	99.35	99.13	99.29	99.16	100.03	99.66	99.96	99.88	100.01	99.96	99.54	99.44	100.73	101.01
Zr	420.0	431.0	435.0	430.0	331.0	399.8	394.9	399.2	428.3	405.0	378.4	388.9	397.5	393.9	394.3	392.7	390.9	382.6	402.0	401.0
Nb	21.0	22.0	22.0	22.0	19.7	18.8	18.8	20.6	21.4	18.9	19.1	19.5	19.5	19.8	18.8	19.6	18.5	17.8	22.0	20.0
Sr	182.0	151.0	132.0	154.0	115.0	193.3	179.9	157.6	137.4	185.0	178.5	197.4	195.5	193.0	208.3	198.7	159.1	171.1	189.0	181.0
Rb	229.0	216.0	205.0	206.0	222.0	186.8	190.0	213.6	193.8	186.0	172.2	178.2	181.9	180.6	182.8	187.5	207.9	200.1	195.0	184.0
Y	67.0	67.0	67.0	66.0	58.0	54.6	56.8	62.7	65.3	55.0	55.9	53.8	56.0	54.8	54.6	60.0	52.8	51.4	54.0	54.0
Ba	1468.0	1454.0	1407.0	1389.0	923.0	1306.7	1280.0	1310.1	1262.4	1249.0	1164.0	1263.0	1266.0	1187.0	1263.0	1239.0	1255.9	1352.3	1290.0	1215.0
Sc	13.0	13.0	13.0	14.0	8.6	9.4	10.4	10.8	11.6	13.5	11.8	10.9	12.4	10.5	10.9	11.5	7.6	7.6	13.0	13.0
Ga	22.0	21.0	21.0	21.0	19.0	20.8	20.3	19.9	19.5	n.d.	21.3	22.5	21.2	21.5	22.0	22.3	18.8	19.4	n.d.	n.d.
Ni	1.0	2.0	3.0	2.0	2.0	1.5	3.3	3.1	2.4	3.0	n.d.	n.d.	n.d.	n.d.	n.d.	n.d.	0.4	0.0	13.0	12.0
Th	32.0	30.0	29.0	29.0	31.0	25.2	25.3	28.2	27.7	24.0	24.0	25.7	24.8	23.1	25.5	23.9	28.3	27.4	n.d.	n.d.
Pb	33.0	22.0	30.0	30.0	36.0	28.1	25.5	28.8	22.8	32.0	23.1	24.3	25.0	27.3	24.8	24.4	26.7	28.1	n.d.	n.d.
U	7.0	8.1	7.9	7.7	7.1	6.3	5.5	5.5	6.1	8.0	5.1	4.2	5.2	5.9	4.4	6.7	7.2	6.7	n.d.	n.d.
Ce	175.0	176.0	179.0	179.0	155.0	153.6	158.1	165.5	176.9	130.0	150.0	152.0	156.0	151.0	151.0	157.0	154.5	148.2	n.d.	143.0
Nd	70.0	70.0	73.0	76.0	60.0	65.4	65.9	74.3	78.1	66.0	68.0	69.0	70.0	66.0	67.0	68.0	66.1	64.3	n.d.	59.0
La	79.0	83.0	85.0	93.0	73.0	78.9	78.0	82.7	85.3	68.0	75.0	78.0	77.0	75.0	75.0	76.0	78.4	74.7	n.d.	n.d.
V	18.0	22.0	22.0	18.0	15.0	25.0	27.5	17.9	16.0	38.0	39.9	38.8	41.2	37.3	33.3	36.4	15.4	15.9	35.0	43.0
Cr	< 5	< 5	5.0	6.0	< 5	5.1	3.6	2.8	0.2	1.0	n.d.	n.d.	n.d.	n.d.	n.d.	n.d.	4.1	4.4	n.d.	n.d.
Mol. Na+K/Al	0.802	0.826	0.794	0.800	0.864	0.761	0.745	0.796	0.784	0.776	0.713	0.720	0.754	0.730	0.754	0.761	0.793	0.788	0.733	0.769
Mol Al/Na+K+Ca	0.986	0.966	1.047	0.951	0.987	0.933	0.935	0.951	0.929	0.909	0.928	0.945	0.908	0.916	0.919	0.914	0.955	0.962	0.983	0.893
Mg/Mg+Fe	0.259	0.295	0.322	0.208	0.251	0.243	0.262	0.237	0.201	0.259	0.257	0.272	0.260	0.240	0.248	0.241	0.243	0.236	0.238	0.176

¶ - analysis from Giles (1980)

sections of the Yardea and Eucarro Dacites are listed in Table 5.2 and illustrated in Figure 5.4a and b. In the case of the Yardea Dacite there is no systematic variation for most elements between the vitrophyric samples and those from the main part of the unit which could be attributed to element mobility. Indeed there is often less variation observed for the more mobile elements Na_2O, K_2O, Ba and Rb than for elements such as MnO, MgO, P_2O_5, Ni and Sr. The differences between samples may be better explained by different crystal contents than by alteration. This is illustrated by comparing two samples taken from adjacent sites within the vitrophyre (samples Y1A and B) which have a similar state of preservation, but which exhibit differences in composition in the same order of magnitude as those seen between the vitrophyre and the main part of the Yardea Dacite. For the Eucarro Dacite a comparison was made between a sample from the vitrophyre and a sample from the lower part of the main unit. The differences between the two samples are small, and again the amount of variation of elements such as MgO, MnO and Sc are often greater than or similar to that exhibited by the more mobile elements Na_2O, K_2O, Rb and Ba. It is not possible to chemically compare the vitrophyre and the granophyric core of the Eucarro Dacite because as described in a later section this unit is zoned chemically from top to bottom. In contrast to most samples from the mature phase volcanism, a few samples of Paney Rhyolite exhibit evidence of addition of K_2O and removal of Na_2O during devitrification as has been described by Lipman (1965) and Scott (1971). In addition many of the Paney analyses have more MgO and less CaO than the general trend at a given silica content, which may in part be due to chloritization.

Looking at the chemical trends exhibited by the mature phase volcanics as a group, elements such as K_2O, Na_2O, Ba and Rb which are particularly susceptible to secondary mobilization and movement after emplacement exhibit regular trends with only moderate scatter consistent with them having suffered little post-eruptive movement of these mobile elements. The only exceptions are the few samples of Paney Rhyolite discussed previously. In addition there is no apparent correlation between loss on ignition and either Na_2O or K_2O concentrations for the mature phase volcanics as perhaps would be expected if the distribution of these elements had been affected by alteration. Also, as noted in Chapter 4, the matrices of both the Yardea and Eucarro vitrophyres appear not to have undergone the extreme loss of Na_2O and gain of K_2O often seen in devitrified glasses (Lipman, 1965; Noble, 1971).

The above chemical information provides a cogent argument that movement of mobile elements was minimal during devitrification and that with few exceptions the chemical variations observed are primary in origin. The high temperatures of the magmatic products, coupled with their anhydrous nature (Chapter 4) and their subaerial mode of eruption would have resulted in rapid welding and low porosity, which may have restricted fluid movement through the volcanic pile, thus limiting elemental mobility.

Table 5.2 - Chemical variation between samples from the vitrophyres and main portions of both the Eucarro and Yardea Dacites

Sample No. *Unit*	*884-Eu5* *Eucarro Dacite*	*884-Eu7* *Eucarro Dacite (v)*	*Eu7(v)-Eu5*	*884-Y1A* *Yardea Dacite (v)*	*884Y1B* *Yardea Dacite (v)*	*884-Y32* *Yardea Dacite*	*Y1A(v)-Y32*	*Y1B(v)-Y32*	*Y1B(v)-Y1A(v)*	*884-Y31* *Yardea Dacite (v)*	*884-Y36* *Yardea Dacite*	*Y31(v)-Y36*
SiO2	71.62	71.35	-0.27	66.71	66.93	66.51	0.20	0.42	0.22	67.41	67.57	-0.16
TiO2	0.37	0.40	0.03	0.79	0.74	0.78	0.01	-0.04	-0.05	0.73	0.68	0.05
Al2O3	13.09	13.27	0.18	13.75	13.57	13.95	-0.20	-0.38	-0.18	14.13	13.55	0.58
Fe2O3	3.44	3.60	0.16	5.60	5.29	5.51	0.09	-0.22	-0.31	5.13	5.18	-0.05
MnO	0.09	0.08	-0.01	0.12	0.14	0.12	0.00	0.02	0.02	0.11	0.12	-0.01
MgO	0.33	0.22	-0.11	1.06	1.24	0.99	0.07	0.25	0.18	0.83	0.66	0.17
CaO	1.12	1.13	0.01	2.19	2.06	2.49	-0.30	-0.43	-0.13	2.42	2.18	0.24
Na2O	3.22	3.26	0.04	3.32	3.17	3.26	0.06	-0.09	-0.15	3.44	3.25	0.19
K2O	5.49	5.52	0.03	4.96	4.90	4.65	0.31	0.25	-0.06	4.70	4.87	-0.17
P2O5	0.06	0.06	0.00	0.22	0.19	0.22	0.00	-0.03	-0.03	0.20	0.18	0.02
LOI	0.47	0.34		0.86	1.33	0.87				0.52	1.05	
Total	99.30	99.23		99.58	99.56	99.35				99.62	99.29	
Zr	465.2	499.5	34.30	412.0	419.0	394.9	17.10	24.10	7.00	399.8	428.3	-28.50
Nb	25.2	25.7	0.50	19.2	19.6	18.8	0.40	0.80	0.40	18.8	21.4	-2.60
Sr	74.6	78.2	3.60	229.0	140.0	179.9	49.10	-39.90	-89.00	193.3	137.4	55.90
Rb	223.0	221.1	-1.90	205.0	197.0	190.0	15.00	7.00	-8.00	186.8	193.8	-7.00
Y	70.0	71.4	1.40	57.0	58.0	56.8	0.20	1.20	1.00	54.6	65.3	-10.70
Ba	1036.0	1252.0	216.00	1189.0	1034.0	1280.0	-91.00	-246.00	-155.00	1306.7	1262.4	44.30
Sc	6.0	7.0	1.00	12.0	13.0	10.4	1.60	2.60	1.00	9.4	11.6	-2.20
Ga	20.3	20.3	0.00	21.0	21.0	20.3	0.70	0.70	0.00	20.8	19.5	1.30
Ni	0.0	0.0	0.00	6.0	5.0	3.3	2.70	1.70	-1.00	1.5	2.4	-0.90
Th	36.4	36.2	-0.20	27.0	29.0	25.3	1.70	3.70	2.00	25.2	27.7	-2.50
Pb	35.7	33.6	-2.10	27.0	32.0	25.5	1.50	6.50	5.00	28.1	22.8	5.30
U	7.1	8.9	1.80	7.8	6.0	5.5	2.30	0.50	-1.80	6.3	6.1	0.20
Ce	200.8	195.7	-5.10	158.0	161.0	158.1	-0.10	2.90	3.00	153.6	176.9	-23.30
Nd	87.1	86.8	-0.30	67.0	70.0	65.9	1.10	4.10	3.00	65.4	78.1	-12.70
La	97.1	95.3	-1.80	79.0	78.0	78.0	1.00	0.00	-1.00	78.9	85.3	-6.40

(v) indicates sample is from the vitrophyre

5.3.4 - Major Elements

The entire mature phase eruptive sequence displays reasonably coherent trends from 65-75% SiO_2. TiO_2, P_2O_5, Fe_2O_3*, form the most linear arrays, whereas those of MgO, CaO, and Al_2O_3 are more scattered. Some of this scatter in the latter three elements may be due to the small range of these elements in the mature phase volcanics amplifying variation on the graphs, however much of the scatter is interpreted to be due to the preferential retention in the magma, at any particular level in the chamber, of glomerophenocrysts primarily composed of plagioclase and pyroxene. This is supported by the dominance of these minerals in the glomerporphyritic clots observed in the volcanics (see Chapter 4), and also by the fact that the scatter in these elements is greatest in the Yardea Dacite, interpreted as being due to the crystal rich nature of this lithology which would render it highly viscous and more likely to retain phenocrysts than the less phenocrystic Eucarro and Nonning. Those elements controlled by other phases, e.g. the alkalis, P_2O_5, TiO_2 and Fe_2O_3* , which are controlled by alkali feldspar, apatite and titanomagnetite respectively, and which are less common in glomerporphyritic clots, have inherently less scatter.

Fe_2O_3*, MgO, CaO, Al_2O_3, TiO_2 and P_2O_5 all decrease monotonically with increasing SiO_2 content. The observed variations are Fe_2O_3* from 6-2.3%, MgO from 1.25-0.05%, CaO from 2.8-0.15%, Al_2O_3 from 14-11%, TiO_2 from 0.86-0.2%, and P_2O_5 0.25-0.01%. These trends are readily explicable by removal of observed mineral phases, CaO by plagioclase, Al_2O_3 by plagioclase ± sanidine, P_2O_5 by apatite, MgO by pyroxene, Fe_2O_3* by pyroxene + titanomagnetite, and TiO_2 by Fe-Ti oxides. Many of these negative linear major element trends have an inflexion at approximately 69-70% SiO_2, which is interpreted as a change in the proportions of phenocryst phases where sanidine for the first time became part of the fractionating sequence, and as a consequence the proportions of the other minerals in the fractionating assemblage changed.

Discounting those samples obviously affected by alkali mobility, Na_2O concentrations are relatively constant throughout most of the sequence at around 3.3-3.5%, with a small decrease down to 2.5% apparent only in samples with more than 73% SiO_2 . However the low number of samples at high SiO_2 means this inflexion cannot be positively identified as genetically produced rather than an artifact of sampling. If an inflexion indeed exists, the decrease is likely to be linked to rather sodic plagioclases being fractionated at higher SiO_2.

The sole major element which has a positive correlation with SiO_2 is K_2O. Again disregarding the few samples with high, alteration induced levels, K_2O increases strongly with increasing SiO_2 in the Yardea samples from 4.2 to 5.4%. The pattern then flattens from approximately 69% SiO_2 upwards, and although K_2O still increases, the rate of

Figure opposite:

Figure 5.2 - Major element oxide variations with SiO_2 for the mature phase volcanics. Symbols: filled squares - Nonning Rhyodacite and Eucarro Dacite, triangles - Yannabie Rhyodacite, open squares - Paney Rhyolite, circles - Yardea Dacite.

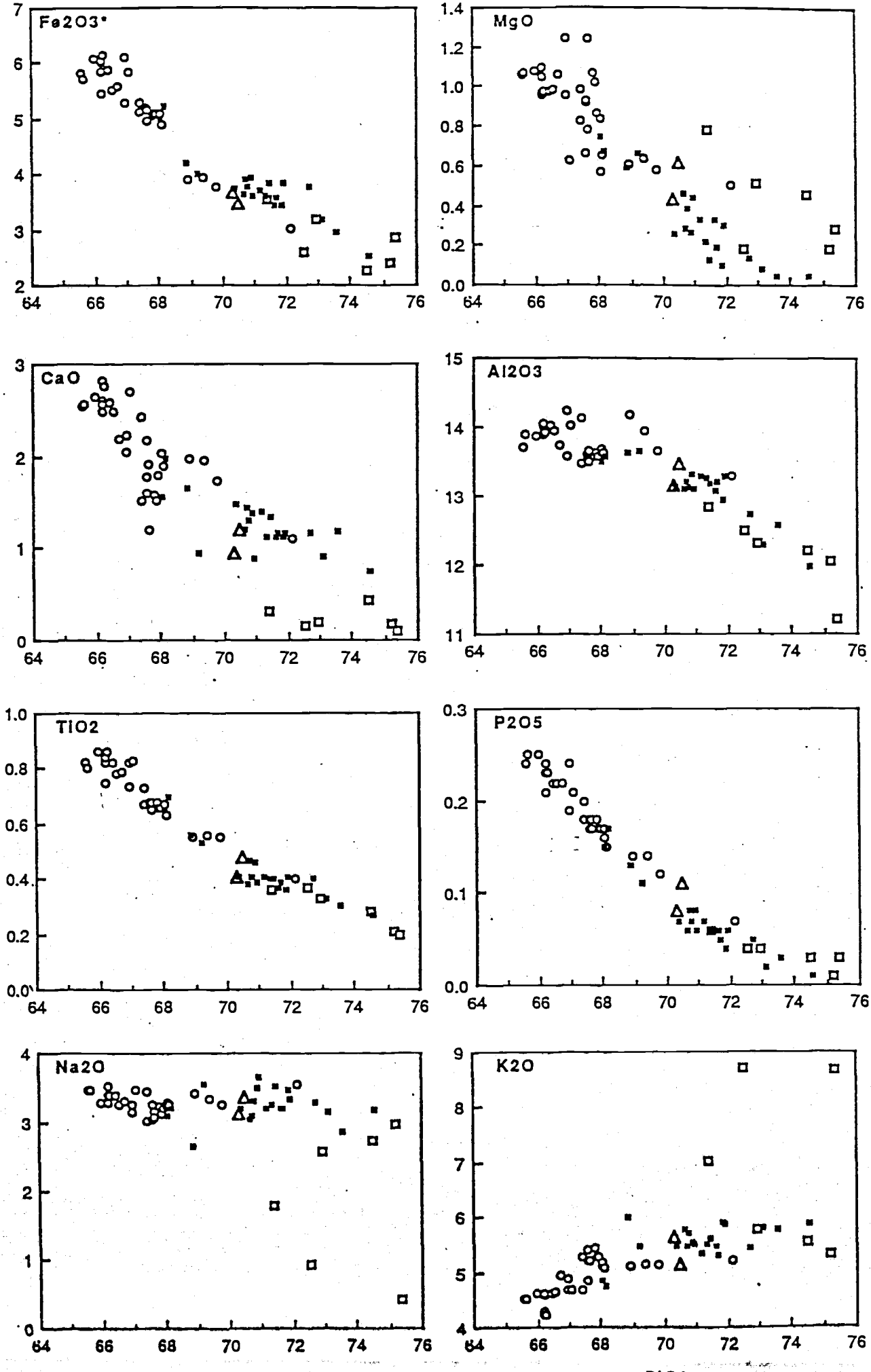
Fe2O3*
MgO
CaO
Al2O3
TIO2
P2O5
Na2O
K2O
SIO2
SIO2

increase is relatively small from 5.4-6.0%. This change in slope is where sanidine became a major fractionating phase, for although present in all samples, sanidine only becomes the dominant mineral phase in rocks which are rhyodacitic or rhyolitic (>68-69% SiO_2). Four samples of the Yardea Dacite do not follow the general pattern of strong K_2O enrichment, these samples all have more than 68% SiO_2, and are indeed the only samples of this unit that are this siliceous. These samples have lower than expected levels of K_2O and are considered not to have formed by simple fractionation from the Yardea magma. This point will be expanded and clarified in a later section.

There is an apparent dearth of samples plotting in the 68-70% SiO_2 range. The lack of Eucarro Dacite and Nonning Rhyodacite samples in this range is considered to be due to sampling bias. The Yardea Dacite is considered to have $SiO_2 \leq 68\%$ except in isolated samples such as those discussed above.

5.3.5 - Trace Elements

Systematic variations are seen in most of the trace element compositions for the mature phase volcanism. The compatible trace elements Sr and Sc decrease in a linear fashion with increasing SiO_2, the former from 200ppm to 25ppm and the latter from 15ppm to 4ppm. These patterns fit the mineralogical evidence that the phases likely to control their concentrations, plagioclase and pyroxene respectively, were crystallizing throughout the evolution of the magmas. The only other trace element which exhibits a negative correlation with increasing SiO_2 is V which decreases from 44ppm to 1ppm, however unlike Sc and Sr the trend is not strictly linear, instead it strongly inflects at 69-70% SiO_2. Samples lower in SiO_2 than this define a steep slope, indicating rapid removal of magnetite, whereas within the more silicic samples the trend is much flatter, reaffirming the interpretation made from major element trends that magnetite comprised a proportionately lesser part of the fractionating assemblage for these rocks due to sanidine having joined the fractionating assemblage.

All other trace elements analysed increase with increasing differentiation. La, Ce and Nd all increase in a linear fashion up to 75% SiO_2. The two samples above this point appear indicate a rapid enrichment in rare earths above this SiO_2 level, which may be real, as high silica rhyolites may contain high REE concentrations. Alternatively the apparent enrichment may be bias caused by the low sample density in this region. Some apparently anomalously low values are recorded for La and Nb for rhyodacitic samples from the Paney Rhyolite. These are the same samples which have undergone severe alteration and alkali mobilization, and although rare earths are generally considered to be relatively immobile it may be that they have been remobilised during alteration. Excluding these samples the ranges for the analysed rare earths are as follows, La 68-163ppm, Ce 130-313ppm and Nd 58-140ppm.

Figures opposite and overleaf:

Figure 5.3a & b- Trace element variations with SiO_2 for the mature phase volcanics. Symbols as for Figure 5.1.

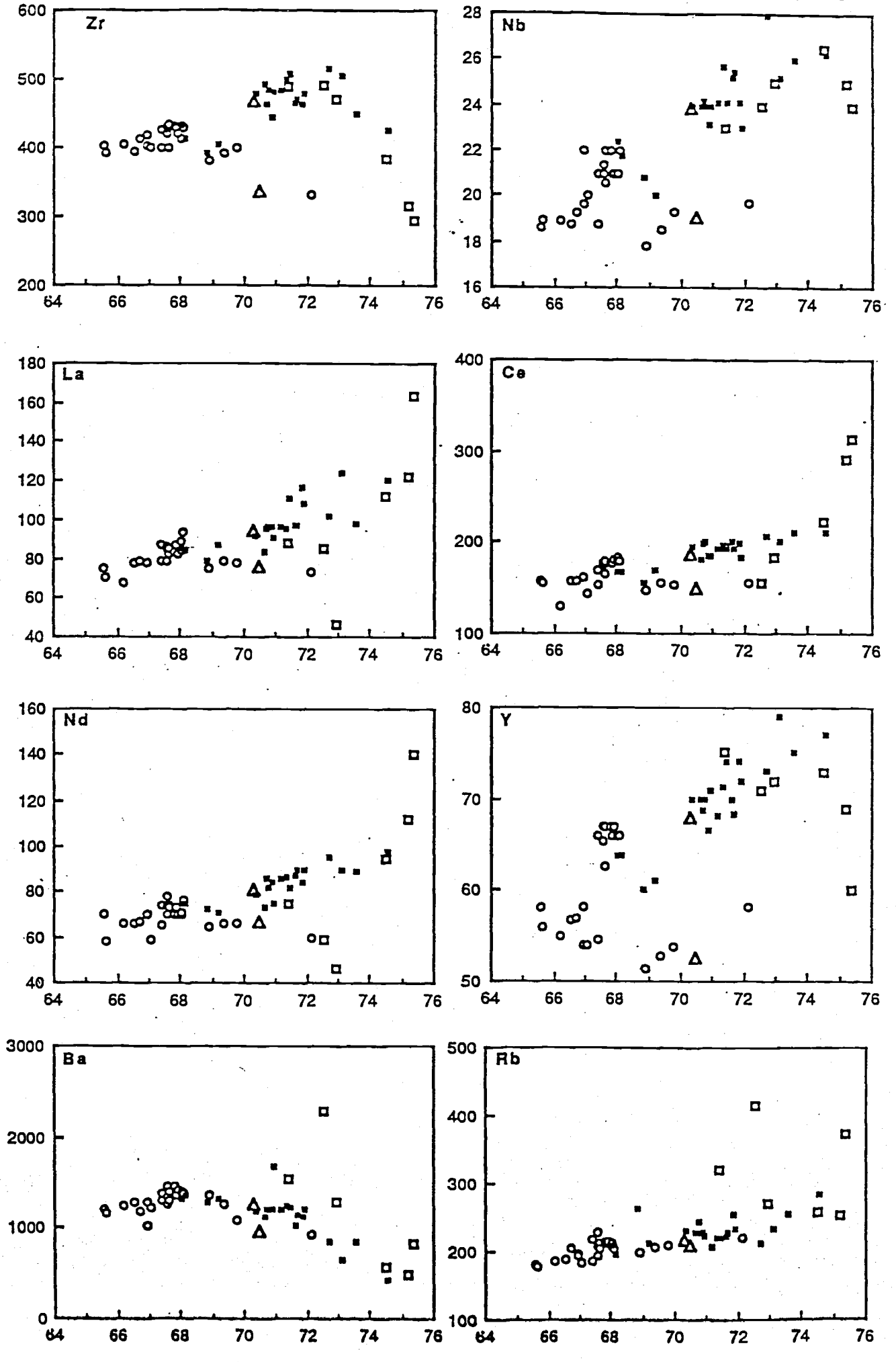
Zr
Nb
La
Ce
Nd
Y
Ba
Rb
SiO2
SiO2

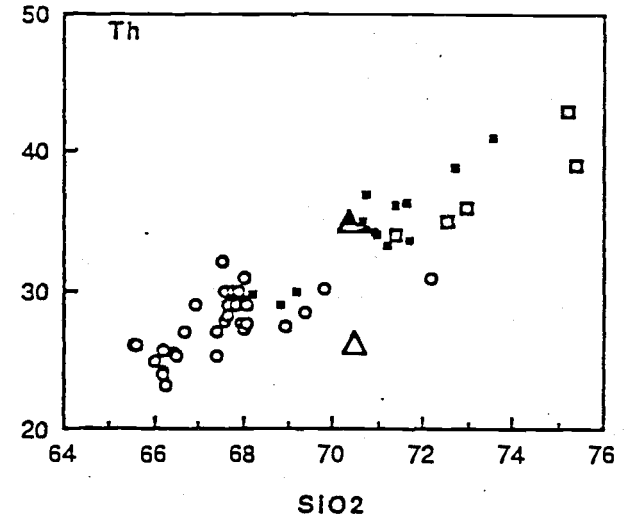
Th
50
40
30
20
64
66
68
70
72
74
76
SIO2

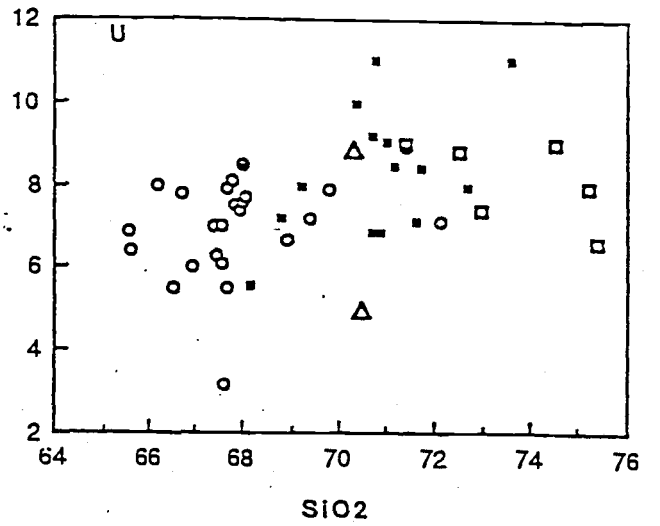
U
12
10
8
6
4
2
64
66
68
70
72
74
76
SIO2

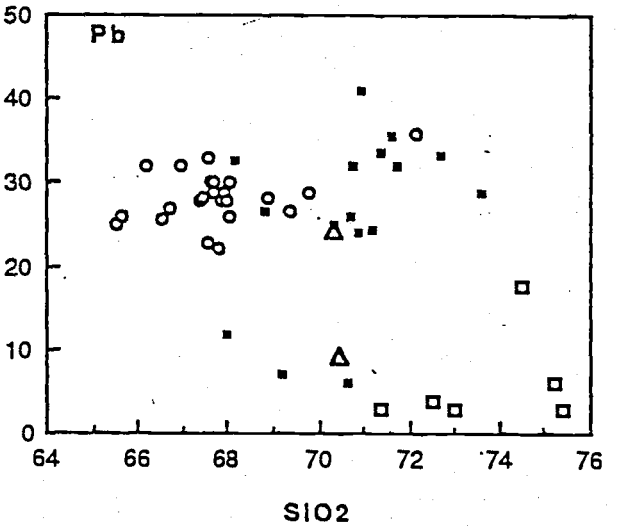
Pb
50
40
30
20
10
0
64
66
68
70
72
74
76
SIO2

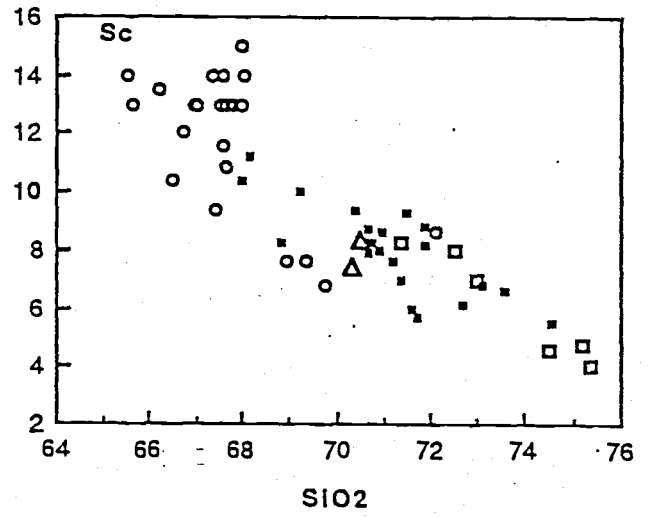
Sc
16
14
12
10
8
6
4
2
64
66
68
70
72
74
76
SIO2

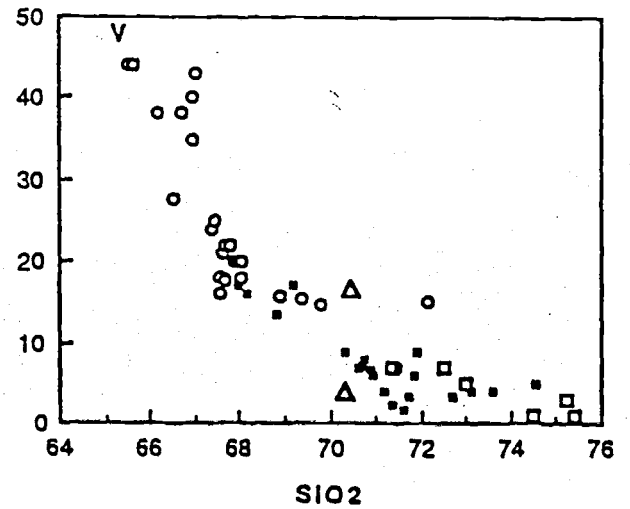
V
50
40
30
20
10
0
64
66
68
70
72
74
76
SIO2

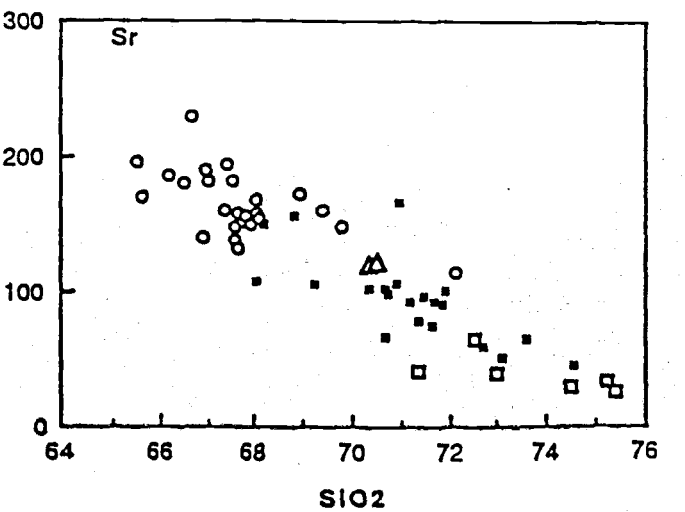
Sr
300
200
100
0
64
66
68
70
72
74
76
SIO2

Figure 5.4 - Diagrams comparing the chemistry of the Eucarro and Yardea basal vitrophyres with the main portions of the same unit. Note the lack of systematic differences between vitrophyre and main body.

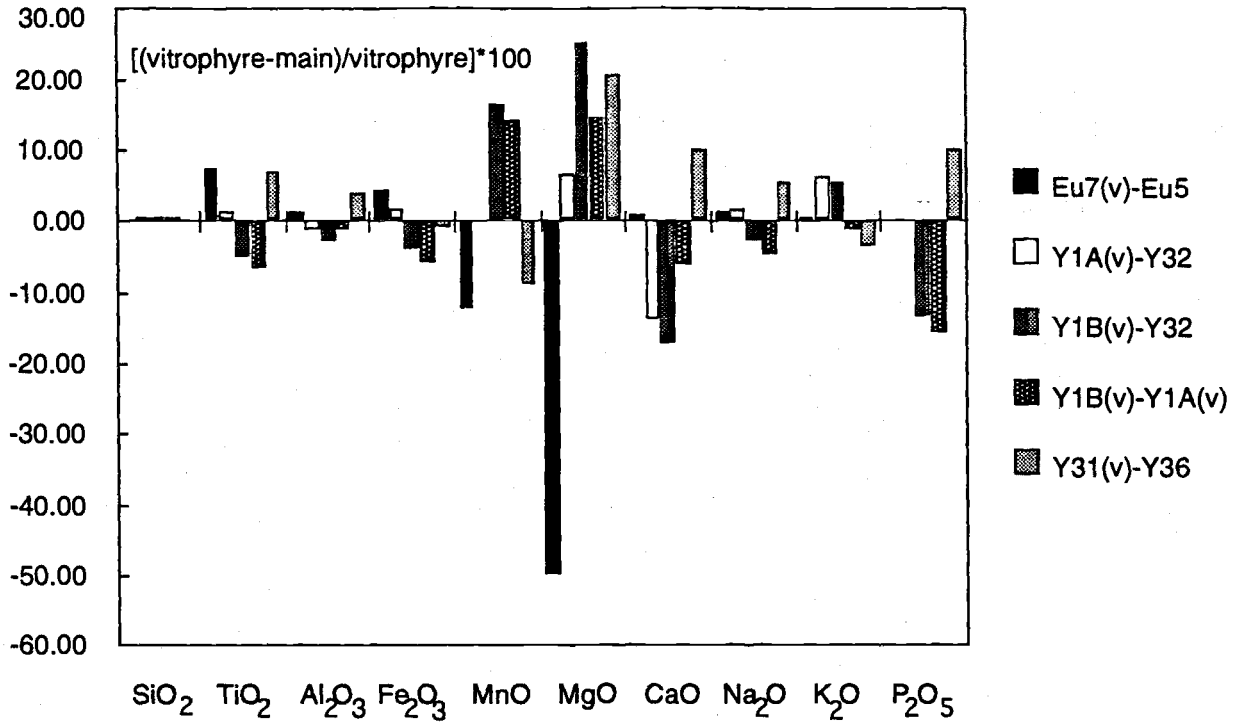
30.00
20.00
10.00
0.00
-10.00
-20.00
-30.00
-40.00
-50.00
-60.00
[(vitrophyre-main)/vitrophyre]*100
SiO2 TiO2 Al2O3 Fe2O3 MnO MgO CaO Na2O K2O P2O5
Eu7(v)-Eu5
Y1A(v)-Y32
Y1B(v)-Y32
Y1B(v)-Y1A(v)
Y31(v)-Y36

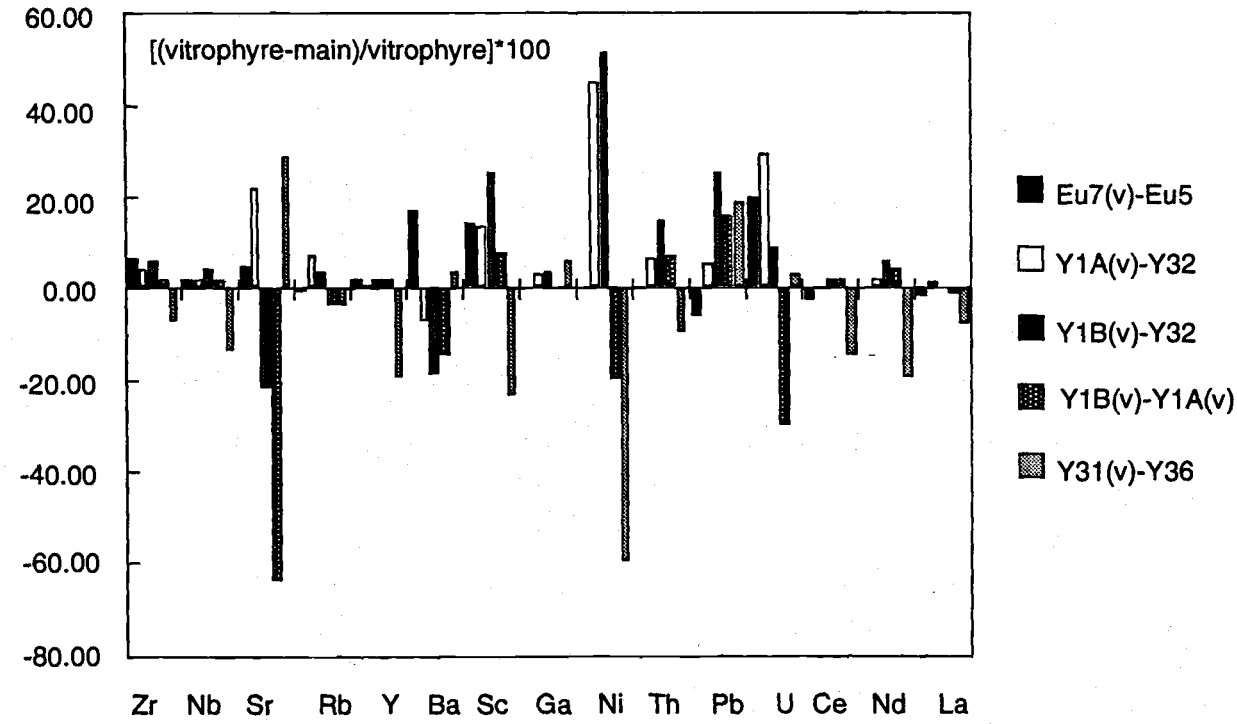
60.00
40.00
20.00
0.00
-20.00
-40.00
-60.00
-80.00
[(vitrophyre-main)/vitrophyre]*100
Zr Nb Sr Rb Y Ba Sc Ga Ni Th Pb U Ce Nd La
Eu7(v)-Eu5
Y1A(v)-Y32
Y1B(v)-Y32
Y1B(v)-Y1A(v)
Y31(v)-Y36

Of the highly charged incompatible elements (Y, Nb, Zr), Y and Nb both increase with increasing silica content to approximately 74%, above which they appear to decrease. As only four samples in the database have more than 74% SiO_2, it is difficult to ascertain whether the decrease at these silica levels does in fact exist. Zr also has a distinct inflexion, rising from 390ppm in the most mafic Yardea to a maximum of just over 500ppm between 72 and 73% SiO_2, after which levels decrease to approximately 300ppm at 75% SiO_2. The decrease in Zr, Nb and Y at high SiO_2 is considered to indicate the onset of accessory phase fractionation, zircon certainly and possibly others. A group of analyses, comprised of the four Yardea samples with more than 68% SiO_2 and one sample of Yannabie Rhyodacite, plot below the main trend on each of the SiO_2 variation diagrams of Zr, Nb and Y. These samples are considered to have been contaminated by assimilation of material from the country rock capping the magma chamber. All of the four Yardea samples in this group are from the basal 'vitrophyre', which is likely to have been at the top of the Yardea magma chamber and readily contaminated by roof rock. Likewise the Yannabie sample, being from an eruptive unit of low volume from the uppermost part of the pre-Yardea chamber, would be easily subject to country rock contamination.

Rb exhibits typically incompatible behaviour, increasing from 180-280ppm with increasing SiO_2 (excluding samples which show evidence of alkali mobility). Th demonstrates a similar incompatibility, with concentrations varying from 23ppm in mafic Yardea Dacite to 43ppm in the rhyolitic portion of the Paney rhyolite. Ignoring those samples which have experienced movement of alkalis, Ba initially increases, from 1164ppm up to a maximum of 1460ppm at ≈68% SiO_2, above which it decreases in a curvilinear manner in more differentiated rocks down to approximately 500ppm at 74-75% SiO_2.

Pb values are relatively constant for the mature phase at between 20 and 35 ppm, with the exception of a number of samples with low values <12ppm all of which are likely to have suffered post-emplacement Pb movement. Of all the trace elements analysed, U defines the most diffuse pattern, one of vague enrichment with increasing SiO_2.

REE patterns for the Nonning Rhyodacite, the Eucarro Dacite and the Yardea Dacite are illustrated in Figure 5.5. The chemical similarity of the Nonning and Eucarro is confirmed by their near identical patterns. The Yardea pattern is a similar shape, but a little less enriched overall, and with a slightly smaller Eu anomaly, as might be expected if it had fractionated less plagioclase. The increase in REE content from the Yardea to the Eucarro and Nonning is not accompanied by relative LREE enrichment, La/Yb remains relatively constant at about 14.

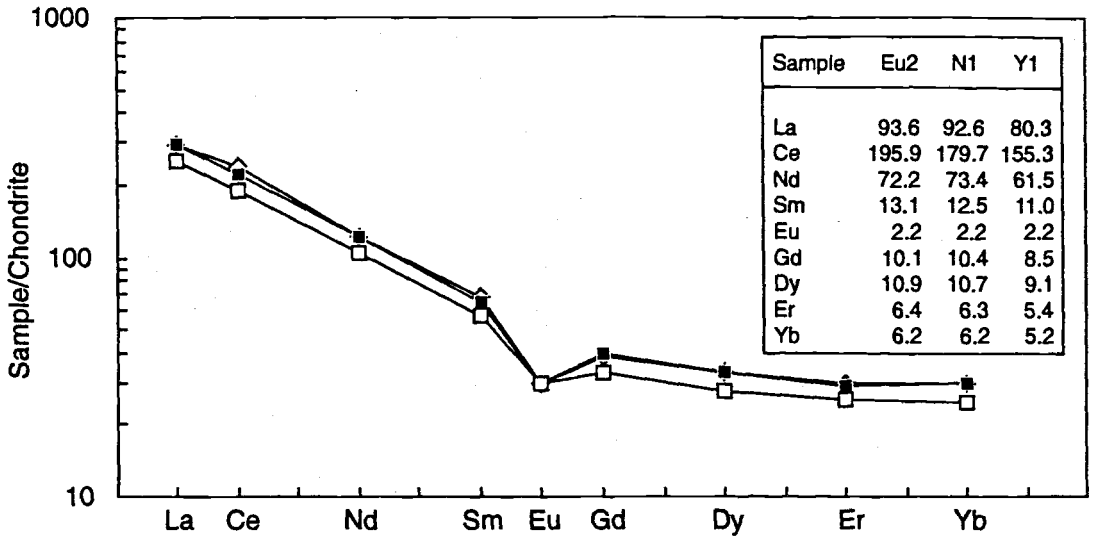

Sample	Eu2	N1	Y1
La	93.6	92.6	80.3
Ce	195.9	179.7	155.3
Nd	72.2	73.4	61.5
Sm	13.1	12.5	11.0
Eu	2.2	2.2	2.2
Gd	10.1	10.4	8.5
Dy	10.9	10.7	9.1
Er	6.4	6.3	5.4
Yb	6.2	6.2	5.2

Figure 5.5 - Rare earth patterns normalized to chondrite for representative samples of the Nonning Rhyodacite and the Eucarro and Yardea Dacites. Inset is a table of the rare earth concentrations in ppm. The rare earth concentrations were measured by isotope dilution using techniques as described in Turner *et al.*, (1993). Symbols : open squares, 884-Y1A; filled squares, 884-N1; open diamonds, 884-Eu2.

5.4 - Radiogenic isotopes

Nd and Sr isotopic determinations were carried out on ten and six samples respectively of the mature phase volcanic sequence. Samples from the 'vitrophyres' and main sections of both the Eucarro and Yardea Dacite were included, and samples considered to have suffered major alteration after emplacement were excluded.

Measured $^{143}Nd/^{144}Nd$ and $^{87}Sr/^{86}Sr$ values are presented in Table 5.3, as are Nd, Sm, Rb and Sr concentrations measured by isotope dilution, calculated initial Sr isotopic ratios and initial ε_{Nd} values. The Sr results are variable, those samples containing less than 100ppm Sr have improbably low calculated initial ratios. It is considered that, as for the volcanics of the developmental phase (Chapter 2), samples which have less than 100ppm Sr do not yield correct initial Sr ratios, unlike those with higher Sr concentrations. Only two samples analysed for Sr isotopes fulfil this requirement, both are from the Yardea Dacite, and they produce initial Sr ratios of approximately 0.7034.

ε_{Nd} values are relatively constant, with most samples plotting in a range between -3.8 and -4.5. Two values however plot outside of the main spread of analyses. One of these is from the Eucarro vitrophyre with an ε_{Nd} value of -5.8, whereas the other anomalous value is ε_{Nd} of -2.2 for the most silicic sample of Yardea Dacite (72% SiO_2).

Table 5.3 - Isotopic data for mature phase Gawler Range volcanics

Unit	*Sample number*	*SiO2 %*	*143Nd/144 Ndm ±2s*	*Nd ppm*	*Sm ppm*	*147Sm/144Nd*	*143Nd/144Nd(T)**	*epsNd(T)**	*TDM*	*Sr ppm*	*Rb ppm*	*Rb/Sr*	*87Sr/86Sr m ±2s*	*87Rb/86Sr*	*87Sr/86Sr (1592Ma.)*
Yardea	884-Y4	65.53	0.511577 ± 25	60.52	11.56	0.1155	0.510368	-4.58	2.19	194.5	179.1	0.921	0.764446 ± 3	2.667	0.70348
Yardea	884-Y10	68.02	0.511593 ± 33	68.52	13.07	0.1154	0.510385	-4.25	2.17	165.6	208.4	1.258	0.78767 ± 10	3.686	0.70341
Yardea	884-Y19	72.14	0.511648 ± 14	58.42	10.70	0.1108	0.510489	-2.22	2.00	n.d	n.d	n.d	n.d	n.d	n.d
Yardea	884-Y49	66.43	0.511567 ± 16	60.19	11.01	0.1107	0.510409	-3.79	2.11	n.d	n.d	n.d	n.d	n.d	n.d
Nonning	884-N1	70.66	0.511517 ± 10	71.27	12.46	0.1058	0.510410	-3.76	2.09	n.d	n.d	n.d	n.d	n.d	n.d
Eucarro	884-EU1	73.58	0.511509 ± 15	78.90	14.26	0.1093	0.510365	-4.65	2.16	61.9	248.0	4.008	0.963961 ± 3	11.741	0.69552
Eucarro	884-EU2	70.73	0.511544 ± 18	71.08	13.30	0.1131	0.510360	-4.74	2.19	88.7	234.9	2.650	0.868375 ± 2	7.763	0.69089
Eucarro	884-EU7	71.35	0.511529 ± 30	70.82	13.70	0.1170	0.510304	-5.83	2.29	89.7	220.0	2.454	0.868583 ± 2	7.187	0.70425
Eucarro	849-38	73.09	0.511523 ± 13	78.17	13.94	0.1079	0.510394	-4.07	2.12	n.d	n.d	n.d	n.d	n.d	n.d
Pancy	884-P6	75.19	0.511514 ± 12	89.78	16.28	0.1097	0.510366	-4.62	2.16	33.5	245.7	7.328	1.163307 ± 2	21.465	0.67254

n.d indicates not determined
** calculated to 1592 Ma.*

5.5 - Causes of the Chemical Variation

Chemical patterns in volcanic systems may be the result of magmatic processes only, however the magmatic signature may be significantly modified by emplacement effects and/or post-emplacement alteration. In order to identify the magmatic variation, the likely presence and effect of the other mechanisms must first be assessed.

5.5.1 - Post-emplacement alteration

As noted in section 5.3.3, there is little evidence to suggest that post-emplacement element mobility has significantly affected the chemistry of the mature phase volcanics. The few samples of Paney Rhyolite which show evidence of considerable post-emplacement alteration such as that documented by Lipman (1965) and Noble (1971) are easily identified by their high K_2O, Rb, Ba and low Na_2O (and possibly also low Pb) contents. These samples have been excluded from the data base during the further consideration of causes of chemical variability.

5.5.2 - Modification of Magmatic Chemistry by Emplacement Processes

As discussed in Chapter 3 the major units of the mature phase volcanism are considered to have features consistent with their having erupted as ignimbrites and it is therefore possible that the initial chemical variation produced by magmatic processes may have been modified by physical fractionation during eruption. The concentration of crystals and loss of glass during some eruptions has been convincingly demonstrated (Lipman, 1967; Walker, 1972; Sparks and Walker, 1977) and has been used to account for the chemical variation seen in at least one very large volume ignimbrite (Whitney and Stormer, 1985). The similarity in matrix compositions for the Eucarro and Yardea Dacites (Chapter 4) would seem to indicate that ash winnowing is a possible mechanism for development of the chemical patterns observed. Winnowing would result in linear arrays on chemical variation diagrams due to the loss of the glass component as ash, as discussed by Whitney and Stormer (1985), however the curved trends exhibited by the mature phase rocks in silica variation plots of Zr and Ba cannot be produced by this mechanism. In addition, no correlated variation between crystal concentration and chemical composition, which might arise from winnowing, has been noted in either the Eucarro or Yardea Dacite. Instead each unit has relatively constant proportions of crystals regardless of the whole rock composition. These points argue strongly against crystal winnowing during eruption being a major cause of the observed chemical variation.

5.5.3 - Major element constraints on fractional crystallization processes

Crystal fractionation from more mafic members of the mature phase volcanism is considered to be the most viable process for the derivation of the more silicic types. Major element modelling has successfully reproduced the variation seen within and between the various units with small residuals. The modelling was carried out using a least squares approximation, following the method of Bryan *et al.* (1969). Calculations which replicated the chemical variation by extracting mineral assemblages which were a good approximation of the observed modal mineralogical proportions were considered successful. The preferred models are listed in Table 5.4.

The most mafic Yardea composition was used as the parent for differentiation to the most silicic Yardea (excluding those samples considered to have undergone contamination from wall rocks). Generation of silicic Eucarro Dacite was modelled from mafic Eucarro and also from silicic Yardea compositions, with mineral proportions in the latter calculation being in general less satisfactory. Rhyolite of the Paney Rhyolite was derived in turn from silicic Eucarro.

The relative proportions of minerals removed by the modelling were very dependent on the amounts of K_2O in the selected parent and daughter and the compositions of both sanidine and plagioclase chosen for removal. Reasonable models were readily developed for the intra-Yardea models which removed various proportions of plagioclase and/or sanidine. The preferred best fit models within the Yardea compositions did not remove sanidine, which is consistent with the lack of Ba depletion in the Yardea, as all sanidine analysed contained relatively large amounts of Ba. Plagioclase in these models exceeds 60% of the extracted mineral assemblage and while substitution of various plagioclase compositions did not drastically change the proportion of plagioclase subtracted, it did alter the relative amounts of pigeonite and augite removed. More calcic plagioclase resulted in the removal of less augite and more pigeonite. The favoured models removed subequal amounts of the two pyroxene types, in line with the modal mineralogy of the unit.

All intra-Eucarro models calculated removed a far greater proportion of plagioclase (45-55%) than sanidine (17-19%). Those inferred to most accurately reproduce the actual assemblage again removed approximately equal amounts of pigeonite and augite, in accordance with observed pyroxene populations.

The quality of fit and mineral proportions in the generation of silicic Eucarro from silicic Yardea was the most highly dependent of all modelling on the relative endmember rock compositions chosen. Mineral assemblages subtracted by various models ranged from sanidine dominant through those with proportionate amounts of the two feldspars to plagioclase dominant. This variation in turn had a controlling effect on the relative

percentages of augite and pigeonite removed, with the amounts of plagioclase and augite being antithetic.

Paney Rhyolite was derived from silicic Eucarro, and was equally successful when the subtracted mineral assemblage contained the ferromagnesian silicate pairs augite+pigeonite and augite+olivine. The lack of preserved mafic silicates in the Paney disallows the identification of either model as being more correct, however the occurrence of olivine in some of the most siliceous Eucarro samples perhaps indicates an olivine bearing assemblage was present in the most fractionated products of the mature phase chamber. The choice of mafic silicates has little effect on the overall proportions of minerals removed. For all these models feldspars constitute over 80% of the subtracted assemblage, but for the first time sanidine is in every case the dominant mineral, exceeding 40%, and plagioclase more than 35% of the minerals removed. The percentage of olivine and pigeonite removed in the respective calculations where they were used is approximately equal.

In most models the mineral compositions which produced the best fits and most realistic mineral proportions were those of the parent rather than the differentiate. The titano-magnetite composition used throughout was the titanium rich inclusion in pyroxene from the Yardea Dacite considered to best compositionally approximate an original high temperature phase. Ilmenite was never successfully included in the modelling, but as it has only ever been identified in trace amounts this was not considered to represent a major problem.

5.5.4 - Trace element constraints

The major element models outlined above were used as the foundation in attempts to reproduce the trace element variations seen in the mature phase volcanism. Mineral proportions calculated using the major element data were combined with published mineral K_Ds to yield bulk rock partition coefficients for each of the trace elements modelled. The trace element chemistry of the calculated crystallization product was then calculated by the substitution of the bulk rock partition coefficients and the amount of crystallization (from the major element modelling) into the standard Rayleigh fractionation equation.

Trace element fractionation models were calculated to test the major element models. One set of mineral distribution coefficients was used for the dacitic to rhyolitic models (Y1, Y2, E1, E2) while a second set was used for the rhyolite to high silica rhyolite models (P1, P2). As very little partition coefficient data is available for pigeonite in silicic rocks, values for orthopyroxene were substituted. The mineral partition coefficients used are given in Appendix C together with the results of the modelling, and the results are summarised in Table 5.3. One constant result of the modelling was the

inability of any of the models to replicate Sc concentrations in the fractionated product, with calculated values typically about half of the required value. The reason for this is problematical, however recent experimental work on mafic rocks has revealed that partition coefficients for Sc in low Ca pyroxenes vary not only between orthopyroxene and pigeonite but also vary within each pyroxene type, by up to a factor of 4, with the Ca content of the pyroxene (Nielsen *et al.*, 1992). This, coupled with the strong dependence of partition coefficients on melt composition and temperature, means that the partition coefficients used for Sc are likely to be prone to a considerable degree of error. It is also obvious that substitution of orthopyroxene partition coefficients for those of pigeonite is inadequate, however until data for pigeonite in silicic rocks becomes available, little more can be done. Apart from Sc, the trace element modelling produces good fits for both the intra-Yardea models Y1 and Y2, however of the two models an overall better fit was produced by model Y1. This model removed approximately equal amounts of augite and pigeonite from the parent, in agreement with the the relative proportions of these minerals observed in the Yardea Dacite (Chapter 4), whereas the less successful model Y2 removed more pigeonite than augite. Model E1 produced a serious mismatch in levels of Ba, with the calculated values almost 400ppm below the required level, due to the large proportion of sanidine removed by this model. Model E1, which removes more plagioclase than sanidine and approximately equal proportions of augite and pigeonite, produces the best fit of the models for silicic Eucarro, and these mineral proportions are consistent with those documented for the unit (Chapter 4). The models P1 and P2, which attempt to derive high silica Paney Rhyolite from rhyolitic Eucarro, are moderately successful, with higher levels of Zr, Y, Th, and lower levels of the REE in the calculated product than required. The high Zr, Y and Th concentrations can be accounted for if a small amount of zircon (which has not been modelled) was added to the fractionating assemblage. The discrepancy in the rare earths for models P1 and P2 is greatest for Ce, however the reason for this mismatch is uncertain.

Many of the K_D values used in the modelling were in the low range of published values. Reasons for this may be: 1) the high temperatures of these volcanics may induce trace element Kds which are lower, similar to values more generally associated with intermediate rocks, due to the temperature dependence of partition coefficients; 2) recent microprobe (Michael, 1988) and ion microprobe (Sisson, 1991) determinations of partition coefficients of some elements, particularly REEs and incompatible elements, has shown that many of the higher K_D values published previously may be suspect, as these elements are contained in very small accessory mineral grains rather than in major phenocryst phases. This latter point reinforces previous ideas that REE and other incompatible elements are controlled by the behaviour of accessory minerals (Gromet and Silver, 1983; Miller and Mittlefeldt, 1982). To minimise the affect of accessory mineral

Table 5.4 - Major and trace element crystal fractionation models

Model #	*Y1*			*Y2*			*E1*			*E2*			*P1*			*P2*		
	Parent	*Daughter Observed*	*Daughter Estimated*	*Parent*	*Daughter Observed*	*Daughter Estimated*	*Parent*	*Daughter Observed*	*Daughter Estimated*	*Parent*	*Daughter Observed*	*Daughter Estimated*	*Parent*	*Daughter Observed*	*Daughter Estimated*	*Parent*	*Daughter Observed*	*Daughter Estimated*
	Y4#	*Y35#*		*Y4#*	*Y12#*		*Y12#*	*Eu21#*		*Eu25#*	*Eu21#*		*Eu21#*	*P6#*		*Eu21#*	*P6#*	
SiO2	67.35	69.16	69.22	67.35	69.11	69.11	69.11	72.78	72.87	69.54	72.78	72.86	72.78	76.51	76.82	72.78	76.51	76.76
TiO2	0.84	0.66	0.72	0.84	0.68	0.71	0.68	0.40	0.46	0.71	0.40	0.40	0.40	0.21	0.14	0.40	0.21	0.21
Al2O3	14.09	13.95	13.89	14.09	13.85	13.83	13.85	13.41	13.56	13.85	13.41	13.65	13.41	12.26	12.44	13.41	12.26	12.42
FeO*	5.40	4.57	4.55	5.40	4.65	4.64	4.65	3.27	3.25	4.78	3.27	3.27	3.27	2.20	2.24	3.27	2.20	2.21
MnO	0.13	0.13	0.10	0.13	0.14	0.10	0.14	0.09	0.08	0.13	0.09	0.07	0.09	0.01	0.05	0.09	0.01	0.04
MgO	1.09	0.80	0.78	1.09	0.85	0.87	0.85	0.19	0.28	0.68	0.19	0.38	0.19	0.18	0.02	0.19	0.18	0.07
CaO	2.62	1.96	1.94	2.62	2.06	2.05	2.06	1.19	1.18	2.01	1.19	1.13	1.19	0.18	0.23	1.19	0.18	0.25
Na2O	3.57	3.24	3.35	3.57	3.29	3.34	3.29	3.25	2.98	3.26	3.25	2.86	3.25	3.03	2.71	3.25	3.03	3.03
K2O	4.67	5.34	5.23	4.67	5.19	5.18	5.19	5.38	5.28	4.86	5.38	5.25	5.38	5.40	5.41	5.38	5.40	5.40
P2O5	0.25	0.18	0.22	0.25	0.16	0.17	0.16	0.05	0.07	0.17	0.05	0.13	0.05	0.01	-0.05	0.05	0.01	0.01
Sum r sqd			0.037			0.006			0.124			0.275			0.272			0.22
F= fraction of liquid remaining			0.874			0.885			0.755			0.818			0.789			0.793
Proportion of mineral phase in total of crystals subtracted																		
Plagioclase			64.59			67.47			29.08			43.04			37.21			38.33
Sanidine			-			-			41.79			24.63			43.93			43.56
Augite			15.18			9.16			11.18			12.71			10.34			9.87
Pigeonite			13.19			14.74			12.29			11.68			2.58			-
Magnetite			5.97			6.77			4.60			7.06			4.95			4.07
Apatite			1.07			1.87			1.06			0.89			0.96			1.24
Olivine			-			-			-			-			-			2.93
Zr	402	399	431	402	412	428	412	470	502	414	470	465	470	315	551	470	315	552
Sr	196	158	153	196	158	150	158	94	87	150	94	103	94	34	41	94	34	41
Rb	182	214	204	182	208	204	208	230	222	197	230	223	230	252	253	230	252	252
Y	58	63	60	58	66	60	66	68	71	64	68	66	68	69	76	68	69	76
Ba	1205	1310	1335	1205	1390	1334	1390	1143	754	1368	1143	1167	1143	496	511	1143	496	523
Sc	14.0	10.8	4.7	14.0	13.0	6.4	13.0	5.7	1.9	11.2	5.7	2.8	5.7	4.8	2.1	5.7	4.8	2.5
Th	26.0	28.2	29.5	26.0	29.0	29.4	29.0	46.6	44.8	34.4	46.6	40.9	46.6	43	58	46.6	43	58
Ce	158.0	165.5	166.2	158.0	183.0	160.8	183.0	193.0	191.2	168	193.0	184.7	193.0	292	218	193.0	292	213
Nd	70.0	74.3	73.2	70.0	70.0	71.5	70.0	90.0	85.2	75	90.0	81.0	90.0	112	101	90.0	112	99
La	75.0	82.7	78.6	75.0	89.0	76.0	89.0	97.0	95.3	84	97.0	94.5	97.0	122	109	97.0	122	106

 # whole rock compositions recalculated to 100% anhydrous
Compositions of phases used in calculations are listed in Table 6.5, along with calculated cumulate compositions for each of the listed models.
- denotes the phase was not included in a calculation.

fractionation, in all models except those attempting to produce the Paney Rhyolite from silicic Eucarro Dacite, the samples chosen to represent products of differentiation had greater REE, Zr, Nb, Y, etc. contents than the parent. As noted above greater difficulty was encountered in reproducing Paney Rhyolite from silicic Eucarro Dacite, due to the removal of indeterminate amounts of zircon.

In summary the chemical variation observed for the mature phase magmas are best modelled by fractional crystallisation in which the relative proportions of minerals removed are similar to the proportions observed in the units (Chapter 4).

5.5.5 - Chemical zonation in the pre-Eucarro and pre-Yardea magma chambers

As documented in earlier sections, the Eucarro Dacite exhibits chemical variation from dacite (68% SiO_2) to rhyolite (72% SiO_2). To assess whether this chemical variation represented zoning, samples Eu20 to Eu 25 were taken as a section through the unit from base to top. Eu20 was sampled at one of the few localities where the basal vitrophyre of the Eucarro is well exposed above the flow folded Bittali Rhyolite of the underlying developmental phase volcanism. Samples Eu21 to Eu 25 were then taken at successively higher stratigraphic levels, with sample Eu25 taken at a point adjacent to, but not directly underlying, the black vitrophyre of the Yardea Dacite, i.e. at the top of the Eucarro Dacite. The samples reveal that the Eucarro Dacite is zoned from a rhyolitic base, through rhyodacite, to a dacitic top, however the full chemical variation is seen only where the sparsely outcropping vitrophyre is exposed, such that the base of the unit is unequivocally located. Combined with evidence that the Eucarro represents a single cooling unit (Chapter 3), this base to top chemical variation indicates that the Eucarro Dacite represents the erupted top of a zoned magma chamber. The wide spacing of the samples prohibits assessment at this point as to whether the zoning was chemically continuous, or discontinous with sharp chemical breaks such as might be expected from a chamber containing double diffusive convection cells (Turner and Campbell, 1986).

The Nonning Rhyodacite is apparently also chemically zoned, although evidence for this at present is limited to general petrology contained in Turner (1975) (carried out before the definition of the unit) and from remote sensing interpretations of Macdonald (1988). It is difficult to assess whether the Yardea Dacite is also chemically zoned, for the generally flat-lying nature of the unit, coupled with the erosion of an unknown amount of its upper part, means that although its base is defined by vitrophyre, the thickness between any given outcrop and the (presumably present but buried) vitrophyre cannot be determined. Therefore it cannot be unequivocally stated that the Yardea magma was zoned from base to top.

Figure opposite:

Figure 5.6a - Enrichment factor diagram for the Eucarro Dacite. The factors are concentrations c the base of the unit divided by those from the top of the unit.

Figure 5.6b - Enrichment factor diagram for the Yardea Dacite. Enrichment factors represent concentrations in more silicic Yardea divided by those in the most mafic Yardea.

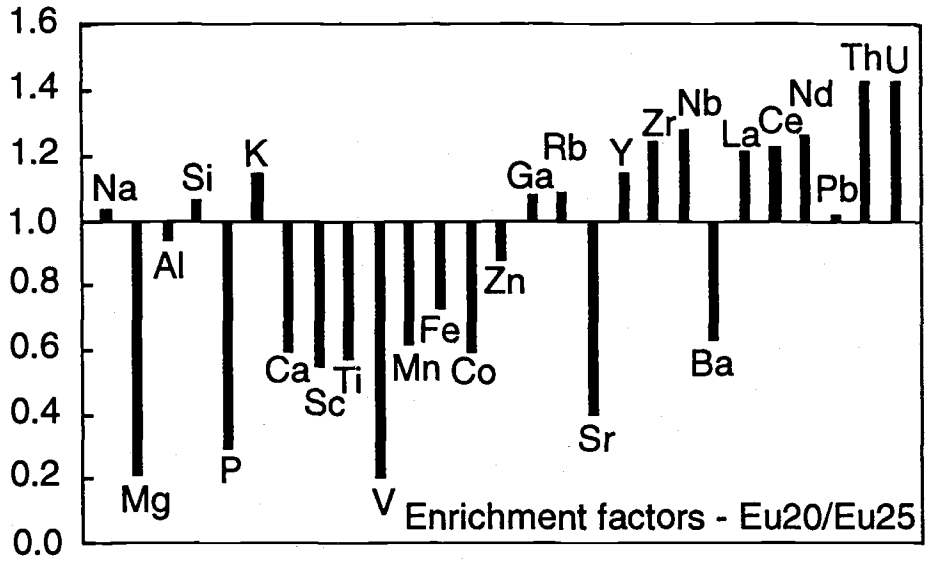
1.6
1.4
1.2
1.0
0.8
0.6
0.4
0.2
0.0
Na
Si
K
Ga
Rb
Y
Zr
Nb
La
Ce
Nd
Pb
Th
U
Al
Zn
Fe
Ca
Sc
Ti
Mn
Co
Ba
Sr
Mg
P
V
Enrichment factors - Eu20/Eu25

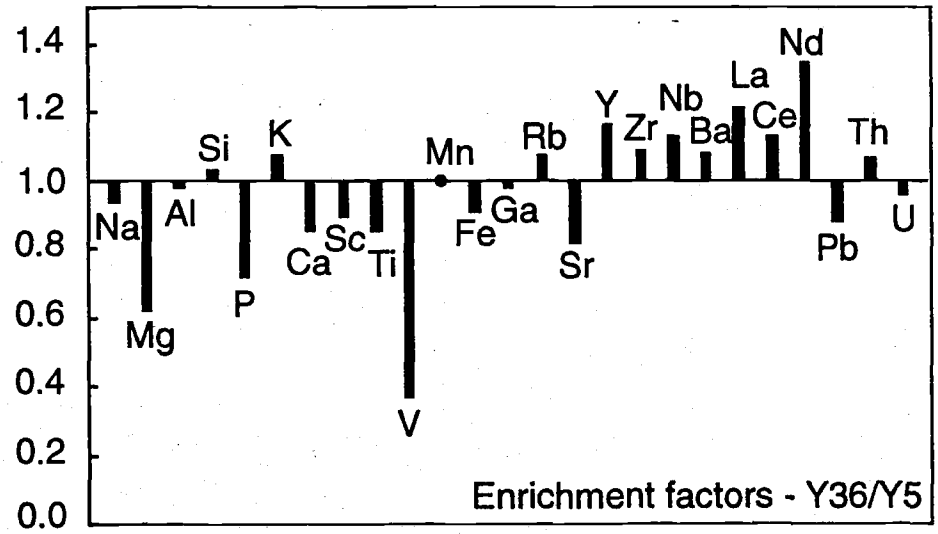
1.4
1.2
1.0
0.8
0.6
0.4
0.2
0.0
Nd
La
Y
Nb
Zr
Ba
Ce
Th
Si
K
Mn
Rb
Na
Al
Sc
Ga
U
Ca
Ti
Fe
Pb
Sr
P
Mg
V
Enrichment factors - Y36/Y5

Figure 5.6a is an enrichment diagram which shows the enrichment factors for the Eucarro Dacite, that is the concentrations in the basal material divided by those at the top of the unit. Although it is not possible to state with certainty that the Yardea Dacite is zoned, a diagram illustrating possible enrichment factors for the Yardea Dacite is presented as Figure 5.6b and the following discussion it is assumed that the Yardea is also zoned. Both diagrams illustrate roofward enrichments in elements which are incompatible in the mineral assemblage modelled as being fractionated, and roofward depletions in elements compatible in the crystallizing phases.

The enrichment factor diagrams reveal roofward enrichments of LREE and Th in both units implying that even though allanite has been observed as an accessory phase in both the Eucarro and Yardea, little allanite fractionation has occurred. Even a small amount of allanite removal would result in depletions of these elements roofward. Zr is enriched roofward in both units, therefore only minor, if any, zircon fractionation can have occurred in either magma. This is in agreement with zircon saturation calculations carried out on the mature phase volcanics following the method of Watson and Harrison (1983). At the temperatures determined for the mature phase volcanics (Chapter 4) most of the magmas would not be saturated in zircon, however in the volumetrically minor Eucarro with >73% SiO2 and the rhyolitic part of the Paney the magmas would be saturated in zircon.

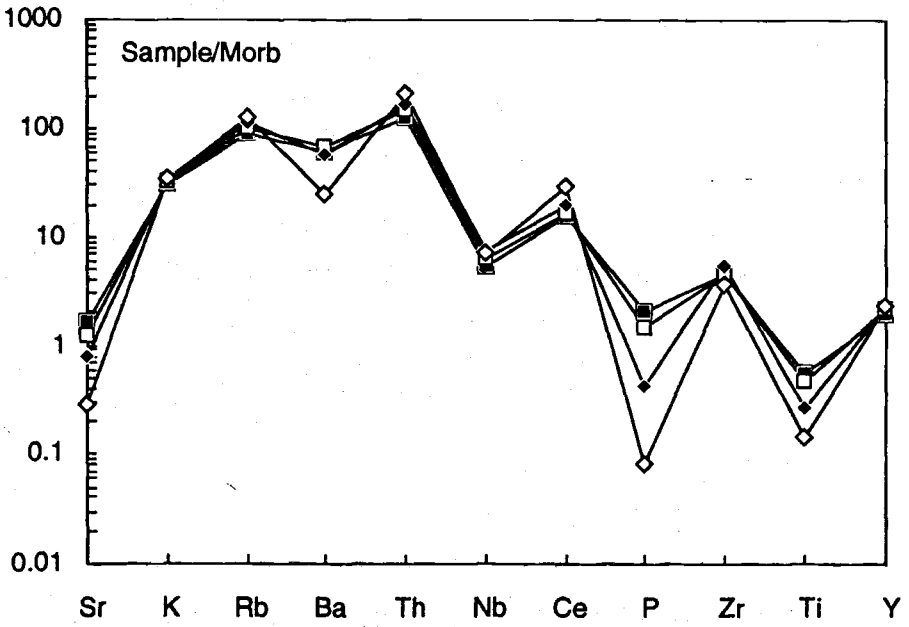

Figure 5.7 - MORB normalized spidergram of representative samples of mature phase volcanics. Normalization factors and element order are taken from Pearce (1983). Symbols: filled squares, Y4; open squares, Eu25; filled diamonds, Eu21; open diamonds, P6.

MORB normalized element diagrams spanning the entire silica range of the mature phase volcanics are illustrated in Figure 5.7 and demonstrate the coherency of the chemistry, with the variations readily explained by the mechanism of fractionation modelled previously. The choice of normalisation diagram was simply governed by the fact that the variation in the mature phase sequence was clearly illustrated, showing the strong depletion of Sr, P and Ti throughout the sequence, the depletion in Ba in the more siliceous samples, and the gradual increase of other elements.

5.6 - Origins of the isotopic variations

Most of the ε_{Nd} isotopic values for the mature phase magmas fall within a narrow range from -3.8 to -4.5. As noted previously two samples have ε_{Nd} values outside of this range. One anomalous value is for the most silicic sample of black Yardea (72% SiO_2), for which there is both mineralogical (Chapter 4), and chemical evidence that it was produced by contamination of the Yardea magma by silicic country rock or a partial melt thereof. It is interesting to note that this contamination has resulted in the sample having an ε_{Nd} value of -2.2, considerably higher than the range for those considered to be uncontaminated. The contaminant must be reasonably silicic, with high V, Sr, and Ca, low REE, Y, Th, K, Zr and Nb, and a high ε_{Nd} value relative to the Yardea Dacite. The required contaminant type is therefore somewhat unusual, however a lithology which fits the required chemical and isotopic constraints is the Waganny Dacite of the Southern Gawler Range developmental volcanic area (Chapter 2). The chemistry and Nd isotopic character of this anomalous sample of Yardea Dacite has been modelled by bulk assimilation of approximately 45% of a rhyodacitic member of the Waganny Dacite from Toondoolya Bluff, followed by 10% fractional crystallization. The contamination is thought to have had to be introduced in the magma chamber rather than as a consequence of the eruptive process because this anomalous Yardea sample contains a disequilibrium pyroxene assemblage.

The other anomalous sample comes from the basal Eucarro 'vitrophyre' and yields an ε_{Nd} value of -5.8. Unlike the example above, it exhibits no chemical or mineralogical evidence for contamination. However the uppermost Eucarro magma, with approximately 72% SiO_2, would have been compositionally little different to a contaminant of granitic country rock or a partial melt thereof. Contamination would therefore not greatly affect the chemical character of the magma and not induce the chemical or mineralogical changes seen in the contaminated Yardea Dacite, however it would alter the isotopic character of the sample.

Both of the contaminated samples come from the basal vitrophyres and contamination of the mature phase units appears to be limited to these samples which were

at or near the top of the magma chamber prior to eruption, where the magma assimilated roof rock, or a partial melt of the chamber roof. The contaminants have highly variable Nd isotopic character, however this is not unexpected for the basement underneath the province is probably heterogeneous, as is illustrated by the isotopic variation in the developmental phase volcanism (Chapter 2).

This contamination was apparently localised, for it occurs only in some samples from the vitrophyres, whereas other samples from these basal sections have isotopic characteristics within the main mature phase range. This may indicate that evidence of contamination may only have been preserved in small areas adjacent to the roof where the contaminated magma was not immediately swept into the main magma volume.

5.7 Origin of the parental magma

The ability of fractional crystallization modelling to reproduce the observed chemical variations, when considered together with the tight clustering of most of the isotopic data from this phase of volcanism, argues strongly for all of the units discussed in this chapter as products of differentiation from a single, periodically tapped magma chamber. Alternative scenarios, such as each of the major mature phase units developing in a separate magma chamber, would seem unlikely given that in documented cases of this type, the eruptive units tend to be isotopically variable (e.g. Riciputi and Johnson, 1990). The mature phase magma chamber is interpreted to have initially contained an isotopically and chemically homogenous parental magma, which evolved the observed chemical and mineralogical variation (Chapter 4) over time.

The question then arises whether the magma which was ultimately parental to the entire mature phase sequence was more mafic than any of the observed compositions, or rather was itself dacitic. Petrographic observations such as the development of reasonably coarse augite lamellae in pigeonite (and vice versa) in pyroxenes from glomerophenocrysts, remnants of pigeonite in augite which are more mafic than the main spread of analyses, and the presence of more calcic plagioclase and more potassic sanidine within glomerophenocrysts (see Chapter 4), are considered to be compelling evidence for the fractionation hypothesis and for the parental magma having been more mafic than the least siliceous Yardea Dacite (i.e. with <65% SiO_2). This is further substantiated by the occurrence of a set of magmatic inclusions within the Yardea Dacite which may suggest that the parental mature phase magma was andesitic in composition (see Chapter 6). Therefore models for the origin of the parental magma must produce a high temperature magma (T>1000°C), andesitic to low silica dacite in composition (62-65% SiO_2).

5.7.1 Derivation by crustal melting

Partial melting of crustal lithologies provides a simple mechanism for producing large volumes of silicic magma. Possible crustal sources for the mature phase volcanics must reside at lower to middle crustal depths, for pressures of ≈ 5 kilobars calculated from pyroxenes in the Eucarro Dacite indicate that the top of the magma chamber was at ≥8-15 km depth (Chapter 4), and therefore melting to produce the magmas must have been deeper than this, within the mid- to lower crust. Possible crustal sources include mafic or silicic granulites, broadly granitic material and previously emplaced mafic intrusive material.

If the mature phase volcanics were produced by anatexis of mid- to lower crustal lithologies, the estimated large volumes of magma (Chapter 3) require partial melting of substantial volumes of crust. The composition of such a large crustal volume may best be approximated by the estimated compositions of bulk and lower crust of Taylor and McLennan (1985). Modelling has therefore been undertaken to determine whether partial melting of either bulk or lower crust could yield magmas with the chemical composition of the most mafic Yardea Dacite. The modelling assumes equilibrium partial melting, such that the melt is in equilibrium with the crystalline residue in the source region up until segregation takes place. The concentration of any given element is calculated by the equilibrium melting equation Cl=Co/(F+D-FD) where Cl and Co are the concentrations of the element in the melt and the source respectively, D is the bulk partition coefficient of the element and F is the degree of melting. For each of the sources considered the minimum degree of partial melting has been estimated assuming that Th is a totally incompatible element (Bulk D=0), such that the equilibrium melting equation approximates Cl=Co/F, which allows the amount of melting, F, to be determined. The minimum amounts of melting required by the Th concentrations have been calculated as 13% and 3% for the average bulk crust and average lower crust of Taylor and McLennan respectively. In addition for each of the source compositions the composition of a 30% melt has been calculated, which is at the low end of values of critical melt percentages (CMP, the proportion of melt necessary to allow segregation of a silicic magma from its source) given by Wickham (1985), van der Molen and Paterson (1979), Marsh (1981) and Miller *et al.* (1988).

5.7.1.1. Melting bulk crust of intermediate composition

Figure 5.8a &b are primitive mantle normalised (PMN) diagrams showing the chemistry of the Yardea Dacite, together with the patterns for 13%, 18% and 30% melts of bulk crust for two different postulated residues. Figure 5.9a and b compares the REE patterns of the same melts with that of the Yardea Dacite, again for two different residues. The proportions of residual minerals were selected to after reviewing the experimental data

Figure 5.8a&b- Primitive mantle normalised diagrams comparing the Yardea Dacite with partial melts of bulk crust.

Figure 5.9a&b - REE pattern of the Yardea Dacite compared with those of partial melts of bulk crust.

a)

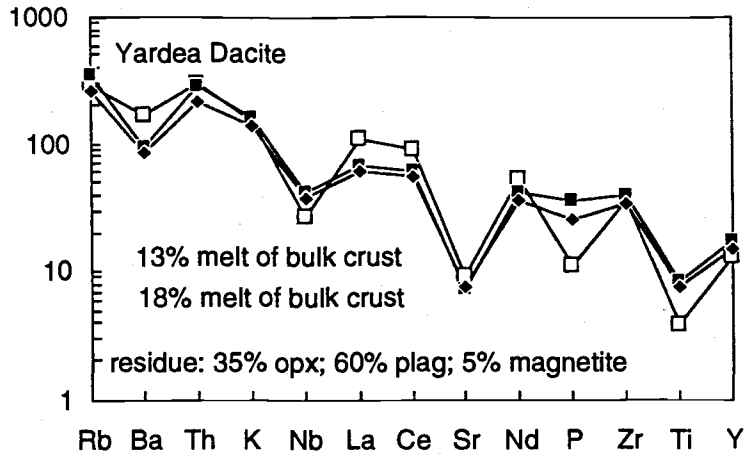
1000
100
10
1
Yardea Dacite
13% melt of bulk crust
18% melt of bulk crust
residue: 35% opx; 60% plag; 5% magnetite
Rb Ba Th K Nb La Ce Sr Nd P Zr Ti Y

b)

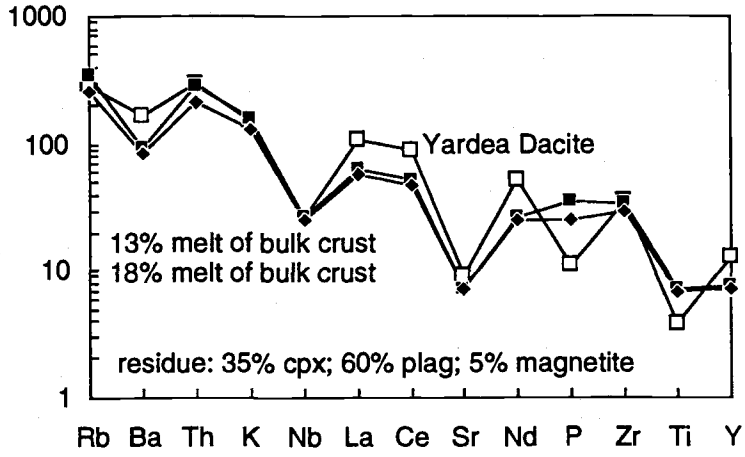
1000
100
10
1
Yardea Dacite
13% melt of bulk crust
18% melt of bulk crust
residue: 35% cpx; 60% plag; 5% magnetite
Rb Ba Th K Nb La Ce Sr Nd P Zr Ti Y

a)

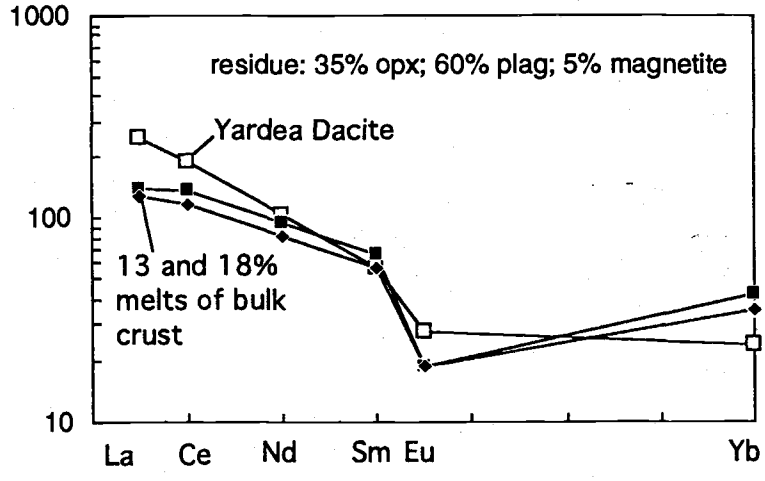
1000
100
10
residue: 35% opx; 60% plag; 5% magnetite
Yardea Dacite
13 and 18%
melts of bulk
crust
La Ce Nd Sm Eu Yb

b)

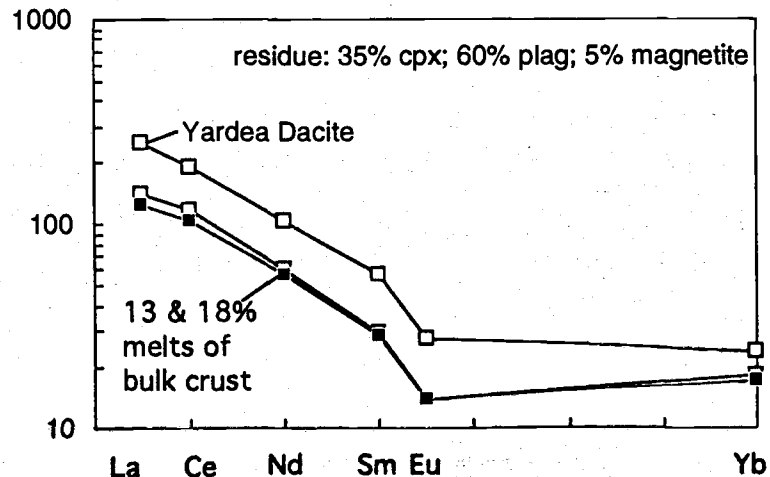
1000
100
10
residue: 35% cpx; 60% plag; 5% magnetite
Yardea Dacite
13 & 18%
melts of
bulk crust
La Ce Nd Sm Eu Yb

on fluid absent melting of intermediate crustal lithologies (e.g. Rutter and Wyllie, 19; Skjerlie and Johnson, 1992) and the partition coefficients used were those listed for intermediate rocks in Feeley and Grunder (1991). As can be seen from Figures 5.8 and 5.9, regardless of whether the pyroxene in the residue is orthopyroxene or clinopyroxene, the modelled melts cannot replicate the chemistry of the Yardea Dacite, particularly the levels of the REE. None of the melts attain anywhere near the high levels of LREE observed in the Yardea Dacite, nor do they show the required LREE enrichment, with $(La/Yb)_N$ of the 13% melt = 3.4 and 7.3 for the clinopyroxene and orthopyroxene bearing residues respectively, compared with $(La/Yb)_N$ of 10.2 for the Yardea Dacite. The melting models also have trouble reproducing the amount of Eu in the Yardea Dacite, for all the models have much too low levels of Eu.

Any partial melt of intermediate composition crustal rocks will have plagioclase in the melt residue, and experimental work indicates that it will be the dominant residual phase (Skjerlie end Johnson, 1992; Rutter and Wyllie, 1988). As Eu will be preferentially partitioned into the residual plagioclase, the melt will be heavily depleted in Eu. If the melt contained significant amount of restitic plagioclase carried up from the source, this could possibly explain the smaller than expected Eu anomaly. However there is not petrographic evidence from the mature phase volcanics to suggest that any of the plagioclase crystals have a residual origin, rather all indications are that the plagioclase grains are phenocrysts crystallised from a melt. A crustal source of intermediate composition which could produce a partial melt compositionally similar to the Yardea Dacite would therefore have to be much more LREE enriched than bulk crust *and* have a positive Eu anomaly. Such lithologies are uncommon in the crust (Taylor and McLennan, 1985; Vielzeuf *et al.*, 1990). For example if the positive Eu anomaly were the result of the source itself having undergone a previous melt depletion event, the source would be depleted rather than enriched in LREE. It is therefore considered that the parental mature phase magma cannot have been produced by the simple mechanism of partial melting intermediate composition continental crust.

See p. 162

5.7.1.2. Melting mafic lower crust

Another possible source for the production of the parental mature phase magma by anatexis is mafic lower crust. The modelling undertaken to assess whether the parental mature phase magma could have been produced by partial melting of mafic crustal material used as the source composition the average lower crust composition of Taylor and McLennan (1985). The proportions and compositions of residual phases in two possible residual assemblages are those appropriate for a melt of temperature >1000°C as determined by the fluid absent melting experiments of Rushmer (1991), while the partition coefficients used are taken from Feeley and Grunder (1991). The minimum degree of

melting of this source has been calculated as 3%, estimated assuming Th is totally incompatible as discussed previously.

Figure 5.10 a &b show the PMN patterns for the Yardea Dacite and for 3% and 30% melts of average lower crust calculated for the two different residues. Figure 5.11 a & b illustrate the REE patterns of these 3% and 30% melt of average lower crust compared with that of the Yardea Dacite. The figures illustrate that although a 3% melt of average lower crust shows some chemical similarities to the Yardea Dacite, the calculated melt contains neither the required levels of REE, nor the degree of LREE enrichment. A 3% melt of lower crust has only half the La of the Yardea Dacite, and $(La/Yb)_N$ of 5.9-7.1 compared to $(La/Yb)_N$ of the Yardea Dacite of 10.2. The levels of Eu in the calculated melts are also far too low, with the 3% melts of lower crust having only between 54 and 64% of the Eu observed in the Yardea Dacite. As all experimental vapour-absent melting of mafic lithologies have plagioclase as the dominant residual phase, it is difficult if not impossible to produce a melt with the required level of Eu. For a mafic lower crustal source to yield a melt like the Yardea Dacite it would have to be both enriched in LREE and have a positive Eu anomaly. As stated in the previous section, it is difficult to create a source which fulfils these characteristics, for a source residual after a previous partial melting event may have a positive Eu anomaly, but would be depleted in LREE. If the positive Eu anomaly was the result of cumulus feldspar, an allied strong LREE enrichment would be unlikely.

Another point against a lower crustal mafic source for the mature phase volcanics is the problem of extracting such a small volume of silicic melt from its source. A 3% melt is an order of magnitude lower than the 30-50% melt commonly quoted for the CMP (Wickham, 1985; van der Molen and Paterson, 1979; Marsh, 1981; Miller *et al.*, 1988). Tectonic related mechanisms for extracting low melt percentages from their source, such as tectonic pumping, are not realistic in this case because of the anorogenic setting of the Gawler Range volcanism.

The chemical and mechanical arguments outlined above weigh strongly against the mature phase volcanics having been produced by partial melting of either intermediate or mafic lower crust. A further point against a partial melting model is provided by isotopic data on granulitic basement rocks from the Gawler Craton, which may be considered as exhumed equivalents of mid- to lower crustal lithologies. The ε_{Nd} of the mature phase volcanics is higher than the majority of Archaean and Palaeoproterozoic rocks exposed on the Gawler Craton which may be considered to represent possible source lithologies at mid- to lower crustal depths (Table 2.4; Figure 5.12). This isotopic constraint provides added weight to the previous arguments that the mature phase volcanism cannot be the product of simple crustal fusion.

Figure 5.10a&b- Primitive mantle normalised diagrams comparing the Yardea Dacite with partial melts of mafic lower crust.

Figure 5.11a&b - REE pattern of the Yardea Dacite compared with those of partial melts of mafic lower crust crust.

a)

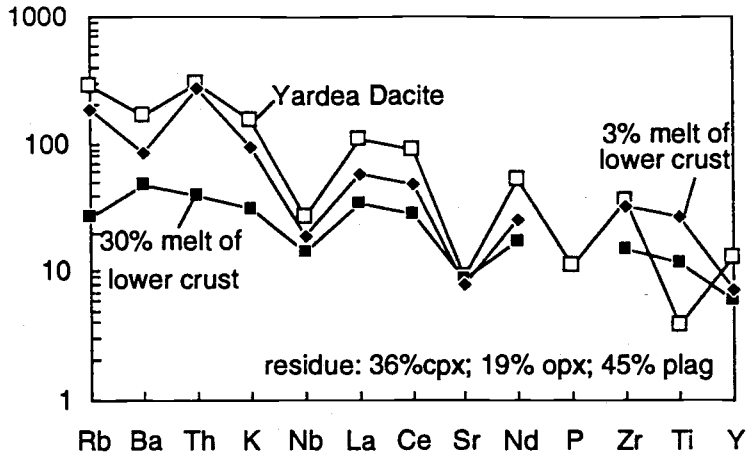
1000
100
10
1
Yardea Dacite
3% melt of lower crust
30% melt of lower crust
residue: 36%cpx; 19% opx; 45% plag
Rb Ba Th K Nb La Ce Sr Nd P Zr Ti Y

b)

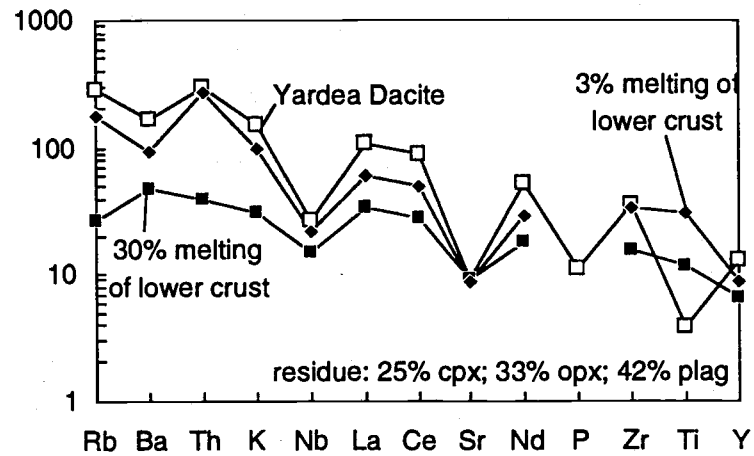
1000
100
10
1
Yardea Dacite
3% melting of lower crust
30% melting of lower crust
residue: 25% cpx; 33% opx; 42% plag
Rb Ba Th K Nb La Ce Sr Nd P Zr Ti Y

a)

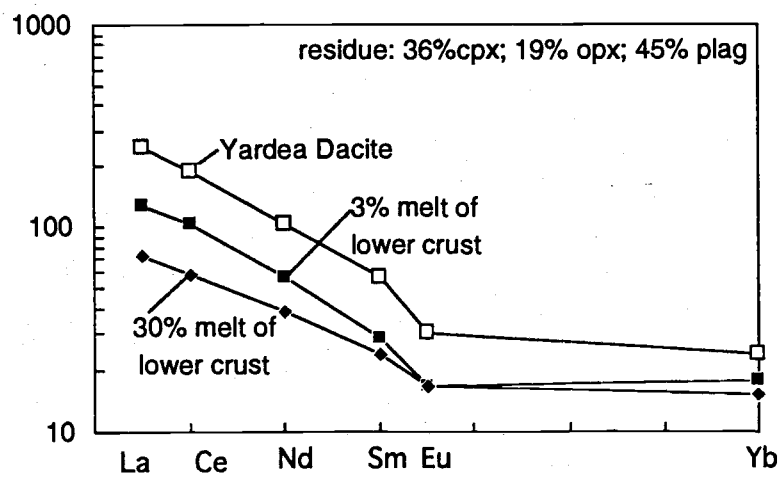
1000
100
10
residue: 36%cpx; 19% opx; 45% plag
Yardea Dacite
3% melt of lower crust
30% melt of lower crust
La Ce Nd Sm Eu Yb

b)

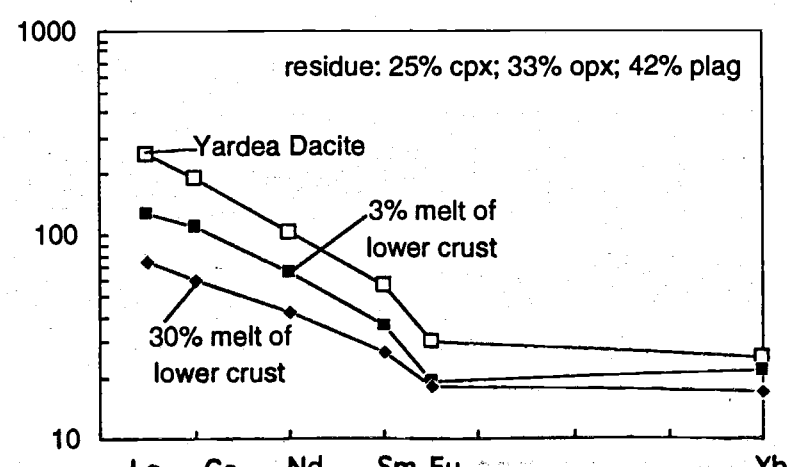
1000
100
10
residue: 25% cpx; 33% opx; 42% plag
Yardea Dacite
3% melt of lower crust
30% melt of lower crust
La Ce Nd Sm Eu Yb

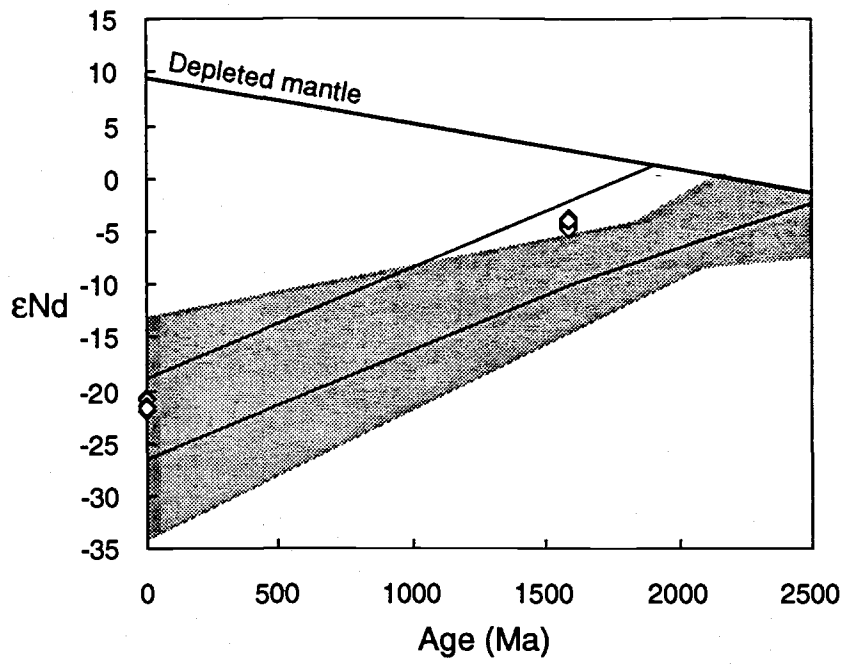

Figure 5.12 - Nd evolution curve for the mature phase volcanics. Diamond symbols represent the mature phase volcanics. The field for Archaean basement rocks is shaded and the field for Palaeoproterozoic rocks is outlined.

5.7.2 - Fractionation of mantle derived mafic melt

The most compelling evidence against the mature phase magmas having formed via crystal fractionation of a mafic melt from the mantle is provided by their isotopic characteristics compared with those of basaltic rocks from the developmental phase which are considered to represent mantle melts (Chapter 2). All of the basalts have ε_{Nd} values between -1.8 and -3.5, whereas the average value obtained for the mature phase (excluding the one sample from the Yardea with an anomalous isotopic value) is -4.6. This indicates that simple fractional crystallisation from contemporary mantle derived mafic magma cannot be an acceptable process for producing the mature phase volcanics.

5.7.3 - Assimilation-Fractional Crystallisation

Fractionation of a basaltic parent combined with concomittant crustal contamination is an alternative mechanism for producing silicic magmas which has been invoked for several large volume silicic volcanic provinces, e.g. the San Juan volcanic field (Riciputi and Johnson, 1990) and the Timber Mountain/Oasis Valley volcanic centre (Farmer *et al.*, 1991). Modelling AFC processes is not an easy task given the number of variables in the AFC equation, including the chemical and isotopic composition of both the source and assimilant, and the mineral partition coefficients chosen. Given that the

production of such a large volume of felsic magma is unlikely to have resulted from interaction between a single mafic magma and a single crustal contaminant, the modelling outlined below was undertaken to determine if the AFC process could produce magmas which were chemically and isotopically like the most mafic Yardea Dacite.

In modelling AFC, the parental mafic starting endmember chosen was the Nuckulla Basalt from Lake Everard which has the highest εNd of any of the Gawler Range basaltic rocks (Chapter 2). The assimilant used in the calculations was the Kokatha rhyolite RH3, which was chosen because it was highly siliceous and significantly enriched in incompatible elements, both of which would be features of a partial melt of silicic crustal rocks and because it has a Nd isotopic value which is approximately in the middle of the range exhibited by the basement rocks of the Gawler Craton. The proportions of minerals in the fractionating assemblage were chosen such that they were consistent with mineralogical observations of the Yardea Dacite and the basalts of the developmental phase. The fractionating assemblage used was 0.070 olivine, 0.555 plagioclase, 0.184 clinopyroxene, 0.150 pigeonite, 0.034 magnetite and 0.007 apatite. As illustrated in Figure 5.13, AFC with low r values (rate of assimilation/rate of crystallisation) of 0.2 reproduces quite well the chemistry of the Yardea Dacite when F, the fraction of original melt remaining, is approximately 0.4-0.5. The poor fit for Ti and P in the models may be due to relatively poorly known partition coefficients for these elements in magnetite and apatite respectively. Of the two sets of partition coeffiecients used, the lower values for the REE of Honjo and Leeman (1987) more closely reproduce the elemental concentrations of the Yardea Dacite than do those of Feeley and Grunder (1991). However even using the Feeley and Grunder values, the results of the AFC modelling more closely resemble the Yardea Dacite than do any of the melting models outlined above. Although choosing a different assimilant may change the calculated r value, if it is granitic in composition the r will nevertheless be small, i.e. the mantle component will be dominant.

As no REE pattern is available for the chosen assimilant rhyolite RH3, the amount of Eu in the AFC product cannot be evaluated. However the AFC mechanism for producing the mature phase magmas provides a possible explanation if modelling of the REE produced a higher than expected value for Eu. The mature phase magmas contain 20-40% phenocrysts which are dominantly plagioclase. Inefficient separation of plagioclase from the magma, due to small density differences between plagioclase and melt, could cause higher than expected levels of Eu compared to the other REE.

AFC modelling of Nd isotopes has been carried out using the same endmembers, fractionating assemblage and distribution coefficients, to determine if the mechanism could also produce the isotopic values seen in the mafic Yardea Dacite. As seen in Figure 5.14, the AFC curves for the two sets of partition coefficients bracket theYardea Dacite.

Although the isotopic modelling cannot be considered in any way definitive, it nevertheless is consistent with the chemical modelling and supports an AFC origin for the mature phase magmas.

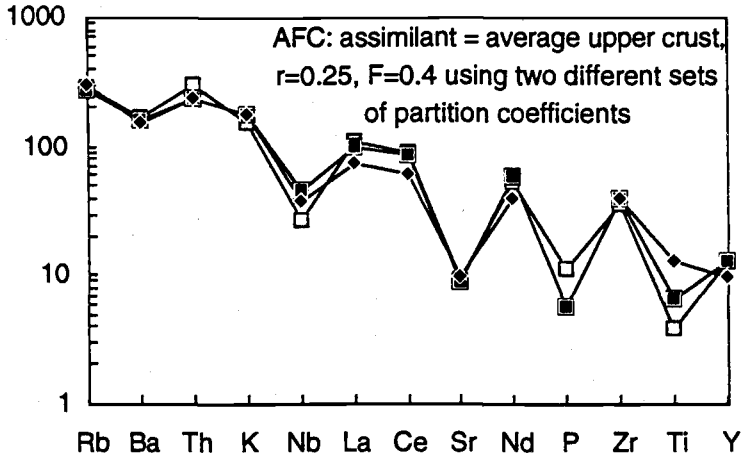

Figure 5.13 - PMN diagram comparing the chemistry of the Yardea Dacite with calculated compositions of melts formed by the AFC process. Basaltic endmenber = Nuckulla Basalt, silicic endmember= rhyolite 908-1. Details of model are in Appendix F.

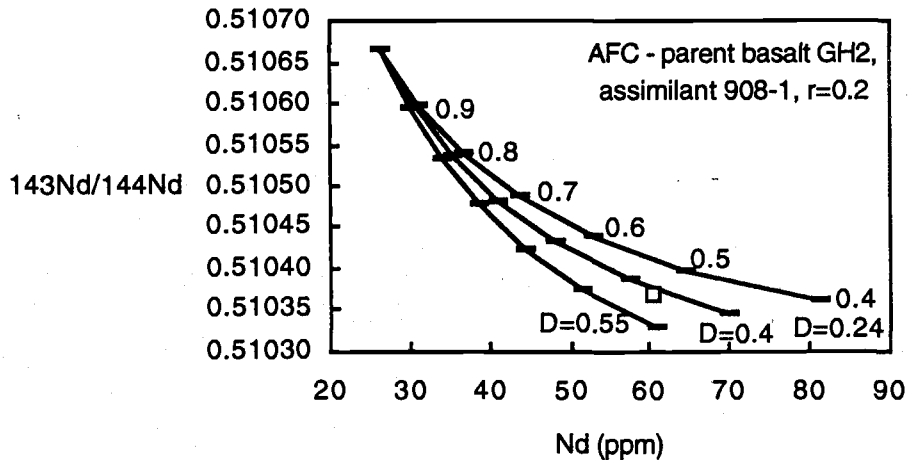

Figure 5.14 - Plot of $^{143}Nd/^{144}Nd$ against Nd (ppm) illustrating the results of AFC modelling using different bulk partition coefficients for Nd. The open square represents Yardea Dacite sample Y4. The curves are AFC curves with ticks at 10% fractionation intervals. The fractionating assemblage is as listed in text. Left hand and right hand curves were generated using the partition coefficients of Feeley and Grunder (1991) and Honjo and Leeman (1987) respectively. The centre curve was calculated using a bulk partition coefficient for Nd intermediate between the two extremes.

5.7.4 - Conclusions and comparison with previous models

Geochemical modelling indicates that the parent magma of mature phase volcanics did not form by partial melting of either intermediate ot mafic mid-to lower continental crust. Partial melting models also encounter melt extraction problems, for all of the melting calculations require melt percentages far below the minimum CMP required to extract a silicic melt from its source. The melting models also fail to reproduce the high REE contents and the degree of LREE enrichment seen in the most mafic Yardea Dacite.

Trace element modelling suggests that the parental mature phase magma formed via an AFC process from a LP basalt, with the assimilant being an incompatible element enriched partial melt derived from the crust. This process more successfully reproduces the high REE contents of the Yardea Dacite. An AFC origin is also consistent with Nd isotopes of the mature phase which lie between the basalts of the developmental phase and the Archaean to Palaeoproterozoic basement rocks.

Two alternative models have recently been proposed for the petrogenesis of the Yardea Dacite. The first model has been proposed as a general model for the production of A-type magmas by Creaser *et al.*, 1991, and for the Yardea Dacite specifically (R. Creaser pers. comm.). The model seeks to produce A-type magmas including the Yardea Dacite by melting crustal rocks of tonalitic to granodioritic composition.

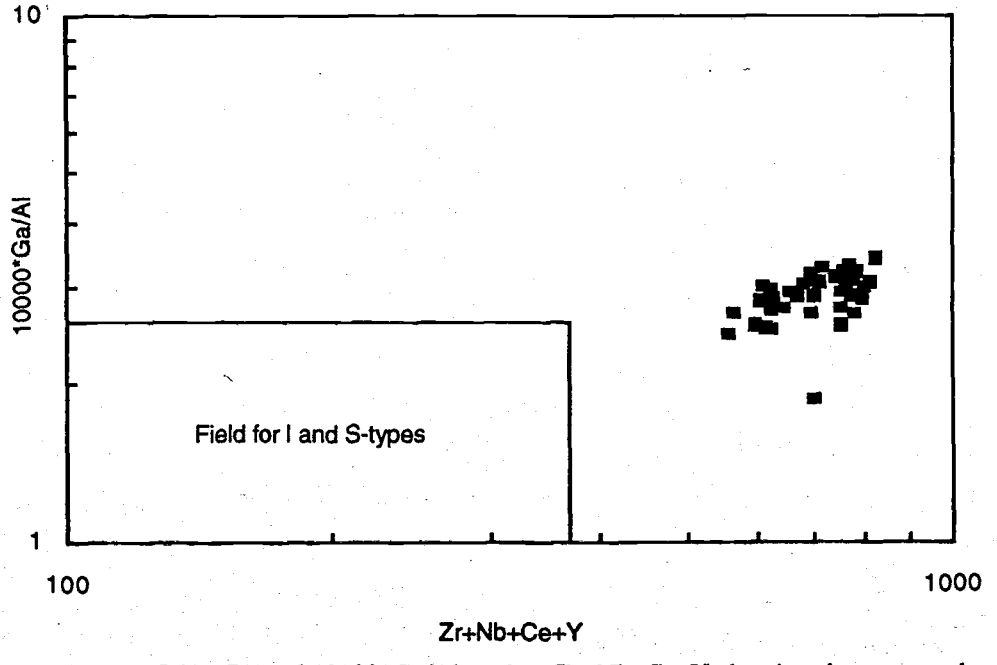

Figure 5.15 - Plot of 10000*Ga/Al against Zr+Nb+Ce+Y showing the mature phase volcanics lie in the field of A-type granites of Whalen *et al.*, (1987).

The mature phase volcanics do fit the criteria for A-type magmas, being enriched in incompatible elements (Figure 5.15), relatively dry, and have an anorogenic setting. However there are several problems with the model of Creaser *et al.* (1991) in producing dry, very hot silicic magmas such as the Yardea. Firstly melting of these broadly granitic crustal rocks should not produce dry magmas, for melt is produced by the breakdown of hydrous phases (biotite, amphibole) within the source, which releases most, if not all, of the volatile content of the source into the magma. Therefore such a melt is not likely to be dry, as is required by both the phase relationships and the degree of crystallisation in the Yardea Dacite (Chapter 4). A second point is that the dehydration breakdown of amphibole and biotite tend to occur at temperatures <950°C (Rutter and Wyllie, 1988; Skjerlie and Johnson, 1992), which are considerably lower than the 1050-1100°C of the Yardea Dacite (Chapter 4). It would seem then that melting of broadly granitic source would produce cooler, less dry magmas than the Yardea Dacite.

A second model suggested that the Yardea Dacite represents an extrusive equivalent of a charnockitic magma type (CMT), whose magmas are generated by the partial melting of a mafic to intermediate di-normative crustal source that has little hornblende due to a previous dehydration event (Kilpatrick and Ellis, 1992). Such dehydrated sources will melt at the high temperatures required for the Yardea Dacite, however the dehydration of hornblende would produce a less fertile source, which would yield relatively small volumes of melt per volume unit of source (Vielzeuf *et al.*, 1990). It is difficult to reconcile this fact with the considerable volumes of magma estimated to have been produced during the mature phase volcanism (Chapter 3). Kilpatrick and Ellis (1992) list the chemical distinctions of the CMT as coupled enrichments in TiO_2, P_2O_5 and K_2O, and low CaO. However the Yardea Dacite, together with the other mature phase volcanics, are not particularly enriched in TiO_2, P_2O_5 or K_2O and on the discrimination diagrams of Kilpatrick and Ellis (1992) plot within the field defined by Lachlan Fold Belt granites rather than within the main field of the CMT. Therefore these chemical parameters do not require an unusual source type. The Yardea does however have low CaO compared with the Lachlan Fold Belt granites. Kilpatrick and Ellis (1992) attribute the low CaO of the CMT to a lack of biotite in the source, however an AFC model can also explain the low CaO as a chemical feature inherited from the basaltic endmember, for all of the Gawler Range basalts also have low CaO and CaO/Al_2O_3 (<0.47) when compared to MORB and other basalt types. Assimilation and fractionation of an assemblage dominated by plagioclase and clinopyroxene would further lower CaO in the resultant mature phase silicic magmas.

Reproducing the REE patterns of the Yardea Dacite presents another problem for the models of both Creaser *et al.* (1991) and Kilpatrick and Ellis (1992). As was discussed in section 5.7.1 melting of a crustal source, either mafic or intermediate, would

result in a plagioclase rich residue, and the resultant melts would contain far lower levels of Eu than those seen in the Yardea Dacite. In addition unless the source was characterised by high REE contents and strong LREE enrichment, it would be difficult to attain the high REE levels of the Yardea Dacite by partial melting.

5.8 -Summary and a model for the pre-Eucarro and pre-Yardea magma chambers

The mature phase volcanics exhibit systematic chemical variation, but are isotopically homogenous with two exceptions. Major and trace element modelling are consistent with the mature phase volcanics being related by crystal-liquid fractionation of the observed phenocryst assemblages from a low silica dacitic or andesitic parent magma. The chemical, isotopic and mineralogic data for the mature phase volcanics which have been presented above and in the preceding chapter are consistent with them representing periodic eruptions from a single, large, evolving magma chamber. Mineralogical and chemical data can be synthesized to produce models for the mature phase magma chamber at two points in its evolutionary history, immediately prior to the eruptions which formed the Eucarro and Yardea Dacites. Figure 5.16 is a schematic representation of the models.

There is good evidence that the Eucarro represents the eviscerated contents of a zoned magma chamber, sections taken through the unit exhibit systematic changes in mineralogy and mineral composition, as outlined in Chapter 4, which is linked to chemical variation. The pre-Eucarro chamber contained a magma column which was both compositionally and mineralogically zoned from a cooler, rhyolitic top with a larger proportion of dissolved volatiles to a hotter, dacitic lower portion containing less volatiles. In a limited volume of the rhyolitic magma, probably at the very top of the chamber, igneous amphibole was stabilized in preference to pyroxene as a result of increased volatile content in the melt which may or may not have been associated with lower temperature. In the entirety of the erupted portion of the magma the fluid content of the magma was low, X_{fluid} in the magma being less than 0.25 where pyroxene was stabilized and only exceeding this value in the small amphibole bearing magma volume. Phenocryst content of the magma was relatively unchanged with depth in the chamber, indicating that fluid concentration near the chamber roof did not reach levels sufficient to depress the liquidus. Crystallization had resulted in the concentration of fluid at the top of the massive magma chamber.

After the eruption of the Eucarro Dacite, minor volume eruptions (in the form of the Yannabie Rhyodacite and the Paney Rhyolite) suggest periodic leakage from the chamber, but the subsequent eruption of the Yardea Dacite without a highly differentiated top indicates

the eruption rate exceeded the rate at which regeneration of the zoning could occur. The Yannabie Rhyodacite is more siliceous than the upper Eucarro Dacite, indicating that evolved melt was pooling at the top of the magma chamber as a result of ongoing fractionation processes. The intermingled rhyolitic and rhyodacitic components of the small volume Paney Rhyolite, both of which are more siliceous than the preceding Yannabie Rhyodacite, suggests both that in the repose time between these two eruptive events, evolved magmas continued to collect at the top of the magma chamber, and also that the volume of these evolved magmas was small, such that the eruption process was able to draw down through compositional interfaces which may have been the result of double diffusive processes.

The Yardea Dacite shows some chemical variability, however because it is a flat lying sheet whose upper section has been eroded, and for which no vertical sections are known, an interpretation that it is a zoned unit is admittedly tenuous, it may simply be the monotonous 'dominant volume' (Smith, 1979) of the magma system. Nevertheless it is considered possible that some degree of zoning was present as the observed chemical variation does not correlate with varying phenocryst proportions, i.e. much of the variation does not appear to be due to changes in the crystal/matrix ratio. If the Yardea chamber was zoned, it is a chemical and mineralogical extension of, rather than a repetition of, the zoning observed in the Eucarro Dacite. Therefore much of the mature phase chemical variation may have been established before the mature system began its cycle of eruption. The almost entirely dacitic character of the Yardea Dacite indicates that in the repose time prior to its eruption no highly siliceous cap formed on the magma chamber. The model for the Yardea therefore shows inferred gradations in temperature and silica content with depth (Figure 5.16). The fluid content of the Yardea magma was very low even at the top of the chamber, a remarkable fact considering the remnant magma in the chamber after the eruption of the Eucarro underwent another 15-20% crystallization prior to the expulsion of the Yardea. The fluid in the Yardea magma was halogen rich, as evidenced by high F and Cl contents in the fine amphibole rims on pyroxene. Due to preservation problems, primary amphibole has only been noted from the vitrophyre, which would have been close to the roof of the chamber. It may be therefore that crystallization and magma chamber processes had combined to enrich the roofward magma in halogen rich fluid and therefore limited the stabilization of amphibole to this portion of the chamber only. High amounts of halogens are likely to have stabilized amphibole to much higher than normal temperatures.

Geochemical and isotopic modelling suggest the parental mature phase magma formed by AFC processes from a LP basalt, similar to those erupted in the developmental phase. The AFC models indicate the parental mature phase magma evolved by a combination of low amount of assimilation (r=0.2) of a silicic partial melt of crust and approximately 50-60% fractionation of a phenocryst assemblage dominated by plagioclase

and pyroxene. Several crustal melting models have been assessed and all encounter problems with replicating the high REE contents of the most mafic Yardea Dacite, and also require relatively small degrees of melting which make melt segregation from the source difficult.

After the eruption of the Yardea magma, the massive magma chamber continued to crystallize, passing through the critical crystallinity level beyond which magma can no longer erupt, possibly because the thermal anomaly which had provided the heat for initiation of and continuation of volcanism of entire system was waning.

Figure opposite:

Figure 5.16 - Schematic representations of the mature phase magma chamber at two points in its evolution a) prior to the eruption of the Eucarro Dacite and b) prior to the eruption of the Yardea Dacite with intensive parameters of the chamber as estimated from mineralogical data. Circled numbers represent the percent SiO_2 in the chamber at a given position. Estimated vertical scale is several kilometres, and approximate horizontal scale is $\geq$ 25 kilometres.

The pre- Eucarro magma chamber

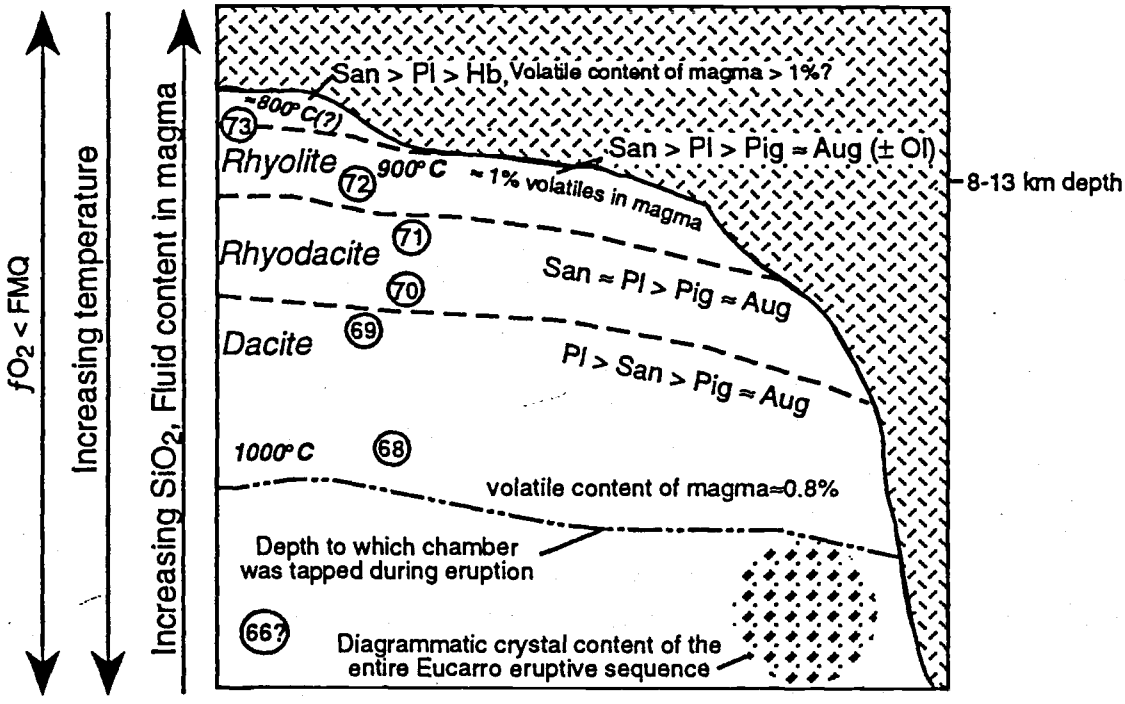

The pre-Yardea magma chamber

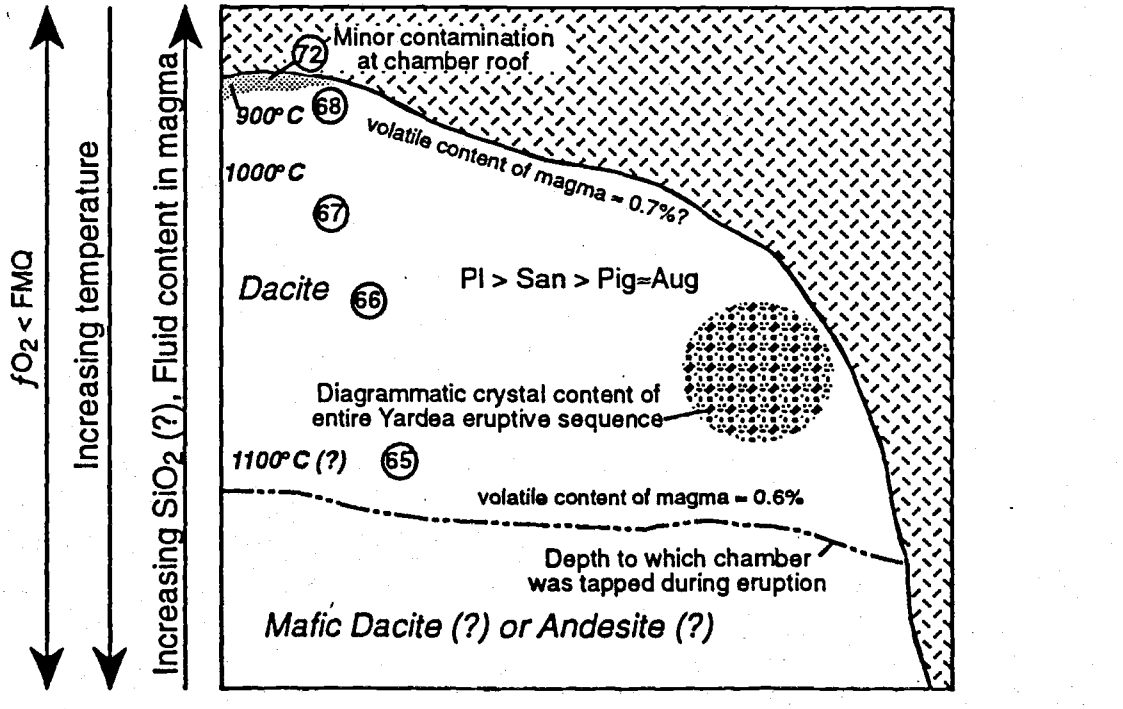

Chapter 6 - Magmatic inclusions in the mature phase volcanics

6.1 - Introduction

Magmatic inclusions in volcanic rocks can yield information on aspects of the magma system which may be otherwise unobtainable. For example inclusions may reveal the action of processes such as magma mixing or hybridization (e.g. Bacon and Metz, 1984), or recharge of a magma chamber (e.g. Druitt and Bacon, 1988) which are not evident from studying the volcanics alone. Alternatively in some silicic volcanic systems, magmatic inclusions may be the only record of contemporaneous mafic magma (e.g. Varga *et al.*, 1990).

Magmatic inclusions have been identified in the Yardea and Eucarro Dacites of the mature phase volcanic sequence and this chapter describes the inclusions and attempts to determine their origin and what they reveal about the mature phase magma system.

6.2 - Occurrence of inclusions

Mafic inclusions in the Yardea have previously been described as lithic fragments of solid basaltic material (Giles, 1980) presumably ripped up from the basement or from earlier Gawler Range eruptions. Although xenoliths of this type do occur along with many other types of lithic fragments (Chapter 3), the inclusions discussed in this chapter are of a separate and distinct origin. Inclusions have been found in both the Yardea and Eucarro Dacites, and may be present in all of the ignimbritic mature phase units, although they have yet to be identified in the Nonning or Yannabie Rhyodacites.

Two groups of inclusions have been identified, which have been named type 1 and type 2. The two inclusion groups are differentiated by their distinctive petrographic appearances, and the division is reinforced by distinct chemical and isotopic characteristics. The Eucarro Dacite contains rare type 1 inclusions but to date no type 2 inclusions have been identified in this unit. Both types of inclusion occur in the Yardea Dacite, where their distribution is irregular, being abundant at some localities and entirely absent at others. Field observations also indicate that the two inclusion types have mutually exclusive distribution within the Yardea Dacite, for localities may contain either type 1 or type 2 inclusions, not both, or alternatively no inclusions at all. At only one

Figures opposite:

Figure 6.1a - Large Type 1 mafic inclusion in the Yardea Dacite. Hammer is approximately 30 centimetres in length.

Figure 6.1b - Type 1 mafic inclusions in the Yardea Dacite. At least eight inclusions of varying sizes are present in this photograph. Lens cap is approximately 6 centimetres in diameter.

Figure 6.1c - Type 2 inclusion in the Yardea Dacite. Note the few large phenocrysts of potassium feldspar within the inclusion. Lens cap is approximately 6 centimetres in diameter.

Figure 6.1d - Type 2 inclusions in the Yardea Dacite. Arrowed are two inclusions, one inclusion is above the lens cap, the second is below and slightly to the left of the lens cap. Lens cap is approximately 6 centimetres in diameter.

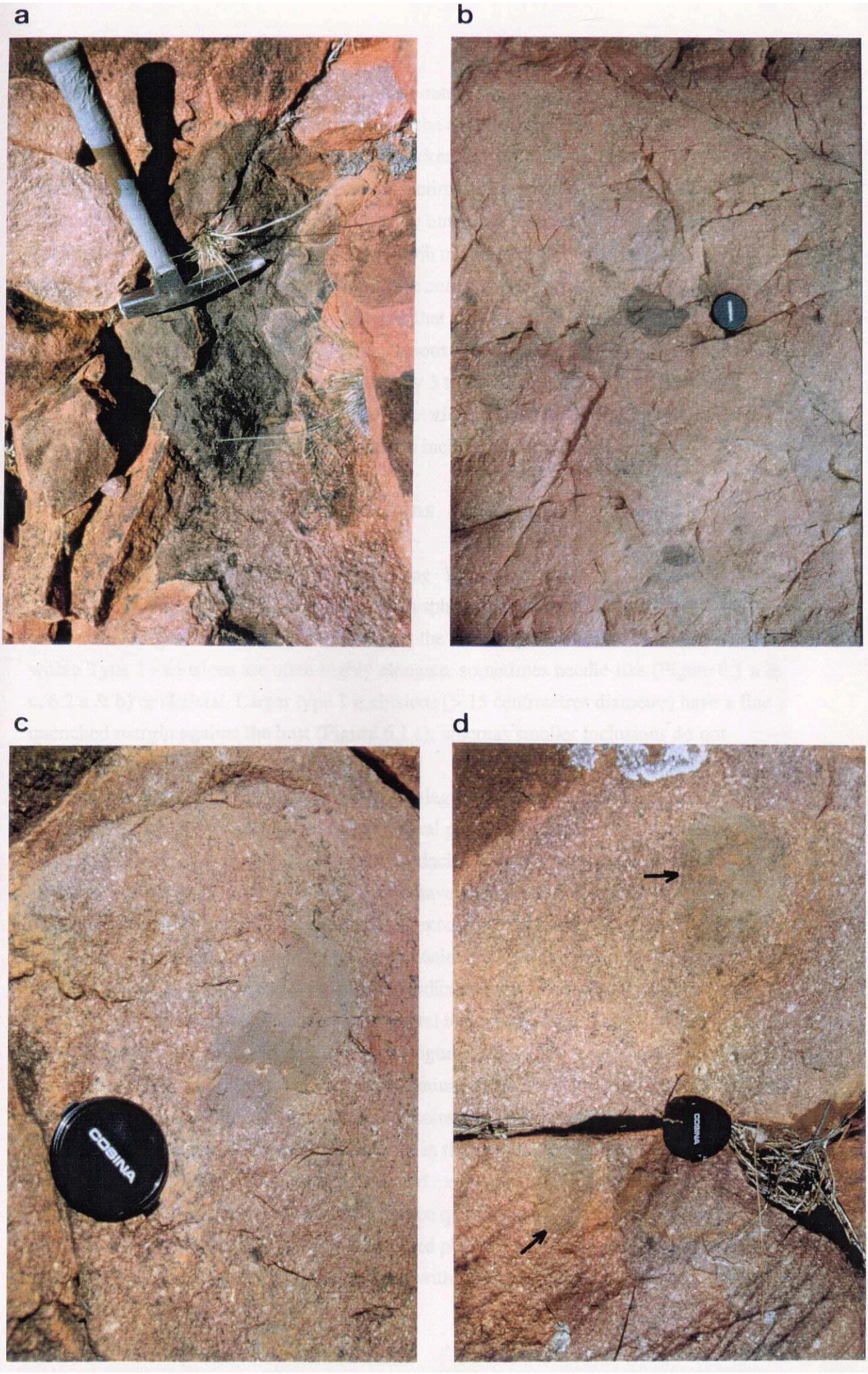
a
b
c
d
COBINA
COBINA

locality does an inclusion of type 1 occur in an outcrop together with several inclusions of type 2, however in this case the assignation to the type 1 category is doubtful.

Type 1 inclusions are conspicuously darker than the host dacite and range in size from approximately ≤ 1 centimetre up to 40 centimetres in diameter (Figures 6.1 a & b). Although they have not been observed in every outcrop, close inspection has revealed small type 1 inclusions in approximately 25-30% of samples of Yardea Dacite collected, and it is therefore considered that they are quite common but where small they are difficult to see in outcrop. It is therefore quite possible that smaller inclusions of this type occur but have not yet been identified. Type 2 inclusions are similar in colour to their host (Figure 6.1c & d) and vary from approximately 3 to 20 centimetres in diameter.

The following descriptions and interpretations are heavily based on the inclusions from the Yardea Dacite, for the majority of the inclusions come from this unit.

6.3 - Description of the inclusions

6.3.1 - Petrographic description of type 1 inclusions

Type 1 inclusions range in shape from spheroidal to amoeboid and typically have crennulate margins which are convex towards the host (Figure 6.2a, b). Mineral textures within Type 1 inclusions are often highly elongate, sometimes needle-like (Figure 6.1 a & c, 6.2 a & b) or skeletal. Larger type 1 inclusions (> 15 centimetres diameter) have a fine quenched margin against the host (Figure 6.1 c), whereas smaller inclusions do not (Figure 6.3a&b).

The inclusions originally consisted of plagioclase, augite, pigeonite, iron-oxide, apatite and glass, however many of these mineral phases have undergone alteration subsequent to their incorporation into the host dacite. Acicular pyroxenes up to 1 centimetre in length (Figure 6.2b, 6.3a and b) have almost ubiquitously been replaced by clays and chlorite (Figure 6.2d). Herringbone exsolution textures preserved by the replacement clays attest to the presence of pigeonite, and rare augite grains which contain 001 lamellae of chlorite (replacing pigeonite) indicate that a primary mineral phase was less calcic augite. Plagioclase occurs as euhedral to subhedral, moderately elongate to acicular grains up to 5 millimetres in length (Figure 6.2 a,c,d), is ubiquitously sericitized and/or turbid (Figures 6.2d and 6.3b). Iron-titanium oxide minerals, which commonly have skeletal morphology, have undergone exsolution and/or oxidization. The elongate minerals produced a felty, interlocking texture in the inclusions which was set in a groundmass of small pyroxene, plagioclase and oxide grains with small amounts of interstitial glass which has devitrified to produce quartz and alkali feldspar(?)(Figures 6.2c, 6.3a & b). Occasionally tabular to rounded phenocrysts of plagioclase and alkali feldspar up to 3 millimetres in diameter occur within type 1 inclusions, and form a

Figures opposite:

Figure 6.2a - Type 1 inclusion in Yardea Dacite. Note the irregular margin convex towards host and needle like minerals in the inclusion, very different to those in the host. Just above centre, a phenocryst has apparently been almost engulfed into the inclusion. Width of view is approximately 11 centimetres.

Figure 6.2b - Type 1 inclusion in Yardea Dacite. Note irregular margin and two feldspar phenocrysts in upper part, and small gabbroic fragment just below centre of inclusion. Width of rock slab is approximately 3.5 centimetres.

Figure 6.2c - Photograph of thin section showing the margin of a Type 1 inclusion. Note thin finely quenched edge of inclusion immediately adjacent to the host Yardea Dacite.

Figure 6.2d - Photomicrograph showing the texture of a Type 1 inclusion. Note the preservation of herringbone exsolution texture of in what was pigeonite, now replaced by iron rich clays. Plagioclases (p) are highly sericitized and oxide minerals (o) are unmixed and/or oxidized. Width of view 2mm.

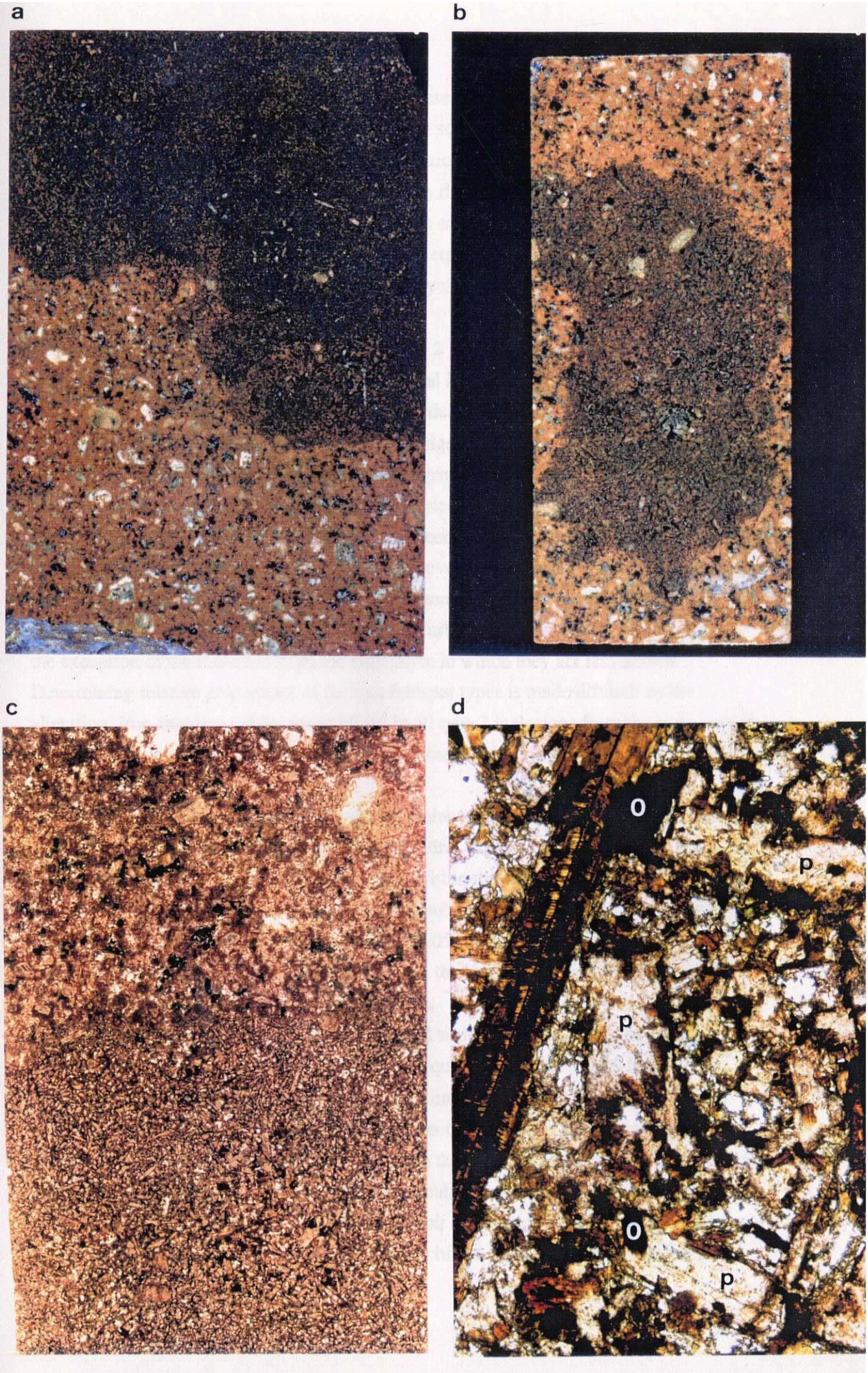
a
b
c
d
O
p
p
O
p

population distinct from the more common elongate plagioclases previously described. Rare xenoliths of gabbroic material are present in some inclusions (Figure 6.2b).

The inclusions do not exhibit any systematic increase in grain size from margin to core such as that reported for similar inclusions in rhyodacite described by Heiken and Eichelberger (1980). Nor do any of the inclusions exhibit notable deviations from the highly elongate to skeletal crystal shapes to more equant morphologies as detailed by Stimac *et al.* (1990) for andesitic inclusions in rhyolite.

6.3.2 - Petrographic description of type 2 inclusions

Type 2 inclusions are spherical to elliptical in shape, with smooth margins which have occasional lobate protrusions convex towards the host (Figure 6.4a). The inclusions contain plagioclase, potassium feldspar, augite, pigeonite, iron-titanium oxides, apatite and varying amounts of matrix made up of intergrowths of potassium feldspar and quartz. In all but one section, which comes from the Yardea vitrophyre, alteration has obscured some of the original mineralogy. Pigeonite has been totally altered to clays, however the preservation of herringbone exsolution textures reveals that it was originally present in the inclusions. Augite although often preserved has sometimes been partially altered to chlorite. Plagioclase and potassium feldspar are turbid and sericitized in all sections with the exception of the inclusion from the vitrophyre in which they are less altered. Determining relative proportions of the two feldspar types is made difficult by the alteration. Iron-titanium oxides are oxidized in all type 2 inclusions from the main part of the Yardea Dacite whereas in the inclusion from the Yardea vitrophyre they are unoxidised but are highly exsolved.

With the exception of apatite, mineral grains in type 2 inclusions are squat to mildly elongate. Feldspars are euhedral to subhedral, equant to tabular (Figure 6.3c), their average size varies from inclusion to inclusion within the range 0.5-1mm with rare grains up to 5mm in diameter. Pyroxenes are typically subhedral, stubby to slightly elongate (Figure 6.4c & d) and most range in size from 0.05mm-0.5 mm, while rare grains range up to 2 mm in length. Apatite grains are acicular, the largest of which (approximately 1mm in length) have hollow cores (Figure 6.4b).

Type 2 inclusions contain matrix material which is interstitial to the crystal phases (Figure 6.4c & d) and is dominantly made up of quartz and potassium feldspar. The proportion of matrix material varies from approximately 15% to 35% of the inclusion volume, and its texture mimics that of the host dacite, i.e. where the dacite has a graphic or granophyric matrix, this texture is also seen in the interstitial material of the inclusions, and when the dacite groundmass has a microgranular texture again so does the interstitial material. Type 2 inclusions do not typically exhibit a fine grained chilled margin adjacent to the host, nor does the host dacite ever appear chilled against the inclusions.

Figures opposite:

Figure 6.3a - Photograph of thin section of Yardea Dacite containing both a Type 1 inclusion and a metasedimentary lithic fragment. Note needle-like form of (now altered) pyroxenes (p) in the inclusion compared with those in the host. Width of view 2 centimetres.

Figure 6.3b - Photograph of a Type 1 inclusion in Yardea Dacite. Note highly elongate, acicular (now altered) pyroxenes in inclusion and apparent minor disaggregation of inclusion indicated by the arrow. Width of view 2 centimetres.

Figure 6.3c - Type 2 inclusion in Yardea Dacite. Note large feldspar phenocrysts.
Scale bar is 10 millimetres.

Figure 6.3d - Photograph of a Type 2 inclusion in Yardea Dacite showing the generally elongate nature of plagioclase grains within the inclusion and their generally small size compared to feldspar phenocrysts in the host. Width of view 2 centimetres.

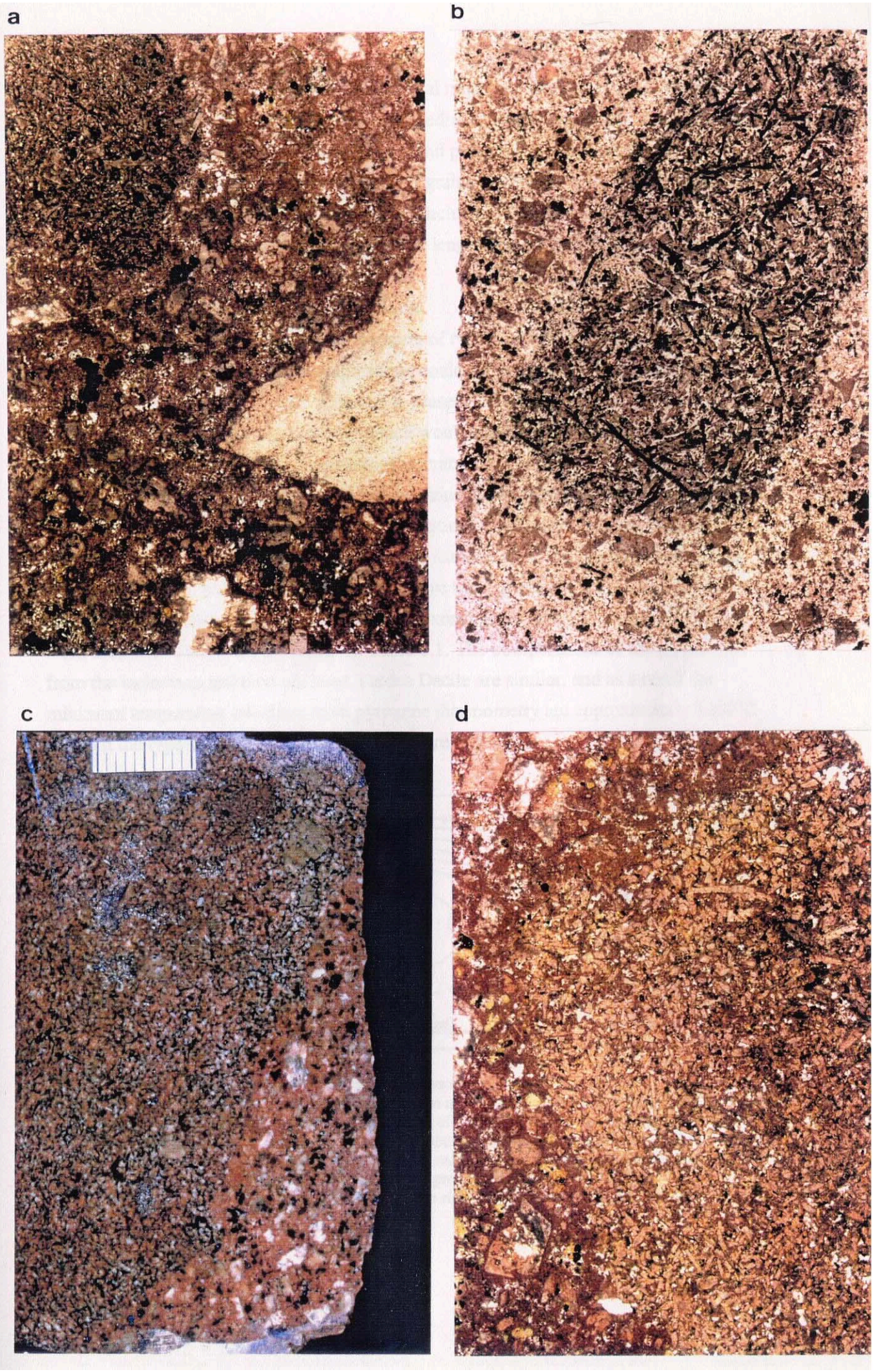
a
b
c
d

The elongate, acicular and skeletal crystal morphologies observed in the type 1 and 2 inclusions are very different from the euhedral to subhedral crystal shapes of the phenocrysts in the dacites: tabular plagioclase and potassium feldspar grains; equant pyroxenes and iron oxides; and stumpy apatite grains. Phenocrysts in the dacites are also considerably larger than those in either of the inclusions (Figure 6.6.2a-c, 6.3a-d), e.g. feldspars in the dacites are commonly >5mm in length and may reach 8mm (Chapter 4).

6.3.3 - Temperatures of the inclusions

Direct determination of the temperature of type 1 inclusions is difficult due to the lack of primary minerals whose compositions could be used for geothermometry. The only pyroxene found in a Type 1 inclusion is present as remnant 001 augite lamellae in chlorite from an exsolved pigeonite (?) which would not represent the original composition or yield a primary magmatic temperature by pyroxene thermometry.

Within type 2 inclusions most augite grains do not contain exsolution lamellae and therefore are likely to have retained compositions which yield original magmatic temperatures by pyroxene thermometry. In one sample, from the vitrophyre at the base of the Yardea Dacite, both pigeonite and augite have been preserved within a type 2 inclusion. Representative compositions of pyroxenes from type 2 inclusions and also from their host dacites are presented in Table 6.1. The compositions of the pyroxenes from the inclusions and from the host Yardea Dacite are similar, and as a result the minimum temperature estimates from pyroxene thermometry are approximately 1000°C for both the type 2 inclusion and the host (Figure 6.5).

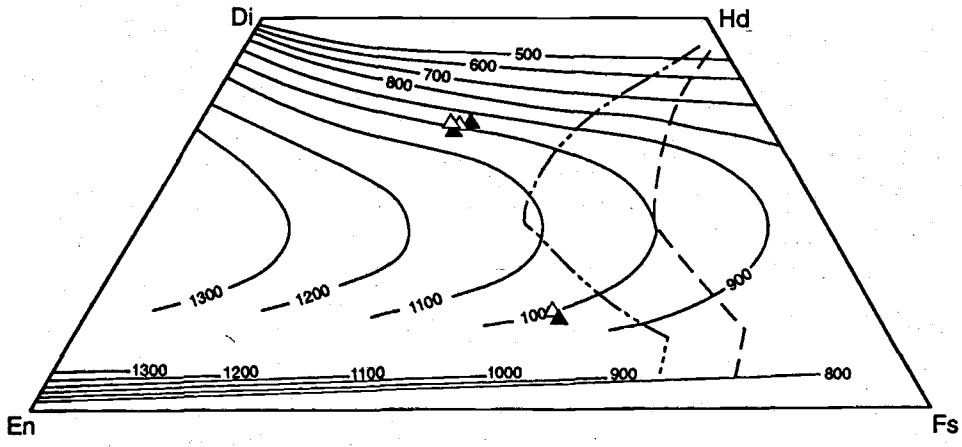

Figure 6.5 - Projection of analyses of pyroxenes from type 2 inclusions and their host Yardea Dacite onto the pyroxene quadrilateral. Pyroxene compositions were recalculated according to the method of Lindsley (1983) and temperature isotherms are from the same source. Symbols: filled triangles, pyroxenes in the host Yardea Dacite; open triangles, pyroxenes in type 2 inclusions. Dashed and dot-dash curves represent the limit of the prohibited zone at 5kb and 1atm respectively (from Lindsley, 1983), to the right of which pyroxenes are no longer stable.

Figures opposite:

Figure 6.4a - Type 2 inclusion in Yardea Dacite showing lobate margin convex towards host. Width of view 4 centimetres.

Figure 6.4b - Photomicrograph of Type 2 inclusion. Plagioclase grains (p) are altered and brownish, original pyroxene is partly to wholly replaced by chlorite, clear areas are occupied by graphic intergrowth of quartz and potassium feldspar. Note hollow apatite needle at centre left. Width of view 2 millimetres.

Figure 6.4c - Photomicrograph of Type 2 inclusion dominated by pyroxene (c) and plagioclase (p) grains with only a small amount of graphically crystallized silicic melt (indicated by arows). Crossed polars, width of view 2 millimetres.

Figure 6.4d - Similar photomicrograph to Figure 5.6c but containing a much larger proportion of graphically crystallized silicic melt. Crossed polars, width of view 2 millimetres.

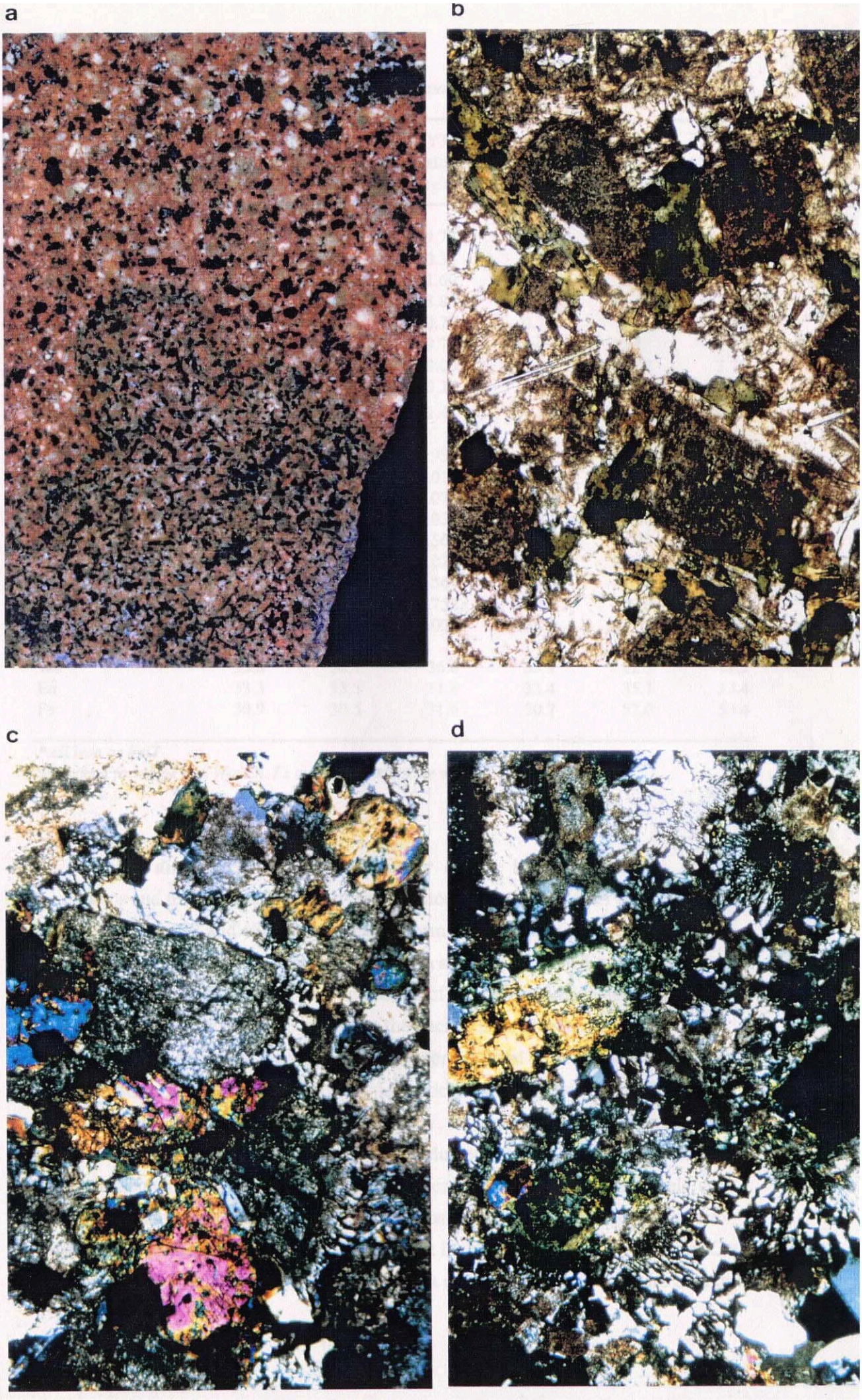
a
b
c
d

Table 6.1 - Pyroxene compositions in type 2 inclusions and their host Yardea Dacite

Sample	Mi2 inclusion augite	Mi2 host Yardea augite	Y31 inclusion augite	Y31 host Yardea augite	Y31 inclusion pigeonite	Y31 host Yardea pigeonite
SiO2	49.77	49.51	49.77	50.71	50.49	49.59
TiO2	0.49	0.41	0.37	0.35	0.19	0.23
Al2O3	1.61	1.42	1.60	1.01	0.45	0.32
FeO*	19.62	18.87	18.83	18.74	31.47	32.33
MnO	0.65	0.75	0.77	0.74	1.28	1.31
MgO	10.34	10.32	9.77	10.69	12.12	11.93
CaO	17.54	17.74	18.03	17.34	4.02	3.70
Na2O	0.50	0.32	0.27	0.29	0.08	0.09
Total	100.52	99.34	99.41	99.87	100.10	99.50
Si	1.916	1.928	1.938	1.959	1.990	1.981
Ti	0.014	0.012	0.011	0.010	0.006	0.007
Al	0.073	0.065	0.074	0.046	0.021	0.015
Fe3+	0.082	0.065	0.050	0.039	0.000	0.008
Fe2+	0.550	0.549	0.563	0.566	1.039	1.072
Mn	0.021	0.025	0.025	0.024	0.043	0.044
Mg	0.593	0.599	0.567	0.616	0.714	0.710
Ca	0.724	0.740	0.752	0.718	0.170	0.158
Na	0.037	0.024	0.021	0.022	0.006	0.007
Wo	35.8	36.1	36.6	35.9	12.3	11.2
En	33.3	33.3	31.8	33.4	35.7	35.4
Fs	30.9	30.5	31.6	30.7	52.0	53.4

** all iron as FeO*
Structural formulae and Wo, En, Fs calculated using the method of Lindsley (1983)

6.3.4 - Major and trace element chemistry of the inclusions

Major and trace element data for the inclusions and some of their host dacites are presented as Table 6.2 and variation diagrams form Figures 6.6, 6.7 and 6.8. The geochemical data presented in Table 6.2 includes a selection of type 1 and 2 inclusions, and some of their host dacites and a serial section of a type 1 inclusion and its host. A more detailed discussion of the chemistry of the dacites is in Chapter 5.

Type 1 inclusions are basaltic andesite in composition with 53-59% SiO_2 whereas type 2 inclusions range from 61-66% SiO_2, i.e. andesite to low silica dacite. Plotted against SiO_2, Fe_2O_3*, TiO_2, MgO, MnO, P_2O_5, V, Sc and Zn all decrease in linear to curvilinear fashion in arrays which have type 1 inclusions at the highest concentrations, with type 2 inclusions and the host dacites at progressively lower elemental levels. All other elements show more complex behaviour when plotted against SiO_2 with the two inclusion types plotting as separate groups. Type 2 inclusions have higher levels of CaO, Al_2O_3 and Sr than either those of type 1 or the host dacites. Na_2O and K_2O are both quite

Table 6.2 - Chemical analyses of representative inclusions and host dacite

Sample Number	*Y15-MI*	*Y25-MI*	*Y30-MI*	*Y31-MI*	*Y36-MI*	*Eu11-MI*	*Eu25-MI*	*Y43-MiA*	*Y43-MiB*	*Y43-MiC*	*Y43-MiD*	*Y43-MiE*	*YX*
Sample Type	*i*	*i*	*i*	*i*	*i*	*i*	*i*	*i*	*i*	*i*	*i*	*i*	*i*
Inclusion type§	*1*	*2*	*1*	*2*	*1*	*1*	*1*	*1*	*1*	*1*	*1*	*1*	*1*
SiO2	55.28	65.71	54.36	61.56	57.83	56.65	57.71	55.42	54.78	54.98	55.95	57.89	53.95
TiO2	2.17	0.71	1.99	1.19	1.93	1.52	1.62	2.19	2.14	2.10	2.03	1.91	2.32
Al2O3	13.92	14.09	15.04	14.35	13.72	14.64	13.85	14.58	14.47	14.32	14.25	14.07	14.44
Fe2O3*	10.99	6.42	10.73	7.84	10.36	11.46	10.53	12.00	11.66	11.69	11.35	10.37	11.42
MnO	0.33	0.14	0.19	0.18	0.38	0.30	0.29	0.45	0.45	0.47	0.45	0.41	0.25
MgO	2.06	1.51	2.98	1.48	1.90	1.94	2.29	2.76	2.77	2.70	2.59	2.32	3.74
CaO	4.08	1.14	2.81	3.92	4.04	3.81	4.39	3.29	3.30	3.23	3.12	3.02	3.21
Na2O	3.26	3.75	3.74	3.49	3.86	3.13	3.59	3.49	3.40	3.38	3.42	3.60	2.89
K2O	3.56	4.31	3.25	3.79	2.84	5.12	2.49	3.74	3.77	3.71	3.74	3.53	3.78
P2O5	1.17	0.17	1.01	0.43	0.88	0.47	0.34	1.03	1.02	1.00	0.95	0.89	1.13
LOI	1.98	1.74	2.99	0.54	1.57	0.90	1.99	2.72	2.67	2.63	2.55	2.28	3.05
Total	98.80	99.69	99.09	98.77	99.31	99.94	99.09	101.67	100.43	100.21	100.40	100.29	100.18
Zr	351.0	384.4	396.0	278.4	384.6	421.1	309.4	375.9	375.7	375.1	384.1	386.6	332.9
Nb	21.6	20.0	15.8	21.6	17.3	17.6	12.8	16.7	16.8	17.0	17.5	18.7	15.0
Sr	200.6	99.2	101.1	265.9	183.7	147.4	195.8	182.4	184.4	186.8	191.7	204.9	107.2
Rb	166.3	177.5	133.3	155.9	131.0	232.4	133.4	159.8	163.3	160.3	156.1	148.3	157.7
Y	104.8	63.0	87.1	61.1	78.9	77.5	58.0	71.6	71.6	71.5	72.7	75.1	69.6
Ba	1283.0	843.0	679.0	947.0	746.0	968.0	594.0	1102.0	1166.0	1171.0	1138.0	1020.0	909.6
Sc	25.9	11.9	20.9	14.7	21.6	23.0	23.6	24.2	24.1	24.2	23.1	21.8	22.4
Ga	24.1	23.2	30.6	21.4	23.0	29.3	29.2	22.6	24.8	21.0	21.5	22.9	27.9
Ni	n.a.	n.a.	n.a.	n.a.	n.a.	n.a.	n.a.	n.a.	n.a.	n.a.	n.a.	n.a.	6.3
Th	16.8	25.0	12.5	21.0	15.1	14.5	11.4	11.8	12.2	11.4	13.7	15.8	18.1
Pb	26.4	55.1	49.3	23.9	26.6	23.5	31.5	62.9	59.4	46.4	40.2	30.6	123.6
U	3.6	6.6	2.1	5.1	4.1	3.2	3.5	4.5	2.3	2.8	3.5	3.4	1.9
Ce	220.0	133.0	161.0	152.0	166.0	182.0	129.0	154.0	152.0	153.0	161.0	163.0	163.6
Nd	105.0	62.0	81.0	70.0	81.0	86.0	54.0	74.0	72.0	75.0	76.0	77.0	83.5
La	107.0	68.0	76.0	77.0	83.0	91.0	66.0	80.0	74.0	76.0	76.0	84.0	81.2
V	39.6	45.1	61.1	58.9	38.4	90.3	110.4	94.2	94.3	90.6	87.8	78.1	152.7
Cr	n.a.	26.0	n.a.	3.0	n.a.	n.a.	n.a.	n.a.	n.a.	n.a.	n.a.	n.a.	0.0
Zn	202.7	125.4	184.6	112.7	155.8	344.7	212.7	182.6	174.5	181.0	173.8	169.0	238.0

** - all iron as Fe2O3*
n.a. indicates element not analysed
§ inclusion types are defined in the text
i = inclusion, h = host dacite
Y43-MiA to MiE and Y43-MiF to MiH represent a serial section from the core to rim of a single type 1 inclusion and its adjacent host dacite respectively (each piece for analysis was approx. 10-12mm thick).

Table 6.2 - (continued)

Sample Number	*Y48-Mi-1*	*Y48-Mi-2*	*Y49-Mi-4*	*Y49-Mi-5*	*Y48*	*Y49*	*Y15*	*Y31*	*Y36*	*Eu11*	*Eu25*	*Y43-MiF*	*Y43-MiG*	*Y43-MiH*
Sample Type	*i*	*i*	*i*	*i*	*h*	*h*	*h*	*h*	*h*	*h*	*h*	*h*	*h*	*h*
Inclusion type	*2*	*2*	*2*	*1 (?)*										
SiO2	63.30	61.57	61.98	58.59	66.24	66.43	67.56	67.41	67.57	71.17	68.18	68.11	67.97	68.03
TiO2	1.05	1.31	1.38	1.46	0.86	0.82	0.68	0.73	0.68	0.41	0.70	0.70	0.68	0.64
Al2O3	14.92	14.33	14.80	13.80	13.93	14.03	13.60	14.13	13.55	13.30	13.58	13.66	13.61	13.66
Fe2O3*	6.61	8.60	8.08	10.76	6.13	5.89	5.20	5.13	5.18	3.72	5.21	5.21	5.17	5.19
MnO	0.15	0.17	0.20	0.23	0.12	0.12	0.13	0.11	0.12	0.10	0.13	0.11	0.12	0.12
MgO	1.40	1.46	1.65	2.64	0.98	0.98	0.92	0.83	0.66	0.33	0.67	0.97	0.91	0.85
CaO	3.54	3.76	3.38	4.75	2.77	2.58	1.59	2.42	2.18	1.41	1.97	1.58	1.66	1.63
Na2O	4.11	3.77	3.92	3.19	3.40	3.40	3.06	3.44	3.25	3.20	3.20	3.12	3.18	3.31
K2O	3.62	3.67	3.50	3.20	4.23	4.61	5.42	4.70	4.87	5.34	4.76	5.25	5.27	5.34
P2O5	0.35	0.48	0.54	0.34	0.23	0.22	0.18	0.20	0.18	0.07	0.17	0.18	0.18	0.18
LOI	1.28	1.43	1.27	1.36	0.99	0.93	1.27	0.52	1.05	0.56	0.80	1.17	1.22	1.29
Total	100.33	100.55	100.70	100.32	99.88	100.01	99.61	99.62	99.29	99.61	99.37	100.06	99.97	100.24
Zr	276.0	239.0	325.5	332.4	393.9	394.3	420.0	399.8	428.3	485.2	414.4	423.7	419.2	417.7
Nb	24.0	22.1	27.3	16.1	19.8	18.8	21.0	18.8	21.4	24.1	21.8	23.7	24.1	23.6
Sr	253.5	249.1	451.4	403.5	193.0	208.3	182.0	193.3	137.4	93.1	149.5	176.9	156.1	157.7
Rb	150.6	146.8	163.0	134.5	180.6	182.8	229.0	186.8	193.8	207.2	196.8	209.0	209.5	208.3
Y	52.7	61.6	60.9	53.5	54.8	54.6	67.0	54.6	65.3	68.1	63.8	63.9	63.9	65.6
Ba	1032.0	1159.0	1072.0	1120.0	1187.0	1263.0	1468.0	1306.7	1262.4	1206.7	1368.0	1446.0	1432.0	1364.0
Sc	15.7	18.3	17.3	21.8	10.5	10.9	13.0	9.4	11.6	7.6	11.2	11.3	11.7	10.8
Ga	18.8	21.9	19.7	20.6	21.5	22.0	22.0	20.8	19.5	19.1	21.3	19.6	19.4	18.9
Ni	n.a.	n.a.	n.a.	n.a.	n.a.	n.a.	1.0	1.5	2.4	0.0	n.a.	n.a.	n.a.	n.a.
Th	16.2	15.4	18.0	14.1	23.1	25.5	32.0	25.2	27.7	33.3	29.9	27.6	27.6	27.3
Pb	20.7	19.6	23.3	26.2	27.3	24.8	33.0	28.1	22.8	24.5	32.7	25.9	18.5	21.3
U	5.5	4.3	3.3	4.0	5.9	4.4	7.0	6.3	6.1	8.5	5.6	7.1	6.2	7.5
Ce	141.0	159.0	157.0	127.0	151.0	151.0	175.0	153.6	176.9	193.3	168.0	166.0	176.0	174.0
Nd	63.0	71.0	77.0	62.0	66.0	67.0	70.0	65.4	78.1	85.8	75.0	75.0	80.0	76.0
La	69.0	78.0	77.0	68.0	75.0	75.0	79.0	78.9	85.3	96.0	84.0	81.0	83.0	86.0
V	57.6	66.1	60.6	291.3	37.3	33.3	18.0	25.0	16.0	4.0	16.1	23.3	20.4	19.7
Cr	n.a.	n.a.	n.a.	n.a.	n.a.	n.a.	<5	5.1	0.2	0.0	n.a.	n.a.	n.a.	n.a.
Zn	88.5	107.5	111.2	131.7	83.9	89.6	n.a.	n.a.	n.a.	n.a.	n.a.	102.5	99.6	96.3

Figure opposite:

Figure 6.6 - Major element silica variation diagrams for the mafic inclusions from the Yardea and Eucarro Dacites. Symbols: larger crosses, type 1 inclusions; small crosses, type 2 inclusions; open circles, Yardea and Eucarro Dacite hosts; open triangles, HPT and IPT basaltic andesites from the Kokatha developmental volcanic area; open squares, cumulates calculated as resulting from the fractionation of the mature phase volcanics; filled squares, cumulates calculated as resulting from the fractionation of the Yardea Dacite only (see text for discussion).

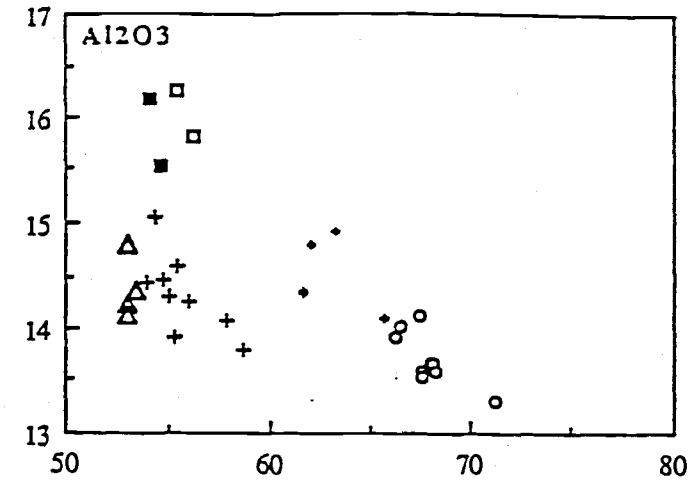
Al2O3
17
16
15
14
13
50
60
70
80

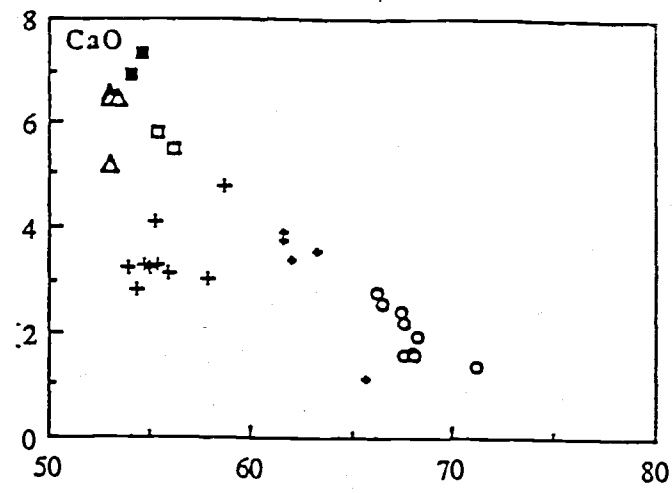
CaO
8
6
4
2
0
50
60
70
80

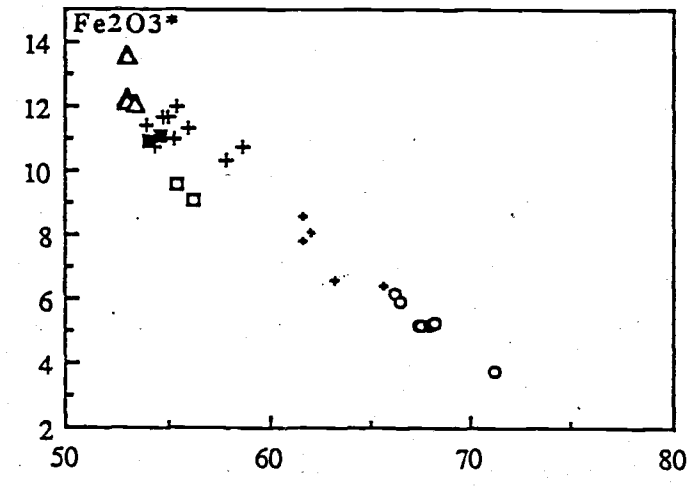
Fe2O3*
14
12
10
8
6
4
2
50
60
70
80

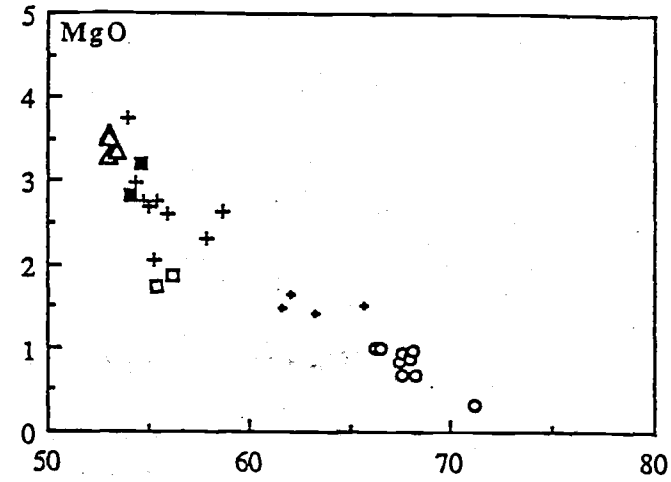
MgO
5
4
3
2
1
0
50
60
70
80

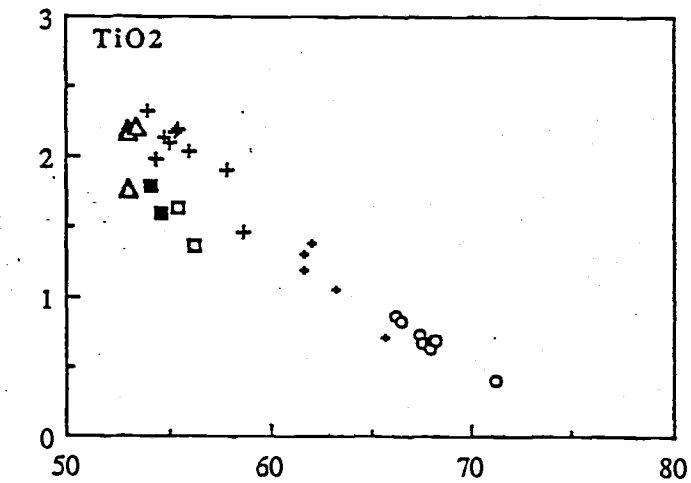
TiO2
3
2
1
0
50
60
70
80

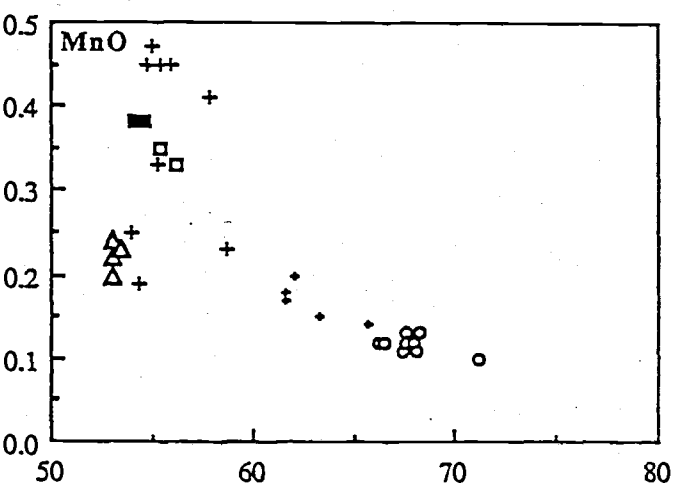
MnO
0.5
0.4
0.3
0.2
0.1
0.0
50
60
70
80

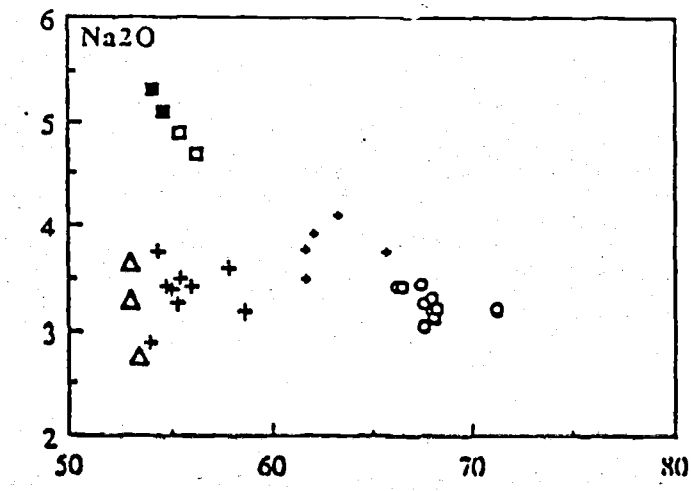
Na2O
6
5
4
3
2
50
60
70
80
SiO2

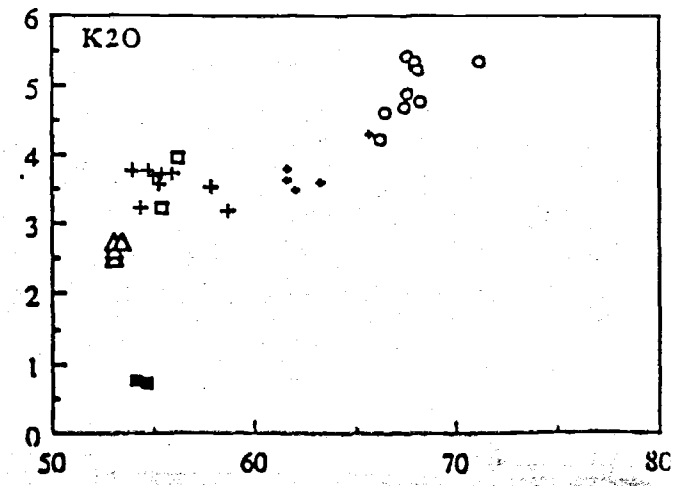
K2O
6
5
4
3
2
1
0
50
60
70
80
SiO2

Figure opposite:

Figure 6.7 - Trace element silica variation diagrams for the mafic inclusions from the Yardea and Eucarro Dacites. Symbols: larger crosses, type 1 inclusions; small crosses, type 2 inclusions; open circles, Yardea and Eucarro Dacite hosts; open triangles, HPT and IPT basaltic andesites from the Kokatha developmental volcanic area.

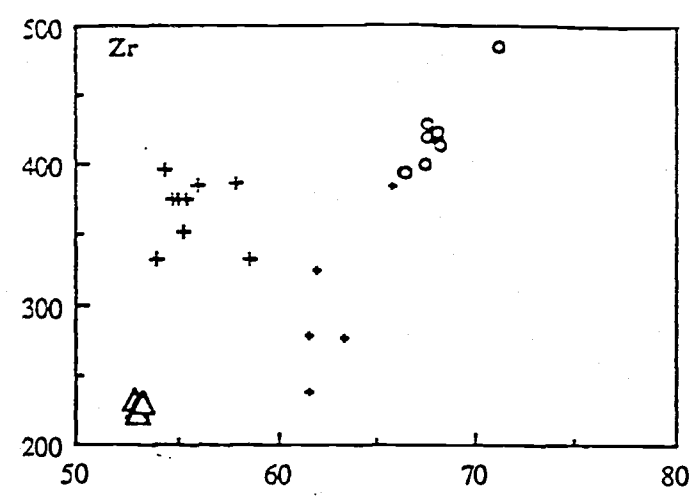
Zr
500
400
300
200
50
60
70
80

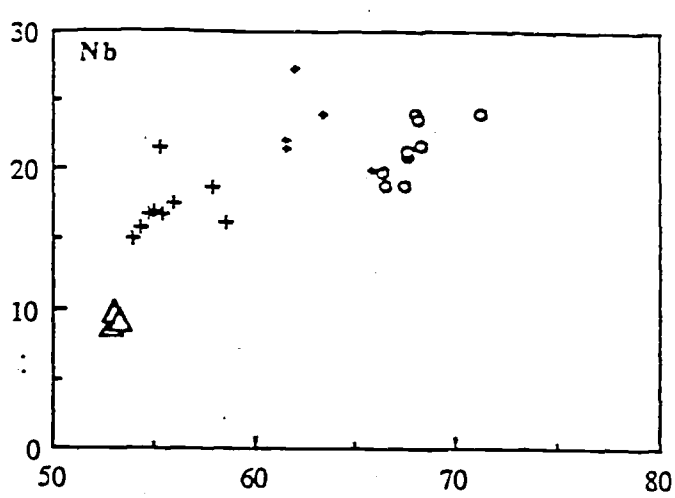
Nb
30
20
10
0
50
60
70
80

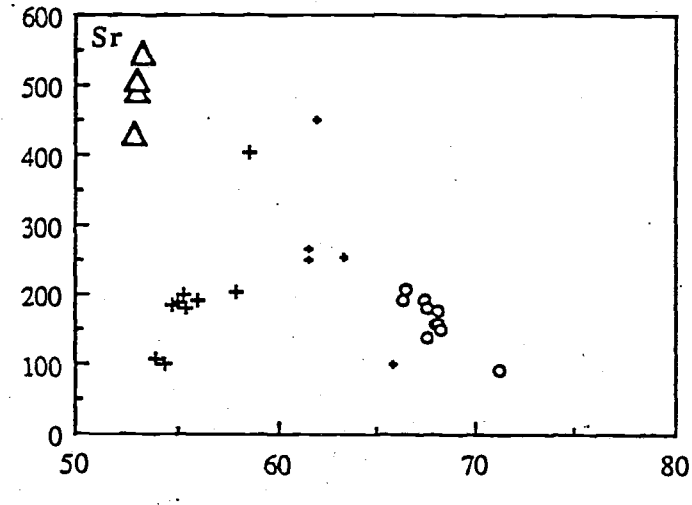
Sr
600
500
400
300
200
100
0
50
60
70
80

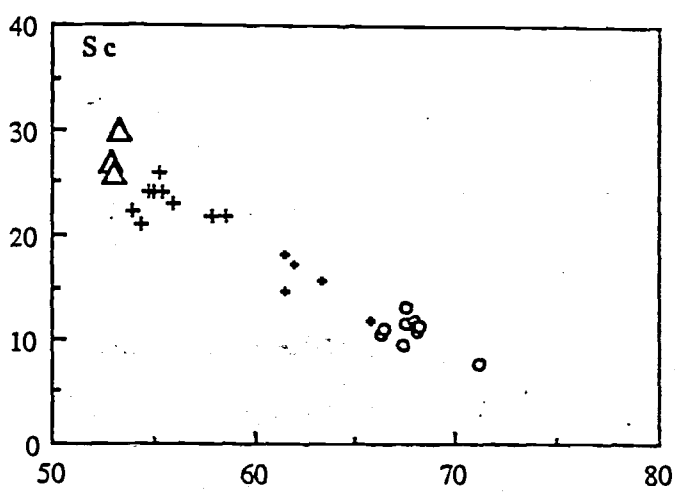
Sc
40
30
20
10
0
50
60
70
80

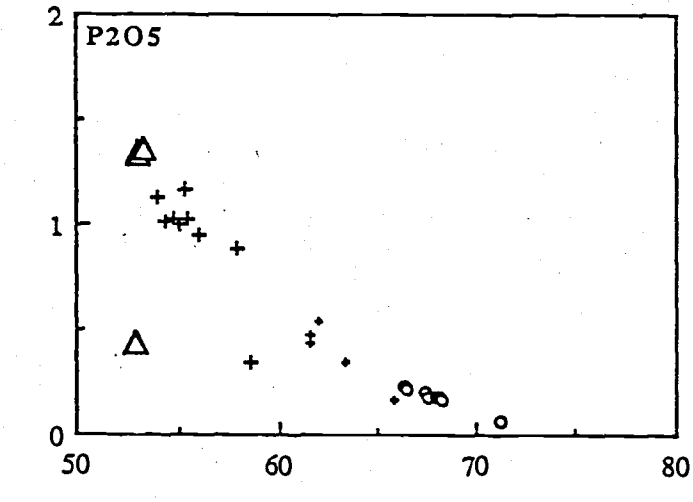
P2O5
2
1
0
50
60
70
80

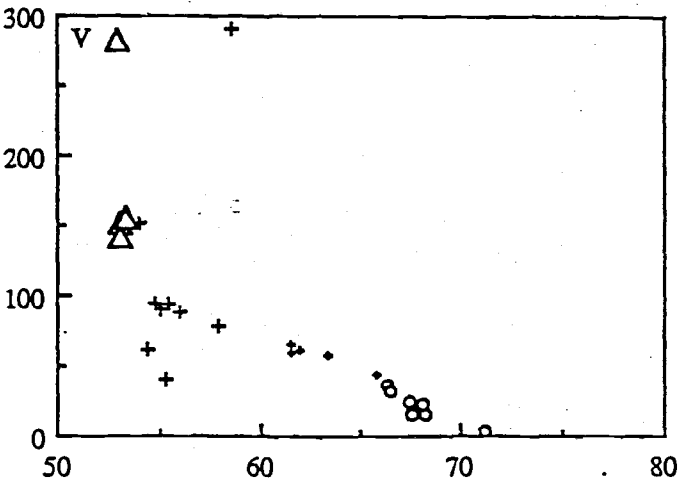
V
300
200
100
0
50
60
70
80

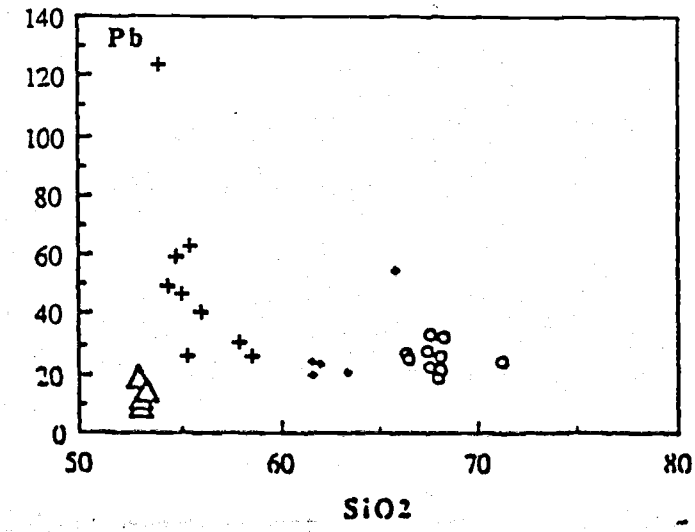
Pb
140
120
100
80
60
40
20
0
50
60
70
80
SiO2

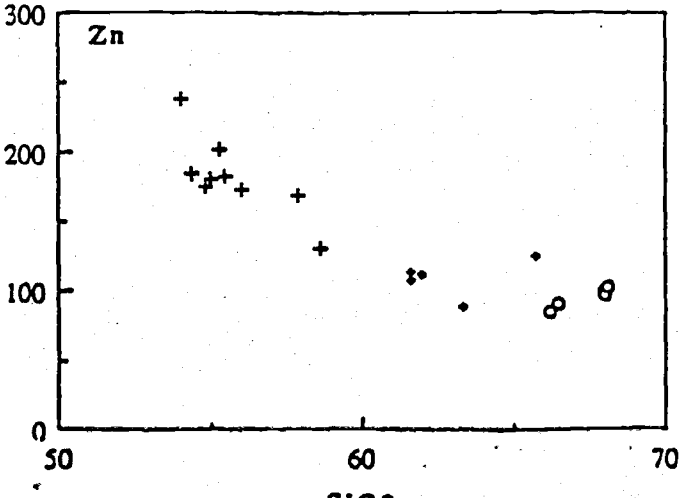
Zn
300
200
100
0
50
60
70
SiO2

Figure opposite:

Figure 6.8 - Trace element silica variation diagrams for the mafic inclusions from the Yardea and Eucarro Dacites. Symbols as for Figure 6.7.

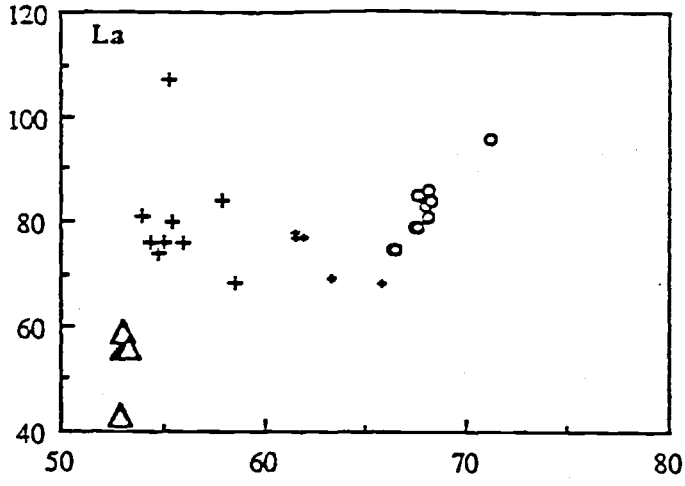
La
120
100
80
60
40
50
60
70
80

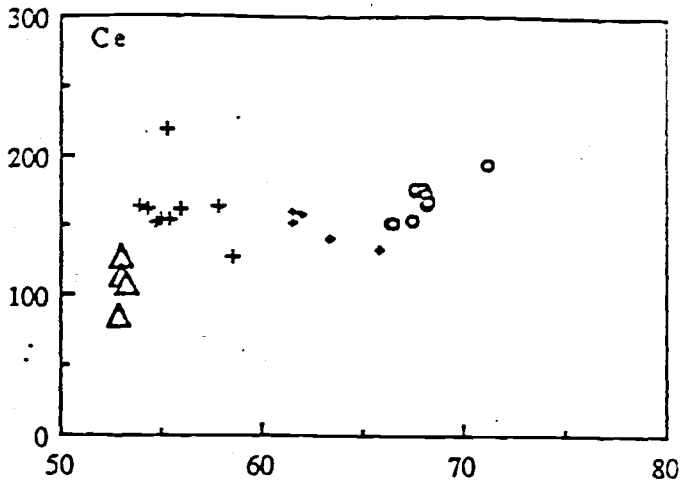
Ce
300
200
100
0
50
60
70
80

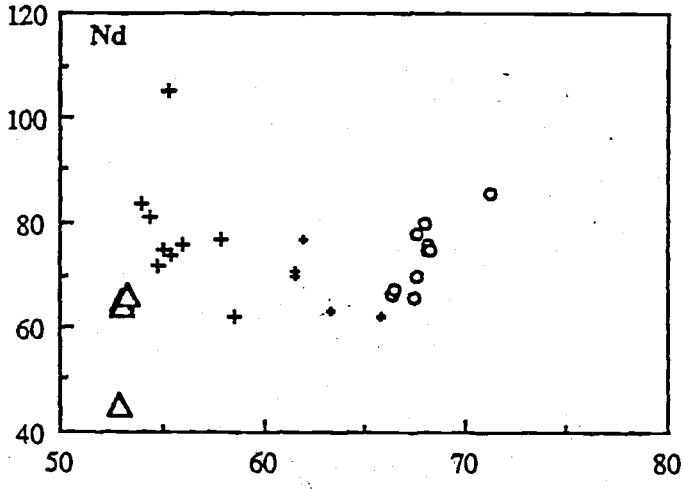
Nd
120
100
80
60
40
50
60
70
80

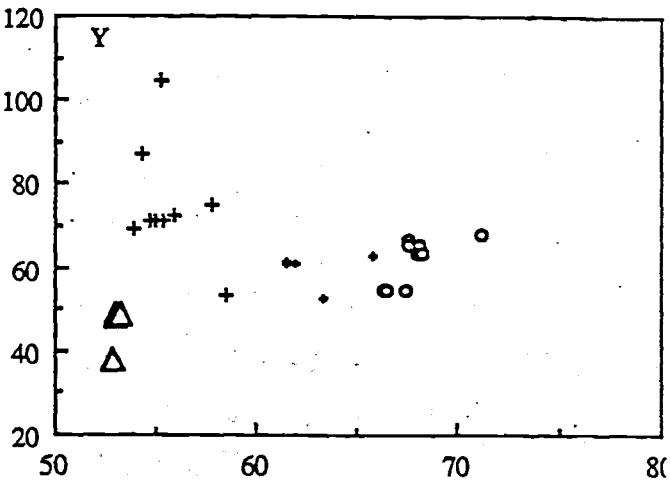
Y
120
100
80
60
40
20
50
60
70

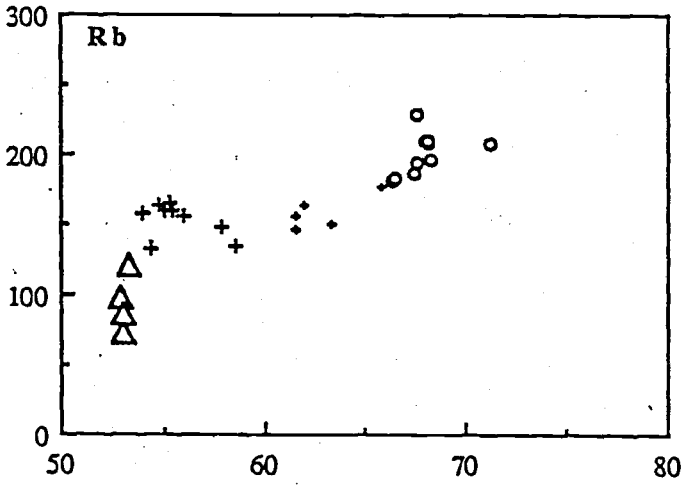
Rb
300
200
100
0
50
60
70
80

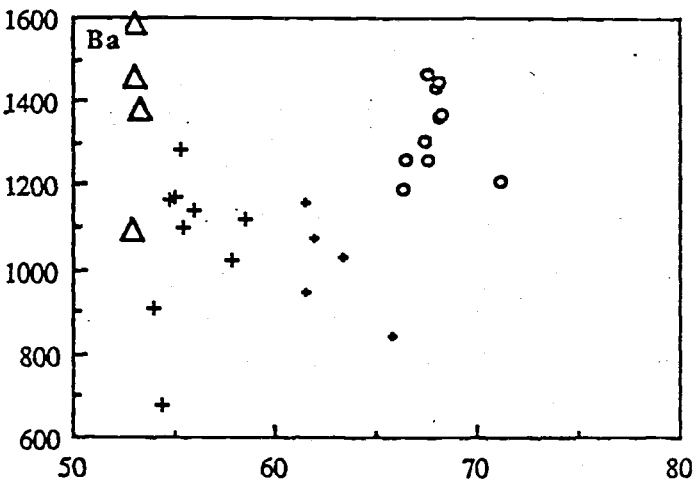
Ba
1600
1400
1200
1000
800
600
50
60
70
80

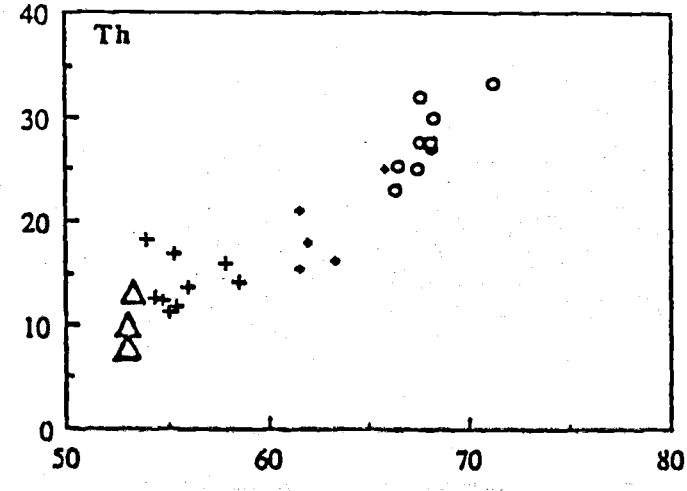
Th
40
30
20
10
0
50
60
70
80
SiO2

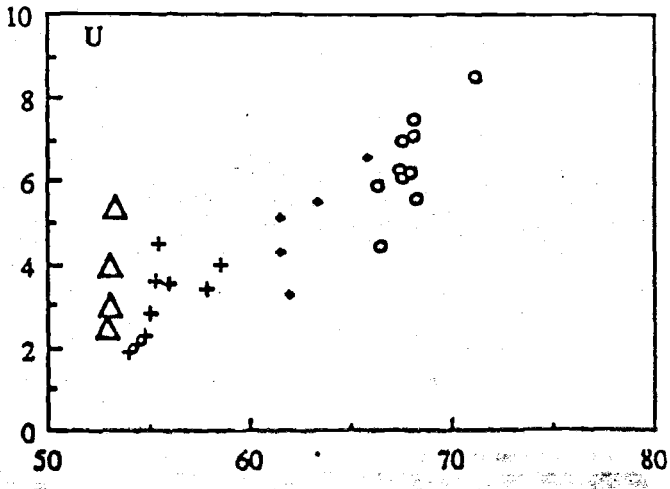
U
10
8
6
4
2
0
50
60
70
80
SiO2

scattered which may be due to post-eruptive mobility. With increasing SiO_2, Rb, Th and U all increase in a curvilinear fashion with type 1 inclusions and the dacites having the lowest and highest concentrations respectively. Type 2 inclusions have the lowest levels of Zr but high levels of Nb compared with type 1 or the dacites. Both inclusion groups and the dacites have similar levels of La, Ce and Nd, but whereas the dacites exhibit a well defined positive correlation with increasing SiO_2, the type 2 inclusions form a crude negative correlation, and the type 1 inclusions plot as a cluster. Ba may exhibit the same type of behaviour but is highly scattered when plotted against SiO_2. Type 1 inclusions have the highest levels of Y.

A series of slabs for analysis were cut radially from the core of a type 1 inclusion to its rim and into the adjacent host dacite. The inclusion was approximately 20 centimetres in diameter, and each slab was 10-12 millimetres thick. The analyses are presented in Table 6.2, with the serial sections denoted Y43-MiA to MiH. Y43-MiA to MiE are the sequence from inclusion core to rim and Y43MiF-MiH are from the host. Extreme care was taken to make certain that no host adhered to the inclusion and vice versa for the two slabs taken either side of the interface. The chemical data for the serial section is presented as Figure 6.9.

Elements which are enriched in the dacite relative to the inclusion tend to increase slightly from the inclusion core towards the rim, e.g. Nb, Th, Zr, and the REEs, whereas the opposite occurs for most elements which are relatively depleted in the dacite, e.g. CaO, TiO_2, MgO, P_2O_5, V, Sc. It would seem that limited interaction has occurred for most elements, with possibly a small amount of diffusion (or felsic melt penetration into interstices of the inclusion?) resulting in the patterns observed. The only element to show a strong diffusional gradient is Pb which steadily declines from inclusion core to rim and into the host. The elements Ba, Rb and Sr however do not conform to any variation of the types previously mentioned. Ba, Rb, and K_2O (the latter is not illustrated) have higher concentrations in the dacite than the inclusion, however the lowest level of each of these elements occurs at the inclusion rim. The opposite is seen for Sr, where a concentration maximum occurs at the inclusion rim, with higher levels than either in the inclusion core or dacite host. The reason for these elemental distributions is rather problematical. One possibility is that during alteration of the inclusions (which in most type 1 inclusions has resulted in almost total replacement of the original minerals), movement of these elements has occurred differentially along the inclusion margin. As a result of these analyses, it is considered that the cores of larger type 1 inclusions are unmodified by diffusional or other types of exchange with the host dacite melt either at the time of, or after, their incorporation into the dacite.

The inclusion core analyses have some chemical similarities to the HP and IP basaltic andesites from Kokatha, with relatively high levels of P_2O_5, TiO_2, and Fe_2O_3*

Figures opposite and overleaf:

Figure 6.9 - Plots of a serial section from the core to rim of a type 1 inclusion and the adjacent host Yardea Dacite. Each point represents an analysis of a slab 10-12 millimetres thick.

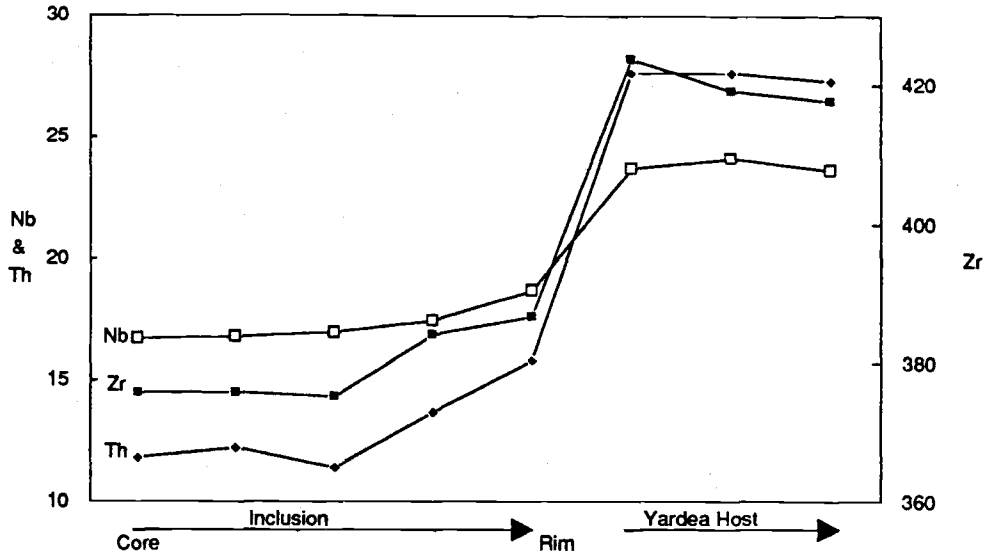
30
25
20
15
10
Nb & Th
Nb
Zr
Th
420
400
380
360
Zr
Inclusion
Core
Rim
Yardea Host

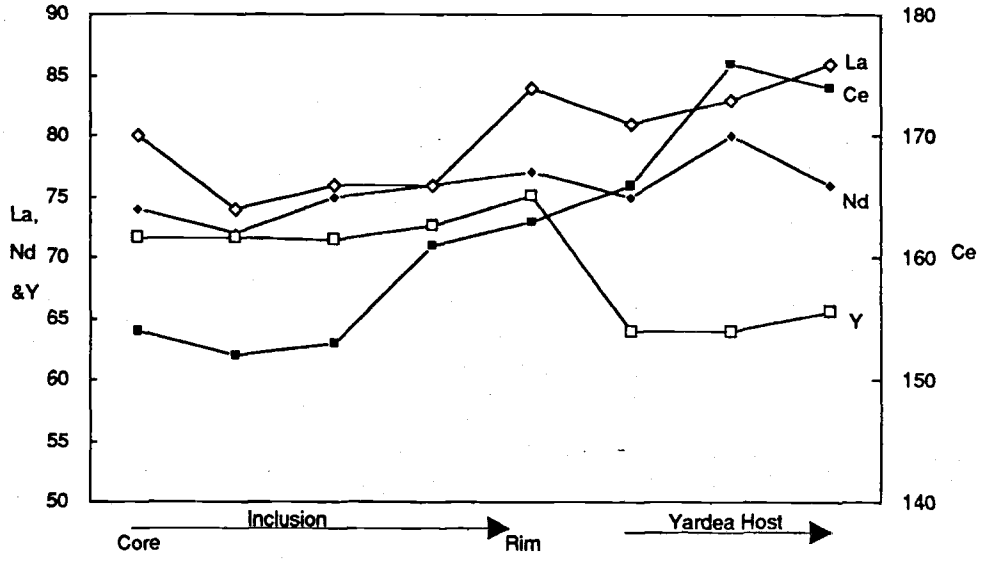
90
85
80
75
70
65
60
55
50
La, Nd &Y
La
Ce
Nd
Y
180
170
160
150
140
Ce
Inclusion
Core
Rim
Yardea Host

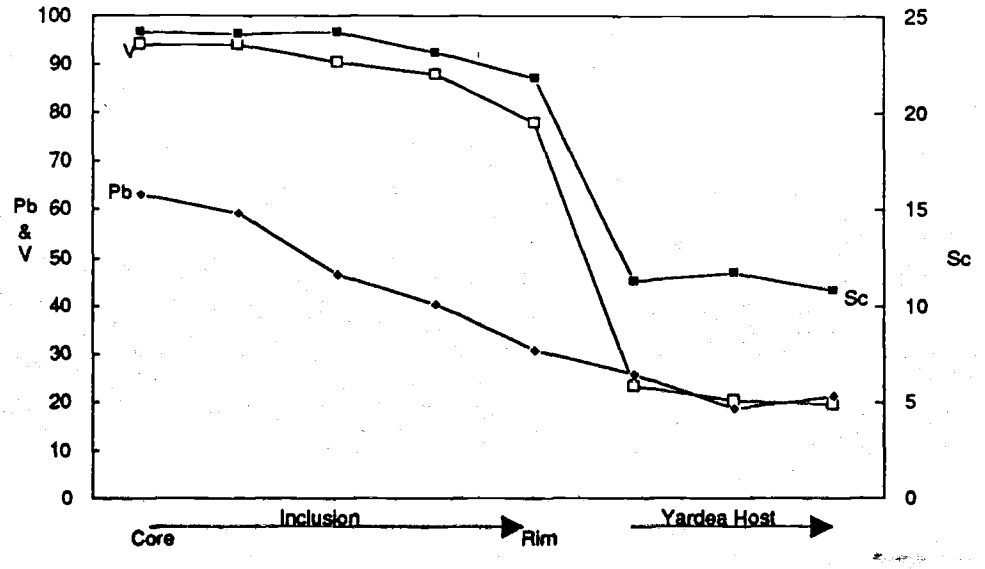
100
90
80
70
60
50
40
30
20
10
0
Pb & V
V
Pb
25
20
15
10
5
0
Sc
Inclusion
Core
Rim
Yardea Host

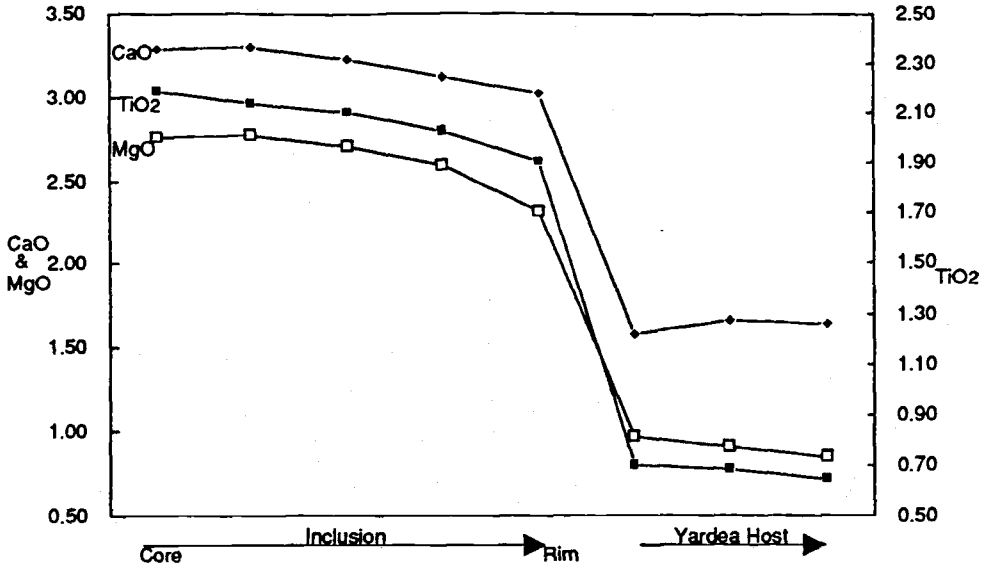
CaO
TiO2
MgO
CaO & MgO
TiO2
Core
Inclusion
Rim
Yardea Host

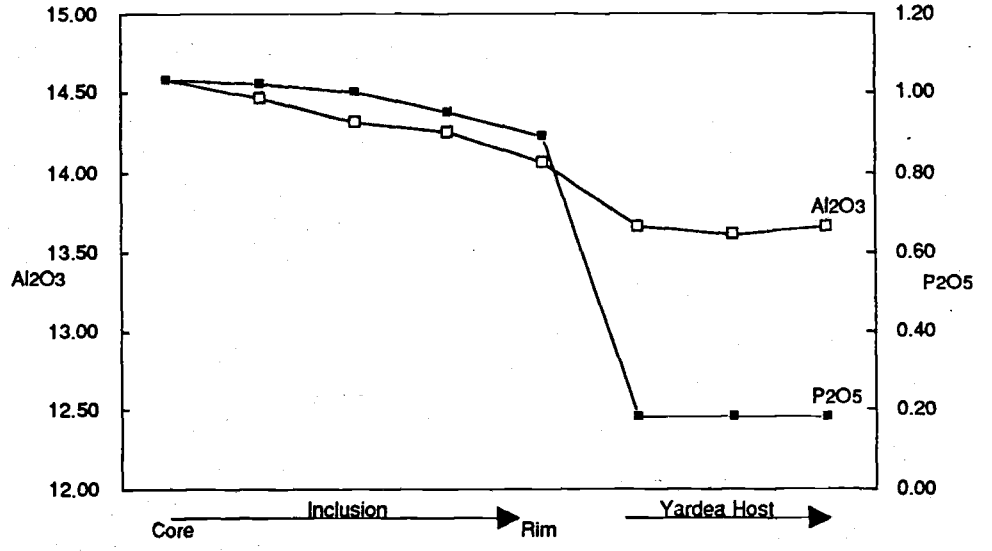
Al2O3
P2O5
Core
Inclusion
Rim
Yardea Host

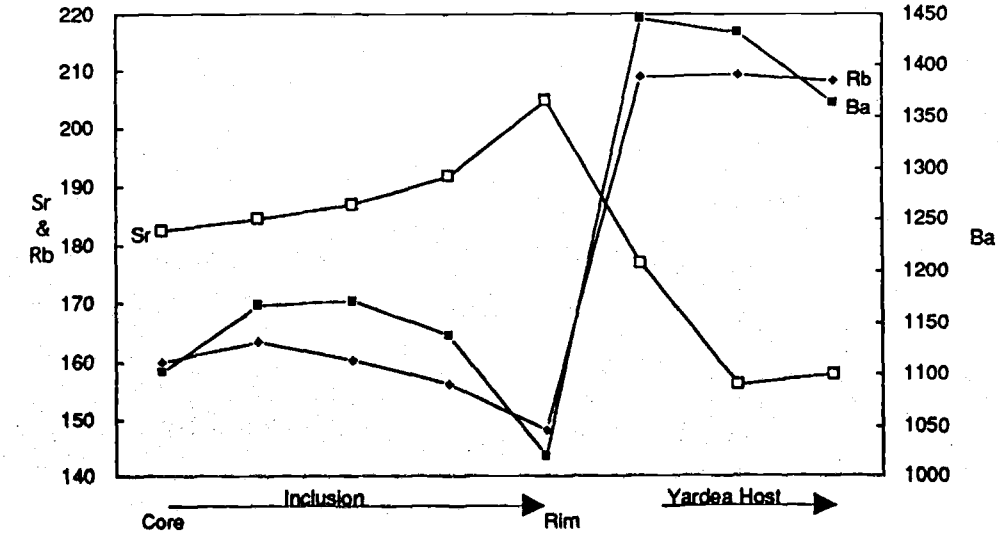
Sr
Rb
Ba
Sr & Rb
Core
Inclusion
Rim
Yardea Host

together with low levels of MgO (Figure 6.6). However systematic chemical differences are seen between the Kokatha basaltic andesites and the inclusions. The inclusions are enriched in most incompatible elements including Zr, Nb,Th, Pb, REEs, Y, and depleted in CaO and Sr relative to HP and IP basaltic andesites (Figures 6.6, 6.7 and 6.8).

6.3.5 - Isotopic data for the inclusions and the Yardea Dacite

The inclusions were not analysed for Sr isotopes because of the highly variable nature of results for samples with low Sr levels (see Chapter 2), thought to be due to post-emplacement element mobility, which renders this isotopic system ineffective for comparing the inclusions and host dacites. Sm-Nd isotopic systematics have proven to be robust in the Gawler Range volcanics (Chapter 2), and therefore Nd isotopic determinations were carried out on a representative sample of each inclusion type and on three samples of Yardea Dacite from localities where inclusions were present. The results are presented in Table 4.3. The type 1 and type 2 inclusions yielded εNd values of -2.5, and -3.1 respectively. Values for the Yardea Dacite ranged from -3.8, for the host to the type 2 inclusion, to -4.6 (Figure 6.10).

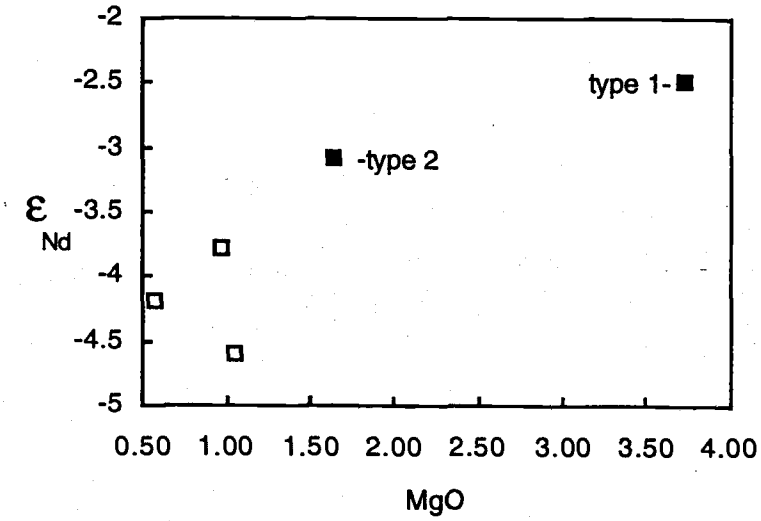

Figure 6.10 - Plot of εNd against MgO for type 1 and 2 inclusions and their host Yardea Dacite. Symbols: open squares, Yardea Dacite; filled squares, inclusions.

Table 6.3 - Isotopic data for magmatic inclusions and the host Yardea Dacite

Sample number	*Sample type*	*Nd ppm*	*Sm ppm*	*143/144 Nd measured*	*Sm/Nd*	*147Sm/144Nd*	*Tchur (Ga)*	*TDm (Ga)*	*143Nd/144Nd (1.592 Ga)*	*epsilon Nd (1.592Ga)*
Y4	Yardea Dacite	60.52	11.56	0.511577 ±25	0.1910	0.1155	2.04	2.19	0.510368	-4.6
Y10	Yardea Dacite	68.52	13.07	0.511593 ±33	0.1979	0.1154	2.01	2.17	0.510385	-4.2
Y49	Yardea Dacite Host	60.19	11.01	0.511567 ±16	0.1830	0.1107	1.94	2.11	0.510409	-3.8
Y49-Mi-4	Type 2 inclusion	75.42	13.87	0.511609 ±12	0.1840	0.1113	1.88	2.06	0.510444	-3.1
YX	Type 1 inclusion	68.04	13.90	0.511768 ±16	0.2043	0.1236	1.86	2.08	0.510475	-2.5

All samples are prefixed 884-
Error on measured 143Nd/144Nd ratio is calculated as 2 standard error of the mean
Y4 contains small type 1 inclusions; no inclusions have been found in Y10
All Yardea Dacite samples were carefully checked to ensure the analysed fraction was inclusion and xenolith ree

6.4 - Origin of the inclusions

Inclusions in felsic volcanic rocks have been interpreted in a number of ways including that they represent

- lithic fragments from basement lithologies
- restite from crustal melting processes
- the products of liquid immiscibility
- disrupted cumulates from magma chamber crystallization processes
- quenched contemporaneous magma more mafic than the host

In this section the mineralogic, petrographic, chemical and isotopic features of the two types of inclusions will be discussed in order to determine their origin and what implications or information they yield on the Gawler Range magmatic system.

6.4.1 - Origin of the type 1 inclusions

A number of features of the type 1 inclusions indicate they were molten when incorporated into the host dacite. First, their crennulate margins, convex towards the host, are typical of mafic magma quenched by contact with a lower temperature silicic magma as has been documented in commingled magmas in the subvolcanic to plutonic environment (e.g. Marshall and Sparks, 1984; Cook, 1988; Wiebe, 1993). Second, the acicular to skeletal morphology of crystals is indicative of some degree of undercooling, although the exact temperature differential (ΔT) between the two magmas cannot be determined. A continuum of crystal morphologies exists, directly related to the degree of undercooling (Lofgren, 1974; Donaldson, 1976), however complexities such as the effect of magma composition and controls on nucleation prevent any precise correlation between ΔT and crystal morphology. Third, evidence for limited mixing between basaltic andesite inclusion and dacite is indicated by small patches of less mafic material at the margins of some inclusions (Figure 6.2a, 6.3b). The interpretation of the larger, squat feldspar grains within the inclusions is that they represent crystals incorporated from the dacite, which supports mixing or commingling having occurred between two melts. The origin of these crystals is confirmed by occasional grains 'caught in the act' of being enveloped (Figure 6.2a). These grains are interpreted as having been included from the dacite, both because potassium feldspar is an unlikely precipitating phase from a magma which is of basaltic andesite composition, and because their rounded shapes indicate resorption has occurred as a response to instability within the chemical environment of the inclusion. Other studies in both the volcanic and plutonic environment have reached similar conclusions on the origin for feldspar xenocrysts on the basis of mineral and whole rock chemistry (e.g. Varga *et al.*, 1990), or igneous microstructures (e.g. Vernon, 1990).

Although the magmatic temperature of the basaltic andesite magma cannot be determined directly, some qualitative information of the thermal contrast can be obtained. Undercooling, indicated by the crystal morphologies within the inclusion, demands the basaltic andesite melt must have been hotter than the dacitic magma. However all but the largest inclusions lack the fine grained margins which are typical of mafic melt quenched in more silicic magma of considerably lower temperature, i.e. a large temperature contrast, ΔT (Bacon, 1986). This indicates at most a moderate thermal contrast between the two magmas.

Whole rock chemistry suggests the basaltic andesite magma parental to the type 1 inclusions was similar to but more evolved than the HP basaltic andesites from Kokatha. The higher concentrations of incompatible elements in the type 1 inclusions may have occurred by fractionation or assimilation of felsic crustal material with or without concomitant fractional crystallization. If simple fractionation was the cause, as the inclusions have much the same silica content as the HP lavas, it is necessary to invoke a fractionating assemblage dominated by pyroxene and/or plagioclase which would have little leverage to induce rapid change in silica levels. This is quite plausible however as these minerals are indeed the main mineralogical components of both the inclusions and the HP basaltic andesite lavas. In addition the fact that the εNd of the type 1 inclusion (-2.5) is no lower than that of the HP and IP basaltic andesites (-3.5 and -3.0 respectively) could be thought to be evidence against significant crustal contamination of the parent magma. However a small amount of crustal contamination cannot be ruled out as the cause of high Pb and low Sr levels in the type 1 inclusions compared to the HP mafic lavas (Figure 6.7).

The evidence for the type 1 inclusions to have formed by the incorporation of molten basaltic andesite magma into dacitic magma is strong. Alternative explanations are inconsistent with the features of the inclusions. A cumulate, restitic or accidental lithic origin is discounted by the skeletal to acicular crystal morphology within the inclusions, and the indications of a molten state at the time of incorporation, while the different Nd isotopic character of dacite and type 1 inclusions rules out the formation of the latter by liquid immiscibility.

6.4.2 - Origin of the type 2 inclusions

The formation of type 2 inclusions by the process of liquid immiscibility is discounted by both chemical and isotopic data. Experimental studies in immiscible liquids indicate that higher levels of REEs and HFSEs would be expected in the mafic phase of two immiscible melts relative to the felsic phase (Ryerson and Hess, 1978), however the opposite relationship is true for the mafic type 2 inclusions and the Yardea Dacite. Also inclusion Y49-Mi4 has an ε_{Nd} value of -3.1 which is slightly but distinctly higher than its

host Yardea Dacite which has a value of -3.8, whereas liquids related by immiscibility would have the same isotopic composition.

Textural and chemical considerations discount an origin of the type 2 inclusions as restitic material or modified source rocks within the dacitic melts. Such restitic inclusions have been described as having igneous or meta-igneous textures (e.g. Chen *et al.*, 1990; Griffin *et al.*, 1978; White and Chappell, 1977). There is no hint of the type 2 inclusions having metamorphic textures, rather the euhedral forms of the crystals (Figures 6.4b,c & d), tabular plagioclases and prismatic pyroxenes, argues for them having precipitated from a melt. The non-linear arrays of some elements for the inclusions and their host dacites (e.g. Zr and the REEs) also disallows a restite origin, as linear elemental variation is a fundamental prediction in the restite model (Chappell *et al.*, 1987).

Simple mixing models between basaltic andesite magma of the type 1 inclusions and Yardea Dacite also fail to explain the chemical characteristics of the type 2 inclusions. For simple bulk mixing any mixture should lie in a straight line between the two endmembers, however type 2 inclusions do not lie on mixing chords between the positions occupied by type 1 inclusions and the dacites on silica variation diagrams for Zr, Ba, Na_2O, Al_2O_3, CaO or Sr. Likewise AFC processes between the same endmembers can be discounted because the type 2 inclusions do not lie on any probable mixing curve between Yardea Dacite and the type 1 inclusions on a diagram of $^{143}Nd/^{144}Nd$ v 1/Nd (Figure 6.11).

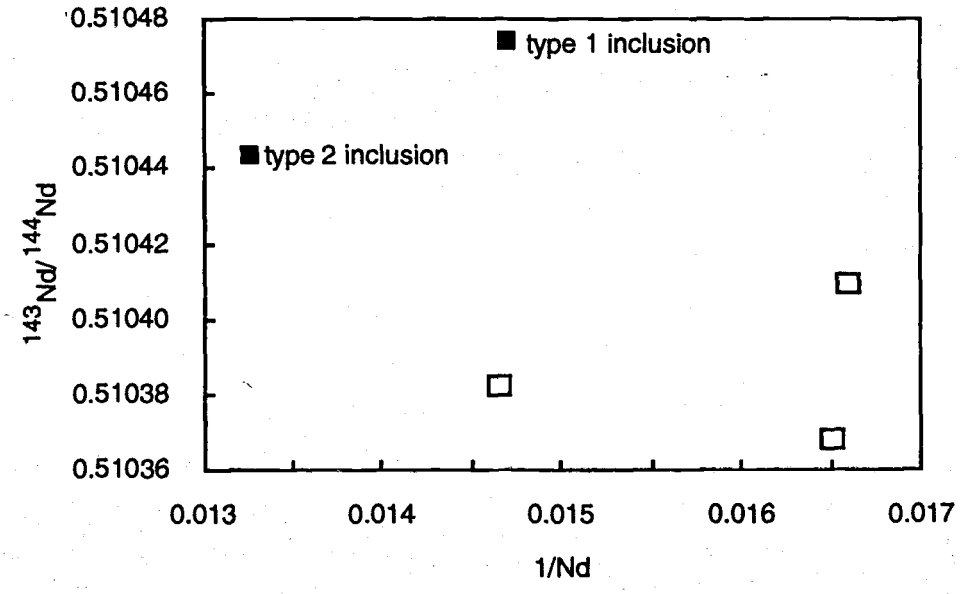

Figure 6.11 - Plot of $^{143}Nd/^{144}Nd$ against 1/Nd for the Yardea Dacite and inclusions. Symbols: open squares, Yardea Dacite; solid squares, inclusions.

Two origins which may explain the chemical and physical features of the type 2 inclusions are 1) they represent cumulates from the fractionation of the Yardea Dacite or of the mature phase in general, or 2) they are highly crystallised portions of a more mafic member of the mature phase fractionation sequence.

In order to test the cumulate hypothesis, cumulate compositions were calculated both for the intra-Yardea crystal fractionation models Y1 and Y2, and for the entire fractionation sequence from Yardea Dacite to Paney Rhyolite. The cumulate compositions were calculated using the fractionation models from Table 5.2, and these compositions are listed in Table 6.4. The major element plots which comprise Figure 6.7 illustrate that the type 2 inclusions do not plot near the cumulates but rather appear to lie on a chord between the cumulates and the Yardea Dacite for most elements. A possibility then examined was that the type 2 inclusions represented cumulates infiltrated by a high silica/potassium melt phase such as that represented by the matrix of the Yardea Dacite. However when bulk mixing calculations were done between the cumulates and the composition of phenocryst free Yardea melt (from Chapter 4), the results generally required greater than 30-40% of the melt phase, which is more than the amount of interstitial material observed in the inclusions. Another point which weighs against the type 2 inclusions being cumulates derived from the fractionation of the most siliceous Yardea from the most mafic Yardea is that modelling of this sequence did not include the fractionation of potassium feldspar (Chapter 5), and type 2 inclusions contain significant proportions of potassium feldspar grains.

The other alternative is that type 2 inclusions represent a partially crystallized, more mafic member of the mature phase fractional crystallization sequence as represented by the Yardea and Eucarro Dacites. Such an origin accounts quite well for most of the chemical variations illustrated in Figures 6.6, 6.7 and 6.8. The ε_{Nd} values of the type 2 inclusion and the host Yardea Dacite are within analytical error of one another at -3.1±0.5 and -3.8± 0.5 respectively. Therefore it cannot be unequivocally stated whether the more negative ε_{Nd} value of the Yardea with respect to the type 2 inclusion indicates that addition of crust accompanied differentiation from andesite to dacite. This is however a possibility, but the added amount of crust would be small (due to the considerably more negative ε_{Nd} values of basement material - see Chapter 2) and the following comments on the chemistry should still hold. A member of a fractionation sequence more mafic than any of the erupted Yardea Dacite would be expected to have lower levels of incompatible elements (e.g. Zr, Ba, U, Rb), and higher concentrations of elements compatible in the fractionating assemblage of pyroxene + plagioclase + Fe-Ti oxides + apatite (e.g. Ca, Al, Fe, Mg, Ti, Sc, Sr, P, V, Nb). As noted in Chapter 5 although the Yardea contains phenocrysts of potassium feldspar, chemical affects associated with fractionation of this

Table 6.4 - Calculation of cumulate compositions formed by fractionation of the mature phase volcanic sequence

Model Y1								
Mineral proportions in calculated residue		0.6459 Plagioclase	0.1518 Augite	0.1319 Pigeonite	0.0597 Magnetite	0.0107 Apatite		Cumulate composition
Mineral compositions	SiO2	61.78	52.09	51.30	0.72	0.24		54.62
	TiO2	0.00	0.23	0.14	25.68	0.00		1.59
	Al2O3	23.65	0.93	0.54	0.85	0.02		15.54
	FeO	0.42	18.57	30.90	64.94	0.27		11.05
	MnO	0.00	0.67	1.23	1.99	0.00		0.38
	MgO	0.13	9.96	12.24	0.22	0.06		3.22
	CaO	5.53	17.33	4.12	0.00	53.97		7.32
	Na2O	7.73	0.33	0.33	0.20	0.00		5.10
	K2O	1.14	0.00	0.00	0.00	0.00		0.74
	P2O5	0.00	0.00	0.00	0.10	41.14		0.45
Model Y2								
Mineral proportions in calculated residue		0.6746 Plagioclase	0.0916 Augite	0.1474 Pigeonite	0.0677 Magnetite	0.0187 Apatite		
Mineral compositions	SiO2	61.78	52.09	51.30	0.72	0.24		54.06
	TiO2	0.00	0.23	0.14	25.68	0.00		1.78
	Al2O3	23.65	0.93	0.54	0.85	0.02		16.18
	FeO	0.42	18.57	30.90	64.94	0.27		10.94
	MnO	0.00	0.67	1.23	1.99	0.00		0.38
	MgO	0.13	9.96	12.24	0.22	0.06		2.82
	CaO	5.53	17.33	4.12	0.00	53.97		6.93
	Na2O	7.73	0.33	0.33	0.20	0.00		5.31
	K2O	1.14	0.00	0.00	0.00	0.00		0.77
	P2O5	0.00	0.00	0.00	0.10	41.14		0.78
Model E1								
Mineral proportions in calculated residue		0.2734 Plagioclase	0.4244 Sanidine	0.13 Augite	0.1194 Pigeonite	0.0483 Magnetite	0.0046 Apatite	
Mineral compositions	SiO2	60.69	64.04	51.66	48.16	0.72	1.18	56.28
	TiO2	0.13	0.00	0.23	0.17	25.68	0.00	1.33
	Al2O3	24.57	19.05	1.03	0.35	0.85	0.01	15.02
	FeO	0.20	0.00	18.41	37.47	64.94	1.08	10.06
	MnO	0.00	0.00	0.76	1.59	1.99	0.00	0.38
	MgO	0.00	0.00	10.01	6.56	0.22	0.04	2.10
	CaO	6.53	0.42	17.74	5.44	0.00	53.72	5.17
	Na2O	6.90	4.92	0.32	0.00	0.20	0.00	4.03
	K2O	1.29	9.90	0.00	0.00	0.00	0.00	4.55
	P2O5	0.00	0.00	0.00	0.00	0.10	40.46	0.19
Model E2								
Mineral proportions in calculated residue		0.4788 Plagioclase	0.1883 Sanidine	0.1235 Augite	0.1313 Pigeonite	0.0725 Magnetite	0.0057 Apatite	
Mineral compositions	SiO2	60.69	64.04	51.66	48.16	0.72	1.18	53.88
	TiO2	0.13	0.00	0.23	0.17	25.68	0.00	1.97
	Al2O3	24.57	19.05	1.03	0.35	0.85	0.01	15.59
	FeO	0.20	0.00	18.41	37.47	64.94	1.08	12.00
	MnO	0.00	0.00	0.76	1.59	1.99	0.00	0.45
	MgO	0.00	0.00	10.01	6.56	0.22	0.04	2.11
	CaO	6.53	0.42	17.74	5.44	0.00	53.72	6.42
	Na2O	6.90	4.92	0.32	0.00	0.20	0.00	4.28
	K2O	1.29	9.90	0.00	0.00	0.00	0.00	2.48
	P2O5	0.00	0.00	0.00	0.00	0.10	40.46	0.24
Model P1								
Mineral proportions in calculated residue		0.3721 Plagioclase	0.4393 Sanidine	0.1038 Augite	0.0258 Pigeonite	0.0495 Magnetite	0.0096 Apatite	
Mineral compositions	SiO2	60.54	64.21	50.21	48.16	0.72	1.18	57.24
	TiO2	0.00	0.00	0.19	0.17	25.68	0.00	1.30
	Al2O3	23.11	18.53	0.62	0.35	0.85	0.01	16.86
	FeO	0.00	0.00	26.38	37.47	64.94	1.08	6.93
	MnO	0.00	0.00	1.07	1.59	1.99	0.00	0.25
	MgO	0.00	0.00	6.15	6.56	0.22	0.04	0.82
	CaO	6.15	0.51	15.17	5.44	0.00	53.72	4.74
	Na2O	8.00	4.95	0.39	0.00	0.20	0.00	5.20
	K2O	2.08	10.09	0.00	0.00	0.00	0.00	5.21
	P2O5	0.00	0.00	0.00	0.00	0.10	40.46	0.39

Calculated bulk cumulate compositions for fractionation of the mature phase magma sequence

	using models a+c+e§	using models b+d+e§
SiO2	56.27	55.35
TiO2	1.37	1.64
Al2O3	15.82	16.26
FeO	9.11	9.60
MnO	0.33	0.35
MgO	1.87	1.73
CaO	5.49	5.82
Na2O	4.70	4.91
K2O	3.95	3.24
P2O5	0.32	0.43

§ bulk cumulates calculated by multiplying the cumulate produced by each model by that fraction of the total amount of crystallization the same model produced, (taken from Table 4.2).

phase is only seen in magmas that have more than 68-69% SiO_2, which excludes most of the Yardea.

Table 6.5 - Calculation of cumulate-matrix mixtures

Model Y1

	Cumulate composition*	Average Yardea matrix	Cumulate - matrix mixes 10% matrix	20% matrix	25% matrix	30% matrix	40% matrix
SiO2	54.62	76.34	56.79	58.97	60.05	61.14	63.31
TiO2	1.59	0.25	1.45	1.32	1.25	1.18	1.05
Al2O3	15.54	12.12	15.20	14.85	14.68	14.51	14.17
FeO	11.05	1.06	10.05	9.05	8.55	8.05	7.05
MnO	0.38	0.00	0.34	0.31	0.29	0.27	0.23
MgO	3.22	0.25	2.93	2.63	2.48	2.33	2.03
CaO	7.32	0.79	6.67	6.02	5.69	5.36	4.71
Na2O	5.10	3.05	4.89	4.69	4.59	4.48	4.28
K2O	0.74	5.84	1.25	1.76	2.01	2.27	2.78
P2O5	0.45	0.00	0.40	0.36	0.33	0.31	0.27

Model Y2

	Cumulate composition*	Average Yardea matrix	Cumulate - matrix mixes 10% matrix	20% matrix	25% matrix	30% matrix	40% matrix
SiO2	54.06	76.34	56.29	58.52	59.63	60.75	62.97
TiO2	1.78	0.25	1.63	1.47	1.40	1.32	1.17
Al2O3	16.18	12.12	15.77	15.36	15.16	14.96	14.55
FeO	10.94	1.06	9.95	8.96	8.47	7.98	6.99
MnO	0.38	0.00	0.34	0.30	0.28	0.26	0.23
MgO	2.82	0.25	2.56	2.31	2.18	2.05	1.79
CaO	6.93	0.79	6.32	5.71	5.40	5.09	4.48
Na2O	5.31	3.05	5.08	4.85	4.74	4.63	4.40
K2O	0.77	5.84	1.28	1.78	2.04	2.29	2.80
P2O5	0.78	0.00	0.70	0.62	0.58	0.54	0.47

** from Table 6.4*

Chemical variations which are not readily explicable by either model are those exhibited by La, Ce and Nd, and in particular the latter. Resolution of this problem is difficult and must await further, more detailed work on the inclusions.

The current database on the type 2 inclusions does not allow discrimination between the two models outlined above for their origin. However regardless of whether the type 2 inclusions are accumulative or a partly crystallized more primitive member of the mature phase fractionation sequence, they do indicate that the Yardea Dacite is itself a fractionate of a more mafic (andesitic?) precursor. Either of the postulated origins for the type 2 inclusions accounts for the lack of any evidence of chilling of either inclusion or host at their interface and for their chemical relationship to the Yardea. On the current data set it is considered that the type 2 inclusions are best interpreted as representing a

disaggregated crystal mush which was disrupted and included in the Yardea Dacite by the eruptive process. This mush was composed of a network of plagioclase, pigeonite, augite, magnetite, potassium feldspar and apatite grains, plus an interstitial phase rich in incompatible elements which was liquid at the time of eruption. The correlation in crystallization textures between this interstitial material and the matrix of the host dacite signifies the liquid state of both at the time of eruption. Occasional lobate margins on type 2 inclusions attest to the fact that they were able to plastically deform after their disaggregation and incorporation into the Yardea magma volume.

6.5 - Summary and discussion of the inclusions in the mature phase dacites

The inclusions found within the mature phase, and particularly the last erupted unit the Yardea Dacite, have been interpreted to have two separate and distinct origins.

The basaltic andesitic type 1 inclusions were incorporated into their host dacites as blobs of magma after which rapid crystallization took place at an unknown degree of undercooling. Little chemical transfer or equilibration occurred between the type 1 inclusions and their host dacites. The actual mechanism for the formation of the type 1 inclusions cannot be easily determined. Possibilities include the forceful injection of mafic magma into a magma chamber, which is considered to be a possible eruption trigger (Sparks *et al.*, 1977), the disruption and incorporation of a lower mafic layer into overlying felsic magma by the magma chamber dynamics of a violent eruption, or mixing initiated by a density inversion when any of a number of processes result in a lower mafic melt changing from more dense to less dense than the overlying felsic magma (see Huppert *et al.* 1983, 1984 and Turner *et al.*, 1983 for discussions of this mechanism). Regardless of how the basaltic andesite became intermingled with the dacite, the result was quenched mafic blobs within the dacite. As noted by Sparks and Marshall (1986), variation of mafic-felsic magma interaction ranges from the formation of inclusions where both magmas maintain their physical and chemical integrity, through intimate mingling producing banded lavas or pumice, to complete hybridization with the resultant volcanics having mixed phenocryst populations. It has been estimated that basaltic magma must make up more than 50 volume % of intermingled mafic and felsic magmas for mixing to occur (Sparks and Marshall, 1986), a proportion which would be difficult to achieve in a very large volume magma chamber such as that represented by the Yardea-Eucarro system by the introduction of mafic magma via any of the mechanisms outlined above. As a result, mixing was prohibited and the introduced mafic magma formed quenched inclusions.

The presence of the type 1 inclusions has important implications for the development of the mature phase volcanism. Firstly they indicate that contemporary mafic magma was present during the evolution of the mature phase magma chamber. This is important because recent modelling (Huppert and Sparks, 1988) has shown that silicic magma chambers crystallize in time spans of 10^3 years, which is orders of magnitude faster than estimates of the time taken to develop and/or produce chemical zoning in large volume silicic magma chambers which are in the range of 10^5-10^6 years (Hildreth *et al.*, 1991, Shaw, 1985; Smith, 1979; Wolff *et al.*, 1990). Therefore external heat input, via hot, mafic magmas is necessary to maintain develop and maintain this sort of large volume silicic system and the type 1 inclusions provide the only direct evidence for such continued heat input during the mature phase. To date the type 1 inclusions in the Yardea and Eucarro Dacites are the only recognised occurrence of quenched mafic inclusions in large volume silicic ignimbrites. In addition, the magma from which the type 1 inclusions were derived has been shown to have considerable similarities to the HP basaltic andesites from Kokatha, but with enrichments in many incompatible elements which are thought to be the result of fractionation ± the incorporation of a small degree partial melt of a crustal lithology. The evolution of the mature phase magmas is however considered to be linked not to this HP type magma but rather formed by AFC processes ultimately based on a LP basaltic parent (Chapter 5). Both HP and LP mafic magmas may have been produced throughout the evolution of the province. This is quite reasonable if the interpretation that the mafic magmas represent members of a mixing continuum derived from lithospheric and asthenospheric sources, as suggested in Chapter 2, is correct. The fact that this HP type of mafic magma occurs both in the developmental phase, at Kokatha, and also in the mature phase indicates that the sub-continental mantle lithosphere was still acting as a magma source towards the end of the volcanism, and had not been 'eroded' or replaced by upwelling asthenosphere as has been documented in some extensional volcanic provinces (e.g. Perry *et al.*, 1988; Daley and DePaolo, 1992).

The second type of inclusion present in the Yardea have been interpreted to represent crystal mushes which are either cumulates produced by the fractionation of the mature phase magmas or by crystallization of magma more mafic than the preserved erupted Yardea, a precursor to the Yardea in the mature phase fractionation sequence.

Recent theoretical modelling of crystallization in convecting magma chambers (Worster *et al.*, 1990) provides a neat mechanism for the formation of crystal mushes, and a possible explanation for the two types of inclusions not having been found at the same localities. In a magma chamber which is being cooled from above (as most if not all chambers must be), a mushy layer of connected crystals and interstitial melt forms near the roof of chambers below a solid crystal crust. Although this mushy layer forms at the roof, most of the crystallization nevertheless occurs at the floor. The presence and

thickness of the mushy layer is dependant on a number of fluid dynamical factors including the composition, temperature and thickness of magma and the presence and rate of convective flow in the chamber (Worster *et al.*, 1990). Although the modelling was carried out on a Di-An system, chemically much simpler than that being considered here, it is suggested that the type 2 inclusions may well have formed from such a layer disrupted by the evisceration of the magma chamber in the eruption which produced the Yardea Dacite. The finer grain size of the inclusions compared with the host dacite may be a function of their crystallization having taken place at the upper, cooler part of the chamber.

If the type 2 inclusions represent a diaggregated crystal mush from the top of the magma chamber, and the type 1 inclusions are quenched mafic magma introduced by some mechanism from somewhere beneath the Yardea magma volume, it is not surprising that they have mutually exclusive distributions within the Yardea Dacite. If the eruption which produced the Yardea Dacite tapped progressively deeper levels of the magma chamber, it could be expected that the type 2 inclusions would be torn from the crystal mush and expelled from the chamber at a relatively early stage in the eruption, whereas the lower levels of the chamber would be tapped later, and the more mafic type 1 inclusions would be contained in this later stage material.

The work of Worster *et al.* (1990) also allows a speculative comment on why the type 2 inclusions may occur only in the Yardea Dacite. Convection in a magma chamber inhibits the growth of a mushy layer at the top of a magma chamber by increasing the heat transfer from the melt into the roof. Given that the Yardea was considerably more viscous than the earlier Eucarro Dacite (see calculations in Chapter 3), and this higher viscosity would slow convection (Huppert and Sparks, 1988), the magma in the pre-Eucarro chamber would be expected to convect more rapidly than that in the pre-Yardea magma chamber. As a result the Eucarro magma chamber would have had a lesser thickness (or even absence) of mushy layer than the Yardea. Consequently type 2 inclusions are absent, or are rare and have not thus far been observed in the Eucarro Dacite.

The discovery of inclusions in the Yardea and Eucarro Dacites is important for although many recent studies have revealed magmatic inclusions in silicic volcanic provinces (Bacon and Metz, 1984; Bacon, 1986; Druitt and Bacon, 1988 and 1989; Davidson *et al.*, 1990; Varga *et al.*, 1990), most inclusions have been reported to be hosted by felsic lavas. Only rarely have such inclusions been reported in ignimbritic rocks (e.g. Stimac *et al.*, 1990), and as yet no occurrences have been described from ignimbrites of the large volume category (>1000km^3) to which the Yardea and Eucarro belong. Further work on these inclusions may help our understanding of magma chamber processes in large volume magma chambers.

Chapter 7 - The fundamental role of mafic magma in the generation of the Gawler Range volcanic province and implications for crustal growth

7.1 - Introduction

The role ascribed to mafic magma in the generation of felsic magmas has been the subject of considerable debate. Some petrologists consider that mafic magmas act as a heat source for crustal anatexis but have little or compositional input to the felsic melts (e.g. Chappell *et al.*, 1987; Chappell and Stephens, 1988). At the other extreme some silicic volcanic and plutonic rocks have been interpreted to have formed by extreme differentiation of parental, mantle-derived mafic magmas which had minimal or no interaction with crustal lithologies (e.g. Sparks, 1988; Musselwhite *et al.*, 1989). Many recent studies have invoked models which occupy middle ground between these two endmember extremes and attribute the generation of felsic magma to process(es) which combine mantle and crustal sources.

Direct evidence of coeval mafic melts in dominantly felsic magmatic systems is often absent (e.g. Riccuputi and Johnson, 1990). In the Gawler Range volcanic province, the occurrence of basalts and basaltic andesites in three of the four exposed developmental centres (Chapter 2), and the type 1, basaltic andesitic inclusions in the Yardea Dacite (Chapter 6) are evidence that mafic magmas existed throughout the evolution of the province, however they do not provide evidence for the large volumes of mantle derived mafic magma which are required to have been emplaced within the crust at Gawler Range time by the interpretation that both the developmental and mature phase volcanics are the result of mantle dominated AFC processes. The first section of this chapter presents evidence for a very large mafic body underlying the Gawler Range volcanic province at depth. The second part of the chapter gives an overview of the evolution of the Gawler Range volcanism and presents a model for the evolution of the province, which concludes that the Gawler Range magmatism resulted in major addition to the crust and lithospheric modification.

7.2 - Evidence for a large volume of contemporaneous mafic magma in the mid-crust region beneath the Gawler Ranges

Most large volume felsic volcanic provinces have associated negative gravity signatures which have been variously attributed to the underlying presence of a zone of melt beneath currently active areas (e.g. Yellowstone, Smith and Christiansen, 1980; Smith and Braile, 1984) or to silicic intrusives of batholithic proportions underlying provinces which are no longer active (e.g. the San Juan Volcanic Field, Steven and Lipman, 1976). Positive gravity anomalies associated with dominantly felsic volcanic provinces are also recognised although this is a less common phenomenon. Examples include the western central Snake River Plain (Lum *et al.*, 1989) and the Caddilac Mountain Granite (Wiebe, 1992). The dominantly felsic Gawler Range volcanic province falls into this category and is characterized by a distinct positive gravity anomaly, indicating the presence of a dense body at depth (Figure 7.1). This is interpreted to be a large gabbroic body which recent calculations from the gravity data indicate lies at a depth of approximately 13 kilometres (Zhiqun Shi, 1993). The shape of the gravity high closely correlates with the known distribution of the Gawler Range Volcanics (Figure 7.1). An apophysis from the main gabbroic body as defined by the gravity data runs off to the southwest towards the coast, and undeformed gabbro was intersected in a number of shallow holes drilled by the South Australian Department of Mines in the early 1960s on local gravity highs. The positions of these holes are shown on Figure 7.1. The mineralogy of the gabbros is typically orthopyroxene + clinopyroxene + plagioclase + magnetite + apatite ± olivine ± late formed hornblende and/or biotite. No foliation or deformational fabric is present in any of the gabbros.

In order to ascertain whether the apophysis, and by inference the main gabbroic body, was temporally related to the Gawler Range volcanism, a five point Sm-Nd mineral isochron, and a six point Rb-Sr isochron were determined on a two-pyroxene gabbro from one of these drill holes, Inkster IR2 (Table 7.1, Figures 7.2a and b). This particular gabbro contains early formed cumulate orthopyroxene and clinopyroxene, later formed cumulate plagioclase and apatite, set in an intercumulus assemblage of plagioclase, titanomagnetite, hornblende and biotite. The sample chosen was fresh, with only occasional, very minor sericitic alteration of plagioclase.

The Sm-Nd isochron (Figure 7.2a) yielded an initial ratio of 0.510540 and an age of 1589±293 Ma. Although there is considerable error on the age, in part due to the relatively small Sm/Nd variation exhibited by the minerals, the MSWD of 1.26 suggests that an age of approximately 1590 Ma. may be correct. The age is very close to the U-Pb ages for both the developmental and mature phases of the Gawler Range volcanism (these

Figure opposite:

Figure 7.1 - Map showing contoured gravity data illustrating the gravity high associated with the Gawler Range volcanic province. The open circles represent the positions of drill holes which intersected undeformed gabbro. The crossed circle indicates the Inkster hole, from which a two-pyroxene gabbro was selected for isotopic analysis.

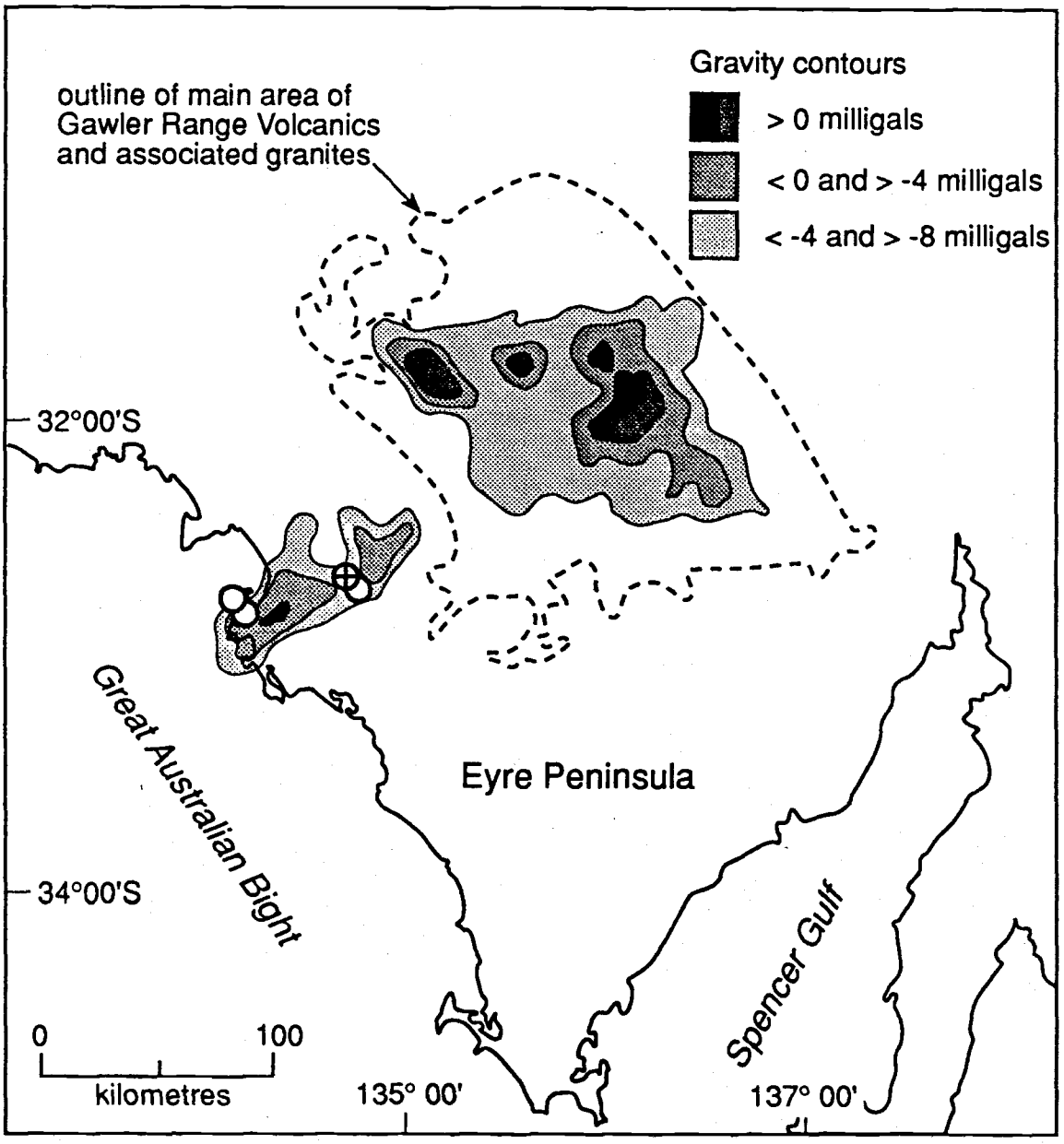
Gravity contours
> 0 milligals
< 0 and > -4 milligals
< -4 and > -8 milligals
outline of main area of
Gawler Range Volcanics
and associated granites
32°00'S
34°00'S
Great Australian Bight
Eyre Peninsula
Spencer Gulf
0
100
kilometres
135° 00'
137° 00'

ages are 1591±3 Ma. for the Waganny Dacite and 1592±3 Ma. for the Yardea Dacite; Fanning *et al.*, 1986, 1988).

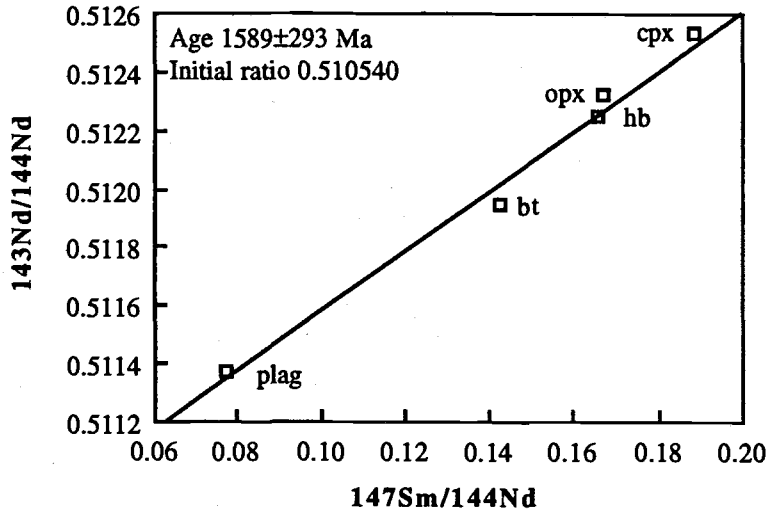

Figure 7.2a: Sm-Nd mineral isochron determined on the two pyroxene gabbro from drillhole Inkster IR2.

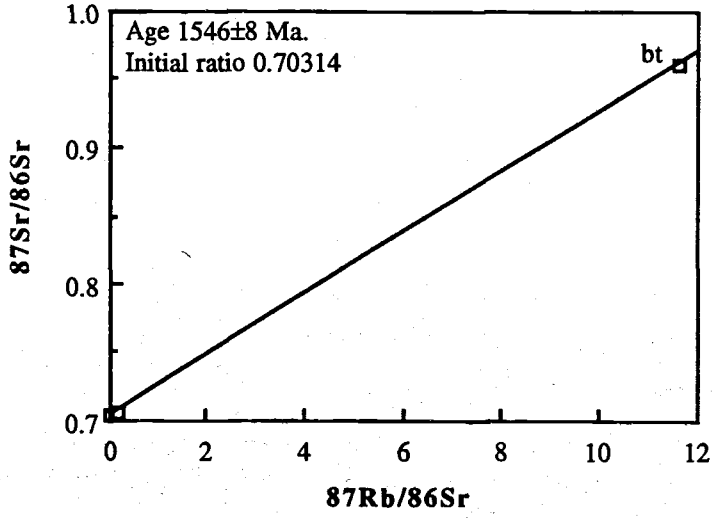

Figure 7.2b: Rb-Sr mineral isochron determined on the two pyroxene gabbro from drillhole Inkster IR2.

Table 7.1 - Isotopic data for gabbro mineral isochrons

Mineral	*Nd (ppm)*	*Sm (ppm)*	*147Sm/144Nd*	*143Nd/144Nd (m)*
Clinopyroxene	18.75	5.84	0.1888	0.512538 ±28
Orthopyroxene	2.43	0.67	0.1655	0.512251 ±21
Hornblende	36.64	10.09	0.1667	0.512325 ±16
Biotite	1.15	0.28	0.1427	0.511950 ±44
Plagioclase	2.45	0.31	0.0773	0.511375 ±34

Model 1 isochron yields an age of 1589±293Ma. Initial ratio = 0.510540. MSWD = 1.26

	Rb (ppm)	*Sr (ppm)*	*87Rb/86Sr*	*87Sr/86Sr (m)*
Clinopyroxene	1.7	60.6	0.0832	0.70507 ±4
Orthopyroxene	0.6	36.0	0.1537	0.70577 ±5
Hornblende	11.5	284.9	0.1175	0.70598 ±1
Biotite	293.6	73.2	11.6370	0.96145 ±3
Plagioclase	1.4	1690.1	0.0024	0.70341 ±2
Apatite	0.1	434.2	0.0006	0.70341 ±1

Model 3 isochron yields an age of 1546±8 Ma. Initial ratio = 0.70314. MSWD=1

(m) denotes the measured isotopic ratio
Errors in isotope ratios are quoted as ±2 sigma S.E.

The Rb-Sr isochron (Figure 7.2b) yielded an age of 1546±8 Ma which is a little older than the range of Rb/Sr ages, 1510-1529 Ma, previously reported for the volcanism in the Gawler Range province (Webb *et al.*, 1986). The initial Sr ratio for this isochron is 0.70314, a value slightly lower than any obtained for whole rock isotopic determinations on basalts from the Kokatha, Lake Everard and Tarcoola developmental volcanic areas. The Rb/Sr isochron is controlled by the biotite point and the younger age for this isochron compared with that from the Sm/Nd system could be due to the lower closure temperature of biotite for Sr compared with Nd, or to minor re-equilibration in the Rb-Sr system.

As a result of this isotopic work, the crystallization age of the Inkster gabbro, and by inference at least an approximation of the age of the large mid-crustal gabbroic body, is given by the Nd-Sm age of approximately 1590 Ma. Thus the intrusion of this large volume of mafic magma is considered to have been contemporaneous with the period of dominantly silicic volcanism in the Gawler Range province.

The bulls-eye coincidence of the mid-crustal gabbroic body and the known distribution of the Gawler Range Volcanics (Figure 7.1), together with the indications that the two magmatic events were contemporaneous, argues strongly for the magmatism in the Gawler Ranges having been initiated by the input into the continental crust of a large volume of mantle-derived mafic magma. The position of the gabbroic body at approximately 16 kilometres depth correlates well with the minimum estimated depth of phenocryst formation of the Eucarro Dacite (a minimum depth of approximately 8-13 kilometres, Chapter 4). The preferred interpretation of this information is that the gabbro represents the mafic magma which ponded beneath the large, mature phase silicic magma chamber, and which provided the the requisite heat for the development and maintenance of felsic magmatism for the amount of time necessary to develop massive felsic magma chambers, suggested to be in the region of 10^6 years (Shaw, 1985; Wolff *et al.*, 1990).

Chemical and isotopic data discussed in Chapters 2 and 4 indicate that mafic magma provided a significant source component for both the developmental and mature phases of the Gawler Range volcanism, and the large volume of mantle magma required is indeed present beneath the Gawler Ranges. Therefore considerable crustal addition occurred during this period of magmatism. The exact volume of material added is difficult to estimate, mainly because of the difficulty in estimating the volume of the volcanic units. However an absolute minimum estimate can be made using the mature phase units alone. Using as a starting point the AFC modelling for producing the Yardea Dacite which was outlined in Chapter 5, the amount of crust involved is approximately 10-12%. If the volcanics of the mature phase represent only 10% of the amount of magma in the mature phase system, an erupted to intrusive ratio which has been suggested for other silicic magma chambers (Smith, 1979; Shaw, 1985), then the total amount of mature phase magma would be between approximately 40,000km^3 and 225,000km^3 (calculated from the volumes estimated in Chapter 3. The amount of mafic mantle derived magma needed to produce the silicic mature phase magmas would therefore be in the order of 35,000-200,000 km^3. Although these figures cannot be said to be rigorously constrained, they do nevertheless indicate that the Gawler Range volcanism was accompanied by large scale addition of mafic mantle derived magma to the crust.

7.3 - A model for the Gawler Range volcanism

The data presented above and in the previous chapters suggest that mafic mantle derived magma played an important role in the generation of the Gawler Range volcanic province, both providing a heat flux into the crust from the mantle which initiated crustal

melting, and itself being an important source component for the resultant magmatism, both mafic and felsic.

7.3.1 The developmental phase

The basalts of the developmental phase are themselves interpreted as having been derived by mixing between two mantle sources, a contemporary asthenospheric melt and an enriched component from the mantle lithosphere. This latter component is interpreted to have been separated from the convecting asthenosphere for some considerable time, time needed for it to develop an εNd signature much lower than the contemporary convecting mantle. Various degrees of melting of this lithospheric mantle, coupled with mixing with asthenospheric mantle, formed a complex array of magmas with similar chemical signatures (as evidenced by primitive mantle normalized element patterns), but with varying absolute elemental concentrations.

The correlation of εNd values in the developmental volcanics with chemical parameters implies mixing relationships between these mafic, mantle derived magmas and continental crust. Modelling of the mixing indicates that bulk mixing cannot account for the isotopic and chemical variation of the developmental volcanics. The felsic developmental volcanic rocks are considered to be best modelled by the fractional crystallization of enriched basalts (which themselves have both lithospheric and asthenospheric components) with concomitant assimilation of crustal materials. The actual amount of assimilation which occurs is dependant on a number of interacting factors such as the volume of mafic melt input into the crust in any single event, the crustal temperature and the residence time. Increases in any of these factors will tend to produce an increase in the amount of crust assimilated.

Mafic melt continued to be input into the various developmental magmatic systems, generally ponding beneath the less dense silicic magmas, but occasionally, when inputs exceeded 50% of the silicic hybrid magma volume, mixing was able to reset the isotopic evolution of the chamber (Sparks and Marshall, 1986), as seen in the Kokatha sequence.

Two possible models have been proposed for the variations in Nd isotope arrays seen from centre to centre of the developmental phase volcanism. The first model postulates that the crustal assimilant in each province was similar, of broadly granitic composition and Archaean in age, and that the observed variation therefore was due to different ratios of assimilation/fractional crystallization from centre to centre, with the amount of assimilation decreasing in centres as you move southward. This could possibly be caused by lesser volumes of basalt being involved in each centre as you move south, for this is a factor in the amount of assimilation which takes place, as determined by Vosage *et al.* (1990). The second model proposes that the crustal assimilant decreases in

age as you move southward from Kokatha, through Lake Everard, to Toondoolya Bluff, and that the amount of assimilation in each province is relatively similar. This second model is similar to that proposed by Chauvel *et al.*(1987) for a crust forming event in the Proterozoic of Canada, where a progressive decrease in εNd values in granites towards a portion of Archaean craton was interpreted to indicate the mixing of an increasing amount of an Archaean component with new, mantle-derived Proterozoic material. It is not possible at present to determine which of the two models is correct for the Gawler Ranges. Isotopic analysis of basement rock from the Lake Everard and Toondoolya Bluff areas would solve the dilemma, but are at present unobtainable without drilling.

Driven by continued injection of basaltic melts into the crust, larger volumes of felsic magma were formed as the province developed. This is consistent with modelling of the generation of silicic magmas by Huppert and Sparks (1988) which shows that when a volume of basalt is emplaced into the crust, the volume of silicic magma produced by crustal melting increases over time while the basaltic layer cools. In addition, successive injection of basaltic magma will initiate a larger amount of crustal melting than the last, as the crust will be heated by previous basalt inputs. Assimilation/fractional crystallization continued to be the dominant differentiation mechanism, and the developmental chambers therefore contained hybrid magmas.

7.3.2 The mature phase

Two characteristics of the mature phase volcanism which are among the factors distinguishing it from the products of the preceding developmental phase are its isotopic homogeneity and the fact that the units all form a single chemical sequence. It seems unlikely that each unit of the mature phase developed in a separate chamber, which just by chance had developed identical isotopic values derived from a complex combination of sources, and in addition exhibited systematic chemical variation with all other units. A much more realistic scenario, and indeed the preferred one, is the mature phase volcanics represent the periodic tapping of an isotopically homogeneous, chemically and mineralogically stratified magma reservoir (Chapter 5).

The formation of the mature phase magma chamber could have occurred in a number of ways. For example, it may simply have formed by AFC processes initiated by a new influx of mafic magma into the crust, following solidification of the developmental phase reservoirs, and have no direct relationship with the earlier phase of magmatism. However an alternative origin for the mature phase magma chamber provides a simple and elegant explanation of many of the features of the mature phase volcanism. This model suggests that the developmental phase magma chambers became larger due to continued mafic magma input and that the felsic

magma volume increased until it initiated the coalescence of a number of relatively small, developmental chambers into a single very large volume chamber.

A physical repercussion of the formation of this new, much larger, chamber was the chemical and isotopic homogenization of the magma it contained. The magma volumes which were contained in the smaller volume chambers would have been thoroughly mixed together upon the formation of the much larger mature phase chambers because the increase in chamber dimensions would induce vigorous convection. Whether convection occurs, and what type of convection occurs, is determined by the thermal Rayleigh number (Ra), where

$$Ra=\rho g\alpha T L^3/\kappa\nu$$ (e.g. Turner and Campbell, 1986, Equation 2, p261; see also p263 and p329) where ρ is the density, g is the acceleration due to gravity, α is the coefficient of thermal expansion, T is the temperature difference between two boundaries, L is the distance between them, κ is the thermal diffusivity and ν is the kinematic viscosity. It can be clearly seen that the dominant parameter in this equation is that relating to the size of the chamber which is raised to the third power; an increase in the dimensions of the magma chamber would result in vigorous convection, and in turn in chemical and isotopic homogenization of the magma chamber. Figure 7.3 illustrates that at the temperatures of interest (>1000°C) an increase in the size of a magma chamber will cause convection, and that for a large chamber the convection will probably be turbulent. Turbulent convection would rapidly homogenise the magma. It should be noted that the developmental phase magmas were crystal poor, as would have been the resultant homogenised magma. It is possible that the magma which resulted from this homogenization had the silicic andesitic composition of the type 2 inclusions in the Yardea Dacite. If so the lack of large phenocrysts in these inclusions may also indicate that the magma which was parental to the mature phase volcanics had a low crystal content. The formation of the mature phase magma chamber by coalsecence of several smaller developmental phase magma chambers explains not only the isotopic homogeneity of the mature phase, but also the fact that the isotopic values are approximately at the middle of the isotopic range exhibited by the entire developmental phase.

Differences between the silicic units of the developmental phase and the mature phase are predominantly the much larger size and the greater average phenocryst content of the latter. The larger volume of the mature phase units is attributable to the greater size of the final magma chamber. The smaller average phenocryst content in the developmental magmas may have been due to a closer juxtaposition of the felsic magmas and underlying mafic melts in the smaller chambers, resulting in superheated felsic melts. Alternatively it could be a result of higher water contents of the developmental magmas which suppressed crystallisation. The latter possibility provides a neat explanation not only for the different crystal contents of the two phases, but also for the dry nature of the mature phase. As

volatiles tend to be collect at the top of magma chambers, the magmas which remained behind in the developmental chambers after eruption of their volcanic sequences would have been relatively 'dry'. The parental mature phase magma which formed by homogenisation of the remaining magmas would therefore also have been quite dry.

Following the formation of the mature phase magma chamber and the accompanying production of a chemically and isotopically homogeneous parent magma, the mature phase chamber then evolved by fractional crystallization (or convective fractionation) from this homogeneous parent magma. It developed a more siliceous cap which was zoned from dacite to rhyolite. This upper zoning may be have been continuous, or the product of a number of chemically distinct, stratified convecting cells produced by double-diffusive convection (also known as multi-component convection; e.g. Sparks *et al.*, 1984; Turner and Campbell, 1986). Which of these types of zoning was present in the mature phase chamber cannot be determined with the current sample distribution, much more detailed sampling of the zoned units (i.e. the Eucarro Dacite and Nonning Rhyodacite) is required. Pyroxene thermometry from the Eucarro Dacite indicates that at least the upper part of the Eucarro magma volume cooled during its formation (Chapter 4). This cooling may have resulted in the upper part of the pre-Eucarro magma chamber changing from turbulent to steady convection (Figure 7.3), which would assist the formation of double diffusive convective cells.

The dominant volume (Hildreth, 1981) beneath the zoned cap was dacitic in composition, and evidence indicates that during the eruptive period of the mature phase chamber, a second zoned silicic cap was not formed, either because the eruption rate exceeded the rate at which chemical zoning was formed (which is suggested to be $>10^5$ years for large volume systems by Wolff *et al.*, 1990), or because the fractionation mechanism became inhibited by increasing crystallinity of the magma. The magma in the mature phase chamber may have continued to assimilate crust, however only minor manifestations of assimilation are seen in the isotopes of the mature phase volcanics. The lack of isotopic change with time of the mature phase magma chamber differs from many other large volume silicic magma systems such as Yellowstone (Hildreth *et al.*, 1991), the Sawatch Range (Johnson and Fridrich, 1990), the San Juan Mountains (Colluci *et al.*, 1991; Riciputi and Johnson, 1990), the Timber Mountain-Oasis Valley complex (Farmer *et al.*, 1991) and the Latir volcanic field (Johnson *et al.*, 1990). Each of these systems exhibits variation of ε_{Nd} either with time or with SiO_2. Although less commonly reported, some volcanic units do appear not to have undergone interaction with wall rocks after the formation of a large magma chamber. One such units is the Kalamazoo Tuff in the northern Basin and Range Province (Gans *et al.*, 1989).

The attainment and maintenence of isotopic homogeneity for such a large volume of relatively hot magma is remarkable considering the length of time required to develop

such a system, which is in the order of millions of years (Smith, 1979; Shaw, 1985). One explanation for this may be that little contamination of the magmas was occurring, possibly because after the movement of the magma into the upper crust, it was enclosed by wall rocks which were far below their solidi and therefore less likely to melt. A similar explanation was used by Gans *et al.* (1989) to explain the lack of contamination of the Kalamazoo Tuff. Another possibility is that little of the peripheral, contaminated material was erupted. Another possibility is that the magma chamber walls were lined by a crystal mush of such as that suggested to have given rise to the type 2 inclusions in the Yardea Dacite. This crystal mush may have prevented all but minor instances of contamination. Alternatively vigorous convection may have thoroughly mixed the contaminated magma into the main magma volume, although if this were so then the magma which was retained in the chamber longest, i.e. the Yardea magma, should be the most contaminated. As this is not the case, it is considered unlikely that this mechanism was operating. It is difficult to evaluate the other listed possibilities, therefore the reason for the apparent lack of contamination of the mature phase magmas must remain problematical.

7.3.3 Mafic magmatism in the mature phase

As described in Chapter 2 the developmental phase of volcanism in the Gawler Ranges contains the only exposed mafic volcanism of the province. This has been ascribed to the relative ease of penetration of mafic melts to the surface by brittle fracturing of the crust. With continued development of the province, and particularly once the large mature phase magma chamber had formed, further eruption of basalt was hindered by the presence of this very large amount of less dense felsic magma. The more dense mafic melts were prevented from rising any further and were therefore forced to pond at the base of the felsic magma. As a result of this density barrier, no mafic or intermediate magmas erupted following the formation of the mature phase magma chamber. A similar cessation of mafic activity is also observed in some other felsic volcanic provinces e.g. the Inyo Craters volcanic chain (Metz and Mahood, 1991), and the Timber Mountain/Oasis Valley volcanic centre (Byers *et al.*, 1989; Broxton *et al.*, 1989). In other provinces mafic or intermediate magmas may erupt peripherally to the main felsic magma reservoir, in areas where the crust has not undergone enough melting to arrest the rising melts e.g. Yellowstone (Hildreth *et al.*, 1990) and the San Juan volcanic field (Askren *et al.*, 1991).

Mafic magma continued to be input into the system after the formation of the mature phase chamber. This is evident from the type 1 basaltic andesitic inclusions found in the Yardea and Eucarro Dacites, and is also necessary to maintain silicic magmatism over the large periods of time (10^5-10^6 years) required to form, and chemically zone, large volume silicic magma chambers (Smith, 1979; Shaw, 1985; Wolff *et al.*, 1990). Resetting or changing of the isotopic character of the mature phase chamber did not occur,

as it had in the earlier, smaller developmental chambers, because of the very large volume of mafic magma which would be needed to exceed 50% of the chamber volume and cause mixing (Sparks and Marshall, 1986).

In some large felsic volcanic provinces, basalts erupt only after the cessation of the major or most voluminous felsic activity, e.g. the Hinsdale formation which succeeded the major ignimbritic activity in the San Juan volcanic region (Steven and Lipman, 1976; Askren *et al.*, 1991), the basaltic volcanism which followed the massive outpourings of rhyolitic magma in the Central Snake River Plain (Lum *et al.*, 1989) and the andesite and basalt lavas which overlie the Latir volcanic field (Johnson and Lipman, 1988). Basaltic magmas in this situation breach the surface when solidification of the preceding felsic magma has proceeded to the point where it will fail in a brittle manner.

There is no indication that basalts erupted following end of the mature phase volcanism in the Gawler Ranges. The cessation of volcanism and the highly crystalline nature of the Yardea Dacite may indicate that the thermal anomaly which initiated and maintained the magmatism had waned by the late stages of the mature phase magmatism and little basalt was being produced. According to the calculations of Huppert and Sparks (1988), without continued injections of basalt, the ponded mafic magma beneath the province would have solidified well before the overlying silicic magma chamber was fully crystalline.

The Gawler Range volcanic province is one of few instances in which continued basaltic magmatism can be demonstrated to have occurred throughout the life of such a large volume felsic volcanic province, and to have contributed not only heat but also source components to the felsic magmas. This continued input of mantle derived material, combined with the interpretation that most if not all of the felsic magmatism contained a considerable mantle derived component (Chapters 2 and 5) indicates that there was significant crustal growth during this period of magmatism. The evolution of the province would have resulted in a gradual hybridization of the crust under the Gawler Ranges, by the repeated intrusion of large volumes of mafic magma (combined with subsequent AFC processes), resulting in increasing ε_{Nd} and decreasing $^{87}Sr/^{86}Sr$ in the crust, as described by Johnson (1991) for several provinces in the western United States. The type of mafic magma-crust interaction and the resultant lower crustal lithologies and structure may have been similar to that observed in the Ivrea Zone (Vosage *et al.*, 1990; Sinigoi *et al.*, 1991).

One unresolved problem is what initiated the basaltic flux from the mantle. This question is rather tricky, even in still active areas like Yellowstone where despite extensive data of all types, it is still unclear whether the magmatism is related to a hotspot or to the propagating tip of a structural accomodation zone between two extensional provinces (Hildreth *et al.*, 1991). Asthenospheric input is necessary in the Gawler Ranges to explain the high temperatures reported for some of the basalts (>1350°C, Robertson, 1989). One

possible model is that outlined in a recent paper by Barley and Groves (1992) in which the voluminous anorogenic magmatism occurs at times where supercontinents had formed and in the early stages of supercontinent breakup. They envisage that supercontinents act as thermal blankets to the underlying mantle and upwelling zones result in the production of anorogenic magmatism. The very large amount of anorogenic magmatism which occurs in the Proterozoic is attributed by Barley and Groves (1992) to the higher mantle temperatures at this time of first supercontinent formation compared with later episodes, which resulted in a larger amount of anorogenic magma production.

7.3.4 Summary

The evolution of the Gawler Range volcanic province is interpreted to have occurred in two phases. In the first or developmental phase, chemically and isotopically heterogeneous sequences of magmas were erupted from several spatially separate centres. At each of these centres the dominantly silicic volcanics were produced by AFC processes from LREE enriched basalts.

The developmental phase was ended by the coalescence of several magma chambers to form a single, large magma chamber. The formation of this chamber induced turbulent convection, which resulted in an isotopically heterogeneous magma volume of andesitic composition. The mature phase volcanics then formed from this parental magma by crystal-liquid fractionation processes, apparently with little associated assimilation. Therefore the mature phase volcanics are not interpreted to have formed directly by an AFC process, but rather to be the result of a complicated sequence of AFC, magma homogenisation and fractionation.

Thus all of the silicic magmas of the Gawler Range volcanism formed directly or indirectly by the AFC process, and modelling indicates that they contain more mantle derived component than crust. The unusually high incompatible element contents of the silicic Gawler Range volcanics is the result of the AFC process from the already enriched, mantle derived, mafic endmember. Recent detailed studies of several large volume, caldera related ignimbrites (e.g. Hildreth *et al.*, 1991; Farmer *et al.*, 1991) reveal that they were also produced by AFC from a basaltic parent, which may indicate that this is an important mechanism in producing large volume silicic magmas.

Figures 7.3 and 7.4 are cartoons which attempt to illustrate the development of the Gawler Range volcanic province as summarised here.

Figure opposite:

Figure 7.3 - Cartoon illustrating the evolution of the Gawler Range volcanic province in the developmental stage

Figure overleaf:

Figure 7.4 - Cartoon illustrating stages in the evolution of the Gawler Range volcanic province in the mature phase.

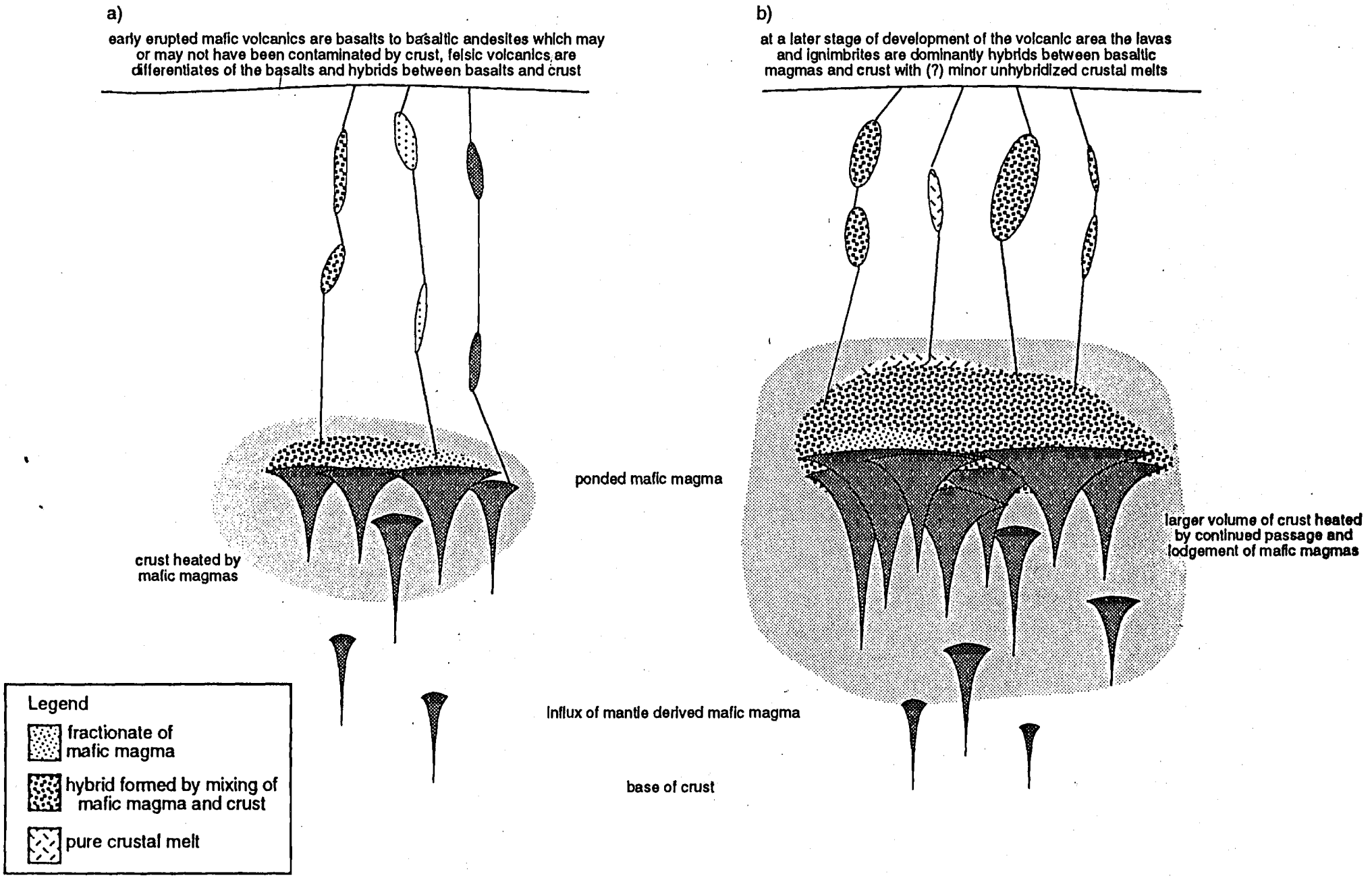
a)
early erupted mafic volcanics are basalts to basaltic andesites which may or may not have been contaminated by crust, felsic volcanics are differentiates of the basalts and hybrids between basalts and crust
b)
at a later stage of development of the volcanic area the lavas and ignimbrites are dominantly hybrids between basaltic magmas and crust with (?) minor unhybridized crustal melts
ponded mafic magma
crust heated by mafic magmas
larger volume of crust heated by continued passage and lodgement of mafic magmas
influx of mantle derived mafic magma
base of crust
Legend
fractionate of mafic magma
hybrid formed by mixing of mafic magma and crust
pure crustal melt

a) the mature phase chamber prior to tapping of upper zoned region

b) the mature phase chamber after the evisceration of the Yardea Dacite

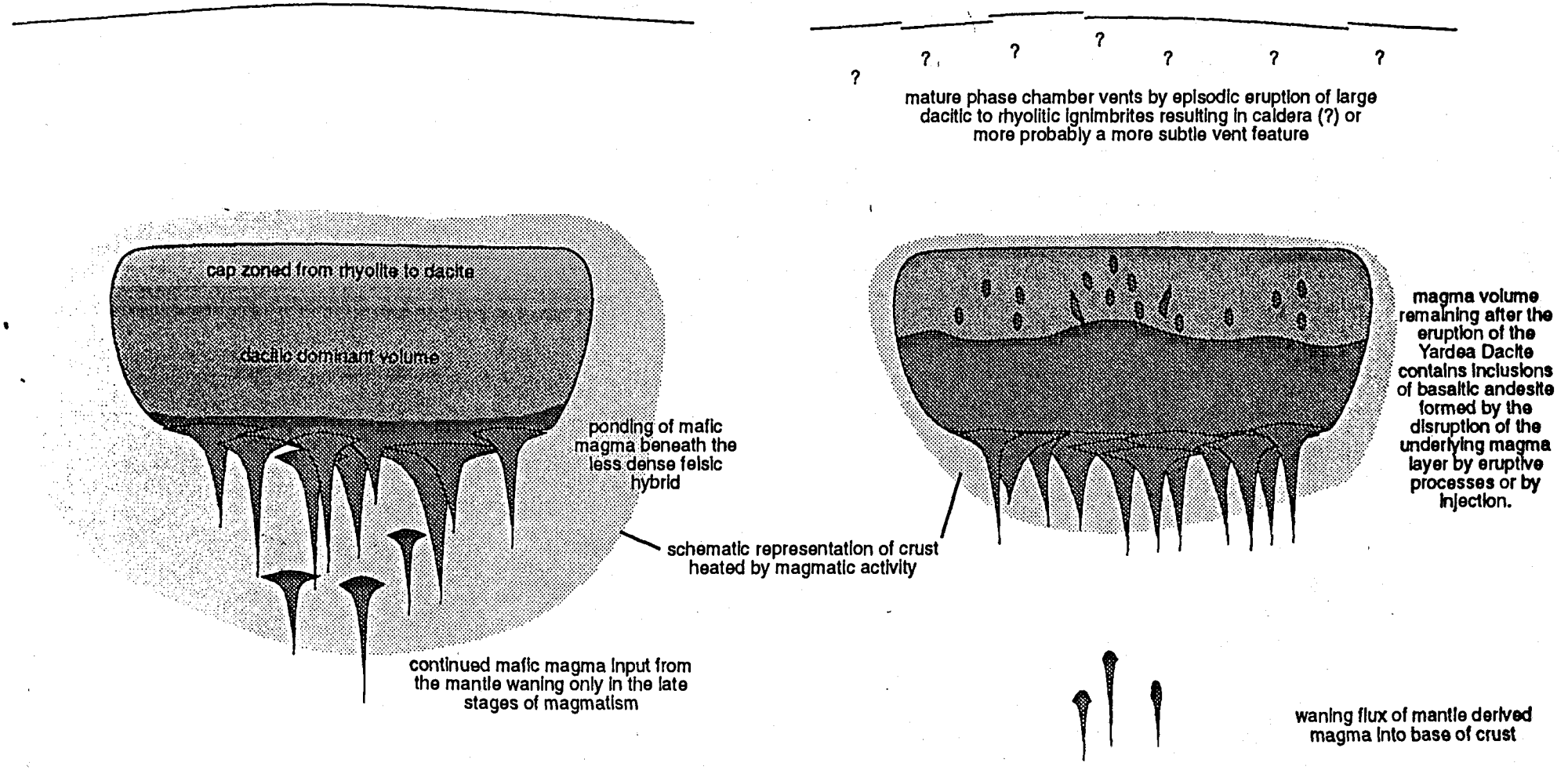

Addendum to references

Anderson (1985): should read Anderson and Lindsley (1985), see main reference list.

Bacon C.R., and Hirschmann, M.M., 1988: Mg/Mn partitioning as a test for equilibrium between co-existing oxides. Am. Mineral., 73:57-61.

Branney, M.J., Kokelaar, B.P., 1992: A reappraisal of ignimbrite emplacement: particulate to non-particulate flow transitions during progressive aggradation of high -grade ignimbrite. Bull Volcanol, 54: 504-520.

Cas, R.A.F., 1978. Silicic lavas in Paleozoic flyschlike deposits in New South Wales, Australia: Behaviour of deep subaqueous silicic flows: Geol. Soc. Am. Bull, 89: 1708-1714.

Creaser, R.A., Price, R.C., and Wormald, R.J., 1991: A-type granites revisited: Assessment of a residual source model. Geology, 19:163-166.

Francis, P.W., Sparks, R.S.J., Hawkesworth, C.J., Thorpe, R.S., Pyle, D.M., Tait, S.R., Mantovani, M.S., and McDermott, F., 1989: Petrology and geochemistry of volcanic rocks of the Cerro Galan caldera, northwest Argentina. Geol. Mag., 126: 515-547.

Henry, C.D., Price, J.G., Parker, D.F., Wolff, J.A., 1989: Mid-Tertiary silicic alkalic magmatism of Trans-Pecos Texas: rheomorphic tuffs and extensive silicic lavas. In: Capin CE, Zidek J (eds) Field excursions to volcanic terrains in the western United States I: Southern Rocky Mountain region. New Mex Bur Mines Min Res Mem 46:231-274.

Hildreth, W., Halliday, A.N., and Christiansen, R.L. Irving, A.J., and Frey, F.A., 1978: The distribution of trace elements between garnet megacrysts and volcanic liquids of kimberlitic to rhyolitic composition. Geochim. Cosmochim. Acta, 42: 771-787.

Kilpatrick, J.A., and Ellis, D.J., 1992: C-type magmas: igneous charnokites and their extrusive equivalents. Trans. Roy. Soc. Edinburgh: 83, 155-164.

Lipman, P.W., Christansen, R.L., and Van Alstine, R.E., 1969: Retention of alkalis by calc-alkalic rhyolites during crystallization and hydration. Am.Mineral., 54: 286-291.

McBirney, A.R., Baker, B.H., and Nilson, R.H., 1985: Liquid fractionation. Part 1: Basic principles and experimental simulations. J. Volc. Geotherm. Res., 24: 1-24.

Smith, R.B., and Braile, L.W., 1984: Crustal structure and evolution of an explosive silicic system at Yellowstone National Park. In:: Explosive volcanism: Inception, Evolution and Hazards. Washington D.C., National Academy Press, pp 96-109.

Smith, R.B., and Christiansen, R.L., 1980: Yellowstone Park as a window on the Earth's interior. Sci. Am., 242:104-117.

Sparks, R.S.J., Wilson, L., and Hulme, G., 1978: Theoretical modelling of the generation, movement and emplacement of pyroclastic flows by column collapse. J. Geophys. Res., 83:1727-1739.

Turner, S.P., Univ.Adelaide PhD Thesis

Vielzeuf, D., Clemens, J.D., Pin, C., and Moinet, E., 1990: Granites, granulites and crustal differentiation. In: Vielzeuf, D., and Vidal, Ph.,(Eds), Granulites and Crustal Evolution. NATO ASI series C311, Kluwer Academic Publishers, Netherlands, pp 59-85.

Zhiqun, Shi., 1993: Interpretation of regional aeromagnetic and gravity data from surveys carried out over the Eyre Peninsula, South Australia. Univ.Adelaide PhD Thesis

References

Allègre, C.J., Dupre, B., Lambret, B., and Richard, P., 1981: The subcontinental versus suboceanic debate, I. Lead-Neodymium-Strontium isotopes in primary alkali basalts from a shield area: the Ahaggar volcanic suite. *Earth Planet. Sci. Lett.*, **52**: 85-92.

Allègre, C.J., Dupre, B., Richard, P., Rousseau, D., and Brooks, C., 1982: Subcontinental versus suboceanic mantle, II. Nd-Sr-Pb isotopic comparison of continental tholeiites with mid-ocean ridge tholeiites, and the structure of the continental lithosphere. *Earth Planet. Sci. Lett.*, **57**: 25-34.

Allen, R.L., 1988: False pyroclastic textures in altered silicic lavas, with implications for volcanic-associated mineralization. *Econ. Geol.*, **83**: 1424-1446.

Anderson, J.L., 1983: Proterozoic anorogenic granite plutonism of North America. *In*: Medaris, L.G., Jr., Byers, C.W., Mickelson, D.M., and Shanks, W.C., (eds.) Proterozoic Geology: Selected papers from an international Proterozoic symposium: *Geol. Soc. Am. Mem.*, **161**: 133-154.

Anderson, D.J., and Lindsley, D.H., 1985: New (and final!) models for Ti-magnetite/ilmenite geothermometer and oxygen barometer. *EOS*, **66**: 416.

Arculus, R.J., 1987: The significance of source versus process in the tectonic controls of magma genesis. *J. Volc. Geotherm. Res.*, **32**: 1-12.

Arndt, N.T., and Goldstein, S.L., 1987: Use and abuse of crust-formation ages. *Geology*, **15**: 893-895.

Arth, J.G., 1976: Behaviour of trace elements during magmatic processes-A summary of theoretical models and their applications. *J. Res. U.S. Geol. Surv.*, **4**: 41-47.

Askren, D.R.R., Whitney, J.A., and Roden, M.A., 1991: Petrology and geochemistry of the Huerto Andesite, San Juan volcanic field, Colorado. *Contrib. Mineral. Petrol.*,**107**: 373-386.

Bacon, C.R., 1986: Magmatic inclusions in silicic and intermediate volcanic rocks. *J. Geophys. Res.*, **91**: 6091-6112.

Bacon, C.R., and Druitt T.H., 1988: Compositional evolution of the zoned calcalkaline magma chamber of Mount Mazama, Crater Lake, Oregon.*Contrib. Mineral. Petrol.*, **98**: 224-256.

Bacon, C.R., and Metz, J., 1984: Magmatic inclusions in rhyolites, contaminated basalts and compositional zonation beneath the Coso volcanic field, California. *Contrib. Mineral. Petrol.*, **85**: 346-365.

Barley, M.E., and Groves, D.I., 1992: Supercontinent cycles and distribution of metal deposits through time. *Geology*, **20**: 291-294.

Barth, A.P., Wooden, J.L., May, D.J., 1992: Small scale heterogeneity of Phanerozoic lower crust: evidence from isotopic and geochemical systematics of mid-Cretaceous granulite

gneisses, San Gabriel Mountains, southern California. *Contrib. Mineral. Petrol.*, **109**: 394-407.

Blissett, A.H., 1975: Rock units in the Gawler Range Volcanics, South Australia. *Q. Geol Notes, Geol. Surv. S. Aus.*, **55**: 2-14.

Blissett, A.H., 1986: Subdivision of the Gawler Range Volcanics in the Gawler Ranges. *Q. Geol. Notes, Geol. Surv. S. Aus.* **99**, 3-11.

Blundy, J.D., and Holland, T.J.B., 1990: Calcic amphibole equilibria and a new amphibole-plagioclase geothermometer. *Contrib. Mineral. Petrol.*, **104**: 208-224.

Bonnichsen, B. and Kauffman, D.F., 1987: Physical features of rhyolite lava flows in the Snake River Plain volcanic province, southwestern Idaho. *Geol. Soc. Am. Spec. Pap.* **212**

Bowden, P., and Kinnaird, J., 1992: A-type granites in Africa (abstract). *Eos Trans. AGU*, **73(14)**, Spring Meeting Suppl.: 348.

Branch, C.D., 1978: Evolution of the middle Proterozoic Chandabooka Caldera, Gawler Range acid volcano-plutonic province, South Australia. *Geol. Soc. Aust. J.*, **25**: 199-216.

Branney, M.J., Kokelaar, B.P., and McConnell, B.J., 1992: The Bad Step Tuff: a lava-like rheomorphic ignimbrite in a calc-alkaline piecemeal caldera, English Lake District. *Bull. Volcanol.*, **54**: 187-199.

Broxton, D.E., Warren, R.G., Byers, F.M., and Scott, R.B., 1989: Chemical and mineralogic trends within the Timber Mountain-Oasis Valley caldera complex, Nevada: Evidence for multiple cycles of chemical evolution in a long lived silicic magma chamber. *J. Geophys. Res.*, **94:** 5961-5986.

Bryan, W.B., Finger, L.W., and Chayes, F., 1969: Estimating proportions in petrographic mixing equations by least squares approximation. *Science*, **163**: 926-927.

Byers, F.M.Jr., Carr, W.J., and Orkild, P.P., 1989: Volcanic centres of southwestern Nevada: Evolution of understanding, 1960-1988. *J. Geophys. Res.*, **94**: 5908-5924.

Carlson, R.W., 1991: Physical and chemical evidence on the cause and source characteristics of flood basalt volcanism. *Aust. J. Earth Sci.*, **38**: 525-544.

Carmichael, I.S. E., 1967: The iron-titanium oxides of salic volcanic rocks and their associated ferromagnesian silicates. *Contrib. Mineral. Petrol.*, **14:** 36-64.

Carmichael, I.S.E., 1992: The redox states of basic and silicic magmas: a reflection of their source regions? *Contrib. Mineral. Petrol.*, **106**: 129-141.

Carmichael, I.S.E., Turner, F.J., and Verhoogen, J., 1974: *Igneous petrology.* McGraw-Hill, 739 pp.

Cas, R.A.F., and Wright, J.V., 1987: Volcanic successions; modern and ancient. Allen & Unwin, London. 528pp.

Chappell, B.W., 1984: Source rocks of I- and S-type granites in the Lachlan Fold Belt, southeastern Australia. *Phil. Trans. R. Soc. Lond.*, **A310**: 693-707.

Chappell, B.W., and White, A.J.R., 1974: Two contrasting granite types. *Pacific Geol.*, **8**: 173-174.

Chappell, B.W., and White, A.J.R., 1984: I- and S-type granites in the Lachlan Fold Belt, southeastern Australia. *In:* Xu Keqin and Tu Guangchi (Eds), *Geology and Granites and their Metallogenic Relations.*, pp. 87-101. Beijing Science Press.

Chappell, B.W., and Stephens, W.E., 1988: Origin of infracrustal (I-type) granite magmas. *Trans. R. Soc. Edin.*, **79**: 71-86.

Chappell, B.W., White, A.J.R., and Wyborn, D., 1987: The importance of residual source material (restite) in granite petrogenesis. *J. Pet.*, **28**: 1111-1138.

Chauvel, C., Arndt, N.T., Kielinczuk, S., and Thom, A., 1987: Formation of Canadian 1.9 Ga old crust: (1) Nd isotopic data. *Can. J. Earth Sci.*, **24**: 396-406.

Chen, Y.D., Price, R.C., White, A.J.R., and Chappell, B.W., 1990: Mafic inclusions from the Glenbog and Blue Gum granite suites, southeastern Australia. *J. Geophys. Res.*, **95**: 17757-17785.

Clemens, J.D., Holloway, J.R., and White, A.J.R., 1986: Origin of an A-type granite: experimental constraints. *Am. Min.*, **71**: 317-324.

Collins, W.J., Beams, S.D., White, A.J.R., and Chappell, B.W., 1982: Nature and origin of A-type granites with particular reference to southeastern Australia. *Contrib. Mineral. Petrol.*, **80**: 189-200.

Colucci, M.T., Dungan, M.A., Ferguson, K.M., Lipman, P.W., and Moorbath, S., 1991: Precaldera lavas of the southeast San Juan volcanic field: Parent magmas and crustal interactions. *J. Geophys. Res.*, **96**: 13413-13434.

Cook, N.D.J., 1988: Diorites and associated rocks in the Anglem Complex at the Neck, northwestern Stewart Island:an example of magma mingling. *Lithos*, **21**:247-262.

Cowley, W.M., and Fanning, C.M., 1991: Low-grade Archaean metavolcanics in the northern Gawler Craton. *Q. Geol. Notes, Geol. Surv. S.Aust.*, **119**: 2-17.

Cowley, W.M., and Martin, A.R., 1991: Kingoonya 1:250,000 Geology Map Sheet SH 53-11.

Cox, K.G., and Hawkesworth, C.J., 1984: Relative contributions of crust and mantle to flood basalt magmatism, Mahabaleshwar area, Deccan Traps. *Phil. Trans. Roy. Soc. Lond.*, **A310**: 627-641.

Cox, K.G., Bell, J.D., and Pankhurst, R.J., 1979: *The interpretation of igneous rocks.* George Allen and Unwin, London, 450 p.

Creaser, R.A., Price, R.C., and Wormald, R.J., 1991: A-type granites revisited: Assesment of a residual source model. *Geology*, **19**: 163-166.

Creaser, R.A., and White, A.J.R., 1991: Yardea Dacite - Large volume, high temperature volcanism from the Middle Proterozoic of South Australia. *Geology*, **19**: 48-51.

Crisp, J.A., 1984: Rates of magma emplacement and volcanic output. *J. Volcanol. Geotherm. Res.*, **20**: 177-211.

Crock, J.G., Lichte, F.E., and Wildeman, T.R., 1984: The group separation of the rare earth elements and Yttrium from geologic materials by cation-exchange chromatography. *Chem. Geol.*, **45**: 149-163.

Daley, E.E., and DePaolo, D.J., 1992: Isotopic evidence for lithospheric thinning during extension: Southern Great Basin. *Geology*, **20**: 104-108.

Daly, S., 1985: Tarcoola 1:250,000 Geology Map SH 53-10.

Daly, S.J., and Fanning, C.M., 1990: Archaean geology of the Gawler Craton. *In*: Glover, J.E., and Ho, S.E., (Compilers), *Third International Archaean Symposium. Extended abstracts*: 91-92.

Davidson, J.P., DeSilva, S.L., Holden, P., and Halliday, A.N., 1990: Small-scale disequilibrium in a magmatic inclusion and its more silicic host. *J. Geophys. Res.*, **95**: 17,661-17,675.

Defant, J.M., and Nielsen, R.L., 1990: Interpretation of open system petrogenetic processes: Phase equilibria constraints on magma evolution. *Geochim. Cosmochim. Acta*, **54**: 87-102.

DePaolo, D.J., 1981: Trace element and isotopic effects of combined wallrock assimilation and fractional crystallization. *Earth Planet. Sci. Lett.*, **53**: 189-202.

DePaolo, D.J., 1988: *Neodymium isotope geochemistry.* Springer-Verlag, Berlin. p. 187.

Donaldson, C.H., 1976: An experimental investigation of olivine morphology: *Contrib. Mineral. Petrol.*, **57**: 187-213.

Druitt, T.H., and Bacon, C.R., 1988: Compositional zonation and cumulus processes in the Mount Mazama magma chamber, Crater Lake, Oregon. *Trans. Roy. Soc. Edin.*, **79** : 289-297.

Druitt, T.H., and Bacon, C.R., 1989: Petrology of the zoned calcalkaline magma chamber of Mount Mazama, Crater Lake, Oregon. *Contrib. Mineral. Petrol.*, **101**: 245-259.

Duncan, A.R., 1987: The Karroo igneous province - a problem area for inferring tectonic setting from basalt geochemistry. *J. Volcanol. Geotherm. Res.*, **32**: 13-34.

Eby, G.N., 1990: The A-type granitoids: A review of the occurrence and chemical characteristics and speculations on their petrogenesis. *Lithos.*, **26**: 115-134.

Eichelberger, J.C., and Westrich, H.R., 1992: Volatile behaviour in silicic magmas during and after eruption (abstract). *Eos Trans. AGU*, **73 (14)**, Spring Meeting Suppl.

Ekren, E.B., Anderson, R.E., Rogers, C.L. and Noble,D.C., 1971: Geology of northern Nellis Air Force Base Bombing and Gunnery Range. *U.S. Geol. Surv. Prof. Pap.* **651**.

Ekren, E.B., McIntyre, D.H., and Bennett, E.H, 1984: High-temperature, large-volume, lavalike ash-flow tuffs without calsderas in southwestern Idaho. *U.S.G.S. Prof. Pap.* **1272.**

Ellam, R., and Cox, K.G., 1989: A Proterozoic lithospheric source for Karoo magmatism: evidence for the Nuanetsi picrites. *Earth Planet. Sci. Lett.*, **92**: 207-218.

Ellam, R.M., and Cox, K.G., 1991: An interpretation of Karoo picrite basalts in terms of interaction between asthenospheric magmas and the mantle lithosphere. *Earth Planet. Sci. Lett.*, **105**: 330-342.

Ellam, R.M., and Hawkesworth, C.J., 1988: Elemental and isotopic variations in subduction related basalts: evidence for a three component model. *Contrib. Mineral. Petrol.*, **98**: 72-80.

Erlank, A.J., Allsopp, D.L., Hawkesworth, C.J., and Menzies, M.A., 1982: Chemical and isotopic characterization of upper mantle metasomatism in peridotite nodules from the Bulfontein kimberlite. *Terrra Cognita*, **2**: 261-263.

Erlank, A.J., Marsh, J.S., Duncan, A.R., Miller, R.McG., Hawkesworth, C.J., Betton, P.J., and Rex, D.C., 1984: Geochemistry and petrogenesis of the Etendeka volcanic rocks from SWA/Namibia. *Spec. Publ. Geol. Soc. S.Afr.*, **13**:195-245.

Erlank, A.J., Waters, F.G., Hawkesworth, C.J., Haggerty, H.L., Allsopp, R.S., Rickard, R.S., and Menzies, M.A., 1987: Evidence for mantle metasomatism in peridotite nodules from the Bultfontein Floors, Kimberley, South Africa. *In*: Mantle metasomatism, Menzies, M.A., and Hawkesworth, C.J., (eds.) pp221-311, Academic Press, London.

Fanning, C.M., 1975: Petrology, structure and geochronology of some high grade metamorphic rocks at Fishery Bay and Cape Carnot, Southern Eyre Peninsula.*Univ. Adelaide Hons. Thesis, (unpubl.).*

Fanning, C.M., Blissett, A.H., Flint, R.B., Ludwig, K.R. and Parker, A.J., 1986: A refined geological history for the Southern Gawler Craton through U-Pb zircon dating of acid volcanics, and correlations with northern Australia. *Geol. Soc. Aust. Abstracts*, **15**, 67-68.

Fanning, C.M., Flint, R.B., Parker, A.J., Ludwig, K.R., and Blissett, A.H., 1988: Refined Proterozoic evolution of the Gawler Craton, South Australia, through U-Pb zircon geochronology. *Precamb. Res.*, **40/41**: 363-386.

Fanning, C.M., Flint, R.B., and Preiss, W.V., 1983: Geochronology of the Pandurra Formation. *Q. Geological Notes, Geol. Surv. S.Aust.*, **88**: 11-16.

Farmer, G.L., Broxton, D.E., Warren, R.G., and Pickthorn, W., 1991: Nd, Sr, and O isotopic variations in metaluminous ash-flow tuffs and related volcanic rocks at the Timber Mountain/Oasis Valley caldera complex, SW Nevada: implications for the origin and evolution of large volume silicic magma bodies. *Contrib. Mineral. Petrol.*, 109: 53-68.

Feeley, T.C., and Grunder, A.L., 1991: Mantle contribution to the evolution of Middle Tertiary silicic magmatism during early stages of extension: the Egan Range volcanic complex, east-central Nevada. *Contrib. Mineral. Petrol.*, **106**: 154-169.

Fitton, J.G., James, D., and Leeman, W.P., 1991: Basic magmatism associated with Late Cenozoic extension in the western United States: compositional variations in space and time. *J. Geophys. Res.*, **96**: 13,693-13,711.

Foden, J.D., 1983: The petrology of the calc-alkaline lavas of Rindjani volcano, East Sunda Arc: a model for island arc petrogenesis. *J.Pet.*, **24**: 98-130.

Foden, J.D., and Green, D.H., 1992:Possible role of amphibole in the origin of andesite: some experimental and natural evidence.*Contrib. Mineral. Petrol.*, **109**: 479-493.

Foden, J.D., Turner, S.P., and Morrison, R.S., 1990: The tectonic implications of Delamerian magmatism in South Australia and western Victoria. *In:* Jago, J.B., and Moore, P.J., (Eds), *The evolution of a Late Precambrian-Early Cambrian Palaeozoic rift complex: The Adelaide Geosyncline. Geol. Soc. Aust. Spec. Publ.* no. 16, pp. 465-482.

Foland, K.A., Raczek. I, Henderson, C.M.B., and Hofmann, A.W., 1988: Petrogenesis of the magmatic complex at Mount Ascutney, Vermont, U.S.A.: *Contrib. Mineral. Pet.*, **98**: 408-416.

Francis, P.W., O'Callaghan, L., Kretzschmar, G.A., Thorpe, R.S., Sparks, R.S.J., Page, R.N., de Barrio, R.E., Gillou, G., and Gonzalez, O.E., 1983: The Cerro Galan ignimbrite. *Nature*, **301**: 51-53.

Frey, F.A., Green, D.H., and Roy, S.D., 1978: Integrated models of basalt petrogenesis: A study of quartz tholeiites to olivine melilites from south-eastern Australia utilising geochemical and experimental petrological data. *J.Petrol.*, **19**: 463-513.

Fujimaki, H., Tatsumoto, M, and Aoki, K., 1984: Partition coefficients of Hf, Zr and REE between phenocrysts and groundmasses. *J.Geophys. Res.*, **89** (supplement), B662-B672.

Gallagher, K. and Hawkesworth, C.J., 1992: Dehydration melting and the generation of continental flood basalts. *Nature*, **358**: 57-59.

Gans, P.B., Mahood, G.A., and Schermer, E., 1989: Synextensional magmatism in the Basin and Range Province. *Geol. Soc. Am. Spec. Pap.*, 233.

Giles, C.W., 1980: A comparative study of Archaean and Proterozoic felsic volcanic associations in southern Australia. *University of Adelaide PhD thesis (unpubl.)*

Giles, C.W., 1988: Petrogenesis of the Proterozoic Gawler Range Volcanics, South Australia. *Precamb. Res.*, **40/41**: 407-427.

Green, J.C., and Fitz, T.J.III, 1993: Extensive felsic lavas and rheoignimbrites in the Keweenawan Midcontinent Rift plateau volcanics, Minnesota: petrographic and field recognition. *J. Volcanol. Geotherm. Res.*, **54**: 177-196.

Griffin, T.J., White, A.J.R., and Chappell, B.W., 1978: The Moruya Batholith and geochemical contrasts between the Moruya and Jindabyne suites. *J. Geol. Soc. Aust.*, **25**: 235-247.

Gromet, L.P., and Silver, L.T., 1983: Rare earth element distributions among minerals in a granodiorite and their petrogenetic implications. *Geochim. Cosmochim. Acta*, **34**: 331-376.

Grove, T.L., and Juster, T.C., 1989: Experimental investigations of low-Ca pyroxene stability and olivine-pyroxene-liquid equilibria at 1-atm in natural basaltic and andesitic liquids. *Contrib. Mineral. Petrol.*, **103**: 287-305.

Grunder, A.L., and Mahood, G.A., 1988: Physical and chemical models of zoned silicic magmas: The Loma Seca Tuff and Calabazos caldera, southern Andes. *J. Pet.*, **29**: 831-867.

Hammarstrom, J.M., and Zen, E-an., 1986: Aluminium in hornblende: an empirical igneous geobarometer. *Am. Miner.*, **71**: 1297-1313.

Hawkesworth, C.J., Kempton, P.D., Rogers, N.W., Ellam, R.M., and van Calsteren, P.W., 1990: Continental mantle lithosphere, and shallow level enrichment processes in the Earth's mantle. *Earth Planet. Sci. Lett.*, **96**: 256-268.

Heiken, G., and Eichelberger, J.C., 1980: Eruptions at Chaos Crags, Lassen Volcanic National Park. *J. Volcanol. Geotherm. Res.*, **7**: 443-481.

Henry, C.D., Price, J.C., Rubin, J.N., and Laubach, S.E., 1990: Case study of an extensive silicic lava: the Bracks Rhyolite, Trans-Pecos Texas. *J. Volcanol. Geotherm. Res.*, **43**: 113-132.

Henry, C.D., Price, J.C., Rubin, J.N., Parker, D.F., Wolff, J.A., Self, S., Franklin, R.R., and Barker, D.S., 1988: Widespread, lava-like rocks of Trans-Pecos Texas. *Geology*, **16**: 509-512.

Henry, C.D., and Wolff, J.A., 1992: Distinguishing strongly rheomorphic tuffs from extensive silicic lavas. Bull. Volcanol., 54: 171-186.

Hergt, J.M., Chappell, B.W., McCulloch, M.T., McDougall, I., and Chivas, A.R., 1989: Geochemical and isotopic constraints on the origin of the Jurassic dolerites of Tasmania. *J. Pet.* **30**: 841-883.

Hergt, J.M., Peate, D.W., and Hawkesworth, C.J., 1991: The petrogenesis of Mesozoic Gondwana low-Ti flood basalts. *Earth Planet. Sci. Lett.*, **105**: 134-138.

Hildreth, W., 1979: The Bishop Tuff. Evidence for the origin of compositional zonation in silicic magma chambers. *In* Chapin, C.E., and Elston, W., (Eds.) *Ash-flow Tuffs.* Spec. Pap. Geol. Soc. Am., **180**: 43-75.

Hildreth, W., 1981: Gradients in silicic magma chambers: implications for lithospheric magmatism. *J. Geophys. Res.*, **86** B11: 10153-10192.

Hildreth, W., Halliday, A.N., and Christiansen, R.L., 1991: Isotopic and chemical evidence concerning the genesis and contamination of basaltic and rhyolitic magma beneath the Yellowstone Plateau volcanic field. *J. Petrol.*, **32**: 63-138.

Hildreth, W.E., and Moorbath, S., 1988: Crustal contributions to arc magmatism in the Andes of Central Chile. *Contrib. Mineral. Petrol.*, **98**, 455-499.

Hogan, J.P., and Gilbert, M.C., 1992: Reversely zoned A-type sheet granites of the Southern Oklahoma Aulacogen, U.S.A. (abstract). *Eos Trans. AGU*, **73 (14)**, Spring Meeting Supp.: 354.

Hollister, L.S., Grissom, G.C., Peters, E.K., Stowell, H.H., and Sisson, V.B., 1987: Confirmation of the empirical correlation of Al in hornblende with pressure of solidification of calc-alkaline plutons. *Am. Mineral.*, **72**: 231-239.

Honjo, N., Bonnichsen, B., Leeman, W.P., and Stormer, J.C., 1992: Mineralogy and geothermometry of high temperature rhyolites from the central and western Snake River Plain. *Bull. of Volcanol.*, **54**: 220-237.

Honjo, N., and Leeman, W.P., 1987: Origin of hybrid ferrolatite lavas from Magic Reservoir eruptive centre, Snake River Plain, Idaho.*Contrib. Mineral. Petrol.*, **96**: 163-177.

Huppert, H.E., and Sparks, R.S.J., 1980: The fluid dynamics of a basaltic chamber replenished by influx of hot, dense ultrabasic magma. *Contrib. Mineral. Petrol.*, **75**: 279-289.

Huppert, H.E., and Sparks, R.S.J., 1988: The generation of granitic magmas by intrusion of basalt into continental crust. *J. Pet.*, **29**: 599-624.

Huppert, H.E., Sparks, R.S.J., and Turner, J.S., 1983: Laboratory investigations of viscous effects in replenished magma chambers. *Earth Planet. Sci. Lett.*, **65**: 377-381.

Huppert, H.E., Sparks, R.S.J., and Turner, J.S., 1984: Some effects of viscosity on the dynamics of replenished magma chambers. *J. Geophys. Res.*, **89**: 6857-6877.

Irvine, T.N., and Baragar, W.R.A., 1971: A guide to the chemical classification of the common volcanic rocks. *Can. J. Earth Sci.*, **8**: 523-548.

Ishii, T., 1975: The relations between temperature and composition of pigeonire in some lavas and their applications to geothermometry. Min. J., 8: 48-57.

Jack, R.L., 1912: The geology of portions of the counties of Le Hunte, Robinson and Dufferin with special reference to underground water supplies. *Bull. Geol. Surv. S. Aust.*, **1**: 37pp.

Jack, R.L., 1917: The geology of the Moonta and Wallaroo Mining district. *Bull. Geol. Surv. S. Aust.*, **6**: 135pp.

Jagodzinski, E., 1985: The geology of the Gawler Range volcanics in the Toondoolya Bluff area, and U-Pb dating of the Yardea Dacite at Lake Acraman. *University of Adelaide Honours thesis (unpubl.)*

Johnson, C.M., 1991: Large-scale crust formation and lithosphere modification beneath Middle to Late Cenozoic calderas and volcanic fields, western North America. *J. Geophy. Res.*, **96**: 13,485-13,507.

Johnson, C.M., 1990: Non-monotonic chemical and O, Sr, Nd and Pb isotope zonations and heterogeneity in the mafic- to silicic-composition magma chamber of the Grizzly Peak Tuff, Colorado. *Contrib. Mineral. Petrol.*, **105**: 677-690.

Johnson, C.M., and Lipman, P. W., 1988: Origin of metaluminous and alkaline volcanic rocks of the Latir volcanic field, northern Rio Grande rift, New Mexico. *Contrib. Mineral. Petrol.* **100**: 107-128.

Johnson, C.M., Lipman, P.W., and Czamanske, G.K., 1990: H,O,Sr, Nd, and Pb isotope geochemistry of the Latir volcanic field and cogenetic intrusions, New Mexico, and relations between evolution of a continental magmatic centre and modifications of the lithosphere. *Contrib. Mineral. Petrol.*, **104**: 99-124.

Johnson, M.C., and Rutherford, M.J., 1989a: Experimental calibration of the aluminium-in-hornblende geobarometer with application to Long Valley caldera (California) volcanic rocks. *Geol.* **17**: 837-841.

Johnson M.C., and Rutherford, M.J., 1989b: Experimentally determined conditions in the Fish Canyon Tuff, Colorado, magma chamber. *J. Pet.*, **30**: 711-737.

Jolly, W.T., Dicken, A.P., and Wu, Tsai-Way, 1992: Geochemical stratigraphy of the Huronian continental volcanics at Thessalon, Ontario: contributions of two-stage crustal fusion. *Contrib. Mineral. Petrol.*, **110**:411-428.

Kempton, P.D., Fitton, J.G., Hawkesworth, C.J., and Ormerod, D.S, 1991: Isotopic and trace element constraints on the composition and evolution of the lithosphere beneath the Southwestern United States. *J. Geophys. Res.*, **96**:13,713-13,735.

Kilinic, I.A., Carmichael, I.S.E., Rivers, M.L., and Seck, R.O., 1983: The ferric-ferrous ratio of natural silicate liquids equilibrated in air. *Contrib. Mineral. Petrol.*, **83**: 136-140.

King, P.L., Chappell, B.W., and White, A.J.R., 1992: A-type granites of the Lachlan Fold Belt, Eastern Australia (abstract). *Eos Trans. AGU,* **73(14),** Spring Meeting Supp.: 346-347.

Knutson, J., Donnelly, T.H., Eadington, P.J., and Tonkin, D.G., 1992: Hydrothermal alteration of mid-Proterozoic basalts, Stuart Shelf, South Australia, a possible source for Cu-mineralization. *Econ. Geol.*, **87**: (in press).

Kuroda, N., Shiraki, K., and Urano, H., 1988: Ferropigeonite quartz dacites from Chichi-jima, Bonin Islands: Latest differentiates from boninite-forming magma. *Contrib. Mineral Petrol.*, **100**: 129-138.

Leake, B.E., 1978: Nomenclature of amphiboles. *Am. Min.*, **63**: 1023-1052.

Leat, P.T., Thompson, R.N., Dickin, A.P., Morrison, M.A., and Hendry, G.L., 1989: Quaternary volcanism in northwestern Colorado: Implications for the roles of asthenosphere and lithosphere in the genesis of continental basalts. *J. Volcanol. Geotherm. Res.*, **37**:291-310.

LeBas, M.J., LeMaitre, R.W., Streckheisen, A., and Zannetin, B., 1986: A chemical classification of volcanic rocks based on the total alkali-silica diagram. *J. Pet.*, **27**: 745-750.

Lindsley, D.H., 1983: Pyroxene thermometry. *Am. Min.*, **68**: 477-493.

Lipman, P.W., 1965: Chemical comparison of glassy and crystalline volcanic rocks. *Spec. Pap. Geol. Soc. Am.*, **81**: 260-261.

Lipman, P.W., 1967: Mineral and chemical variations within an ash-flow sheet from the Aso Caldera, southwestern Japan. *Contrib. Mineral. Petrol.*, **16**: 300-327.

Lipman, P.W., 1984: The roots of ash-flow calderas in western North America: Windows into the tops of granite batholiths. *J. Geophys. Res.*, **89**: 8801-8841.

Lofgren, G.E., 1974: An experimental study of plagioclase morphology: Isothermal crustallization. *Am. J. Sci.*, **274**: 243-273.

Loiselle, M.C., and Wones, D.R., 1979: Characteristics and origin of anorogenic granites. *Geol. Soc. Am. Bull. Abs. Prog.*, **92**: 468.

Luhr, J.F., and Carmichael, I.S.E., 1980: The Colima volcanic complex, Mexico I. Post -caldera andesites from Colima volcano. *Contrib. Mineral., Petrol.*, **71**: 343-372.

Lum, C.C.L., Leeman, W.P., Foland, K.A., Kargel, J.A., and Fitton, J.G., 1989: Isotopic variations in continental basaltic lavas as indicators of mantle heterogeneity: Examples from the Western U.S. Cordillera, *J. Geophys. Res.*, **94**: 7,871-7,884.

Luth, W.C., Jahns, R.H., and Tuttle, O.F., 1964: The granite system at pressures of 4 to 10 kilobars. *J. Geophys. Res.*, **69**: 759-773.

Maaløe, S., and Wyllie, P.J., 1975: Water content of a granite magma deduced from the sequence of crystallization determined experimentally under water-undersaturated conditions. *Contrib. Mineral. Petrol.*, **52**: 175-179.

Macdonald, D.R., 1988: The assessment of Landsat Multispectral Scanner and Thematic Mapper for geological investigation using four examples from South Australia. *University of Adelaide Hons Thesis (unpubl.).*

Mahood, G.A., 1981: Chemical evolution of a Pleistocene rhyolitic centre: Sierra La Primavera, Jalisco, Mexico. *Contrib. Mineral. Petrol.*, **77**:129-149.

Mahood, G.A., and Halliday, A.N., 1988: Generation of high-silica rhyolite: A Nd, Sr, and O isotopic study of Sierra La Primavera, Mexican Neovolcanic belt. *Contrib. Mineral. Petrol.*, **100**: 183-191.

Manning, D.A.C., and Pichavant, M., 1983: The role of fluorine and boron in the generation of granitic melts. *In:* Atherton, M.P., and Gribble, C.D., (Eds), *Migmatites, melting and metamorphism.* Shiva pp. 94-110.

Marsh, B.D., 1981: On the crystallinity, probability of occurrence, and rheology of lava and magma. *Contrib. Mineral. Petrol.*, **78**: 85-98.

Marshall, L.A., and Sparks, R.S.J., 1984: Origin of some mixed-magma and net-veined ring intrusions. *J. Geol. Soc. London*, **141**:171-182.

Martin, D., 1990: Crystal settling and in situ crystallization in aqueous solutions and magma chambers. *Earth Planet. Sci. Lett.* **96**: 336-348

Martin, R.F., and Bonin, B., 1976: Water and magma genesis: the association hypersolvus granite-subsolvus granite. *Can. Min.* **14**: 228-237.

McBirney, A.R., and Murase, T., 1984: Rheological properties of magmas. *Ann. Rev. Earth Planet. Sci.*, **12**: 337-357.

McCulloch, M.T., 1987: Sm-Nd isotopic constraints on the evolution of Precambrian crust in the Australian continent. *In:* Kroner, A., (Ed.), *Proterozoic lithospheric evolution. Am. Geophys. Union.* Geodynamics series, #17 pp. 115-130.

McKenzie, D.P., 1989: Some remarks on the movement of small melt fractions in the mantle. *Earth Planet.Sci. Lett.*, **95**: 53-72.

McMillan N.J., and Dungan, M.A., 1988: Open system magmatic evolution of the Taos Plateau volcanic field, northern New Mexico:3. Petrology and geochemistry of andesite and dacite. *J. Pet.*, **29**: 527-557.

Menzies, M.A., 1983: Mantle ultramafic xenoliths in alkaline magmas: evidence for mantle heterogeneity modified by magmatic activity. *In:* Hawkesworth, C.J., and Norry, M.J., (Eds), *Continental basalts and mantle xenoliths.* Shiva, Nantwich, U.K., pp. 92-110.

Menzies , M.A., and Halliday, A.R., 1988: Lithospheric domains beneath the Archaean and Proterozoic crust of Scotland. *J. Petrol. Spec. Vol.*

Menzies, M.A., Halliday, A.N., Palacz, Z., Hunter, R., Upton, B., Aspen, P., and Hawkesworth, C.J., 1987: Evidence from mantle xenoliths for an enriched lithospheric keel under the Outer Hebrides. *Nature*, **325**, 44-47.

Menzies, M.A., Leeman, W.P., and Hawkesworth, C.J., 1983: Isotope geochemistry of Cenozoic volcanic rocks reveals mantle heterogeneity below western USA. *Nature,* **303**, 205-209.

Metz, J.M., and Mahood, G.A., 1991: Development of the Long Valley, California, magma chamber recorded in precaldera rhyolite lavas of Glass Mountain. *Contrib. Mineral. Petrol.*, **106**: 379-397.

Michael, P.J., 1988: Partition coefficients for the rare earth elements in mafic minerals of high silica rhyolites: The importance of accessory mineral inclusions. *Geochim. Cosmochim. Acta*, **52**: 275-282.

Miller, C.F., and Mittlefehldt, D.W., 1982: Depletion of light rare earth elements in felsic magmas. *Geology*, **10**: 129-133.

Miller, C.F., Watson, E.B. and Harrison, T.M., 1988: Perspectives on the source, segregation and transport of granitoid magmas. *Trans. R. Soc. Edin. Earth Sci.*, **79**: 135-156.

Milner, S.C., Duncan, A.R., and Ewart, A., 1992: Quartz latite rheoignimbrite flows of the Etendeka Formation, north-west Namibia. *Bull. Volcanol.*, **54**: 200-219.

Milner, S.C., and Ewart, A., 1989: The geology of the Goboboseb Mountain volcanics and their relationship to the Messum Complex. *Communs. Geol. Surv. Namibia*, **5**: 31-40.

Morgan, L.A., Doherty, D.J. and Leeman, W.L., 1984: Ignimbrites of the eastern Snake River Plain: evidence for major caldera forming eruptions. *J. Geophys. Res.*, **89**: 8665-8678.

Mortimer, G.E., 1984: Granitoids and basaltic dykes, southern Eyre Peninsula. *University of Adelaide PhD thesis (unpubl.).*

Musselwhite, D.S., DePaolo, D.J., and McCurry, M., 1989: The evolution of a silicic magma system: isotopic and chemical evidence from the Woods Mountains Volcanic Center, eastern California. *Contrib. Mineral. Petrol.*, **101**: 19-29.

Nagasawa, H., 1970: Rare earth concentrations in zircon and apatite, and their host dacites and granites. *Earth Planet. Sci. Lett.*, **9**: 359-364.

Nagasawa, H., and Schnetzler, C.C., 1971: Partitioning of rare earth, alkali, and alkaline earth elements between phenocrysts and acidic igneous magmas. *Geochim. Cosmochim. Acta.*, **35**: 953-967.

Naney, M.T., Phase equilibria of rock forming ferromagnesian silicates in granitic systems. *Am. J. Sci.*, **283**: 993-1033.

Nash, W.P., and Crecraft, H.R., 1985: Partition coefficients for trace elements in silicic magmas. *Geochim. Cosmochim. Acta.*, **49**: 2309-2322.

Nekvasil, H., 1988: Calculation of equilibrium crystallization paths of compositionally simple hydrous felsic melts. *Am. Min.*, **73**: 956-965.

Nekvasil, H., 1991: Feldspar crystallization trends in granitic and syenitic magmas. *In*: B. Chappell (ed.), Second Hutton Symposium on granites and related rocks, Canberra, A.C.T., *BMR Record 1991/25*, p 74.

Nielson, D.L. and Hulen, J.B., 1984: Internal geology and evolution of the Redondo Dome, Valles Caldera, New Mexico. *J. Geophys. Res.*, **89**: 8695-8711.

Nielsen, R.L., Gallahan, W.E., and Newberger, F., 1992: Experimentally determined mineral-melt partition coefficients for Sc, Y and REE for olivine, orthopyroxene, pigeonite, magnetite and ilmenite. *Contrib. Mineral. Petrol.*, **110**: 488-499.

Noble, D.C., 1970: Loss of sodium from crystallized comendite welded tuffs of the Miocene Grouse Canyon Member of the Belted Range Tuff, Nevada. *Bull. Geol. Soc. Am.* **81**: 2677-2687.

Ormerod, D.S., Hawkesworth, C.J., Rogers, N.W., Leeman, W.P., and Menzies, M.A., 1988: Tectonic and magmatic transitions in the western Great Basin, USA. *Nature*, **333**: 349-353.

Ormerod, D.S., Rogers, N.W., and Hawkesworth, C.J., 1991: Melting in the lithospheric mantle: Inverse modelling of alkali-olivine basalts from the Big Pine Volcanic Field, California. *Contrib. Mineral. Petrol.*, **109**: 305-317.

Parker, A.J., and Lemon, N.M., 1982: Reconstruction of Early Proterozoic stratigraphy of the Gawler Craton, South Australia. *J. Geol. Soc. Aust.*, **29**: 221-238.

Parker, A.J., Fanning, C.M. and Flint, R.B., 1985: Geology . *In:* Twidale,C.R., Tyler, M.J. and Davies, M., (Eds.), *Natural history of Eyre Peninsula.* Royal Society of S. Aust.

Peacock, M.A., 1931: Classification of igneous rock series. *J.Geol.*, **39**: 54-67.

Pearce, J.A., 1983: The role of sub-continental lithosphere in magma genesis at active continental margins. *In:* Hawkesworth, C.J., and Norry, M.J., (Eds), *Continental Basalts and Mantle Xenoliths,* Shiva Geology Series, pp. 230-249.

Pearce, J.A., and Norry, M.J., 1979: Petrogenetic implications of Ti, Zr, Y and Nb variations in volcanic rocks. *Contrib. Mineral. Petrol.*, **69**: 33-47.

Peate, D.W., Hawkesworth, C.J., Mantovani, M.S.M., and Shukowsky, W., 1990: Mantle plumes and flood basalt stratigraphy in the Paraná, South America. *Geology*, **18**: 1223-1226.

Perry, F.V., Baldridge, W.S., and DePaolo, D.J., 1988: Chemical and isotopic evidence for lithospheric thinning beneath the Rio Grand rift. *Nature*, **332**: 432-434.

Philpotts, J.A., and Schnetzler, C.C., 1970: Phenocryst-matrix partition coefficients for K, Rb, Sr, and Ba, with applications to anorthosite and basalt genesis. *Geochim. Cosmochim. Acta.*, **34**: 307-322.

Piccoli, P.M., and Candela, P.A., 1992: A model calculation for the estimation of Chlorine and Fluorine in magmatic systems: an example from the Bishop Tuff. *Eos Trans. AGU*, **73 (14)**, Spring Meeting Suppl.: 367.

Pinkerton, H., and Stevenson, R.J., 1992: Methods of determining the rheological properties of magmas at sub-liquidus temperatures. *J. Volcanol. Geotherm. Res.*, **53**: 47-66.

Richard, P., Shimizu, N., and Allegre, C.J., 1976: $^{143}Nd/^{144}Nd$, a natural tracer: an application to oceanic basalts. *Earth Planet. Sci. Lett.*, **31**: 269-278.

Richardson, S.H., Erlank, A.J., and Hart, S.R., 1985: Kimberlite-borne garnet peridotite xenoliths from old enriched subcontinental mantle lithosphere. *Earth Planet. Sci. Lett.*, **75**: 116-128.

Riciputi, L. R., and Johnson, C.M., 1990: Nd- and Pb-isotope variations in the multicyclic central caldera cluster of the San Juan volcanic field, Colorado, and implications for crustal hybridization. *Geology*, **18**: 975-978.

Robertson, B.D., 1989: The geology, petrology and geochemistry of the volcanics in the Kokatha region, Gawler Ranges, South Australia. *University of Adelaide Honours thesis (unpubl.)*

Robinson, P., 1980: The composition space of terrestrial pyroxenes - internal and external limits. *In*: Prewett, C.T. (ed.), *Pyroxenes. Mineral. Soc. Am. Rev. Min.*,**7**: 419-494.

Rudnick, R.L., and Presper, T., 1990: Geochemistry of intermediate/- to high-pressure granulites. *In:* Vielzuef, D., and Vidal, Ph., (Eds), *Granulites and crustal evolution.* NATO ASI series C 311, Kluwer Academic Publishers, Netherlands pp, 523-550.

Rushmer, T., 1991: Partial melting of two amphibolites: contrasting experimental results under fluid absent conditions.*Contrib. Mineral. Petrol.*, **107**: 41-59.

Rutherford, M.J., and Devine, J.D., 1988: The May 18, 1980, eruption of Mount St. Helens III: Stability and chemistry of amphibole in the magma chamber. *J. Geophys. Res.*, **93**: 11,949-11,959.

Rutherford, M.J., Sigurdsson, H., Carey, S., and Davis, A., 1985: The May 18, 1980, eruption of Mount St. Helens. I. Melt composition and phase equilibria. *J. Geophys. Res.*, **90**: 2,929-2,947.

Rutter M.J., and Wyllie, P.J., 1988: Melting of vapour absent tonalite at 10kbar to simulate dehydration melting in the deep crust. *Nature*, **331**: 159-160.

Ryerson, F.J., and Hess, P.C., 1978: Implications of liquid-liquid distribution coefficients to mineral-liquid partitioning. *Geochim. Cosmochim. Acta.*, **42**: 921-932.

Salters, V.J.M., and Shimizu, N., 1988: Worldwide occurrence of HFSE-depleted mantle. *Geochim. et Cosmochim. Acta.*, **52**: 2177-2182.

Sandiford, M., and Powell, R., 1990: Some isostatic and thermal consequences of the vertical strain geometry in convergent orogens. *Earth Planet. Sci. Lett.*, **98**: 154-165.

Schminke, H.U., and Swanson, D.A., 1967: Laminar viscous flowage structures in ash-flow tuffs from Gran Canaria, Canary Islands. *J. Geol.*, **75**: 641-664.

Schnetzler, C.C., and Philpotts, J.A., 1970: Partition coefficients of rare earth elements between igneous matrix material and rock forming mineral phenocrysts II. *Geochim. Cosmochim. Acta.*, **34**: 331-340.

Schuraytz, B.C., Vogel, T.A., and Younker, L.W., 1989: Evidence for dynamic withdrawal from a layered magma body: the Topopah Spring Tuff, Southwestern Nevada. *J. Geophys. Res.*, **94**: 5925-5942.

Scott, R.B., 1971: Alkali exchange during devitrification and hydration of glasses in ignimbrite cooling units. *Geology*, **79**: 100-110.

Sharma, M., Basu, A.R., Cole, R.B., and DeCelles, P.G., 1991: Basalt-rhyolite volcanism by MORB-continental crust interaction:Nd,Sr-isotopic and geochemical evidence from southern San Joaquin Basin, California. *Contrib. Mineral. Petrol.*,**109**:159-172.

Shaw, H.R., 1972: Viscosities of magmatic silicate liquids: an empirical method of prediction. *Am. J. Sci.*, **272**: 870-893.

Shaw, H.R., 1985: Links between magma-tectonic rate balances, plutonism and volcanism. *J. Geophys. Res.*, **90**: 11275-11288.

Shaw, H.R., and Swanson, D.A., 1970: Eruption and flow rates of flood basalts. *Proc. 2nd CFB Symp.*: 271-299.

Sheridan, M., 1979: The emplacement of pyroclastic flows: a review. *In*: Chapin, C.E. and Elston, W.E. (eds.), Ash Flows,*Spec. Pap. Geol. Soc. Am.*, **180**: 125-134.

Sinigoi, S., Antonini, P., Demarchi, G., Longinelli, A., Mazzucchelli, M., Negrini, L., and Rivalenti, G., 1991: Interactions of mantle and crustal magmas in the southern part of the Ivrea Zone (Italy). *Contrib. Mineral. Petrol.*, **108**: 385-395.

Sisson, T.W., 1991: Pyroxene-high silica rhyolite trace element partition coefficients measured by ion microprobe. *Geochim. Cosmochim. Acta*, **55**: 1575-1585.

Skjerlie, K.P., and Johnston, A.D., 1992: Vapour-absent melting at 10 kbar of a biotite- and amphibole-bearing tonalitic gneiss: Implications for the generation of A-type granites. *Geology*, **20**: 263-266.

Smith, R.L., 1979: Ash-flow magmatism. *Spec. Pap. Geol. Soc. Am.*, **180**: 5-26.

Smith, R.B., and Braile, L.W., 1983: Crustal structure and evolution of an explosive silicic volcanic system at Yellowstone National Park. *In*: Boyd, F.R. (ed.), *Explosive Volcanism*: 96-109.

Sparks, R.S.J., 1988: Petrology and geochemistry of the Loch Ba ring-dyke, Mull (N.W. Scotland): an example of the extreme differentiation of tholeiitic magmas. *Contrib. Mineral. Petrol.*, **100**: 446-461.

Sparks, R.S.J., Sigurdsson, H., and Wilson, L., 1977: Magma mixing: a mechanism for triggering acid explosive eruptions. *Nature*, **267**: 315-318.

Sparks, R.S.J., Huppert, H.E., and Turner, J.S., 1984: The fluid dynamics of evolving magma chambers. *Phil. Trans. R. Soc. Lond.*, **A310**, 511-534.

Sparks, R.S.J., Francis, P.W., Hamer, R.W., Pankhurst, R.J., O'Callaghan, L.O., Thorpe, R.S., and Page, R., 1985: Ignimbrites of the Cerro Galan caldera, N.W. Argentina. *J. Volcanol. Geotherm. Res.*, **24**: 205-248.

Sparks, R.S.J., and Marshall, L.A., 1986: Thermal and mechanical constraints on mixing between mafic and silicic magmas. *J. Volcanol. Geotherm. Res.*, **29**: 99-124.

Sparks, R.S.J., and Walker, G.P.L., 1977: The significance of vitric enriched ignimbrites. *J. Volcanol. Geotherm. Res.*, **2**: 329-341.

Stasiuk, M.V., Jaupart, C., and Sparks, R.S.J., 1993: Influence on cooling on lava-flow dynamics. *Geology*, **21**: 335-338.

Steven, T.A., and Lipman, P.W., 1976: Calderas of the San Juan volcanic field, southwestern Colorado. *Prof. Pap. U.S. Geol. Surv.*, **958**.

Steven, T.A., Rowley, P.D. and Cunningham, C.G., 1984: Calderas of the Marysvale Volcanic Field, West Central Utah. *J. Geophys. Res.*, **89**: 8751-8764.

Stimac, J.A., Pearce, T.H., Donnelly-Nolan, J.M., and Hearn, B.C. Jr., 1990: The origin and implications of undercooled andesitic inclusions in rhyolites, Clear Lake Volcanics, California. *J. Geophys. Res.*, **95**: 17,729-17,746.

Sun, S.S., and McDonough, W.F., 1989: Chemical and isotopic systematics of oceanic basalts: implications for mantle composition and processes. *In*: Saunders, A.D., and Norry, M.J., (eds.) *Magmatism in ocean basins, Geol. Soc. Lond. Spec. Pub.*,**42**: 313-345.

Taylor, S.R., and McClennan, S.M., 1985: *The continental crust: its composition and evolution.* Hallam, A. (Ed). Blackwell Scientific Publications, 312pp.

Thompson, R.N., 1983: Thermal aspects of the origin of Hebridean Tertiary acid magmas. II. Experimental melting behaviour of the granites at 1 kbar PH_2O. *Min. Mag.*, **47**: 111-121.

Thompson, R.N., Leat, A.P., Dickin, A.P., Morrison, M.A., Hendry, G.L., and Gibson, S.A., 1990: Strongly potassic mafic magmas from lithospheric mantle sources during continental extension and heating: Evidence from Miocene minettes of northwest Colorado, U.S.A., *Earth Planet. Sci. Lett.*, **98**: 139-153.

Thompson, R.N., Morrison, M.A., Dickin, A.P., and Hendry, G.L., 1983: Continental flood basalts...arachnids role OK? *In:* Hawkesworth, C.J., and Norry, M.J., (Eds), *Continental basalts and mantle xenoliths.* Shiva, Nantwich, pp. 158-185.

Thompson, R.N., Morrison, M.A., Dickin, A.P., Gibson, I.L., and Harmon, R.S., 1986: Two contrasting styles of interaction between basic magmas and continental crust in the British Tertiary Province. *J. Geophys. Res.*, **91**: 5985-5997.

Thompson, R.N., and Morrison, M.A., 1988: Asthenospheric and lower-lithospheric mantle contributions to continental extensional magmatism: an example from the British Tertiary Province. *Chem. Geol.*, **68**: 1-15.

Tollo, R.P., 1992: Tectonic and petrogenic significance of rift-related alkaline granitoids, Blue Ridge Province, Virginia and North Carolina (abstract). *Eos Trans. AGU*, **73 (14)**, Spring Meeting Suppl., 347.

Turner, A.R., 1975: The petrology of the eastern Gawler Ranges volcanic complex. *Geol. Surv. S. Aust. Bull.*, **45**.

Turner, J.S., and Campbell, I.H., 1986: Convection and mixing in magma chambers. *Earth Sci. Rev.* **23**: 255-352.

Turner, J.S., Huppert, H.E., and Sparks, R.S.J., 1983: An experimental investigation of volatile exsolution in evolving magma chambers. *J. Volcanol. Geotherm. Res.*, **16**: 263-277.

Turner, S.P., 1991: Late orogenic, mantle derived bimodal magmatism in the southern Adelaide Foldbelt, South Australia. *Uni. Adelaide PhD. thesis (unpubl.).*

Turner, S.P., Foden, J.D., and Morrison, R.S., 1992a: Derivation of some A-type magmas by fractionation of basaltic magmas: an example from the Padthaway Ridge, South Australia. *Lithos*, **28**: 151-179.

Turner, S.P., Foden, J.D., Sandiford, M., and Bruce, D., 1993: Sm-Nd isotopic evidence for the provenance of sediments from the Adelaide Fold Belt and southeastern Australia with implications for episodic crustal addition. *Geochim. Cosmochim. Acta.*, **57**:1837-1856.

Tuttle, O.F., and Bowen, N.L., 1958: Origin of granite in the light of experimental studies in the system $NaAlSi_3O_8$-$KAlSi_3O_8$-SiO_2-H_2O. *Geol. Soc. Amer. Mem.*, **74**.

van der Molen, I., and Paterson, M.S., 1979: Experimental deformation of partially melted granite.*Contrib. Mineral. Petrol.*, **70**: 229-318.

Varga, R.J., Bailey, R.A., and Suemnicht, G.A., 1990: Evidence for 600 year-old basalt and magma mixing at Inyo Craters volcanic chain, Long Valley Caldera, California. *J. Geophys. Res.*, **95**: 21,441-21,450.

Varga, R.J., and Smith, B.M., 1984: Evolution of the Early Oligocene Bonanza Caldera, Northeast San Juan Volcanic Field, Colorado. *J. Geophys. Res.*, **89**: 8679-8694.

Vernon, R.H., 1990: Crystallization and hybridism in microgranitoid enclave magmas: microstructural evidence. *J. Geophys. Res.*, **95**: 17849-17859.

Vielzeuf, D., and Vidal, Ph., 1990: *Granulites and crustal evolution.* NATO ASI series C 311, Kluwer Academic Publishers, Netherlands.

Vosage, H., Hoffman, A. W., Mazzucchelli, M., Rivalenti, G., Sinigoi, S., Raczek, I., and Demarchi, 1990: Isotopic evidence from the Ivrea Zone for a hybrid lower crust formed by magmatic underplating. *Nature*, **347**: 731-736.

Walker, G.L., 1972: Crystal concentration in ignimbrites. *Contrib. Mineral. Petrol.*, **36**: 135-146.

Walker, G.L., 1973: Lengths of lava flows. *Philos. Trans. Roy. Soc. London*, **A 274:** 107-118.

Walker, G.L., 1983: Ignimbrite types and ignimbrite problems. *J. Volcanol. Geotherm. Res.*, **17**: 65-88.

Walker, G.L., Heming, R.F., and Wilson, C.J.N., 1980: Low-aspect ratio ignimbrites. *Nature*, **283**: 286-287.

Ware, N.G., 1981: Computer programs and calibration with the PIBS technique for quantitative electron probe analysis using a lithium-drifted silicon detector. *Comput. Geosci.*, **7**: 167-184.

Warren, R.G., Byres, F.M., Broxton, D.E., Freeman, S.H., and Hagan, R.C., 1989: Phenocryst abundances and glass and phenocryst compositions as indicators of magmatic environments of large volume ash flow sheets in Southwestern Nevada. *J. Geophys. Res.*, **94**: 5987-6020.

Warshaw, C.M., and Smith, R.L., 1988: Pyroxenes and fayalites in th Bandalier Tuff, New Mexico: temperatures and comparison with other rhyolites. *Am. Min.*, **73**: 1025-1037.

Waters, F.G., and Erlank, A.J., 1988: Assessment of vertical extent and distribution of mantle metasomatism below Kimberly, South Africa. *J. Petrol.* Special Lithosphere Issue, 185-204.

Watson, E.B. and Harrison, T.M., 1983: Zircon saturation revisited : temperature and composition effects in a variety of crustal magma types. *Earth Planet. Sci Lett.*, **64**: 295-304.

Weaver, B.L., Hogan, J.P., Gilbert, M.C., and Lambert, D.D., 1992: Origin of A-type granites from the Southern Oklahoma Aulacogen: The importance of crystal fractionation of mafic magmas (abstract). *Eos Trans. AGU*, **73(14)**, Spring Meeting Supp., 347.

Webb, A.W., Thompson, B.P., Blissett, A.H., Daly, S.J., Flint, R.B., and Parker, A.J., 1986: Geochronology of the Gawler Craton, South Australia. *Aust. J. Earth. Sci.*, **33**: 119-143.

Whalen, J.B., Currie, K.L., and Chappell, B.W., 1987: A-type granites: geochemical characteristics, discrimination and petrogenesis.*Contirb. Mineral. Petrol.*, **95**: 407-419.

White, A.J.R., and Chappell, B.W., 1977: Ultrametamorphism and granitoid genesis. *Tectonophysics*, **43**: 7-22.

White, A.J.R., and Chappell, B.W., 1983: Granitoid types and their distribution in the Lachlan Fold Belt, southeastern Australia. *Geol. Soc. Am. Mem.*, **159**: 21-34.

White, R.S., and McKenzie, D.P., 1989: Magmatism at rift zones: the generation of volcanic continental margins and flood basalts. *J. Geophys. Res.*, **94**: 7685-7730.

Whitney, J.A., 1975: The effects of pressure, temperature and X_{H_2O} on phase assemblage in four synthetic rock compositions. *J. Geol.*, **83**: 1-31.

Whitney, J.A., Dorais, M.J., Stormer, J.C.,Jr., Kline, S.W. and Mattey, D.J., 1988: Magmatic conditions and development of chemical zonation in the Carpenter Ridge Tuff, Central San Juan Volcanic Field, Colorado. *Am. J. of Sci.*, **288-A**, 16-44.

Whitney, J.A., and Stormer, J.C., 1985: Mineralogy, petrology and magmatic conditions from the Fish Canyon Tuff, Central San Juan volcanic field, Colorado. *J. Pet.*, **26**: 726-762.

Wickham, S.M., 1987: The segregation and emplacement of granitic magmas. Geol. Soc. London Journal, 144: 281-297.

Wickham, S.M., Litvinovsky, B.A., Zanvilevich, A.N., and Alberts, A.D., 1992: A-type granitoid magmatism in East-Central Asia (abstract)., *Eos Trans. AGU*, **73 (14)**, Spring Meeting Suppl.: 346.

Wiebe, R.A., 1992: Basaltic replenishments into a floored granitic magma chamber: the Cadillac Mountain Granite, Coastal Maine (abstract). *Eos Trans AGU*, **73 (14)**, Spring Meeting Suppl.: 347.

Wiebe, R.A., 1993: Basaltic injections into floored silicic magma chambers. *Eos Trans. AGU*, **74**: 1-3.

Wolff, J.A., Wörner, G., and Blake, S., 1990: Gradients in physical parameters in zoned felsic magma bodies: implications for evolution and eruptive withdrawal. *J. Volcanol. Geotherm. Res.*, **43**: 37-55.

Wones, D.R., 1972: Stability of biotite: a reply. *Am. Min.*, **57**: 316-317.

Woods, A.W., 1988: The fluid dynamics and thermodynamics of eruption columns. *Bull. Volcanol.*, **50**: 169-193.

Worster, M.G., Huppert, H.E., and Sparks, R.S.J., 1990: Crystallization in convecting magma chambers cooled from above. *Earth Planet. Sci. Lett.*, **101**: 78-89.

Wyborn, 1988: Petrology, geochemistry and origin of a major Australian 1880-1840 Ma felsic volcano-plutonic suite: a model for intracontinental felsic magma generation. *Precambrian Res.*, **40/41**: 37-60.

Wyborn, L.A.I., Warren, R.G., and Drummond, B.J., 1991: Proterozoic granite types in Australia: implications for lower crustal structure and evolution. *Extended abstracts, Second Hutton Symposium on granites and related rocks. (in press).*

Wyborn, L.A.I., Page, R.W., and McCulloch, M.T., 1988: Petrology, geochronology and isotope geochemistry of the post-1820 Ma granites of the Mount Isa Inlier: mechanisms for the generation of proterozoic anorogenic granites. *Precamb. Res.*, **40/41**: 509-541.

Zhiqun, S., 1992: Interpretation of regional aeromagnetic and gravity data from surveys carried out over the Eyre Peninsula, South Australia. *Univ. Adelaide PhD Thesis (in prep.)*

Appendix A: AMG coordinates of sample locations

AMG coordinates for samples collected for this thesis.
All listed samples are prefixed 884- and are stored at the Department of Geology and Geophysics, University of Adelaide. Sample locations of samples prefixed 849-, 908-, or E can be found in Jagodzinski (1985), Robertson (1989) and Giles (1980) respectively.

	Eastings	Northings
Lake Everard area		
GH1	493 350	6 489 250
GH2	492 500	6 489 400
GH4	517 400	6 480 450
GH5	521 150	6 484 900
GH8	483 450	6 492 200
GH10	511 500	6 486 850
GH11	499 800	6 487 150
GH14	507 000	6 493 900
GH15	536 050	6 495 350
GH18	523 650	6 493 300
GH20	505 150	6 496 500
Kokatha		
K3	521 300	6 543 050
K4	520 400	6 543 900
K5	520 750	6 543 500
K7	519 850	6 544 300
K8	519 800	6 544 750
K10	524 700	6 544 300
K11	524 000	6 542 900
K12	524 350	6 541 300
K13	525 150	6 541 800
K14	524 950	6 541 350
K15	524 650	6 541 250
K16	526 300	6 539 800
K17	525 750	6 539 500
K18	525 400	6 540 000
K19	535 300	6 539 450
K20	531 250	6 549 700
K21	531 250	6 549 750
K22	531 400	6 549 400
K23	529 300	6 548 700
K25	524 450	6 542 050
K26	522 000	6 543 750
Tarcoola		
T1-T11	463 250 - 464500	6 621 000- 6 621 900
T15-22	461 050- 461800	6 629 600- 6 630 350
T27	454 400	6 646 450
T28	454 950	6 646 800
T29	451 450	6 644 750
T30	451 000	6 644 300
T31	452 750	6 644 200
T32	435 000	6 639 950
T34	429 850	6 638 950
T35	426 400	6 639 500
Southern Gawler Ranges		
Bi2	628 600	6 386 400
Bi5	628 250	6 381 850
Bi6	543 300	6 385 050
PaO1	542 850	6 382 600

	Eastings	Northings
Mature phase volcanics		
Eu1	516 750	6 435 400
Eu2	500 620	6 433 700
Eu3	536 050	6 393 950
Eu4	657 500	6 643 000
Eu5	543 850	6 385 350
Eu7	543 600	6 385 200
Eu10	528 300	6 424 950
Eu11	501 050	6 453 200
Eu20	517 650	6 424 850
Eu21	517 700	6 424 900
Eu22	518 900	6 425 500
Eu23	522 450	6 424 650
Eu24	524 800	6 424 400
Eu25	526 250	6 423 900
N1	658 900	6 639 700
N2	647 000	6 396 500
Yan2	530 250	6 422 650
Yan4	640 285	6 625 300
P1	538 500	6 394 650
P2	538 600	6 394 500
P3	537 000	6 394 750
P5	538 500	6 395 000
P6	540 750	392 700
YR1	504 850	6 451 850
Y	6076 800	6 401 500
Y1A	607 900	6 401 350
Y1B	608 350	6 401 200
Y2	585 300	6 414 650
Y4	556 950	6 410 740
Y5	556 950	6 410 740
Y10	571 350	6 396 800
Y11	571 300	6 396 650
Y12	571 150	6 396 400
Y13	571 400	6 395 950
Y14	571 150	6 395 500
Y15	571 150	6 395 350
Y16	571 050	6 395 200
Y17	571 000	6 395 150
Y18	571 450	6 394 700
Y19	571 750	6 394 000
Y31	531 450	6 422 700
Y32	531 450	6 422 700
Y35	515 500	6 454 900
Y36	553 000	6 396 600
Y43	579 000	6 422 450
Y45	541 850	6 431 450
Y46	540 350	6 430 800
Y47	539 200	6 429 800
Y48	535 300	6 426 750
Y49	532 150	6 425 300
Y50	530 550	6 425 050
WA3	529 200	6 457 750
WA4	529 150	6 457 600
A2	529 250	457 750

Appendix B: Analytical techniques and uncertainties

Appendix B.

Analytical techniques and uncertainties

Electron microprobe analyses

Polished sections were coated with approximately 250 um of carbon. Multiple analyses of each grain were carried out using a KEVEX 7000 series energy dispersive system (EDS) attached to a JEOL 733 analyser.

Analysis conditions used were 15 KV accelerating voltage and 5 nA electron beam current. Data was corrected on-line using PIBS style software (Ware, 1981). Calibration of the EDS system was carried out using pure copper as a primary standard and olivine and kaersutite as secondary standards.

Fluorine and chlorine analyses were carried out using the JEOL wave length dispersive system (WDS). WDS analysis conditions were 15 KV accelerating voltage and 2 nA electron beam current.

Detection limits are:

Element	Detection limit (wt%)
Na_2O	0.0511
MgO	0.0517
Al_2O_3	0.0590
SiO_2	0.0623
P_2O_5	0.0750
SO_3	0.1037
Cl	0.0406
Fe_2O_3	0.0072
K_2O	0.0565
CaO	0.0737
TiO_2	0.1191
V_2O_3	0.1216
Cr_2O_3	0.1366
MnO	0.1435
NiO	0.2412
F	0.0479 - 0.0870

Whole rock chemical analysis

Samples were trimmed to remove weathered edges and crushed using a jaw crusher. Crushed samples were then ground in a Siebtechnic tungsten carbide mill. Powders for major element analysis were ignited overnight at 960 °C; for each sample 280 mg of ignited sample, 20 mg of sodium nitrate and 1.5 g of flux were mixed and used to produce a fused button.

SiO_2, Al_2O_3, Fe_2O_3, MnO, MgO, CaO, Na_2O, K_2O, TiO_2 and P_2O_5 concentrations were determined using a programable Siemens SRS XRF calibrated on international standards. Na_2O analyses were performed on 50-60 mg of sample digested and made up to 100 ml. Concentrations were determined by atomic absorption on a Varian Techtron atomic absorption spectrophotometer. In-house standards were run with all samples and the following is given as a guide to the precision of the major element analyses:

Element	+/- %
SiO_2	0.6 rel.
TiO_2	1.5 rel. +/- 0.01% abs.
Al_2O_3	1.0 rel.
Fe_2O_3	1.0 rel.
MnO	+/- 0.01% abs.
MgO	1.0 rel +/- 0.10% abs.
CaO	0.5 rel. +/- 0.02% abs.
Na_2O	2.2 rel.
K_2O	1.5 rel. +/-0.01 abs.
P_2O_5	+/- 0.01% abs.

Trace elements abundances (Sr, Rb, Y, Zr, Nb, Ba, Sc, Ni, V, Ga, La, Ce, Nd, U, Pb, Th, Cr) were determined on a Siemens XRF using pressed pellets produced using approximately 5 g of unignited powder. For trace element analyses, the lower limit of detection (LLD) is used as a measure of the precision of the data. It is defined statistically as that concentration which gives a count-rate equal to three times the standard deviation of the nett count-rate for peak minus background. This means that if an element is present in this amount, then there is a 99.7% probability of it being detected. Obviously, with less stringent statistical criteria the LLD values will be reduced. Because the LLD is

dependent on the mass absorption of the individual sample the following LLD's are given for a typical basaltic rock and a typical rhyolitic rock from the thesis work.

Element	LLD (+/- ppm)	
	basalt	rhyolite
Cr	5.6	5.2
Ni	2.9	2.1
Sc	1.1	0.9
V	2.3	1.6
Pb	2.9	2.3
Rb	1.1	0.9
Sr	1.0	0.8
Ba	3.9	2.7
Ga	2.2	1.7
Nb	1.7	1.4
Zr	2.1	1.7
Y	1.2	1.1
Th	2.5	2.0
U	3.1	2.4
La	4.1	2.8
Ce	8.6	6.2
Nd	5.0	3.7

Rare earth element analysis

Selected samples were analysed for the rare earth elements (REE) La, Ce, Nd, Sm, Eu, Gd, Dy, Er and Yb. 500 mg of sample was spiked with a multi element spike and disolved for several days in a teflon bomb using HF and HCl_4O. The REE were seperated following the cation exchange column techniques of Crock *et al.* (1984), firstly on a HNO_3 based column and then on a HCl based column. The samples were run, at The University of Adelaide Department of Geology and Geophysics, on a Thompson thermal ion solid source mass spectrometer. The mass spectrometry methods are described in:

Nesbitt, R.W., and Stanley, J., (Eds), Compilation of analytical geochemistry reports 1973-1979, Research Report #3, 1980. The Department of Geology and Geophysics, University of Adelaide.

In-run ratio variance was less than 0.2% and the following results were obtained for BCR-1:

La	25.29
Ce	54.33
Nd	27.82
Sm	6.25
Eu	1.90
Gd	6.45
Dy	6.07
Er	3.48
Yb	3.25

Rb-Sr and Nd-Sm isotope analysis

The same samples run for rare earths were also analysed for their Nd and Sr isotopic compositions. Approximately 100 mg of unspiked sample was digested for several days in a teflon bomb using HF and then converted to a chloride using 3 N HCl. Sr and Nd were then separated from the sample solution using a two stage cation exchange column proceedure essentially the same as that described by Richard *et al.* (1976). The resulting Sr and Nd samples were loaded onto single tantalum and double rhenium filaments (respectively) and analysed for their isotopic compositions, at the University of Adelaide Department of Geology and Geophysics, on a Finnigan Mat 261 thermal ion, solid source, mass spectrometer. Data blocks of 10 scans each were run untill acceptable in run statistics were achieved (8-16 blocks for Sr using a double collector, and 15-35 blocks for Nd using a single collector). The following results were obtained for duplicate samples and standards where (n) indicates the number of analyses (errors quoted are 2 standard errors of the mean of in-run statistics):

	$^{143}Nd/^{144}Nd$ (measured)	error	$^{87}Sr/^{86}Sr$ (measured)	error
La Jolla	0.511838	± 0.000021 (3)		
E & A			0.708001	± 0.000037 (1)
NBS SRM 987			0.710234	± 0.000025 (10)
BHVO-1	0.512968	± 0.000035 (2)	0.703426	± 0.000027 (2)
BCR-1	0.512507	± 0.000024 (1)	0.704679	± 0.000044 (2)

Average procedural blanks during the course of isotope analysis were as follows:

Rb	0.5 ng
Sr	1.1 ng
Nd	0.09 ng
Sm	0.06 ng

$^{147}Sm/^{143}Nd$ was calculated using the concentrations obtained from the rare earth analyses. $^{87}Rb/^{86}Sr$ was calculated from accurate Rb and Sr analyses obtained from an extended XRF routine.

Constants used in isotope work are:

$^{87}Rb/^{85}Rb = 0.38571$

$^{88}Sr/^{86}Sr = 8.3752$

$\lambda_{Rb} = 1.42 \times 10^{-11} y^{-1}$

Bulk Earth $^{87}Rb/^{86}Sr = 0.0827$

Bulk Earth $^{87}Sr/^{86}Sr = 0.7045$

Bulk Earth $^{147}Sm/^{143}Nd = 0.1967$

Depleted mantle $^{147}Sm/^{143}Nd = 0.2157$

$\lambda_{Sm} = 6.54 \times 10^{-12} y^{-1}$

Bulk earth $^{143}Nd/^{144}Nd = 0.512638$

Depleted mantle $^{143}Nd/^{144}Nd = 0.513108$

Nd isotopic compositions normalized to $^{146}Nd/^{144}Nd = 0.721903$

Average error in $\varepsilon Nd \pm 0.5$, error in Nd model age < 40Ma.

Appendix C: Least Squares modelling for some developmental phase volcanics

Mineral compositions and assimilant compositions used in least squares modelling

Minerals	Plagioclase 1	Plagioclase 2	Augite 1	Augite 2	Pigeonite	Magnetite	Apatite	Olivine	Sanidine
Source	a	a	a	a	a	b	b	c	b
SiO2	53.32	55.21	55.23	53.00	52.63	0.72	0.24	40.00	65.69
TiO2	0.00	0.00	0.20	0.29	0.14	25.68	0.00	0.00	0.00
Al2O3	28.41	26.56	2.28	0.77	1.94	0.85	0.02	0.00	19.04
FeO*	1.23	1.11	7.49	14.19	23.61	64.94	0.27	15.00	0.27
MnO	0.00	0.00	0.25	0.54	0.89	1.99	0.00	0.00	0.00
MgO	0.23	0.20	18.87	13.36	12.42	0.22	0.06	45.00	0.00
CaO	11.41	9.19	12.41	18.05	5.96	0.00	53.97	0.00	0.46
Na2O	5.03	6.15	0.46	0.29	0.33	0.20	0.00	0.00	3.54
K2O	0.11	0.14	0.00	0.00	0.50	0.00	0.00	0.00	11.12
P2O5	0.00	0.00	0.00	0.00	0.00	0.00	41.14	0.00	0.00
	99.74	98.56	97.19	100.49	98.42	94.60	95.70	100.00	100.12

sources of mineral compositions: a) Robertson, 1989 minerals from Kokatha basaltic rocks; b) from this work, Chapter 4, minerals from the Yardea Dacite c) estimated composition

Assimilan	partial melt	466-256
SiO2	77.12	69.57
TiO2	0.16	0.64
Al2O3	12.29	14.86
FeO*	1.87	3.21
MnO	0.06	0.04
MgO	0.21	2.06
CaO	0.53	1.31
Na2O	2.45	2.77
K2O	5.29	5.46
P2O5	0.03	0.09

Solutions to AFC models by least squares mixing

Kokatha cycle 1 volcanism - basalt to rhyodacite

Model - K1a

Parent = 908-123
Assimilant = 466-256

	Actual daughter 908-80	Calculated daughter	Difference
SiO2	70.56	71.06	-0.49
TiO2	0.48	0.55	-0.07
Al2O3	14.69	14.8	-0.12
FeO*	2.89	2.89	0
MnO	0.09	-0.14	0.24
MgO	0.5	0.48	0.02
CaO	1.17	1.09	0.08
Na2O	4.66	4.46	0.2
K2O	4.88	4.62	0.26
P2O5	0.08	0.19	-0.11
		Sum r squared =	0.444

Fractionating phases	%
Olivine	8.05
Plagioclase 1	52.02
Augite 1	16.76
Pigeonite	18.29
Titanomagnetite	4.08
Apatite	0.80

F=0.27
r=0.16

Model K1b

Parent = 908-123
Assimilant = partial melt

	Actual daughter 908-80	Calculated daughter	Difference
SiO2	70.56	71.23	-0.66
TiO2	0.48	0.58	-0.11
Al2O3	14.69	14.81	-0.12
FeO*	2.89	2.89	0.01
MnO	0.09	-0.15	0.24
MgO	0.5	0.47	0.03
CaO	1.17	1.04	0.13
Na2O	4.66	4.56	0.11
K2O	4.88	4.32	0.56
P2O5	0.08	0.26	-0.18
		Sum r squared =	0.896

Fractionating phases	%
Olivine	6.80
Plagioclase 1	50.82
Augite 1	18.60
Pigeonite	19.23
Titanomagnetite	3.83
Apatite	0.72

F=0.29
r=0.11

Kokatha cycle 2 volcanism - basalt to andesite

Model K2a
Parent = 908-123
Assimilant = 466-256

	Actual daughter 908-18	Calculated daughter	Difference
SiO2	60.99	61.3	-0.31
TiO2	1.04	1.14	-0.10
Al2O3	14.25	14.34	-0.08
FeO*	8.24	8.24	0.00
MnO	0.16	0.17	-0.01
MgO	3.01	3.01	0.01
CaO	5.55	5.47	0.08
Na2O	3.68	3.46	0.22
K2O	2.85	2.52	0.33
P2O5	0.22	0.36	-0.13
		Sum r squared =	0.293

Fractionating phases	%
Olivine	21.8
Plagioclase 1	59.84
Augite 1	16.11
Titanomagnetite	1.89
Apatite	0.36

F=0.64
r=0.35

Model K2b
Parent = 908-123
Assimilant = partial melt

	Actual daughter 908-18	Calculated daughter	Difference
SiO2	60.99	61.42	-0.44
TiO2	1.04	1.08	-0.40
Al2O3	14.25	14.35	-0.10
FeO*	8.24	8.28	-0.04
MnO	0.16	0.17	-0.01
MgO	3.01	3.00	0.01
CaO	5.55	5.46	0.09
Na2O	3.68	3.51	0.17
K2O	2.85	2.34	0.52
P2O5	0.22	0.39	-0.17
		Sum r squared =	0.702

Fractionating phases	%
Olivine	19.05
Plagioclase 1	56.93
Augite 1	21.88
Titanomagnetite	1.92
Apatite	0.22

F=0.65
r=0.26

Model K2c
Parent = 908-123
Assimilant = partial melt

	Actual daughter 908-18	Calculated daughter	Difference
SiO2	60.99	61.36	-0.37
TiO2	1.04	1.14	-0.10
Al2O3	14.25	14.32	-0.07
FeO*	8.24	8.25	-0.01
MnO	0.16	0.16	0.01
MgO	3.01	3.00	0.01
CaO	5.55	5.45	0.10
Na2O	3.68	3.60	0.08
K2O	2.85	2.33	0.52
P2O5	0.22	0.39	-0.17
		Sum r squared =	0.468

Fractionating phases	%
Olivine	17.00
Plagioclase 1	56.68
Augite 1	18.87
Pigeonite	5.05
Titanomagnetite	2.04
Apatite	0.36

F=0.61
r=0.16

Kokatha cycle 2 volcanism - andesite to dacite

Model K2d
Parent = 908-18
Assimilant = 466-256

	Actual daughter 908-64	Calculated daughter	Difference
SiO2	65.48	65.57	-0.10
TiO2	1.00	0.99	0.10
Al2O3	14.20	14.22	-0.02
FeO*	6.38	6.39	-0.02
MnO	0.16	0.04	0.12
MgO	1.62	1.62	0.01
CaO	3.04	3.05	-0.01
Na2O	4.14	4.13	0.01
K2O	3.70	3.71	-0.01
P2O5	0.28	0.27	0.00
		Sum r squared =	0.036

Fractionating phases	%
Plagioclase 1	40.53
Augite 2	22.34
Pigeonite	21.50
Titanomagnetite	3.63
Apatite	0.22
Sanidine	11.78

F=0.66
r=0.15

Model K2e
Parent = 908-18
Assimilant = 466-256

	Actual daughter 908-64	Calculated daughter	Difference
SiO2	65.48	65.81	-0.33
TiO2	1.00	0.91	0.09
Al2O3	14.20	14.29	-0.09
FeO*	6.38	6.45	-0.08
MnO	0.16	0.03	0.14
MgO	1.62	1.52	0.11
CaO	3.04	3.1	-0.06
Na2O	4.14	3.97	0.17
K2O	3.70	3.71	-0.01
P2O5	0.28	0.22	0.05
		Sum r squared =	0.198

Fractionating phases	%
Plagioclase 2	41.97
Augite 2	22.69
Pigeonite	18.31
Titanomagnetite	4.27
Apatite	0.50
Sanidine	12.26

F=0.62
r=0.02

Model K2f
Parent = 908-18
Assimilant = partial melt

	Actual daughter 908-64	Calculated daughter	Difference
SiO2	65.48	65.62	-0.14
TiO2	1.00	0.94	0.06
Al2O3	14.20	14.22	-0.02
FeO*	6.38	6.42	-0.04
MnO	0.16	0.05	0.11
MgO	1.62	1.57	0.05
CaO	3.04	3.07	-0.03
Na2O	4.14	4.14	0.00
K2O	3.70	3.72	-0.02
P2O5	0.28	0.25	0.03
		Sum r squared =	0.042

Fractionating phases	%
Plagioclase 1	41.68
Augite 2	24.27
Pigeonite	21.00
Titanomagnetite	4.02
Apatite	0.35
Sanidine	8.68

F=0.68
r=0.09

Model K2g
Parent = 908-18
Assimilant = partial melt

	Actual daughter 908-64	Calculated daughter	Difference
SiO2	65.48	65.55	-0.07
TiO2	1.00	0.89	0.11
Al2O3	14.20	14.35	-0.15
FeO*	6.38	6.43	-0.06
MnO	0.16	0.07	0.10
MgO	1.62	1.62	0.00
CaO	3.04	3.11	-0.07
Na2O	4.14	3.77	0.37
K2O	3.70	4.02	-0.32
P2O5	0.28	0.20	0.08
		Sum r squared =	0.304

Fractionating phases	%
Plagioclase 2	48.04
Augite 2	29.80
Pigeonite	17.30
Titanomagnetite	4.28
Apatite	0.58

F=0.72
r=0.22

Lake Everard volcanism

Model G1a
Parent = 844-GH2
Assimilant = partial melt

	Actual daughter 884-GH8	Calculated daughter	Difference
SiO2	62.21	62.44	-0.23
TiO2	1.33	1.35	-0.02
Al2O3	14.43	14.41	0.02
FeO*	7.07	7.09	-0.02
MnO	0.21	0.05	0.16
MgO	2.93	2.93	0.00
CaO	3.01	2.99	0.01
Na2O	3.16	3.55	-0.39
K2O	4.94	4.82	0.11
P2O5	0.72	0.37	0.35
		Sum r squared =	0.367

Fractionating phases	%
Olivine 2	2.05
Plagioclase 1	62.45
Augite 1	11.81
Pigeonite	21.69
Titanomagnetite	2.00

F=0.37
r=0.42

Model G1b
Parent = 844-GH2
Assimilant = partial melt

	Actual daughter 884-GH8	Calculated daughter	Difference
SiO2	62.21	62.59	-0.38
TiO2	1.33	1.40	-0.07
Al2O3	14.43	14.52	-0.09
FeO*	7.07	7.09	-0.02
MnO	0.21	0.06	0.15
MgO	2.93	3.04	-0.12
CaO	3.01	2.83	0.18
Na2O	3.16	3.47	-0.31
K2O	4.94	4.67	0.27
P2O5	0.72	0.33	0.39
		Sum r squared =	0.548

Fractionating phases	%
Plagioclase 1	61.66
Augite 1	14.26
Pigeonite	22.91
Titanomagnetite	1.17

F=0.40
r=0.54

Model G1c
Parent = 844-GH2
Assimilant = 466-256

	Actual daughter 884-GH8	Calculated daughter	Difference
SiO2	62.21	62.47	-0.26
TiO2	1.33	1.33	0.00
Al2O3	14.43	14.47	-0.05
FeO*	7.07	7.10	-0.04
MnO	0.21	0.09	0.12
MgO	2.93	2.94	-0.01
CaO	3.01	3.03	-0.02
Na2O	3.16	3.27	-0.11
K2O	4.94	4.99	-0.05
P2O5	0.72	0.30	0.42
		Sum r squared =	0.278

Fractionating phases	%
Olivine 2	6.61
Plagioclase 1	67.70
Augite 1	8.00
Pigeonite	15.91
Titanomagnetite	1.78

F=0.39
r=0.84

Model G2a
Parent = 844-GH2
Assimilant = partial melt

	Actual daughter 884-GH11	Calculated daughter	Difference
SiO2	60.41	60.29	0.12
TiO2	1.02	0.85	0.16
Al2O3	17.4	17.24	0.16
FeO*	5.7	5.77	-0.07
MnO	0.18	-0.08	0.27
MgO	3.17	2.89	0.28
CaO	2.44	2.95	-0.51
Na2O	4.58	4.37	0.21
K2O	4.55	5.21	-0.66
P2O5	0.53	0.51	0.03
		Sum r squared =	0.963

Fractionating phases	%
Plagioclase 1	55.67
Augite 1	17.32
Pigeonite	22.80
Titanomagnetite	4.21

F=0.35
r=0.20

Model G2b
Parent = 844-GH2
Assimilant = 466-256

	Actual daughter 884-GH11	Calculated daughter	Difference
SiO2	60.41	60.44	-0.03
TiO2	1.02	0.88	0.14
Al2O3	17.4	17.41	-0.01
FeO*	5.7	5.77	-0.07
MnO	0.18	-0.04	0.23
MgO	3.17	3.02	0.15
CaO	2.44	2.82	-0.38
Na2O	4.58	4.09	0.49
K2O	4.55	5.19	-0.64
P2O5	0.53	0.42	0.12
		Sum r squared =	0.909

Fractionating phases	%
Plagioclase 1	55.21
Augite 1	19.20
Pigeonite	21.24
Magnetite	4.35

F=0.33
r=0.39

Model G3a
Parent = 844-GH2
Assimilant = partial melt

	Actual daughter 884-GH5	Calculated daughter	Difference
SiO2	60.08	60.24	-0.16
TiO2	1.23	1.21	0.02
Al2O3	15.39	15.48	-0.09
FeO*	7.45	7.48	-0.03
MnO	0.18	0.08	0.11
MgO	3.40	3.41	-0.01
CaO	4.01	4.06	-0.04
Na2O	3.84	3.62	0.22
K2O	3.94	4.09	-0.15
P2O5	0.48	0.33	-0.15
		Sum r squared =	0.142

Fractionating phases	%
Olivine 2	1.17
Plagioclase 1	60.55
Augite 1	15.25
Pigeonite	20.69
Titanomagnetite	2.34

F=0.48
r=0.45

Model G3b
Parent = 844-GH2
Assimilant = partial melt

	Actual daughter 884-GH5	Calculated daughter	Difference
SiO2	60.08	60.30	-0.22
TiO2	1.23	1.23	0.00
Al2O3	15.39	15.53	-0.14
FeO*	7.45	7.48	-0.03
MnO	0.18	0.08	0.10
MgO	3.40	3.46	-0.06
CaO	4.01	3.99	0.02
Na2O	3.84	3.59	0.25
K2O	3.94	4.03	-0.09
P2O5	0.48	0.31	0.17
		Sum r squared =	0.182

Fractionating phases	%	0.1824
Plagioclase 1	59.93	
Augite 1	16.89	
Pigeonite	21.23	
Titanomagnetite	1.95	

F=0.50
r=0.52

Model G4a

Model G4b

Parent = 844-GH5
Assimilant = partial melt

	Actual daughter 884-GH10	Calculated daughter	Difference
SiO2	66.01	66.11	-0.10
TiO2	0.93	1.02	-0.09
Al2O3	14.75	14.83	-0.08
FeO*	4.67	4.64	0.02
MnO	0.17	0.07	0.10
MgO	2.24	2.32	-0.08
CaO	1.96	1.94	0.03
Na2O	3.99	3.78	0.21
K2O	4.97	4.94	0.03
P2O5	0.32	0.36	-0.04
		Sum r squared =	0.089

Fractionating phases	%
Plagioclase 2	41.60
Augite 2	3.82
Pigeonite	30.73
Titanomagnetite	4.40
Apatite	1.31
Sanidine	18.14

F=0.65
r=0.43

Parent = 844-GH5
Assimilant = 416-143

	Actual daughter 884-GH10	Calculated daughter	Difference
SiO2	66.01	66.10	-0.09
TiO2	0.93	1.04	-0.11
Al2O3	14.75	14.84	-0.10
FeO*	4.67	4.63	0.03
MnO	0.17	0.04	0.14
MgO	2.24	2.35	-0.11
CaO	1.96	1.93	0.04
Na2O	3.99	3.75	0.24
K2O	4.97	4.94	0.03
P2O5	0.32	0.37	-0.05
		Sum r squared =	0.125

Fractionating phases	%
Plagioclase 2	41.29
Augite 2	3.38
Pigeonite	26.39
Titanomagnetite	4.65
Apatite	1.18
Sanidine	22.56

F=0.49
r=0.58

Mineral partition coefficients

	Olivine	Plag	Cpx	Opx	Tmag	Ap	Sanidine
Nd	0.0034	0.14	0.7	0.2	0.45	31.1	0.04

Bulk partition coefficients calculated from results of Least Squares Modelling

	Kokatha cycle 1 volcanism - basalt to rhyodacite				Kokatha cycle 2 volcanism - basalt to andesite				
	Model - K1a	Model K1b	Model K2a	Model K2b	Model K2c	Model K2d	Model K2e	Model K2f	Model K2g
Nd	0.49	0.48	0.32	0.31	0.34	0.35	0.43	0.40	0.51

	Model G1a	Model G1b	Model G1c	Model G2a	Model G2b	Model G3a	Model G4a	Model G4b
Nd	0.22	0.24	0.19	0.26	0.27	0.24	0.58	0.53

Appendix D: Plagioclase analyses from the mature phase volcanics

Plagioclase analyses and structural formulae - Eucarro and Yardea Dacites

Sample	Eu7 core	Eu7 core	Eu7 core	Eu7 core	Eu7 core	Eu7 core	Eu7 mid-grain	Eu7 mid-grain	Eu7 mid-grain	Eu7 mid-grain	Eu7 mid-grain	Eu7 mid-grain	Eu7 mid-grain	Eu7 mid-grain	Eu7 mid-grain	Eu7 mid-grain	Eu7 mid-grain	Eu7 rim	Eu7 rim	Eu7 rim	Eu7 rim	Eu7 rim
SiO2	61.31	61.78	61.44	61.86	62.21	61.24	62.68	61.20	62.02	62.34	62.59	61.34	61.84	62.36	62.61	62.25	61.82	62.94	62.49	62.87	62.05	62.22
Al2O3	24.08	23.76	23.96	23.82	23.22	23.33	23.30	23.78	23.51	23.38	23.13	24.30	23.40	23.30	22.98	23.63	22.82	23.33	23.66	23.22	23.57	23.49
FeO	0.22	0.31	0.29	0.26	0.21	0.39	0.18	0.36	0.27	0.29	0.23	0.23	0.20	0.25	0.15	0.19	0.41	0.15	0.19	0.26	0.34	0.33
MgO	0.20	0.11		0.15						0.13				0.08						0.10	0.14	0.12
CaO	6.12	5.05	5.77	5.57	5.40	6.07	4.96	5.71	5.31	4.92	4.81	6.01	5.37	5.01	5.03	5.20	5.23	4.91	5.14	4.75	5.14	5.32
Na2O	7.04	7.64	7.33	7.06	7.08	6.89	7.36	7.23	7.37	7.64	7.77	7.02	7.50	7.31	7.61	7.97	7.30	7.95	8.08	8.18	7.54	7.83
K2O	1.33	1.54	1.46	1.04	2.15	1.71	1.80	1.79	1.79	1.53	1.62	1.37	1.68	1.93	1.72	0.98	1.79	0.88	0.58	0.79	1.48	0.93
Total	100.30	100.19	100.25	99.76	100.27	99.63	100.28	100.07	100.27	100.23	100.15	100.27	99.99	100.24	100.10	100.22	99.37	100.16	100.14	100.17	100.26	100.24
Si	10.905	10.996	10.941	11.013	11.080	10.989	11.124	10.940	11.038	11.076	11.128	10.908	11.036	11.091	11.141	11.045	11.104	11.141	11.067	11.135	11.029	11.042
Al	5.048	4.985	5.029	4.998	4.875	4.934	4.874	5.010	4.932	4.896	4.847	5.093	4.922	4.884	4.820	4.942	4.831	4.867	4.939	4.847	4.938	4.914
Fe	0.033	0.046	0.043	0.039	0.031	0.059	0.027	0.054	0.040	0.043	0.034	0.034	0.030	0.037	0.022	0.028	0.062	0.022	0.028	0.039	0.051	0.049
Mg	0.053	0.029	0.000	0.040	0.000	0.000	0.000	0.000	0.000	0.034	0.000	0.000	0.000	0.021	0.000	0.000	0.000	0.000	0.000	0.026	0.037	0.032
Ca	1.166	0.963	1.101	1.062	1.031	1.167	0.943	1.094	1.013	0.937	0.916	1.145	1.027	0.955	0.959	0.989	1.007	0.931	0.975	0.901	0.979	1.012
Na	2.428	2.637	2.531	2.437	2.445	2.397	2.533	2.506	2.543	2.632	2.679	2.420	2.595	2.521	2.626	2.742	2.543	2.729	2.775	2.809	2.599	2.694
K	0.302	0.350	0.332	0.236	0.488	0.391	0.407	0.408	0.406	0.347	0.367	0.311	0.382	0.438	0.390	0.222	0.410	0.199	0.131	0.178	0.336	0.211
Total	19.936	20.005	19.976	19.825	19.950	19.938	19.909	20.012	19.971	19.965	19.972	19.911	19.992	19.947	19.958	19.967	19.956	19.889	19.916	19.936	19.969	19.953
An	29.9	24.4	27.8	28.4	26.0	29.5	24.3	27.3	25.6	23.9	23.1	29.5	25.6	24.4	24.1	25.0	25.4	24.1	25.1	23.2	25.0	25.8
Ab	62.3	66.8	63.9	65.2	61.7	60.6	65.2	62.5	64.2	67.2	67.6	62.4	64.8	64.4	66.1	69.4	64.2	70.7	71.5	72.2	66.4	68.8
Or	7.7	8.9	8.4	6.3	12.3	9.9	10.5	10.2	10.3	8.9	9.3	8.0	9.5	11.2	9.8	5.6	10.4	5.1	3.4	4.6	8.6	5.4

Sample	Eu7 rim	Eu7 rim	849-36 core	849-36 core	849-36 core	849-36 mid-grain	849-36 mid-grain	849-36 mid-grain	849-36 mid-grain	849-36 rim	849-36 rim	849-36 rim	Eu21 core	Eu20 core	Eu21 rim	Eu20 rim	Eu20 rim	Y31 core	Y31 core	Y31 core	Y31 core	Y31 rim
SiO2	62.65	62.61	62.10	61.65	61.92	61.75	62.47	61.91	61.84	62.83	62.73	61.94	60.56	61.67	62.02	61.56	61.69	60.69	61.29	60.78	60.89	61.21
Al2O3	23.18	22.59	23.15	23.23	23.60	23.07	23.08	22.71	23.04	22.75	22.81	23.04	24.20	23.50	23.54	23.79	23.46	24.57	23.99	24.38	25.09	24.26
FeO	0.25	0.28	0.39	0.28	0.25	0.23	0.37	0.31	0.18	0.22	0.27	0.19	0.01	0.22	0.14	0.40	0.16	0.20	0.30	0.30	0.30	0.35
MgO	0.15												0.03						0.09	0.11		
CaO	4.68	5.00	5.83	5.94	6.11	5.53	5.25	5.46	5.77	4.90	5.33	5.34	6.34	5.48	5.14	5.34	5.56	6.53	5.99	6.57	6.85	6.27
Na2O	8.29	8.35	6.74	7.09	7.07	7.02	7.75	6.90	7.09	7.66	7.45	7.58	7.39	6.99	7.32	7.24	7.36	6.90	7.11	6.98	6.90	7.25
K2O	0.79	0.87	1.87	1.76	1.70	1.82	1.30	2.28	1.83	1.47	1.63	1.27	1.38	2.00	1.67	1.67	1.63	1.29	1.32	1.11	0.93	0.90
Total	99.99	99.70	100.08	99.95	100.65	99.42	100.22	99.57	99.75	99.83	100.22	99.36	99.91	99.86	99.83	100.00	99.86	100.18	100.09	100.23	100.96	100.24
Si	11.121	11.168	11.075	11.023	10.992	11.078	11.104	11.116	11.068	11.190	11.153	11.094	10.839	11.025	11.060	10.985	11.021	10.820	10.924	10.830	10.764	10.886
Al	4.850	4.749	4.866	4.896	4.938	4.878	4.836	4.806	4.861	4.776	4.780	4.864	5.105	4.952	4.948	5.004	4.940	5.163	5.040	5.120	5.228	5.086
Fe	0.037	0.042	0.058	0.042	0.037	0.035	0.055	0.047	0.027	0.033	0.040	0.028	0.001	0.033	0.021	0.060	0.024	0.030	0.045	0.045	0.044	0.052
Mg	0.040	0.000	0.000	0.000	0.000	0.000	0.000	0.000	0.000	0.000	0.000	0.000	0.008	0.000	0.000	0.000	0.000	0.000	0.024	0.029	0.000	0.000
Ca	0.890	0.956	1.114	1.138	1.162	1.063	1.000	1.050	1.107	0.935	1.015	1.025	1.216	1.050	0.982	1.021	1.064	1.247	1.144	1.254	1.298	1.195
Na	2.853	2.888	2.331	2.458	2.434	2.442	2.671	2.402	2.461	2.645	2.568	2.633	2.565	2.423	2.531	2.505	2.549	2.385	2.457	2.412	2.365	2.500
K	0.179	0.198	0.425	0.401	0.385	0.416	0.295	0.522	0.418	0.334	0.370	0.290	0.315	0.456	0.380	0.380	0.371	0.293	0.300	0.252	0.210	0.204
Total	19.970	20.000	19.870	19.959	19.948	19.912	19.961	19.943	19.941	19.912	19.926	19.935	20.049	19.939	19.922	19.955	19.970	19.938	19.934	19.942	19.909	19.923

An	22.7	23.6	28.8	28.5	29.2	27.1	25.2	26.4	27.8	23.9	25.7	26.0	29.7	26.7	25.2	26.1	26.7	31.8	29.3	32.0	33.5	30.6
Ab	72.7	71.5	60.2	61.5	61.1	62.3	67.4	60.4	61.7	67.6	65.0	66.7	62.6	61.7	65.0	64.1	64.0	60.8	63.0	61.5	61.1	64.1
Or	4.6	4.9	11.0	10.0	9.7	10.6	7.4	13.1	10.5	8.5	9.4	7.4	7.7	11.6	9.8	9.7	9.3	7.5	7.7	6.4	5.4	5.2

Plagioclase analyses and structural formulae - Eucarro and Yardea Dacites

Sample	Y31 rim	Y31 rim	Y31 rim	A2 core	A2 core	A2 core	A2 core	A2 core (resorbed)	A2 core (resorbed)	A2 core	A2 core	A2 core	A2 mid-grain	A2 mid-grain	A2 mid-grain	A2 mid-grain	A2 mid-grain	A2 rim	A2 rim	A2 rim	A2 rim	A2 rim
SiO2	61.05	61.33	61.33	60.54	59.92	60.58	61.29	60.57	60.39	59.82	60.40	59.64	61.18	60.12	60.18	60.53	59.87	61.46	60.63	61.46	61.07	61.00
Al2O3	24.29	24.09	24.18	23.59	23.98	24.00	23.60	24.39	24.94	24.97	24.96	24.74	23.68	23.98	23.70	24.93	25.12	23.60	24.04	23.68	23.80	24.63
FeO	0.34	0.32	0.39	0.22	0.32	0.19	0.35	0.29	0.21	0.23	0.44	0.26	0.29	0.26	0.25	0.21	0.24	0.36	0.37	0.25	0.30	0.14
MgO			0.13						0.19	0.18	0.10	0.09				0.11						
CaO	6.34	6.22	6.14	6.36	6.84	6.69	6.39	6.90	6.99	6.84	6.79	6.86	6.45	6.90	6.75	6.79	7.05	6.19	6.85	6.14	6.67	6.33
Na2O	7.26	7.25	7.58	6.83	6.60	7.03	7.09	7.05	6.73	6.99	6.77	6.62	6.94	6.62	6.80	6.87	6.71	7.37	7.07	7.26	7.16	7.09
K2O	1.00	1.05	0.80	1.46	1.17	1.25	1.45	0.94	1.27	1.25	1.12	1.17	1.36	1.24	1.39	1.33	1.10	1.08	0.98	1.17	1.09	1.30
Total	100.28	100.26	100.55	99.00	98.83	99.74	100.17	100.14	100.72	100.28	100.58	99.38	99.90	99.12	99.07	100.77	100.09	100.06	99.94	99.96	100.09	100.49
Si	10.865	10.910	10.881	10.924	10.834	10.858	10.942	10.808	10.727	10.685	10.738	10.729	10.939	10.841	10.869	10.745	10.696	10.962	10.845	10.965	10.902	10.835
Al	5.096	5.051	5.056	5.017	5.111	5.070	4.966	5.130	5.221	5.257	5.230	5.246	4.990	5.097	5.045	5.216	5.290	4.961	5.069	4.980	5.008	5.157
Fe	0.051	0.048	0.058	0.033	0.048	0.028	0.052	0.043	0.031	0.034	0.065	0.039	0.043	0.039	0.038	0.031	0.036	0.054	0.055	0.037	0.045	0.021
Mg	0.000	0.000	0.034	0.000	0.000	0.000	0.000	0.000	0.050	0.048	0.027	0.024	0.000	0.000	0.000	0.029	0.000	0.000	0.000	0.000	0.000	0.000
Ca	1.209	1.186	1.167	1.230	1.325	1.285	1.222	1.319	1.330	1.309	1.293	1.322	1.236	1.333	1.306	1.292	1.350	1.183	1.313	1.174	1.276	1.205
Na	2.505	2.501	2.608	2.390	2.314	2.443	2.454	2.439	2.318	2.421	2.334	2.309	2.406	2.315	2.381	2.365	2.324	2.549	2.452	2.512	2.478	2.442
K	0.227	0.238	0.181	0.336	0.270	0.286	0.330	0.214	0.288	0.285	0.254	0.268	0.310	0.285	0.320	0.301	0.251	0.246	0.224	0.266	0.248	0.295
Total	19.953	19.934	19.985	19.930	19.902	19.971	19.967	19.954	19.966	20.039	19.941	19.937	19.924	19.910	19.959	19.979	19.947	19.955	19.958	19.934	19.957	19.954
An	30.7	30.2	29.5	31.1	33.9	32.0	30.5	33.2	33.8	32.6	33.3	33.9	31.3	33.9	32.6	32.6	34.4	29.7	32.9	29.7	31.9	30.6
Ab	63.6	63.7	65.9	60.4	59.2	60.9	61.3	61.4	58.9	60.3	60.1	59.2	60.9	58.9	59.4	59.8	59.2	64.1	61.5	63.6	61.9	62.0
Or	5.8	6.1	4.6	8.5	6.9	7.1	8.2	5.4	7.3	7.1	6.5	6.9	7.8	7.3	8.0	7.6	6.4	6.2	5.6	6.7	6.2	7.5

Sample	A2 rim	A2 rim	A2 rim	WA4 core	WA4 core	WA4 core	WA4 core	WA4 core	WA4 core	WA4 core	WA4 mid-grain	WA4 mid-grain	WA4 mid-grain	WA4 mid-grain	WA4 mid-grain (resorbed)	WA4 rim	WA4 rim	WA4 rim	WA4 rim	WA4 rim	WA4 rim	WA4 rim
SiO2	60.49	60.02	61.10	60.26	60.33	60.07	60.67	58.27	61.02	60.41	60.35	60.33	60.19	60.68	59.78	60.80	60.85	61.06	60.83	60.54	60.74	60.93
Al2O3	24.81	24.69	24.28	24.76	24.31	25.03	24.51	26.22	24.52	24.68	24.62	25.01	24.99	24.80	24.89	24.49	24.60	24.16	24.12	24.66	24.14	24.34
FeO	0.19	0.25	0.28	0.17	0.28	0.27	0.21	0.23	0.27	0.27	0.27	0.17	0.26	0.22	0.25	0.14	0.19	0.19	0.21	0.38	0.29	0.31
MgO		0.13					0.19		0.15		0.10	0.09			0.24				0.16		0.15	
CaO	6.78	6.90	5.96	6.64	6.26	7.09	6.38	8.36	6.44	6.65	6.65	6.77	6.72	6.64	6.73	6.25	6.34	5.84	5.89	6.40	6.01	6.20
Na2O	6.84	6.93	7.35	7.23	7.13	7.02	6.94	6.47	7.12	6.99	7.05	6.83	6.76	7.32	6.98	7.31	7.27	7.87	7.45	7.18	7.79	7.30
K2O	1.30	1.11	1.27	0.96	1.28	1.12	1.43	0.89	1.05	1.17	1.22	1.15	1.21	1.18	1.21	1.23	1.20	0.90	1.23	1.02	0.96	1.19
Total	100.41	100.03	100.24	100.02	99.59	100.60	100.33	100.44	100.57	100.17	100.26	100.35	100.13	100.84	100.08	100.22	100.45	100.02	99.89	100.18	100.08	100.27
Si	10.770	10.735	10.881	10.762	10.827	10.695	10.809	10.423	10.829	10.780	10.768	10.739	10.742	10.766	10.694	10.834	10.820	10.888	10.872	10.795	10.845	10.854
Al	5.207	5.205	5.097	5.212	5.142	5.253	5.147	5.528	5.129	5.191	5.178	5.248	5.257	5.186	5.248	5.144	5.156	5.078	5.081	5.183	5.080	5.111
Fe	0.028	0.037	0.042	0.025	0.042	0.040	0.031	0.034	0.040	0.040	0.040	0.025	0.039	0.033	0.037	0.021	0.028	0.028	0.031	0.057	0.043	0.046
Mg	0.000	0.035	0.000	0.000	0.000	0.000	0.050	0.000	0.040	0.000	0.027	0.024	0.000	0.000	0.064	0.000	0.000	0.000	0.043	0.000	0.040	0.000
Ca	1.293	1.322	1.137	1.271	1.204	1.353	1.218	1.602	1.225	1.271	1.271	1.291	1.285	1.262	1.290	1.193	1.208	1.116	1.128	1.223	1.150	1.183
Na	2.361	2.403	2.538	2.504	2.481	2.423	2.398	2.244	2.450	2.419	2.439	2.357	2.339	2.518	2.421	2.526	2.507	2.721	2.582	2.482	2.697	2.522
K	0.295	0.253	0.288	0.219	0.293	0.254	0.325	0.203	0.238	0.266	0.278	0.261	0.275	0.267	0.276	0.280	0.272	0.205	0.280	0.232	0.219	0.270
Total	19.955	19.991	19.984	19.993	19.989	20.018	19.978	20.036	19.950	19.967	20.001	19.946	19.937	20.033	20.031	19.997	19.991	20.036	20.018	19.971	20.073	19.986

An	32.7	33.2	28.7	31.8	30.3	33.6	30.9	39.6	31.3	32.1	31.9	33.0	33.0	31.2	32.4	29.8	30.3	27.6	28.3	31.1	28.3	29.8
Ab	59.8	60.4	64.0	62.7	62.4	60.1	60.8	55.4	62.6	61.1	61.2	60.3	60.0	62.2	60.7	63.2	62.9	67.3	64.7	63.1	66.3	63.4
Or	7.5	6.4	7.3	5.5	7.4	6.3	8.2	5.0	6.1	6.7	7.0	6.7	7.1	6.6	6.9	7.0	6.8	5.1	7.0	5.9	5.4	6.8

Plagioclase analyses and structural formulae - Eucarro and Yardea Dacites

Sample	Eu2 core	Eu2 core	Eu2 core	Eu2 core	Eu2 core	Eu2 core	Eu2 mid-grain	Eu2 mid-grain	Eu2 rim	Eu2 rim	Eu2 rim	Eu2 rim	Eu2 rim	Eu2 rim	Eu2 rim	Eu5 core	Eu5 core	Eu5 core	Eu5 mid-grain	Eu5 mid-grain	Eu5 mid-grain	Eu5 mid-grain
SiO2	62.32	60.46	61.61	61.69	62.30	62.41	62.02	61.46	63.07	62.22	62.24	62.94	63.98	63.40	62.29	62.47	62.54	62.06	62.43	62.51	62.44	62.50
Al2O3	23.84	24.83	23.98	24.24	23.66	23.38	24.14	24.19	23.18	23.81	23.70	23.25	22.62	22.82	23.71	23.20	23.19	23.65	23.18	23.31	23.31	23.52
FeO	0.12	0.21	0.27	0.18	0.22	0.21		0.28			0.26	0.22	0.16	0.22	0.24	0.27	0.13	0.35	0.34	0.26	0.22	0.14
MgO			0.10												0.11							
CaO	5.24	6.62	6.07	5.89	5.47	4.33	5.63	5.95	5.00	5.47	5.44	4.95	4.10	4.77	5.36	5.19	4.98	5.37	5.16	5.12	5.19	5.02
Na2O	8.00	7.50	7.57	7.76	7.86	7.95	7.73	7.73	8.54	8.03	8.03	8.47	8.96	8.37	7.95	7.51	7.54	7.62	7.61	7.57	7.69	7.72
K2O	0.67	0.57	0.72	0.62	0.75	0.74	0.71	0.67	0.39	0.55	0.62	0.49	0.45	0.52	0.57	1.75	1.78	1.21	1.48	1.51	1.41	1.18
Total	100.19	100.19	100.32	100.38	100.26	99.02	100.23	100.28	100.18	100.08	100.29	100.32	100.27	100.10	100.23	100.39	100.16	100.26	100.20	100.28	100.26	100.08
Si	11.037	10.765	10.935	10.930	11.040	11.148	10.983	10.913	11.150	11.029	11.028	11.128	11.283	11.216	11.032	11.097	11.120	11.024	11.100	11.098	11.089	11.092
Al	4.977	5.211	5.017	5.062	4.942	4.922	5.039	5.063	4.830	4.974	4.949	4.845	4.702	4.758	4.950	4.858	4.860	4.952	4.858	4.878	4.879	4.920
Fe	0.018	0.031	0.040	0.027	0.033	0.031	0.000	0.042	0.000	0.000	0.039	0.033	0.024	0.033	0.036	0.040	0.019	0.052	0.051	0.039	0.033	0.021
Mg	0.000	0.000	0.026	0.000	0.000	0.000	0.000	0.000	0.000	0.000	0.000	0.000	0.000	0.000	0.029	0.000	0.000	0.000	0.000	0.000	0.000	0.000
Ca	0.994	1.263	1.154	1.118	1.039	0.829	1.068	1.132	0.947	1.039	1.033	0.938	0.775	0.904	1.017	0.988	0.949	1.022	0.983	0.974	0.988	0.955
Na	2.747	2.589	2.605	2.666	2.701	2.753	2.654	2.661	2.927	2.760	2.759	2.904	3.064	2.871	2.730	2.587	2.600	2.625	2.624	2.606	2.648	2.657
K	0.151	0.129	0.163	0.140	0.170	0.169	0.160	0.152	0.088	0.124	0.140	0.110	0.101	0.117	0.129	0.397	0.404	0.274	0.336	0.342	0.319	0.267
Total	19.924	19.989	19.941	19.942	19.924	19.852	19.905	19.962	19.943	19.926	19.947	19.957	19.948	19.899	19.922	19.966	19.952	19.949	19.951	19.937	19.955	19.910
An	25.5	31.7	29.4	28.5	26.6	22.1	27.5	28.7	23.9	26.5	26.3	23.7	19.7	23.2	26.2	24.9	24.0	26.1	24.9	24.8	25.0	24.6
Ab	70.6	65.0	66.4	67.9	69.1	73.4	68.4	67.5	73.9	70.3	70.2	73.5	77.8	73.8	70.4	65.1	65.8	66.9	66.6	66.4	67.0	68.5
Or	3.9	3.3	4.2	3.6	4.3	4.5	4.1	3.8	2.2	3.2	3.6	2.8	2.6	3.0	3.3	10.0	10.2	7.0	8.5	8.7	8.1	6.9

Sample	Eu5 mid-grain	Eu5 mid-grain	Eu5 mid-grain	Eu5 mid-grain	Eu5 mid-grain	Eu5 rim	Eu5 rim
SiO2	62.78	62.69	62.62	62.20	62.39	63.43	62.76
Al2O3	23.34	23.22	23.25	23.48	23.40	23.22	23.41
FeO	0.15	0.21	0.19	0.31	0.23	0.12	0.13
MgO		0.16	0.11	0.10	0.11	0.12	0.13
CaO	5.09	4.78	4.68	5.39	5.25	4.44	4.85
Na2O	7.97	8.33	8.47	7.44	8.28	8.53	8.53
K2O	0.55	0.61	0.65	1.37	0.65	0.48	0.40
Total	99.88	100.00	99.97	100.29	100.31	100.34	100.21
Si	11.131	11.118	11.113	11.046	11.056	11.182	11.100
Al	4.878	4.854	4.864	4.915	4.888	4.825	4.880
Fe	0.022	0.031	0.028	0.046	0.034	0.018	0.019
Mg	0.000	0.042	0.029	0.026	0.029	0.032	0.034
Ca	0.967	0.908	0.890	1.026	0.997	0.839	0.919
Na	2.740	2.865	2.915	2.562	2.845	2.916	2.925
K	0.124	0.138	0.147	0.310	0.147	0.108	0.090
Total	19.862	19.956	19.986	19.932	19.996	19.918	19.968

An	25.2	23.2	22.5	26.3	25.0	21.7	23.4
Ab	71.5	73.2	73.8	65.7	71.3	75.5	74.3
Or	3.2	3.5	3.7	8.0	3.7	2.8	2.3

Appendix E: Trace element fractionation models for the mature phase

TRACE ELEMENT CALCULATIONS - FRACTIONAL CRYSTALLIZATION MODEL #Y1

F= 0.874 (F - fraction of melt remaining, taken from major element modelling)

Mineral	Plagioclase	Sanidine	Augite	Pigeonite	Magnetite	Apatite	Calc WR KD	Parent Conc	Daughter conc	Calc Daughter
Propn. fractionating assemblage	0.646	0	0.152	0.132	0.06	0.011		Y4	Y35	
Zr	0.36	0.05	0.5	0.22	2.4	0.00	0.482	402	399.2	431.1
Sr	4.4	3.87	0.08	0.01	0.00	0.39	2.860	196	157.6	152.6
Rb	0.2	1.2	0.03	0.00	0.00	0.11	0.135	182	213.6	204.5
Y	0.04	0.1	2.6	0.5	2	13.1	0.751	58	62.7	60.0
Ba	0.36	7.2	0.03	0.00	0.00	0.05	0.238	1205	1310	1335.3
Sc	0.04	0.02	44	18	1.5	0.1	9.181	14	10.8	4.7
Th	0.03	0.02	0.09	0.02	0.09	2.5	0.069	26	28.2	29.5
Ce	0.2	0.04	0.36	0.26	1.1	31	0.625	158	165.5	166.2
Nd	0.2	0.02	0.94	0.2	1.65	25	0.672	70	74.3	73.2
La	0.3	0.07	0.23	0.2	0.9	31	0.650	75	82.7	78.6

TRACE ELEMENT CALCULATIONS - FRACTIONAL CRYSTALLIZATION MODEL #Y2

F= 0.885 (F - fraction of melt remaining, taken from major element modelling)

Mineral	Plagioclase	Sanidine	Augite	Pigeonite	Magnetite	Apatite	Calc WR KD	Parent Conc	Daughter conc	Calc Daughter
Propn. fractionating assemblage	0.675	0	0.092	0.147	0.068	0.019		Y4	Y12	
Zr	0.36	0.05	0.5	0.22	2.4	0.00	0.485	402	412	428.1
Sr	4.4	3.87	0.08	0.01	0.00	0.39	2.986	196	158	150.0
Rb	0.2	1.2	0.03	0.00	0.00	0.11	0.140	182	208	204.4
Y	0.04	0.1	2.6	0.5	2	13.1	0.725	58	66	60.2
Ba	0.36	7.2	0.03	0.00	0.00	0.05	0.247	1205	1390	1333.7
Sc	0.04	0.02	44	18	1.5	0.1	6.825	14	13	6.4
Th	0.03	0.02	0.09	0.02	0.09	2.5	0.085	26	29	29.4
Ce	0.2	0.04	0.36	0.26	1.1	31	0.870	158	183	160.8
Nd	0.2	0.02	0.94	0.2	1.65	25	0.838	70	70	71.5
La	0.3	0.07	0.23	0.2	0.9	31	0.903	75	89	76.0

Mineral partition coefficient data have been chosen from ranges compiled from:
Arth (1976), Duncan and Taylor (1968), Irving and Frey (1978), Leeman and Phelps (1981), Mahood (1981), Nagasawa (1970), Nash and Crecraft (1985), Noble and Hedge (1970), Fujimaki and Tatsumoto (1984), Nagasawa and Schnetzler (1971), Philpotts and Schnetzler (1970), Schnetzler and Philpotts (1970), Onuma et al. (1968), Pearce and Norry (1979), Sisson (1991).

TRACE ELEMENT CALCULATIONS - FRACTIONAL CRYSTALLIZATION MODEL # E2

F= 0.818 (F - fraction of melt remaining, from major element modelling)

Mineral	Plagioclase	Sanidine	Augite	Pigeonite	Magnetite	Apatite	Calculated	Parent Conc	Daughter conc	Calc Daughter
Propn. fractionation assemblage	0.43	0.246	0.127	0.117	0.071	0.009	whole rock KD	Eu25	Eu21	
Zr	0.36	0.05	0.5	0.22	2.4	0.00	0.4267	414.4	470	465.0
Sr	4.4	3.87	0.08	0.01	0.00	0.39	2.8589	149.5	93.7	102.9
Rb	0.2	1.2	0.03	0.00	0.00	0.11	0.3860	196.8	230	222.6
Y	0.04	0.1	2.6	0.5	2	13.1	0.8280	63.8	68.4	66.0
Ba	0.36	7.2	0.03	0.00	0.00	0.05	1.7927	1368	1143	1166.6
Sc	0.04	0.02	44	18	1.5	0.1	7.8192	11.2	5.7	2.8
Th	0.03	0.02	0.09	0.02	0.09	2.5	0.1336	34.4	46.6	40.9
Ce	0.2	0.04	0.36	0.26	1.1	31	0.5291	168	193	184.7
Nd	0.2	0.02	0.94	0.2	1.65	25	0.6189	75	90	81.0
La	0.3	0.07	0.23	0.2	0.9	31	0.4127	84	97	94.5

MODEL # E1

F= 0.755 (F - fraction of melt remaining, from major element modelling)

Mineral	Plagioclase	Sanidine	Augite	Pigeonite	Magnetite	Apatite	Calculated	Parent Conc	Daughter conc	Calc Daughter
Propn. fractionation assemblage	0.291	0.418	0.112	0.123	0.046	0.011	whole rock KD	Y12	Eu21	
Zr	0.36	0.05	0.5	0.22	2.4	0.00	0.3191	414.4	470	501.8
Sr	4.4	3.87	0.08	0.01	0.00	0.39	2.9125	149.5	93.7	87.3
Rb	0.2	1.2	0.03	0.00	0.00	0.11	0.5644	196.8	230	222.4
Y	0.04	0.1	2.6	0.5	2	13.1	0.6422	63.8	68.4	70.5
Ba	0.36	7.2	0.03	0.00	0.00	0.05	3.1183	1368	1143	754.3
Sc	0.04	0.02	44	18	1.5	0.1	7.2321	11.2	5.7	1.9
Th	0.03	0.02	0.09	0.02	0.09	2.5	0.0613	34.4	46.6	44.8
Ce	0.2	0.04	0.36	0.26	1.1	31	0.5388	168	193	191.2
Nd	0.2	0.02	0.94	0.2	1.65	25	0.5473	75	90	85.2
La	0.3	0.07	0.23	0.2	0.9	31	0.5493	84	97	95.3

Mineral partition coefficient data have been chosen from ranges compiled from:
Arth (1976), Duncan and Taylor (1968), Irving and Frey (1978), Leeman and Phelps (1981), Mahood (1981), Nagasawa (1970), Nash and Crecraft (1985), Noble and Hedge (1970), Fujimaki and Tatsumoto (1984), Nagasawa and Schnetzler (1971), Philpotts and Schnetzler (1970), Schnetzler and Philpotts (1970), Onuma et al. (1968), Pearce and Norry (1979), Sisson (1991).

TRACE ELEMENT CALCULATIONS - FRACTIONAL CRYSTALLIZATION MODEL # P1

F= 0.789 (F - fraction of melt remaining, from major element modelling)

Mineral Propn. fractionating assemblage	Plagioclase 0.372	Sanidine 0.439	Augite 0.104	Pigeonite 0.026	Magnetite 0.0495	Apatite 0.0096	Calculated whole rock KD	Parent Conc Eu21	Daughter conc P6	Calc Daughter
Zr	0.36	0.05	0.5	0.22	2.4	0.00	0.3324	470	315	550.6
Sr	6.8	4.5	0.08	0.01	0.00	0.39	4.5174	93.7	34	40.7
Rb	0.2	1.2	0.03	0.00	0.00	0.11	0.6054	230	252	252.5
Y	0.04	0.1	2.6	0.5	2	13.1	0.5669	68.4	69	75.8
Ba	0.36	9.7	0.03	0.00	0.00	0.05	4.3958	1143	496	511.1
Sc	0.04	0.02	44	18	1.5	0.1	5.1429	5.7	4.8	2.1
Th	0.03	0.02	0.09	0.02	0.09	2.5	0.0583	46.6	43	58.3
Ce	0.2	0.04	0.36	0.26	1.1	31	0.4882	193	292	217.9
Nd	0.2	0.02	0.94	0.2	1.65	25	0.5078	90	112	101.1
La	0.3	0.07	0.23	0.2	0.9	31	0.5136	97	122	108.9

TRACE ELEMENT CALCULATIONS - FRACTIONAL CRYSTALLIZATION MODEL # P2

F= 0.793 (F - fraction of melt remaining, from major element modelling)

Mineral Propn. fractionating assemblage	Plagioclase 0.383	Sanidine 0.436	Augite 0.099	Pigeonite 0.000	Magnetite 0.041	Apatite 0.012	Olivine 0.029	Calculated whole rock KD	Parent Conc Y12	Daughter conc Eu21	Calc Daughter
Zr	0.36	0.05	0.5	0.22	2.4	0.00	0	0.3076	470	315	551.9
Sr	6.8	4.5	0.08	0.01	0.00	0.39	0	4.5790	93.7	34	40.9
Rb	0.2	1.2	0.03	0.00	0.00	0.11	0	0.6041	230	252	252.1
Y	0.04	0.1	2.6	0.5	2	13.1	0	0.5555	68.4	69	75.8
Ba	0.36	9.7	0.03	0.00	0.00	0.05	0	4.3707	1143	496	523.0
Sc	0.04	0.02	44	18	1.5	0.1	4.8	4.5819	5.7	4.8	2.5
Th	0.03	0.02	0.09	0.02	0.09	2.5	0.276	0.0708	46.6	43	57.8
Ce	0.2	0.03	0.36	0.26	1.1	31	0.93	0.5694	193	292	213.3
Nd	0.2	0.01	0.94	0.2	1.65	25	0.77	0.5640	90	112	99.6
La	0.3	0.07	0.23	0.2	0.9	31	1.08	0.6084	97	122	106.2

Mineral partition coefficient data have been chosen from ranges compiled from:
Arth (1976), Duncan and Taylor (1968), Irving and Frey (1978), Leeman and Phelps (1981), Mahood (1981), Nagasawa (1970), Nash and Crecraft (1985), Noble and Hedge (1970), Fujimaki and Tatsumoto (1984), Nagasawa and Schnetzler (1971), Philpotts and Schnetzler (1970), Schnetzler and Philpotts (1970), Onuma et al. (1968), Pearce and Norry (1979), Sisson (1991).

Appendix F: Data used for melting and AFC modelling of the mature phase.

Data used for melting and AFC calculations

Partition coefficients, from Feeley and Grunder, 1991

	La	Ce	Nd	Sm	Eu	Yb
Plagioclase	0.29	0.18	0.14	0.12	1.13	0.04
Opx	0.2	0.2	0.2	0.2	0.2	0.3
Quartz	0	0	0	0	0	0
Cpx	0.23	0.36	0.7	1.3	1.2	1.4
Magnetite	0.29	0.35	0.45	0.55	0.53	0.26
Apatite	25	31	31.1	40	27.3	21

Compositions used for REE melting calculations, from Taylor and McLennan, 1985

	La	Ce	Nd	Sm	Eu	Yb
Lower Crust	11	23	12.7	3.17	1.17	2.2
Bulk Crust	16	33	16	3.5	1.1	2.2

Residues for melting calculations
Melt of Bulk crust
residue 1: 60% plag; 35% cpx; 5% magnetite
residue 2: 60% plag; 35% opx; 5% magnetite

Melting lower crust
residue 1: 25%cpx;33%opx;42%plag
residue 2: 36%cpx;19%opx;45%plag

Partition coefficients
(from Feeley & Grunder, 1991; except those for olivine from Honjo and Leeman, 1987 and those for K and Ti from Pearce and Norry, 1979)

	Rb	Ba	Th	K	Nb	La	Ce	Sr	Nd	P	Zr	Ti	Y
Olivine	0.0055	0.0055	0.0055	0.0075	0.013	0.0019	0.0022	0.011	0.0034	0.01	0.0105	0.03	0.006
Plagioclase	0.02	0.48	0.01	0.17	0.03	0.29	0.18	3	0.14		0.01	0.04	0.04
Clinopyroxene	0.01	0.03	0.02	0.03	1	0.23	0.36	0.08	0.7		0.34	0.3	1.4
Orthopyroxene	0.02	0	0.02	0.02	0.3	0.2	0.2	0.01	0.2		0.2	0.1	0.3
Magnetite	0	0	0.06	0	3	0.29	0.35	0	0.45		0.63	7.5	0.26
Apatite	0.11	0.05	2.5	0	0.01	25	31	0.39	31.1		0		21
Quartz	0.009	0.032	0.014	0.009	0.001	0.014	0.02	0.001	0.012	0.001	0.08	0.001	0.001

Partition coefficients from Honjo &Leeman, 1987

	Rb	Ba	Th	K	Nb	La	Ce	Sr	Nd	P	Zr	Ti	Y
Olivine	0.0055	0.0055	0.0055	0.0075	0.013	0.0019	0.0022	0.011	0.0034	0.01	0.0105	0.03	0.006
Plagioclase	0.185	0.355	0.0055	0.21	0.013	0.17	0.1255	3.09	0.0915	0.0075	0.0155	0.055	0.035
Clinopyroxene	0.0055	0.1505	0.007	0.042	0.105	0.052	0.103	0.129	0.236	0.009	0.255	0.65	0.35
Magnetite	0.0055	0.0055	0.28	0.0055	0.6	0.0255	0.0255	0.0055	0.0255	0.0255	0.25	12.5	0.35
Apatite	0.026	0.026	2	0.0055	0.026	15	15	3	15	220	0.026	0.0055	20

Fractionating assemblage used for calculations

using partition coefficients a)
note: orthopyroxene partition coefficients used for pigeonite

Olivine	0.07
Plagioclase	0.555
Pigeonite	0.15
Clinopyroxene	0.184
Magnetite	0.034
Apatite	0.007

using partition coefficients b) -
note: all pyroxene as clinopyroxene

Olivine	0.07
Plagioclase	0.555
Clinopyroxene	0.334
Magnetite	0.034
Apatite	0.007

Rock compositions used in melting and AFC calculations
GH2 basalt and 908-1 rhyolite from Chapter 2: Bulk, uupper and lower crustal estimates from Taylor and McLennan, 1985.

GH2	56	482	6.2	14195	8.9	28	63	450	35	961	162	6894	28
908-1	185	919	23	43248	14.1	67	133	41	50	131	266	959	35
Bulk Crust	32	250	3.5	9131	11	16	33	260	16	437	100	5396	20
Upper crust	112	550	10.7	28223	25	30	64	350	26	874	190	2998	22
Lower crust	5.3	150	1.06	2822	6	11	23	230	12.7	568	70	5995	19

GEOLOGICAL SETTING OF THE GAWLER RANGE VOLCANICS

SCALE
1:500 000

KILOMETRES 10 0 10 20 30 40 50 KILOMETRES

PRINTED IN AUSTRALIA
D. J. WOOLMAN, GOVERNMENT PRINTER
SOUTH AUSTRALIA

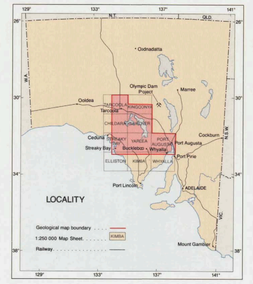

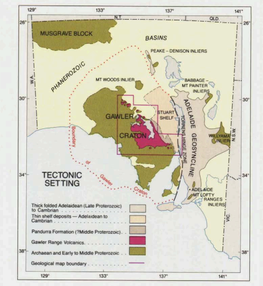

REFERENCE

CAINOZOIC

QUATERNARY

- Qs — Aeolian quartz sand and gypsiferous sand. Includes vegetated inland seif dunes. (Pleistocene to Holocene).
- Ql — Inland saline and gypsiferous lacustrine mud, silt and sand. Tidal-flat sediments bordering Spencer Gulf. (Pleistocene to Holocene).
- Qp — Thin red-brown and yellow-brown soil veneer on alluvial and colluvial clay, sand and gravel. Calcareous and ferruginous duricrusts (calcrete and ferricrete). (Pleistocene to Holocene).

TERTIARY

- Tsi — Silcrete (siliceous duricrust). Mainly "terrazzo" type with angular fragments of quartz in cryptocrystalline siliceous matrix.
- T — Undifferentiated Tertiary sediments, including equivalents of Eocene Pidinga Formation and Garford Formation (Miocene-Early Pliocene).

MESOZOIC

EARLY CRETACEOUS TO LATE JURASSIC

- J-K — Algebuckina Sandstone, Bulldog Shale.

PERMIAN TO CARBONIFEROUS

- CP — Boorthanna Formation, Stuart Range Formation, Mount Toondina Formation. — Sub-surface only (TARCOOLA region).

PALAEOZOIC

CAMBRIAN

STUART SHELF (West of Spencer Gulf) — ADELAIDE GEOSYNCLINE (East of Spencer Gulf)

- € — HAWKER GROUP (Andamooka Limestone).

PROTEROZOIC

LATE PROTEROZOIC — 900 Ma

ADELAIDEAN

	STUART SHELF (West of Spencer Gulf)	ADELAIDE GEOSYNCLINE (East of Spencer Gulf)
MARINOAN	Ewt — WILPENA GROUP (Tent Hill Formation: Equivalent to ABC Range Quartzite and Brachina Formation).	Ew — WILPENA GROUP (Brachina Formation, ABC Range Quartzite, Bunyeroo Formation and Wonoka Formation).
STURTIAN—MARINOAN	Eu — UMBERATANA GROUP (Whyalla Sandstone). — BURRA GROUP absent	Eu — UMBERATANA GROUP (Appila Tillite, Tapley Hill Formation, Brighton Limestone, undifferentiated Willochra Subgroup and Elatina Formation).
WILLOURAN—TORRENSIAN	Eb — CALLANNA GROUP (Backy Point Formation). Ebv—Beda Volcanics and related ? feeder-dykes (? Gairdner Dyke Swarm).	Eb — CALLANNA GROUP and BURRA GROUP. Ebv—Basic volcanics in Depot Creek.

NORTHWEST — GAWLER CRATON — SOUTHEAST

- E2p — Pandurra Formation. Red feldspathic sandstone and pebbly grit. Some bands of micaceous shale and siltstone.

TARCOOLA REGION — GAWLER RANGE VOLCANO—PLUTONIC PROVINCE — CORUNNA—MYALL CREEK—? ROOPENA

INTRUSIVE PHASE

- E2vb — Willabbie Volcanics (Tarcoola region — possibly related to Gawler Range Volcanics). Dykes of porphyritic rhyolite and rhyodacite; dacite, andesite, basalt.
- E2rh — HILTABA SUITE. Pink and reddish unfoliated leucocratic granite and adamellite.
- E2rd — Red-brown porphyritic rhyolite and rhyodacite plugs and dykes. Probably related to Gawler Range Volcanics.

GAWLER RANGE VOLCANICS "GOUGER"

KOKATHA AREA
- E2cb — Chandabooka Dacite.

NW LAKE GAIRDNER AREA
- E2cb — Chandabooka Dacite.

LAKE EVERARD AREA
- E2yd — Yardea Dacite.

GAWLER RANGES
- E2yd — Yardea Dacite. E2yb — "Black" dacite.
- E2pa — Paney Rhyolite.
- E2yb — Yannable Rhyodacite.
- E2ry — Eucarro Dacite. Porphyritic dacite at Mt Sturt, etc.
- E2ny — Nonning Rhyodacite.
- E2bl — Bittali Rhyolite.
- E2wa — Waganny Dacite.
- E2rb — Rhyolite 7km NE of Mt Sturt and 10km NW of "Buckleboo".
- E2nn — Nonning Rhyodacite.
- E2rp — Roopena Volcanics.
- E2pm — Porphyritic dacite, rhyodacite and rhyolite.

GAWLER RANGE VOLCANICS "OLDER"
- E2cb — Carnding Rhyodacite.
- E2ra — Ealbara Rhyolite.
- E2rk — Konkaby Basalt.
- ? — Tarcoola Formation.
- Muckanippie Dioritic Complex.

CHITANILGA VOLCANIC COMPLEX
- E2rk — Red rhyodacite and rhyolite.
- E2ra — Potassic andesite.
- E2rb — Basaltic andesite.
- ? E2sd — ? Lake Gairdner Rhyolite equivalent.
- E2sd — Lake Gairdner Rhyolite.
- E2ra — Basalt.
- E2rb — Red and grey rhyodacite and rhyolite.
- E2rbc — Basalt, andesite. Interlayered rhyodacite and dacite.

GLYDE HILL VOLCANIC COMPLEX
- E2rw — Whyeela Dacite.
- E2rb — Yantea Rhyodacite. Buckyburn Dacite.
- E2rw — Wheppool Rhyolite. Baldry Rhyolite. Arburree Rhyolite. Mangaroongah Dacite. Childera Dacite.

- E2p — Metadolerite dykes S of Mt Sturt.

EARLY PROTEROZOIC — 1600 Ma

- Ep — LINCOLN COMPLEX — Quartzofeldspathic gneiss and migmatite. Foliated and non-foliated granitoids.
- Eh — HUTCHISON GROUP — MIDDLEBACK SUBGROUP Ferruginous jaspilite, quartzite and gneiss; quartz-mics schist; dolomitic marble.
- Eww — Warrow Quartzite — Massive to flaggy siliceous,micaceous and feldspathic quartzite with some pebble conglomerate; leucogneiss.

ARCHAEAN — 2500 Ma

- AEp — MULGATHING COMPLEX (NW part of Gawler Craton).
- AEs — SLEAFORD COMPLEX (S part of Gawler Craton). — Garnetiferous foliated quartz-feldspar-biotite gneiss; augen gneiss; granulite; banded iron formation; amphibolite; metabasalt including pillow-lava.

- Emy — Myola Volcanics (west of Whyalla).
- Em — Moonabie Formation — Volcaniclastic pebbly grit and sandstone.
- Pc — Corunna Conglomerate.

GEOCHRONOLOGICAL AGE (Rb–Sr; U–Pb). Ma = 1 Million years before present. ($\lambda^{87}Rb = 1.42 \times 10^{-11}\ yr^{-1}$) — HILTABA SUITE Rb–Sr 1477 ± 34 Ma

GEOLOGICAL BOUNDARY

VOLCANIC LAYERING — INCLINED, VERTICAL; HORIZONTAL, INCLINED (INFERRED FROM COLUMNAR JOINTING)

FAULT — OBSERVED; INFERRED

BOREHOLE INTERSECTING CONCEALED GAWLER RANGE VOLCANICS — 6035 WW 7 (Rig 17)

HYDROGRAPHICAL FEATURE — DRAINAGE (intermittent); SWAMP

MANGROVE; PLAYA LAKE

RELIEF FEATURE — TRIANGULATION STATION; IDENTIFIED POINT (elevation in metres); TOPOGRAPHIC CONTOURS (100 metre interval); SAND DUNE

CULTURAL FEATURE — RAILWAY WITH STATION OR SIDING; HIGHWAY WITH ROUTE NUMBER; MAIN ROAD; SECONDARY ROAD; TRACK; DOG FENCE; HOMESTEAD

GEOLOGICAL COMPILATION BASED ON 1:250 000 GEOLOGICAL SERIES
(Geological Survey of South Australia, Department of Mines and Energy).

PUBLISHED MAP SHEETS

CHILDARA, SHEET SH 53-14. Blissett, A.H., 1977.

GAIRDNER, SHEET SH 53-15. Blissett, A.H., 1977.

PORT AUGUSTA, SHEET SI 53-4. Dalgarno, C.R., Johnson, J.E., Forbes, B.G. and Thomson, B.P., 1968, (with additions and amendments).

TARCOOLA, SHEET SH 53-10. Daly, S.J., 1985.

WHYALLA, SHEET SI 53-8. Parker, A.J., 1983.

UNPUBLISHED MAP SHEETS

ELLISTON, SHEET SI 53-6. Flint, R.B. (in progress).

KIMBA, SHEET SI 53-7. Flint, R.B.,Rankin, L.R. and Parker, A.J. (in progress).

KINGOONYA, SHEET SH 53-11. Cowley, W.M. and Martin,A.R. (in progress); Miller, G.C. (Amoco Minerals Australia Company), 1980, (Map revised, 1983). S.A.DME. open file Env. 3726 (unpublished).

STREAKY BAY, SHEET SI 53-2. Flint, R.B.,and Blissett, A.H. (in progress).

YARDEA, SHEET SI 53-3. Blissett, A.H., Parker, A.J. and Crooks, A.F. (in preparation).

RADIOMETRIC AGES

Rb – Sr — Webb, A.W., Thomson, B.P., Blissett, A.H., Daly, S.J., Flint, R.B. and Parker, A.J., 1986. Geochronology of the Gawler Craton, South Australia. *Aust. J. Earth Sci.* Vol. 33, pp. 119-143.

U – Pb — HILTABA SUITE. Cooper, J.A., Mortimer, G.E., Rosier, C.M. and Uppill, R.K., 1985. Gawler Range magmatism — further isotopic age data. *Aust. J. Earth Sci.* Vol. 32, pp. 115–123.

GAWLER RANGE VOLCANICS. Fanning, C.M., Blissett, A.H., Flint, R.B., Ludwig, K.R. and Parker, A.J., 1986. A refined geological history for the southern Gawler Craton through U-Pb zircon dating of acid volcanics and correlations with Northern Australia. Abstracts 8th Aust. geol. Conv, Geol. Soc. Aust., Adelaide, pp. 67-68.

Transverse Mercator Projection. Australian Map Grid.

Compiled by A.H. Blissett, M.Sc.

B.G. Forbes, Ph.D., Chief Geologist, Regional Geology Branch.

Cartography by the Drafting Branch, Department of Mines and Energy.

Compiled under the direction of R.K. Johns, M.Sc., Director-General, Department of Mines and Energy.

Issued under the authority of the Honourable R.G. Payne, M.P., Minister of Mines and Energy.

Published 1987

Bibliographic Reference: Blissett, A.H. (Compiler), 1987. Geological Setting of the Gawler Range Volcanics, Geological Atlas Special Series, 1:500 000.S. Aust. Dept. Mines and Energy.